2.5 GEOLOGY, SEISMOLOGY, AND GEOTECHNICAL ENGINEERING

{This section of the U.S. EPR FSAR is incorporated by reference with the following departure(s) and/or supplement(s).

This section presents information on the geological, seismological, and geotechnical engineering properties of the CCNPP3 site. Section 2.5.1 describes basic geological and seismologic data, focusing on those data developed since the publication of the Final Safety Analysis Report (FSAR) for licensing CCNPP Units 1 and 2. Section 2.5.2 describes the vibratory ground motion at the site, including an updated seismicity catalog, description of seismic sources, and development of the Safe Shutdown Earthquake (SSE) and Operating Basis Earthquake (OBE) ground motions. Section 2.5.3 describes the potential for surface faulting in the site area, and Section 2.5.4 and Section 2.5.5 describe the stability of surface materials at the site.

Appendix D of Regulatory Guide 1.165, "Geological, Seismological and Geophysical Investigations to Characterize Seismic Sources," (NRC, 1997) provides guidance for the recommended level of investigation at different distances from a proposed site for a nuclear facility.

- The site region is that area within 200 mi (322 km) of the site location (Figure 2.5-1).
- The site vicinity is that area within 25 mi (40 km) of the site location (Figure 2.5-2).
- The site area is that area within 5 mi (8 km) of the site location (Figure 2.5-3).
- The site is that area within 0.6 mi (1 km) of the site location (Figure 2.5-4).

The terms, site region, site vicinity, site area, and site, are used in Sections 2.5.1 through 2.5.3 to describe these specific areas of investigation. These terms are not applicable to other sections of the FSAR.

The geological and seismological information presented in this section was developed from a review of previous reports prepared for the existing units, published geologic literature, interpretation of aerial photography, and a subsurface investigation and field and aerial reconnaissance conducted for preparation of this application. Previous site-specific reports reviewed include the Preliminary Safety Analysis Report (BGE, 1968) and the Independent Spent Fuel Storage Installation Safety Analysis Report (CEG, 2005). A review of published geologic literature was used to supplement and update the existing geological and seismological information. In addition, relevant unpublished geologic literature, studies, and projects were identified by contacting the U.S. Geological Survey (USGS), State geological surveys and universities. The list of references used to compile the geological and seismological information is presented in the applicable section.

Field reconnaissance of the site and within a 25 mi (40 km) radius of the site was conducted by geologists in teams of two or more. Two field reconnaissance visits in late summer and autumn 2006 focused on exposed portions of the Calvert Cliffs, other cliff exposures along the west shore of Chesapeake Bay, and roads traversing the site and a 5 mi (8 km) radius of the CCNPP site. Key observations and discussion items were documented in field notebooks and photographs. Field locations were logged by hand on detailed topographic base maps and with hand-held Global Positioning System (GPS) receivers.

Aerial reconnaissance within a 25 mi (40 km) radius of the site was conducted by two geologists in a top-wing Cessna aircraft on January 3, 2007. The aerial reconnaissance investigated the geomorphology of the Chesapeake Bay area and targeted numerous previously mapped geologic features and potential seismic sources within a 200 mi (322 km) radius of the CCNPP site (e.g., Mountain Run fault zone, Stafford fault system, Brandywine fault zone, Port Royal fault zone, and Skinkers Neck anticline). The flight crossed over the CCNPP site briefly but did not circle or approach the site closely in order to comply with restrictions imposed by the Federal Aviation Administration. Key observations and discussion items were documented in field notebooks and photographs. The flight path, photograph locations, and locations of key observations were logged with hand-held GPS receivers.

The investigations of regional and site physiography and geomorphology, geologic history, and stratigraphy (Sections 2.5.1.1.1 through 2.5.1.1.3, and Sections 2.5.1.2.1 through 2.5.1.2.3) were conducted by Bechtel Power Corporation. The investigations of regional and site tectonics and structural geology (Sections 2.5.1.1.4 and 2.5.1.2.4) were conducted by William Lettis and Associates. Paul C. Rizzo Associates, Inc. completed the evaluation of vibratory ground motion for the CCNPP site (Section 2.5.2). This evaluation was accomplished through a Probabilistic Seismic Hazard Analysis (PSHA), the results of which are used to determine uniform hazard response spectra (UHRS) and ground motion response spectra (GMRS) for the site. Paul C. Rizzo Associates, Inc. also completed a review of recent (post-2010) publications directly related to the principal tectonic structures in the site region, as identified in Section 2.5.1.1.4. These more recent publications indicate no evidence of tectonic or geologic instability within the site vicinity.

This section is intended to demonstrate compliance with the requirements of paragraph c of 10 CFR 100.23, "Geologic and Seismic Siting Criteria" (CFR, 2007).}

2.5.1 Basic Geologic and Seismic Information

The U.S EPR FSAR includes the following COL Item in Section 2.5.1:

> A COL applicant that references the U.S. EPR design certification will use site-specific information to investigate and provide data concerning geological, seismic, geophysical, and geotechnical information.

This COL Item is addressed as follows:

{This section presents information on the geological and seismological characteristics of the site region (200 mi (322 km) radius), site vicinity (25 mi (40 km) radius), site area (5 mi (8 km) radius) and site (0.6 mi (1 km) radius). Section 2.5.1.1 describes the geologic and tectonic characteristics of the site region. Section 2.5.1.2 describes the geologic and tectonic characteristics of the site vicinity and location. The geological and seismological information was developed in accordance with the following NRC guidance documents:

- Regulatory Guide 1.70, Section 2.5.1, "Basic Geologic and Seismic Information," (NRC, 1978)
- Regulatory Guide 1.206, Section 2.5.1, "Basic Geologic and Seismic Information," (NRC, 2007) and
- Regulatory Guide 1.165, "Identification and Characterization of Seismic Sources and Determination of Safe Shutdown Earthquake Ground Motion," (NRC, 1997).

2.5.1.1 Regional Geology (200 mi (322 km) radius)

This section discusses the physiography, geologic history, stratigraphy, and tectonic setting within a 200 mi (322 km) radius of the site. The regional geologic map and explanation as shown in Figure 2.5-5 and Figure 2.5-6 contain information on the geology, stratigraphy, and tectonic setting of the region surrounding the CCNPP site (Schruben, 1994). Summaries of these aspects of regional geology are presented to provide the framework for evaluation of the geologic and seismologic hazards presented in the succeeding sections.

Sections 2.5.1.1.1 through 2.5.1.1.4 are added as a supplement to the U.S. EPR FSAR.

2.5.1.1.1 Regional Physiography and Geomorphology

The CCNPP site lies within the Coastal Plain Physiographic Province as shown in Figure 2.5-1 (Fenneman, 1946). The area within a 200 mi (322 km) radius of the site encompasses parts of five other physiographic provinces. These are the: Continental Shelf Physiographic Province, which is located east of the Coastal Plain Province, and the Piedmont, Blue Ridge, Valley and Ridge and Appalachian Plateau physiographic provinces, which are located successively west and northwest of the Piedmont Province (Thelin, 1991).

Each of these physiographic provinces is briefly described in the following sections. The physiographic provinces in the site region are shown on Figure 2.5-1 (Fenneman, 1946). A map showing the physiographic provinces of Maryland, as depicted by the Maryland Geological Survey (MGS), is shown on Figure 2.5-7.

2.5.1.1.1.1 Coastal Plain Physiographic Province

The Coastal Plain Physiographic Province extends eastward from the Fall Line (the physiographic and structural boundary between the Coastal Plain Province and the Piedmont Province) to the coastline as shown in Figure 2.5-1. The Coastal Plain Province is a low-lying, gently-rolling terrain developed on a wedge-shaped, eastward-dipping mass of Cretaceous, Tertiary, and Quaternary age as shown in Figure 2.5-5 and Figure 2.5-6, which are unconsolidated and semi-consolidated sediments (gravels, sands, silts, and clays), that thicken toward the coast. This wedge of sediments attains a thickness of more than 8,000 ft (2,430 m) along the coast of Maryland (MGS, 2007). In general, the Coastal Plain Province is an area of lower topographic relief than the Piedmont Province to the west. Elevations in the Coastal Plain Province of Maryland range from near sea level to 290 ft (88 m) above sea level near the District of Columbia - Prince Georges County line (Otton, 1955).

Four main periods of continental glaciation occurred in the site region during the Pleistocene. Glaciers advanced only as far south as northeastern Pennsylvania and central New Jersey as shown in Figure 2.5-5 and Figure 2.5-6. However, continental glaciation affected sea level and both coastal and fluvial geomorphic processes, resulting in the landforms that dominate the Coastal Plain Province.

In Maryland, the MGS subdivides the Coastal Plain Physiographic Province into the Western Shore Uplands and Lowlands regions, the Embayment occupied by the Chesapeake Estuary system, and the Delmarva Peninsula Region on the Eastern Shore of the Chesapeake Bay as shown in Figure 2.5-7. In the site region and vicinity, geomorphic surface expression is a useful criterion for mapping the contacts between Pliocene and Quaternary. These geomorphic features appear to be mappable only on the more detailed county (1:62500) or quadrangle (1:2400) scales. For example, geomorphic surface expression is one of the criteria used by McCartan (McCartan, 1989b) to map the contact between Pliocene and Quaternary units in

St. Mary's County. Constructional surface deposits define the tops of estuarine and fluvial terraces and erosional scarps correspond with the sides of old estuaries (McCartan, 1989a) (McCartan, 1989b). In some areas, the physiographic expression of terraces that might have formed in response to alternate deposition and erosion during successive glacial stages is poorly defined (Glaser, 1994) (Glaser, 2003c). Sea levels were relatively lower during glacial stages than present-day, and relatively higher than present-day during interglacial stages. Deposition and erosion during periods of higher sea levels led to the formation of several discontinuous Quaternary-age stream terraces that are difficult to correlate (McCartan, 1989a). The distribution of Quaternary surficial deposits in the CCNPP site area and site location is discussed in Section 2.5.1.2. Northeast of the Chesapeake Bay, the Western Shore Uplands Region consists of extensive areas of relatively little topographic relief, less than 100 ft (30 m). The Western Shore Lowlands Region located along the west shore of Chesapeake Bay and north of the Western Shore Uplands Region as shown in Figure 2.5-7 is underlain by interbedded quartz-rich gravels and sands of the Cretaceous Potomac Group and gravel, sand, silt and clay of the Quaternary Lowland deposits. During glacial retreats, large volumes of glacial melt-waters formed broad, high energy streams such as the ancestral Delaware, Susquehanna, and Potomac Rivers that incised deep canyons into the continental shelf. Southwest of the Chesapeake Bay, marine and fluvial terraces developed during the Pliocene and Pleistocene. As a result of post-Pleistocene sea level rise, the outline of the present day coastline is controlled by the configuration of drowned valleys, typified by the deeply recessed Chesapeake Bay and Delaware Bay. Exposed headlands and shorelines have been modified by the development of barrier islands and extensive lagoons (PSEG, 2002).

2.5.1.1.1.2 Continental Shelf Physiographic Province

The Continental Shelf Physiographic Province is the submerged continuation of the Coastal Plain Province and extends from the shoreline to the continental slope as shown in Figure 2.5-1. The shelf is characterized by a shallow gradient of approximately 10 ft/mi (1.9 m/ km) to the southeast (Schmidt, 1992) and many shallow water features that are relics of lower sea levels. The shelf extends eastward for about 75 to 80 mi (121 to 129 km), where sediments reach a maximum thickness of about 40,000 ft (12.2 km) (Edwards, 1981). The eastward margin of the continental shelf is marked by the distinct break in slope to the continental rise with a gradient of approximately 400 ft/mi (76 m/km) (Schmidt, 1992).

2.5.1.1.1.3 Piedmont Physiographic Province

The Piedmont Physiographic Province extends southwest from New York to Alabama and lies west of, and adjacent to, the Coastal Plain Physiographic Province as shown in Figure 2.5-1. The Piedmont is a rolling to hilly province that extends from the Fall Line in the east to the foot of the Blue Ridge Mountains in the west as shown in Figure 2.5-1. The Fall Line is a low east-facing topographic scarp that separates crystalline rocks of the Piedmont Province to the west from less resistant sediments of the Coastal Plain Province to the east (Otton, 1955) (Vigil, 2000). The Piedmont Province is about 40 mi (64 km) wide in southern Maryland and narrows northward to about 10 mi (16 km) wide in southeastern New York.

Within the site region, the Piedmont Province is generally characterized by deeply weathered bedrock and a relative paucity of solid rock outcrop (Hunt, 1972). Residual soil (saprolite) covers the bedrock to varying depths. On hill slopes, the saprolite is capped locally by colluvium (Hunt, 1972).

In Maryland, the Piedmont Province is divided into the Piedmont Upland section to the east and the Piedmont Lowland section to the west, which is referred to as a sub-province in some publications as shown in Figure 2.5-7. The Piedmont Upland section is underlain by

metamorphosed sedimentary and crystalline rocks of Precambrian to Paleozoic age. These lithologies are relatively resistant and their erosion has resulted in a moderately irregular surface. Topographically higher terrain is underlain by Precambrian crystalline rocks and Paleozoic quartzite and igneous intrusive rocks. The Piedmont Lowland section is a less rugged terrain containing fault-bounded basins filled with sedimentary and igneous rocks of Triassic and Early Jurassic age.

2.5.1.1.1.4 Blue Ridge Physiographic Province

The Blue Ridge Physiographic Province is bounded on the east by the Piedmont Province and on the west by the Valley and Ridge Province as shown in Figure 2.5-1. The Blue Ridge Province, aligned in a northeast-southwest direction, extends from Pennsylvania to northern Georgia. It varies in approximate width from 5 mi (8 km) to more than 50 mi (80 km) (Hunt, 1967). This province corresponds with the core of the Appalachians and is underlain chiefly by more resistant granites and granitic gneisses, other crystalline rocks, metabasalts (greenstones), phyllites, and quartzite along its crest and eastern slopes.

2.5.1.1.1.5 Valley and Ridge Physiographic Province

The Valley and Ridge Physiographic Province lies west of the Blue Ridge Province and east of the Appalachian Plateau Province as shown in Figure 2.5-1. This is designated as the Valley and Ridge Province in Maryland as shown in Figure 2.5-7. Valleys and ridges are aligned in a northeast-southwest direction in this province, which is between 25 and 50 mi (40 and 80 km) wide. The sedimentary rocks underlying the Valley and Ridge Province are tightly folded and, in some locations, faulted. Sandstone units that are more resistant to weathering are the ridge formers. Less resistant shales and limestones underlie most of the valleys as shown in Figure 2.5-5 and Figure 2.5-6. The Great Valley Section of the province as shown in Figure 2.5-7, to the east, is divided into many distinct lowlands by ridges or knobs, the largest lowland being the Shenandoah Valley in Virginia. This broad valley is underlain by shales and by limestones that are prone to dissolution, resulting in the formation of sinkholes and caves. Elevations within the Shenandoah Valley typically range between 500 and 1,200 ft (152 and 366 m) msl. The western portion of the Valley and Ridge Province is characterized by a series of roughly parallel ridges and valleys, some of which are long and narrow (Lane, 1983). Elevations within the ridges and valleys range from about 1,000 to 4,500 ft (305 to 1,372 m) msl (Bailey, 1999).

2.5.1.1.1.6 Appalachian Plateau Physiographic Province

Located west of the Valley and Ridge Province, the Appalachian Plateau Physiographic Province includes the western part of the Appalachian Mountains, stretching from New York to Alabama as shown in Figure 2.5-1. The Allegheny Front is the topographic and structural boundary between the Appalachian Plateau and the Valley and Ridge Province (Clark, 1992). It is a bold, high escarpment, underlain primarily by clastic sedimentary rocks capped by sandstone and conglomerates. In eastern West Virginia, elevations along this escarpment reach 4,790 ft (1,460 m) (Hack, 1989). West of the Allegheny Front, the Appalachian Plateau's topographic surface slopes gently to the northwest and merges imperceptibly into the Interior Low Plateaus. Only a small portion of this province lies within 200 mi (322 km) of the CCNPP site as shown in Figure 2.5-1.

The Appalachian Plateau Physiographic Province is underlain by sedimentary rocks such as sandstone, shale, and coal of Cambrian to Permian age as shown in Figure 2.5-5 and Figure 2.5-6. These strata are generally subhorizontal to gently folded into broad synclines and anticlines and exhibit relatively little deformation. These sedimentary rocks differ significantly from each other with respect to resistance to weathering. Sandstone units tend to be more

resistant to weathering and form topographic ridges. The relatively less resistant shales and siltstones weather preferentially and underlie most valleys. The Appalachian Plateau is deeply dissected by streams into a maze of deep, narrow valleys and high narrow ridges (Lane, 1983). Limestone dissolution and sinkholes occur where limestone units with high karst susceptibility at or near the ground surface.

2.5.1.1.2 Regional Geologic History

The geologic and tectonic setting of the CCNPP site region is the product of a long, complex history of continental and island arc collisions and rifting. The geologic history, as deduced from subsurface exploration, rock and rock / sediment exposures, structural and stratigraphic relationships, and geophysical evidence, spans a period of more than one billion years (1000 Ma). The geologic history includes the formation of the Grenville Mountains, the Appalachian Mountains, and associated island arc and microcontinental terranes that have been accreted to the existing mid-Atlantic continental margin. The top of the Grenville Mountains have been eroded and buried beneath younger rocks, but their bases underlie much of the eastern North America continental margin. Exposed remnants of the Grenville Mountains are found where overlying rocks have been worn away by erosion and the scraping action of glaciers. In the northeast, the Grenville rocks are exposed in the Adirondacks, the Hudson and Jersey Highlands, Manhattan and Westchester in New York, the Green Mountains of Vermont, the Reading Prong of Pennsylvania, and the Berkshire Hills of Massachusetts. The Appalachian Mountains include deformed rock of the Appalachian Plateau, Valley and Ridge, Blue Ridge, and rocks of the New England physiographic provinces, including Proterozoic through Paleozoic metamorphosed thrust sheets and plutons. The Appalachian Mountains are disrupted by subsequent development of Mesozoic (Late Triassic and Early Jurassic) rift basins filled with igneous and sedimentary rocks, and basalt dikes and sills that intruded both rift basins and surrounding Piedmont crystalline basement exposed in the hilly, subdued topography of the Piedmont physiographic province. The eastward dipping clastic wedge of Cenozoic sediments overlaps some of the Piedmont and New England physiographic provinces and covers the entire Coastal Plain province. This variation in lithologies results in varied terrane that is reflected in the physiographic provinces of the region, as shown in Figure 2.5-1.

This geologic history of the region is discussed within the context of tectonostratigraphic terranes shown in Figure 2.5-9. Episodes of continental collisions have produced a series of accreted terranes separated, in part, by low angle detachment faults or juxtaposed by higher-level normal faulting. Episodes of extension have reactivated many earlier structures and created new ones. The deformation of these terranes through time imparts a pre-existing structural grain in the crust that is important for understanding the current seismotectonic setting of the region.

Sources of seismicity may occur in the overlying, exposed terranes or along structures within the North American basement buried beneath the accreted terranes or overthrust plates. Therefore, regional seismicity may not be related to any known surface structure. Intervening episodes of continental rifting have produced high angle normal or transtensional faults that either sole downward into detachment faults or penetrate entirely through the accreted terranes and upper crust. Understanding the geologic history, including the evolution and the geometry of these crustal faults, is important for identifying potentially active faults and evaluating the distribution of historical seismicity within the tectonic context of the site region. Based on the geologic history presented here, the seismic implications of geologic structures and the current state of strain in the region are discussed in Sections 2.5.1.1.2.8, 2.5.1.1.3.2.1, and 2.5.2.2.

Major tectonic events recognized in the site region include five compressional orogenies (Grenville, Potomac, Taconic, Acadian and Alleghany) and two extensional episodes (Late Precambrian rifting to produce the Iapetus Ocean and Mesozoic rifting to produce the Atlantic Ocean)(Faill, 1997a). Extension probably occurred, perhaps of less scale and duration, between each of the compressional episodes (resulting in the opening of the Rheic and Theic oceans, for example). These compressional and extensional episodes began to be recognized in the 1970s through 1980s and are depicted in Figure 2.5-8, modified from Hatcher, 1987. While direct evidence of these deformational events is visible in the Appalachian Plateau, Valley and Ridge, Blue Ridge, Piedmont and New England physiographic provinces, other evidence is buried beneath the Coastal Plain sediments in the site region and is inferred based on geophysical data, as described in Section 2.5.1.1.4.3, and borehole data as described in Section 2.5.1.1.3. The site region is located currently on the passive, trailing margin of the North American plate following the last episode of continental extension and rifting. The current stress regime of this region is discussed in Section 2.5.1.1.4.2. The history of orogenic events is described below.

2.5.1.1.2.1 Grenville Orogeny

The earliest compressional event (orogeny) recorded in the exposed rocks of the mid-Atlantic continental margin is the Grenville orogeny. Prior to the Grenville compressional event, a 'supercontinental' landmass known as Hudsonland (also known as Columbia) is postulated to have included the Laurentian craton (Pesonen, 2003). On the basis of purely paleomagnetic data, this supercontinent consisted of Laurentia, Baltica, Ukraine, Amazonia and Australia and perhaps also Siberia, North China and Kalahari. Hudsonland existed from 1830 Ma to ca. 1500–1250 Ma (Pesonen, 2003). The interior of the Laurentian craton experienced plutonism in the 1740 to 1504 Ma time frame and Hudsonland began to split apart and volcanic arcs were formed between 1300 and 1250 Ma. A composite arc belt or microcontinent was formed by about 1200 Ma in the Panthalassa-type ocean basin. (Carr, 2000; Murphy, 2004). This set the stage for the Grenville orogeny.

The Grenville orogeny occurred during Middle Proterozoic time, approximately one billion years ago (1000 Ma). Two phases of compression are recognized, from ca. 1080-1030 Ma and 1010-980 Ma (Carr, 2000). A composite arc or micro-continent was thrust over the eastern Laurentian margin. The uplifted terranes were dissected and exhumed by normal faulting before ca. 1040 Ma. Despite a long pre-Grenvillian tectonic and plutonic history, the present crustal architecture and much of the seismic reflectivity were acquired during the 1080-980 Ma phase of compression and extension (Carr, 2000).

The Grenville orogeny was the result of the convergence of the ancestral North American craton (Laurentia) with proto-African tectonic plates. During this orogeny, various terranes were accreted onto the edge of Laurentia, forming the Grenville Mountains (Faill, 1997a) and the supercontinent of Rodinia (Thomas, 2006). The Grenville Mountains were likely the size of the present day Himalayas (Carr, 2004). Convergence around the periphery of the Laurentian craton produced a series of mountain ranges offset by transform boundaries.

Intrusive Grenville rocks of the north-central Appalachians are exposed in the Piedmont physiographic province of central Maryland, southeastern Pennsylvania and northern New Jersey (Figure 2.5-201). In the north-central (Maryland and Pennsylvania) Appalachians, these massifs are separated by the Pleasant Grove-Huntingdon Valley shear zone (PGHV) into external and internal massifs (Figure 2.5-201)(Faill, 1997a). External massifs include the Reading Prong, Honey Brook Upland, Mine Ridge, and Trenton Prong. The stratigraphy of the external massifs is described in more detail in Section 2.5.1.1.3.1.1. Internal massifs include the Brandywine and Baltimore massifs (Figure 2.5-204). The stratigraphy of the internal massifs is

described in more detail in Section 2.5.1.1.3.1.2. Other small external massifs are recognized throughout the area (Faill, 1997a).

External massifs are allochthonous massifs that were emplaced by Taconic or Alleghany age thrusts and are now surrounded by Paleozoic and Mesozoic age rocks. External basement massifs (closer to the foreland) in the central and northern Appalachians expose Mesoproterozoic rocks that are likely derived from the nearby craton and mark the eastern edge of Laurentia. They are important because they record the Neoproterozoic rifting of Rodinia (Figure 2.5-205) and the Paleozoic collisions of arcs and continents that eventually formed the supercontinent of Pangea (Karabinos, 2008 and Hatcher, 2004). Internal basement massifs are located in the internal parts of an orogen and can be derived from a number of sources, not necessarily from the nearby craton (Hatcher, 2004).

The Grenville orogeny was followed by several hundred million years of tectonic quiescence, during which time the Grenville Mountains were eroded and their basement rocks exposed. The stratigraphy of Grenville remnants found within a 200-mile (322-kilometer) radius of the CCNPP site is described in more detail in Sections 2.5.1.1.3.1. Eventually, the supercontinent of Laurentia underwent a major rifting episode that led to the opening of the Iapetus Ocean (Figure 2.5-8) in late Precambrian time, 590–550 Ma (van Staal, 1998). Evidence of rifting can be found in the presence of metamorphosed mafic dikes (for example, the Chesnutt Hill Formation in the western New Jersey Highlands) (Gates, 2004) and the Catoctin and Swift Run formations in central Virginia (Bartholomew, 2004). Continued rifting produced a great basin off the Laurentian margin (the Theic or Rheic oceans) (Figure 2.5-203 and Figure 2.5-206) in which thousands of meters of quartz arenites and limestones/dolomites, including stromatolites, were deposited in shallow (e.g. Frederick Valley Chilhowee Group Weverton Formation) to deep waters (e.g. Great Valley Chilhowee Group Loudon Formation) on the continental slope and shelf platform (Cleaves, 1968) (Cecil, 2004). Further offshore in the deep water of the continental rise, fine-grained rocks (such as the Westminster terrane) were deposited as carbonates interspersed with turbidite deposits. Turbidites of the Potomac terrane were deposited even further offshore in a trench setting (Southworth, 2004). As discussed in Section 2.5.1.1.2.4, all of these units were metamorphosed, deformed, and intruded by plutons in the Ordovician Taconian orogeny (Drake, 1989) (Figure 2.5-9).

2.5.1.1.2.2 Late Precambrian Rifting

Following the Grenville orogeny, crustal extension and rifting began during Late Precambrian time, which caused the separation of the North America and African plates and created the proto-Atlantic Ocean (Iapetus Ocean). Rifting is interpreted to have occurred over a relatively large area, sub-parallel to the present day Appalachian mountain range (Faill, 1997a) (Wheeler, 1996). This period of crustal extension is documented by the metavolcanics of the Catoctin, Swift Run, and Sams Creek formations (Schmidt, 1993). During rifting, the newly formed continental margin began to subside and accumulate sediment. Initial sedimentation resulted in an eastward thickening wedge of clastic sediments consisting of graywackes, arkoses, and shales deposited unconformably on the Grenville basement rocks. In the Blue Ridge and western Piedmont, the Weverton and Sugarloaf Mountain quartzites represent late Precambrian to early Cambrian fluvial and beach deposits. Subsequent sedimentation included a transgressive sequence of additional clastic sediments followed by a thick and extensive sequence of carbonate sediments. Remnants of the rocks formed from these sediments can be found within the Valley and Ridge Province and Piedmont Province (Fichter, 2000). In the western Piedmont, the sandy Antietam Formation was deposited in a shallow sea. In the Valley and Ridge Province, a carbonate bank provided the environment of deposition for the thick carbonates ranging from the Cambrian Tomstown Dolomite through the Ordovician Chambersburg Formation. In the eastern Piedmont, the Setters Formation (quartzite and

interbedded mica schist) and the Cockeysville Marble have been interpreted as metamorphosed beach and carbonate bank deposits that can be correlated from Connecticut to Virginia. Accumulation of this eastward thickening wedge of clastic and carbonate sediments is thought to have occurred from the Middle to Late Cambrian into Ordovician time (PSEG, 2002).

2.5.1.1.2.3 Late Precambrian to Early Cambrian Orogenies (Potomac/Penobscot Orogeny)

The Potomac orogeny is the earliest Paleozoic age orogeny recorded in the north-central Appalachians. It is recognized along the western margin of the Piedmont province and is considered distinct from the Penobscot orogeny of the northern Appalachians and the Virgilian orogeny of Northern Carolina (Hibbard and Samson, 1995). The orogeny is dated from Late Cambrian to Early Ordovician and occurred a considerable distance from the North American continental margin, as the magmatic arc(s) in the Theic ocean (including the Jefferson and Smith River terranes) were obducted over the Brandywine microcontinent (Figure 2.5-207). The orogeny started with the magmatic arcs overriding the forearc sediments of the White Clay nappe and the Liberty Complex. The Wilmington Complex in Delaware and southeast Pennsylvania overrode the Glenarm Wissahickon Formation of the White Clay nappe (Figure 2.5-200, Figure 2.5-201 and Figure 2.5-202) and the Potomac-Philadelphia terrane. This obduction created the peak metamorphism of the Potomac orogeny in this part of the north-central Appalachians and possibly generated the Arden Pluton within the Wilmington Complex (Faill, 1997a).

This obduction of the combined Wilmington Complex (Figure 2.5-202), White Clay nappe and Philadelphia terrane over the Brandywine microcontinent continued for some time, although petrologic and microprobe evidence indicates that the schists of the White Clay nappe had cooled somewhat before the amalgamate was thrust over the Brandywine microcontinent on the Doe Run fault (Figure 2.5-200 and Figure 2.5-201). The weight of the obduction is considered to have caused the microcontinent to descend (Figure 2.5-207) raising temperatures and pressures in the massifs, especially in the West Chester massif, which occupied the lowest structural level in the amalgamation (Faill, 1997a).

Around the Baltimore microcontinent, a similar amalgamation was occurring. The westward advancing magmatic arc (James Run volcanics) and ophiolites (Baltimore Mafic Complex) produced a precursory mélange (Morgan Run Formation and the potentially equivalent Sykesville Formation) (Figure 2.5-200 and Figure 2.5-201) in the accretionary wedge to the west. The accretionary wedge and magmatic arc were obducted onto the eastern portion of the Baltimore microcontinent which subsequently became submerged (Figure 2.5-200 and Figure 2.5-201). During the thrusting, the Morgan Run Formation was elevated and provided a source of clasts for the associated Sykesville diamictite. The Ellicott City Granodiorite (west of Baltimore) was subsequently emplaced deep within the thickened crust between the Baltimore Mafic complex and metasediments (Faill, 1997a).

The southward extension of the Potomac Orogeny is represented by the Cambrian age Chopawamsic metavolcanics and associated mélanges of an accretionary / forearc complex. The one difference between the north-central and southern portions of the Appalachian orogeny is that micro-continents are not generally associated with the north-central Chopawamsic or Jefferson terranes (Figure 2.5-9). The Sauratown Mountains anticlinorium and the Goochland terrane of the eastern Piedmont may have a similar history to that of the north-central Appalachians. Lithic and metamorphic evidence of the Goochland gneisses indicate that the Goochland terrane was probably derived from the North American craton (Laurentian

origin) and had an emplacement history quite different from that of the Baltimore and Brandywine internal massifs (Faill, 1997a).

2.5.1.1.2.4 Taconic Orogeny

The Taconic orogeny occurred during Middle to Late Ordovician time and was caused by continued collision of micro-continents and volcanic arcs with the eastern North America margin along an eastward dipping subduction zone during progressive closure of the Iapetus Ocean (Figure 2.5-8). Taconic terranes are preserved today in the Piedmont in a series of belts representing island-arcs and micro-continents. They include the Chopawamsic terrane, the Carolina / Albemarle arc, the Goochland-Raleigh terrane, and the Sussex Terrane, directly west of the CCNPP site, as shown in Figure 2.5-9. These terranes are thought to have collided with, and accreted to, eastern North America craton at different times during the Taconic orogeny (Horton, 1991; Glover, 1997). Closer to the CCNPP site, the central Piedmont in Northern Virginia, Maryland, and Pennsylvania contains several belts of rocks whose age is unknown and/or whose relation to the pre- or synorogenic rocks of the Taconic orogen is uncertain (Drake, 1999). These stratigraphic units include the Wissahickon Formation, which is now recognized in the Potomac Valley as three distinct lithotectonic assemblages (Drake, 1999). Other stratigraphic units, whose ages range from Late Proterozoic to Late Ordovician and contain indications of Taconic deformation, include various units in the Ijamsville Belt, the Glenarm Group Belt, which includes the Baltimore Gneiss, the Potomac terrane that was thrust over the Glenarm Group belt, and the Baltimore mafic complex to the east as shown in Figure 2.5-9 (Horton, 1989) (Fichter, 2000). Additional details on the complex stratigraphy of the Taconic orogen in the Piedmont were described by Drake (Drake, 1999).

Accretion of the island-arcs and micro-continents to the eastern margin of North America created a mountain system, the Taconic Mountains, that became a major barrier between the Iapetus Ocean to the east and the carbonate platform to the west. The growth of this barrier transformed the area underlain by carbonate sediments to the west into a vast, elongate sedimentary basin, the Appalachian Basin. The present day Appalachian Basin extends from the Canadian Shield in southern Quebec and Ontario Provinces, Canada, southwestward to central Alabama, approximately parallel to the Atlantic coastline (Colton, 1970). The formation of the Appalachian Basin is one of the most significant consequences of the Taconic orogeny in the region defined by the Valley and Ridge Province and Appalachian Plateau Province. The Taconic mountain system was the source of most of the siliclastic sediment that accumulated in the Appalachian Basin during Late Ordovician and Early Silurian time. Many of these units are preserved closest to the CCNPP site in the Valley and Ridge Province. A continent-wide transgression in Early Silurian time brought marine shales and carbonate sedimentation eastward over much of the basin, and a series of transgressions and regressions thereafter repeatedly shifted the shoreline and shallow marine facies. Carbonate deposition continued in the eastern part of the basin into Early Devonian time (Faill, 1997b).

The type region of the Taconic orogeny in the northern Appalachians records the obduction of one or more volcanic arcs onto the eastward-dipping Ordovician Laurentian (Iapetan) margin. However, the southern Appalachians record late Cambrian initiation of a westward dipping subduction zone and Ordovician development of an arc-backarc system along the Laurentian margin, reflecting an extensional, not collisional, orogenesis. The limit of this Middle Ordovician extensional regime is currently unknown, but determining its northeastern extent is important in paleotectonic reconstructions of the Laurentian margin for the early Paleozoic (Barineau, 2008).

2.5.1.1.2.5 Acadian Orogeny

The Acadian orogeny began in early Devonian time and ended at the beginning of Mississippian time. Accretion of a composite Goochland-Avalonia terrane to Laurentia at c. 421 Ma and the subsequent accretion of Meguma between 400 and 390 Ma were probably responsible for the Acadian orogeny and continuing Devonian orogenesis (van Staal, 1998). The 1 billion year old (1000 Ma) Goochland terrane, possibly a displaced fragment of Laurentia (Bartholomew and Tollo, 2004) had been sutured to the Avalonia terrane in the Taconian orogeny (Sheridan, 1993).

At its peak, the orogeny produced a continuous chain of mountains along the east coast of North America and brought with it associated volcanism and metamorphism. The Acadian orogeny ended the largely quiescent environment that dominated the Appalachian Basin during the Late Ordovician and into the Silurian, as vast amounts of terrigenous sediment from the Acadian Mountains were introduced into the basin and formed the Catskill clastic wedge in Pennsylvania and northeastern New York as shown in Figure 2.5-5, Figure 2.5-6, and Figure 2.5-8. Vast amounts of terrigenous sediment from the Acadian Mountains were introduced into the Catskill foreland basin during the Middle and Late Devonian and formed the Catskill clastic wedge sequence in Pennsylvania and New York. Thick accumulations of clastic sediments belonging to the Catskill Formation are spread throughout the Valley and Ridge Province (Faill, 1997b). The Catskill clastic wedge is representative of fluctuating shorelines and prograding alluvial environments along the western margin of the Acadian upland. This regressional sequence is represented in the sedimentary record with turbidites, slope deposits, alternating shallow marine and nonmarine sediments and alluvial plain fining-upward sequences (Walker, 1971, Faill, 1997b and USGS, 2008). The pebbles and sand grains of the Catskill Formation in New York, Pennsylvania and Maryland are mostly composed of metamorphic and granitic rock fragments, feldspar, mica and quartz. The red color is due to the presence of a small percentage of iron oxide between the grains (Dolt and Batten, 1988). The regressive sequence in the region is bounded above and below by marine transgressions which are represented by basal black shale overlain by gray shales and mudstones capped by small amounts of siltstone (Bridge, 1994; Huber, 2000). The Catskill clastic wedge was the site of the greatest accumulation of sediment in the region depositing as much as 7,000 feet of sediment (Stoffer, 2003). The sediments are the thickest in the east and grow progressively thinner westward and southward into the central Appalachian Basin region (Figure 2.5-200). In general, the Acadian Orogeny was superimposed upon terranes affected or formed by the Taconic Orogeny (Figure 2.5-200).

By Mississippian time, the Acadian Mountains had been denuded because the source material for the Catskill Delta was depleted and sedimentation ceased.

2.5.1.1.2.6 Allegheny Orogeny

The Allegheny orogeny occurred during the Late Carboniferous Period and extended into the Permian Period. The orogeny represents the final convergent phase in the closing of the Iapetus Ocean in the Paleozoic Era (Figure 2.5-8). Metamorphism and magmatism were significant events during the early part of the Allegheny orogeny. The Allegheny orogeny was caused by the collision of the North American and proto-African plates, and it produced the Allegheny Mountains. As the African continent was thrust westward over North America, the Taconic and Acadian terranes became detached and also were thrust westward over Grenville basement rocks (Mulley, 2004). The northwest movement of the displaced rock mass above the thrust was progressively converted into the deformation of the rock mass, primarily in the form of thrust faults and fold-and-thrust structures, as seen in the Blue Ridge and Piedmont Plateau Provinces. The youngest manifestation of the Allegheny orogeny was northeast-trending strike-slip faults

and shear zones in the Piedmont Province. The extensive, thick, and undeformed Appalachian Basin and its underlying sequence of carbonate sediments were deformed and a fold-and-thrust array of structures, long considered the classic Appalachian structure, was impressed upon the basin. The tectonism produced the Allegheny Mountains and a vast alluvial plain to the northwest. The Allegheny Front along the eastern margin of the Appalachian Plateau Province is thought to represent the westernmost extent of the Allegheny orogeny. Rocks throughout the Valley and Ridge Province are thrust faulted and folded up to this front, whereupon they become relatively flat and only slightly folded west of the Allegheny Front (Faill, 1998).

2.5.1.1.2.7 Early Mesozoic Extensional Episode (Triassic Rifting)

Crustal extension during Early Mesozoic time (Late Triassic and Early Jurassic) marked the opening of the Atlantic Ocean (Figure 2.5-8). This extensional episode produced numerous local, closed basins ("Triassic basins") along eastern North America continental margin (Figure 2.5-9) (Faill, 1998). The elongate basins generally trend northeast, parallel to the pre-existing Paleozoic structures (Figure 2.5-10). The basins range in length from less than 20 mi (32 km) to over 100 mi (161 km) and in width from less than 5 mi (8 km) to over 50 mi (80 km). The basins are exposed in the Piedmont Lowland of Maryland and Northern Virginia and are also buried beneath sediments of the Coastal Plain and the continental shelf. The exposed and buried Mesozoic basins are described more fully in Section 2.5.1.1.3.4.

Generally, the Mesozoic rift basins are asymmetric half-grabens with principal faults located along the western margin of the basins. Triassic and Jurassic rocks that fill the basins primarily consist of conglomerates, sandstones, and shales interbedded with basaltic lava flows. At several locations, these rocks are cross-cut by basaltic dikes. The basaltic rocks are generally more resistant to erosion and form local topographically higher landforms. The Mesozoic rift basins along the length of the North American Atlantic margin are related to one of the largest intrusive systems in the world, the Central Atlantic Magmatic Province (CAMP) (de Boer, 2003). The CAMP intrusives were emplaced before the breakup of Pangea, during the embryonic stage of continental rifting. Correlative dike swarms are found in the western and southeastern margins of the African continental margin and the northern part of the South American continental margin (representing the "Early Jurassic Circum-Atlantic Dike System") (de Boer, 2003). The dikes of the Circum-Atlantic swarm show a convergence pattern, with a focal point near the present-day Blake Plateau, near Florida (present coordinates).

Subsidence of the rift basins was initiated ca. 230 Ma prior to the magmatic event. Dike intrusion began in the northern (New England) section of the North American continental margin. Most of the dikes along the length of the CAMP were emplaced between 205 and 195 Ma. Similar ages are found for dike swarms in Iberia, Africa and South America. de Boer (2003) summarizes various models proposed for the production of the voluminous magma that created the dike swarms. One proposal has a single hotspot plume, located near Florida (present coordinates) beneath the Blake Plateau. Another model proposed two hot spots, one off Florida and the other in the Gulf of Maine. Another model proposes that magmas were derived from multiple, rather than localized, sources below the rift valleys. The results of de Boer (2003) analyses of the anisotropy of magnetic susceptibility across the CAMP suggest that the overall radiating pattern of the circum-Atlantic dikes support a plume source in the vicinity of the Blake Plateau (de Boer, 2003).

The episode of crustal extension that produced the Mesozoic rift basins of the mid-Atlantic region is believed to have ended and the Atlantic margin stabilized as a passive margin before Eocene time (see discussion in Section 2.5.1.1.4.1.2).

2.5.1.1.2.8 Cenozoic History

The Early Mesozoic extensional episode gave rise to the Cenozoic Mid-Atlantic spreading center. The Atlantic seaboard presently represents the trailing passive margin related to the spreading at the Mid-Atlantic ridge. Ridge push forces resulting from the Mid-Atlantic spreading center are believed to be responsible for the northeast-southwest directed horizontal compressive stress presently observed along the Atlantic seaboard.

During Cenozoic time, as the Atlantic Ocean opened, the newly formed continental margin cooled and subsided, leading to the present day passive trailing divergent continental margin. As the continental margin developed, continued erosion of the Appalachian Mountains produced extensive sedimentation within the Coastal Plain. The Cenozoic history of the Atlantic continental margin, therefore, is preserved in the sediments of the Coastal Plain Province, and under water along the continental shelf. The geologic record consists of a gently east-dipping, seaward-thickening wedge of sediments, caused by both subsidence of the continental margin and fluctuations in sea level. Sediments of the Coastal Plain Province cover igneous and metamorphic basement rocks and Triassic basin rift deposits.

During the Quaternary Period much of the northern United States experienced multiple glaciations interspersed with warm interglacial episodes. The last (Wisconsinan) Laurentide ice sheet advanced over much of North America during the Pleistocene. The southern limit of glaciation extended into parts of northern Pennsylvania and New Jersey, but did not cover the CCNPP site vicinity (Figure 2.5-5). South of the ice sheet, periglacial environments persisted throughout the site region (Conners, 1986). Present-day Holocene landscapes, therefore, are partially the result of geomorphic processes, responding to isostatic uplift, eustatic sea level change, and alternating periglacial and humid to temperate climatic conditions (Cleaves, 2000).

Recent studies demonstrate that widespread uplift of the central Appalachian Piedmont and subsidence of the Salisbury Embayment represents first-order, flexural isostatic processes driven by continental denudation and offshore deposition. Studies indicate that the mid-Atlantic margin experiences an average, long-term denudation rate of approximately 33 ft (10 m) per million years, and the Piedmont has been flexurally upwarped between 115 to 427 ft (35 to 130 m) in the last 15 million years (Pazzaglia, 1994). This Piedmont upwarp and basin subsidence are accommodated primarily by a convex-up flexural hinge, physiographically represented by the Fall Zone. The current state of resulting stress on the Atlantic margin lithosphere is discussed more fully in Section 2.5.1.1.2.8 and 2.5.1.1. 4.4.

2.5.1.1.3 Regional Stratigraphy

This section contains information on the regional stratigraphy within a 200-mile (322-km) radius of the CCNPP site. The regional geology and generalized stratigraphy within this area is shown on Figure 2.5-5 and described in Figure 2.5-6. For an illustration of regional stratigraphy, see Figure 2.5-209 through Figure 2.5-212. In this FSAR section, the description of pre-Silurian (pre-Taconian) stratigraphic units is organized by tectonostratigraphic affinity to Laurentian continental characteristics or by affinity to oceanic, island arc, or exotic microcontinent terranes. Figure 2.5-9 provides one interpretation of these tectonostratigraphic terranes within a 200-mile radius of the CCNPP site. The pre-Silurian terranes are described in FSAR sections 2.5.1.1.3.1, The Laurentian Realm, 2.5.1.1.3.2, The Iapetan Realm, and 2.5.1.1.3.3, The Peri- Gondwanan Realm. Silurian through Jurassic stratigraphic units are described in Section 2.5.1.1.3.4, The Pangean Realm. Finally, post-rifting Cretaceous, Tertiary and Quaternary sediments that drape the basement rocks across the Piedmont, Coastal Plains, and continental shelf of the mid-Atlantic margin are described in Section 2.5.1.1.3.5, Post-Pangean Sediments.

Sections 2.5.1.1.3.1 through 2.5.1.1.3.5 are supported by corresponding stratigraphic columns that correlate regional stratigraphic names across the 200-mile (322 kilometer) radius of the CCNPP site. The stratigraphic units that comprise the Laurentian, Iapetan, and Peri-Gondwanan realms are correlated in Figure 2.5-209 and Figure 2.5-210. The description of stratigraphic units in FSAR Sections 2.5.1.1.3.1 through 2.5.1.1.3.3 refer to the map symbols on Figure 2.5-9. The post-Silurian through Jurassic stratigraphic units described in Section 2.5.1.1.3.4 are regionally correlated in Figure 2.5-211. The Cretaceous through Holocene stratigraphic units described in Section 2.5.1.1.3.5 are regional correlated in Figure 2.5-212.

A tectonostratigraphic map such as Figure 2.5-9 is by definition interpretive; both of the nature of boundaries, and in terms of the nature of tectonostratigraphic units. Some of the affinities depicted in Figure 2.5-9, which was based on work through 1991, have subsequently been questioned (Glover 1997, for example). According to Hibbard, the pre-Silurian Appalachian orogen is composed of three realms: Laurentian, Iapetan, and peri-Gondwanan (Hibbard, 2007). The three realms acquired their defining geologic character before the Late Ordovician. The Laurentian realm is composed of all rocks deposited either on or immediately adjacent to ancient proto-North America supercontinent known as Rodinia (see discussion in Section 2.5.1.1.2.1) at the close of the Grenville orogeny. The Laurentian realm formed the western flank of the Appalachian orogen. The Iapetan realm is a collection of terranes of oceanic and volcanic arc affinity that were caught between the Laurentian and peri-Gondwanan realm during Appalachian orogenesis. The peri-Gondwanan realm along the southeastern flank of the orogen formed near the supercontinent Gondwana and is exotic with respect to Laurentian elements. Only one terrane within a 200-mile (322-kilometer radius of the CCNPP site, the Raleigh-Goochland terrane, defies easy classification into this scheme. For the present discussion, it will be placed in the Iapetan realm.

According to Hibbard (2006), the Laurentian realm is represented by terranes found west of the Pleasant Grove-Huntington Valley fault system (Figure 2.5-23) (incorrectly referred to as the Pleasant Valley shear zone on the Hibbard 2006 map). Peri-Laurentian and Iapetan realm terranes are found west of the Central Piedmont shear zone (including the Spotsylvania fault). The Peri-Gondwanan realm (Carolina and related terranes) is found east of the Central Piedmont shear zone (Figure 2.5-23). See Section 2.5.1.1.4.4.2.1, Appalachian Structures, for a description of these two regional structures.

2.5.1.1.3.1 The Laurentian Realm

The stratigraphic units within a 200-mile (322-kilometer) radius of the CCNPP site provide a history of the growth of the proto-North American continental margin within the past billion years. It is a history of recycling and redistribution of Mesoproterozoic crust of Laurentia, accretion and subsequent deformation of oceanic crust, volcanic arcs and microcontinents related to ancient oceans, and probable capture and subsequent deformation of portions of other micro-continents and terranes (such as the Pan-African Avalon terrane in the northern Appalachians and Suwannee terrane in the southern Appalachians) by the North American continental margin.

Precambrian-age Grenville rocks of the north-central Appalachians outcrop in central Maryland, southeastern Pennsylvania and northern New Jersey (Figure 2.5-209 and Figure 2.5-210). These exposures are metamorphic massifs that were emplaced on Taconic or Allegheny orogenic thrusts and are now surrounded by Paleozoic and Mesozoic age rocks. In the north-central Appalachians these massifs are separated by the Pleasant Grove-Huntingdon Valley shear zone (Figure 2.5-23) into external and internal massifs (Figure 2.5-201) (Faill 1997a). External basement massifs are blocks of older crust that are incorporated into the more external (foreland-ward) parts of an orogen, whereas internal basement massifs are blocks of

older crust that are located in the internal parts of an orogen (Hatcher, 1983). External massifs are more likely to be derived from the nearby craton, but internal massifs can be derived from a variety of locales, not necessarily from the nearby craton, so they can be either proximally derived or parts of exotic terranes, such as the remains of the microcontinent that originated from the South America craton (Gondwana) (Faill, 1997a) (Figure 2.5-203).

Laurentian Terrane (Undivided): Tectonostratigraphic Map (Figure 2.5-9) Unit "L"

Almost half of the exposed landmass within a 200-mile (322-kilometer) radius of the CCNPP site is composed of ancestral North America, or Laurentia terrane together with probable related terranes deformed during the Grenville orogeny (see Section 2.4.1.1.2.1). The undifferentiated Laurentian terrane shown in Figure 2.5-9 includes a number of Mesoproterozoic massifs, rift-related Late Proterozoic clastic sedimentary and volcanic sequences, and deformed Paleozoic shelf and platform strata.

Chesapeake Terrane: Tectonostratigraphic Map (Figure 2.5-9) Unit "ch"

The character of the Chesapeake terrane and its position at the outer limits of the mid-Atlantic continental margin has raised a great deal of interest regarding its affinities. The detected presence of the Chesapeake terrane in boreholes along the central Atlantic Coast implies some relationship to the broad gravity low [tectonostratigraphic map (Figure 2.5-9) unit "g3"] known as the Salisbury gravity anomaly (Faill 1998). Gravity and magnetic data, seismic reflection profiles, and drill hole data are interpreted to indicate that Laurentian crust of Grenville age underlies the New Jersey Coastal Plain as far south as Cape May (Maguire, 1999). The tectonostratigraphic map (Figure 2.5-9) indicates that this terrane continues south beneath the coast of Virginia to about the Virginia-North Carolina line. Rb/Sr age dates indicate that the basement terrane was created 1025±0.035 Ma. Basement lithologies are similar to exposed Grenville-age rocks of the Appalachians and perhaps most importantly, the TiO_2 and Zr/P_2O_5 composition of metagabbro in the Chesapeake terrane overlap those of Proterozoic mafic dikes in the New Jersey Highlands. These findings support the interpretation that Laurentian basement extends southeast as far as the continental shelf in the U.S. mid-Atlantic region. The subcrop of Laurentian crust under the mid-Atlantic Coastal Plain implies unroofing by erosion of the younger Carolina (Avalon) supracrustal terrane. Dextral-transpression fault duplexes may have caused excessive uplift in the Salisbury Embayment area during the Alleghanian orogeny (Sheridan, 1999).

2.5.1.1.3.1.1 External Massifs

Grenville basement rocks are exposed in the cores of en echelon massifs which are interpreted to be allochthonous (Rankin, 1989) or para-autochthonous (Drake, 1989) and have been carried westward (current coordinates) by Taconian thrusting.

The external massifs include the Reading Prong, Honey Brook Upland, Mine Ridge, Trenton Prong and Blue Ridge massifs (Figure 2.5-201 and Figure 2.5-202). Following are brief descriptions of these massifs from Faill (1997a).

Reading Prong: Tectonostratigraphic Map (Figure 2.5-9) Unit "L," Located Immediately East of the Hamburg Terrane

The Reading Prong extends from western New England southwestward across southern New York, northern New Jersey, and terminates in the vicinity of Reading, Pennsylvania in the "Little" South Mountain (Figure 2.5-201). Rocks of the Reading Prong consist of a variety of metamorphic and igneous rocks including quartzofeldspathic and calcareous metasediments,

sodium-rich gneisses and amphibolites, granites and mafic plutonic rocks. The terrane, extending from the New Jersey Highlands to Reading, Pennsylvania, is underlain by a Middle Proterozoic assemblage of intrusive plutonic rocks and migmatites, metasediments, rocks of probable volcaniclastic origin and charnockitic rocks of unknown origin (Drake, 1989).

The Hexenkopf complex is part of the Reading Prong in Pennsylvania. It apparently represents the oldest basement rocks of the Reading Prong and is overlain by the Losee Metamorphic Suite, a largely sodic plagioclase and quartz series of granofels, granitoid, and foliated rocks. The Losee Suite is overlain in turn by a sequence of quartzofeldspathic and calcareous metasedimentary rocks. The rocks in this part of the Reading Prong are considered to be a part of Laurentia, and resemble the rocks of the Honey Brook massif but not the rocks in the internal or other external massifs to the south.

Honey Brook Upland: Tectonostratigraphic Map (Figure 2.5-9) Unit "L," Located South of the Reading Prong and Immediately North of the Westminster Terrane

The Honey Brook Upland consists mainly of amphibolite to granulite facies, felsic to mafic gneisses having sedimentary, volcanic and/or volcaniclastic protoliths. The graphitic metasediments are interlayered with felsic gneisses in some areas. These rocks are somewhat similar to the rocks of the Reading Prong and the Adirondacks in northern New York, but the lenticular ultramafites in both the Honey Brook Uplands and Mine Ridge are not present in the Reading Prong. The Honey Brook Upland, Mine Ridge and the Trenton Prong are the southeastern most external basement massifs in the central Appalachians (Drake,1989). The Honey Brook Upland overlies undated, but presumably Middle Proterozoic rocks.

Granulite gneisses appear to be the oldest rocks in the massif, and are associated with, and probably intruded by, the Honey Brook anorthosite. The layered gneiss has both light and dark phases which are interpreted to be metamorphosed volcanics (Rankin, 1989). The layered gneiss appears to be younger than the granulite gneiss and the anorthosite. Amphibolite is found within both the layered gneiss and in the Pickering Gneiss, a coarsely crystalline highly variable rock characterized by abundant graphite and pods of marble. The intrusive rocks that characterize the Reading Prong are missing from the Honey Brook Upland.

Mine Ridge: Tectonostratigraphic Map Unit "L" (Undifferentiated), Located Immediately South and West of the Honey Brook Upland, and Appalachian Orogen Map (Figure 2.5-201)

The Mine Ridge massif consists of amphibolite-facies felsic to mafic gneisses mixed with sedimentary and volcaniclastic protoliths and is similar to parts of the Honey Brook Upland. The presence of ultramafites in both the Mine Ridge and Honey Brook is considered to indicate either a Precambrian age oceanic provenance or tectonic emplacement along offshore and continental margin rocks. There is no evidence in the literature that there are intrusives in the Mine Ridge Anticline.

Trenton Prong: Tectonostratigraphic Map (Figure 2.5-9) Unit "L" Located just South of the Newark Basin near Trenton, New Jersey and Appalachian Orogen Map (Figure 2.5-201) Unit "13"

The Trenton Prong (or Trenton massif) consists of Grenville-age graphitic schists and intermediate grade gneiss with some mafic gneiss and the lithologies are similar to the schists and gneiss of the Honey Brook. The Trenton Prong contains Mesoproterozoic metagabbro, charnockite, and metadacite/tonalite, unconformably overlain by biotite-bearing quartzo-feldspathic gneiss, calc-silicate gneiss, and minor marble. (Maguire, 1999). The rocks are unconformably overlain on the south by the Cambrian Chickies quartzite (Figure 2.5-209 and Figure 2.5-210).

Blue Ridge Anticlinorium: Tectonostratigraphic Map (Figure 2.5-9) Unit "L," Located Immediately West of the Mountain Run Fault

The Blue Ridge Anticlinorium contains the largest area of exposed Laurentian crust in the Appalachians. The Grenville rocks south of Pennsylvania are dominantly derived from plutonic igneous rocks with locally stratified rock protoliths. The interpretation of these local protoliths is questionable as they could be strongly deformed dikes as well as metasedimentary rocks (Rankin, 1989). The northern-most exposure of Grenville rocks in the Blue Ridge complex occurs in northern Virginia and Maryland, north of the Potomac River.

Above the Grenville basement rocks of the Blue Ridge Anticlinorium terrane, a clastic wedge began to form in late Precambrian time. It was intruded by basalts, presumably related to the lapetan rifting. The resulting terrane consists of stratified metasedimentary rocks and meta-basalts of Late Precambrian and Early Paleozoic age. The earliest sediments were siliciclastic and quartzose deposits derived from the Laurentian craton to the northwest (current coordinates). These sediments include the Chilhowee Formation within the Catoctin rift basins, the Hardyston quartzite in the Reading Prong, the Chickies, Harpers and Araby formations in Maryland, and the Weverton, Loudon, Antietam, and Harpers formations in Virginia. Some of these clastic sediments were trapped on the continental margin but some were deposited on the continental slope and deeper water in the Theic Ocean (Faill, 1997a). The clastic wedge progressively overlapped the Grenville basement rocks exposed to the northwest. Siliciclastic sediments were eventually replaced by carbonate deposition during the Early Cambrian. The eastern (present coordinates) margin of the shelf spalled large fragments of carbonate shelf deposits downslope, forming a slope-facies Conestoga Limestone. The carbonate bank, with local influx of sand and silt from the northwest (present coordinates), persisted for the next 100 ma. The carbonates varied in thickness across the platform, reflecting the impact of epeirogenic structural arches and basins (Faill, 1997a). In addition, the shelf-to-bank transition appears to have migrated back and forth in the central Laurentian continental margin because of the superposition of shelf over bank (such as slope-facies Vintage Limestone over Chilhowee clastics in Pennsylvania and slope-facies Conestoga over shelf carbonates further to the northwest (Faill, 1997a).

Eventually, the carbonate bank began to subside at different rates across its area probably also due to epeirogenic movements of the crust and the proximity to the shelf edge. This disparate subsidence produced locally different depositional environments, where contrasting carbonate sequences accumulated. These differences are reflected in the character of the Cumberland Valley, Lebanon Valley, Schuylkill and Lehigh Valley sequences (Figure 2.5-209 and Figure 2.5-210).

The initial closing of the Theic Ocean began in Middle Cambrian but the approaching tectonism did not affect the carbonate shelf until Middle Ordovician. Initial shelf response to the closure of the Theic Ocean was the Knox unconformity (Figure 2.5-200 and Figure 2.5-201). The magnitude of the Knox unconformity decreases from northwest to southeast and may be non-existent from central Pennsylvania to northern Virginia because the stratigraphic section there appears to be uninterrupted (Faill, 1997a).

The Late Precambrian to Ordovician clastic wedge sediments and igneous intrusives were deformed during three successive orogenies (the Taconic, the Acadian and the Alleghanian (see FSAR Sections 2.5.1.1.2.4 through 2.5.1.1.2.6). Throughout those orogenic events, post-Silurian sediments were shed across the uplifted terranes and deposited in basins resulting from orogenic crustal flexure and faulting. These post-Silurian sediments are described in FSAR Sections 2.5.1.1.3.4.

The stratigraphic units of the Valley and Ridge physiographic province of the central Appalachians are composed of Grenvillian crystalline basement rocks overlain by pre-Silurian clastic and carbonate bank deposits similar to those of the Blue Ridge described above. The initial clastic and carbonate bank deposits may have eroded from the northern Valley and Ridge (represented by the Knox unconformity). Further south, in the Virginia and North Carolina portions of the Valley and Ridge, deposition was continuous (Faill, 1997a) through the Lower Devonian, as the effects of the closure of Iapetus moved progressively westward in the Taconic orogeny. The stratigraphy of these post-Silurian units is described in Section 2.5.1.1.3.3.1.

2.5.1.1.3.1.2 Internal Massifs or Peri-Laurentian Microcontinents

The Internal Massifs in the north-central Appalachians include the Brandywine massifs in southeastern Pennsylvania and the Baltimore massifs in central Maryland. Following are descriptions of these massifs from Faill (1997a).

Brandywine Massifs: Laurentian Margin Map (Figure 2.5-202) Unit "2"

The Brandywine massifs include the West Chester, Avondale, and Woodville bodies and possibly the gneiss in the Mill Creek "dome" (Figure 2.5-202). These four massifs comprise the Brandywine terrane of southern Pennsylvania.

The West Chester massif consists predominantly of quartzofeldspathic granulites of variable composition and pyroxene granulites of dioritic to olivine-gabbroic composition, metamorphosed to granulite facies during the Grenville orogeny and later recrystallized to amphibolite facies. There is little information available on the gneisses of the Avondale, Woodville and Miller Creek massifs. The Brandywine gneisses of the internal massifs are quite different lithologically from the gneisses of the external massifs in that they lack large Precambrian age intrusions, charnockitic rocks are not present in the massifs and Late Precambrian dikes in the internal massifs do not have the Catoctin-affinity chemistry present in the dikes in the gneisses north of the Pleasant Grove-Huntingdon Valley shear zone. These differences are considered to infer that the massifs may not have been derived from the ancestral North America craton (Laurentia) but from the remains of a microcontinent that originated from the South America craton (West Gondwana) (Faill, 1997a).

The gneisses of the Avondale, Woodville and Miller Creek massifs are unconformably overlain by a siliciclastic and carbonate sequence of the Setters and Cockeysville Formations, which constitute the lower part of the Glenarm Group. This group was originally defined to include the Wissahickon schist, Peters Creek Formation, Cardiff Conglomerate, and Peach Bottom Slate and underlie much of the Piedmont Province in Maryland, Delaware, Pennsylvania, and New Jersey and under the Coastal Plain to the southeast. The age of the Glenarm Group remains indeterminate, although Late Precambrian to Early Paleozoic is now generally assumed for most of the group.

Baltimore Massifs: Tectonostratigraphic Map (Figure 2.5-9) Unit "ib"

The Baltimore Massifs lie in central Maryland clustered around the city of Baltimore (Figure 2.5-201). Seven gneiss-cored anticlines compose the Baltimore gneisses, which consist largely of layered quartzofeldspathic gneiss of granitic to granodioritic composition and are considered to be metamorphosed felsic and intermediate to mafic volcaniclastic rocks. Subordinate lithologies include amphibolite, augen gneiss, biotitehornblende gneiss and massive granitic gneiss. These gneisses are thought to represent multiple episodes of deformation in recumbent folds. These rocks are typically surrounded by carbonate and

perhaps the basal clastics, forming a link between the Mesoproterozoic basement and the Avondale anticline of the Brandywine massif to the north.

Like the Brandywine gneisses, the Baltimore gneisses are different lithologically from the gneisses of the external massifs in that they lack the large Precambrian-age intrusions and charnockitic characteristics, indicating that the Baltimore massifs may also have been derived from the remains of a microcontinent that originated from the South American craton.

The Baltimore massifs, like several of the Brandywine massifs, are overlain unconformably by the lower Glenarm, Setters and Cockeysville Formations. In Maryland, the Cockeysville Formation is overlain by the Loch Raven schist. The Baltimore massifs and their sedimentary cover comprise the Baltimore terrane (Figure 2.5-201).

2.5.1.1.3.1.3 Laurentian Rift Sequences

Catoctin Rift

The Catoctin rift (Figure 2.5-204 and Figure 2.5-206) is part of the Late Precambrian age intracontinental rift system sub-parallel to the eastern margin of the Laurentian craton. Rocks of the Catoctin rift are largely associated with the Blue Ridge massif, as mapped from Charlottesville, Virginia to south central Pennsylvania. The exposed rock of the Catoctin rift in Virginia, Maryland and Pennsylvania include the volcanic rocks of the Catoctin Formation (Schmidt, 1993) and the overlying sedimentary clastics of the Chilhowee Group. In Virginia and Maryland, the Catoctin volcanics are mostly basalts and are present on both flanks of the Blue Ridge anticlinorium (known in Maryland as the South Mountain). In Maryland, the volcanics overlie the Precambrian-age Grenville basement rocks whereas south of the Potomac River the Catoctin volcanics are underlain by rift-filling sediments of the Fauquier Group. Northward into Pennsylvania the volcanics are predominantly rhyolite and form the exposed core of South Mountain. Catoctin volcanics are not present above the gneisses of the Honey Brook, Reading Prong and Trenton Prong massifs, suggesting that these massifs were outside the Catoctin rift. Metabasalt dikes in these eastern massifs, however, are geochemically very similar to the Catoctin volcanics of South Mountain in Pennsylvania.

Rome Trough

The Rome Trough extends from eastern Kentucky northeastward through West Virginia and southwestern Pennsylvania and disappears in north central Pennsylvania (Figure 2.5-204 and Figure 2.5-206)(Faill, 1997a). It is the result of crustal extension that occurred primarily during Middle and Late Cambrian time. The trough is bounded on the northwest and southeast by steep normal faults that become listric at depth where they merge with the thrusts that originated during the Grenville orogeny. In the north-central Appalachians, the lithology of the sediments that fill the trough is unknown. Correlative rocks outside the trough, however, consist of dolomite, limestone, sandstone and shale.

2.5.1.1.3.1.4 Laurentian Continental and Shelf Sediments

Early Cambrian-Early Ordovician Passive Margin Sequences

The oldest deposits on the Laurentian continental margin are Late Precambrian to Early Cambrian age siliciclastic and quartzose sediments derived from the exposed craton to the northwest (current coordinates). Continued subsidence of the continental margin through the Cambrian caused the quartzose facies to transgress westward and a carbonate shelf to develop

behind (Figure 2.5-206). Once the carbonate shelf formed, supplies of siliciclastic sediment from the Laurentian craton slowed (Faill, 1997a).

In southern Virginia, the basal siliciclastic and quartzose sediments are Early Cambrian in age and become progressively younger to the northwest. In northwestern Pennsylvania the oldest of these rocks are Middle Cambrian in age and in southern Ohio they are Early Ordovician. The Chilhowee sequence which is thickest in the Catoctin rift becomes progressively thinner toward the shelf edge (Figure 2.5-206). The Hardyston quartzite in the Reading Prong and the Lowerre quartzite in the Manhattan Prong in southern New York are much thinner across the New Jersey arch and into southern New England (Cheshire Quartzite) and thicken again in west central Connecticut (Faill, 1997a).

In Maryland, the first sediments deposited were sands which later became the Weverton and Sugarloaf Mountain quartzites. These were deposited during the Late Precambrian or Early Cambrian time followed by the Harpers, Urbana and Ijamsville formations. Sands and thin mud of the Setters Formation were deposited on the shelf edge together with the sands of the Antietam Formation. Farther offshore, mud and silt deposits would later become the Araby and Cash Smith formations (Schmidt, 1993).

Siliciclastic deposition near the shelf edge of the north-central Appalachians was replaced by carbonate deposition during the Early Cambrian (Figure 2.5-206), indicative of either a decreased volume of siliciclastic deposits and/or a northwestward migration of the shoreline. In Maryland and Virginia, the carbonate-rimmed continental shelf graded into a carbonate ramp. In Maryland, the thick accumulations of limestones and dolomites include all of the formations between the Tomstown Dolomite and the Chambersburg formations, with the exception of the Waynesboro Formation (Schmidt, 1993). In southern New York, the shelf edge in the Manhattan Prong is represented by the Inwood Marble, which is correlated with the Wappinger Limestone, north of the Manhattan Prong. The carbonate bank edge or rim presently lies roughly along a line from White Marsh Valley north of Philadelphia to Lancaster and southwestward through Hanover and then through Frederick, Maryland (Figure 2.5-201). The current location of the carbonate bank edge in the latter area is due to thrusting during the Taconic and Alleghany orogenies (Faill 1997a).

Late Ordovician Drowning Margin Sequences

Subsidence of the continental shelf was not uniform. In northwestern Pennsylvania, the clastic/carbonate sequence thickens considerably to the southwest (Figure 2.5-206). The sequence becomes thinner to the north in southeastern New York as well as to the west and northwest and thickens again farther north in the Champlain Valley. Near the shelf edge, the sequence thins to the northeast over the New Jersey arch and to the southwest over the Virginia arch. These thinner sequences and the inferred arches have been related to the New York and Virginia promontories (Faill, 1997a).

An unconformity extending from eastern Pennsylvania to western Massachusetts during the Early and Middle Cambrian produced locally different environments of deposition. The variations are shown in several stratigraphic sequences including the Cumberland Valley, Lebanon Valley, Schuylkill, and Lehigh Valley sequences (Figure 2.5-204 and Figure 2.5-201). While initial tectonic events in the Theic Ocean may have started in the Middle Cambrian, it was not until the Middle Ordovician that the carbonate shelf was significantly affected. The Knox unconformity developed as a result of flexural bulge during the Middle Ordovician. Rocks as old as Late Cambrian were eroded and subsequently overlain by Chazyan carbonates. The magnitude of the unconformity decreases to the southeast and is possibly absent from central Pennsylvania to northern Virginia where the stratigraphic sequence is uninterrupted. The

Blackriveran unconformity affected Llanvirn to Early Caradoc rocks along the shelf margin from south-central Pennsylvania into New Jersey. In west-central New York and southeastern Ontario it occurs as an east-west trending arch under Lake Ontario and into the southwestern Adirondacks where approximately 1 km of shelf sequence from the Upper Cambrian age Potsdam Formation to the top of the Beekmantown Group was eroded form the arch crest. The arch was then unconformably overlain by the widespread Lowville Formation (Blackriveran) and Trenton units (Faill, 1997a).

2.5.1.1.3.2 The Iapetan Realm

Based on a compilation of core and cutting descriptions from wells that penetrated the buried basement complex in the Maryland Coastal Plain and on regional magnetic and gravity data, Hansen (1986) interprets three distinct belts of crystalline rock underlying Cretaceous sediments (Figure 2.5-11). The "Inner Belt" has lithologies and geophysical characteristics similar to the adjacent, exposed Piedmont. As such, this belt appears to be similar to rocks that had been mapped as part of the Wissahickon Group, Baltimore Mafic Complex and the James Run Formation. Rocks of the Middle Belt do not crop out in Maryland but, based on along-strike projections, appear to be similar to the Fredericksburg Complex and Petersburg Granite in Virginia. Although schist or phyllite was logged in borehole CH-BE 57 (Figure 2.5-11), and CH-DA 6-14 toward the southeast, this belt appears to consist of more gneissic and granitic rocks. The Middle Belt in Maryland appears to be characterized by a relatively smooth, anomaly-free, magnetic gradient. The Outer Belt contains diverse lithologies such as gneisses, schists, mafic intrusives and metavolcanics rocks. En echelon geophysical anomalies are truncated at the contact with the Middle Belt. Hansen (1986) interpret the geophysical data as indicating that the Outer Belt may have been accreted to the main North American plate subsequent to the Taconic Orogeny.

2.5.1.1.3.2.1 Iapetan Slope and Abyssal Deposits

2.5.1.1.3.2.1.1 Iapetan Continental Slope and Rise Deposits

Hamburg Terrane: Tectonostratigraphic Map (Figure 2.5-9) Unit "ah"

The Hamburg terrane is an allochthonous continental slope and rise sequence of the Laurentian margin. The Hamburg terrane, located in southeastern Pennsylvania, is one of the southernmost of the Taconic klippen that are so prominent in the central and northern Appalachians (Figure 2.5-9) (Hatcher, 2007). Like the Westminster terrane, the rocks of the Hamburg terrane are Late Proterozoic to Early Cambrian in age. The Hamburg terrane has been tectonically thickened and has been inferred to represent an Early Paleozoic subduction complex. The terrane is composed of alternating sequences of sandstone, siltstone, olive-green mudstone (~85%), and red, purple and light green mudstone, deep water limestone, and radiolaria-bearing siliceous mudstone and chert. Minor proportions of pebble and boulder conglomerate and mafic intrusive and extrusive igneous rocks are also present (Lash, 1989). The generally coarsening-upward sequence has been interpreted as reflecting a migration from an abyssal plain on oceanic crust to a trench (Lash, 1989). Later analyses of the pebble/boulder conglomerate and intrusive and extrusive igneous rocks suggest that minor portions of the Hamburg terrane are para-autochthonous, with deposition of Late Ordovician siliciclastics and igneous rocks produced and erupted during complex plate interactions with subduction of the Laurentian margin beneath the Taconic arc (Figure 2.5-209 and Figure 2.5-210, Middle Ordovician). The Hamburg terrane was emplaced into the foreland basin (Martinsburg formation) on the Yellow Breeches fault (Figure 2.5-23) early in the Taconic orogeny (Ganis, 2005).

During Early and Middle Cambrian the transition between continental shelf and slope shifted back and forth. This shifting is evident from the presence of Vintage Limestone over Chilhowee clastics in southern Lancaster County and the Conestoga Formation over shelf carbonates farther to the northwest (Figure 2.5-206). The presence of Upper Cambrian and Ordovician shelf carbonates in central Lancaster County, however, indicate that this slope edge did not shift any further to the north (Faill, 1997a).

In Maryland, the transition between continental shelf and slope is considered to be somewhat different. From Early Cambrian to Middle Ordovician the slope edge migrated eastward towards the Octoraro Sea. The change from deep to shallow water facies of the Upper Cambrian Frederick limestone suggests a carbonate ramp rather than a reef rim. To the northeast, the correlative transition during Late Cambrian to Middle Ordovician is hidden under Westminster terrane siliciclastics south of the Martic Line in Pennsylvania and under Mesozoic and/or Cenozoic age rocks farther east in New Jersey (Figure 2.5-201). This lack of exposure of shelf to slope deposits within the north-central Appalachians led to a decade long controversy over whether the Martic Line represents a conformable contact or a thrust fault (Faill, 1997a).

The Martic Line, east of the Susquehanna River, is the surface trace of the contact between the Lower Paleozoic carbonates of Chester and Lancaster Valleys and the siliciclastic rocks to the south (Figure 2.5-201). West of the Susquehanna River, west of Long Level in York County and southwestward into Maryland, the Martic Line does not correspond to the siliciclastic-carbonate boundary but rather was mapped between two predominantly pelitic assemblages. It is now generally considered that the Martic Line along the south edge of Chester Valley represents an early Taconic thrust fault which carried the Lower Paleozoic Octoraro Formation over the Conestoga Formation and the other Lower Paleozoic carbonates (Figure 2.5-201) with superposed late Alleghany transpressional shear zones. Along the Martic Line trace southwest of Mine Ridge, the relations are complicated by multiple thrusts and repetitious stratigraphy. An apparent break in the Conestoga Formation supports the interpretation of a thrust fault. West of the Susquehanna River the southern edge of the carbonate shelf is hidden under the Alleghany-age Stoner thrust sheet. The Martic Line disappears farther southwestward under the southeastern portion of the Gettysburg basin. It reappears in central Maryland as a thrust fault between the slope shales and siltstones of the Cash Smith and Araby formations below and the slightly older Ijamsville and Urbana Formations above (Faill, 1997a).

2.5.1.1.3.2.1.2 Iapetan Abyssal Deposits

Octoraro Sea

Translational movement in the Theic Ocean positioned the Brandywine and Baltimore microcontinents east (present coordinates) of the Laurentian craton creating the Octoraro Sea (Figure 2.5-206), its size throughout the Cambrian was mainly dependent on the positions of these microcontinents. The apparent absence of carbonate shelf deposits southeast of the Martic Line is considered to indicate that the Octoraro Sea had already formed by the Early Cambrian. The Peters Creek Formation occupied the southeastern part of the sea and suggests a continental source consisting of interlayered sequences of quartzites, psammites, and pelites. The Jonestown Basalt in the Hamburg klippe and the Sams Creek Metabasalt in the western Piedmont of Maryland (Schmidt, 1993) and Pennsylvania suggest either an oceanic or highly-attenuated transitional continental/oceanic source (Faill, 1997a).

The sediments and volcanics deposited in the Octoraro Sea now make up the Westminster terrane (Figure 2.5-201). It is comprised of three segments, the Martinsburg segment, the Octoraro segment, and the Peters Creek segment. The Martinsburg segment includes the

Urbana, Ijamsville, and Marburg Formations. The Octoraro segment includes Sams Creek, Gillis, Pretty Boy, and the Octoraro formations and is separated from the Marburg segment in Maryland by the Linganore thrust. The Peters Creek segment includes the Peters Creek Formation only (Faill, 1997a; Schmidt, 1993).

Westminster Terrane: Tectonostratigraphic Map (Figure 2.5-9) Unit "aw"

The Westminster terrane of Maryland and Pennsylvania includes rocks previously described as Ijamsville-Pretty Boy-Octoraro terrane (Horton, 1989). This terrane consists of pelitic schist or phyllite, characterized by albite porphyroblasts, and a green and purple phyllite unit.

The rocks of the Westminster terrane have been interpreted to be a slope-rise deep-water prism related to the initial rifting of the Theic Ocean. At some point during the initial rifting, the Brandywine and Baltimore microcontinents (Section 2.5.1.1.3.1.1.2) moved independently within the Theic Ocean between the eastern cratonic margin and developing magmatic arc(s) (Figure 2.5-203). The Octoraro Sea is a proposed arm of the Theic Ocean, between the Laurentian margin and the South American craton (Faill, 1997a). The sediments that accumulated in the sea, mostly from the microcontinents, now constitute the Westminster terrane (Figure 2.5-201).

The rocks are probably correlative with rocks in the Hamburg terrane of Pennsylvania (Drake, 1989; Horton, 1991). The Westminster terrane rocks were metamorphosed to greenschist facies, assembled as a thrust sheet, and finally folded and contractually inverted during the Taconic orogeny (Southworth, 2006).

The Westminster terrane is comprised of three segments, the Marburg segment, the Octoraro segment, and the Peters Creek segment (Figure 2.5-201). The Marburg includes the Urbana, Ijamsville, and Marburg formations. The Octoraro segment includes Sams Creek, Gillis, Pretty Boy, and the Octoraro formations and is separated from the Marburg segment in Maryland by the Linganore thrust. The Peters segment includes the Peters Creek Formation only (Figure 2.5-209 and Figure 2.5-210) (Faill, 1997a; Schmidt, 1993).

While the metamorphic overprint of Westminster terrane rocks shows evidence of Early Silurian and Middle Devonian thermal events, the highest temperature steps of the age spectrum of these rocks record ages that are consistent with cooling from Grenvillian metamorphism (Mulvey, 2004). The Westminster terrane is thought to have been thrust over the unmetamorphosed, Cambro-Ordovician Frederick Valley Limestone along the Martic Line fault onto the Laurentian margin during the Ordovician Taconic orogeny. (Mulvey, 2004). Later, rocks of the Potomac terrane were transported westward onto rocks of the Westminster terrane along the Pleasant Grove fault (Figure 2.5-23). The Pleasant Grove fault is a ductile shear zone as much as 0.6 to 1.2 mi (1 to 2 km) wide that initially formed as a thrust fault during deformation associated with the Ordovician Taconian orogeny (Drake, 1989).

Theic Ocean

The Theic Ocean beyond the Brandywine and Baltimore microcontinents was an oceanic basin. Parts of several separate structural bodies that existed in the Theic Ocean were obducted onto the North American continental margin during the Taconic orogeny, some of which were assembled during the Potomac orogeny. These structural bodies each represent a different Theic component and include the Philadelphia terrane, the Wilmington Complex, White Clay nape and Cecil Amalgamate (Figure 2.5-202). Following are descriptions of these structural bodies from Faill (1997a).

Philadelphia Terrane

The Philadelphia terrane in southeastern Pennsylvania (Figure 2.5-201 and Figure 2.5-202) consists mostly of the Wissahickon Formation, a group of schists and gneisses whose pelitic and psammitic layering indicate accumulation of siliciclastic sediments in a basin environment, possibly as turbidites. The general homogeneity of the Wissahickon throughout the Philadelphia terrane indicates that the part of the Theic Ocean from which the terrane came was an open basin. The lack of true amphibolites in the terrane indicates that it developed at some distance from any magmatic source. The presence of Springfield Granodiorite and Lima Granite in the Wissahickon Formation suggest a possible affinity with the Ellicott City Granodiorite in Baltimore, Maryland. The present northern contact of the Philadelphia terrane is the Huntington Valley fault (Figure 2.5-201). Initial contacts of the Philadelphia terrane were considered to be thrust faults but the evidence to support this has either been obscured, covered or destroyed by later deformation. The southeastern boundary of the terrane is hidden under Coastal Plain sediments. The early contact between the terrane and the Brandywine terrane to the west was obscured by Taconic shearing along the Rosemont fault. The contact with the White Clay nappe farther south is hidden under the Wilmington Complex.

White Clay Nappe

The White Clay Nappe (Figure 2.5-201 and Figure 2.5-202) consists of pelitic and psammitic schists and gneisses of the "Glenarm Wissahickon," so named because in the past they have been related to the Wissahickon of the Philadelphia terrane and formed part of the Glenarm Series. The White Clay Nappe schists and gneisses are lithologically similar to the metasedimentary micaceous and quartzose schists and gneisses of the Wissahickon Formation of the Philadelphia terrane. However, they are separated from the Philadelphia terrane by the Rosemont fault and so associated with ultramafic bodies. On the northwest side, the nappe rocks are in fault contact with the Brandywine massifs, they overlie the Cockeysville and Setters Formations in the western part of the massifs and lie directly on massif gneisses in the east. Evidence suggests that the White Clay nappe was probably generated out of the accretionary wedge that accumulated in front of the northwestward moving magmatic arc. The nappe rocks were subsequently carried on the Doe Run thrust over the massifs of the Brandywine terrane.

Cecil Amalgamate

The Cecil Amalgamate lies mostly in Maryland, southeast of the Westminster and Baltimore terranes and southwest of the White Clay nappe (Figure 2.5-202). A portion of it, the Liberty Complex, lies between the Westminster and Baltimore terranes (Figure 2.5-201). It occupies northern Cecil County, eastern and northern Harford County, and southern Baltimore County. The Liberty Complex crosses northern Baltimore County into Carroll County where it passes southward into the Potomac terrane, which is a complex of thrust sheets and sedimentary mélanges that extend southward into northern Virginia. The Cecil Amalgamate consists of five separate lithic assemblages, the Liberty Complex, the Baltimore Mafic Complex, a metasedimentary sequence, the James Run Formation and the Port Deposit Tonalite. All of these five separate assemblages, while quite distinct lithologically, all have characteristics that relate them to a magmatic arc origin.

The Liberty Complex is the northwestern-most assemblage of the Cecil Amalgamate and consists of the Morgan Run Formation and the younger Sykesville Formation. The assemblage is considered to represent an accretionary wedge accumulated in front of a westward advancing magmatic arc. Fragments of basalt, amphibolite and ultramafics from the magmatic arc were deposited in the Morgan Run schist, while blocks from the Morgan Run were incorporated into the Sykesville metadiamictitic mélange. The combined

Morgan Run-Sykesville assemblage was thrust over the Baltimore terrane to its present location between Baltimore and Westminster terranes.

The Baltimore Mafic Complex lies southeast of the Baltimore and Westminster terranes and includes the Aberdeen block (Figure 2.5-201). It consists of a layered sequence of ultramafic, cumulate mafic and mafic intrusives, and volcanic rocks. It has many of the characteristics of an ophiolite sequence, but evidence suggests that it may not be derived from typical depleted oceanic crust as it contains contamination from continental material. The Baltimore Mafic Complex probably developed in a magmatic arc setting over a subduction zone with its contamination coming from subducted continental sediment from nearby microcontinents.

South of the main body of the Baltimore Complex (Figure 2.5-201) lies a belt of metasedimentary rocks which consist of pelitic schists, diamictites, and metagraywackes. The clasts in the diamictites are reported to match lithically the metavolcanics of the James Run Formation and the felsic rocks of the Port Deposit Tonalite indicating that they accumulated in close proximity to both.

The James Run Formation is the southeastern-most belt of the Cecil Amalgamate (Figure 2.5-201) and consists of a sequence of mostly felsic to intermediate rocks of bimodal volcanic, hypabyssal, and volcaniclastic origin. The rocks of the James Run Formation have been associated with the Chopawamsic terrane because of the lithological similarities between the James Run rocks and the rocks of the Chopawamsic terrane. However, an alternate interpretation is that the James Run Formation has a greater chemical affinity to the Baltimore Mafic Complex than to the Chopawamsic Formation (Faill, 1997a).

Within the metasedimentary belt and the James Run Formation is the Port Deposit Tonalite, a metamorphosed felsic pluton (Figure 2.5-201). It has a gradational contact with the James Run Formation and is chemically similar to these volcanics. It is considered to be the extrusive equivalent of the James Run and pre-dates the Taconic orogeny; a post-Taconic shallow granodiorite/granite (the Basin Run Granitoid) reportedly lies to the northwest.

2.5.1.1.3.2.2 Iapetan Oceanic Crust Remnants

Variously sized bodies of ultramafic rocks are found within the Baltimore Gneiss, all parts of the Wissahickon Formation, and the Peters Creek Schist and variably tectonized schist. They are primarily serpentinite, ranging in color from dark green to yellow-green. Steatite, chlorite-talc schist, anthophyllite schist, pyroxenite, and norite are also present. The relationships between the ultramafic and surrounding rocks, and between the ultramafic bodies themselves, are unclear. The age of these rocks is also uncertain. The largest bodies lie along and near the Rosemont Fault. Other concentrations of ultramafic rocks are close to the boundary between the Avondale Anticline and West Chester Massif, and to the Cream Valley Fault. The remaining small bodies are scattered through the surrounding rocks with no apparent pattern. Examples of possible obducted oceanic crust include the Bel Air-Rising Sun terrane [Tectonostratigraphic map (Figure 2.5-9) unit “ob”] and the Sussex terrane [Tectonostratigraphic map (Figure 2.5-9) unit “os”].

A newly identified remnant of the Siluro-Devonian ocean crust is the Cat Square terrane (Merchat, 2007). The Cat Square terrane is located just south of the Virginia-North Carolina border southwest of the Milton terrane. It is bound on the west by the Brevard fault zone (southern extension of the Bowens Creek fault) and on the east by the central Piedmont suture (Figure 2.5-23). The terrane consists of metapsammite and pelitic schist that was intruded by Devonian anatectic granitoids. Rare mafic and ultramafic rocks occur in the eastern Cat Square

terrane. The metapsammite and pelitic schist may represent turbidites derived from approaching highlands on both sides of the closing ocean.

2.5.1.1.3.2.3 Iapetan Volcanic Arc Terranes

The volcanic arcs accreted along the mid-Atlantic margin of North America consist of a collection of terranes that generally display first-order similarities with respect to lithic content and depositional-crystallization ages; however, each of these terranes records differences with respect to the proportions of different rock types, isotopic signatures of magmatic rocks, and tectonothermal histories that distinguish one terrane from another. The components of the zone can be crudely divided on the basis of tectonothermal imprint. Some elements have remained at upper crustal levels throughout their history, experiencing mainly low-grade metamorphism and simple structural imprints and thus are designated "suprastructural" terranes; primary structures are commonly preserved in these terranes, thus allowing for the establishment of stratigraphic sequences (Hibbard, 2003). Suprastructural terranes include the Wilmington, Chopawamsic, Milton, Carolina / Albemarle, Spring Hope, and Roanoke Rapids terranes (Figure 2.5-9). Locally some of these terranes display higher grade metamorphism and complex structural geometries. The accreted island arc terranes are described in the following paragraphs.

Wilmington Terrane: Tectonostratigraphic Map (Figure 2.5-9) Unit "cw"

The Wilmington terrane consists of granulite grade felsic to mafic gneisses presently exposed in northern Delaware and adjacent Pennsylvania (Figure 2.5-201 and Figure 2.5-202). The complex is considered to have formed in the lower portion of a magmatic arch that developed over an eastward dipping subduction zone in the Iapetan basin as early as the Middle Cambrian. Its emplacement over the Philadelphia terrane, White Clay nappe, and Brandywine Avondale massif occurred during the Late Proterozoic-Early Cambrian Potomac orogeny (Faill, 1997a).

Chopawamsic and Milton Terranes: Tectonostratigraphic Map (Figure 2.5-9) Unit "vcp" and "um," Respectively

The Early Cambrian Chopawamsic terrane and its southeastward extensions, the Milton terrane, comprise a broad central part of the Piedmont Province extending from southeast Delaware to North Carolina. The Chopawamsic and Milton terranes consist predominantly of meta-sedimentary and meta-volcanic rocks. The Chopawamsic terrane includes the Ta River (Virginia) and James Run (Maryland) metamorphic suites (Figure 2.5-209 and Figure 2.5-210). The Ta River and James Run metamorphic suites consist of a sequence of amphibolites and amphibole-bearing gneisses with subordinate ferruginous quartzites and biotite gneiss. Rocks of the Ta River Metamorphic Suite are generally thought to be more mafic and to have experienced higher-grade regional metamorphism than the rocks of the Chopawamsic Formation (Spears, 2002).

The Chopawamsic and Milton terranes are interpreted to be vestiges of island-arcs that were accreted to ancestral North America during the Taconic orogeny (Figure 2.5-208). The terranes consist of sequences of felsic, intermediate and mafic meta-volcanic rocks with subordinate meta-sedimentary rocks. The Chopawamsic and Milton terranes (and others described later in this section) are regarded as exotic, or suspect, terrains that formed ocean-ward from the Laurentian continental margin. Recent U-Pb studies consistently yield Ordovician ages for Chopawamsic volcanic rocks. Rb-Sr and U-Pb dating of granite plutons give late Ordovician ages (Spears, 2002). Detrital zircon ages for the Arvonia and Quantico overlap sequences indicate deposition in early Devonian/late Silurian.

Figure 2.5-9, based on the Horton map (1991) correctly shows the regional extent of the Milton terrane as a southern extension of the Chopawamsic terrane. However, the map legend indicates that the Milton terrane represents an accreted portion of continental crust, distinct from the volcanic arc affinity of the Chopawamsic terrane. Subsequent analytical work shows conclusively that the Milton terrane rocks are isotopically, geochemically, and geochronologically equivalent to the Chopawamsic terrane in the central Virginia Piedmont (Henika, 2006).

Within the 200-mile (322-kilometer) radius of the CCNPP site, the Chopawamsic transitions to the Milton terrane south-southeast of Richmond, Virginia (Figure 2.5-9). The Chopawamsic and Milton terranes are bounded on the west by the Brookneal northeast-trending dextral shear zone (Figure 2.5-23) and its northern extension, the Chopawamsic thrust fault (Figure 2.5-23). Further south, the Milton terrane is overlain on the east by sediments of the Mesozoic Dan River-Danville Basin (tectonostratigraphic map unit "Mz_3"), bounded to the west by a down-to-the-east normal fault. To the east, the Goochland terrane overrides the Chopawamsic and Milton terranes along the Spotsylvania thrust fault. The Chopawamsic and Milton terranes, as well as the contiguous Potomac terrane on the east, are intruded by the Ordovician Occoquan pluton (tectonostratigraphic map unit "p_1"), the Ellisville pluton (tectonostratigraphic map unit "p_2"), and Tanyard Branch pluton (tectonostratigraphic map unit "p_3"). These are "stitching" plutons whose age dates provide a maximum age of terrane assembly (Howell, 1995) (see discussion of Paleozoic plutons in Section 2.5.1.1.3.2.2). Unconformably overlying the Chopawamsic and Milton terranes and their intruded plutons are in-folded remnants of a Paleozoic overlap sequences, the Arvonia Formation (tectonostratigraphic map unit "O_1") and Quantico Formation (tectonostratigraphic map unit "O_2"), consisting of slates, phyllites, schists, and quartzites (see description of Paleozoic overlap sequences in Section 2.5.1.1.3.2.1)

2.5.1.1.3.2.4 Iapetan Disrupted (Infrastructural) Terranes

Some terranes have been subjected to either middle or lower crustal conditions at some time(s) during their history and are thus considered as "infrastructural" terranes; most of these terranes are imprinted by both amphibolite facies or higher metamorphism and complex deformational geometries primary structures have generally been obliterated in these terranes, thus precluding the establishment of any stratigraphy (Hibbard, 2003). Terranes with infrastructural character within a 200-mile (322-kilometer) radius of the CCNPP site include Potomac composite terrane, the Jefferson terrane, the Smith River terrane, the Falls Lake, and Raleigh - Goochland terranes.

Potomac Composite Terrane: Tectonostratigraphic Map (Figure 2.5-9) Unit "dp"

The Potomac terrane is characterized by a stack of mainly metaclastic thrust sheets and intervening mélanges with ophiolitic remnants (Horton, 1989). The Potomac terrane has been divided into the Mather Gorge, Sykesville, and Laurel formations. The protoliths of the three formations were interpreted to be Neoproterozoic to Early Cambrian distal slope deposits and olistostromes (Drake, 1989). The three formations are separated by major north-northeast–striking faults (Drake, 1989). Multiple foliations are common and composite foliations are strongest in phyllonitic rocks close to these fault zones.

The relationship between the Smith River allochthon and the Potomac terrane is unknown, although it is likely that the north end of the Smith River allochthon structurally overlies the Potomac terrane. Slices of the Potomac Terrane from central Virginia to the New York Bight appear to have been dextrally transposed along the Brookneal shear zone in Virginia (Figure 2.5-23) and its continuation northeastward.

Jefferson Terrane: Tectonostratigraphic Map (Figure 2.5-9) Unit "dje"

The Jefferson terrane contains mainly metaclastic rocks with subordinate amphibolite and meta-ultramafic rocks that structurally underlie the allochthon. The age of rocks in the Jefferson terrane is unknown, although traditionally they have been viewed to be Neoproterozoic to early Paleozoic (Faill, 1997a). The terrane has been thrust over the Laurentia cover sequence on the Creek Fault and was, in turn, overthrust by the Smith River terrane by the Chatham Fault (Figure 2.5-9).

Smith River Terrane: Tectonostratigraphic Map (Figure 2.5-9) Unit "ds"

The Smith River allochthon is in a southern Appalachian belt of metaclastic rocks that has traditionally been considered to be of peri-Laurentian origin. Th-U-Pb monzonite ages confirm that the allochthon was involved in an Early Cambrian tectonothermal event, and the presence of ca. 1000 Ma Detrital zircons indicate that the terrane is exotic with respect to adjacent Laurentian rocks and could have a Gondwanan source, because Detrital and xenocrystic zircons of this age are also found in Appalachian peri-Gondwanan crustal elements (Hibbard, 2003). The allochthon may form a new link between the Appalachians and the Pampean terrane of western South America; in addition, its position in the orogen has implications for recent models of the opening of the Iapetus (Hibbard, 2003).

The Smith River terrane includes the structurally underlying Bassett Formation and the structurally overlying Fork Mountain Formation; the contact between the units appears to be conformable, although there is no evidence preserved that indicates their stratigraphic sequence (Conley, 1973). Both units are dominated by biotite paragneiss; the Fork Mountain Formation also includes matrix-supported breccias that have been favorably compared to some of the mélanges in the Potomac terrane (Horton, 1989). The only age constraint for these units is that they are intruded by the Martinsville intrusive suite. (Hibbard, 2003)

Falls Lake Terrane: Tectonostratigraphic Map (Figure 2.5-9) Unit "df"

The Falls Lake terrane is a small allochthonous unit found in Grenville County, North Carolina, just at the limit of the 200-mile (322-kilometer) radius of the CCNPP site. The western boundary of the Falls Lake terrane is thrust over the eastern edge of the upper greenschist facies Carolina/ Albemarle arc along the ductile normal Upper Barton Creek fault while western boundary of the Spring Hope terrane is thrust over the eastern boundary of the Falls Lake terrane along the Nutbush Creek Fault (Figure 2.5-9 and Figure 2.5-23). In Grenville County, a greenschist facies pluton of the Carolina / Albemarle terrane contains a variety of relict igneous features including greenstone, metagabbro, and meta-ultramafic blocks similar to the amphibolite facies Falls Lake terrane.

Goochland or Raleigh / Goochland Terrane: Tectonostratigraphic Map (Figure 2.5-9) Unit "cg"

The Goochland terrane (also known as the Raleigh-Goochland terrane of Hibbard, 2003) stretches southward from Fredericksburg, Virginia, to the North Carolina state line east of the Spotsylvania fault (discussed in Section 2.5.1.1.4.4.2) (Frye, 1986) (Figure 2.5-9). The Goochland belt (Virginia) is composed predominantly of granulite facies (high grade) metamorphic rocks and the Raleigh belt (North Carolina) is composed of sillimanite (very high grade) metamorphic rocks (Hibbard, 2007). The Goochland-Raleigh terrane is interpreted to be a microcontinent that was accreted to ancestral North America during the Taconic orogeny. Some geologists believe that the micro-continent was rifted from ancestral North America during the proto-Atlantic rifting while others believe that it formed outboard of ancestral North America (exotic or suspect terrane). Rocks of the Goochland-Raleigh belt are considered to be the oldest rocks

of the Piedmont Province and bear many similarities to the Grenville age rocks of the Blue Ridge Province (Spears, 2002).

The Po River Metamorphic Suite and the Goochland terrane, that lie southeast of the Spotsylvania fault, make up the easternmost part of the Goochland-Raleigh terrane. The Po River Metamorphic Suite was named after the Po River in the Fredericksburg area and comprises amphibolite grade (high grade) metamorphic rocks, predominantly biotite gneiss and lesser amounts of hornblende gneiss and amphibolite (Pavlides, 1989). The age of this unit is uncertain, but it has been assigned a provisional age of Precambrian to Early Paleozoic (Pavlides, 1980). The Goochland terrane was first studied along the James River west of Richmond, Virginia, and contains the only dated Precambrian rocks east of the Spotsylvania fault. It is a Precambrian granulite facies (high grade) metamorphic terrane.

2.5.1.1.3.3 The Peri-Gondwanan Realm

2.5.1.1.3.3.1 Peri-Gondwanan Microcontinents

Avalonia or the Avalon terrane has been identified as a microcontinent of peri-Gondwanan affinity (Faill, 1998). Remnants of Avalonian continental crust are not found within the 200-mile (322-kilometer) radius of the CCNPP site. However, exposures in the northern Appalachians indicate that the Carolina volcanic arc terrane was accreted to the Avalonia terrane before the amalgamated microcontinent impinged of the North Atlantic continental margin. The impingement of the amalgamated microcontinent added to the intensity of the collision during the Alleghanian orogeny. Only southeastward (current coordinates) translated portions of the Carolina arc are found within the 200-mile radius of the CCNPP site. Therefore, the discussion of this terrane is limited to the volcanic arc terranes described in the next section (Section 2.5.1.1.3.3.2). The other identified peri-Gondwanan microcontinent, the Suwannee terrane of the southern Appalachians, is only found outside the 200-mile radius of the CCNPP site and is not discussed further.

2.5.1.1.3.3.2 Peri-Gondwanan Volcanic Arcs

Carolina Terrane: Tectonostratigraphic Map (Figure 2.5-9) Unit "vca"

The Carolina terrane extends southward from southern Virginia to central Georgia, while the Eastern Slate belt is located predominantly in North Carolina, east of the Goochland-Raleigh belt (Figure 2.5-9). Both the Carolina and Eastern Slate belts are composed of greenschist facies (low grade) metamorphic rocks (Hackley, 2007), including metagraywacke, tuffaceous argillites, quartzites, and meta-siltstones (Glover, 1997). The Carolina and Eastern Slate belts are interpreted to be island-arcs that were accreted to ancestral North America during the Taconic orogeny. The island-arcs are interpreted to have been transported from somewhere in the proto-Atlantic Ocean, and are therefore considered to be exotic or suspect terranes. Rocks of the Carolina and Eastern Slate belts generally are considered to be Early Paleozoic in age. Granitic and gabbro-rich plutons that intrude the belts generally are considered to be Middle to Late Paleozoic in age).

New analytical work shows that the Milton terrane and Carolina terrane are distinct and unrelated crustal blocks, separated by a significant shear zone, the Hyco shear zone, a segment of the central Piedmont shear zone (Henika, 2006).

Hatteras Terrane: Tectonostratigraphic Map (Figure 2.5-9) Unit "uh"

The Hatteras terrane is a pluton-rich belt of amphibolite metamorphic grade metaigneous rocks that range in composition from tonalite gneiss with mafic amphibolite layers through quartz monzonite to granite to cordierite-bearing granite. The rocks have a compositional range appropriate for magmatic arcs on continental crust. The western boundary is an abrupt transition to greenschist facies volcaniclastic rocks and may be a fault. Rb/Sr whole-rock ages of 583±46 Ma for the granite and 633±61 Ma for the quartz monzonite. Except for the younger age, the Hatteras terrane is compositionally similar to the eastern high-grade continental basement of the mid-Atlantic states. The plutonic and sub-volcanic to volcanic nature and age span of the Hatteras terrane rocks is consistent with those of the Carolinian terrane (Glover, 1997).

In the Carolinas, magmatic arc rocks are continuous across the Piedmont and under the coastal plain from west of Charlotte, North Carolina, to Cape Hatteras. In Virginia the Piedmont nappes of Goochland Grenville basement are warped into an antiformal structure that plunges southward beneath the Carolinian terrane magmatic arc rocks near Raleigh North Carolina (Glover, 1997). Glover (1997) goes on to state that "The Carolinian terrane is broken by faults and interrupted by Mesozoic basins (Keppie, 1989), but there is little evidence to suggest that it comprises more than a single exotic terrane. Recent maps of the Atlantic Coastal Plain basement (Thomas, 1989; Keppie; 1989) generally agree. Horton (1991), however, split Carolinia into five terranes but consider several to be possible extensions of adjacent volcanic 'terranes.'" Based on the Glover (1997) analysis, this FSAR section groups the Chopawamsic and Milton terranes, the Carolina / Albemarle arcs, and the Hatteras terrane together as possibly correlative accreted volcanic arc terranes built on continental crust.

2.5.1.1.3.4 The Pangean Realm

2.5.1.1.3.4.1 Paleozoic Pangean Sediments

The Paleozoic orogenies eventually led to the formation of the Pangean supercontinent by Late Paleozoic time. The closure of the Iapetus/Theic oceans beginning in the Middle Ordovician was accompanied by the loading onto the Rodinian (see discussion in FSAR Sections 2.5.1.1.3 and 2.5.1.1.2.1) continental margin of thrust sheets. These thrust sheets included microcontinental, abyssal and volcanic arc terranes. This loading likely led to a crustal bulge that uplifted the cratonward portion of carbonate platform in the northern Appalachians causing erosion (the Knox unconformity) of carbonate platform sediments that were shed westward into a foreland basin. On the opposite side of the bulge, subsidence was occurring. Twenty-plus ash falls that thickened southwestward were deposited across the carbonate shelf of the orogenic belt during the Upper Ordovician (the Millbrig K-bentonite, for example). Based on thicknesses of these units, the source of these volcanic deposits is believed to have been off the coast of South Carolina (present coordinates), from a magmatic arc or the Baltica continent colliding with Laurentia (Faill, 1997a).

As the Taconic orogeny reached greater intensity in the central Appalachians, the Brandywine and Baltimore microcontinents began to impinge on the Laurentian margin, leading to subsidence along the continental shelf. Carbonate shelf deposition was replaced by pelitic sedimentation Martinsburg and Reedville formations (Figure 2.5-209 and Figure 2.5-210). Pelitic units were soon replaced by coarser siliciclastic sediments (Bald Eagle, Juniata and Tuscarora formations) derived from uplifted terranes to the southeast (Figure 2.5-211) (Faill, 1997a). The start of regional deposition of these coarse siliciclastics ended the 100 ma of carbonate shelf deposition on the Laurentian margin. The area of subsidence widened during the Taconic orogeny, spreading northwestward with deposition of the Reedsville shale, for

example. Deposition of these marine units spread as far westward (current coordinates) as far north as Ontario and as far west as the Mid-continent (Faill, 1997a). As the Octoraro Sea continued to close, crustal fragments and supracrustal rocks were thrust onto the Laurentian margin, generating several nappes and producing widespread metamorphism. Events associated with the collapse of the Octoraro basin included the development of the Martic thrust, emplacement of the Hamburg klippe, creation of the Reading meganappe system, and the obduction onto the Laurentian margin of microcontinent/magmatic arc packages, previously assembled within the Octoraro basin (Faill, 1997a).

East of the Susquehanna river, oceanic basin sediments were thrust over the Conestoga slope and carbonate shelf sediments. Further south, in south-central Pennsylvania and central Maryland, equivalent Octoraro and related sediments were thrust over pelitic and carbonate slope deposits along the Linganore thrust fault. A deeper thrust, probably still affecting Octoraro basin sediments but not oceanic crust, provided the mechanism by which the Reading meganappe system was emplaced. (Faill,1997a). The depth limit of this thrust is based on the lack of ophiolitic material in the resulting nappe. This lower thrust fault, however, was probably responsible for the inclusion of slivers of Laurentian continental basement into the interleaved and stacked thrust sheets.

The Appalachian basin developed as a consequence of the Taconic orogeny, which produced a crustal downwarp cratonward of new highlands to the west (present coordinates) uplifted as a result of crustal bulging. The initial deposits in the basin included molasse deposits of conglomerate, sandstone, siltstone, and shales of the Shagawunk Formation and its lateral facies, the Bloomsburg delta. A series of transgressions and regressions repeatedly shifted the shore zone and shallow marine facies. The lagoonal-tidal Wills Creek and laminated limestones of the Tonolway formations (Figure 2.5-211) accumulated in the Late Silurian. The Appalachian basin continued to receive sediments nearly uninterrupted through the remainder of the Paleozoic. Sedimentation in the basin accelerated as a result of Silurian through Permian orogenies.

The Acadian orogeny (Figure 2.5-8) was caused by the collision of the microcontinent Avalon with eastern North America during the Middle to Late Devonian Period. At its peak, the orogeny produced a continuous chain of mountains along the east coast of North America and brought with it associated volcanism and metamorphism. The Acadian orogeny ended the largely quiescent environment that dominated the Appalachian Basin during the Late Ordovician and into the Silurian, as vast amounts of terrigenous sediment from the Acadian Mountains were introduced into the basin and formed the Catskill clastic wedge in central Pennsylvania and northeastern New York (Figure 2.5-200). Vast amounts of terrigenous sediment from the Acadian Mountains were introduced into the Catskill foreland basin during the Middle and Late Devonian and formed the Catskill clastic wedge sequence in Pennsylvania and New York. Thick accumulations of clastic sediments belonging to the Catskill Formation are spread throughout the Valley and Ridge Province (Faill, 1997b). The Catskill clastic wedge is representative of fluctuating shorelines and prograding alluvial environments along the western margin of the Acadian upland. This regressional sequence is represented in the sedimentary record with turbidites, slope deposits, alternating shallow marine and non-marine sediments and alluvial plain fining-upward sequences (Walker, 1971, Faill, 1997b and USGS, 2008). The pebbles and sand grains of the Catskill Formation in New York, Pennsylvania and Maryland are mostly composed of metamorphic and granitic rock fragments, feldspar, mica and quartz. The red color is due to the presence of a small percentage of iron oxide between the grains (Dolt, 1988). The regressive sequence in the region is bounded above and below by marine transgressions which are represented by basal black shale overlain by gray shales and mudstones capped by small amounts of siltstone (Bridge, 1994 and Huber, 2000). The Catskill clastic wedge was the site of the greatest accumulation of sediment in the region, depositing as

much as 7,000 feet of sediment (Stoffer, 2003). The sediments are the thickest in the east and grow progressively thinner westward and southward into the central Appalachian Basin region (Figure 2.5-200). In general, the Acadian Orogeny was superimposed upon terranes affected or formed by the Taconic Orogeny (Dolt, 1988) (Figure 2.5-200).

The Catskill clastic wedge in the central Appalachians is overlain by cyclothems of the Mississippian Pocono Group (Figure 2.5-211), consisting predominantly hard gray massive sandstones, with some shale. In the Eastern Panhandle of Maryland, the Pocono Group has been divided into the Hedges, Purslane, and Rockwell formations unconformably overlain by the Greenbrier and Mauch Chunk formations. The Mississippian stratigraphic units in northern Virginia and West Virginia, and western Maryland/Delaware include the Rockville and Burgoon/ Purslane Sandstone unconformably overlain by the Greenbrier and Mauch Chunk formations.

Sediments of the Mississippian Pocono Group are overlain by cyclothems in the Pennsylvanian Pottsville Group (Figure 2.5-211). The Pottsville Group consists predominantly of sandstones, some of which are conglomeratic, interbedded with thin shales and coals. In eastern Pennsylvania, the Pennsylvanian stratigraphic units include the Pottsville Group and overlying Allegheny, Glenshaw, Casselman, and Monongahela formations. In Maryland and Delaware, the Pennsylvanian stratigraphic units consist of the Pottsville Group and overlying Allegheny, Conemaugh and Monongahela formations. The Pottsville Group is known only from the southwestern portion of Virginia and the southeastern portion of West Virginia (outside the 200-mile (322-kilometer) radius of the CCNPP site). There, the Pottsville is known as the Pocahontas, New River, and Kanawha formations (Stewart 2002). Interestingly, in the Late Mississippian Mauch Chunk Group north of Bluefield, Virginia at the state border with West Virginia, evidence is found of a paleoseismite, including clastic sand dikes and slumps, probably associated with the Alleghany orogeny (Stewart 2002).

2.5.1.1.3.4.2 Late Paleozoic Plutons

Late Paleozoic plutons were the result of the final orogeny (the Alleghany orogeny) that contributed to the formation of the Pangean supercontinent. Plutonism was widespread across the Appalachian orogen. Some of the plutons were intruded into paraautochthonous and allochthonous terranes that had been accreted during previous orogenies and provide a means of dating the minimum age of emplacement of the thrusted units. These plutons are termed "stitching" plutons. Some of the major "stitching" plutons and the terranes they affected are described below.

Occoquan Pluton: Tectonostratigraphic Map (Figure 2.5-9) Unit "p_1"

The Occoquan pluton is a granite-granodiorite-tonalite body that is medium- to coarsegrained with rare xenoliths and exhibits moderate to strong metamorphic foliation and mineral lineation by quartz rods and mica layers. The pluton intrudes the upper part of the Wissahickon Schist and the Chopawamsic Formation.

Ellisville Pluton: Tectonostratigraphic Map (Figure 2.5-9) Unit "p_2"

The Ellisville pluton is a large granodiorite body that intrudes the high metamorphic grade rocks of the Hatcher Complex and the lower-grade rocks of the Chopawamsic Formation. Most of the pluton is porphyritic granodiorite with minor foliation, but the body is sheared along the southern margin along the James River.

2.5.1.1.3.4.3 Mesozoic Rift Sequences

The Mesozoic rift basins within a 200-mile (322-kilometer) radius of the CCNPP site are identified collectively in Figure 2.5-9 as map unit "Mz_3" and individually in Figure 2.5-10 with numeric designators.

As described in the subsection on Cenozoic History (Section 2.5.1.1.2.8), early Mesozoic rifting and opening of the Atlantic Ocean was followed by sea floor spreading and the continued opening of the Atlantic Ocean during Cenozoic time. Continued erosion of the Appalachian Mountains and the exposed Piedmont produced extensive sedimentation within the Coastal Plain Province that includes the CCNPP site region.

The non-marine and marine sediments deposited in the Coastal Plain Physiographic Province overlie what are most likely foliated metamorphic or granitic rocks, similar to those cropping out in the Piedmont approximately 50 mi (80 km) to the northwest (Figure 2.5-5 and Figure 2.5-6). A combination of erosion, downwarping, and faulting resulted in an undulatory, east-dipping basement surface with local slope variations that underlies the Coastal Plan Province. The Pre-Cretaceous basement bedrock is only encountered in the Coastal Plain Province by borings designed to characterize deep aquifers above the underlying basement rock. Hansen (Hansen, 1986) indicates that most of the borings that penetrate coastal plain sediments and extend to the underlying basement have encountered metamorphic or igneous rocks. For example, well DO-CE 88 in Dorchester County located approximately 24 mi (39 km) east of the CCNPP site was drilled into gneissic basement rock at 3,304 ft (1,007 m) in depth (Figure 2.5-11). Based on the characteristics summarized in Section 2.5.1.1.3.2.1, this lithology is within the Outer Belt of the terranes underlying the Coastal Plain sequence. Well QA-EB 110, in Queen Anne's County, located 38 mi (61 km) north of the CCNPP site, was drilled to explore for deep freshwater aquifers. This well was drilled into basement at a depth of 2,518 ft (767 m). The basement rock was only sampled in the drill cuttings and suggests a gneiss/schist from the mineralogy present, (i.e., biotite, chlorite, and clear quartz). This crystalline sample lies within the Middle Belt terrane.

Regional geophysical and scattered borehole data indicate that a Mesozoic basin might be present in the site vicinity, buried beneath Coastal Plain sediments. Triassic clastic deposits, indicative of a possible rift basin, were penetrated in Charles County (well CH-CE 37), located over 20 mi (32 km) west of the site, for an interval of 99 ft (30 m), returning samples of weathered brick red clay and shale. Hansen (1986) reports the occurrence of siltstones, sandstones, and clays in several borings north of this well within Prince Georges County. These samples appear to represent continental deposits within the buried Taylorsville Basin. The Inner Belt as defined by Hansen (Hansen, 1986) may contain portions of a buried Mesozoic basin or basins similar to the Neward-Gettysburg terrane to the Northwest (Figure 2.5-9). Section 2.5.1.1.4.4.3 contains further discussions of potential Mesozoic extensional (rift) basins buried beneath coastal plain sediments.

Diabase was cored in the closest deep boring (SM-DF 84) to the CCNPP site that penetrated the Pre-Cretaceous basement. The boring is located in Lexington Park, St. Mary's County, about 13 mi (21 km) south of the CCNPP site (Hansen, 1984) (Figure 2.5-11). Hansen (Hansen, 1984) states:

As no other basement lithologies were encountered, it is presently not known whether the diabase is from a sill or dike associated with the rift-basin sediments or whether it is cross-cutting the crystalline rocks. The diabase is apparently a one-pyroxene (augite) rock, which Fisher (1964) suggests is evidence of rapid, undifferentiated crystallization in a relatively thin intrusive body, such as a dike.

The occurrence of Mesozoic rift-basin rocks in St. Mary's and Prince George's County are further discussed (Hansen, 1986): "The basins that occur in Maryland are all half-grabens with near-vertical border faults along the western sides. The strata generally strike north-easterly, but, in places, particularly in the vicinity of cross-faults, strike may diverge greatly from the average."

Exposed Mesozoic rift basins found within a 200-mile (322-kilometer) radius of the CCNPP site include the Culpepper Basin, the Deep River Basin, the Gettysburg Basin, the Newark Basin, the Oatlands-Studley Basin, the Richmond Basin, and the Taylorsville Basin. Buried Mesozoic rift basins, inferred from geophysical studies or borehole drilling within a 200-mile radius of the CCNPP site, include New York Bight Basin, the Queen Anne Basin, the Delmarva Basin, the Norfolk Basin, and other unnamed basins identified in Figure 2.5-9 and Figure 2.5-10. All of the exposed rift basins identified above belong to the Newark Supergroup. Instead of describing individual stratigraphic units within each basin, the following is a brief description of the rift basin formation associated with the Eastern North America Magmatic Province (discussion in Section 2.5.1.1.2.7), and a more specific discussion of the Newark Basin Supergroup lithologies.

The Newark Supergroup consists largely of poorly-sorted non-marine sediments deposited within rift basins along the mid-Atlantic margin. The typical lithologies are conglomerate, arkosic sandstone, siltstone, and shale. Most of the strata are red beds that feature ripple marks, mud cracks, and rain drop imprints; dinosaur footprints are common, though actual body fossils are very rare. Some of the strata are detailed to the level of varves, with indications of Milankovitch cycles. The Triassic stratigraphy of a typical Newark Group basin consists of a basal fluvial unit overlain by lacustrine strata. The deepest lakes occur near the base of the lacustrine succession and then gradually shoal upward. This Triassic sequence is referred to as the "tripartite stratigraphy" (Schlische, 2003a) (Schlische, 2003b). The tripartite stratigraphy is generally overlain by an Early Jurassic age sequence of lava flows and intercalated lacustrine (commonly deep-water) strata overlain in turn by shallow lacustrine strata and, in some cases, by fluvial strata (Schlische, 2003a) (Schlische, 2003b). Based on basin geometry, onlap geometry, and major stratigraphic transitions, the basins grow wider, longer, and deeper through time. Sediment supply appears to keep pace with basin subsidence. Transition from fluvial to lacustrine appears to be a consequence of gradual growth of basin length and width (Schlische, 2003a) (Schlische, 2003b).

The Mesozoic rift basins along the length of the North American Atlantic margin are related to the Eastern North America Magmatic Province (de Boer, 2003). Subsidence of the rift basins was initiated ca. 230 Ma. The orientation of the rift basin follows the general axis of deformation of the Appalachian orogen, including changes along strike related to promontories and recesses. This likely indicates that crustal thinning took advantage of pre-existing deep crustal features such as a major translithospheric suture zone, possibly related to the edge of the Grenvillian basement.

2.5.1.1.3.5 Post-Pangean Sediments

2.5.1.1.3.5.1 Upper Mesozoic Stratigraphic Units

Regionally, coastal plain deposits lap onto portions of the eastern Piedmont. (Mixon, 2000). East of the Fall Line, the Coastal Plain sediments range from Early Cretaceous to Quaternary in age and consist of interbedded silty clays, sands, and gravels that were deposited in both marine and non-marine environments. These sediments dip and thicken toward the southeast. Whereas the basement surface dips southeast at about 100 ft/mi (18.9 m/km) in Charles County, west of the CCNPP site, a marker bed in the middle of the Cretaceous Potomac Group dips southeast at about 50 ft/mi (9.5 m/km) (McCartan, 1989a). This wedge of unlithified sediments consists of Early Cretaceous terrestrial sediments and an overlying sequence of

well-defined, Late Cretaceous, marine stratigraphic units. These units from oldest to youngest are summarized in the following paragraphs.

The Lower Cretaceous strata of the Potomac Group consists of a thick succession of variegated red, brown, maroon, yellow, and gray silts and clays with interstratified beds of fine to coarse gray and tan sand. The Potomac Group occurs on Proterozoic to Cambrian metamorphic and igneous rocks in the Washington DC area (McCartan,1990) In the Baltimore-Washington area, the Potomac Group is subdivided from oldest to youngest into the Patuxent, Arundel, and Patapsco Formations. This subdivision is recognizable in the greater Washington-Baltimore area where the clayey Arundel Formation is easily recognized and separates the two dominantly sandy formations (Hansen, 1984). This distinction is less pronounced to the east and southeast where the Potomac Group is divided into the Arundel/Patuxent formations (undivided) and the overlying Patapsco Formation. At Lexington Park, Maryland, the clayey beds that dominate the formation below a depth of 1,797 ft (548 m) are assigned to the Arundel/Patuxent Formations (undivided) (Hansen, 1984).

At the Lexington Park well, located about 13 mi (21 km) south of the CCNPP site (Figure 2.5-11), about 30 ft (9 m) of a denser, acoustically faster, light gray, fine to medium clayey sand occurs at the base of the Potomac Group and might represent an early Cretaceous, pre-Patuxent Formation. These sediments might correlate with the Waste Gate Formation encountered east of Chesapeake Bay in the DOE Crisfield No. 1 well (Hansen, 1984).

The Patapsco Formation contains interbedded sands, silts, and clays, but it contains more sand than the overlying Arundel/Patuxent Formations (undivided). The contact is marked by an interval dominated by thicker clay deposits. The Arundel/Patuxent Formations (undivided) are marked by the absence of marine deposits. The Mattaponi Formation was proposed (Cederstrom, 1957) for the stratigraphic interval immediately above the Patapsco Formation. An identified interval (Hansen, 1984) as the Mattaponi (?) is now recognized as part of the upper Patapsco Formation.

The Upper Cretaceous Magothy Formation (Figure 2.5-212) is approximately 200 ft (61 m) thick in northern Calvert County but becomes considerably thinner southward at the CCNPP site and pinches out south of the site and north of wells in Solomons and Lexington Park, Maryland (Hansen, 1996) (Achmad, 1997) (Figure 2.5-13). This pattern also appears to reflect thicker deposition in the Salisbury Embayment. The Magothy Formation is intermittently exposed near Severna Park, Maryland, and in the interstream area between the Severn and Magothy Rivers. This outcrop belt becomes thinner to the south in Prince Georges County. The Magothy consists mainly of lignitic or carbonaceous light gray to yellowish quartz sand interbedded with clay layers. The sand is commonly coarse and arkosic and in many places is cross bedded or laminar. Pyrite and glauconite occur locally (Otton, 1955).

The upper Cretaceous Matawan and Monmouth formations (Figure 2.5-212) are exposed in Anne Arundel County, Maryland. While the Matawan is absent in Prince Georges County, the Monmouth crops out in a narrow belt near Bowie, Maryland. Exposures of these formations have not been identified in Charles County. These formations are inseparable in sample cuttings and drillers' logs and are undifferentiated in southern Maryland (Otton 1955) (Hansen, 1996). They consist mainly of gray to grayish-black micaceous sandy clay and weather to a grayish brown. Glauconite is common in both formations and fossils include fish remains, gastropods, pelecypods, foraminifera, and ostracods. The presence of glauconite and this fossil fauna indicate that the Matawan and Monmouth are the oldest in a sequence of marine formations. These formations range in thickness from a few feet or less in their outcrop area to more than 130 ft (40 m) at the Annapolis Water Works (Otton, 1955). The formations thin to the west and average about 45 ft (14 m) in Prince Georges County. The combined formations along

with the Brightseat Formation form the Lower Confining Beds (Section 2.4.12) that become progressively thinner from southern Anne Arundel County through Calvert County to St. Mary's County where this hydrostratigraphic unit appears to consist mainly of the Brightseat Formation (Hansen, 1996).

2.5.1.1.3.5.2 Tertiary Stratigraphic Units

The Brightseat Formation is exposed in a few localities in Prince Georges County and contains foraminifera of Paleocene age (Figure 2.5-212). This unit is relatively thin [up to about 25 ft (8m)] but occurs widely in Calvert and St. Mary's counties. It is generally medium and olive gray to black, clayey, very fine to fine sand that is commonly micaceous and / or phosphatic (Otton, 1955; Hansen, 1996). It can be distinguished from the overlying Aquia Formation by the absence or sparse occurrence of glauconite. It generally contains less fragmental carbonaceous material than the underlying Cretaceous sediments (Otton, 1955). The Brightseat Formation is bounded by unconformities with a distinct gamma log signature that is useful for stratigraphic correlation (Hansen, 1996). The Late Paleocene Aquia Formation (Figure 2.5-212) was formerly identified as a greensand due to the ubiquitous occurrence of glauconite. This formation is a poorly to well sorted, variably shelly, and glauconitic quartz sand that contains calcareous cemented sandstone and shell beds. The Aquia Formation was deposited on a shoaling marine shelf that resulted in a coarsening upward lithology. This unit has been identified in the Virginia Coastal Plain and underlies all of Calvert County and most of St. Mary's County, Maryland (Hansen, 1996). The Aquia Formation forms an important aquifer as discussed in Section 2.4.12. The Late Paleocene Marlboro Clay (Figure 2.5-212) was formerly considered to be a lower part of the early Eocene Nanjemoy Formation but is now recognized as a widely distributed formation. The Marlboro Clay extends approximately 120 mi (193 km) in a northeast-southwest direction from the Chesapeake Bay near Annapolis, Maryland to the James River in Virginia. Micropaleontological data indicate a late Paleocene age although the Eocene-Paleocene boundary may occur within the unit (Hansen, 1996). The Marlboro Clay is one of the most distinctive stratigraphic markers of the Coastal Plain in Maryland and Virginia. It consists chiefly of reddish brown or pink soft clay that changes to a gray color in the subsurface of southern St. Mary's and Calvert Counties. Its thickness ranges from 40 ft (12 m) in Charles County to about 2 ft (60 cm) in St. Mary's County (Otton, 1955). However, the thickness is relatively constant from Anne Arundel County south through the CCNPP site to Solomons and Lexington Park, Maryland (Figure 2.5-13). The apparent localized thickening in Charles County might represent a local depocenter rather than a broader downwarping of the Salisbury Embayment relative to the Norfolk Arch (Figure 2.5-12).

The lower part of the overlying Early Eocene Nanjemoy Formation (Figure 2.5-212) is predominantly a pale-gray to greenish gray, glauconitic very fine muddy sand to sandy clay. This formation becomes coarser upward from dominantly sandy silts and clays to dominantly clayey sands. The gradational contact between the two parts of the Nanjemoy is defined on the basis of geophysical log correlations (Hansen, 1996). In southern Maryland the Nanjemoy Formation ranges in thickness from several ft in its outcrop belt to as much as 240 ft (73 m) in the subsurface in St. Mary's County (Otton, 1955) (Figure 2.5-13).

The Middle Eocene Piney Point Formation (Figure 2.5-212) was recognized (Otton, 1955) as a sequence of shelly glauconitic sands underlying the Calvert Formation in southern Calvert County. The contact with the underlying Nanjemoy Formation is relatively sharp on geophysical logs, implying a depositional hiatus or unconformity (Hansen, 1996). The Piney Point Formation ranges in thickness from 0 ft (0 m) in central Calvert County to about 90 ft (27 m) at Point Lookout at the confluence of the Potomac River and Chesapeake Bay (Hansen, 1996). The Piney Point Formation contains distinctive carbonate-cemented interbeds of sand and shelly sand that range up to about 5 ft (1.5 m) in thickness (Hansen, 1996) and a

characteristic fauna belonging to the Middle Eocene Jackson Stage (Otton, 1955). This unit is recognizable in the subsurface in Charles, Calvert, St. Mary's, Dorchester, and Somerset Counties in Maryland and in Northumberland and Westmoreland Counties in Virginia but has not been recognized at the surface (Otton,1955). The work of several investigators were summarized (Hansen, 1996) who identified a 1 to 4 ft (30 to 122 cm) thick interval of clayey, slightly glauconitic, fossiliferous olive-gray, coarse sand containing fine pebbles of phosphate. This thin interval of late Oligocene age occurs near the top of the Piney Point Formation and appears to correlate with the Old Church Formation in Virginia. This formation appears to thicken downdip between Piney Point and Point Lookout (Hansen, 1996). The absence of middle Oligocene deposits in most of the CCNPP site region indicates possible emergence or non-deposition during this time interval. Erosion or nondeposition during this relatively long interval of time produced an unconformity on the top of the Piney Point Formation that is mapped as a southeast dipping surface in the CCNPP site vicinity (Figure 2.5-14).

Renewed downwarping within the Salisbury Embayment resulted in marine transgression across older Cretaceous and Eocene deposits in Southern Maryland. The resulting Miocene-age Chesapeake Group consists of three marine formations; from oldest to youngest these are the Calvert, Choptank and St. Mary's Formations (Figure 2.5-212). The basal member of the group, the Calvert Formation, is exposed in Anne Arundel, Calvert, Prince Georges, St. Mary's and Charles Counties. Although these formations were originally defined using biostratigraphic data, they are difficult to differentiate in well logs (Hansen, 1996) (Glaser, 2003a). The basal sandy beds are generally 10 to 20 ft (3 to 6 m) thick and consist of yellowish green to greenish light gray, slightly glauconitic fine to medium, quartz sand. The basal beds unconformably overlie older Oligocene and Eocene units and represent a major early Miocene marine transgression (Hansen, 1996). The overlying Choptank and St. Mary's formations are described in greater detail in Section 2.5.1.2.3.

The Upper Miocene Eastover Formation and the Lower to Upper Pliocene Yorktown Formation occur in St. Mary's County and to the south in Virginia (McCartan, 1989b) (Ward, 2004). These units appear to have not been deposited to the north of St. Mary's County and that portion of the Salisbury Embayment may have been emergent (Ward, 2004).

Surficial deposits in the Coastal Plain consist, in general, of two informal stratigraphic units: the Pliocene-age Upland deposits and the Pleistocene to Holocene Lowland deposits (Figure 2.5-212). McCartan (McCartan, 1989b) recognized that an Upper Pliocene sand with gravel cobbles and boulders that blankets topographically high areas in the southeast third of St. Mary's County. The Upland Deposits are areally more extensive in St. Mary's County than in Calvert County (Glaser, 1971). The map pattern has a dendritic pattern and since it caps the higher interfluvial divides, this unit is interpreted as a highly dissected sediment sheet whose base slopes toward the southwest (Glaser, 1971) (Hansen, 1996). This erosion might have occurred due to differential uplift during the Pliocene or down cutting in response to lower base levels when sea level was lower during period of Pleistocene glaciation.

2.5.1.1.3.5.3 Plio-Pleistocene and Quaternary Stratigraphic Units

As stated previously, surficial deposits in the Coastal Plain consist, in general, of two informal stratigraphic units: the Pliocene-age Upland deposits and the Pleistocene to Holocene Lowland deposits. McCartan (1989b) differentiates three Upper Pleistocene estuarine deposits, Quaternary stream terraces, Holocene alluvial deposits and colluvium in St. Mary's County. The Lowland deposits in southern Maryland were laid down in fluvial to estuarine environments (Hansen, 1996) and are generally found along the Patuxent and Potomac River valleys and Chesapeake Bay. These deposits occur in only a few places along the eastern shore of Chesapeake Bay. The Lowland deposits extend beneath Chesapeake Bay and the Potomac

River filling deep, ancestral river channels with 200 ft (61 m) or more of fluvial or estuarine sediments (Hansen, 1996). These deep channels and erosion on the continental slope probably occurred during periods of glacial advances and lower sea levels. Deposition most likely occurred as the glaciers retreated and melt waters filled the broader ancestral Susquehanna and Potomac Rivers.

2.5.1.1.4 Regional Tectonic Setting

In 1986, the Electric Power Research Institute (EPRI) developed a seismic source model for the Central and Eastern United States (CEUS), which included the CCNPP site region (EPRI, 1986). The CEUS is a stable continental region characterized by low rates of crustal deformation and no active plate boundary conditions. The EPRI source model included the independent interpretations of six Earth Science Teams and reflected the general state of knowledge of the geoscience community as of 1986. The seismic source models developed by each of the six teams were based on the tectonic setting and the occurrence, rates, and distribution of historical seismicity. The original seismic sources identified by EPRI (1986) are thoroughly described in the EPRI study reports (EPRI, 1986).

In a post-EPRI (1986) review of earthquakes in major and minor stable continental regions worldwide, Johnston et al. (Johnston, 1994) found that the majority of seismic energy release and the largest earthquakes in stable continental regions have occurred in areas of extended (i.e., thinned, or rifted) crust, and particularly within crust rifted during the Mesozoic and/or Cenozoic. Wheeler (Wheeler, 1995; Wheeler, 1996) and Ebel and Tuttle (Ebel, 2002) similarly (and more specifically) argued that many earthquakes in central and eastern North America have been concentrated on late Proterozoic or early Paleozoic normal faults of the extended lapetan passive margin.

In another study, Schulte and Mooney (Schulte, 2005) reassessed the Johnston et al. (Johnston, 1994) findings using a much larger earthquake catalog. This revised catalog consisted of 1,373 earthquakes (excluding 152 non-tectonic events) with moment magnitudes greater than or equal to 4.5, and represented a 58% increase (approximately) in the number of crustal events considered, relative to the catalog used by Johnston et al. (Johnston, 1994). Schulte and Mooney (Schulte, 2005) also concluded that the largest earthquakes ($M \geq 7.0$) have occurred predominantly within rifts (i.e., in extended crust) but noted that extended stable continental regions were characterized by only slightly more moderately sized ($M \geq 4.5$) earthquakes than non-extended stable continental regions.

More recently, seismic sources in the CCNPP site region have been addressed in the Central and Eastern United States Seismic Source Characterization for Nuclear Facilities (CEUS SSC) Project (EPRI/DOE/NRC, 2012). The CEUS SSC integrates data used in the development of the previous EPRI models, new data generated over the last two decades (e.g., Johnston, 1994; Schulte, 2005) and hazard analyses that were developed in conjunction with licensing actions for proposed and existing nuclear power plants. Detailed descriptions of the CEUS SSC Project history and the CEUS SSC earthquake catalog and source model are provided in Sections 2.5.2.1 through 2.5.2.3.

The CCNPP site is located largely within the Extended Continental Crust–Atlantic Margin (ECC-AM) seismotectonic zone of the CEUS SSC. This zone extends from Georgia to Nova Scotia and includes onshore portions of the Piedmont and Coastal Plain physiographic provinces as well as most of the offshore continental shelf region (EPRI/DOE/NRC, 2012). The ECC-AM includes several major faults and shear zones, most of which are related to the accretion of terranes during Paleozoic Appalachian orogenic events. Prominent examples include the Brevard fault zone in Georgia, South Carolina, and North Carolina, and the Central Piedmont

suture of Georgia, the Carolinas, and Virginia. Faults also commonly bound the Mesozoic rift basins throughout the ECC-AM. The location and geometry of these rift basins are interpreted to have been controlled mainly by existing Paleozoic structures. Cretaceous and younger faults within the ECC-AM, in turn, are predominantly oriented north-south to northeast-southwest.

Several fault systems within the ECC-AM source zone provide evidence for Cenozoic activity (EPRI/DOE/NRC, 2012). These include the Stafford fault system in northeastern Virginia (Mixon, 1977) (Newell, 1985), the Brandywine fault system in southwestern Maryland (Jacobeen, 1972), and the Everona-Mountain Run fault zone and Hopewell/Dutch Gap fault in central Virginia (Pavlides, 1983) (Pavlides, 1994) (see Sections 2.5.1.1.4.1.2 and 2.5.1.1.4.4.5). These faults typically strike north to northeast, exhibit steep dips, and displace sedimentary rocks of Late Cretaceous to Miocene age (typically, 100 to 5.3 Ma) (EPRI/DOE/NRC, 2012). Late Cenozoic (i.e., Quaternary) movement along the faults mapped in the ECC-AM is difficult to assess, largely as a result of poor exposure and relatively small displacements. Seismicity within the ECC-AM, like most of the CEUS, is spatially variable, with moderate concentrations of earthquake activity separated by areas of very low seismicity. The most prominent zones of seismicity are located in central Virginia, and the greater New York City and Philadelphia areas. Additional clusters of seismicity occur in the Charleston, South Carolina area, the Piedmont region of South Carolina and Georgia, and New England.

The following sections describe the tectonic setting of the site region (with limited reference to the CEUS SSC) by discussing the: (1) plate tectonic evolution of eastern North America at the latitude of the site, (2) origin and orientation of tectonic stress, (3) gravity and magnetic data and anomalies, (4) and principal tectonic features.

2.5.1.1.4.1 Plate Tectonic Evolution of the Atlantic Margin

The Late Precambrian to Recent plate tectonic evolution of the site region is summarized in Section 2.5.1.1.2 and in Figure 2.5-8. Fundamental understanding about the timing and architecture of major orogenic events was clear by the early 1980's, after a decade or more of widespread application of plate tectonic theory to the evolution of the Appalachian orogenic belt (e.g., (Rodgers, 1970) (Williams, 1983)). Major advances in understanding of the plate tectonic history of the Atlantic continental margin include the organization of lithostratigraphic units and how they relate to the timing and kinematics of Paleozoic events (e.g., (Hatcher, 1989) (Hibbard, 2006) (Hibbard, 2007)) and the refinement of the crustal architecture of the orogen and passive margin (e.g., (Hatcher, 1989) (Glover, 1995b) (Klitgord, 1995)).

The following subsections divide the regional plate tectonic history into: (1) Late Proterozoic and Paleozoic tectonics and assembly of North American continental crust, (2) Mesozoic rifting and passive margin formation, and (3) Cenozoic vertical tectonics associated with exhumation, deposition, and flexure.

2.5.1.1.4.1.1 Late Proterozoic and Paleozoic Plate Tectonic History

Although details about the kinematics, provenance, and histories of lithostratigraphic units within the Appalachian orogenic belt continue to be debated and reclassified (e.g., (Hatcher, 1989) (Horton, 1991) (Glover, 1995b) (Hibbard, 2006)), it is well accepted that plate boundary deformation has occurred repeatedly in the site region since middle Proterozoic time. Two complete Wilson cycles, the paired large-scale events of suturing of continents to form supercontinents and rifting to breakup the supercontinents and form ocean basins, occurred twice during this time period (see Fig. 2.5-8). Numerous studies have been published reviewing in detail the individual tectonic events that comprised these two Wilson cycles (e.g., (Faill,

1997a) (Faill, 1997b) (Faill, 1998) (Hatcher, 2007) (Thomas, 2006) (Whitmeyer, 2007)). The largest-scale events that comprised these Wilson cycles are:

- The Grenville orogeny: The Grenville orogeny marked the beginning of the first Wilson cycle with the suturing of numerous tectonic blocks to Laurentia forming the supercontinent Rodinia. The orogeny occurred over a prolonged period of time extending from approximately 1.3 to 1.0 Ga.

- Rodinia breakup and opening of Iapetus Ocean: This stage of rifting marks the completion of the first Wilson cycle. Extension began as early as approximately 760 to 650 Ma with major rifting occurring around 620 to 550 Ma. The final stages of minor rifting are thought to have been completed by approximately 530 Ma.

- The Appalachian orogeny: The Appalachian orogeny is a broad term used to describe the successive collisional episodes that mark the beginning of the second Wilson cycle and resulted in the formation of Pangea. Three main compressive, orogenic episodes led to the formation of Pangea: Taconic (Ordovician-Silurian), Acadian (Devonian-Mississippian), and Alleghanian (Mississippian-Permian). However, some researchers also explicitly identify the Avalonian (Late Proterozoic-Cambrian), Potomac (pre-Early Ordovician) and Penobscot (Cambrian-Ordovician) orogenies and periods of subduction as key compressional events in the formation of Pangea.

- Pangea breakup and opening of the Atlantic Ocean: The breakup of Pangea during Jurassic time marks the end of the second Wilson cycle.

Evidence for most of these compressive tectonic events are preserved in the geologic record based on foreland strata, deformation structures, and metamorphism (Figure 2.5-8). Synrift basins, normal faults, and postrift strata associated with the opening of the Iapetus and Atlantic Ocean basins record the break-up of the supercontinents. The principal structures that formed during the major events are relevant to the current seismic hazards in that: (1) they penetrate the seismogenic crust, (2) they subdivide different crustal elements that may have contrasting seismogenic potential, and (3) their associated lithostratigraphic units make up the North American continental crust that underlies most of the site region. Many of the principal structures are inherited faults that have been reactivated repeatedly through time. Some are spatially associated with current zones of concentrated seismic activity and historical large earthquakes. For example, the 1811 - 1812 New Madrid earthquake sequence ruptured a failed Late Proterozoic rift that also may have been active in the Mesozoic (Ervin, 1975).

During the interval between opening of the Iapetus Ocean and opening of the Atlantic Ocean, the eastern margin of the ancestral North America continent was alternately (1) an active rift margin accommodating lithospheric extension with crustal rift basins and synrift strata and volcanism; (2) a passive continental margin accumulating terrestrial and shallow marine facies strata; and (3) an active collisional margin with accretion of microcontinents, island arcs, and eventually the African continent. Major Paleozoic mountain building episodes associated with the collision and accretion events included the Taconic, Acadian, and Allegheny Orogenies. More localized collisional events in the site region include the Avalon, Virgilina and Potomac (Penobscot) orogenies (Hatcher, 1987) (Hatcher, 1989) (Glover, 1995b) (Hibbard, 1995) (Drake, 1999) (Figure 2.5-8). The geologic histories of these orogenies are described in Section 2.5.1.1.2.

Tectonic structures developed during the interval between the Late Proterozoic and Triassic Periods are variable in sense of slip and geometry. Late Proterozoic and early Cambrian rifting associated with the breakup of Rodinia and development of the Iapetus Ocean formed east-dipping normal faults through Laurentian (proto-North American) crust (Figure 2.5-16 and

Figure 2.5-17). Late Proterozoic extended crust of the Iapetan margin probably underlies the Appalachian fold belt southeastward to beneath much of the Piedmont Province (Wheeler, 1996). Paleozoic compressional events associated with the Taconic, Acadian, and Allegheny orogenies formed predominantly west-vergent structures that include (1) Valley and Ridge Province shallow folding and thrusting within predominantly passive margin strata, (2) Blue Ridge Province nappes of Laurentian crust overlain by Iapetan continental margin deposits, (3) Piedmont Province thrust-bounded exotic and suspect terranes including island arc and accretionary complexes interpreted to originate in the Iapetan Ocean, and (4) Piedmont Province and sub-Coastal Plain Province east-dipping thrust, oblique, and reverse fault zones that collectively are interpreted to penetrate much of the crust and represent major sutures that juxtapose crustal elements (Hatcher, 1987) (Horton, 1991) (Glover, 1995b) (Hibbard, 2006) (Figure 2.5-16 and Figure 2.5-17). Many investigators recognize significant transpressional components to major faults bounding lithostratigraphic units (Hatcher, 1987) (Glover, 1995b) (Hibbard, 2006) (Figure 2.5-8 and Figure 2.5-16).

2.5.1.1.4.1.2 Mesozoic and Cenozoic Passive Margin Evolution

The current Atlantic passive continental margin has evolved since rifting initiated in the Early Triassic. The progression from active continental rifting to sea-floor spreading and a passive continental margin included: (1) initial rifting and hot-spot plume development, (2) thinning of warm, buoyant crust with northwest-southeast extension, normal faulting and deposition of synrift sedimentary and volcanic rocks, and (3) cooling and subsidence of thinned crust and deposition of postrift sediments on the coastal plain and continental shelf, slope, and rise (Klitgord, 1988) (Klitgord, 1995). The transition between the second (rifting) and third (drifting) phases during the Late Triassic and Early Jurassic marked the initiation of a passive margin setting in the site region, in which active spreading migrated east away from the margin (Withjack, 1998) (Withjack 2005). As the thinned crust of the continental margin cooled and migrated away from the warm, buoyant crust at the mid-Atlantic spreading center, horizontal northwest-southeast tension changed to horizontal compression as gravitational potential energy from the spreading ridge exerted a lateral "ridge push" force on the oceanic crust. Northwest-southeast-directed postrift shortening, manifested in Mesozoic basin inversion structures, provides the clearest indication of this change in stress regime (Withjack, 1998) (Schlische, 2003a) (Schlische, 2003b). The present-day direction of maximum horizontal compression (east-northeast to west-southwest) is rotated from this hypothesized initial postrift direction.

The crustal structure of the passive continental margin includes areas of continental crust, (Iapetan-extended crust (Wheeler, 1996)), rifted continental crust, rift-stage (transitional) crust, marginal oceanic crust, and oceanic crust (Klitgord, 1995) (Figure 2.5-18 and Figure 2.5-19). Rifted continental crust is crust that has been extended, faulted, and thinned slightly. In the site region, rifted-continental crust extends from the western border faults of the exposed synrift Danville, Scottsville, Culpeper, Gettysburg, and Newark basins to the basement hinge zone, approximately coincident with the seaward edge of the continental shelf (Klitgord, 1995) (Figure 2.5-12 and Figure 2.5-19). Rifted crust also includes exposed and buried Upper Triassic to Lower Jurassic basins within the eastern Piedmont and Coastal Plain Provinces, including the Richmond, Taylorsville, and Norfolk basins (LeTourneau, 2003) (Schlische, 2003a) (Schlische, 2003b) (Figure 2.5-10). Several additional basins with poorly defined extent also underlie the Coastal Plain and Continental Shelf and are shown directly east and northeast of the site (Figure 2.5-10). Buried synrift basins are delineated based on sparse drillhole data, magnetic and gravity anomalies, and seismic reflection data (e.g., (Benson, 1992)). Figure 2.5-19 shows east-dipping basin-bounding faults that penetrate the seismogenic crust and have listric geometries at depth. Many of the synrift normal faults within the site region are interpreted as Paleozoic thrust faults reactivated during Mesozoic rifting. The Mesozoic basins are discussed

further in Section 2.5.1.1.4.4.3 as well as the hypothesized Queen Anne basin shown as lying beneath the site (Figure 2.5-10) as one alternate interpretation of basement lithology.

Rift-stage (transitional) crust is extended continental crust intruded by mafic magmatic material during rifting. In the site region, this crustal type coincides with the basement hinge zone and postrift Baltimore Canyon Trough (Klitgord, 1995) (Figure 2.5-12). The basement hinge zone is defined where pre-Late Jurassic basement abruptly deepens seaward from about 1 to 2.5 mi (1.6 to 4 km) to more than 5 mi (8 km). Overlying this lower crustal unit seaward of the basement hinge zone is the Jurassic volcanic wedge, representing a period of excess volcanism and is greater than 65 mi (105 km) wide and 1 to 5 mi (1.5 to 8 km) thick. The wedge is identified on seismic reflection lines as a prominent sequence of seaward-dipping reflectors. The East Coast magnetic anomaly (ECMA) coincides with the seaward edge of the wedge (Figure 2.5-18) (Section 2.5.1.1.4.3.2).

The last transitional crustal unit between continental and oceanic crust is marginal oceanic crust (Klitgord, 1995) (Figure 2.5-18). Marginal oceanic crust is located east of the ECMA where the Jurassic volcanic wedge merges with the landward edge of oceanic crust. Here, the transition from rifting to sea-floor spreading created a thicker than normal oceanic crust with possible magmatic underplating.

A postrift unconformity separates synrift from postrift deposits and represents the change in tectonic regime in the Middle Jurassic from continental rifting to the establishment of the passive margin ("drifting"). Sedimentary rocks below the unconformity are cut by numerous faults. In contrast, the rocks and strata above the unconformity accumulated within the environment of a broadly subsiding passive margin and are sparsely faulted. Sediments shed from the faulted blocks of the rifting phase and from the core of the Allegheny orogen accumulated on the coastal plain, continental shelf, slope, and rise above the postrift unconformity and contributed to subsidence of the cooling postrift crust by tectonic loading.

Postrift deformation is recorded in synrift basins and within postrift strata as normal faults seaward of the basement hinge zone and as contractional features landward of the basement hinge zone. Extensive normal faulting penetrates the postrift strata (and upper strata of the volcanic wedge) of the marginal basin overlying the volcanic wedge (Figure 2.5-18 and Figure 2.5-19). This set of faults is thought to have been caused by sediment loading on the outer edge of the margin due to differential compaction of the slope-rise deposits relative to adjacent carbonate platform deposits (Poag, 1991) (Klitgord, 1995). These faults are interpreted as margin-parallel structures that bound large mega-slump blocks and are not considered active tectonic features (Poag, 1991).

The evidence for postrift shortening and positive basin inversion (defined as extension within basins followed by contraction) is well documented in several Atlantic margin basins, including the Newark, Taylorsville, and Richmond basins in the site region (LeTourneau, 2003) (Schlische, 2003a) (Schlische, 2003b) (Withjack, 2005) (Figure 2.5-10). Contractional postrift deformation is interpreted to record the change in stress regime from horizontal maximum extension during rifting to horizontal maximum compression during passive margin drifting. Much of the site region was under a state of northwest-southeast maximum compression by Late Triassic and Early Jurassic time (Withjack, 1998) (Schlische, 2003a) (Withjack, 2005). This deformation regime may have persisted locally into the Cenozoic based on the recognized early Cenozoic contractional growth faulting associated with the northeast-striking Brandywine fault system (Jacobeen, 1972) (Wilson, 1990), Port Royal fault zone (Mixon, 1984) (Mixon, 2000) and Skinkers Neck anticline (Mixon, 1984) (Mixon, 2000) (Section 2.5.1.1.4.4.4). The present-day stress field of east-northeast to west-southwest maximum horizontal compression (Zoback, 1989a) is rotated from the hypothesized Jurassic and Cretaceous northwest-southeast orientation. The

east-northeast to west-southwest maximum horizontal stress direction is consistent with resolved dextral transpressive slip locally documented on the northeast-striking Stafford fault system (Mixon, 2000), a recognized Tertiary tectonic feature (Section 2.5.1.1.4.4.4.1).

2.5.1.1.4.1.3 Cenozoic Passive Margin Flexural Tectonics

Tectonic processes along the Atlantic passive continental margin in the Cenozoic Era include vertical tectonics associated with lithospheric flexure. Vertical tectonics are dominated by: (1) cooling of the extended continental, transitional, and oceanic crust as the spreading center migrates eastward, and (2) the transfer of mass from the Appalachian core to the Coastal Plain and Continental Shelf, Slope, and Rise via erosion. Erosion and exhumation of the Allegheny crustal root of the Piedmont, Blue Ridge, Valley and Ridge, and Appalachian Plateau Provinces has been balanced by deposition on and loading of the Coastal Plain and offshore provinces by fluvial, fluvial-deltaic, and marine sediment transport. Margin-parallel variations in the amount of uplift and subsidence have created arches (e.g. South New Jersey and Norfolk Arches) and basins or embayments (e.g. Salisbury Embayment) along the Coastal Plain and Continental Shelf (Figure 2.5-12).

Flexural zones show both passive-margin-normal and passive-margin-parallel trends. Flexure normal to the passive margin is clearly recorded in the basement hinge zone (Figure 2.5-19). The vertical relief across the offshore basement hinge zone accounts for a change in postrift sediment thickness from 1 to 2.5 mi (1.6 to 4 km) to over 5 mi (8 km) and indicates lateral changes in tectonic loading (Klitgord, 1995). It has been proposed that the downwarping of the margin in the vicinity of the main depocenter of the Baltimore Canyon Trough led to the flexural uplift of the Coastal Plain units to the west (Watts, 1982). However, more recent studies show that sea-level variations since the Cretaceous are compatible with the present elevations of exposed Coastal Plain strata and thus do not support flexural uplift of the Coastal Plain (e.g., (Pazzaglia, 1993a) (Pazzaglia, 1993b) (Pazzaglia, 1994)).

A simple elastic model of Cenozoic flexural deformation across the Atlantic passive margin has been used to approximate the response of rifted continental crust to surface erosion of the Piedmont and deposition on the Coastal Plain and Continental Shelf (Pazzaglia, 1994) (Figure 2.5-12 and Figure 2.5-19). The boundary between areas of net Cenozoic erosion and deposition, the Fall Line, marks the flexural hinge between uplift and downwarping. Geologic correlation and longitudinal profiles of Miocene to Quaternary river terraces on the Piedmont with deltaic and marine equivalent strata on the Coastal Plain provide data for model validation (Pazzaglia, 1993a) (Pazzaglia, 1993b). A one-dimensional elastic plate model replicates the form of the profiles and maintenance of the Fall Line with flexure driven by exhumation of the Piedmont and adjacent Appalachian provinces coupled with sediment loading in the Salisbury Embayment and Baltimore Canyon Trough (Pazzaglia, 1994). Model results suggest a long-term denudation rate of approximately 33 ft (10 m) per million years and about 115 to 426 ft (35 to 130 m) of upwarping of the Piedmont in the last 15 million years.

The flexural hinge zones (Fall Line and basement hinge zone) do not appear to be seismogenic. The spatial association between the Fall Line and observed Cenozoic faults such as the Stafford and Brandywine fault systems is commonly attributed to the fact that those faults are recognizable where Cenozoic cover is thin and there is greater exposure of bedrock compared to areas farther east toward the coast (e.g., (Wentworth, 1983)). It is suggested (Pazzaglia, 1994) that low rates of contractional deformation on or near the hinge zone documented on Cenozoic faults may be a second-order response to vertical flexure and horizontal compressive stresses.

Along-strike variations in the amount of epeirogenic movement along the Atlantic continental margin has resulted in a series of arches and embayments identified based on variations in thickness of Coastal Plain strata from Late Cretaceous through Pleistocene time. The Salisbury Embayment is a prominent, broad depocenter in the site region, and coincides with Chesapeake Bay and Delaware Bay (Figure 2.5-12). In general, it appears that downwarping associated with the Salisbury Embayment (Figure 2.5-12) began early in the Cretaceous and continued intermittently throughout the Cretaceous and Tertiary periods. Deposition apparently kept pace, resulting in a fluvial-deltaic environment. Biostratigraphic data from test wells on the west side of Chesapeake Bay indicate that Upper Cretaceous sediments reach maximum thickness in Anne Arundel County and show progressive thinning to the south. This appears to reflect deposition within the downwarping, northwest-trending Salisbury Embayment during the Cretaceous (Hansen, 1978). At the margins of the Salisbury Embayment are the South New Jersey Arch to the northeast and the Norfolk Arch to the south. Both arches are broad anticlinal warps reflected in the top of basement and overlying sediments. Thinning and overlapping within the Upper Cretaceous interval suggests that the northern flank of the Norfolk Arch was tectonically active during late Cretaceous time (Hansen, 1978) (Figure 2.5-12). The processes that form and maintain the arches and embayments are poorly understood. Poag (2004), however, uses new basement data obtained from seismic reflection profiles and exploratory boreholes in the region of the main Chesapeake Bay impact crater to show that the Norfolk Arch is not as well expressed as originally interpreted by earlier authors (Brown, 1972) using limited data. Previous elevation differences cited as evidence for the basement arch appear to be due to a subsidence differential between the impact crater and the adjacent deposits (Poag, 2004) (Section 2.5.1.1.4.4.4). Regardless, no published hypothesis was found suggesting causality between epeirogenic processes maintaining these specific arches and the embayment and potentially seismogenic structures, and there is no spatial association of seismicity with the basement arches. Thus, it is concluded that these features are not capable tectonic sources.

2.5.1.1.4.2 Tectonic Stress in the Mid-Continent Region

Ambient tectonic stress in the CEUS region is generally characterized by northeast-southwest directed horizontal compression. This stress orientation is consistent with buoyancy driven ridge-push forces resulting from continuous seafloor spreading in the mid-Atlantic (Zoback, 1980) (Zoback, 1989a) (Zoback, 1989b). Richardson and Reding (Richardson, 1991) performed numerical modeling of stress in the continental U.S. interior, and considered the contribution to total tectonic stress to be from three classes of forces:

- Horizontal stresses that arise from gravitational body forces acting on lateral variations in lithospheric density. These forces commonly are called buoyancy forces. Richardson and Reding emphasize that what is commonly called ridge-push force is an example of this class of force. Rather than a line-force that acts outwardly from the axis of a spreading ridge, ridge-push arises from the pressure exerted by positively buoyant, young oceanic lithosphere near the ridge against older, cooler, denser, less buoyant lithosphere in the deeper ocean basins (Turcotte, 2002). The force is an integrated effect over oceanic lithosphere ranging in age from about 0 to 100 million years (Dahlen, 1981). The ridge-push force is transmitted as stress to the interior of continents by the elastic strength of the lithosphere.

- Shear and compressive stresses transmitted across major plate boundaries (strike-slip faults and subduction zones).

- Shear tractions acting on the base of the lithosphere from relative flow of the underlying asthenospheric mantle.

Richardson and Reding (Richardson, 1991) concluded that the observed northeast-southwest trend of principal stress in the CEUS dominantly reflects ridge-push body forces. They estimated the magnitude of these forces to be about 2 to 3 X 10^{12} N/m (i.e., the total vertically integrated force acting on a column of lithosphere 1 m wide), which corresponds to average equivalent stresses of about 40 to 60 MPa distributed across a 30 mi (50 km) thick elastic plate. The fit of the model stress trajectories to data was improved by the addition of compressive stress (about 5 to 10 MPa) acting on the San Andreas Fault and Caribbean plate boundary structures. The fit of the modeled stresses to the data further suggested that shear stresses acting on these plate boundary structures is in the range of 5 to 10 MPa.

Richardson and Reding (Richardson, 1991) noted that the general northeast-southwest orientation of principal stress in the CEUS also could be reproduced in numerical models that assume a shear stress, or traction, acting on the base of the North American plate. Richardson and Reding (Richardson, 1991) and Zoback and Zoback (Zoback, 1989) do not favor this as a significant contributor to total stress in the mid-continent region. A basal traction predicts or requires that the horizontal compressive stress in the lithosphere increases by an order of magnitude moving east to west, from the eastern seaboard to the Great Plains. Zoback and Zoback (Zoback, 1989) noted that the state of stress in the southern Great Plains is characterized by north-northeast to south-southwest extension, which is contrary to this prediction. They further observed that the level of background seismic activity is generally higher in the eastern United States than in the Great Plains, which is not consistent with the prediction of the basal traction model that compressive stresses (and presumably rates of seismic activity) should be higher in the middle parts of the continent than along the eastern margin.

Subsequent statistical analyses of stress indicators confirmed that the trajectory of the maximum compressive principal stress is uniform across broad continental regions at a high level of statistical confidence. In particular, the northeast-southwest orientation of principal stress in the CEUS is statistically robust, and is consistent with the theoretical trend of compressive forces acting on the North American plate from the mid-Atlantic ridge (Zoback, 1992) (Coblentz, 1995) (Hurd, 2012) as well as mantle flow beneath the continent (Ghosh, 2012). However, localized variations in the regional stress field are also observed across the CEUS (e.g., Kim, 2005). These variations generally result from geoid perturbations related to sediment loading and/or de-glaciation, or from lateral lithospheric heterogeneities (Hurd, 2012). For example, Mazzotti and Townend (Mazzotti, 2010) provided an analysis of the state of stress in ten CEUS seismic zones, and reported a systematic 30 to 50 degrees clockwise rotation of the earthquake-generating stress relative to the regional stress in six of the zones (including central Virginia). On the basis of stress magnitude measurements and calculations, Mazzotti and Townend (Mazzotti, 2010) suggested that this pattern may be due to the interaction of stresses generated by post-glacial rebound with local stress concentrators, such as weak faults (notably, again, in central Virginia).

2.5.1.1.4.3 Gravity and Magnetic Data and Features of the Site Region and Site Vicinity

Maps of the gravity and magnetic fields in North America by the Geological Society of America (GSA), as part of the Society's DNAG project (Tanner, 1987) (Hinze, 1987) are widely available in digital form via the internet (Hittelman, 1994). A magnetic anomaly map of North America was published in 2002 that featured improved reprocessing of existing data and compilation of a new and more complete database (Bankey, 2002) (Figure 2.5-20).

These maps present the potential field data at 1:5,000,000-scale, and thus are useful for identifying and assessing gravity and magnetic anomalies with wavelengths on the order of

tens of kilometers or greater (Bankey, 2000) (Hittelman, 1994). Regional gravity anomaly maps are based on Bouguer gravity anomalies onshore and free-air gravity anomalies offshore. The primary sources of magnetic data reviewed for this CCNPP Unit 3 study are from aeromagnetic surveys onshore and offshore (Bankey, 2002), and the DNAG datasets available digitally from the internet (Hittelman, 1994).

Large-scale compilations (1:2,500,000-scale) of the free-air anomalies offshore and Bouguer anomalies onshore were published in 1982 by the Society of Exploration Geophysicists (Lyons, 1982). The DNAG magnetic anomaly maps were based on a prior analog map of magnetic anomalies of the U.S. published in the early 1980's (Zietz, 1982) (Behrendt, 1983) (Sheridan, 1988a) (Sheridan, 1988b).

In addition, the DNAG Continent-Ocean transect program published a synthesis of gravity and magnetic data with seismic and geologic data (Klitgord, 1995). Transect E-3, which crosses the site region, is presented in Figure 2.5-16 and Figure 2.5-17. Much of the seismic and geophysical data through the Piedmont region was reanalyzed from a geophysical survey conducted along Interstate I-64 in Virginia (Harris, 1982).

Discussion of the gravity and magnetic anomalies is presented in the following sections.

2.5.1.1.4.3.1 Gravity Data and Features

Gravity data compiled at 1:5,000,000-scale for the DNAG project provide documentation of previous observations that the gravity field in the site region is characterized by a long-wavelength, east-to-west gradient in the Bouguer gravity anomaly over the continental margin (Harris, 1982) (Hittelman, 1994) (Figure 2.5-21). The free-air gravity anomaly shows broad gravity lows over offshore oceanic crust near the continental margin and over the broad marginal embayments. Offshore marginal platforms are marked by shorter-wavelength, higher-amplitude gravity highs and lows. The present shelf edge is marked by a prominent free-air gravity anomaly that also corresponds to the continent-ocean boundary (Sheridan, 1988a) (Sheridan, 1988b) (Klitgord, 1995).

Bouguer gravity values increase eastward from about -80 milligals (mgal) in the Valley and Ridge Province of western Virginia to about +10 mgal in the Coastal Plain Province, corresponding to an approximately 90 mgal regional anomaly across the Appalachian Orogen (Figure 2.5-17 and Figure 2.5-21). This regional gradient is called the "Piedmont gravity gradient" (Harris, 1982), and is interpreted to reflect the eastward thinning of the North American continental crust and the associated positive relief on the Moho discontinuity with proximity to the Atlantic margin.

The Piedmont gravity gradient is punctuated by several smaller positive anomalies with wavelengths ranging from about 15 to 50 mi (25 to 80 km), and amplitudes of about 10 to 20 mgal. Most of these anomalies are associated with accreted Taconic terranes such as the Carolina/Chopawamsic terrane (Figure 2.5-17). Collectively, they form a gravity high superimposed on the regional Piedmont gradient that can be traced northeast-southwest on the 1:5,000,000-scale DNAG map relatively continuously along the trend of the Appalachian orogenic belt through North Carolina, Virginia, and Maryland (Figure 2.5-21). The continuity of this positive anomaly diminishes to the southwest in South Carolina, and the trend of the anomaly is deflected eastward in Maryland, Pennsylvania, and Delaware.

The short-wavelength anomalies and possible associations with upper crustal structure are illustrated by combining gravity profiles with seismic reflection data and geologic data (Harris, 1982) (Glover, 1995b). In some cases, short-wavelength positive anomalies are associated with

antiformal culminations in Appalachian thrust sheets. For example, there is a positive anomaly associated with an anticline at the western edge of the Blue Ridge nappe along the Interstate I-64 transect (Harris, 1982) (Figure 2.5-17). The anomaly is presumably due to the presence of denser rocks transported from depth and thickened by antiformal folding in the hanging wall of the thrust.

The Salisbury geophysical anomaly (SGA) is a paired Bouguer gravity anomaly and magnetic high that is located along the west side of the Salisbury Embayment (Klitgord, 1995) (Figure 2.5-17, Figure 2.5-18, Figure 2.5-20, and Figure 2.5-21). The SGA is located about 10 mi (16 km) west of the CCNPP site (Figure 2.5-22). The anomaly is expressed most clearly as a magnetic lineation that separates a zone of short-wavelength, high-amplitude magnetic lineations to the west from a zone of low-amplitude, long-wavelength anomalies to the east. The gravity data show the SGA to form the western margin of a broad gravity low that extends seaward to the basement hinge zone. The anomaly takes the form of a north-northeast-trending gravity high having about 30 mgal relief (Johnson, 1973). The anomaly has also been named the Sussex-Curioman Bay trend (Levan, 1963) or the Sussex-Leonardtown anomaly (Daniels, 1985), and is believed to reflect an east-dipping mafic rock body associated with a suture zone buried beneath coastal plain sediments (Figure 2.5-17). The SGA is interpreted (Klitgord, 1995) to mark the likely location of the Taconic suture that separates the Goochland terrane on the west from a zone of island arc and oceanic metavolcanics formed in the Iapetus Ocean on the east. The SGA is shown (Horton, 1991) to be associated with the buried Sussex terrane is a probable mafic mélange that was interpreted by Lefort and Max (Lefort, 1989) to mark the Alleghenian "Chesapeake Bay suture" (Figure 2.5-16).

The offshore portions of the site region contain a prominent, long-wavelength free-air gravity anomaly associated with the transition from continental to oceanic crust (Sheridan, 1988a) (Sheridan, 1988b) (Klitgord, 1995) (Figure 2.5-19). This anomaly is large (75 to 150 mgal peak to trough) and is 45 to 80 mi (72 to 129 km) wide. Variations in the amplitude and shape of the anomaly along the Atlantic margin are due to seafloor relief, horizontal density variations in the crust, and relief on the crust-mantle boundary (Sheridan, 1988a) (Sheridan, 1988b) (Klitgord, 1995).

In summary, gravity data confirm and provide additional documentation of previous observations of a gradual "piedmont gravity gradient" across the Blue Ridge and Piedmont Provinces of Virginia and a prominent gravity anomaly at the seaward margin of the continental shelf. Shorter-wavelength anomalies such as the SGA also are recognized in the data. The "piedmont gravity gradient" is interpreted to reflect eastward thinning of the North American crust and lithosphere. The free-air anomaly at the outer shelf edge is interpreted as reflecting the transition between continental and oceanic crust. Second-order features in the regional field, such as the Salisbury geophysical anomaly and the short discontinuous northeast-trending anomaly east of the site, primarily reflect density variations in the upper crust associated with the boundaries and geometries of Appalachian thrust sheets and accreted terranes.

2.5.1.1.4.3.2 Magnetic Data and Features

Magnetic data compiled for the 2002 Magnetic Anomaly Map of North America reveal numerous northeast-southwest-trending magnetic anomalies, generally parallel to the structural features of the Appalachian orogenic belt (Bankey, 2002) (Figure 2.5-20). Unlike the gravity field, the magnetic field is not characterized by a regional, long-wavelength gradient that spans the east-west extent of the site region. A magnetic profile along Interstate-64 published to accompany a seismic reflection profile (Harris, 1982) shows anomalies with wavelengths of about 6 to 30 mi (10 to 48 km). It has been concluded (Harris, 1982) that

anomalies in the magnetic field primarily are associated with upper-crustal variations in magnetic susceptibility and, unlike the gravity data, do not provide information on crustal-scale features in the lithosphere.

Prominent north- to northeast-trending magnetic anomalies in the CCNPP site region include the interior New York-Alabama, Ocoee, and Clingman lineaments, the Coastal Plain Salisbury geophysical anomaly and nearshore Brunswick magnetic anomaly, and the offshore East Coast magnetic anomaly (King, 1978) (Klitgord, 1988) (Klitgord, 1995) (Bankey, 2002) (Figure 2.5-20). The offshore Blake Spur magnetic anomaly is outside the site region.

King and Zietz (1978) identified a 1,000 mi (1,600 km) long lineament in aeromagnetic maps of the eastern U.S. that they referred to as the "New York-Alabama lineament" (NYAL) (Figure 2.5-20). The NYAL primarily is defined by a series of northeast-southwest-trending linear magnetic anomalies in the Valley and Ridge province of the Appalachian fold belt that systematically intersect and truncate other magnetic anomalies. The NYAL is located about 160 mi (257 km) northwest of the CCNPP site.

The Clingman lineament is an approximately 750 mi (1,200 km) long, northeast-trending aeromagnetic lineament that passes through parts of the Blue Ridge and eastern Valley and Ridge provinces from Alabama to Pennsylvania (Nelson, 1981). The Ocoee lineament splays southwest from the Clingman lineament at about latitude 36°N (Johnston, 1985a). The Clingman-Ocoee lineaments are sub-parallel to and located about 30 to 60 mi (48 to 97 km) east of the NYAL. These lineaments are located about 60 mi northwest of the CCNPP site.

King and Zietz (King, 1978) interpreted the NYAL to be a major strike-slip fault in the Precambrian basement beneath the thin-skinned fold-and-thrust structures of the Valley and Ridge province, and suggested that it may separate rocks on the northwest that acted as a mechanical buttress from the intensely deformed Appalachian fold belt to the southeast. Shumaker (Shumaker, 2000) interpreted the NYAL to be a right-lateral strike-slip fault that formed during an initial phase of Late Proterozoic continental rifting that eventually led to the opening of the Iapetus Ocean.

More recent work by Steltenpohl (Steltenpohl, 2010) indicates that the right-lateral strike-slip motion along the NYAL has displaced anomalies attributed to Grenville orogenesis by approximately 130 mi (220 km). Precise timing of the movement was not provided, but it was suggested to have occurred during either a relatively late, post-contractional stage of the Grenville orogeny, during the late Neoproterozoic to Cambrian rifting of Laurentia, or during Appalachian movements.

The Clingman lineament also is interpreted to arise from a source or sources in the Precambrian basement beneath the accreted and transported Appalachian terranes (Nelson, 1981). Johnston (Johnston, 1985a) observed that the "preponderance of southern Appalachian seismicity" occurs within the "Ocoee block", a Precambrian basement block bounded by the NYAL and Clingman-Ocoee lineaments (the Ocoee block was previously defined by (Johnston, 1985b)). Based on the orientations of nodal planes from focal mechanisms of small earthquakes, it was noted (Johnston, 1985) that most events within the Ocoee block occurred by strike-slip displacement on north-south and east-west striking faults, Johnston (Johnston, 1985a) did not favor the interpretation of seismicity occurring on a single, through-going northeast-southwest-trending structure parallel to the Ocoee block boundaries.

The Ocoee block lies within a zone defined by Wheeler (Wheeler, 1995) (Wheeler, 1996) as extended continental crust of the Late Proterozoic to Cambrian Iapetan terrane. Synthesizing geologic and geophysical data, Wheeler (Wheeler, 1995) mapped the northwest extent of the

Iapetan normal faults in the subsurface below the Appalachian detachment, and proposed that earthquakes within the region defined by Johnston and Reinbold (Johnston, 1985b) as the Ocoee block may be the result of reactivation of Iapetan normal faults as reverse or strike-slip faults in the modern tectonic setting.

The East Coast magnetic anomaly (ECMA) is a prominent, linear, segmented magnetic high that extends the length of the Atlantic continental margin from the Carolinas to New England (Figure 2.5-20). The anomaly is about 65 mi (105 mi) wide and has an amplitude of about 500 nT. This anomaly approximately coincides with the seaward edge of the continental shelf, and has been considered to mark the transition from continental to oceanic crust. Klitgord et al. (Klitgord, 1995) note that the anomaly is situated above the seaward edge of the thick Jurassic volcanic wedge and lower crustal zone of magmatic under plating along the boundary between rift-stage and marginal oceanic crust (Figure 2.5-18 and Figure 2.5-19). The ECMA is not directly associated with a capable tectonic feature, and thus is not considered as a seismic source.

The Brunswick magnetic anomaly (BMA) is located along the basement hinge zone offshore of the Carolinas, at the southern portion of the site region about 200 mi (322 km) from the CCNPP site (Figure 2.5-20). The lineament is narrower and has less amplitude than the ECMA (Klitgord, 1995). The BMA may continue northward along the hinge zone of the Baltimore Canyon Trough, but the magnetic field there is much lower in amplitude and the lineament is diffuse. The BMA is not directly related to a fault or other tectonic structure, and thus is not a potential seismic source.

The Blake Spur magnetic anomaly (BSMA) is located east of the site region above oceanic crust, about 290 mi (465 km) from the CCNPP site (Figure 2.5-20). The BSMA is a low-amplitude magnetic anomaly that lies subparallel to the East Coast magnetic anomaly (Klitgord, 1995). The BSMA probably formed during the Middle Jurassic as the midocean ridge spreading center shifted to the east. The BSMA coincides with a fault-bounded, west-side-down scarp in oceanic basement. Since its formation, the BSMA has been a passive feature in the Atlantic crust, and thus is not a potential seismic source.

The Salisbury geophysical anomaly (SGA), as mentioned above, is a paired Bouguer gravity and magnetic anomaly along the west side of the Salisbury embayment that is located about 10 mi (16 km) of the CCNPP site (Figure 2.5-22). The anomaly is expressed in the magnetic data as a lineament separating short-wavelength, high-amplitude magnetic lineations to the west from a zone of low-amplitude, long-wavelength anomalies to the east. The contrast in magnetic signature is related to the juxtaposition of terranes of contrasting affinity beneath coastal plain sediments, and in particular the mafic to ultramafic rocks and mélange termed the Sussex terrane by Horton et al. (Horton, 1991) and believed to represent alternatively a Taconic (Glover, 1995b) or Alleghenian (Lefort, 1989) suture (Figure 2.5-16). Lower intensities to the west are associated with the Goochland terrane, which represents continental basement (Figure 2.5-17).

Discrete magnetic lows associated with the Richmond and Culpeper basins are discernible on the 2002 North America magnetic anomaly map (Bankey, 2002) (Figure 2.5-22). Basaltic and diabase dikes and sills are a component of the synrift fill of the exposed basins in the Piedmont and of the Taylorsville basin (Schlische, 2003a) (Schlische, 2003b) (Klitgord, 1995). The distinctive, elongate magnetic anomalies associated with these igneous bodies within the synrift basins of the Piedmont are also used beneath the Coastal Plain to delineate the Taylorsville, Queen Anne, and other synrift basins (e.g., (Benson, 1992)). The elongate magnetic anomalies are less prevalent in the magnetic field east of the Salisbury geophysical anomaly. Either the eastern rift basins do not contain as much volcanic material as the western set of rift basins or the depth to this volcanic material is considerably greater (Klitgord, 1995). Small,

circular magnetic highs across the coastal plain have been interpreted as intrusive bodies (Horton, 1991) (Klitgord, 1995).

Approximately 5 to 7 mi (8 to 11 km) east of the CCNPP site is an unnamed short, discontinuous weak to moderate northeast-trending magnetic anomaly that aligns subparallel to the SGA (Figure 2.5-22). Similar features to the south have been interpreted as granitic intrusive anomalies, whereas Benson (1992) interprets the feature as being bound by a Mesozoic basin (Figure 2.5-10). A deep borehole (SM-DF-84, Figure 2.5-11) drilled near the southern margin of this feature encountered Jurassic (?) volcanic rocks (dated at 169 ± 8 million years old) related to Mesozoic rifting, or perhaps basic metavolcanic rocks accreted to North America as part of the Brunswick Terrane (Hansen, 1986).

A magnetic profile along an approximately west-northwest to east-southeast transect through central Pennsylvania (Glover, 1995b) (Figure 2.5-17) indicates that paired high and low magnetic anomalies are associated with the margins of crustal units. Many of these anomalies have very high amplitudes and short wavelengths. For example, there is a 400-600 nT anomaly associated with the western margin of the Blue Ridge thrust nappe. Similarly, along a continuing transect line through Virginia, Glover and Klitgord (Glover, 1995a) show a 1500-2000 nT anomaly associated with the western edge of the Potomac mélange. This transect crosses the Salisbury geophysical anomaly where it is expressed as an 600 nT anomaly (Figure 2.5-17).

2.5.1.1.4.4 Principal Tectonic Structures

In the sections below, specific tectonic features in the site region and their evidence of Cenozoic activity are discussed. This discussion is based largely on a review of existing published literature by Crone and Wheeler (Crone, 2000) and Wheeler (Wheeler, 2005) (Wheeler, 2006), and field studies performed for this COL. Specifically, this investigation included the following steps:

1. The references of Crone and Wheeler (Crone, 2000) (Wheeler, 2005) (Wheeler, 2006), were used as screening tools to initially characterize and identify possible late Cenozoic structures within a 200-mile-radius of the site. The references were obtained and reviewed for structures located within a 200-mile-radius, as well as a few located directly outside of the 200-mile-radius. An internal internet- and library-based reference search for authors and topics related to potential Cenozoic seismogenic structures along the East Coast of the United States was performed to capture studies that post-date this work, as well as references the authors missed during their own compilation (e.g., (Hansen, 1986) (Kidwell, 1997) (McCartan, 1995) (Pazzagllia, 1993a)).

2. To complement the comprehensive literature search, UniStar geologists contacted regional and local experts with field experience in Virginia, Maryland, Pennsylvania, Washington, D.C. and Calvert County, Maryland. At the U.S. Geological Survey in Reston, Virginia, both in-person and over-the-phone interviews were performed with experts regarding previously known and unknown potential seismic sources in the region. Experts contacted to discuss their knowledge on the structural and geologic setting of Chesapeake Bay and the eastern seaboard of the United States included Richard Harrison, David Russ, David Powars, Wayne Newell, Lucy McCartan, Wylie Poag, Milan Pavich, and Steve Schindler of the U.S. Geological Survey. In addition, UniStar geologists visited the Maryland Geological Survey (MGS) and discussed similar topics with John Wilson who provided references related to studies performed by former MGS geologist Harry Hansen. In-house experts Scott Lindvall and Ross Hartleb, who worked on numerous similar nuclear-related sites in the southeast, were contacted to provide a

summary of potential regional seismic sources (i.e., Charleston, etc.). In addition, UniStar geologists contacted Dr. Susan Kidwell to discuss a detailed biostratigraphy and basin analysis of the Miocene Coastal Plain section exposed along Calvert Cliffs, and her basis for inferring a hypothetical fault at Moran Landing. Dr. Steve Obermier (retired from the U.S. Geological Survey) and Dr. Martitia Tuttle (an expert in paleoliquefaction investigations in the Central-Eastern United States) were contacted to discuss their knowledge of liquefaction-related features, if any, along the East Coast near the CCNPP site. UniStar also spoke with Martin Chapman of Virginia Tech, and Duane Braun of Bloomsberg University, Pennsylvania.

3. To independently evaluate the information collected through the literature searches and interviews, UniStar conducted field reconnaissance of: (a) previously mapped geologic features and potential seismic sources within a 200-mi-radius of the site, (b) site vicinity geomorphology and Quaternary geology with respect to neotectonic deformation, and (c) local cliff exposures for evidence of faulting and/or folding. Reconnaissance of key potential structures was conducted during and after consultation with local experts and literature review. Field reconnaissance was performed on the Stafford, Brandywine, Port Royal, Skinkers Neck, Mountain Run, Hazel Run, Fall Hill, Dumfries, Fall Line, Upper Marlboro, and Hillville fault zones. Field reviews of faults were followed by aerial reconnaissance. Dr. David Powars of the U.S. Geological Survey provided UniStar geologists with a tour of the Rock Creek fault zone and recent exposures of ancient gravels at the National Cathedral. The location of field stops and the aerial reconnaissance flight path are shown on Figure 2.5-215. UniStar geologists performed reconnaissance of several hypothesized faults/folds that were not evaluated by Crone (Crone, 2000) or Wheeler (Wheeler, 2005) (Wheeler, 2006). UniStar geologists attended a three-day field trip affiliated with the 2006 Annual Meeting of the Geological Society of America and lead by Dr. Frank Pazzaglia titled, "Rivers, glaciers, landscape evolution, and active tectonics of the central Appalachians, Pennsylvania and Maryland" (Pazzaglia, 2006). The field trip was attended by a diverse group of geologists and geomorphologists. The trip afforded UniStar geologists the opportunity to engage with other regional experts on questions pertaining to the Quaternary and structural geology and tectonic framework of the Chesapeake Bay region (a portion of the field trip route is depicted in Figure 2.5-215).

4. Previously mapped structures and tectonic-related geomorphology were evaluated utilizing aerial photography within a 5-mi-radius of the site and LiDAR data that encompassed St. Mary's, Charles, and Calvert Counties, Maryland (a map depicting some of the LiDAR data reviewed is provided in Figure 2.5-26). Multiple flights of fluvial terraces mapped previously by McCartan (McCartan, 1989a) (McCartan, 1989b) were evaluated where the Hillville and inferred Kidwell faults would project across fluvial surfaces of the Patuxent and Potomac Rivers. Lastly, aerial reconnaissance of many of the structures listed above was performed to assess their geomorphic expression and lateral continuity, if any (Figure 2.5-215).

For discussion purposes, principal tectonic structures within the 200 mi (322 km) CCNPP site region were divided into five categories based on their age of formation or most recent reactivation. These categories include Late Proterozoic, Paleozoic, Mesozoic, Tertiary, and Quaternary. Late Proterozoic, Paleozoic, and Mesozoic structures are related to major plate tectonic events and generally are mapped regionally on the basis of geological and/or geophysical data. Late Proterozoic structures include normal faults active during post-Grenville rifting and formation of the Iapetan passive margin. Paleozoic structures include thrust and reverse faults active during Taconic, Acadian, Alleghanian, and other contractional orogenic

events. Mesozoic structures include normal faults active during break-up of Pangaea and formation of the Atlantic passive margin.

Tertiary and Quaternary structures within the CCNPP site region are related to the tectonic environment of the Atlantic passive margin. This passive margin environment is characterized by southwest- to northeast-oriented, horizontal principal compressive stress, and vertical crustal motions. The vertical crustal motions associated with loading of the coastal plain and offshore sedimentary basins and erosion and exhumation of the Piedmont and westward provinces of the Appalachians. Commonly, these structures are localized, and represent reactivated portions of older bedrock structures. Zones of seismicity not clearly associated with a tectonic feature are discussed separately in Section 2.5.1.1.4.5.

2.5.1.1.4.4.1 Late Proterozoic Tectonic Structures

Extensional structures related to Late Proterozoic-Early Cambrian rifting of the former supercontinent Rhodinia and formation of the Iapetan Ocean basin are located along a northeast-trending belt between Alabama and Labrador, Canada, and along east-west-trending branches cratonward (Wheeler, 1995) (Johnston, 1994) (Figure 2.5-23). Major structures along this northeast-trending belt include the Reelfoot rift, the causative tectonic feature of the 1811-1812 New Madrid earthquake sequence. Within the 200 mi (322 km) site region, a discrete Late Proterozoic feature includes the New York-Alabama lineament (King, 1978) (Shumaker, 2000)(Steltenpohl, 2010). The Rome Trough (Ervin and McGinnis, 1975) is located directly outside the 200-mile (322 km) site region. Within the eastern Piedmont physiographic province, extended crust of the Iapetan passive margin extends eastward beneath the Appalachian thrust front approximately to the eastern edge of Paleozoic crust extended during the Mesozoic (Johnston, 1994) (Wheeler, 1996) (Figure 2.5-15). This marks the western boundary of major Paleozoic sutures that juxtapose Laurentian crust against exotic crust amalgamated during the Paleozoic orogenies (Wheeler, 1996) (Figure 2.5-16 and Figure 2.5-17). At its closest approach, the area of largely intact and slightly extended Iapetan crust is located about 70 mi (113 km) northwest of the CCNPP site (Figure 2.5-23).

Seismic zones in eastern North America spatially associated with Iapetan normal faults include the Giles County seismic zone of western Virginia, and the Charlevoix, Quebec seismic zone, both of which are located outside the CCNPP site region (Wheeler, 1995) (Figure 2.5-23). Because the Iapetan structures are buried beneath Paleozoic thrust sheets and/or strata, their dimensions are poorly known except in isolated, well studied cases.

2.5.1.1.4.4.2 Paleozoic Tectonic Structures

The central and western portions of the CCNPP site region encompass portions of the Piedmont, Blue Ridge, Valley and Ridge, and Appalachian Plateau physiographic provinces (Figure 2.5-1). Structures within these provinces are associated with thrust sheets, shear zones, and sutures that formed during convergent and transpressional Appalachian orogenic events of the Paleozoic Era. Tectonic structures of this affinity exist beneath the sedimentary cover of the Coastal Plain and Continental Shelf Provinces. Paleozoic structures shown on Figure 2.5-23 include: (1) sutures juxtaposing allochthonous (tectonically transported) rocks against proto-North American crust, (2) regionally extensive Appalachian thrust faults and oblique-slip shear zones, and (3) a multitude of smaller structures that accommodated Paleozoic deformation within individual blocks or terranes (Figure 2.5-16, Figure 2.5-17, and Figure 2.5-18). The majority of these structures dip eastward and sole into either a low angle thrust or the low angle, basal Appalachian decollement (Figure 2.5-17). Below the decollement are rocks that form the North American basement complex (Grenville or Laurentian crust).

Researchers have observed that much of the sparse seismicity in eastern North America occurs within the North American basement below the basal decollement. Therefore, seismicity within the Appalachians may be unrelated to the abundant, shallow thrust sheets mapped at the surface (Wheeler, 1995). For example, seismicity in the Giles County seismic zone, located in the Valley and Ridge Province, is occurring at depths ranging from 3 to 16 mi (5 to 25 km) (Chapman, 1994), which is generally below the Appalachian thrust sheets and basal decollement (Bollinger, 1988).

2.5.1.1.4.4.2.1 Appalachian Structures

Paleozoic faults within 200 mi (322 km) of the CCNPP site and catalog seismicity are shown on Figure 2.5-23 and Figure 2.5-24 (see section 2.5.2 for a complete discussion on seismicity). Paleozoic faults with tectonostratigraphic units are shown on Figure 2.5-16, Figure 2.5-17 and Figure 2.5-18. Faults mapped within the Appalachian provinces (Piedmont, Blue Ridge, Valley and Ridge) are discussed in this section along with postulated Paleozoic faults in the Coastal Plain that are buried by Cenozoic strata. Paleozoic faults are discussed below from west to east across the CCNPP site region.

Major Paleozoic tectonic structures of the Appalachian Mountains within 200 mi (322 km) of the site include the Little North Mountain-Yellow Breeches fault zone, the Hylas shear zone, the Mountain Run-Pleasant Grove fault system, the Brookneal shear zone, and the Central Piedmont shear zone (including the Spotsylvania fault) (Figure 2.5-23). These structures bound lithotectonic units as defined in recent literature (Horton, 1991) (Glover, 1995b) (Hibbard, 2006) (Hibbard, 2007).

The northeast-striking Little North Mountain fault zone is located within the eastern Valley and Ridge Physiographic Province of western Virginia, eastern Maryland, and southern Pennsylvania (Figure 2.5-16 and Figure 2.5-23). The fault zone forms the tip of an upper level thrust sheet that attenuated Paleozoic shelf deposits of the Laurentian continental margin during the Alleghenian Orogeny (Hibbard, 2006). The east-dipping Little North Mountain thrust sheet soles into a decollement (Figure 2.5-17). This decollement represents an upper-level detachment above a deeper decollement about 5 mi (8 km) deep (Glover, 1995b) (Figure 2.5-17). The Little North Mountain fault and Yellow Breeches fault to the northeast mark the approximate location of the westernmost thrusts that daylight within the Valley and Ridge Province (Figure 2.5-23). Farther west, thrust ramps branching from the deeper decollement rarely break the surface and overlying fault-related folds control the morphology of the Valley and Ridge Province.

The Little North Mountain-Yellow Breeches fault zone is not considered a capable tectonic source. The decollement associated with the Little North Mountain thrust is relatively shallow, suggesting that the fault probably does not penetrate to seismogenic depths. No seismicity is attributed to the Little North Mountain-Yellow Breeches fault zone and published literature does not indicate that it offsets late Cenozoic deposits or exhibits geomorphic expression indicative of Quaternary deformation. Therefore, this Paleozoic fault is not considered to be a capable tectonic source.

The Hylas shear zone, active between 330 and 220 million years ago during the Alleghenian orogeny, comprises a 1.5 mi (2.4 km) wide zone of ductile shear fabric and mylonites located 71 mi (115 km) southwest of the site (Bobyarchick, 1979, Gates, 1989). The Hylas shear zone also locally borders the Mesozoic Richmond and Taylorsville basins and appears to have been reactivated during Mesozoic extension to accommodate growth of the basin (Figure 2.5-10) (LaTourneau, 2003; Hibard, 2006). Discussions of the post-Paleozoic reactivation of the Hylas shear zone are presented in Section 2.4.1.1.4.4.3, Mesozoic Tectonic Structures, and in

Section 2.4.1.1.4.4.4, Tertiary Tectonic Structures. Based on review of published literature and historical seismicity, there is no reported geomorphic expression, historical seismicity, or Quaternary deformation along the Hylas shear zone, and thus this feature is not considered to be a capable tectonic source.

The Mountain Run-Pleasant Grove fault system is located within the Piedmont Physiographic Province in Virginia and Maryland and may extend to near Newark, New Jersey (Hibbard, 2006) (Figure 2.5-17 and Figure 2.5-23). This fault system extends across the entire site region and juxtaposes multiple-tectonized, allochthonous rocks and terranes to the east against the passive margin rocks of North American affinity to the west. Included in this fault system are portions of the Bowens Creek fault, the Mountain Run fault zone, the Pleasant Grove fault, and the Huntingdon Valley fault (Horton, 1991; Mixon, 2000; Hibbard, 2006). Fault zones along this fault system exhibit mylonitic textures, indicative of the ductile conditions in which it formed during the Paleozoic Era. Locally the allochthonous rocks are the Potomac composite terrane (Horton, 1991), which consists of a stack of thrust sheets containing tectonic mélange deposits that include ophiolites, volcanic arc rocks, and turbidites. This east-dipping thrust probably shallows to a decollement, and is shown to be truncated by the Brookneal shear zone (Figure 2.5-17) (Glover, 1995b). In the site region, the southeastern boundary of the Mesozoic Culpeper basin locally is bounded by the Mountain Run fault zone (Mixon, 2000), suggesting that portions of the Paleozoic thrust fault system may have been reactivated since the Paleozoic (Figure 2.5-10). Discussions of the Culpeper basin and local reactivation of portions of the Mountain Run-Pleasant Grove fault system are included in Section 2.5.1.1.4.4.3.

Within the Mountain Run-Pleasant Grove fault system, only local portions of the Mountain Run fault zone have been identified with possible late Cenozoic tectonic activity (Crone, 2000) (Wheeler, 2006). These portions of the Mountain Run fault zone are discussed in Section 2.5.1.1.4.4.5.2. For other faults within the Mountain Run-Pleasant Grove fault system, published literature does not indicate that it offsets late Cenozoic deposits or exhibits geomorphic expression indicative of Quaternary deformation, and no seismicity has been attributed to it. Therefore, these faults are not considered to be capable tectonic sources.

The Brookneal shear zone is located within the Piedmont in Virginia and probably extends beneath the Coastal Plain across Virginia and Maryland to within about 50 mi (80 km) of the site (Figure 2.5-16 and Figure 2.5-23). The dextral-reverse shear zone is the northern continuation of the Brevard zone, a major terrane boundary extending from Alabama to North Carolina (Hibbard, 2002). The Brookneal shear zone juxtaposes magmatic and volcaniclastic rocks of the Chopawamsic volcanic arc to the east against the Potomac mélange to the west. This east-dipping thrust possibly truncates the Mountain Run fault at about 2.5 mi (4 km) depth, then flattens to a decollement at about 4 to 5 mi (6 to 8 km) depth that dips gently eastward beneath the surface trace of the Spotsylvania fault (Figure 2.5-17) (Glover, 1995b). Southwest of the site region, the Mesozoic Danville basin locally overlies the Brookneal shear zone. The depositional contact defining the southeastern margin of the Danville basin crosses the Brookneal shear zone and is unfaulted, suggesting that the Paleozoic fault was not reactivated as a normal fault during Triassic rifting. The Brookneal shear zone is not considered a capable tectonic source. No seismicity is attributed to it and published literature does not indicate that it offsets late Cenozoic deposits or exhibits geomorphic expression indicative of Quaternary deformation. Therefore, this Paleozoic fault is not considered to be capable tectonic source.

The northeast-striking Spotsylvania fault has been mapped in the Virginia piedmont as far north as Fredericksburg and beneath the Coastal Plain in eastern Virginia and Maryland (Hibbard, 2006) (Horton, 1991) (Glover, 1995b) (Figure 2.5-16, Figure 2.5-17 and Figure 2.5-23). At its closest approach, the fault is about 40 mi (64 km) northwest of the site (Figure 2.5-16). The fault juxtaposes terranes of different affinity, placing Proterozoic continental rocks of the

Goochland terrane to the east against Early Paleozoic (Ordovician) volcanic arc rocks of the Chopawamsic terrane to the west (Glover, 1995b)(Hibbard, 2006) (Figure 2.5-9). The Spotsylvania fault is a Late Paleozoic dextral-reverse fault active during the Alleghenian orogeny (Pratt, 1988; Bailey, 2004). The fault is the northern continuation of the Central Piedmont shear zone, a zone of ductile and brittle shear that accommodated thrust and right-lateral movement of various exotic volcanic arc terranes to the east against rocks of the Piedmont domain (including the Chopawamsic terrane) to the west (Hibbard, 1998; Hibbard, 2000; Bailey, 2004; Hibbard, 2006). The Hyco shear zone, the part of the Central Piedmont shear zone located directly southeast of the Spotsylvania fault (Hibbard, 1998; Bailey, 2004), is partially located within the 200-mile site region (Figure 2.5-9 and Figure 2.5-23). The east-dipping Spotsylvania fault and Hyco shear zone likely penetrate the crust at gentle to intermediate angles (Hibbard, 1998; Pratt, 1988; Glover, 1995b), and the Spotsylvania fault may truncate the basal Appalachian decollement and higher decollement of the Brookneal shear zone (Figure 2.5-17) (Glover, 1995b).

Specific studies of the Spotsylvania fault by Dames and Moore (DM, 1977b) demonstrate that it exhibits negligible vertical deformation of a pre- to early-Cretaceous erosion surface and is not related to Tertiary faulting along the younger Stafford fault zone (Section 2.5.1.1.4.4.4). The fault was determined by the NRC (AEC) to be not capable within the definition of 10 CFR 100, Appendix A (CFR, 2006). Nonetheless, it should be noted that Horton (Horton, 2011) more recently indicated that recurrent Cretaceous to Cenozoic movements have occurred on steep coastal-plain faults rooted in basement structures associated with the Hylas and Spotsylvania fault zones. Horton (Horton, 2011) provides no specific data related to these movements, or evidence for the timing of the movements. Exhaustive literature reviews completed as part as part of the CCNPP Unit 3 investigation yielded no evidence for potential Quaternary activity within these fault zones, nor has any seismicity been attributed to them. Accordingly, the Hylas and Spotsylvania fault zones are not considered capable tectonic sources.

2.5.1.1.4.4.2.2 Coastal Plain Structures

Major Paleozoic tectonic structures beneath the Coastal Plain in the 25 mi (40 km) CCNPP site vicinity include faults bounding the Sussex terrane west of the site and unnamed faults mapped seaward of the CCNPP site by Glover and Klitgord (Glover, 1995a) (Figure 2.5-16, Figure 2.5-17 and Figure 2.5-23). These fault zones, cited here as the western and eastern zones, are interpreted to dip steeply east, penetrate the crust, and juxtapose lithostratigraphic terranes.

The western fault zone coincides with the margins of the Sussex Terrane of Horton (Horton, 1991) (Figure 2.5-16 and Figure 2.5-17). The narrow Sussex Terrane and potential bounding faults are delimited in part by the Salisbury geophysical anomaly, a positive gravity and magnetic high described in Section 2.5.1.1.4.3. The eastern fault zone is shown to extend from coastal North Carolina to southern Delaware, trending north along the eastern part of southern Chesapeake Bay before branching into two splays that trend northeast across the Delmarva Peninsula (Figure 2.5-16 and Figure 2.5-23). The regional crustal cross section shows the fault zone as dipping east at moderate to steep angles (Figure 2.5-17).

Recent abstracts presented by Powars and Horton (Powars, 2010a) and Powars et al. (Powars, 2011) suggest the possibility that river channel deflections in parts of the Coastal Plain may coincide with underlying Paleozoic faults. For example, Powars et al. (Powars, 2011) suggested that meander bends and deflections of the James River locally coincide with the eastern boundary of the Petersburg Granite, and with the boundaries of the Taylorsville rift basin, Sussex terrane, and Chesapeake block in the underlying basement, and that major bends in the Potomac River coincide with western and eastern boundaries of the Goochland terrane.

Smaller bends in the Potomac River were similarly described as coincident with the boundaries of the Taylorsville basin, Sussex terrane, and Chesapeake block. Powars (Powars, 2011) also noted that the Rappahannock and Patuxent Rivers display meander loops or sharp bends coincident with structural boundaries in the basement, and that the Chickahominy and Choptank Rivers also change course at fault boundaries.

To date, this work by Powars and Horton (Powars, 2010a) and Powars et al. (Powars, 2011) remains unpublished, and consequently cannot be fully evaluated. Nonetheless, it alludes only to "modern geomorphic expressions" and never explicitly states that offsets are related to Quaternary movement along faults. Given the paucity of seismicity attributed to these Coastal Plain faults in the CEUS SSC (EPRI/DOE/NRC, 2012) and a lack of specific evidence for Quaternary deformation, the Paleozoic Coastal Plain structures in the CCNPP site region and site vicinity (e.g., faults bounding the Sussex terrane west of the site and unnamed faults mapped seaward of the CCNPP site by Glover and Klitgord (Glover, 1995a)) are not considered to be capable tectonic sources.

Other Paleozoic faults mapped by Hibbard (Hibbard, 2006) within the 200 mi (322 km) site region are smaller features that typically are associated with larger Paleozoic structures and accommodate internal deformation within the intervening structural blocks (Figure 2.5-23). No seismicity is attributed to these faults and published literature does not indicate that any of these faults offset late Cenozoic deposits or exhibit geomorphic expression indicative of Quaternary deformation. Therefore, these Paleozoic structures in the site region are not considered to be capable tectonic sources.

2.5.1.1.4.4.3 Mesozoic Tectonic Structures

A series of elongate rift basins of early Mesozoic age are exposed in a belt extending from Nova Scotia to South Carolina and define an area of crust extended during the Mesozoic (Figure 2.5-10)(Benson, 1992). These Mesozoic rift basins, also commonly referred to as Triassic basins, exhibit a high degree of parallelism with the surrounding structural grain of the Appalachian orogenic belt. The parallelism generally reflects reactivation of pre-existing Paleozoic structures (Ratcliffe, 1986a) (LeTourneau, 2003) (Schlische, 2003a) (Schlische, 2003b). The rift basins formed during extension and thinning of the crust as Africa and North America rifted apart to form the modern Atlantic Ocean (Section 2.5.1.1.4.1.2) (Withjack, 2005).

Generally, the rift basins are asymmetric half-grabens with the primary rift-bounding faults on the western margin of the basin (Figure 2.5-10, Figure 2.5-18 and Figure 2.5-19) (Benson, 1992) (Schlische, 1990) (Withjack, 1998) (Schlische, 2003a) (Schlische, 2003b). The rift-bounding normal faults are interpreted by some authors to be listric at depth and merge into Paleozoic low -angle detachments (Crespi, 1988) (Harris, 1982) (Manspeizer, 1988). Other authors interpret rift-bounding faults to penetrate deep into the crust following deep crustal fault zones (Wentworth, 1983) (Pratt, 1988) (Klitgord, 1995) (Figure 2.5-19).

Within the 200 mi (322 km) CCNPP site region, rift basins with rift-bounding faults on the western margin include the exposed Danville, Richmond, Culpeper, Gettysburg, and Newark basins, and the buried Taylorsville, Norfolk, hypothesized Queen Anne, and other smaller basins (Figure 2.5-10). As discussed below, most of the above-mentioned basins are bound by reactivated Paleozoic thrust or reverse faults (e.g. the Richmond basin and the Paleozoic Hylas shear zone) (Figure 2.5-10 and Figure 2.5-23). Field data also indicate that the Ramapo Fault was reactivated with both strike-slip and dip-slip displacement during Paleozoic orogenies and Mesozoic extension (Ratcliff, 1971). The principal basins within the site region are discussed below in further detail.

The Culpepper, Gettysburg, and Newark basins (i.e. the composite Birdsboro basin of Faill [2003]) form an east- to northeast-trending band of mostly exposed Mesozoic basins located 60 to 125 miles west, northwest, and north of the CCNPP Unit 3 site (Figure 2.5-10). These basins are asymmetric half-grabens bounded on the west or northwest by a series of interconnected east- to southeast-dipping fault zones (Lindholm, 1978) (Hibbard, 2006). The fault bounding the western margin of the Culpeper basin was observed to follow a well-developed foliation in metamorphic rocks by Lindholm (1978), indicating to him that the Mesozoic faulting was controlled by Paleozoic structure. However, a named Paleozoic fault zone associated with the western margin of the Culpeper basin is not clearly identified in the published literature. The southeast margin of the Culpeper basin is locally in fault contact with the Paleozoic Mountain Run fault zone (Mixon, 2000) (Hibbard, 2006) (Figure 2.5-10). This southeast-dipping fault contact probably represents post-Triassic, east-side up movement, although the total post-Triassic throw on the fault is limited and does not seem to strongly influence the basin architecture (Mixon, 2000). The Mountain Run fault zone is discussed further in FSAR sections 2.5.1.1.4.4.2.1 and 2.5.1.1.4.4.5.2.

The Gettysburg and Newark basins are bounded on their northwestern margins by southeast-dipping faults with a recognized Paleozoic history. The Gettysburg basin is bounded by the Shippenburg and Carbaugh-Marsh Creek faults (Root, 1989). The Newark basin is at least partially bounded by the Ramapo Fault zone (Ratcliffe, 1985) (Ratcliffe, 1986a) (Schlische, 1992). Detailed studies of these basin-bounding faults confirm they formed as a result of reactivation of Paleozoic faults or metamorphic structures (Ratcliffe, 1985) (Root, 1989) (Schlische, 1993) (Swanson, 1986). None of these basinbounding faults have demonstrable associated Quaternary seismic activity or conclusive evidence for recent fault activity (Section 2.5.1.1.4.4.5). The northeast-striking, narrow Danville basin (also grouped with the larger Dan River-Danville basin) is located about 170 miles southwest of the CCNPP Unit 3 site (Figure 2.5-10). The primary basin-bounding fault is located on the northwest margin of the basin and dips southeast (Benson, 1992) (Hibbard, 2006), creating a highly asymmetric cross-section (Schlische, 2003a) (Schlische, 2003b). Swanson (1986) summarizes evidence suggesting the main basin-bounding fault reactivated ductile Paleozoic faults, specifically the Stony Ridge fault zone, a probable northern extension of the Paleozoic Chatham fault. The Danville basin and the basin-bounding Chatham fault separates the Smith River Terrane on the northwest against the Milton terrane on the southeast within the central portion of the basin, but farther northeast the fault and basin are located within the Potomac terrane as mapped by Horton (1991).

The northeast-striking Richmond Taylorsville basins are located about 80 miles and 30 miles west and southwest of the CCNPP Unit 3 site, respectively within central Virginia and Maryland (Figure 2.5-10). The Richmond basin is subaerially exposed and its extent is well defined by mapping. In contrast, the Taylorsville basin is mainly buried beneath the coastal plain and its extent is constrained by limited geologic mapping, multiple seismic lines, boreholes, and interpretation of gravity and aeromagnetic data (Milici, 1995) (LeTourneau, 2003). The extent of the buried portions of the Taylorsville basin is well-defined in Virginia, but poorly constrained within Maryland based on limited subsurface data (Jacobeen, 1972) and a lack of seismic lines.

Where exposed, both the Taylorsville and Richmond basins are bounded on the west by the northeast-striking, southeast-dipping Paleozoic Hylas shear zone (Section 2.5.1.1.4.4.2.1) (Figure 2.5-10 and Figure 2.5-23). Bobyarchick and Glover (Bobyarchick,1979) argue that the Hylas shear zone was reactivated as an extensional fault to accommodate the growth of the Richmond and Taylorsville basins during Mesozoic rifting based on a 220 million year old phase of brittle extensional deformation mapped throughout the fault zone. Evidence for later Mesozoic and early Tertiary inversion of the Taylorsville basin is based on interpretation of seismic reflection profiles (LeTourneau, 2003) and the coincidence of the eastern margin of the

Taylorsville basin with contractional structures that disrupt the Cretaceous and early Tertiary coastal plain sediments (i.e. Skinker's Neck anticline, Port Royal fault zone, and Brandywine fault zone) (Section 2.5.1.1.4.4.4) (Figure 2.5-25).

The extension of the basin bounding fault of the Taylorsville basin (Hylas shear zone) beneath the CCNPP site can be hypothesized based on a range of possible down-dip geometries. The northwestern boundary of the Taylorsville basin is approximately 27 to 30 miles (44 to 48 km) northwest of the CCNPP site (Figure 2.5-10) (Schlische, 1990)(Benson, 1992). Available crustal-scale cross sections provide a range of dip angles from 20 degrees (Withjack 1998) (Schlische, 2003a) to 25 degrees (Glover, 1995) (Klitgord, 1995) (Figure 2.5-17 and Figure 2.5-19) to 30 degrees (Pratt, 1988). Based on this range in dip angle the Hylas shear zone would be 10-11 mi (16-18 km), 12-14 mi (20-22 km), and 15-17 mi (25-28 km) beneath the CCNPP site within crystalline bedrock. The thickness of the seismogenic upper crust (i.e. depth to the Moho) is variable in these cross sections and is typically depicted as either 9 mi (15 km) thick (Schlische, 1990)(Schlische, 2003a) or 18-25 mi (30-40 km thick). The 9 mi (15 km) thick model suggests that the Hylas shear zone should sole into the Moho before the fault extends beneath the CCNPP site.

Data constraining the location of the buried Queen Anne basin with respect to the CCNPP Unit 3 Site are sparse and thus the geometry and continuity of the basin are unclear. Seismic reflection studies (Hansen, 1988)(Benson, 1992), borehole data (Hansen, 1978) (Figure 2.5-11), and gravity and magnetic signatures (Benson, 1992)(Hansen, 1988)(Figure 2.5-23) were used to characterize the limits of the Queen Anne basin. These data permit multiple interpretations of the location of a basin at or near the CCNPP Site (Klitgord, 1988) (Schlische, 1990) (Horton, 1991) (Bensen, 1992) (Klitgord 1995) (Withjack 1998) (LeTourneau, 2003) (Figure 2.5-10, Figure 2.5-12, Figure 2.5-16, and Figure 2.5-22).

The delineation of the Queen Anne basin by Benson (1992) (shown on Figure 2.5-10) is derived from a seismic reflection profile (Hansen, 1988) approximately 40 mi (64 km) northeast of the site, "extensive proprietary seismic reflection profiling" data south of CCNPP, a borehole located about 13 mi (21 km) southwest of the site, and aeromagnetic and gravity data. The Queen Anne basin was first named and imaged by Hansen (1988) in the TXC-10C Vibroseis profile located 40 mi (64 km) northeast of the CCNPP site. This seismic line crosses the eastern boundary of west-dipping Triassic basin deposits above high-angle west-side-down faults offsetting crystalline basement (Hansen, 1988), but does not cross the western boundary of the basin. The Coastal Plain section is not deformed by the underlying faults. As discussed below, Benson (1992) extends the Queen Anne basin to the south based on the presence of proprietary seismic lines. Although Benson (1992) did not review the data, he inferred, based on the local concentration of these proprietary seismic lines, that they were acquired to better image a known Tertiary basin. A borehole located about 13 mi (21 km) southwest of the CCNPP Unit 3 site encountered a diabase dike at depth (Benson, 1992). Although suggestive, Benson (1992) acknowledges that the diabase dike may or may not be associated with a Mesozoic basin. Benson (1992) summarizes: "The areas of inferred buried rift basins/synrift rocks shown in this map might best be considered as areas where efforts should be concentrated to verify their presence or absence." To convey this uncertainty, Benson (1992) shows the southern extension of the Queen Anne basin with a dashed and queried boundary, whereas to the north-northeast of the site the basin boundary is depicted as a solid line where geophysical data are available (and verifiable). Subsequent authors have relied upon and modified Benson (1992), yet no new published information is available near the CCNPP site to better constrain the presence or absence of a Triassic basin beneath the site. The Hillville fault (Hansen,1986) may represent a fault along the western margin of the Queen Anne basin or the eastern margin of the Taylorsville basin reactivated during Cretaceous and early Tertiary time. The geometry of this fault is poorly constrained in the vibroseis line by Hansen (1978), which illustrates offset

crystalline basement. There are limited data to constrain its length and no data to constrain its down-dip geometry (Hansen, 1986). In addition, there is no evidence for Quaternary activity of the Hillville fault or any other structure associated with the hypothesized Queen Anne basin.

In summary, there are no specific Mesozoic basin-bounding faults within the site region that have demonstrable associated seismic activity or evidence of recent fault activity. No new data have been developed to demonstrate that any of the Mesozoic basins are currently active, and Crone and Wheeler (Crone, 2000), and Wheeler (Wheeler, 2006) do not recognize any basin-margin faults that have been reactivated during the Quaternary in the site region.

2.5.1.1.4.4.4 Tertiary Tectonic Structures

Several faults were active during the Tertiary Period within the 200 mi (322 km) CCNPP site region (Figure 2.5-25). These faults have been recognized in the western part of the Coastal Plain Province where Tertiary strata crop out in river valleys and where the faults have been investigated using seismic and borehole data. These faults include the relatively well characterized Stafford fault system in Virginia, the Brandywine fault system in Maryland, and the Washington, D.C. fault zone. Additional faults and fault-related folds defined by seismic and borehole data include the Port Royal fault zone and Skinkers Neck anticline in Virginia, and the Hillville fault in Maryland. Tertiary structures that have been proposed but are poorly constrained by data include east-facing monoclines along the western shore of Chesapeake Bay (McCartan, 1995) and a northeast-striking fault in the upper Chesapeake Bay (Pazzaglia, 1993a). In addition, Kidwell (Kidwell, 1997) uses detailed stratigraphic analysis of the Calvert Cliffs area to postulate the existence of several broad folds developed in Miocene strata as well as a poorly constrained postulated fault. All of these structures are located within about 50 mi (80 km) of the site, and the proposed east-facing monoclines of McCartan (McCartan, 1995) are within a few miles of the CCNPP site. Within 25 mi (40 km) of the site, the only fault with documented Tertiary displacement is the Hillville fault (Hansen, 1978) (Hansen, 1986) (Figure 2.5-25).

Several faults associated with the Eocene Chesapeake Bay impact crater have been identified near the mouth of the Chesapeake Bay about 60 mi (97 km) south of the site (Powars, 1999) (Figure 2.5-5). The impact crater formed on a paleo-continental shelf when the Eocene sea in this location was approximately 1,000 ft (305 m) deep. The 35-million year old Chesapeake Bay impact crater is a 56 mi (90 km) wide, complex peak-ring structure. Fault styles observed within the impact include a series of inner and outer ring, post-impact, compaction related growth faults, sin-impact faults that offset Proterozoic and Paleozoic crystalline basement rocks, and syn-impact faults related to secondary craters (Powars, 1999; Poag, 2004; Poag, 2005). These faults and others within the outer and inner ring include normal-faulted slump blocks and compaction faults that extend up-section into upper Miocene and possibly younger deposits. Published literature does not indicate that any faults related to the impact crater are seismogenic or offset Quaternary deposits.

Multiple, fault-bounded secondary craters of Eocene age also have been interpreted from multichannel seismic profiles previously collected by Texaco along the Potomac River and Chesapeake Bay 20 and 40 mi (32 and 64 km) north and northwest of the main Chesapeake Bay impact crater (Poag, 2004). The secondary impact craters have diameters ranging from 0.25 to 2.9 mi (0.4 to 4.7 km). Faults associated with the secondary craters occasionally penetrate Proterozoic and Paleozoic crystalline basement rocks (Poag, 2004). Primarily middle Miocene to Quaternary sediments thicken and sag into the primary and secondary craters. Faults associated with the impact crater are not considered capable tectonic sources and are not discussed further in this section.

Faults and folds mapped within the 200 mi (322 km) CCNPP site region that displace Tertiary Coastal Plain deposits are described below. These structures include the Stafford fault system, Brandywine fault system, National Zoo/Rock Creek faults, Port Royal fault zone, Skinkers Neck anticline, and the Hillville fault. Additional hypothesized Tertiary structures for which compelling geologic or geophysical evidence is lacking are then described. These structures include hypothesized east-facing monoclines along the western shore of Chesapeake Bay near the CCNPP site described by McCartan (McCartan, 1995), a hypothesized fault in the upper Chesapeake Bay mapped by Pazzaglia (Pazzaglia, 1993a), and structures interpreted in Calvert Cliffs by Kidwell (Kidwell, 1997).

2.5.1.1.4.4.4.1 Stafford Fault

The Stafford fault is centered roughly 50 mi (80 km) west of the CCNPP site (Figure 2.5-25). The 42 mi (68 km) long fault system consists of several northeast-striking, northwest-dipping, high-angle reverse to reverse oblique faults including, from north to south, the Dumfries, Fall Hill, Brooke, Tank Creek, Hazel Run, and an unnamed fault (Mixon, 1977). Two additional northeast-striking, southeast-side-down faults, the Ladysmith and the Arcadia faults, are included here as part of the Stafford fault system. These individual faults are 10 to 25 mi (16 to 40 km) long and are separated by 1.2 to 3 mi (2 to 5 km) wide en echelon, left step-overs. The left-stepping pattern and horizontal slickensides found on the Dumfries fault suggest a component of dextral shear on the fault system (Mixon, 1977).

Locally, the Stafford fault system coincides with the Fall Line and a northeast-trending portion of the Potomac River (Figure 2.5-25). Mixon and Newell (Mixon, 1977) suggest that the Fall Line and river deflection may be tectonically controlled. Drilling, trenching, and mapping in the Fredericksburg region showed that most fault movement on any of the four primary faults comprising the Stafford fault system was pre-middle Miocene in age (Mixon, 1978) (Mixon, 1982). Mesozoic and Tertiary movement is documented by displacement of Ordovician bedrock over lower Cretaceous strata along the Dumfries fault and abrupt thinning of the Paleocene Aquia Formation across multiple strands of the fault system (Mixon, 1977). Minor late Tertiary activity of the fault system is documented by an 11-14-inch (28-36 cm) displacement by the Fall Hill fault of a Pliocene terrace deposit along the Rappahannock River (Mixon, 1978) (Mixon, 1982) and an 18 in (46 cm) displacement near the Hazel Run fault of upland gravels of Miocene or Pliocene age (Mixon, 1978). Both offsets suggest southeast-side-down displacement (Mixon, 1978).

Subsequent studies of the Stafford fault system better document the timing of displacement, mostly by refining the age of units. For example, the Rappahannock River terrace deposit was originally cited as Late Pliocene or early Pleistocene. However, later work has revealed that the deposit is Pliocene in age (Mixon, 2000). Similarly, the offset Miocene or Pliocene upland gravels are now interpreted as Pliocene (Mixon, 2000).

More recent geologic and geomorphic analysis of the Stafford fault system for the application of North Anna Power Station Early Site Permit (ESP) to the NRC provides additional constraints on the age of deformation (Dominion, 2004a). Geomorphic analyses (structure contour maps and topographic profiles) of upland surfaces capped by Neogene marine deposits and topographic profiles of Pliocene and Quaternary fluvial terraces of the Rappahannock River near Fredericksburg, Virginia, indicate that these surfaces are not visibly deformed across the Stafford fault system (Dominion, 2004a). In addition, field and aerial reconnaissance of these features during the North Anna ESP indicate that there are no distinct scarps or anomalous breaks in topography on the terrace surfaces associated with the mapped fault traces. The NRC (2005) agreed with the findings of the subsequent study for the North Anna ESP, and stated: "Based on the evidence cited by the applicant, in particular the applicant's examination of the

topography profiles that cross the fault system, the staff concludes that the applicant accurately characterized the Stafford fault system as being inactive during the Quaternary Period." Collectively, this information indicates that the Stafford fault system is not a capable tectonic source.

Powars et al. (Powars, 2010b) suggested that some movements along the Stafford fault system may be more recent, with small offsets (typically less than 3.3 ft (1 m)) of Pliocene and Pleistocene terrace deposits. However, the interpretation of these offsets as tectonic in origin is equivocal, simply because the offsets are so small and could be explained simply by the effects of differential subsidence and/or compaction. Field and aerial reconnaissance performed as part of the CCNPP Unit 3 study, coupled with interpretation of LiDAR data, revealed no anomalous geomorphic features in the site vicinity indicative of potential Quaternary activity along the Stafford fault system. Moreover, no CEUS SSC seismicity or Quaternary deformation has been associated with the fault (EPRI/DOE/NRC, 2012). On this basis, the conclusions developed by Powars et al. (Powars, 2010b) are considered speculative, and the Stafford fault system is therefore not considered a capable tectonic source.

It should be noted that Marple (Marple, 2004a) recently proposed a significantly longer Stafford fault system that extends from Fredericksburg, Virginia to New York City as part of a northeastern extension of the postulated East Coast fault system (ECFS), (Section 2.5.1.1.4.4.5.14). The proposed northern extension of the Stafford fault system is based on: (1) aligned apparent right-lateral deflections of the Potomac (22 mi (35 km) deflection), Susquehanna (31 mi (50 km) deflection) and Delaware Rivers (65 mi (105 km) deflection) (collectively these are named the "river bend trend"), (2) upstream incision along the Fall Line directly west of the deflections, and (3) limited geophysical and geomorphic data. Marple and Talwani (Marple, 2004b) proposed that the expanded Stafford fault system of Marple (Marple, 2004a) was a northeast extension of the ECFS of Marple and Talwani (Marple, 2000). Marple and Talwani (Marple, 2004b) further speculate that the ECFS and the Stafford fault system were once a laterally continuous and through-going fault, but subsequently were decoupled to the northwest and southeast, respectively, during events associated with the Appalachian orogeny.

Data supporting the extended Stafford fault system of Marple (Marple, 2004a) is limited. Marple and Talwani (Marple, 2004b) suggest that poorly located historical earthquakes that occurred in the early 1870's and 1970's lie close to the southwestern bend in the Delaware River and concluded an association between historical seismicity and the postulated northern extension of the Stafford fault system. However, CEUS SSC seismicity data indicates a poor correlation in detail between earthquake epicenters and the expanded Stafford fault system. Moreover, geophysical, borehole and trench data collected by McLaughlin (McLaughlin, 2002) near the Delaware River across the trace of the postulated expanded Stafford fault system of Marple (Marple, 2004a) provide direct evidence for the absence of Quaternary deformation. Accordingly, there is little geologic and seismologic evidence to support this extension of the fault system beyond that mapped by Mixon (Mixon, 2000).

2.5.1.1.4.4.4.2 Brandywine Fault System

The Brandywine fault system is located approximately 30 mi (48 km) west of the site and north of the Potomac River (Figure 2.5-25). The 12 to 30 mi (19 to 48 km) long Brandywine fault system consists of a series of en echelon northeast-trending, southeast-dipping reverse faults with east-side-up vertical displacement. Jacobeen (Jacobeen, 1972) and Dames and Moore (DM, 1973) first described the fault system from Vibroseis™ profiles and a compilation of borehole data as part of a study for a proposed nuclear power plant at Douglas Point along the Potomac River. The fault system is composed of the Cheltenham and Danville faults, which are 4 mi and 8 mi (6 to 13 km) long, respectively. These two faults are separated by a 0.6 to 1 mi

(1 to 1.6 km) wide left step-over (Jacobeen, 1972). Later work by Wilson and Fleck (Wilson, 1990) interpret one continuous 20 to 30 mi (32 to 48 km) long fault that transitions into a west-dipping flexure to the south near the Potomac River. The mapped trace of the Brandywine fault system is generally coincident with (within 1.0 to 2.5 miles (2 to 4 km)) and parallel to the aeromagnetic and gravity anomalies used to define the western boundary of the Taylorsville basin but they do not precisely coincide (Mixon, 1977) (Hansen, 1986) (Wilson, 1990) (Benson, 1992). This observation lead Mixon and Newell (Mixon, 1977) to speculate the origin of the Brandywine fault system may be related to the reversal of a pre-existing zone of crustal weakness (i.e., Taylorsville Basin border fault).

The Brandywine fault system was active in the Early Mesozoic and reactivated during late Eocene and possibly middle Miocene time (Jacobeen, 1972) (Wilson, 1990). Basement rocks have a maximum vertical displacement of approximately 250 ft (76 m) across the fault (Jacobeen, 1972). Also, the Cretaceous Potomac Formation is 150 ft (46 m) thinner on the east (up-thrown) side of the fault indicating syndepositional activity of the fault. The faulting is interpreted to extend upward into the Eocene Nanjemoy Formation 70 ft (21 m) offset (Wilson, 1990), and die out as a subtle flexure developed within the Miocene Calvert Formation (8 ft (2.4 km) flexure) (Jacobeen, 1972).

Wilson and Fleck (Wilson, 1990) speculate that the fault system continues northeast toward the previously mapped Upper Marlboro faults, near Marlboro, Maryland (Figure 2.5-25). Dryden (Dryden, 1932) reported less than 5 ft (1.5 m) of reverse faulting in Pliocene Upland deposits in a railroad cut near Upper Marlboro, Maryland (Prowell, 1983). However, these faults are not observed beyond this exposure. Wheeler (Wheeler, 2006) suggests that the Upper Marlboro faults have a surficial origin (i.e., landsliding) based on the presence of very low dips and geometric relations inconsistent with tectonic faulting. Field reconnaissance conducted as part of this CCNPP Unit 3 study used outcrop location descriptions from Prowell (Prowell, 1983) but failed to identify any relevant exposures associated with the faults of Dryden (Dryden, 1932). Wheeler's (Wheeler, 2006) assessment of the Upper Marlboro fault appears to be consistent with the outcrop described by Dryden (Dryden, 1932) as not being associated with the Brandywine fault system.

Geologic information indicates that the Brandywine fault system was last active during the Miocene. This fault system is identified only in the subsurface and geologic mapping along the surface projection of the fault zone does not show a fault (DM, 1973) (McCartan, 1989a) (McCartan, 1989b). Field and aerial reconnaissance performed as part of this CCNPP Unit 3 study, coupled with interpretation of Light Detection and Ranging (LiDAR) data (see Section 2.5.3.1 for additional information regarding the general methodology), revealed no anomalous geomorphic features indicative of potential Quaternary activity. The Brandywine fault system, therefore, is not a capable tectonic source.

2.5.1.1.4.4.4.3 Port Royal Fault Zone and Skinkers Neck Anticline

The Port Royal fault zone and Skinkers Neck anticline are located about 32 mi (51 km) west of the CCNPP site, south of the Potomac River (Figure 2.5-25). First described by Mixon and Powars (Mixon, 1984), these structures have been identified within the subsurface by: (1) contouring the top of the Paleocene Potomac Formation, (2) developing isopach maps of the Lower Eocene Nanjemoy Formation, and (3) interpreting seismic lines collected in northern Virginia (Milici, 1991) (Mixon, 1992) (Mixon, 2000). The fault and anticline are not exposed in surface outcrop. The Port Royal fault zone is located about 4 to 6 mi (6 to 10 km) east and strikes subparallel to the Skinkers Neck anticline and the Brandywine fault system. In our discussion, we consider the Skinkers Neck anticline to consist of a combined anticline and fault zone, following previous authors.

Mixon and Newell (Mixon, 1977) first hypothesized that a buried fault zone existed beneath Coastal Plain sediments and connected the Taylorsville basin in the north to the Richmond basin in the south along a fault zone coincident with the Brandywine fault zone of Jacobeen (Jacobeen, 1972). The inferred fault of Mixon and Newell (Mixon, 1977) coincides with a gravity gradient used to target exploration studies that led to the discovery of the Port Royal fault and Skinkers Neck anticline in 1984 (Mixon, 1984) (Mixon, 1992).

The Port Royal fault zone consists of a 32 mi (51 km) long, north to northeast-striking fault zone that delineates a shallow graben structure that trends parallel to a listric normal fault bounding the Taylorsville basin (Mixon, 2000) (Milici, 1991). In map view, the fault zone makes a short left-step to the Brandywine fault system (Figure 2.5-25). Along the northern part of the fault zone, near the town of Port Royal, Virginia, the fault is expressed in the subsurface as a 3 mi (5 km) wide zone of warping with a west-side-up sense of displacement. Water well and seismic reflection data show an apparent west-side-up vertical component for the southwestern part of the structure also (Mixon, 1992) (Mixon, 2000) (Milici, 1991).

The Skinkers Neck anticline is located directly west of the Port Royal fault zone and southwest of the mapped terminus of the Brandywine fault system (Figure 2.5-25). The north- to northeast-striking structure is 30 mi (48 km) long and 3 to 5 mi (5 to 8 km) wide, and is defined as an asymmetric, low-amplitude, north-plunging anticline with a west-bounding fault (Mixon, 2000). Locally, Mixon (Mixon, 2000) mapped the feature as two separate, closely-spaced anticlines. Along the west side of the structure, a fault zone strikes north-to-northeast and is interpreted as a fault-bounded, down-dropped block. The Skinkers Neck anticline is not mapped north of the Potomac River by Mixon (Mixon, 1992) (Mixon, 2000). However, McCartan (McCartan, 1989a) shows two folds north of the Potomac River, west of the Brandywine fault system, and along trend with the Skinkers Neck anticline as mapped by Mixon (Mixon, 2000).

The Port Royal fault zone and Skinkers Neck anticline likely are associated with Paleozoic structures that were reactivated in the Early Mesozoic, Paleocene, and possibly middle Miocene (Mixon, 1992) (Mixon, 2000) (McCartan, 1989c). Similar to the Brandywine fault system, these structures closely coincide with the Mesozoic Taylorsville basin (Mixon, 1992) (Milici, 1991). This apparent coincidence with a Mesozoic basin suggests that the Port Royal fault zone and the Skinkers Neck anticline represent possible pre-existing zones of crustal weakness. Post-Mesozoic deformation includes as much as 30 to 33 ft (9 to 10 km) of Paleocene offset, but less than 25 ft (7.6 m) of displacement across the basal Eocene Nanjemoy Formation. Deformation on the order of 5 to 10 ft (1.5 to 3 m) is interpreted to extend upward into the Middle Miocene Calvert and Choptank Formations (Mixon, 1992). The overlying Late Miocene Eastover Formation is undeformed across both the Port Royal fault zone and Skinkers Neck anticline, constraining the timing of most recent activity (Mixon, 1992) (Mixon, 2000).

Both of these structures are mapped in the subsurface as offsetting Tertiary or older geologic units (Mixon, 2000). Field and aerial (inspection by plane) reconnaissance coupled with interpretation of aerial photography (review and inspection of features preserved in aerial photos) and LiDAR data (see Section 2.5.3.1 for additional information regarding the general methodology), conducted during this CCNPP Unit 3 study shows that there are no geomorphic features indicative of potential Quaternary activity along the surface-projection of the fault zone (i.e., along the northern banks of the Potomac River and directly northeast of the fault zone). Accordingly, the Port Royal fault zone and Skinkers Neck anticline are not considered capable tectonic sources.

2.5.1.1.4.4.4.4 Washington, D.C. Fault Zone

Tertiary-age (and younger) faults in Washington, D.C. approach to within about 45 mi (72 km) of the CCNPP site (Figure 2.5-25). Portions of the fault zone were first recognized in an exposure located near Clydesdale Place and Adams Mill Road near the National Zoo, and in a now destroyed exposure on Calvert Street, not far from the Zoo grounds (Darton, 1950). Additional faults were later recognized during construction near the intersection of 18th Street Northwest and California Street, and in drill cores collected in Lafayette Square (near the White House) (Prowell, 2010). These post-Cretaceous faults are primarily northwest striking and southwest dipping with a generally west-side-up (reverse) displacement (Darton, 1950) (Prowell, 1983) (McCartan, 1990) (Fleming, 1998).

Offsets along the Washington, D.C. fault zone range from about 40 ft (about 12 m) near the National Zoo grounds at California Street, to roughly 25 ft (nearly 8 m) at Lafayette Square (Fleming, 1994) (Prowell, 2010). This data suggests that displacements along the Washington, D.C. fault zone generally decrease (diminish) toward the south-southeast and east.

There is no clear indication of the age of the most recent movement (or movements) within the Washington, D.C. fault zone. Most data indicate that these movements affected Cretaceous to Pliocene age strata, and that Quaternary deposits are either not offset, or are only slightly offset (Prowell, 1983; Fleming, 1998). More recently, however, Southworth et al. (Southworth, 2007) suggested that some discrete faults of the Washington, D.C. fault zone near the National Zoo have placed crystalline rocks against Quaternary sediments. Discussion of these possibly more recent movements within the Washington, D.C. fault zone are provided below, in Section 2.5.1.1.4.4.5.15.

2.5.1.1.4.4.5 Hillville Fault Zone

The Hillville fault zone of Hansen (1978) approaches to within 5 mi (8 km) of the site in the subsurface (Figure 2.5-25, Figure 2.5-26, and Figure 2.5-27). The 26 mi (42 km) long, northeast-striking fault zone is composed of steep southeast-dipping reverse faults that align with the east side of the north to northeast trending Sussex-Currioman Bay aeromagnetic anomaly (i.e., SGA, Figure 2.5-11 and Figure 2.5-22) (Hansen, 1986). Based on seismic reflection data collected about 9 mi (15 km) west-southwest of the site, the fault zone consists of a narrow zone of discontinuities that vertically separate basement by as much as 250 ft (76 m) (Hansen, 1978). (Figure 2.5-218). With the exception of the single seismic reflection profile St. M-1 of Hansen (1978) there are no other data to indicate the down-dip geometry of the fault. The strike of the fault is inferred entirely from the coincidence of the fault with the Sussex Currioman Bay aeromagnetic anomaly (Figure 2.5-11)(Hansen, 1986).

The Hillville fault zone delineates a possible Paleozoic suture zone reactivated in the Mesozoic and Early Tertiary. The fault zone is interpreted as a lithotectonic terrane boundary that separates basement rocks associated with Triassic rift basins on the west from low-grade metamorphic basement on the east (i.e., Sussex Terrane/Taconic suture of Glover and Klitgord, (Glover, 1995a) (Figure 2.5-17) (Hansen, 1986). The apparent juxtaposition of the Hillville fault zone with the Sussex-Currioman Bay aeromagnetic anomaly suggests that the south flank of the Salisbury Embayment may be a zone of crustal instability that was reactivated during the Mesozoic and Tertiary. Cretaceous activity is inferred by Hansen (Hansen, 1978) who extends the fault up into the Cretaceous Potomac Group. The resolution of the geophysical data does not allow an interpretation for the upward projection of the fault into younger overlying Coastal Plain deposits (Hansen, 1978). Hansen (Hansen, 1978), however, used stratigraphic correlations (i.e. "pinchouts") of Coastal Plain deposits from borehole data to speculate that the Hillville fault may have been active during the Early Paleocene.

There is no geologic data to suggest that the Hillville fault is a capable tectonic source. Field and aerial reconnaissance, coupled with interpretation of aerial photography and LiDAR data (see Section 2.5.1.1.4.4 for additional information regarding the general methodology), conducted during this COL study shows that there are no geomorphic features indicative of potential Quaternary activity along the surface-projection of the Hillville fault zone. A review of geologic cross sections (McCartan, 1989a) (McCartan, 1989b) (Glaser, 2003b) (Glaser, 2003c) show south-dipping Lower to Middle Miocene Calvert Formation and no faulting along projection with the Hillville fault zone. A structure contour map of the top of the Eocene Piney Point-Nanjemoy Aquifer appears undeformed in the vicinity of the Hillville fault, indicating the likely absence of faulting of this regionally recognized stratigraphic marker (Figure 2.5-14). A geologic cross section prepared by Achmad and Hansen (Achmad, 1997) that intersects the Hillville fault, also shows no demonstrable offset across the contact between the Piney Point and Nanjemoy Formations (Figure 2.5-13). Furthermore Quaternary terraces mapped by McCartan (McCartan, 1989b) and Glaser (Glaser, 2003b) (Glaser, 2003c) bordering the Patuxent and Potomac Rivers were evaluated for features suggestive of tectonic deformation by interpreting LiDAR data and through field and aerial reconnaissance (Figure 2.5-26 and Figure 2.5-27 and Figure 2.5-215). No northeast-trending linear features coincident with the zone of faulting were observed where the surface projection of the fault intersects these Quaternary surfaces. Aerial reconnaissance of this fault zone also demonstrated the absence of linear features coincident or aligned with the fault zone (Figure 2.5-215). The interpretation of the detailed stratigraphic profiles collected along Calvert Cliffs and the western side of Chesapeake Bay provide geologic evidence for no expression of the fault where the projected fault would intersect the Miocene-aged deposits (Kidwell, 1997; see Section 2.5.3 for further explanation). Lastly, abundant shallow seismic reflection data acquired and interpreted by Colman (Colman, 1990) in Chesapeake Bay intersect the northeast projection of the Hillville fault (Figure 2.5-29). Colman (Colman, 1990) makes no mention of encountering the Hillville fault in the interpretations of the seismic data. Therefore, we conclude that the Hillville fault zone is not a capable tectonic source.

2.5.1.1.4.4.4.6 Unnamed Fault beneath Northern Chesapeake Bay, Cecil County, Maryland

Pazzaglia (Pazzaglia, 1993a) proposed a fault in northern Chesapeake Bay that comes to within 70 mi (113 km) north of the site (Figure 2.5-25, and Figure 2.5-216). On the basis of geologic data and assuming that the bay is structurally controlled, Pazzaglia (Pazzaglia, 1993a) infers a 14 mi (23 km) long, northeast-striking fault with a southeast-side up sense of displacement. Pazzaglia (Pazzaglia, 1993a) interprets this fault as beneath the Northeast River and northern Chesapeake Bay based on a vertical elevation difference of the early Pleistocene Turkey Point beds across the bay in Cecil County, Maryland (Figure 2.5-216). Specifically:

> "The Turkey Point beds at Turkey Point, Grove Point, and Betterton lie 6 - 8 m higher than at the mouth of the Susquehanna River…These elevation disparities suggests ~8 m of post-early Pleistocene offset along a northeast-southwest - trending fault beneath the upper Chesapeake Bay."(Pazzaglia, 1993a; p. 1632).

Central to the Pazzaglia (Pazzaglia, 1993a) interpretation of a fault is the argument that the Turkey Point beds exposed in a three meter deep trench on Coudon Farm terrace west of Chesapeake Bay correlate with, and are equivalent to, the Turkey Point beds exposed in a sea cliff at Turkey Point, located 6.2 mi (10 km) to the southeast on the opposite side of the bay (Figure 2.5-216). This fault interpretation assumes that the depositional base of the Turkey Point beds should lie at a very similar elevation over considerable lateral distances. Pazzaglia clarified several key aspects of the fault interpretation during expert interviews. First, he stated that only the Turkey Point and Coudon Farm sites were used to estimate the approximately 20 to 26 ft

(6 to 8 m) of vertical separation. Second, he indicated that there may be original depositional relief on the base of the Turkey Point beds, which could account for the elevation disparity between Coudon Farms and Turkey Point.

Despite the information discussed above, the hypothesized fault from Pazzaglia (Pazzaglia, 1993a) is unconfirmed based on evidence that supports the absence of faulting and the lack of direct supporting geologic evidence. First, the hypothetical fault inferred by Pazzaglia (Pazzaglia, 1993a) is coincident with a fault inferred previously by Higgins (Higgins, 1974) that was re-evaluated by Edwards (Edwards, 1979). Motivated by speculations from Higgins (Higgins, 1974) that the northern Chesapeake Bay magnetic anomaly was created by faulting of Coastal Plain stratigraphy, Edwards (Edwards, 1979) drilled three borings on either side of the magnetic anomaly and compiled existing boring and geophysical data to construct the top-of-basement structure contour map shown in Figure 2.5-216. Based on their findings, Edwards (Edwards, 1979) made several key statements on the absence of a fault, including: "A regional map of the basement surface… does not reveal any structural anomalies… that could not be explained by relict topographic relief on the pre-Coastal Plain surface" (p. 20) and "within the scale of resolution (50 feet) of the data obtained in this project, offset at the base of the Coastal Plain cannot be demonstrated. Thus any fault associated with the shear zone can be dated no younger than Early Cretaceous" (p. 21). Similarly, geologic cross-sections from Benson (Benson, 2006), developed from the borings of Edwards (Edwards, 1979), provide a line of evidence that is inconsistent with faulting beneath the northern part of Chesapeake Bay. Second, geologic mapping by Higgins (Higgins, 1986) along the northeast on-land projection of the inferred fault of Pazzaglia (Pazzaglia, 1993a) does not show any northeast-striking fault(s) near Indian Falls and Northeast (Figure 2.5-217). Likewise, Higgins (Higgins, 1990) report unfaulted Cretaceous deposits along a northeast projection of the inferred fault and state: "No irregularities such as local steepening, flattening, or reversal of the dip of the Coastal Plain strata have been found in Cecil County which would indicate that there has been significant post-depositional tectonic movements." (p. 123).

There is no direct geologic evidence to suggest that this unnamed fault zone from Pazzaglia (Pazzaglia, 1993a) is a capable tectonic source. There is no seismicity spatially associated with this fault zone. Field and aerial reconnaissance conducted to support CCNPP Unit 3 (Figure 2.5-215) and inspection of detailed 'bare earth' LiDAR data (Figure 2.5-217) shows that there are no geomorphic features indicative of potential Quaternary activity along the surface-projection of the unnamed fault. Based on the sum of published literature (Higgins, 1986)(Higgins, 1990), structure contour maps (Edwards, 1979), field and aerial reconnaissance, and reasonable alternate explanations presented by F. Pazzaglia himself, it is concluded that this hypothetical fault is not a capable tectonic source.

2.5.1.1.4.4.4.7 Unnamed Monocline beneath Chesapeake Bay

McCartan (McCartan, 1995) show east-facing monoclinal structures bounding the western margin of Chesapeake Bay approximately 1.8 and 10 mi (2.9 and 16 km) east and southeast, respectively, of the site (Figure 2.5-25). Also, McCartan (McCartan, 1995) interprets an east-facing monocline about 10 mi (16 km) west of the site. The three monoclinal structures are depicted on two cross sections as warping Lower Paleocene to Upper Miocene strata with approximately 60 to 300 ft (18 to 91 m) of relief. The monoclines exhibit a west-side up sense of structural relief that projects upward into the Miocene Choptank Formation (McCartan, 1995). The overlying Late Miocene St. Mary's Formation is not shown as warped. Boreholes shown with the cross sections accompanying the McCartan (MaCartan, 1995) map provide the only direct control on cross section construction. The boreholes are widely spaced and do not appear to provide a constraint on the existence and location of the warps. No borehole data is available directly west of the cliffs and within the bay to substantiate the presence of the warp.

No surface trace or surface projection of the warps is indicated on the accompanying geologic map. Based on text accompanying the map and cross sections, we infer that the cross sections imply two approximately north- to northeast-striking, west-side up structures, of presumed tectonic origin.

McCartan (McCartan, 1995) interpret the existence of the monocline based on three observations in the local landscape. Firstly, the north to northeast-trending western shore of Chesapeake Bay within Calvert County is somewhat linear and is suggestive of structural control (McCartan, 1995). Secondly, land elevation differences west and east of Chesapeake Bay are on the order of 90 ft (27 m), with the west side being significantly higher in elevation, more fluvially dissected, and composed of older material compared to the east side of Chesapeake Bay. On the west side of the bay, the landscape has surface elevations of 100 to 130 ft (30 to 40 m) msl and drainages are incised into the Pliocene Upland Deposits and Miocene-aged deposits of the St. Mary's, Choptank, and Calvert Formations. Along the eastern shoreline of the Delmarva Peninsula, surface elevations are less than 20 to 30 ft (6 to 9 m) msl and the surface exhibits minor incision and a more flat-lying topographic surface. These eastern shore deposits are mapped as Quaternary estuarine and deltaic deposits. Thirdly, variations in unit thickness within Tertiary deposits between Calvert Cliffs and the Delmarva Peninsula are used to infer the presence of a warp. Based on these physiographic, geomorphic and geologic observations, McCartan (McCartan, 1995) infer the presence of a fold along the western shore of Chesapeake Bay (Figure 2.5-25).

Based on the paucity of geologic data constraining the cross sections of McCartan (McCartan, 1995), the existence of the monocline is speculative. The borehole data that constrain the location of the monocline are approximately 18 to 21 mi (29 to 34 km) apart and permit, but do not require the existence of a monocline. McCartan (McCartan, 1995) does not present additional data that are inconsistent with the interpretation of flat-lying, gently east-dipping Miocene strata shown in prior published cross sections north and south of this portion of Chesapeake Bay (Cleaves, 1968) (Milici, 1995) and within Charles and St. Mary's Counties, Maryland (McCartan, 1989a) (McCartan, 1989b) (DM, 1973). No geophysical data are presented as supporting evidence for this feature. In contrast, shallow, high-resolution geophysical data collected along the length of Chesapeake Bay to evaluate the ancient courses of the submerged and buried Susquehanna River provide limited evidence strongly indicating that Tertiary strata are flat lying and undeformed along the western shore of Chesapeake Bay (Colman, 1990) (Figure 2.5-29).

Alternatively, the change in physiographic elevation and geomorphic surfaces between the western and eastern shores of Chesapeake Bay can be explained by erosional processes directly related to the former course of the Susquehanna River, coupled with eustatic sea level fluctuations during the Quaternary (Colman, 1990) (Owens, 1979). Colman and Halka (Colman, 1989) also provide a submarine geologic map of Chesapeake Bay at and near the site which depicts Tertiary and Pleistocene deposits interpreted from high-resolution geophysical profiles. No folding or warping or faulting is depicted on the Colman and Halka (Colman, 1989) map which encompasses the warp of McCartan (McCartan, 1995). Colman (Colman, 1990) utilize the same geophysical data to track the former courses of the Susquehanna River between northern Chesapeake Bay and the southern Delmarva Peninsula. Paleo-river profiles developed from the geophysical surveys that imaged the depth and width of the paleochannels show that the Eastville (150 ka) and Exmore (200 to 400 ka) paleochannels show no distinct elevation changes within the region of the Hillville fault and McCartan (McCartan, 1995) features.

There is no geologic data to suggest that the postulated monocline along the western margin of Chesapeake Bay of McCartan (McCartan, 1995), if present, is a capable tectonic source. Field and aerial reconnaissance, coupled with interpretation of aerial photography and LiDAR data

(see Section 2.5.3.1 for additional information regarding the general methodology), conducted during this COL study, shows that there are no geomorphic features indicative of folding directly along the western shores of Chesapeake Bay. There is similarly no seismicity spatially associated with this structure. These data indicate that the McCartan (McCartan, 1995) warps, if present, most likely do not deform Pliocene to Quaternary deposits and thus are not capable tectonic sources.

2.5.1.1.4.4.4.8 Unnamed Folds and Postulated Fault within Calvert Cliffs, Western Chesapeake Bay, Calvert County, Maryland

The Calvert Cliffs along the west side of Chesapeake Bay provide a 25 mile (40 km) long nearly continuous exposure of Miocene, Pliocene and Quaternary deposits (Figure 2.5-26). Kidwell (1988 and 1997) prepared over 300 comprehensive lithostratigraphic columns along a 25 mi (40 km) long stretch of Calvert Cliffs (Figure 2.5-30). Because of the orientation of the western shore of Chesapeake Bay, the cliffs intersect any previously potential structures (i.e., Hillville fault) trending northeast or subparallel to the overall structural trend of the Appalachians. The cliff exposures provide a 230 ft (70 m) thick section of Cenozoic deposits that span at least 10 million years of geologic time.

On the basis of the stratigraphic profiles, Kidwell (Kidwell, 1997) develops a chronostratigraphic sequence of the exposed Coastal Plain deposits and provides information on regional dip and lateral continuity. The Miocene Choptank Formation is subdivided into two units and is unconformably overlain by the St. Mary's Formation. The St. Mary's Formation is subdivided into three subunits each of which is bound by a disconformity. The youngest subunit is unconformably overlain by the Pliocene Brandywine Formation (i.e., Pliocene Upland gravels). The exposed Coastal Plain deposits strike northeast and dip south-southeast between 1 and 2 degrees. The southerly dip of the strata is disrupted occasionally by several low amplitude broad undulations in the Choptank Formation, and decrease in amplitude upward into the St. Mary's Formation (Figure 2.5-30). Kidwell (Kidwell, 1997) interprets the undulations as monoclines and asymmetrical anticlines. The undulations typically represent erosional contacts that have wavelengths on the order of 2.5 to 5 mi (4 to 8 km) and amplitudes of 10 to 11 ft (about 3 m). Any inferred folding of the overlying Pliocene and Quaternary fluvial strata is very poorly constrained or obscured because of highly undulatory unconformities within these younger sand and gravel deposits. For instance, the inferred folding of the overlying Pliocene and Quaternary channelized sedimentary deposits consist of intertidal sand and mud-flats, tidal channels and tidally-influenced rivers exhibit as much as 40 ft (12 m) of erosional elevation change (Figure 2.5-30).

About 1.2 mi (1.9 km) south of the site, Kidwell (Kidwell, 1997) interprets an apparent 6 to 10 ft (2 to 3 m) elevation change in Miocene strata by extrapolating unit contacts across the approximately 0.6 mi (1 km) gap at Moran Landing (Figure 2.5-25 and Figure 2.5-30). Kidwell (Kidwell, 1997) also interprets a 3 to 12 ft (1 to 3.6 m) elevation change in younger, possibly Quaternary, fluvial material across the same gap. Because of the lack of cliff exposures at Moran Landing (only the valley margins), no direct observations of these elevation changes can be made. Kidwell (Kidwell,1997) explains the differences in elevation of the Miocene-Quaternary stratigraphy by hypothesizing the existence of a fault at Moran Landing that strikes northeast and accommodates a north-side down sense of separation. However, the postulated fault of Kidwell (Kidwell, 1997) is not shown on any of Kidwell's (Kidwell, 1997) cross- sections, or any published geologic map. In addition, Hansen (Hansen, 1978) does not describe faulting in seismic reflection line St. M-2 that intersects the inferred southwest projection of the hypothesized Kidwell (Kidwell, 1997) fault (Figure 2.5-27).

The observations of offset younger gravels do not provide any evidence for the existence of a fault because the surface on which the gravels are deposited is an erosional unconformity with extensive variable relief (Kidwell, 1997). Observations made during field reconnaissance, as part of the FSAR preparation, confirmed that this contact was an erosional unconformity with significant topography north and south of Moran Landing consistent with stratigraphic representations in the Kidwell (Kidwell, 1997) profiles. The relatively small elevation change in the Miocene units over such an extensive horizontal distance is at best weak evidence for faulting within the Miocene deposits. For example, subtle elevation variations in Miocene strata characterized along a near-continuous exposure south of Moran Landing contain similar vertical and lateral dimensions as to the inferred elevation change across Moran Landing; however, the features are interpreted as subtle warps and not faults by Kidwell (Kidwell, 1997). On the basis of association with similar features to the south and the lack of a continuous exposure, there is little to no evidence to support a fault across Moran Landing. The lack of evidence for Quaternary faulting within the observations made by Kidwell (Kidwell, 1997) and the results of the studies undertaken as part of the CCNPP Unit 3 COLA effort (field and aerial reconnaissance, air photo and LiDAR analysis) (see FSAR Section 2.5.3.1), collectively support the conclusion that the hypothesized fault of Kidwell (Kidwell, 1997) is not a capable fault.

2.5.1.1.4.4.5 Quaternary Tectonic Features

In an effort to provide a comprehensive database of Quaternary tectonic features, Crone and Wheeler (Crone, 2000) and Wheeler (Wheeler, 2005) (Wheeler, 2006) compiled geological information on Quaternary faults, liquefaction features, and possible tectonic features in the CEUS. Crone and Wheeler (Crone, 2000) and Wheeler (Wheeler, 2005) evaluated and classified these features into one of four categories (Classes A, B, C, and D; see Table 2.5-1 for definitions (Crone, 2000) (Wheeler, 2005)) based on strength of evidence for Quaternary activity.

Within a 200 mi (322 km) radius of the CCNPP site, Crone and Wheeler (Crone, 2000) and Wheeler (Wheeler, 2005) (Wheeler, 2006) identified 16 potential Quaternary features (Figure 2.5-31). Only one of these features, the Central Virginia seismic zone, was designated as Class A. That is, only one feature within a 200 mi (322 km) radius of the CCNPP site provides relatively clear evidence of seismogenic potential. The remaining features identified by Crone and Wheeler (Crone, 2000) and Wheeler (Wheeler, 2005) (Wheeler, 2006) within the 200 mi (322 km) radius were designated as Class C features, suggesting that the available geologic evidence is insufficient to demonstrate the existence of a tectonic fault, or Quaternary slip or deformation. Literature review, expert interviews, and field reconnaissance completed as part of the CCNPP Unit 3 investigation, identified only one additional potential Quaternary tectonic feature within the site region, namely the Washington, D.C. fault zone.

Sections 2.5.1.1.4.4.5.1 through 2.5.1.1.4.4.5.15, below, provide descriptions for 14 of the 16 potential Quaternary features classified by Crone and Wheeler (Crone, 2000) and Wheeler (Wheeler, 2005) (Wheeler, 2006) as well as the unclassified Washington, D.C. fault zone. These features are identified by reference number in Figure 2.5-31 as follows:

1. Fall lines of Weems (1998) (Class C)
2. Everona fault and Mountain Run fault zone (Class C)
3. Stafford fault system (Class C)
4. Ramapo fault system (Class C)
5. Kingston fault (Class C)

6. New York Bight fault (offshore) (Class C)
7. Cacoosing Valley earthquake (Class C)
8. New Castle County faults (Class C)
9. Upper Marlboro faults (Class C)
10. Lebanon Church fault (Class C)
11. Hopewell fault (Class C)
12. Old Hickory faults (Class C)
13. Stanleytown-Villa Heights faults (Class C)
14. East Coast fault system (Class C)
15. Washington, D.C. fault zone (not classified)

Note that the Class A Central Virginia seismic zone (and associated faults) and Class C Lancaster seismic zone (reference numbers 16 and 17, respectively, in Figure 2.5-31) are discussed separately in Section 2.5.1.1.4.5 (and also in Section 2.5.2).

2.5.1.1.4.4.5.1 Fall Lines of Weems (1998)

Weems (Weems, 1998) examined longitudinal profiles within southeastward and northwestward flowing streams across the Piedmont and Blue Ridge provinces of North Carolina and Virginia and identified numerous fall zones, or short stream segments with anomalously steep gradients, rapids, or waterfalls. Weems (Weems, 1998) observed that the fall zones tend to align from stream to stream, and that the alignments follow curvilinear paths that he termed fall lines, the easternmost of which is located approximately 47 mi (76 km) west of the CCNPP site (Figure 2.5-31). Weems (Weems, 1998) considered several possible origins for these fall lines, including climatic controls and differential rock hardness, but concluded that the fall lines were tectonically controlled.

Crone and Wheeler (Crone, 2000) suggested that this identification of fall zones was subjective, and that the criteria for recognizing them were not very clearly defined. Accordingly, Crone and Wheeler (Crone, 2000) assigned the fall lines a Class C designation. Additional critical review of the fall lines during the North Anna Power Station ESP study (Dominion, 2004b) concluded that that the individual fall zones were not as laterally continuous as reported, and that differential erosion due to variable bedrock hardness rather than Quaternary tectonism was a more likely explanation for the origin of the fall lines. This assessment was supported by the NRC in the Safety Evaluation Report for the North Anna ESP (NRC, 2005). Accordingly, it is concluded here that the fall lines of Weems (Weems, 1998) are not tectonic in origin, and thus are not capable tectonic sources.

2.5.1.1.4.4.5.2 Everona Fault and Mountain Run Fault Zone

The Mountain Run fault zone is located approximately 71 mi (114 km) southwest of the site (Figure 2.5-9). The 75 mi (121 m) long, northeast-striking fault zone is mapped from the southeastern margin of the Triassic Culpeper Basin near the Rappahannock River southwestward to near Charlottesville, in the western Piedmont of Virginia (Pavlides, 1986)

(Horton, 1991). The fault zone consists of a broad zone of sheared rocks, mylonites, breccias, phyllonites, and phyllites up to 2.5 to 3 mi (4 to 5 km) wide (Pavlides, 1989) (Crone, 2000) (Mixon, 2000). Within this broad fault zone are three features that have been identified by Crone and Wheeler (Crone, 2000) as having possible Quaternary tectonic activity. From northeast to southwest, these are: (1) the northwest-facing, 1 mi (1.6 km) long Kelly's Ford scarp, (2) the northwest-facing, 7 mi (11 km) long Mountain Run scarp, and (3) the northwest-dipping fault exposed near the town of Everona, Virginia, named informally the Everona fault (Pavlides, 1983) (Pavlides, 1986) (Pavlides, 1994) (Crone, 2000) (Mixon, 2000) (Figure 2.5-31).

The Mountain Run fault zone is interpreted to have formed initially as a thrust fault upon which back-arc basin rocks (mélange deposits) of the Mine Run Complex were accreted onto ancestral North America at the end of the Ordovician (Pavlides, 1989). This major structure separates the Blue Ridge and Piedmont terranes (Pavlides, 1983) (Figure 2.5-9, Figure 2.5-16, and (Figure 2.5-17). Subsequent reactivation of the fault during the Paleozoic and/or Mesozoic produced strike-slip and dip-slip movements. Horizontal slickenside lineations within phyllite found in borehole samples beneath the alluvium-filled valley of Mountain Run suggest strike-slip movement, whereas small scale folds in the uplands near the scarp suggest an oblique dextral sense of slip (Pavlides, 2000). The timing of the reverse and strike-slip histories of the fault zone, and associated mylonitization and brecciation, is constrained to be pre-Early Jurassic, based on the presence of undeformed Early Jurassic diabase dikes that cut rocks of the Mountain Run fault zone (Pavlides, 2000). The northern portion of the Mountain Run fault zone bounds the southeastern margin of the Culpeper basin (Mixon, 2000) (Figure 2.5-9 and Figure 2.5-10), indicating that the fault locally has been active since the Triassic (Crone, 2000) (Section 2.5.1.1.4.4.3).

Two features within the northeast-striking Mountain Run fault zone are moderately to well-expressed geomorphically (Pavlides, 2000). Two northwest-facing scarps occur along the fault zone, including: (1) the 1 mi (1.6 km) long Kelly's Ford scarp located directly northeast of the Rappahannock River and; (2) the 7 mi (11 km) long Mountain Run scarp located along the southeast margin of the linear Mountain Run drainage. The presence of these two locally conspicuous bedrock scarps in the Piedmont, an area characterized by deep weathering and subdued topography, has led some experts to suggest that the scarps formed due to a Late Cenozoic phase of movement within the fault zone (Pavlides, 2000) (Pavlides, 1983).

Field and aerial reconnaissance, and geomorphic analysis of deposits and features associated with the fault zone, recently performed for the North Anna ESP provide information on the Mountain Run and Kelly's Ford scarps in particular, and the Mountain Run fault zone in general (Dominion, 2004a). In response to NRC comments for the North Anna ESP, geologic cross sections and topographic profiles were prepared along the Mountain Run fault zone across and between the Mountain Run and Kelly's Ford scarps to further evaluate the inferred tectonic geomorphology coincident with the fault zone first proposed by Pavlides (1986). The results of the additional analysis were presented in the response to an NRC Request for Additional Information (RAI) (Dominion, 2004a) and demonstrated that the Mountain Run and Kelly's Ford scarps are probably a result of a differential erosion and not late Cenozoic tectonic activity. Three main findings from the Dominion (2004a) study are summarized below:

- There is no consistent expression of a scarp along the Mountain Run fault zone in the vicinity of the Rappahannock River. The northwest-facing Kelly's Ford scarp is similar to a northwest-facing scarp along the southeastern valley margin of Mountain Run; both scarps were formed by streams that preferentially undercut the southeastern valley walls, creating asymmetric valley profiles.

- There is no northwest-facing scarp associated with the 10 mile (16 km) long portion of the Mountain Run fault zone between the Rappahannock and Rapidan Rivers (i.e., between the Kelly's Ford and Mountain Run scarps). Undeformed late Neogene colluvial deposits bury the Mountain Run fault zone in this region, demonstrating the absence of Quaternary fault activity.

- The northwest-facing Mountain Run scarp southwest of the Rappahannock River alternates with a southeast-facing scarp on the opposite side of Mountain Run valley; both sets of scarps have formed by the stream impinging on the edge of the valley.

Near Everona, Virginia, a small reverse fault, found in an excavation, vertically displaces a "probable Late Tertiary" or "Pleistocene" gravel layer by 5 ft (1.5 m) (Pavlides, 1983) (Manspeizer, 1989) (Crone, 2000). The fault strikes northeast and dips between about 55 and 20 degrees northwest, shallowing up-dip (Manspeizer, 1989) (Crone, 2000) (Bobyarchick, 2007). This isolated fault exposure, called the Everona fault by Crone and Wheeler (Crone, 2000), is located about 0.4 mi (0.6 km) northwest of the Mountain Run scarp (Pavlides, 1983) (Mixon, 2000). There is no surface expression associated with the exposure (Crone, 2000). Crone and Wheeler (Crone, 2000) assessed that the faulting at Everona is likely to be of Quaternary age, but because the likelihood has not been tested by detailed paleoseismological or other investigations, this feature was assigned to Class C.

Wheeler (Wheeler, 2006) similarly concluded that a Quaternary offset could not be demonstrated for the Everona fault, or the scarps in the Mountain Run fault zone.

Based on the findings of Crone and Wheeler (Crone, 2000) and Wheeler (Wheeler, 2006) as well as studies completed for the North Anna Power Station ESP, it is concluded here that the Mountain Run fault zone and Everona fault are not capable tectonic sources. It should be noted, however, that recent models of coulomb stress transfer indicate that the southern portions of the Mountain Run fault zone may have been loaded as a as a result of the 2011 Mineral, Virginia earthquake (Walsh, 2012). Walsh et al. (Walsh, 2012) indicated that the stress changes were too small to have significantly affected seismic hazard on the fault, but suggested that possible repeated events in the Central Virginia Seismic Zone could eventually trigger slip. Additional discussion of the Mineral, Virginia earthquake is provided below, in Section 2.5.1.1.4.5.1.

2.5.1.1.4.4.5.3 Stafford Fault System

The Stafford fault system, first described by Newell (Newell, 1976), is centered roughly 50 mi (80 km) west of the CCNPP site (Figure 2.5-31). The fault system consists of a series of five northeast-striking, northwest-dipping, high-angle reverse faults including, from north to south, the Dumfries, Fall Hill, Hazel Run, and Brooke faults, and an unnamed fault. The Brooke fault also includes the Tank Creek fault located northeast of the Brooke fault (Mixon, 2000). Additional discussion of these faults is provided in Section 2.5.1.1.4.4.4.1.

Field reconnaissance performed for the CCNPP Unit 3 study did not reveal any geologic or geomorphic features indicative of potential Quaternary activity along the fault system. In addition, near the site and along the portion of the Stafford fault mapped by Mixon et al. (Mixon, 2000) no seismicity is specifically attributed to the Stafford fault. Similarly, Wheeler (Wheeler, 2005) does not show the Stafford fault system as a Quaternary structure in his compilation of active tectonic features in the CEUS. The NRC (NRC, 2005) agreed with the findings of the subsequent study for the North Anna ESP, and stated: "Based on the evidence cited by the applicant, in particular the applicant's examination of the topography profiles that cross the fault system, the staff concludes that the applicant accurately characterized the Stafford fault system as being inactive during the Quaternary Period." Based on a review of

existing information for the Stafford fault system, including the response to the NRC RAI for the North Anna ESP, the Stafford fault system is not a capable tectonic source.

2.5.1.1.4.4.5.4 Ramapo Fault System

The Ramapo fault is located in northern New Jersey and southern New York State, approximately 200 mi (320 km) north-northeast of the CCNPP site (Figure 2.5-31, Figure 2.5-213 and Figure 2.5-219). The Ramapo fault is one segment of a system of northeast-striking, southeast-dipping, normal faults that bound the northwest side of the Mesozoic Newark basin (Figure 2.5-10, and Figure 2.5-213), (Drake, 1996) (Ratcliffe, 1971) (Schlische, 1992). Bedrock mapping by Drake et al. (Drake, 1996) shows primarily northwest-dipping Lower Jurassic and Upper Triassic Newark Supergroup rocks in the hanging wall and tightly folded and faulted Paleozoic basement rocks in the footwall of the fault. The Ramapo fault proper extends for 50 mi (80 km) from Peapack, NJ to the Hudson River (Ratcliffe, 1971). To the south the Ramapo fault splays into several fault strands and merges with the Flemington Fault zone. On the north side of the Hudson River the fault splays into several northeast- to east-trending faults in Rockland and Westchester Counties, New York.

Interest in the Ramapo fault as a potential seismogenic fault was initially driven by the work of seismologists at what is now referred to as the Lamont Doherty Earth Observatory in New Jersey. Largely based on earthquake locations generated from local network data, these researchers noticed a spatial association between earthquakes and the Ramapo fault (Aggarwal, 1978) (Kafka, 1985) (Page, 1968). The study of Page et al. (Page, 1968) used the locations of four earthquakes that they located near the Ramapo fault as the basis for concluding that the earthquakes were occurring on the Ramapo fault, and, therefore, the Ramapo was experiencing small slip events. In a later study, Aggarwal and Sykes (Aggarwal, 1978) located 33 earthquakes with magnitudes less than or equal to mb 3.3 that occurred between 1962 and 1977 within the New York - New Jersey region surrounding the Ramapo fault. Based on the locations of these earthquakes, Aggarwal and Sykes (Aggarwal, 1978) also noted a spatial association between the locations of the earthquakes and the Ramapo and related faults. Aggarwal and Sykes (Aggarwal, 1978) described this association as "leav[ing] little doubt that earthquakes in this area occur along preexisting faults" (page 426) (Aggarwal, 1978). In particular, Aggarwal and Sykes (Aggarwal, 1978) focused on the Ramapo fault: (1) noting that over half of the 32 events plot along the Ramapo fault, and (2) concluding that that Ramapo fault is an active fault with the capability of generating large earthquakes. Aggarwal and Sykes (Aggarwal, 1978) based this conclusion on: (1) the spatial association of seismicity; (2) focal mechanisms for earthquakes near the Ramapo fault that show high-angle thrust faulting along roughly northeast trending faults, implying a northwest maximum compressive stress direction; and (3) earthquake hypocenters from within 10 km of the Ramapo fault surface trace that align with a dip of approximately 60°.

Despite the strong insistence from earlier authors that there was little doubt the Ramapo fault is active, numerous studies (Kafka, 1985) (Quittmeyer, 1985) (Seborowski, 1982) (Thurber, 1985) post-dating those of Aggarwal and Sykes (Aggarwal, 1978) and Page et al. (Page, 1968) presented revised analyses of the seismicity that contradict the earlier work and clearly demonstrate that there is considerable uncertainty as to whether or not slip on the Ramapo and related faults is causing the recorded seismicity. Seborowski et al. (Seborowski, 1982) analyzed a sequence of aftershocks in 1980 near the northern end of the Ramapo fault close to Annsville, NY (Figure 2.5-213). Seborowski et al. (Seborowski, 1982) demonstrated that the alignment of these earthquakes and their composite focal mechanism suggest thrusting on a north-northwest trending fault plane. This observation led Seborowski et al. (Seborowski, 1982) to conclude that their observations are not consistent with the conclusion of Aggarwal and Sykes (Aggarwal, 1978) that the Ramapo fault is active because their slip direction and

corresponding maximum compressive stress direction is perpendicular to that hypothesized by Aggarwal and Sykes (Aggarwal, 1978).

Quittmeyer et al. (Quittmeyer, 1985) analyzed another earthquake sequence that occurred in 1983 approximately 7 miles from the sequence analyzed by Seborowski et al. (Seborowski, 1982) and also reanalyzed one of the earthquakes used by Aggarwal and Sykes (Aggarwal, 1978) explicitly to address the discrepancy between the expected slip directions, and thus maximum compressive stress directions, of the Aggarwal and Sykes (Aggarwal, 1978) and Seborowski et al. (Seborowski, 1982) studies. Quittmeyer et al. (Quittmeyer, 1985) demonstrated two main points: (1) a composite fault plane solution for the 1983 earthquake sequence indicates thrust faulting along faults striking northwest with a maximum compressive stress direction oriented to the northeast; and (2) the earthquake analyzed by Aggarwal and Sykes (Aggarwal, 1978) has a non-unique fault plane solution that could be consistent with either the results of Aggarwal and Sykes (Aggarwal, 1978) or consistent with the fault plane solution for the 1983 earthquake sequence. Based on these observations, Quittmeyer et al. (Quittmeyer, 1985) hypothesized the maximum compressive stress direction is directed roughly northeast and implied that the Ramapo fault is not likely a source of earthquakes within the region.

Kafka et al. (Kafka, 1985) presented a revised and extended seismicity catalog for the New York - New Jersey area surrounding the Ramapo fault region extending from 1974 to 1983. Kafka et al. (Kafka, 1985) described this compilation as an improvement over previous catalogs because the increased robustness of the network during that timeframe provides more accurate earthquake locations and uniform magnitude estimates. During this time period, Kafka et al. (Kafka, 1985) recorded a total of 61 earthquakes, all with magnitudes less than or equal to mbLg 3.0. Assuming that their earthquake catalog is complete down to magnitudes of mbLg > 2.0, Kafka et al. (Kafka, 1985) reported that 7 out of 15 earthquakes occur within 10 mi (6 km) of the Ramapo fault. Kafka et al. (Kafka, 1985) describe the remaining earthquakes as occurring around the outside of the Newark basin. Importantly, Kafka et al. (Kafka, 1985) concluded that while "much emphasis was placed on the significance of the Ramapo fault and its relationship to seismicity" (page 1279), the other seismicity occurring throughout the region suggests that "the geologic structures associated with most (if not all) earthquakes in this region are still unknown" (page 1285). In a later publication in which Kafka and Miller (Kafka, 1996) analyze updated seismicity with respect to geologic structures, Kafka and Miller (Kafka, 1996) further discredit the association between seismicity and the Ramapo fault by saying, "…the currently available evidence is sufficient to rule out … a concentration of earthquake activity along the Ramapo fault" (page 83).

Thurber and Caruso (Thurber, 1985) derived new, one- and three-dimensional crustal velocity models of the upper crust in the region of the northern Ramapo fault to provide better earthquake locations in that area. These new velocity models are considered improvements over those used in previous studies (e.g., Aggarwal, 1978). The new models resulted in some changes in depths for the 15 earthquakes examined by Thurber and Caruso (Thurber, 1985). Based on their work, Thurber and Caruso (Thurber, 1985) concluded that: (1) there are significant lateral velocity variations within the region surrounding the Ramapo fault that can impact earthquake locations made using simple velocity models; and (2) "the Ramapo fault proper is not such a salient seismic feature in New York State, unlike the findings of Aggarwal and Sykes" (page 151). As with the Quittmeyer et al. (Quittmeyer, 1985), Seborowski et al. (Seborowski, 1982), and Kafka et al. (Kafka, 1985) studies, these conclusions of Thurber and Caruso (1985) indicate that there is considerable uncertainty surrounding the potential activity of the Ramapo fault.

Primarily triggered by the seismological suggestions that the Ramapo fault is active, geological investigations also were conducted to look for evidence of Quaternary slip on the Ramapo fault. The primary researcher involved in these efforts was Nicholas Ratcliffe of the U.S. Geological Survey. Ratcliffe and his colleagues' work consisted of detailed geologic mapping, seismic reflection profiling, petrographic analysis, borings and core analysis along much of the Ramapo fault and its corollary northern and southern extension (Ratcliffe, 1980) (Ratcliffe, 1983) (Ratcliffe, 1985a) (Ratcliffe 1985b) (Ratcliffe 1986a) (Ratcliffe 1986b) (Ratcliffe 1988) (Ratcliffe 1992). Much of Ratcliffe's work was explicitly focused on investigating the potential relationship between the Ramapo fault and the seismicity that had been noted in the surrounding region (Aggarwal, 1978). The primary conclusions of the cumulative work of Ratcliffe and his colleagues' with respect to the potential for Quaternary slip on the Ramapo fault are:

- The most recent episodes of slip along the Ramapo fault, as determined from rock core samples taken across the fault, were in a normal sense with some along-strike slip motion (i.e., oblique normal faulting). Ratcliffe and others concluded that the evidence for extension across the fault as the most recent slip and the lack of compression (i.e., thrust faulting), as would be required in the modern day stress field (Zoback, 1980) (Zoback, 1989), is evidence that the Ramapo fault has not been reactivated since the latest episode of extension in the Mesozoic.

- The Ramapo fault generally has a dip that is less than that inferred from the earthquake epicenters of Aggarwal and Sykes (Aggarwal, 1978), with the exception of the northernmost end of the fault where the dip measured from borings is approximately 70°. The implication of this observation is that earthquakes near the Ramapo fault hypothesized as being due to slip on the Ramapo fault are more likely occurring within the Proterozoic footwall rocks of the Ramapo fault.

Ratcliffe and his colleagues' results provide additional evidence of the uncertainty with respect to the potential activity of the Ramapo fault because they found positive evidence for a lack of slip along the fault since the Mesozoic.

A fieldtrip guidebook of Kafka et al. (Kafka, 1989) for the New York region briefly discusses geomorphic evidence of the Ramapo fault including valley tilting, concentrations of terraces on only one valley side, and tributary offsets as evidence of Quaternary activity along the Ramapo fault. The use of these observations of Kafka et al. (Kafka, 1989) as evidence supporting Quaternary activity of the Ramapo fault should be treated cautiously based on the following:

- Kafka et al. (Kafka, 1989) present no data or evidence supporting these observations;

- Some of the noted geomorphic features may be older than Quaternary in age; and

- The observations themselves are not necessarily positive evidence of seismogenic, Quaternary faulting.

Newman et al. (Newman, 1987) (Newman, 1983) also presents observations that they interpret as evidence of Quaternary activity along the Ramapo fault. In their studies, Newman et al. (Newman, 1987) (Newman, 1983) constructed marine transgression curves based on radiocarbon dating of peat deposits for a series of tidal marsh sites along the Hudson River where it crosses the Ramapo fault. A total of eleven sites were investigated by Newman et al. (Newman, 1987), six of which were within the Ramapo fault zone as it crosses Hudson River. Of the six sites within the Ramapo fault zone, Newman et al. (Newman, 1987) report that three of the sites show a discontinuity in transgression curves that they conclude reflects Holocene

normal faulting within the Ramapo fault zone. These observations and conclusions of Newman et al. (Newman, 1987) (Newman, 1983) are questionable with respect to the argument for Quaternary faulting along the Ramapo fault because:

- There is considerable uncertainty in the radiocarbon and elevation data used to develop the transgression curves that was not clearly taken into account in testing the faulting or no faulting hypotheses;
- The sense of motion indicated by the transgression curves (normal faulting) is contrary to the current state of stress (reverse faulting is expected);
- Trenching studies across the Ramapo fault have not revealed any evidence of Quaternary faulting (Ratcliffe, 1990) (Stone, 1984); and
- If the inferred offsets within the transgression curves are from fault movement, there is no evidence that the movement could have been accumulated through a seismic slip).

Finally, in an abstract for a regional Geological Society of America meeting, Nelson (Nelson, 1980) reported the results of pollen analysis taken from a core adjacent to the Ramapo fault near Ladentown, NY (Figure 2.5-213). In the brief abstract Nelson (Nelson, 1980) reports that the pollen history can be interpreted as either a "continuous, complete Holocene pollen profile suggesting an absence of postglacial seismicity along the fault" or as a pollen profile with a reversal, potentially suggesting a disruption of the infilling process caused by faulting. In summarizing his work, Nelson (Nelson, 1980) concludes that, "the pollen evidence is equivocal but certainly not strongly suggestive of seismicity."

More recently, another reanalysis of the seismicity within the region surrounding the Ramapo fault has been conducted by Sykes et al. (Sykes, 2008), who compiled a seismicity catalog extending from 1677 through 2006 for the greater New York City - Philadelphia area. This catalog contains 383 earthquakes occurring within parts of New York, Connecticut, Pennsylvania, and New Jersey (Figure 2.5-213). Of these 383 earthquakes, those occurring since 1974 are thought to have the best constraints on location due to the establishment of a more robust seismograph network at that time. Sykes et al. (Sykes, 2008) claim that one of the striking characteristics of their seismicity catalog is the concentration of seismicity within what they refer to as the Ramapo Seismic Zone (RSZ), a zone of seismicity approximately 7.5 mi (12 km) wide extending from the Ramapo fault to the west and from northern New Jersey north to approximately the Hudson River (Figure 2.5-213). The RSZ defined by Sykes et al. (Sykes, 2008) is approximately 200 mi (320 km) from the CCNPP site. All of the instrumentally located earthquakes within the RSZ have magnitudes less than mb 3.0 (Sykes, 2008). The only earthquake with mb > 3.0 is the historical mb 4.3 earthquake of 30 October 1783. However, uncertainty in the location of this earthquake is thought to be as much as 100 km (62 mi) (Sykes, 2008) raising significant suspicion as to whether the event occurred within the RSZ given the small extent of the RSZ relative to the location uncertainty.

From analyzing cross sections of the earthquakes, Sykes et al. (Sykes, 2008) concluded that the earthquakes within the RSZ occur within the highly deformed middle Proterozoic to early Paleozoic rocks to the west of the Mesozoic Newark basin and not the Ramapo fault proper. Figure 2.5-214 shows the Sykes et al. (Sykes, 2008) seismicity from the box in Figure 2.5-213 plotted along a cross section perpendicular to the Ramapo fault with the range of expected dips for the Ramapo fault (approximately 45^{o} near the south end and 70^{o} near the north end) (Ratcliffe, 1980) (Ratcliffe, 1985a) (Sykes, 2008) specifically noted that, with the exception of three earthquakes with magnitudes less than or equal to mb 1.0 that are poorly located, earthquake hypocenters are almost vertically aligned beneath the surface trace of the Ramapo

fault and not aligned with the Ramapo fault at depth (Figure 2.5-214). Instead of associating the earthquakes with the Ramapo fault, Sykes et al. (Sykes, 2008) attributed the observed seismicity within the RSZ to minor slip events on numerous small faults within the RSZ. However, neither Sykes et al. (Sykes, 2008), nor any other researchers (Kafka, 1985) (Wheeler, 2001) (Wheeler, 2005) (Wheeler, 2006) (Wheeler, 2008), have identified distinct faults on which they believe the earthquakes may be occurring thus preventing the characterization of any potentially active faults. Also, Sykes et al. (Sykes, 2008) only vaguely described the geometry of the RSZ and did not provide robust constraints on the geometry of the zone, the orientation of the potentially active faults they interpret to exist within the zone, or the maximum expected magnitude of earthquakes within the zone.

A good summary of the current state of knowledge concerning the capability of the Ramapo fault is provided by Wheeler (Wheeler, 2006). While the Wheeler (Wheeler, 2006) paper did not consider the results of the Sykes et al. (Sykes, 2008) study, Wheeler's (Wheeler, 2006) comments accurately describe the current state of knowledge concerning the capability of the Ramapo fault of RSZ. Wheeler (Wheeler, 2006) states that: "No available arguments or evidence can preclude the possibility of occasional small earthquakes on the Ramapo fault or other strands of the fault system, or of rarer large earthquakes whose geologic record has not been recognized. Nonetheless, there is no clear evidence of Quaternary tectonic faulting on the fault system aside from the small earthquakes scattered within and outside the Ramapo fault system" (page 178). The implication for the CCNPP Unit 3 site is that there is no new information to suggest that the existing characterizations for the Ramapo fault do not adequately capture the current technical opinion with respect to the seismic hazard posed by the Ramapo fault or RSZ.

2.5.1.1.4.4.5.5 Kingston Fault

The Kingston fault is located in central New Jersey, approximately 175 mi (282 km) northeast of the CCNPP site (Figure 2.5-31 and Figure 2.5-219). The Kingston fault is a 7 mi (11 km) long north to northeast-striking fault that offsets Mesozoic basement and is overlain by Coastal Plain sediments (Owens, 1998) (Figure 2.5-220). Stanford (Stanford, 1995) use borehole and geophysical data to interpret a thickening of as much as 80 ft (24 m) of the Pliocene Pensauken Formation across the surface projection of the Kingston fault (Figure 2.5-221). Stanford (Stanford, 1995) interprets the thickening of the Pensauken Formation as a result of faulting rather than fluvial processes. Geologic cross sections prepared by Stanford (Stanford, 2002) do not show that the bedrock-Pensauken contact is vertically offset across the Kingston fault (Figure 2.5-221). Therefore, it seems reasonable to conclude that faulting of the Pensauken Formation is not required and that apparent thickening of the Pliocene gravels may represent a channel-fill from a pre-Pliocene channel (Figure 2.5-221). Wheeler (Wheeler, 2006) reports that the available geologic evidence does not exclusively support a fault versus a fluvial origin for the apparent thickening of the Pensauken Formation. Wheeler (Wheeler, 2005) assigns the Kingston fault as a Class C feature based on a lack of evidence for Quaternary deformation. Given the absence of evidence for Quaternary faulting and the presence of undeformed Pleistocene glaciofluvial gravels overlying the fault trace, we conclude that the fault is not a capable tectonic feature.

2.5.1.1.4.4.5.6 New York Bight Fault

On the basis of seismic surveys, the New York Bight fault is characterized as an approximately 31 mile (50 km) long, north-northeast-striking fault, located offshore of Long Island, New York (Hutchinson, 1985) (Schwab, 1997a) (Schwab, 1997b) (Figure 2.5-31 and Figure 2.5-219). The fault is located about 208 mi (335 km) northeast of the CCNPP site. Seismic reflection profiles indicate that the fault originated during the Cretaceous and continued intermittently with

activity until at least the Eocene. The sense of displacement is northwest-side down and displaces bedrock as much as 357 ft (109 m), and Upper Cretaceous deposits about 236 ft (72 m) (Hutchinson, 1985). High-resolution seismic reflection profiles that intersect the surface projection of the fault indicate that middle and late Quaternary sediments are undeformed within a resolution of 3 ft (1 m) (Hutchinson, 1985) (Schwab, 1997a) (Schwab, 1997b).

The Mesozoic New York Bight basin is located immediately east of the New York Bight fault (Hutchinson, 1985) (Figure 2.5-10). On the basis of seismic reflection data, the basin is interpreted to be structurally controlled by block faulting in the crystalline basement accompanied by syn-rift Mesozoic sedimentation. There is no evidence that the basin bounding faults extend into the overlying Cretaceous sediments. Although not explicitly stated in the published literature (Hutchinson,1985)(Schwab, 1997a) (Schwab, 1997b), the association of the New York Bight fault along the western edge of the New York Bight basin suggests late Cretaceous through Eocene reactivation of the early Mesozoic basin bounding fault.

Only a few, poorly located earthquakes are spatially associated with the New York Bight fault (Wheeler, 2006) (Figure 2.5-31 and Figure 2.5-219). Wheeler (Wheeler, 2006) defines the fault as a feature having insufficient evidence to demonstrate that faulting is Quaternary and assigns the New York Bight fault as a Class C feature. Based on the seismic reflection surveys of Schwab (Schwab, 1997a) (Schwab, 1997b) and Hutchinson (Hutchinson, 1985) and the absence of Quaternary deformation, we conclude that the New York Bight fault is not a capable tectonic source.

2.5.1.1.4.4.5.7 Cacoosing Valley Earthquake Sequence

The 1993 to 1997 Cacoosing Valley earthquake sequence occurred along the eastern margin of the Lancaster seismic zone with the main shock occurring on January 16, 1994, near Reading, Pennsylvania, about 135 mi (217 km) north of the CCNPP site (Seeber, 1998) (Figure 2.5-31). This earthquake sequence also is discussed as part of the Lancaster seismic zone discussion (Section 2.5.1.1.4.5.2). The maximum magnitude earthquake associated with this sequence is an event of mbLg 4.6 (Seeber, 1998). Focal mechanisms associated with the main shock and aftershocks define a shallow subsurface rupture plane confined to the upper 1.5 mi (2.4 km) of the crust. It appears that the earthquakes occurred on a pre-existing structure striking N45°W in contrast to the typical north-trending alignment of microseismicity that delineates the Lancaster seismic zone. Seeber (Seeber, 1998) use the seismicity data, as well as the shallow depth of focal mechanisms, to demonstrate that the Cacoosing Valley earthquakes likely were caused by anthropogenic changes to a large rock quarry. Wheeler (Wheeler, 2006) defines the fault as a feature having insufficient evidence to demonstrate that faulting is Quaternary and assigns the Cacoosing Valley earthquake sequence as a Class C feature. Based on the findings of Seeber (Seeber, 1998), we interpret this earthquake sequence to be unrelated to a capable tectonic source.

2.5.1.1.4.4.5.8 New Castle County Faults

The New Castle faults are interpreted as 3 to 4 mi (4.8 to 6.4 km) long buried north and northeast-striking basement faults (Spoljaric, 1972) (Spoljaric, 1973). The faults are interpreted from structural contours of the top of Precambrian to Paleozoic crystalline basement derived from geophysical and borehole data, and define a 1 mi (1.6 km) wide, N25°E-trending graben in basement rock (Spoljaric, 1973). The faults are located in northern Delaware, near New Castle, about 97 mi (156 km) northeast of the CCNPP site (Figure 2.5-31). The graben is bounded by faults that displace the basement surface on the order of 32 to 98 ft (10 to 30 m) (Spoljaric, 1972). Spoljaric (1973) suggests that the overlying Cretaceous deposits are tilted in a direction consistent with fault deformation; however, no direct evidence is reported to indicate that the

faults extend into the Cretaceous sediments. Sbar (Sbar, 1975) evaluates a 1973 M3.8 earthquake and its associated aftershocks, and note that the microseismicity defines a causal fault striking northeast and parallel to the northeast-striking graben of Spoljaric (Spoljaric, 1973). Subsequently, subsurface exploration by the Delaware Geological Survey (McLaughlin, 2002), that included acquisition of high resolution seismic reflection profiles, borehole transects, and paleoseismic trenching, provides evidence for the absence of Quaternary faulting on the New Castle faults. Wheeler (Wheeler, 2005) characterizes the New Castle County faults as a Class C feature. Based on McLaughlin (McLaughlin, 2002) there is strong evidence to suggest that the New Castle County faults as mapped by Spoljaric (Spoljaric, 1972) are not a capable tectonic source.

2.5.1.1.4.4.5.9 Upper Marlboro Faults

The Upper Marlboro faults are located in Prince George's County, Maryland, approximately 36 mi (58 km) northwest of the CCNPP site (Figure 2.5-31). These faults were first shown by Dryden (Dryden, 1932) as a series of faults offsetting Coastal Plain sediments. The faults were apparently exposed in a road cut on Crain Highway at 3.3 mi (5.3 km) south of the railroad crossing in Upper Marlboro, Maryland (Prowell, 1983). Two faults displace Miocene and Eocene sediments and a third fault is shown offsetting a Pleistocene unit. These faults are not observed beyond this exposure. No geomorphic expression has been reported or was noticed during field reconnaissance for the CCNPP Unit 3 study. Based on a critical review of available literature, Wheeler (Wheeler, 2006) re-interprets the Upper Marlboro faults as likely related to surficial landsliding because of the very low dips and concavity of the fault planes. The Marlboro faults are classified by Crone and Wheeler (Crone, 2000) and Wheeler (Wheeler, 2006), as a Class C feature based on a lack of evidence for Quaternary faulting. Given the absence of seismicity along the fault, lack of published literature documenting Quaternary faulting, coupled with the interpretation of Crone and Wheeler (Crone, 2000) and Wheeler (Wheeler, 2006), we conclude that the Upper Marlboro faults are not a capable tectonic source.

2.5.1.1.4.4.5.10 Lebanon Church Fault

The Lebanon Church fault is a poorly-known northeast-striking reverse fault located in the Appalachian Mountains of Virginia, near Waynesboro, about 119 mi (192 km) southwest of the CCNPP site (Prowell, 1983) (Figure 2.5-31). The fault is exposed in a single road cut along U.S. Route 250 as a small reverse fault that offsets Miocene-Pliocene terrace gravels up to 5 ft (1.5 m) (Prowell, 1983). The terrace gravels overlie Precambrian metamorphic rocks of the Blue Ridge Province. However, an earlier author (Nelson, 1962) considered the gravels to be Pleistocene.

Crone and Wheeler (Crone, 2000) indicated that the offset gravel was likely colluvial in origin, based on unpublished data provided by Prowell, and concluded that it could be Quaternary in age. However, Wheeler (Wheeler, 2006) later suggested that no Quaternary movement on the fault had been demonstrated. Both Crone and Wheeler (Crone, 2000) and Wheeler (Wheeler, 2006) assigned the fault a Class C designation.

As part of this CCNPP Unit 3 study, inquiries with representatives of the Virginia Geological Survey and the USGS indicated that no new information is available for the Lebanon Church fault. Based on these discussions, as well as the existing literature on the fault and a lack of seismicity associated with the fault, it is concluded that the Lebanon Church feature is not a capable tectonic source.

2.5.1.1.4.4.5.11 Hopewell Fault

The Hopewell fault is located in central Virginia, approximately 89 mi (143 km) southwest of the CCNPP site (Figure 2.5-31). The Hopewell fault is a 30 mi (48 km) long, north-striking, steeply east-dipping reverse fault (Mixon, 1989) (Dischinger, 1987). The fault was originally named the Dutch Gap fault by Dischinger (Dischinger, 1987), and was renamed the Hopewell fault by Mixon (Mixon, 1989). The fault displaces a Paleocene-Cretaceous contact and is inferred to offset the Pliocene Yorktown Formation (Dischinger, 1987). Mixon (Mixon, 1989) extend the mapping of Dischinger (Dischinger, 1987), but include conflicting data regarding fault activity. For instance, a cross section presented by Mixon (Mixon, 1989) shows the Hopewell fault displacing undivided upper Tertiary and Quaternary units, whereas the geologic map used to produce the section depicts the fault buried beneath these units. A written communication from Newell (Wheeler, 2006) explains that the Hopewell fault was not observed offsetting Quaternary deposits and the representation of the fault in the Mixon (Mixon, 1989) cross section is an error. Thus, the Hopewell fault zone is assigned as a Class C feature because no evidence is available to demonstrate Quaternary surface deformation. Based on the written communication of Newell (Wheeler, 2006), an absence of published literature documenting Quaternary faulting, and an absence of seismicity spatially associated with the feature, we conclude that the Hopewell fault is not a capable tectonic source.

2.5.1.1.4.4.5.12 Old Hickory Faults

The Old Hickory faults are located near the Fall Line in southeastern Virginia, approximately 115 mi (185 km) south-southwest of the CCNPP site (Figure 2.5-31). Based on mining exposures of the Old Hickory Heavy Mineral deposit, the Old Hickory faults consist of a series of five northwest-striking reverse faults that offset Paleozoic basement and Pliocene Coastal Plain sediments. The northwest-striking reverse faults juxtapose Paleozoic Eastern Slate Belt diorite over the Pliocene Yorktown Formation (Berquist, 1999). Strike lengths range between 330 to 490 ft (100 to 150 m) and are spaced about 164 ft (50 m) apart. Berquist and Bailey (Berquist, 1999) report up to 20 ft (6 m) of oblique dip-slip movement on individual faults, and suggest that the faults may be reactivated Mesozoic structures. There is no stratigraphic or geomorphic evidence of Quaternary or Holocene activity of the Old Hickory faults (Berquist, 1999). Crone and Wheeler (Crone, 2000) and Wheeler (Wheeler, 2006) conclude that "no Quaternary fault is documented" and assign a Class C designation to the Old Hickory faults. Based on the absence of published literature documenting the presence of Quaternary deformation, and the absence of seismicity spatially associated with this feature, we conclude that the Old Hickory faults are not a capable tectonic source.

2.5.1.1.4.4.5.13 Stanleytown-Villa Heights Faults

The postulated Stanleytown-Villa Heights faults are located in the Piedmont of southern Virginia, approximately 223 mi (359 km) southwest of the CCNPP site (Figure 2.5-31). The approximately 660 ft long (201 m long) faults juxtapose Quaternary alluvium against rocks of Cambrian age, and reflect an east-side-down sense of displacement (Crone, 2000). No other faults are mapped nearby (Crone, 2000). Geologic and geomorphic evidence suggests the "faults" are likely the result of landsliding. Crone and Wheeler (Crone, 2000) classify the Stanleytown-Villa Heights faults as a Class C feature based on lack of evidence for Quaternary faulting. Based on the absence of published literature documenting the presence of Quaternary faulting, and the absence of seismicity spatially associated with this feature, we conclude that the Stanleytown-Villa Heights faults are not a capable tectonic source.

2.5.1.1.4.4.5.14 East Coast Fault System

The postulated East Coast fault system (ECFS) of Marple and Talwani (2000) trends N34°E and is located approximately 70 mi (113 km) southwest of the site (Figure 2.5-31). The 370 mi (595 km) long fault system consists of three approximately 125 mi (201 km) long segments extending from the Charleston area in South Carolina northeastward to near the James River in Virginia (Figure 2.5-31). The three segments were initially referred to as the southern, central, and northern zones of river anomalies (ZRA-S, ZRA-C, ZRA-N) and are herein referred to as the southern, central and northern segments of the ECFS. The southern segment is located in South Carolina; the central segment is located primarily in North Carolina. The northern segment, buried beneath Coastal Plain deposits, extends from northeastern North Carolina to southeastern Virginia, about 70 mi (113 km) southwest of the CCNPP site. Marple and Talwani (Marple, 2000) map the northern terminus of the ECFS between the Blackwater River and James River, southeast of Richmond. Identification of the ECFS is based on the alignment of geomorphic features along Coastal Plain rivers, areas suggestive of uplift, and regions of local faulting. The right-stepping character of the three segments, coupled with the northeast orientation of the fault system relative to the present day stress field, suggests a right-lateral strike-slip motion for the postulated ECFS (Marple and Talwani, 2000).

The southern segment of the fault system, first identified by Marple and Talwani (1993) as an approximately 125 mi (201 km) long and 6 to 9 mi (10 to 14.5 km) wide zone of river anomalies, has been attributed to the presence of a buried fault zone. The southern end of this segment is associated with the Woodstock fault, a structure defined by fault-plane solutions of microearthquakes and thought to be the causative source of the 1886 Charleston earthquake (Marple, 2000). The southern segment is geomorphically the most well-defined segment of the fault system and is associated with micro-seismicity at its southern end. This segment was included as an alternative geometry to the areal source for the 1886 Charleston earthquake in the 2002 USGS hazard model (Section 2.5.2) for the National Seismic Hazard Mapping Project (Frankel, 2002).

Crone and Wheeler (Crone, 2000) do not include the central and northern segments of the ECFS in their compilation of potentially active Quaternary faults. The segments also were not presented in workshops or included in models for the Trial Implementation Project (TIP), a study that characterized seismic sources and ground motion attenuation models at two nuclear power plant sites in the southeastern United States (Savy, 2002). As a member of both the USGS and TIP workshops, Talwani did not propose the northern and central segments of the fault system for consideration as a potential source of seismic activity.

Recent geologic and geomorphic analysis of stream profiles across sections of the ECFS, and critical evaluation of Marple and Talwani (Marple, 2000) for the North Anna ESP, provides compelling evidence that the northern segment of the ECFS, which lies nearest to the CCNPP site, has a very low probability of existence (Dominion, 2004b). Wheeler (Wheeler, 2005) states that although the evidence for a southern section of the ECFS is good, there is less evidence supporting Quaternary tectonism along the more northerly sections of the ECFS, and designates the northern portion of the fault system as a Class C feature.

In the Safety Evaluation Report for the North Anna ESP site, the NRC staff agreed with the assessment of the northern segment of the East Coast Fault System (ECFS-N) presented by the North Anna applicant (NRC, 2005). Based on their independent review, the NRC staff concluded that:

- "Geologic, seismologic, and geomorphic evidence presented by Marple and Talwani is questionable."

- "The majority of the geologic data cited by Marple and Talwani in support of their postulated ECFS apply only to the central and southern segments."
- There are "no Cenozoic faults or structure contour maps indicating uplift along the ECFS-N."
- "The existence and recent activity of the northern segment of the ECFS is low."

Despite the statements above, the NRC concluded that the ECFS-N could still be a contributor to the seismic hazard at the North Anna site and should be included in the ground motion modeling to determine the Safe Shutdown Earthquake. The NRC agreed with the 10% probability of existence and activity proposed in the North Anna ESP application. The results of the revised ground motion calculations indicate that the ECFS-N does not contribute to the seismic hazard at the North Anna ESP site. The CCNPP site is approximately 70 mi (113 km) northeast of the ECFS-N, or 7 mi (11 km) further away than the North Anna site is from the ECFS-N. Based on the above discussion and the large distance between the site and the ECFS-N, this fault is not considered a contributing seismic source and need not be included in the seismic hazard calculations for the CCNPP site.

Marple and Talwani (Marple, 2004) suggest a northeast extension of the ECFS of Marple and Talwani (Marple, 2000), based on existing limited geologic, geophysical and geomorphic data. Marple and Talwani (Marple, 2004) postulate that the northern ECFS may step left (northwest) to the Stafford fault system near northern Virginia and southern Maryland (Figure 2.5-31) and thus extending the ECFS along the Stafford fault up to New York. As stated in Section 2.5.1.1.4.4.4.1, the NRC (NRC, 2005) agreed with an analysis of the Stafford fault performed as part of the North Anna ESP application and states: "Based on the evidence cited by the applicant, in particular the applicant's examination of the topography profiles that cross the fault system, the staff concludes that the applicant accurately characterized the Stafford fault system as being inactive during the Quaternary Period."

2.5.1.1.4.4.5.15 Washington, D.C. Fault Zone

As previously discussed, post-Cretaceous-age faults in Washington, D.C. approach to within about 45 mi (72 km) of the CCNPP site (Figure 2.5-25). There is no clear indication of the age of the most recent movement (or movements) along this fault zone. Most data indicate that these movements likely stopped in the later Pliocene (e.g., McCartan, 1990) and this timing is largely consistent with the stress field rotations (to the northeast-southwest) described by Zoback and Zoback (Zoback, 1989a) and Zoback (Zoback, 1992). However, Southworth et al. (Southworth, 2007) have suggested that some discrete faults located near the National Zoo (near the northern mapped extent of the Washington, D.C. fault zone) have placed crystalline rocks against Quaternary sediments. Further south, near Lafayette Square, Quaternary strata show little to no displacement (Prowell, 2010). Radiocarbon dating of un-deformed (un-faulted) glacial-age marsh deposits underlying Lafayette Square suggests that no offset has occurred for at least the last 45,000 years (Knox, 1969).

It cannot be definitively determined if movement along the Washington, D.C. fault zone has occurred with any significant frequency within the Quaternary period. However, it seems unlikely that any activity has occurred within the last approximately 50,000 years. Moreover, no seismicity has been directly associated with the Washington, D.C. fault zone. It is therefore concluded that the Washington, D.C. fault zone does not represent a capable tectonic source.

2.5.1.1.4.5 Seismic Sources Defined by Regional Seismicity

Within 200 mi (322 km) of the CCNP site, two potential seismic sources are defined by a concentration of small to moderate earthquakes. These two seismic sources include the Central Virginia seismic zone in Virginia and the Lancaster seismic zone in southeast Pennsylvania, both of which are discussed below.

2.5.1.1.4.5.1 Central Virginia Seismic Zone

The Central Virginia seismic zone is an area of persistent, low level seismicity in the Piedmont Province (Figure 2.5-31). The zone extends approximately 75 mi (121 km) in a north-south direction and about 90 mi (145 km) in an east-west direction from Richmond to Lynchburg, and is centered roughly on the James River (Bollinger, 1985). The CCNPP site is located 47 to 62 mi (76 to 100 km) northeast of the northern boundary of the Central Virginia seismic zone. Seismicity in the Central Virginia seismic zone is shallow, ranging in depth from about 2 to 8 mi (3 to 13 km) (Wheeler, 1992). Numerous faults in this region have been well mapped, but no earthquakes have been linked specifically to the named faults. Coruh (Coruh, 1988) suggested that seismicity in the central and western parts of the zone may be associated with west-dipping reflectors that form the roof of a detached anti-form, while seismicity in the eastern part of the zone (near Richmond) may be related to a near-vertical diabase dike swarm of Mesozoic age. Nonetheless, seismic hazard assessments in the zone are based primarily on the locations of the earthquakes themselves (GEER, 2011).

Crone and Wheeler (Crone, 2000) and Wheeler (Wheeler, 2006) identified two paleo-liquefaction sites in the Central Virginia seismic zone, and consequently assigned a Class A designation to the zone. These liquefaction sites, located on the James and Rivanna Rivers, were first reported by Obermeier and McNulty (Obermeier, 1998) as part of a systematic search for liquefaction features within the Central Virginia seismic zone. From the close spacing of searched streams, the ages of liquefiable sediments, and the scarcity of liquefaction features, Obermeier and McNulty (Obermeier, 1998) concluded that, for at least the last 2000 to 3000 years, the zone had not had an earthquake larger than about magnitude 7. The paleo-liquefaction sites of Obermeier and McNulty (Obermeier, 1998) reflect pre-historical occurrences of seismicity within the Central Virginia seismic zone, and do not indicate the presence of a specific capable tectonic source. That is, these features cannot be linked to a specific tectonic source (i.e., a fault) and thereby only suggest the presence of a capable tectonic source somewhere within the central Virginia seismic zone.

Until recently, the largest documented earthquake within the Central Virginia seismic zone was the Modified Mercalli Intensity (MMI) VII Goochland County event, with an estimated body wave magnitude of 5.0, recorded on December 23, 1875 (Bollinger, 1985) (EPRI/DOE/NRC, 2012). A roughly comparable (M 4.3) earthquake was recorded on December 9, 2003 (Kim, 2005). The 2003 earthquake was centered near the Spotsylvania fault (discussed in Section 2.5.1.1.4.4.2.1) but the fault was not specifically implicated in the event.

On August 23, 2011, an earthquake with moment magnitude 5.8 occurred in the Central Virginia seismic zone near Mineral, VA. Its focal depth was 6 km and it was caused by reverse faulting on a plane striking northeast and dipping 50° to the east-southeast (Horton, 2012a). The earthquake was felt widely in the east-central and northeastern United States. A post-event report provided by the Geotechnical Extreme Events Reconnaissance (GEER) Association indicated that there were few instances of ground failure produced by the earthquake (GEER, 2011). Only minor liquefaction and slumping was noted along some streams, along with rockfalls, and slope movements in marginally stable slopes. Most of these observations were in the earthquake epicentral region. Green and Lasley (Green, 2012) in an independent study

indicated that only two definite liquefaction features, and one questionable feature were found near the epicenter.

Several well known (i.e., named) faults exist within the vicinity of the 2011 earthquake epicenter, including the previously discussed Spotsylvania shear zone (Section 2.5.1.1.4.4.2.1) and the Chopawamsic fault. However, Spears (Spears, 2012) and others (Hughes, 2012) have argued that these features do not appear to be related to the 2011 earthquake. Instead, structures located elsewhere in Chopawamsic terrane rocks may have contributed to the seismicity, including the Long Branch fault, and other unnamed, poorly mapped structures (Spears, 2012) (Harrison, 2012). Hughes et al. (Hughes, 2012) similarly implicated the Long Branch Fault in the recent Virginia seismicity, and suggested that the earthquake possibly occurred at its intersection with Mesozoic structures. The Long Branch fault zone defines a northeast-striking boundary between the Quantico Formation to the southeast and the Chopawamsic Formation to the northwest, and extends to a point approximately 2 mi (3 km) northwest of Stafford, Virginia.

More specifically, the August 23, 2011 Mineral, Virginia M 5.8 mainshock and the majority of associated aftershock hypocenters define a northeast-southwest trending tabular cluster centered roughly on Yanceyville, Virginia. Horton et al. (Horton, 2012a) (Horton, 2012b) have suggested a best-fit plane to this cluster (the so-named Quail fault zone) that generally strikes north 30° east, and dips 45° southeast. These aftershock hypocenters generally occurred at depths between about 1.2 and 5.0 mi (2 and 8 km) and formed a roughly 0.6 mi (1 km) thick zone that dips approximately 45° southeast (Horton, 2012b).

Horton et al. (Horton, 2012a) (Horton, 2012b) also recognized two August 23, 2011 M 5.8 earthquake aftershock hypocenter clusters to the east of the Quail fault zone. Horton et al. (Horton, 2012b) suggested that the easternmost aftershock cluster, identified as the Fredericks Hall fault, may represent a “strand” of the previously known Lakeside fault zone. The Lakeside fault zone bounds the western edge of the Mesozoic-age Farmville basin, and is generally interpreted as a down-to-the-southeast brittle normal fault (Spears, 2011). The interpreted Fredericks Hall fault zone is also located along a northeastward projection of the Paleozoic-age Little Fork Church fault (Horton, 2012a). The Little Fork Church fault effectively separates rocks of the Chopawamsic formation and Ta River metamorphic suite from adjacent pegmatitic rocks (Spears, 2011). The additional eastern cluster, located north of Cuckoo, Virginia, lies near a poorly described fault (the Ebenezer Church fault) at the eastern contact between a small granitic body and rocks of the Quantico formation (Horton, 2012b).

West of the inferred Quail fault zone, Horton et al. (Horton, 2012a; Horton, 2012b) identified a cluster of steeply dipping aftershock hypocenters that occurred late after the August 23, 2011 mainshock event. This aftershock sequence may define additional movement along some other unknown (possibly antithetic) fault (Horton, 2012b).

Additional assessments by Wolin et al. (Wolin, 2012) suggest that the focal mechanism and aftershock locations for the 2011 Mineral, Virginia earthquake are consistent with reverse faulting on a southeast dipping, northeast-southwest striking fault, and suggested that this fault trend is roughly parallel to numerous mapped structures in the Virginia Piedmont, including the Stafford fault system. It should be noted, however, that the Stafford fault was not implicated by Wolin et al. (Wolin, 2012) as a causative fault in the 2011 earthquake.

The alignment proposed by Wolin et al. (Wolin, 2012) is not inconsistent with the trace of the Long Branch fault, or the best-fit plane of the Mineral, Virginia aftershock clusters described by Horton et al. (Horton, 2012a; 2012b). Nonetheless, no definitive causative relationship between

known fault systems or suspected fault systems (e.g., the Long Branch fault or the Quail fault) and the August 23, 2011 Mineral, Virginia mainshock event and aftershocks can be established.

Additional discussion of the 2011 Mineral, Virginia earthquake and its implication for CEUS SSC seismic sources in the CCNPP site region is provided in Section 2.5.2.1.2.

2.5.1.1.4.5.2 Lancaster Seismic Zone

The Lancaster seismic zone, as defined by Armbruster and Seeber (Armbruster, 1987), of southeast Pennsylvania has been a persistent source of seismicity for at least two centuries. The seismic zone is about 80 mi (129 km) long and 80 mi (129 km) wide and spans a belt of allochthonous Appalachian crystalline rocks between the Great Valley and Martic Line about 111 mi (179 km) northwest of the CCNPP site (Figure 2.5-31). The Lancaster seismic zone crosses exposed Piedmont rocks that include thrust faults and folds associated with Paleozoic collisional orogenies. It also crosses the Newark-Gettysburg Triassic rift basin which consists of extensional faults associated with Mesozoic rifting. Most well-located epicenters in the Lancaster seismic zone lie directly outside the Gettysburg-Newark basin (Scharnberger, 2006). The epicenters of 11 events with magnitudes 3.04 to 4.61 rmb from 1889 to 1994 from the western part of Lancaster seismic zone define a north-south trend that intersects the juncture between the Gettysburg and Newark sub-basins. This juncture is a hinge around which the two sub-basins subsided, resulting in east-west oriented tensile stress. Numerous north-south trending fractures and diabase dikes are consistent with this hypothesis. It is likely that seismicity in at least the western part of the Lancaster seismic zone is due to present-day northeast-southwest compressional stress which is activating the Mesozoic fractures, with dikes perhaps serving as stress concentrators (Armbruster, 1987).

It also is probable that some recent earthquakes in the Lancaster seismic zone have been triggered by surface mining. For instance, the 16 January 1994 Cacoosing earthquake (mb 4.6) is the largest instrumented earthquake occurring in the Lancaster seismic zone (Section 2.5.1.1.4.4.5.7). This event was part of a shallow (depths generally less than 1.5 mi (2.4 km)) earthquake sequence linked to quarry activity (Seeber, 1998). The earthquake sequence that culminated in the January 16 event initiated after a quarry was shut down and the quarry began to fill with water. Seeber (Seeber, 1998) interprets the reverse-left lateral oblique earthquake sequence to be due to a decrease in normal stress caused by quarrying followed by an increase in pore fluid pressure (and decrease in effective normal stress) when the pumps were turned off and the water level increased.

Prior to the Cacoosing earthquake sequence, the 23 April 1984 Martic earthquake (mb 4.1) was the largest instrumented earthquake in the seismic zone and resembles pre-instrumental historical events dating back to the middle 18th century (Armbruster, 1987). The 1984 earthquake sequence appears centered at about 2.8 mi (4.5 km) in depth and may have ruptured a steeply east-dipping, north-to northeast-striking fault aligned subparallel to Jurassic dikes with a reverse-right lateral oblique movement, consistent with east-northeast horizontal maximum compression. These dikes are associated with many brittle faults and large planes of weakness suggesting that they too have an effect on the amount of seismicity in the Lancaster seismic zone (Armbruster, 1987). Most of the seismicity in the Lancaster seismic zone is occurring on secondary faults at high angles to the main structures of the Appalachians (Armbruster, 1987) (Seeber, 1998).

2.5.1.2 Site Geology

Sections 2.5.1.2.1 through 2.5.1.2.6 are added as a supplement to the U.S. EPR FSAR.

2.5.1.2.1 Site Area Physiography and Geomorphology

The CCNPP site area is located within the Western Shore Uplands of the Atlantic Coastal Plain Physiographic Province and is bordered by the Chesapeake Bay to the east and the Patuxent River to the west (Figure 2.5-4 and Figure 2.5-7).

The site vicinity geologic map (Figure 2.5-27 and Figure 2.5-28), compiled from the work of several investigators, indicates that the counties due east from the CCNPP site across Chesapeake Bay are underlain by Pleistocene to Recent sands. Most of the site vicinity is underlain by Tertiary Coastal Plain deposits. Quaternary to Recent alluvium beach deposits and terrace deposits are mapped along streams and estuaries. Quaternary terrace and Lowland deposits are shown in greater detail on the scale of the site area geologic map (Figure 2.5-32). Geologic cross sections in the site area indicate that the Tertiary Upland deposits are underlain by gently dipping Tertiary Coastal Plain deposits described in Section 2.5.1.2.2 (Figure 2.5-33).

The topography within 5 mi (8 km) of the site consists of gently rolling hills with elevations ranging from about sea level to nearly 130 ft (40 m) msl (Figure 2.5-4). The site is well-drained by short, ephemeral streams that form a principally dendritic drainage pattern with many streams oriented in a northwest-southeast direction (Figure 2.5-5). As shown on the site area and site topographic and geological maps, the ground surface above approximately 100 ft (30 m) msl is capped by the Upper Miocene-Pliocene Upland deposits (Figure 2.5-4, Figure 2.5-5, Figure 2.5-32, and Figure 2.5-33). These deposits occupy dissected upland areas of the Cove Point quadrangle in which the CCNPP site is located (Figure 2.5-32 and Figure 2.5-33) (Glaser, 2003a). The longest stream near the site is Johns Creek, which is approximately 3.5 mi (5.6 km) long before it drains into St. Leonard Creek (Figure 2.5-4 and Figure 2.5-34). The ephemeral stream channels near the CCNPP site are either tributary to Johns Creek or flow directly to the Chesapeake Bay. These stream channels maintain their dendritic pattern as they cut down into the underlying Choptank and St. Mary's Formations (Figure 2.5-27, Figure 2.5-32 and Figure 2.5-33).

The Chesapeake Bay shoreline forms the eastern boundary of the CCNPP site and generally consists of steep cliffs with narrow beach at their base. The cliffs reach elevations of about 100 ft (30 m) msl along the eastern portion of the site's shoreline. Narrow beaches whose width depends upon tidal fluctuations generally occur at the base of the cliffs. Field observations indicate that these steep slopes fail along nearly vertical irregular surfaces. The slope failure appears to be caused by shoreline erosion along the base of the cliffs. Shoreline processes and slope failure along Chesapeake Bay are discussed in Section 2.4.9. Approximately 2500 ft (762 m) of the shoreline from the existing CCNPP Units 1 and 2 intake structure southward to the existing barge jetty is stabilized against shoreline erosion. The CCNPP Unit 3 will be constructed at a final grade elevation of approximately 85 ft (26 km) msl and will be set back approximately 1,000 ft (305 m) from the Chesapeake Bay shoreline.

As described in Section 2.5.1.1.1, the Chesapeake Bay was formed toward the end of the Wisconsinan glacial stage, which marked the end of the Pleistocene epoch. As the glaciers retreated, the huge volumes of melting ice fed the ancestral Susquehanna and Potomac Rivers, which eroded older Coastal Plain deposits forming a broad river valley. The rising sea level covered the Continental Shelf and reached the mouth of the Bay about 10,000 years ago. Sea level continued to rise, eventually submerging the area now known as the Susquehanna River Valley prior to sea level dropping to the current elevation. The Bay assumed its present dimensions about 3000 years ago (Section 2.4.9).

2.5.1.2.2 Site Area Geologic History

The site area geologic history prior to the early Cretaceous is inferred from scattered borehole data, geophysical surveys and a synthesis of published information. These data indicate that the rock beneath the Coastal Plain sediments in the site area may be either extended or rifted exotic crystalline magmatic arc material (Glover, 1995b) or, alternatively, Triassic rift basin sediments (Benson, 1992). Although the base of the Coastal Plain section has not been penetrated directly beneath the site with drill holes, regional geologic cross sections developed from geophysical, gravity and aeromagnetic, as well as limited deep borehole stratigraphic data beyond the site area, suggest that the base of the Coastal Plain section is most likely at a depth of about 2,600 ft (792 m) beneath the site (Section 2.5.1.2.3 and Section 2.5.1.2.4).

Tectonic models discussed in Section 2.5.1.1.4.3.1 hypothesize that the crystalline basement was first accreted to the pre-Taconic North American margin during the Paleozoic along a suture that lies about 10 mi (16 km) west of the site (Klitgord, 1995) (Figure 2.5-17 and Figure 2.5-23). These models also suggest this basement is rifted crust that was thinned after accretion during the Mesozoic rifting of Pangea (Section 2.5.1.1.4.1.2). Therefore, the crystalline basement beneath the Coastal Plain sediments in the site area might consist of an accreted nappe-like block of Carolina-Chopawamsic magmatic arc terrane with windows of Laurentian Grenville basement cut by later phase normal faults (Figure 2.5-16 and Figure 2.5-17) (Klitgord, 1995).

As discussed in Section 2.5.1.1.2, Section 2.5.1.1.4.4.3, and Section 2.5.1.2.4, Mesozoic rift basins are exposed in the Piedmont Physiographic Province and are buried beneath Coastal Plain sediments (Figure 2.5-10). Whether or not the CCNPP Site is underlain by a Mesozoic basin (e.g., the Queen Anne Basin) preserved beneath the thick Coastal Plain section is unclear. The available data in the site area include only regional gravity and aeromagnetic data that allow multiple (often contradictory) interpretations of the location of a basin at or near the CCNPP Site beneath the Coastal Plain sediments. For example, Horton (1991) (Figure 2.5-9 and Figure 2.5-16) and Benson (1992) (Figure 2.5-10) show the CCNPP site underlain by the Mesozoic Queen Anne basin, whereas Schlische (1990) (Figure 2.5-22) and Withjack (1998) (Figure 2.5-10) do not show a Mesozoic basin beneath the site. There are no deep boreholes or seismic lines that allow for a definitive interpretation of the presence, geometry, or thickness of a Mesozoic rift basin beneath the CCNPP site. See Section 2.5.1.1.4.4.3 for further discussion regarding the Queen Anne basin.

During the early Cretaceous, sands, clays, sandy clays, and arkosic sands of the Arundel/ Patuxent Formations (undivided) were deposited on the crystalline basement in a continental and fluviatile environment. Individual beds of sand or silt grade rapidly into sediments with different compositions or gradations, both vertically and horizontally, which suggests they were deposited in alluvial fan or deltaic environments. Clay layers containing carbonized logs, stumps and other plant remains indicate the existence of quiet-water, swamp environments between irregularly distributed stream channels. Thicker clays near the top of this unit in St. Mary's County are interpreted to indicate longer periods of interfluvial quiet water deposition (Hansen, 1984).

The overlying beds of the Patapsco Formation are similar to the deposits in the Arundel/ Patuxent (undivided) formations and consist chiefly of materials derived from the eroded crystalline rocks of the exposed Piedmont to the west and reworked Lower Cretaceous sediments. These sediments were deposited in deltaic and estuarine environments with relatively low relief. The Upper Cretaceous Raritan Formation appears to be missing from the site area due either to non-deposition or erosion on the northern flank of the structurally positive Norfolk Arch.

The Magothy Formation represents deposits from streams flowing from the Piedmont and depositing sediments in the coastal margins of the Upper Cretaceous sea. Subsequent uplift and tilting of the Coastal Plain sediments mark the end of continental deposition and the beginning of a marine transgression of the region. This contact is a regional unconformity marked in places by a basal layer of phosphatic clasts in the overlying Brightseat Formation.

During the Early Paleocene Epoch, the Brightseat Formation marks a marine advance in the Salisbury embayment (Ward, 2004). Uplift or sea level retreat is indicated by the burrowed contact (unconformity) of the Brightseat Formation with the overlying Aquia Formation. The marine Aquia Formation which is noted for its high glauconite content and shell beds was deposited in a shoaling marine environment indicated by a generally coarsening upward lithology (Hansen, 1996). A mix of light-colored quartz grains and greenish to blackish glauconite grains and iron staining indicated the change to a sandbank facies in the upper Aquia formation (Hansen, 1996). A marine transgression during the Late Paleocene/Early Eocene into the central portion of the Salisbury Embayment deposited the Marlboro Clay (Ward, 2004). During the Early Eocene, a moderately extensive marine transgression deposited the Potopaco Member of the Nanjemoy Formation. A subsequent transgression deposited the Woodstock Member of the Nanjemoy Formation (Ward, 2004). The most extensive marine transgression during the middle Eocene resulted in the deposition of the Piney Point Formation (Ward, 2004). The site area may have been emergent during the Oligocene as the Late Oligocene Old Church Formation indicates sea level rise and submergence to the north and south of the site area (Ward, 2004). A brief regression was followed by nearly continuous sedimentation in the Salisbury Embayment punctuated by short breaks, resulting in a series of thin, unconformity-bounded beds (Ward, 2004). A series of marine transgressions into the Salisbury Embayment during the Miocene produced the Calvert, Choptank and St. Mary's Formations. Pliocene and Quaternary geologic history is discussed in Section 2.5.1.2.1.

2.5.1.2.3 Site Area Stratigraphy

The CCNPP site area is located on Coastal Plain sediments ranging in age from Lower Cretaceous to Recent, which, in turn, were deposited on the pre-Cretaceous basement. As discussed above in Section 2.5.1.2.2, there is uncertainty regarding whether Mesozoic rift basin deposits underlie the Coastal Plain sediments or whether the Coastal Plain sediments are deposited directly over extended crystalline basement. Figure 2.5-36 is a site-specific stratigraphic column based on correlations by Hansen (Hansen, 1996), Achmad and Hansen (Achmad, 1997) and Ward and Powars (Ward, 2004).

Site specific information on the stratigraphy underlying the CCNPP site is constrained by the total depths of the various borings advanced by site investigators over the years. Figure 2.5-35 shows the locations of the various borings at the site and identifies those completed as either water supply wells or observation wells based on the 2007 drilling program and the plot plan at that time. Many of these borings were drilled to 200 ft (61 m) in total depth; two were advanced to a total depth of 400 ft (122 m). Figure 2.5-92 includes the additional boring locations based on the 2008 drilling program. Only a few scattered borings have been advanced below the Aquia Formation (Figure 2.5-13)(Hansen, 1986). The deepest boring known to have been advanced at the site is CA-Ed 22 which was drilled to a total depth of 789 ft (240 m) and completed as a water supply well in 1968 (Hansen, 1996). This boring penetrates the full Tertiary stratigraphic section and intersects the contact between the Tertiary and the Cretaceous section at the base of the Aquia Formation.

The closest boring which advances to pre-Cretaceous bedrock is approximately 13 mi (21 km) south of the site at Lexington Park in St. Mary's County, (Figure 2.5-11) (Hansen, 1986). This boring cored a Jurassic diabase dike that may have intruded either Triassic rift-basin deposits or

extended crystalline basement (Section 2.5.1.1.3). The few other borings that have reached basement rock near the site are widely scattered (Figure 2.5-11) but the majority indicates that the crystalline basement beneath the site area is likely to be similar to the schists and gneisses found in the Piedmont Physiographic Province approximately 50 mi (80 km) to the west (Figure 2.5-1). Alternatively, this crystalline basement might have been accreted to the exposed Piedmont as a result of continental collision during a Paleozoic orogeny (Section 2.5.1.1.1.4 and Section 2.5.1.2.2).

Coastal Plain sediments were deposited in a broad basement depression known as the Salisbury Embayment extending from eastern Virginia to southern New Jersey (Figure 2.5-12) (Ward, 2004). These sediments were deposited during periods of marine transgression/ regression and exhibit lateral and vertical variation in both lithology and texture.

2.5.1.2.3.1 Lower Cretaceous Potomac Group and pre-Potomac sediments

As discussed in Section 2.5.1.1.3, Hansen and Wilson (Hansen, 1984) assign the lowermost 30 ft (9 m) of the Lexington Park well (SM-Df 84), 13 mi (21 km) south of the CCNPP site (Figure 2.5-11) (Hansen, 1986), to the Waste Gate formation. These sediments are described as gray silts and clays, interbedded with fine to medium silty fine to medium sands. Although these sediments might correlate with the Waste Gate Formation identified in a well in Crisfield, Maryland (Do-CE 88), east of the Chesapeake Bay (Figure 2.5-11), there is no direct evidence indicating whether this unit occurs beneath the CCNPP site.

The Potomac Group is comprised of a sequence of interbedded sands and silty to fine sandy clays. Because this formation was not encountered by any borings drilled at the CCNPP site, the description of these units is based on published data (Hansen, 1984) (Achmad, 1997). Regionally, the Potomac Group consists of, from oldest to youngest, the Patuxent Formation, the Arundel Formation and the Patapsco Formation. These units are considered continental in origin and are in unconformable contact with each other.

The Lower Cretaceous Patuxent Formation consists of a sequence of variegated sands and clays which form a major aquifer in the Baltimore area, approximately 50 mi (80 km) up-dip from the site, but which have not been tested in the vicinity of the site. The nearest well intercepting the Patuxent is approximately 13 mi (21 km) south of the site and here the formation contains much less sand than is found in the upper part of the Potomac Group. The Patuxent is approximately 600 to 700 ft (182 m to 213 m) thick and is overlain by the Arundel/Patapsco formations (undivided)

In the Baltimore area, the Arundel Formation consists of clays which are brick red near the Fall Line. Further down-dip toward the southeast, the color changes to gray and this unit is difficult to separate in the subsurface from those clays present in the underlying Patuxent and overlying Patapsco formations. Consequently, the Arundel and the Patuxent are often undivided (Hansen, 1984) in the literature and referred as the Arundel/Patuxent formations (undivided). Hansen and Wilson (Hansen, 1984) describe the upper portion of the Arundel/ Patuxent formations (undivided) as variegated silty clay with thin very fine sand and silt interbeds that may be as thick as 150 to 200 ft (46 to 61 m) beneath the CCNPP site (Figure 2.5-13). The Arundel Formation is not recognized in southern Maryland (Hansen, 1996).

2.5.1.2.3.2 Upper Cretaceous Formations

The Patapsco formation is the uppermost unit in the Potomac Group and consists of gray, brown and red variegated silts and clays interbedded with lenticular, cross-bedded clayey sands and minor gravels. This formation is a major aquifer near the Fall Line in the Baltimore

area, but the Patapsco is untested near the CCNPP site. The thickness of the Patapsco Formation based on regional correlations is 1,000 to 1,100 ft thick beneath the CCNPP site.

The Mattaponi (?) formation described as overlying the Potomac group in Hansen and Wilson (Hansen, 1984) is no longer recognized by the Maryland Geological Survey. The section formerly assigned to the Mattaponi (?) has been included within the Patapsco Formation.

The Magothy Formation unconformably overlies the Patapsco Formation beneath the site. The Magothy is comprised chiefly of pebbly, medium coarse sand, although there are clayey portions in the upper part (Achmad, 1997). This formation is much thinner at the site than further north in Calvert County and pinches out within a few mi to the south (Achmad, 1997). The Monmouth and Matawan formations have not been differentiated from the Magothy Formation in the site area.

2.5.1.2.3.3 Tertiary Formations

The earliest Tertiary sediments beneath the site are assigned to the Lower Paleocene Brightseat Formation, a thin dark gray sandy clay identified in the deepest boring (CA-Ed 22) at the site as the Lower Confining Unit (Figure 2.5-13). The Brightseat Formation is identified in the gamma log as a higher than normal gamma response below the Aquia sand. According to Ward and Powars (Ward, 2004) the Brightseat Formation marks a marine advance in the Salisbury Embayment and occurs principally in the northeastern portion of the Embayment. This stratigraphic unit was reached by the water supply well CA-Ed 22 in 1968 (Figure 2.5-13). Achmad and Hansen (Achmad, 1997) describe the Brightseat Formation as approximately 10 ft (3 m) thick consisting mainly of very fine sand and clay with a bioturbated fabric. The absence of a bioturbated contact with the underlying beds suggests an unconformable contact.

The Aquia Formation unconformably overlies the Brightseat Formation and consists of clayey, silty, very shelly glauconitic sand (Ward, 2004). Microfossil study has placed the Aquia in the upper Paleocene. In the type section, the Aquia Formation is divided into two members, the Piscataway Creek and the Paspotansa, but at the CCNPP site, these members are not differentiated. Achmad and Hansen (Achmed, 1997) describe the Aquia Formation as approximately 150 ft (46 m) thick. The sand becomes fine-grained in the lower 50 ft (15 m) of the formation.

The Marlboro clay is a silvery-gray to pale-red plastic clay interbedded with yellowish-gray to reddish silt occurring at the base of the Nanjemoy Formation (Ward, 2004). Achmad and Hansen (1997) describe approximately 10 ft (3 m) of clay with thin, indistinct laminae of differing colored silt. Its contact with the underlying Aquia Formation is somewhat gradational while the contact between the Marlboro and the overlying Nanjemoy appears to be sharp indicating that the Nanjemoy unconformably overlies the Marlboro. Microfossil studies indicate the presence of a mixture of very late Paleocene and very early Eocene flora. Based on geophysical logs from CA-Ed 22, the Marlboro clay appears to be approximately 15 ft (4.6 m) thick beneath the CCNPP site (Figure 2.5-13).

At the CCNPP site, the Nanjemoy Formation is divided into the Potapaco and Woodstock members between the overlying Piney Point Formation and the underlying Marlboro clay. The Nanjemoy Formation is described as olive black, very fine grained, well-sorted silty glauconitic sands (Ward, 2004). Based on electric log data, the thickness of the Nanjemoy Formation beneath the CCNPP site is approximately 180 ft (55 m). About 80 ft (24 m) of this unit was penetrated by CCNPP Unit 3 borings, B-301 and B-401 (Figure 2.5-37 and Figure 2.5-38), drilled during the subsurface investigation.

The Piney Point Formation is a thin glauconitic sand and clay unit unconformably overlying the Nanjemoy formation. According to Achmad and Hansen (Achmad, 1997), the Piney Point is approximately 20 ft (6 m) thick at the CCNPP site and extends from about the middle of Calvert County, north of the CCNPP site, toward the south to beyond the Potomac River; increasing in thickness to approximately 130 ft (40 m) at Point Lookout at the confluence of the Potomac River and Chesapeake Bay. Formerly considered late Eocene in age, the Piney Point is assigned to the middle Eocene (Achmad, 1997) (Ward, 2004). The unit has a distinctive natural gamma signature associated with the presence of glauconite and is a useful marker bed.

This distinctive natural gamma signature is present in boring B-301 at a depth of 302 ft (92 m) (205 ft (62 m) msl). This interval is described as dark greenish gray, dense clayey sand grading to very dense silty sands in their bottom 25 ft (8 m). Boring B-401 encountered the Piney Point Formation at a depth of 278 ft (85 m) (-181 ft (-55 m) msl).

According to Hansen (Hansen, 1996), the top of the Piney Point Formation occurs at an approximate elevation of -200 ft (-61 m) msl in the CCNPP site area (Figure 2.5-14). The absence of late Eocene and early Miocene sediments indicate the absence of deposition or erosion for millions of years. A structure contour map of the top of the Piney Point Formation shows an erosion surface that dips gently toward the southeast (Figure 2.5-14).

The Chesapeake Group at the CCNPP site is divided into three marine formations which are, from oldest to youngest, the Calvert Formation, the Choptank Formation and the St. Mary's Formation. These units are difficult to distinguish in the subsurface due to similar sediment types and are undivided at the CCNPP site (Glaser, 2003c). Achmad and Hansen (Achmad, 1997) indicate that the Chesapeake Group is approximately 245 ft (75 m) thick beneath the CCNPP site, based on boring CA-Ed 22 data. Kidwell (Kidwell, 1997) states that the stratigraphic relations within this group are highly complex. Based on cross sections presented in Kidwell (Kidwell, 1997), the contact between the St. Mary's Formation and the underlying Choptank is estimated to be approximately 22 ft (7 m) deep in boring B-301 and at 10 ft (3 m) deep in B-401. The thickness of the Chesapeake Group (undifferentiated) is 280 ft in boring B-301 and 268 ft in B-401. The difference in these thicknesses and that in CA-Ed 22 is attributed to the geophysical log of the latter boring not continuing to the top of the boring and/or difference in the chosen top of the St. Mary's Formation.

Although the formational contacts within the Chesapeake Group are difficult to impossible to identify, there are several strata which are encountered in most of the CCNPP Unit 3 investigation borings. The most persistent of these is the calcite-cemented sand shown in Figure 2.5-42 and probably is one of the units Kidwell (Kidwell, 1997) interprets as the Choptank Formation.

About 20 ft below the base of this cemented sand unit as a second, but much thinner cemented sand which is identified primarily by "N" values (the sum of the blow counts for the intervals 6 to 12 in (15 to 30 cm) and 12 to 18 in (30 to 46 cm) sample intervals in a standard SPT) higher than those immediately above and below.

The base of the Chesapeake Group (Piney Point Formation) is clearly identified in the geophysical log (Figure 2.5-37 and Figure 2.5-38) by the characteristic gamma curve response. Based on the boring log, this gamma curve response appears to be related to calcite-cemented sand.

The surficial deposits consist of two informal stratigraphic units: the Pliocene-age Upland deposits and Pleistocene to Holocene Lowland deposits. The Upland deposits consist of two units deposited in a fluviatile environment. The Upland deposits are areally more extensive in

St. Mary's County than in Calvert County (Glaser, 1971). The outcrop distribution has a dendritic pattern and since it caps the higher interfluvial divides, this unit is interpreted as a highly dissected sediment sheet whose base slopes toward the southwest (Glaser, 1971) (Hansen, 1996). This erosion might have occurred due to differential uplift during the Pliocene or down cutting in response to lower base levels when sea level was lower during periods of Pleistocene glaciation.

2.5.1.2.3.4 Quarternary Formations

The Lowland deposits are considered to consist of three lithologic units. The basal unit is estimated to be 10 to 20 ft (3 to 6 m) thick and is often described as cobbly sand and gravel. This unit may represent high energy stream deposits in an alluvial environment near the base of eroding highlands to the west. The basal unit is overlain by as much as 90 ft (27 m) of bluish gray to dark brown clay that may be silty or sandy (Glaser, 1971) The uppermost of the three units consists of 10 to 30 ft (3 to 9 m) of pale gray, fairly well sorted, medium to coarse sand (Glaser, 1971). The Lowland deposits were laid down in fluvial to estuarine environments (Hansen, 1996) and are generally found along the Patuxent and Potomac River valleys and the Chesapeake Bay. These deposits occur in only a few places along the east shore of Chesapeake Bay.

Sands overlying the Chesapeake Group at the CCNPP site are mapped by Glaser (2003c) as Upland Deposits. Within the CCNPP Unit 3 power block these sands range in thickness from a feather edge in borings on the southern edge, to more than 50 ft in B-405.

Boring B-301 intersected 22 ft (7 m) of silty sand above the contact with the Chesapeake Group, while B-401 has 10 ft (3 m) of silty sand (Figure 2.5-37 and Figure 2.5-38). The sand in both borings grades into a coarser sand unit just above the contact. These sands are attributed to the Upland deposits previously mapped (Glaser, 2003c).

Terrace deposits in the CCNPP site area (Figure 2.5-32 and Figure 2.5-34) consist of interbedded light gray to gray silty sands and clay with occasional reddish brown pockets and are approximately 50 ft (15 m) thick. These units are Pliocene to Holocene in age.

Holocene deposits, mapped as Qal on the site Geologic Map, includes heterogeneous sediments underlying floodplains and beach sands composed of loose sand.

2.5.1.2.4 Site Area Structural Geology

The local structural geology of the CCNPP site area described in this section is based primarily on a summary of published geologic mapping (Cleaves, 1968) (Glaser, 1994) (McCartan, 1995) (Achmad, 1997) (Glaser, 2003b) (Glaser, 2003c), aeromagnetic and gravity surveys (Hansen, 1978) (Hittelman, 1994) (Milici, 1995) (Bankey, 2002), detailed lithostratigraphic profiles along Calvert Cliffs (Kidwell, 1988) (Kidwell, 1997), results of earlier investigations performed at the CCNPP site (BGE, 1968) (CEG, 2005), as well as CCNPP site reconnaissance and subsurface exploration performed for the CCNPP Unit 3 site investigation.

Sparse geophysical and borehole data indicate that the basement consists of exotic crystalline magmatic arc material (Hansen, 1986) (Glover, 1995b) or Triassic rift basin sedimentary rocks (Benson, 1992). Although the basement beneath the site area has not been penetrated with drill holes, regional geologic cross sections developed from geophysical, gravity and aeromagnetic, as well as limited deep borehole data from outside of the CCNPP site area, suggest that the based of the Coastal Plain section is present at a depth of approximately 2,500 ft (762 m) msl (Section 2.5.1.2.2).

Tectonic models hypothesize that the crystalline basement underlying the site was accreted to a pre-Taconic North American margin in the Paleozoic along a suture that lies about 10 mi (16 km) west of the site (Klitgord, 1995) (Figure 2.5-17 and Figure 2.5-23). The plate-scale suture is defined by a distinct north-northeast-trending magnetic anomaly that dips easterly between 35 and 45 degrees and lies about 7.5 to 9 mi (12 to 14.5 km) beneath the CCNPP site (Glover, 1995b) (Figure 2.5-17). Directly west of the suture lies the north to northeast-trending Taylorsville Basin (LeTourneau, 2003) and to the east, the postulated Queen Anne Mesozoic rift basin (Figure 2.5-9) (Benson, 1992). These rift basins are delineated from geophysical data subject to alternate interpretations and a limited number of deep boreholes that penetrate the Coastal Plain section located outside the Site Area, and generally are considered approximately located where buried beneath the Coastal Plain (Jacobeen, 1972) (Hansen, 1986) (Benson, 1992) (LeTourneau, 2003). Because the available geologic information used to constrain the basin locations is sparse, some authors, but not all, depict the CCNPP site area to be underlain by a Mesozoic basin (Klitgord, 1988) (Schlische, 1990) (Horton, 1991) (Benson, 1992) (Klitgord, 1995) (Withjack, 1998) (LeTourneau, 2003) (Figure 2.5-10, Figure 2.5-12, Figure 2.5-16, and Figure 2.5-22). However, based on a review of existing published geologic literature, there is no known basin-related fault or geologic evidence of basin-related faulting in the basement directly beneath the CCNPP site area.

Recent 1:24,000-scale mapping (Glaser, 2003b) (Glaser, 2003c) for Calvert County and St. Mary's County shows the stratigraphy at the CCNPP site area consisting of nearly flat-lying Cenozoic Coastal Plain sediments that have accumulated within the west-central part of the Salisbury Embayment (Figure 2.5-32 and Figure 2.5-33). The Salisbury Embayment is defined as a regional depocenter that has undergone slow crustal and regional downwarping as a result of sediment overburden during the Early Cretaceous and much of the Tertiary. The Coastal Plain deposits within this region of the Salisbury Embayment generally strike northeast-southwest and have a gentle dip to the southeast at angles close to or less than one to two degrees (Figure 2.5-32 and Figure 2.5-33). The gentle southerly dip of the sediments result in a surface outcrop pattern in which the strata become successively younger in a southeast direction across the embayment. The gentle-dipping to flat-lying Miocene Coastal Plain deposits are exposed in the steep cliffs along the western shoreline of Chesapeake Bay and provide excellent exposures to assess the presence or absence of tectonic-related structures.

Local geologic cross sections of the site area depict unfaulted, southeast-dipping Eocene-Miocene Coastal Plain sediments in an unconformable contact with overlying Pliocene Upland deposits (Glaser, 1994) (Achmad, 1997) (Glaser, 2003b) (Glaser, 2003c) (Figure 2.5-13, Figure 2.5-32, and Figure 2.5-33). No faults or folds are depicted on these geologic cross sections. A review of an Early Site Review report (BGE, 1977), i.e. Perryman site, and a review of the Preliminary Safety Analysis Report for the Douglas Point site (Potomac Electric Power Company, 1973), located along the eastern shore of the Potomac River about 45 mi (72 km) west-southwest of the CCNPP site, also reported no faults or folds within a 5 mi (8 km) radius of the CCNPP site. The Updated Final Safety Analysis Report for the Hope Creek site, located in New Jersey along the northern shore of Delaware Bay, also was reviewed for tectonic features previously identified within 5 mi (8 km) of the CCNPP site, yet none were identified (PSEG, 2002). Review of a seismic source characterization study (URS, 2000) for a liquidefied natural gas plant at Cove Point, about 3 mi (5 km) southeast of the site, also identified no faults or folds projecting toward or underlying the CCNPP site area.

On the basis of literature review, and aerial and field reconnaissance, the only potential structural features at and within the CCNPP site area consist of a hypothetical buried northeast-trending fault (Hansen, 1986), two inferred east-facing monoclines developed within Mesozoic and Tertiary deposits along the western shore of Chesapeake Bay (McCartan, 1995), and multiple subtle folds or inflections in Miocene strata and a postulated fault directly south of the

site (Kidwell, 1997) (Figure 2.5-25). The Hillville fault of Hansen and Edwards (Hansen, 1986) and inferred fold of McCartan (McCartan, 1995) and Kidwell (Kidwell, 1997) are described in Sections 2.5.1.1.4.4.4 and Section 2.5.3. As previously discussed in Section 2.5.1.1.4.4.4, none of these features are considered capable tectonic sources, as defined in RG 1.165, Appendix A. Each of these features is discussed briefly below. Only the Hillville fault has been mapped within or directly at the 5 mi (8 km) radius of the CCNPP site area (Figure 2.5-27, Figure 2.5-28, and Figure 2.5-32).

Hillville fault of Hansen and Edwards (Hansen, 1986): The 26 mile long Hillville fault approaches to within 5 mi (8 km) of the CCNPP site (Figure 2.5-32). The fault consists of a northeast-striking zone of steep southeast-dipping reverse faults that coincide with the Sussex-Currioman Bay aeromagnetic anomaly. The style and location of faulting are based on seismic reflection data collected about 9 mi (14 km) west-southwest of the site. A seismic line imaged a narrow zone of discontinuities that vertically separate basement by as much as 250 ft (76 m) (Hansen, 1978). Hansen and Edwards (Hansen, 1986) interpret this offset as part of a larger lithotectonic terrane boundary that separates basement rocks associated with Triassic rift basins on the west and low-grade metamorphic basement on the east. The Hillville fault may represent a Paleozoic suture zone that was reactivated in the Mesozoic and Early Tertiary. Based on stratigraphic correlation between boreholes within Tertiary Coastal Plain deposits, Hansen and Edwards (Hansen, 1986) speculate that the Hillville fault was last active in the Early Paleocene. There is no seismicity spatially associated with this feature (Figure 2.5-25) nor is there any geomorphic evidence of Quaternary deformation. The Hillville fault is not considered a capable tectonic source.

In addition, two speculative and poorly constrained east-facing monoclines along the western margin of Chesapeake Bay are mapped within the 5 mi (8 km) radius of the CCNPP site area. East-facing monoclines (McCartan, 1995): The unnamed monoclines are not depicted on any geologic maps of the area, including those by the authors, but they are shown on geologic cross sections that trend northwest-southeast across the existing site and south of the CCNPP site near the Patuxent River (McCartan, 1995) (Figure 2.5-25). East-facing monoclines are inferred beneath Chesapeake Bay at about 2 and 10 mi (3.2 to 16 km) east and southeast, respectively, from the CCNPP site. Along a northerly trench, the two monoclines delineate a continuous north-trending, east-facing monocline. As mapped in cross section and inferred in plan view, the monoclines trend approximately north along the western shore of Chesapeake Bay. The monoclines exhibit a west-side up sense of structural relief that projects into the Miocene Choptank Formation (McCartan, 1995). The overlying Late Miocene St. Mary's Formation is not shown as warped. Although no published geologic data are available to substantiate the existence of the monoclines, McCartan (McCartan, 1995) believes the distinct elevation change across Chesapeake Bay and the apparent linear nature of Calvert Cliffs are tectonically controlled. CCNPP site and aerial reconnaissance, coupled with literature review, for the CCNPP Unit 3 study strongly support a non-tectonic origin for the physiographic differences across the Chesapeake Bay (Section 2.5.1.1.4.4.4). There is no seismicity spatially associated with this feature, nor is there geologic data to suggest that the monocline proposed by McCartan (McCartan, 1995) is a capable tectonic source.

Multiple subtle folds or inflections developed in Miocene Coastal Plain strata including a postulated fault are mapped in the cliff exposures along the west side of Chesapeake Bay. Kidwell's (Kidwell, 1997) postulated folds and fault: Kidwell (Kidwell, 1988) (Kidwell, 1997) prepared over 300 lithostratigraphic columns along a 25 mi (40 km) long stretch of Calvert Cliffs that intersect much of the CCNPP site (Figure 2.5-30). When these stratigraphic columns are compiled into a cross section, they collectively provide a 25 mi (40 km) long nearly continuous exposure of Miocene, Pliocene and Quaternary deposits. Kidwell's (Kidwell, 1997) stratigraphic analysis indicates that the Miocene Coastal Plain deposits strike northeast and dip very shallow

between 1 and 2 degrees to the south-southeast, which is consistent with the findings of others (McCartan, 1995) (Glaser 2003b) (Glaser, 2003c). The regional southeast-dipping strata are disrupted occasionally by several low amplitude broad undulations developed within Miocene Coastal Plain deposits (Figure 2.5-30). The stratigraphic undulations are interpreted as monoclines and asymmetrical anticlines by Kidwell (Kidwell, 1997). In general, the undulatory stratigraphic contacts coincide with basal unconformities having wavelengths of 2.5 to 5 mi (4 to 8 km) and amplitudes of 10 to 11 ft (approximately 3 meters). Based on prominent stratigraphic truncations, the inferred warping decreases upsection into the overlying upper Miocene St. Mary's Formation. Any inferred folding of the overlying Pliocene and Quaternary fluvial deposits is poorly constrained and can be readily explained by highly variable undulating unconformities.

About 1.2 mi (1.9 km) south of the site, Kidwell (Kidwell, 1997) interprets an apparent 6 to 10 ft (2 to 3 m) elevation change in Miocene strata by extrapolating unit contacts across the approximately 0.6 mile wide (1 km) gap at Moran Landing (Figure 2.5-25 and Figure 2.5-30). Kidwell (Kidwell, 1997) also interprets a 3 to 12 (0.9 to 3.7 m) ft elevation change in younger (Quaternary (?)) fluvial material across this same gap. Because of the lack of cliff exposures at Moran Landing (only the valley margins), no direct observations of these elevation changes can be made. Kidwell (Kidwell, 1997) explains the differences in elevation of the Miocene-Quaternary stratigraphy by hypothesizing the existence of a fault at Moran Landing that strikes northeast and accommodates a north-side down sense of separation. However, the postulated fault of Kidwell (Kidwell, 1997) is not shown on any of Kidwell's (Kidwell, 1997) cross-sections, or any published geologic map (e.g., Glaser, 2003b and 2003c). In addition, Hansen (1978) does not describe faulting in seismic reflection line St. M-2 that intersects the inferred southwest projection of the hypothesized Kidwell (1997) fault (Figure 2.5-27).

The observations of offset younger gravels do not provide any evidence for the existence of a fault because the surface on which the gravels are deposited is an erosional unconformity with extensive variable relief (Kidwell, 1997). Observations made during field reconnaissance, as part of the FSAR preparation, confirmed that this contact was an erosional unconformity with significant topography north and south of Moran Landing consistent with stratigraphic representations in Kidwell (1997) profiles. The observations of several feet of elevation change in the Miocene units over several thousands of feet of horizontal distance is at best weak evidence for faulting within the Miocene deposits. For example, subtle elevation variations in Miocene strata characterized along a near-continuous exposure south of Moran Landing contain similar vertical and lateral dimensions as to the inferred elevation change across Moran Landing; however, the features are interpreted as subtle warps and not faults by Kidwell (1997). On the basis of association with similar features to the south and the lack of a continuous exposure, there is little to no evidence to support a fault across Moran Landing. The lack of evidence for Quaternary faulting within the observations made by Kidwell (Kidwell, 1997), and the results of the studies undertaken as part of the CCNPP Unit 3 COLA effort (field and aerial reconnaissance, air photo and LiDAR analysis) (see FSAR Section 2.5.3.1), collectively support the conclusion that the hypothesized fault of Kidwell (Kidwell, 1997) is not a capable fault.

There is no seismicity spatially associated with the Kidwell (Kidwell, 1997) features, the hypothetical features are not aligned or associated with gravity and magnetic anomalies, nor is there data to indicate that the features proposed by Kidwell (Kidwell, 1997) are capable tectonic sources.

The most detailed subsurface exploration of the site was performed by Dames & Moore as part of the original PSAR (BGE, 1968) for the existing CCNPP foundation and supporting structures. The PSAR study included drilling as many as 85 geotechnical boreholes, collecting downhole geophysical data, and acquiring seismic refraction data across the site. Dames and Moore (BGE,

1968) developed geologic cross sections extending from Highway 2/4 northwest of the site to Camp Conoy on the southeast which provide valuable subsurface information on the lateral continuity of Miocene Coastal Plain sediments and Pliocene Upland deposits (Figure 2.5-32 and Figure 2.5-34). Cross sections C-C′ and D-D′ pre-date site development and intersect the existing and proposed CCNPP site for structures trending north-northeast, parallel to the regional structural grain. These sections depict a nearly flat-lying, undeformed geologic contact between the Middle Miocene Piney Point Formation and the overlying Middle Miocene Calvert Formation at about –200 ft (-61 m) msl (Figure 2.5-41 and Figure 2.5-42).

Geologic sections developed from geotechnical borehole data collected as part of the CCNPP Unit 3 study also provide additional detailed sedimentological and structural relations for the upper approximately 400 ft (122 m) of strata directly beneath the footprint of the site. Similar to the previous cross sections prepared for the site, new geologic borehole data support the interpretation of flat-lying and unfaulted Miocene and Pliocene stratigraphy at the CCNPP site (Figure 2.5-39 and Figure 2.5-43). A cross section prepared oblique to previously mapped northeast-trending structures (i.e., Hillville fault), inferred folds (McCartan, 1995) (Kidwell, 1997), and the fault of Kidwell (Kidwell, 1997) shows nearly flat-lying Miocene and Pliocene stratigraphy directly below the CCNPP site. Multiple key stratigraphic markers provide evidence for the absence of Miocene-Pliocene faulting and folding beneath the site. Minor perturbations are present across the Miocene-Pliocene stratigraphic boundary, as well as other Miocene-related boundaries, however these minor elevation changes are most likely related to the irregular nature of the fluvial unconformities and are not tectonic-related.

Numerous investigations of the Calvert Cliffs coastline over many decades by government researchers, stratigraphers, and by consultants for Baltimore Gas and Electric, as well as investigations for the CCNPP Unit 3, have reported no visible signs of tectonic deformation within the exposed Miocene deposits near the site, with the only exception being that of Kidwell (Kidwell, 1997) (Figure 2.5-44). Collectively, the majority of published and unpublished geologic cross sections compiled for much of the site area and site, coupled with regional sections (Achmad, 1997) (Glaser, 2003b) (Glaser, 2003c) and site and aerial reconnaissance, indicate the absence of Pliocene and younger faulting and folding. A review and interpretation of aerial photography, digital elevation models, and LiDAR data of the CCNPP site area, coupled with aerial reconnaissance, identified few discontinuous north to northeast-striking lineaments. None of these lineaments were interpreted as fault-related, nor coincident with the Hillville fault or the other previously inferred Miocene-Pliocene structures mapped by McCartan (McCartan, 1995) and Kidwell (Kidwell, 1997) (Section 2.5.3). A review of regional geologic sections and interpretation of LiDAR data suggest that the features postulated by Kidwell (Kidwell, 1997), if present, are not moderate or prominent structures, and do not deform Pliocene and Quaternary strata. In summary, on the basis of regional and site geologic and geomorphic data, there are no known faults within the site area, with the exception of the poorly constrained Hillville fault that lies along the northwestern perimeter of the 5 mi (8 km) radius of the site (Hansen, 1986).

2.5.1.2.5 Site Area Geologic Hazard Evaluation

No geologic hazards have been identified within the CCNPP site area. No geologic units at the site are subject to dissolution. No deformation zones were encountered in the exploration or excavation for CCNPP Units 1 and 2 and none have been encountered in the site investigation for CCNPP Unit 3. Because the CCNPP Unit 3 plant site is located at an elevation of approximately 85 ft (26 m) msl and approximately 1,000 ft (305 m) from the Chesapeake Bay shoreline, it is unlikely that shoreline erosion or flooding will impact the CCNPP site.

2.5.1.2.6 Site Engineering Geology Evaluation

2.5.1.2.6.1 Engineering Soil Properties and Behavior of Foundation Materials

Engineering soil properties, including index properties, static and dynamic strength, and compressibility are discussed in Section 2.5.4. Variability and distribution of properties for the foundation bearing soils will be evaluated and mapped as the excavation is completed.

Settlement monitoring will based on analyses performed for the final design.

2.5.1.2.6.2 Zones of Alteration, Weathering, and Structural Weakness

No unusual weathering profiles have been encountered during the site investigation. No dissolution is expected to affect foundations. Any noted desiccation, weathering zones, joints or fractures will be mapped during excavation and evaluated.

2.5.1.2.6.3 Deformational Zones

No deformation zones were encountered in the exploration or excavation for CCNPP Units 1 and 2 and none have been encountered in the site investigation for CCNPP Unit 3. Excavation mapping is required during construction and any noted deformational zones will be evaluated and assessed as to their rupture and ground motion generating potential while the excavations' walls and bases are exposed. Additionally, the NRC will be notified when excavations are open for inspection. No capable tectonic sources as defined by Regulatory Guide 1.165 (NRC, 1997) exist in the CCNPP site region.

2.5.1.2.6.4 Prior Earthquake Effects

Outcrops are rare within the CCNPP site area. Studies of the CCNPP Unit 1 and 2 excavation, available outcrops, and small streams, and extensive exposures along the western shore of Chesapeake Bay have not indicated any evidence for earthquake activity that affected the Miocene deposits. The findings of a field and aerial reconnaissance (Figure 2.5-215), coupled with literature and aerial photography review, as well as discussions with experts in the assessment of paleoliquefaction in the central and eastern United States, indicate the absence of evidence for paleoliquefaction in Maryland. For example, one study entitled "Paleoliquefaction Features along the Atlantic Seaboard" by Amick (1990) searched for paleoliquefaction features in the state of Maryland. This NRC funded study performed a regional paleoliquefaction survey between Cape May, New Jersey and the Georgia/Florida state line, which included portions of the Delmarva Peninsula and Chesapeake Bay. Amick (1990) reported no liquefaction in the Delmarva Peninsula portion of the investigation (Amick, 1990) where Quaternary-aged deposits are ubiquitous. These findings are consistent with Crone (2000) and Wheeler (2005)(2006), which make no reference to paleoliquefaction features in the State of Maryland.

2.5.1.2.6.5 Effects of Human Activities

No mining operations, excessive extraction or injection of ground water or impoundment of water has occurred within the site area that can affect geologic conditions.

2.5.1.2.6.6 Site Ground Water Conditions

A detailed discussion of ground water conditions is provided in Section 2.4.12.

2.5.1.3 References

This section is added as a supplement to the U.S. EPR FSAR.

Achmad, 1997. Hydrogeology, model simulation, and water-supply potential of the Aquia and Piney Point-Nanjemoy Aquifers in Calvert and St. Mary's Counties, Maryland, Department of Natural Resources, Maryland Geological Survey Report of Investigations No. 64, 197 p., G. Achmad and H. Hansen, 1997.

Aggarwal, 1978. Earthquakes, Faults, and Nuclear Power Plants in Southern New York and Northern New Jersey, Science, Volume 200, p 425-429, Y. Aggarwal, and L. Sykes, 1978.

Amick, 1990. Paleoliquefaction features along the Atlantic Seaboard, NUREG/CR-5613, D. Amick, R. Gelinas, G. Maurath, R. Cannon, D. Moore, E. Billington, and H. Kemppmen, October, 1990.

Armbruster, 1987. The 23 April 1984 Martic Earthquake and The Lancaster Seismic Zone In Eastern Pennsylvania, Bulletin of the Seismological Society of America, Volume 77, Number 2, p 877-890, J. Armbruster, and L. Seeber, 1987.

Bailey, 1999. The Geology of Virginia: Generalized Geologic Terrane Map of the Virginia Piedmont and Blue Ridge, Physiographic Map of Virginia, College of William and Mary, Department of Geology, C. Bailey, 1999, Website: www.wm.edu/geology/virginia/phys_regions.html, Date accessed: June 25, 2007.

Bailey, 2004. Strain and vorticity analysis of transpressional high-strain zones from the Virginia Piedmont, USA, in Alsop, G.I., and Holdsworth, R.E., eds., Flow processes in faults and shear zones: Geological Society [London] Special Publication 224, p. 249-264, C. Bailey, B. Frances, and E. Fahrney, 2004.

Barineau, 2008. The Taconic Orogeny: Collisional vs. Accretionary orogenesis in the southern Appalachians. Geological Society of America Abstracts with Programs, Vol. 40, No. 4, p. 68, C. I. Barineau, 2008.

Bartholomew, 2004. Northern ancestry for the Goochland terrane as a displaced fragment of Laurentia, Geology, Volume 32; Number 8, 669-672, M. J. Bartholomew and R. P. Tollo, 2004.

BGE, 1968. Preliminary Safety Analysis Report Calvert Cliffs Nuclear Power Plant Units 1 and 2, Volume 1, Docket 50-317 and 50-318, Baltimore Gas and Electric, 1968.

BGE, 1977. Limited Early Site Review Perryman Site Suitability-Site Safety Report, Volume III, Baltimore Gas and Electric, July 1977.

Bankey, 2002. Magnetic Anomaly Map of North America, U.S. Geological Survey, 1 sheet, scale 1:10,000,000, V. Bankey, A. Cuevas, D. Daniels, C. Finn, I. Hernandez, P. Hill, R. Kucks, W. Miles, M. Pilkington, C. Roberts, W. Roest, V. Rystrom, S. Shearer, S. Snyder, R. Sweeney, and J. Velez, 2002.

Behrendt, 1983. Structural elements of the U.S. Atlantic margin delineated by the second vertical derivative of the aeromagnetic data, U.S. Geological Survey Geophysical Investigation Map GP-956, scale 1:2,500,000, J. Behrendt and M. Grim, 1983.

Benson, 1992. Map of Exposed and Buried Early Mesozoic Rift Basins/Synrift Rocks of the U.S. Middle Atlantic Continental Margin, Delaware Geological Survey Miscellaneous Map Series No. 5, R. Benson, 1992.

Benson, 2006. Internal stratigraphic correlation of the subsurface Potomac Formation, New Castle County, Delaware, and adjacent areas in Maryland and New Jersey, Delaware Geological Survey Report of Investigations No. 71, R.N. Benson, 2006.

Berquist, 1999. Late Cenozoic Reverse Faulting in the Fall Zone, Southeastern Virginia, The Journal of Geology, Volume 107, p 727-732, C. Berquist, Jr and C. Bailey, 1999.

Bobyarchick, 1979. Deformation and Metamorphism in the Hylas Zone and Adjacent Parts of the Eastern Piedmont in Virginia, Geological Society of America Bulletin, Volume 90, p 739–752, A. Bobyarchick and L. Glover, 1979.

Bobyarchick, 2007. Kinematics of the Everona Fault, Central Virginia, Paper No. 33-3, Geological Society of America Southeastern Section 56th Annual Meeting, March 29-30, 2007, Geological Society of America Abstracts with Programs, Volume 39, Number 2, p. 89, A.R. Bobyarchick, 2007.

Bollinger, 1985. Seismicity, Seismic Reflection Studies, Gravity and Geology of the Central Virginia Seismic Zone: Part I. Seismicity, Geological Society of America Bulletin, Volume 96, 49–57, G. Bollinger and M. Sibol, January 1985.

Bollinger, 1988. The Giles County, Virginia, Seismic Zone – Seismological Results and Geological Interpretations, U.S. Geological Survey Professional Paper 1355, G. Bollinger and R. Wheeler, 1988.

Bollinger, 1992. Specification of Source Zones, Recurrence Rates, Focal Depths, and Maximum Magnitudes for Earthquakes Affecting the Savannah River Site in South Carolina, U.S. Geological Survey Bulletin 2017, G. Bollinger, 1992.

Brezinski, 2004. Stratigraphy of the Frederick Valley and its Relationship to Karst Development, Maryland Geological Survey, Report of Investigations Number 75, D. Brezinski, 2004.

Bridge, 1994. Marine transgressions and regressions recorded in Middle Devonian shore-zone deposits of the Catskill clastic wedge, Geological Society of America Bulletin, Volume 106, Number 11, pgs 1440-1458, J.S. Bridge and B.J. Willis, 1994.

Brown, 1972. Structural and stratigraphic framework and spatial distribution of permeability of the Atlantic Coastal Plain, North Carolina to New York, U.S. Geological Survey Professional Paper 796, p 79, P. Brown, J. Miller, and F. Swain, 1972.

Burton, 1985. Attitude, movement history, and structure of cataclastic rocks of the Flemington fault—Results of core drilling near Oldwick, New Jersey, U.S. Geological Survey Miscellaneous Field Studies, Map MF-1781, 1 sheet, W. Burton and N. Ratcliffe, 1985.

Carr, 2000. Geologic transect across the Grenville orogen of Ontario and New York. Canadian Journal of Earth Science 37(2-3): 193–216, S. D. Carr, R. M. Easton, R. A. Jamieson and N. G. Culshaw, 2000.

Carter, 1976. Soil Survey of Louisa County, Virginia, U.S. Department of Agriculture, Soil Conservation Service, J. Carter, March 1976.

Cecil, 2004. Geology of the National Capital Region: Field trip guidebook, Stop 11; Upper Devonian and Lower Mississippian strata on Interstate 68 at Sideling Hill, Md., in Southworth, S., and Burton, W., eds., The Paleozoic record of changes in global climate and sea level; central Appalachian basin: U.S. Geological Survey Circular 1264, p 112- 116, C. B. Cecil, D. K. Brezinski, V. Skema and R. Stamm, 2004.

Cederstrom, 1957. Structural Geology of Southeastern Virginia, American Association of Petroleum Geologists Bulletin, Volume 29, D. Cederstrom, 1957.

CFR, 2007. Geologic and Seismic Siting Criteria, Title 10, Code of Federal Regulations, Part 100.23, 2007.

Chapman, 1994. Seismic Hazard Assessment for Virginia, Virginia Tech Seismological Observatory, Department of Geological Sciences, M. Chapman and F. Krimgold, February 1994.

Clark, 1992. Central Appalachian Periglacial Geomorphology, A Field Excursion Guidebook under the auspices of the 27th International Geographical Congress, Commission on Frost Action Environments, Agronomy Series Number 120, G. Clark, R. Behling, D. Braun, E. Ciolkosz, J. Kite, and B. Marsh, August 1992.

Cleaves, 1968. Geologic Map of Maryland, Maryland Geologic Survey, 1 sheet, scale 1:250,000, E. Cleaves, J. Edwards, Jr, and J. Glaser, 1968.

Cleaves, 2000. Regoliths of the Middle-Atlantic Piedmont and Evolution of a Polymorphic Landscape, Southeastern Geology, Volume 39, Numbers 3 and 4, p 199-122, E. Cleaves, October 2000.

Coblentz, 1995. Statistical Trends in the Intraplate Stress Field, Journal of Geophysical Research, Volume 100, p. 20, 245–20, 255, D. Coblentz, and R. Richardson, 1995.

Colman, 1989. Quaternary Geology of the Southern Maryland Part of the Chesapeake Bay, U.S Geological Survey, MF-1948-C, Scale 1:125,000, 3 plates, S. Colman, and J. Halka, 1989.

Colman, 1990. Ancient channels of the Susquehanna River beneath Chesapeake Bay and the Delmarva Peninsula, Geological Society of America Bulletin, Volume 102, p 1268-1279, S. Colman, J. Halka, C. Hobbs, R. Mixon, and D. Foster, 1990.

Colton, 1970. The Appalachian Basin – Its Depositional Sequences and Their Geologic Relationships, Chapter 2 in Studies of Appalachian Geology: Central and Southern by G. Fisher, F. Pettijohn, J. Reed, Jr, and K. Weaver, Interscience Publishers, G. Colton, 1970.

Conley, 1973. Geology of the Snow Creek, Martinsville East, Price, and Spray Quadrangles: Virginia Division of Mineral Resources Report of Investigations 33, p 71, J. F. Conley and W. S. Henika, 1973.

Conners, 1986. Quaternary Geomorphic Processes in Virginia, in The Quaternary of Virginia – A Symposium Volume, edited by J. McDonald and S. Bird, Virginia Division of Mineral Resources, Publication 75, J. Conners, 1986.

CEG, 2005. Calvert Cliffs Independent Spent Fuel Storage Installation, Updated Environmental Report, Volume 3, Revision 7, Constellation Energy Group, 2005.

Coruh, 1988. Seismogenic Structures in the Central Virginia Seismic Zone, Geology, Volume 16, p 748-751, C.Coruh, G. Bollinger, and J. Costain, August 1988.

Crespi, 1988. Using balanced cross sections to understand early Mesozoic extensional faulting, in A.J., Froelich and G.R. Robinson Jr. eds, Studies of the Early Mesozoic Basins of the Eastern United States, U.S. Geological Survey Bulletin no 1776, P. 220-229, J. Crespi, 1988.

Crone, 2000. Data for Quaternary Faults, Liquefaction Features, and Possible Tectonic Features in the Central and Eastern United States, east of the Rocky Mountain front, U.S. Geological Survey Open-File Report 00-260, A. Crone and R. Wheeler, 2000.

Dahlen, 1981. Isostacy and Ambient State of Stress in the Oceanic Lithosphere, Journal of Geophysical Research, Volume 86, p 7801–7807, F. Dahlen, 1981.

DM, 1973. Supplemental Geologic Data, North Anna Power Station, Louisa County, Virginia, Virginia Electric and Power Company Report, Dames and Moore, August 17, 1973.

DM, 1977a. A Seismic Monitoring Program at the North Anna Site in Central Virginia, January 24, 1974 through August 1, 1977, for Virginia Electric and Power Company, Dames and Moore, September 13, 1977.

DM, 1977b. Lateral Continuity of a Pre- or Early Cretaceous Erosion Surface Across Neuschel's Lineament Northern Virginia, for Virginia Electric and Power Company, Dames and Moore, April 1977.

Daniels, 1985. Geologic Interpretation of Basement Rocks of the Atlantic Coastal Plain, United States Department of Interior Geological Survey Open-File Report 85-655, D. Daniels and G. Leo, 1985.

Darton, 1950. Configuration of the Bedrock Surface of the District of Columbia and Vicinity, Maryland Geological Survey, 4 sheets, scale 1:31,680, N. Darton, 1950.

de Boer, 2003. Evidence for Predominant lateral Magma flow Along Major Feeder-Dike Segments of the Eastern North America Swarm Based Magmatic Fabric, in The Great Rift Valleys of Pangea in Eastern North America, in P.M. Letourneau, and P.E. Olsen. (eds), J.Z. de Boer, R.E. Ernst, A.G. Lindsey, p 189-206.

Dischinger, 1987. Late Mesozoic and Cenozoic Stratigraphic and Structural Framework near Hopewell, Virginia, U.S. Geological Survey Bulletin 1567, p 48, J. Dischinger, 1987.

Dominion, 2004a. Response to 6/1/04 RAI 2.5.1-5, 2.5.1-6, 2.5.3-2, and 2.5.1-5, Letter No. 5, U.S. Nuclear Regulatory Committee, Serial No. 04-347, and Docket No. 52-008, Dominion, 2004.

Dominion, 2004b. Response to 4/15/04 RAI 2.5.1-1 to 2.5.1-4, 2.5.2-2 to 2.5.2-4, and 2.5.3-1, Letter No. 3, U.S. Nuclear Regulatory Committee, Serial No. 04-270, and Docket No. 52-008, Dominion, 2004.

Drake, 1989. The Taconic Orogen, in Hatcher, R.D. William T., and Viele, G.W., eds., The Appalachian –Ouachita Orogen in the United States, DNAG, Volume F-2, p 101-177, A. Drake Jr, A. Sinha, J. Laird, and R. Guy, 1989.

Drake, 1999. Geologic map of the Seneca quadrangle, Montgomery County, Maryland, and Fairfax and Loudon Counties, Virginia, U.S. Geological Survey, Geologic Quadrangle Map GQ-1802, A. Drake Jr, S. Southworth, and K. Lee, 1999.

Drake, 1996. Bedrock Geological Map of Northern New Jersey, U.S. Geological Survey, 2 sheets, scale 1:100,000, A. Drake Jr, R. Volkert, D. Monteverde, G. Herman, H. Houghton, R. Parker, and R. Dalton, 1996.

Dryden, 1932. Faults and joints in the Costal Plain of Maryland, Journal of the Washington Academy of Sciences, Volume 22, p 469-472, A. Dryden Jr, 1932.

Ebel, 2002. Earthquakes in the Eastern Great Lakes Basin from a regional perspective, Tectonophysics, p 17-30, J. Ebel and M. Tuttle, 2002.

Edwards, 1979. New Data Bearing on the Structural Significance of the Upper Chesapeake Bay Magnetic Anomaly; Maryland Geological Survey Report of Investigation No. 30, 44 p. J. Edwards and H. Hansen, 1979.

Edwards, 1981. A Brief Description of the Geology of Maryland, Maryland Geological Survey, Pamphlet Series, J. Edwards Jr, 1981, Website: www.mgs.md.gov/esic/brochures/mdgeology.html, Date accessed: June 25, 2007.

EPRI, 1986. Seismic Hazard Methodology for the Central and Eastern United States, EPRI Report NP-4726, Electric Power Research Institute, July 1986.

EPRI/DOE/NRC, 2012. Technical Report: Central and Eastern United States Seismic Source Characterization for Nuclear Facilities, Electric Power Research Institute, U.S. Department of Energy, and the U.S. Nuclear Regulatory Commission, 2012.

Ervin, 1975. Reelfoot Ridft: reactivated precursor to the Mississippi Embayment, Geological Society of America Bulletin, Volume 86, Number 9, p 1287-1295, C. Ervin and L. McGinnis, 1975.

Faill, 1997a. A Geologic History of the North-Central Appalachians, Part 1, Orogenesis from the Mesoproterozoic through the Taconic Orogeny, Journal of Science, Volume 297, p 551–619, R. Faill, 1997.

Faill, 1997b. A Geologic History of the North-Central Appalachians, Part 2, The Appalachian basin from the Silurian through the Carboniferous, Journal of Science, Volume 297, p 729-761, R. Faill, 1997.

Faill, 1998. A Geologic History of the North-Central Appalachians, Part 3, The Allegheny Orogeny, American Journal of Science, Volume 298, p 131–179, R. Faill, February 1998.

Fenneman, 1946. Physical Divisions of the United States, U.S. Geological Survey, 1:7,000,000-scale map, N. Fenneman and D. Johnson, 1946.

Fichter, 2000. The Geological Evolution of Virginia and the Mid-Atlantic Region: Chronology of Events in the Geologic History of Virginia, Stages A through M, James Madison University, L. Fichter and S. Baedke, September 2000, Website: geollab.jmu.edu/vageol/vahist.html, Date accessed: June 25, 2007.

Fisher, 1964. Triassic Rocks of Montgomery County in Geology of Howard and Montgomery Counties, Maryland Geological Survey, p 10-17, G. Fisher, 1964.

Fleming, 1994. Geologic Map of the Washington West Quadrangle, District of Columbia, Montgomery and Prince Georges Counties, Maryland, and Arlington and Fairfax Counties, Virginia, U.S. Geological Survey, 1 sheet, scale 1:24,000, A. Fleming, A. Drake Jr, and L. McCartan, 1994.

Fleming, 1998. Structure, Age, and Tectonic Setting of a Multiply Reactivated Shear Zone In the Piedmont In Washington, D.C., and Vicinity, Southeastern Geology, Volume 37, Number 3, p. 115-140. A.H. Fleming, and A.A. Drake, Jr., 1998.

Frankel, 2002. Documentation for the 2002 Update of the National Seismic Hazard Maps: U.S. Geological Survey Open-File Report 02-420, A. Frankel, M. Petersen, C. Mueller, K. Haller, R. Wheeler, E. Leyendecker, R. Wesson, S. Harmsen, C. Cramer, D. Perkins, and K. Rukstales, 2002.

Frye, 1986. Roadside Geology of Virginia, Mountain Press Publishing Company, K. Frye, 1986.

Gates, 1989. Alleghanian tectono-thermal evolution of the dextral transcurrent Hylas zone, Virginia Piedmont, U.S.A.: Journal of Structural Geology, v. 11, p. 407-419, A. Gates and L. Glover, 1989.

Gates, 2004. Vestiges of an Iapetan rift basin in the New Jersey Highlands: implications for the Neoproterozoic Laurentian margin Journal of Geodynamics, Volume 37, Issues 3-5, p 381-409, A. E. Gates and R. A. Volkert, 2004.

GEER, 2011. Geotechnical Quick Report on the Affected Region of the 23 August 2011, Geotechnical Extreme Events Reconnaissance (GEER) Association Post-Event Report, October, 2011.

Ghosh, 2012. Plate Motions and Stresses from Global Dynamic Models, Science, Volume 335, Number 6070, p. 838-843, A. Ghosh and W.E. Holt, 2012.

Glaser, 1971. Geology and mineral resources of Southern Maryland: Maryland Geological Survey Report of Investigations No 15, 85 p., J. Glaser, 1971.

Glaser, 1994. Geologic Map of Calvert County, Department of Natural Resources Maryland Geological Survey, scale 1:62,500, J. Glaser, 1994.

Glaser, 2003a. Geologic Map of Prince George's County, Maryland, Maryland Geological Survey, 1 sheet, scale 1:62,500, J. Glaser, 2003.

Glaser, 2003b. Geologic Map of the Broomers Island Quadrangle, Calvert and St. Mary's Counties, Maryland, Maryland Geological Survey, 1 sheet, scale 1: 24,000, J. Glaser, 2003.

Glaser, 2003c. Geologic Map of the Cove Point Quadrangle, Calvert County, Maryland, Maryland Geological Survey, 1:24,000 scale, J. Glaser, 2003c.

Glover, 1995a. E-3 Southwestern Pennsylvania to Baltimore Canyon Trough, Geological Society of America Centennial Continent/Ocean Transect #19, L. Glover III, and K. Klitgord, 1995.

Glover, 1995b. Chapter 1, Tectonics of the central Appalachian orogen in the vicinity of corridor E-3, with implications for tectonics of the southern Appalachians, in L. Glover III and K. Klitgord, Chief Compilers, E-3 Southwestern Pennsylvania to Baltimore Canyon Trough, Geological Society of America Continent/Ocean Transect #19, Explanatory Pamphlet, p 2–49, L. Glover III, J. Costain, and C. Coruh, 1995.

Glover, 1997. Paleozoic collisions, Mesozoic rifting and structure of the Middle Atlantic states continental margin: An "EDGE" Project report, in Glover, L., and Gates, A. E., eds., Central and Southern Appalachian Sutures: Results of the EDGE Project and Related Studies: Boulder, Colorado, Geological Society of America Special Paper 314, L. Glover, R. E. Sheridan, W. S. Holbrook, J. Ewing, M. Talwani, R. B. Hawman, and P. Wang, 1997.

Green, 2012. Liquefaction Resulting from the 2011 Central Virginia Earthquake, Paper No. 5-7, Geological Society of America Southeastern Section 61st Annual Meeting, April 1-2, 2012, Geological Society of America Abstracts with Programs, Vol. 44, No. 4, p. 14, R.A. Green and S. Lasley, 2012.

Hack, 1989. Geomorphology of the Appalachian Highlands, R. Hatcher Jr, W. Thomas, and G. Viele, eds., The Geology of North America, Volume F-2, The Appalachian-Ouachita Orogen in the United States, Geological Society of America, J. Hack, 1989.

Hackley, 2007 Northward extension of Carolina slate belt stratigraphy and structure, south-central Virginia: Results from geologic mapping, American Journal of Science, Volume 325, Number 4, p 749-771, P. C. Hackley, J. D Peper, W. C. Burton and J. W. Horton (Jr), 2007.

Hansen, 1978. Upper Cretaceous (Senonian) and Paleocene (Danian) Pinchouts on the South Flank of the Salisbury Embayment, Maryland and their relationship to antecedent basement structures, Department of Natural Resources Maryland Geological Survey Report of Investigations No. 29, p 36, H. Hansen, 1978.

Hansen, 1984. Summary of Hydrogeologic Data from a Deep (2678 ft.) Well at Lexington Park, St. Mary's County, Maryland, Maryland Geological Survey Open File Report No. 84-02-1, H. Hansen and J. Wilson, 1984.

Hansen, 1986. The Lithology and Distribution of Pre-Cretaceous basement rocks beneath the Maryland Coastal Plain, Department of Natural Resources Maryland Geological Survey Report of Investigations No. 44, p 27, H. Hansen and J. Edwards Jr, 1986.

Hansen, 1988. Buried rift basin underlying coastal plain sediments, central Delmarva Peninsula, Maryland, Geology, Volume 49, p 779-782, H. Hansen, September 1988.

Hansen, 1996. Hydrostratigraphic Framework of the Piney Point-Nanjemoy Aquifer and Aquia Aquifer in Calvert and St. Mary's Counties, Maryland, Maryland Geological Survey, Open-File Report No 96-02-8, p 45, H. Hansen, 1996.

Harris, 1982. Interpretive seismic profile along Interstate I-64 from the Valley and Ridge to the Coastal Plain in central Virginia, United States Geological Survey Oil and Gas Investigations Chart OC-123, L. Harris, W. deWitt Jr, and K. Bayer, 1982.

Harrison, 2011. Geology of the Central Virginia Seismic Zone in the Vicinity of the August, 2011 Earthquakes: What We Know and Don't Know, and Suggested Approaches, Paper Presented at the 83rd Annual Meeting of the Eastern Section of the Seismological Society of America, October 16-18, 2011, Little Rock, Arkansas, R.W. Harrison, J.W. Horton, Jr., M.W. Carter, and J.S. Schindler, 2011.

Harrison, 2012. A Preliminary Assessment of Neotectonic Features in the Central Virginia Seismic Zone, Paper No. 5-6, 61st Annual Meeting of the Southeastern Section of the Geological Society of America, Asheville, North Carolina, 1-2 April 2012, Geological Society of America Abstracts with Programs, Volume 44, Number 4, p. 14, R.W. Harrison, 2012.

Hatcher, 1983. Basement massifs in the Appalachians: their role in deformation during the Appalachian Orogenies, Geological Journal, Volume 18, p 255-265, R. D. Hatcher (Jr), 1983.

Hatcher, 1987. Tectonics of the southern and central Appalachian internides, Annual Reviews of Earth and Planetary Science, Volume 15, p 337–362, R. Hatcher Jr, 1987.

Hatcher, 1989. Alleghenian Orogen, in Hatcher, R.D., William, A., Viele, G., eds., The Appalachian-Ouachita Orogen in the United States, Geological Society of America DNAG, Volume F-2, p 233-318, R. Hatcher, W. Thomas, P. Geiser, A. Snoke, S. Mosher, and D. Wiltschko, 1989.

Hatcher, 2004. Paleozoic structure of internal basement massifs, southern Appalachian Blue Ridge, incorporating new geochronologic, Nd and Dr isotopic, and geochemical data, in Tollo, R. P., Corriveau, L., McLelland, J., and Bartholomew, M.J., eds. Proterozoic tectonic evolution of the Grenville orogen in North America: Boulder, Colorado, Geological Society of America Memoir 197, p 525-547, R. Hatcher (Jr), B. R. Bream, C. F. Miller, J. O. Eckert (Jr), P. D. Fullagar, and C. W. Carrigan, 2004.

Hatcher, 2007. Basement Massifs in the Appalachians: Their role in deformation during the Appalachian Orogenies. Geological Journal, Volume 18, p. 255-265, R. D. Hatcher (Jr), 2007.

Henika, 2006. Geology of the Southside Piedmont, in Virginia Museum of National History Guidebook #6, Henika, W.S., Hibbard, J., and Beard, J. eds, W. S. Henika, J. P. Hibbard, J. Beard, P. Bradley, B. Cattanach, M. Ozdogau, E. Robbins, and P. Thayer, 2006.

Hibbard, 1995. Orogenesis exotic to the Iapetan cycle in the Southern Appalachians, J. Hibbard, C. van Staal, and P. Cawood, eds., Current Perspectives in the Appalachian-Caledonian Orogen, Special Paper - Geological Association of Canada, Volume 41, p 191-206, J. Hibbard and S. Samson, 1995.

Hibbard, 1998. The Hyco shear zone in North Carolina and southern Virginia: implications for the Piedmont zone-Carolina zone boundary in the southern Appalachians: American Journal of Science, v. 298, p. 85-107, J. Hibbard, G. Shell, P. Bradley, S. Samson, and G. Worthman, 1998.

Hibbard, 2000. Docking Carolina: Mid-Paleozoic accretion in the southern Appalachians: Geology, v. 28, p. 127-130, J. Hibbard, 2000.

Hibbard, 2002. The Carolina Zone: overview of Neoproterozoic to early Paleozoic peri-Gondwanan terranes along the eastern flank of the southern Appalachians, Earth Science Reviews, Volume 57, p 299-399, J. Hibbard, E. Stoddard, D. Secor, and A. Dennis, 2002.

Hibbard, 2003. Smith River allochthon: A southern Appalachian peri-Gondwanan terrane emplaced directly on Laurentia? Geology, Volume 31, p. 215-218 J. P. Hibbard, R. J. Tracy and W. S. Henika, 2003.

Hibbard, 2007. A Comparative Analysis of Pre-Silurian Crustal Building Blocks of the Northern and the Southern Appalachian Orogen, American Journal of Science, Volume 307, p 23, J. Hibbard, C. van Staal, and D. Rankin, 2007.

Hibbard, 2006. Lithotectonic map of the Appalachian orogen, Canada – United States of America, Geological Survey of Canada Map 02096A, 2 sheets, Scale1:1,500,000, J. Hibbard, C. van Staal, D. Rankin, and H. Williams, 2006.

Higgins, 1974. Interpretation of aeromagnetic anomalies bearing on the origin of Upper Chesapeake Bay and river course changes in the central Atlantic seaboard region: Speculations; Geology, v. 2 no. 1, p. 73-76, M.W. Higgins, I. Zietz, and G.W. Fisher, 1974.

Higgins, 1986. Geologic Map of Cecil County, State of Maryland, U.S. Geological Survey, 1 sheet, Scale 1:62500, M. Higgins and L. Conant, 1986.

Higgins, 1990. The geology of Cecil County, Maryland; Maryland Geological Survey, Bulletin 37, p. 183, M.W. Higgins, and L.B. Conant, 1990.

Hinze, 1987. Magnetic Anomaly map of North America, Decade of North American Geology (DNAG), Geological Society of America, Scale 1:5,000,000, 5 plates, W. Hinze and P. Hood, 1987.

Hittelman, 1994. Geophysics of North America, National Oceanic and Atmospheric Administration, A. Hittelman, J. Kinsfather, and H. Meyers, 1994.

Horton, 1989. Tectonostratigraphic terranes and their Paleozoic boundaries in the central and southern Appalachians. Geological Society of America, Special paper 230, p 213-245, J. Horton, A. Drake, and D. Rankin, 1989.

Horton, 1991. Preliminary Tectonostratigraphic Terrane Map of the Central and Southern Appalachians, U.S. Geological Survey Miscellaneous Investigations Series Map I-2163, J. Horton, A. Drake, D. Rankin, and R. Dallmeyer, 1991.

Horton, 2011. Exploring Pre-Cretaceous Terranes and Basins beneath the Atlantic Coastal Plain, Paper No. 229-8, 2011 Annual Meeting of the Geological Society of America, Minneapolis, Minnesota, 9-12 October 2011, Geological Society of America Abstracts with Programs, Volume 43, Number 5, p. 550, J.W. Horton, Jr., D.S. Powars, and M.J. Kunk, 2011.

Horton, 2012a. The 2011 Virginia Earthquake: What Are Scientists Learning?, EOS, Transactions, American Geophysical Union, Volume 93, Number 33, p, 317–324, J.W. Horton, and R.W. Williams, 2012.

Horton, 2012b. Faults Delineated by Aftershocks Associated with the 2011 Central Virginia Earthquake and their Tectonic Setting, Paper No. 5-5, 61st Annual Meeting of the Southeastern Section of the Geological Society of America, Asheville, North Carolina, 1-2 April 2012, Geological Society of America Abstracts with Programs, Volume 44, Number 4, p. 14, J.W. Horton, Jr., M.C. Chapman, A.M. Carter, M.W. Carter, R.W. Harrison, R.B. Herrmann, and S.L. Snyder, 2012.

Horton, 2012c. Preliminary Analysis of Magnitude 5.8 Virginia Earthquake Causative Fault and Subsidiary Faults Illuminated by Aftershocks", Paper No. 154-10, 2012 Geological Society of America Annual Meeting, Charlotte, North Carolina, 4-7 November 2012, Geological Society of America Abstracts with Programs, Volume 44, Number 7, p. 381, J.W. Horton, Jr., D.E. McNamara, A.K. Shah, A.K. Gilmer, A.M. Carter, W.C. Burton, R.W. Harrison, M.W. Carter, R. B. Hermann, and S.L. Snyder, 2012.

Howell, 1995. Principles of terrane analysis: new applications for global tectonic, Chapman and Hall, Topics in the Earth Sciences 8, 2nd edition, p 245, D. G. Howell, 1995.

Huber, 2000. Warm Climates in Earth History, Cambridge University Press, p. 480, B.T. Huber, K.G. MacLeod, S.L. Wing, 2000.

Hughes, 2012a. Relict Paleozoic Faults in the Epicentral Area of the August 23, 2011 Virginia Earthquake: Geology in the Ferncliff, VA Quadrangle, Paper No. 5-4, 61st Annual Meeting of the Southeastern Section of the Geological Society of America, Asheville, North Carolina, 1-2 April 2012, Geological Society of America Abstracts with Programs, Volume 44, Number 4, p. 14, S. Hughes and J. Hibbard, 2012.

Hughes, 2012b. Relict Paleozoic Faults in the Epicentral Area of the August 23, 2011 Virginia Earthquake: Assessing Potential Sources of Reactivation with Field Observations, Paper No. 154-7, 2012 Geological Society of America Annual Meeting, Charlotte, North Carolina, 4-7 November 2012, Geological Society of America Abstracts with Programs, Volume 44, Number 7, p. 380, S. Hughes and J. Hibbard, 2012.

Hunt, 1967. Physiography of the United States, W.H. Freeman and Company, p 480, C. Hunt, 1967.

Hunt, 1972. Geology of Soils; Their Evolution, Classification, and Uses, W.H. Freeman and Company, p 344, C. Hunt, 1972.

Hurd, 2012. Intraplate Earthquakes, Regional Stress and Fault Mechanics in the Central and Eastern U.S. and Southeastern Canada, Tectonophysics, In Press, O. Hurd and M.D. Zoback, 2012.

Hutchinson, 1985. New York Bight Fault, Geologic Society of America Bulletin, Volume 96, p. 975-989. D.R. Hutchinson and J.A. Grow, 1985.

Jacobeen, 1972. Seismic Evidence for High Angle Reverse Faulting in the Coastal Plain of Prince Georges and Charles County, Maryland, Maryland Geological Survey, Information Circular No. 13, F. Jacobeen Jr, 1972.

Johnson, 1973. Bouguer gravity of northeastern Virginia and the Eastern Shore Peninsula, Virginia Division of Mineral Resources Report of Investigations 32, p 48, S. Johnson, 1973.

Johnston, 1985a. Seismotectonics of the Southern Appalachians, Bulletin of the Seismological Society of America, Volume 75, Number 1, p 291-312, A. Johnston, D. Reinbold, and S. Brewer, 1985.

Johnston, 1985b. A basement block model for Southern Appalachian seismicity, Geological Society of America - Abstracts with Programs, Volume 17, Number 2, p 97, A. Johnston, and D. Reinbold, 1985.

Johnston, 1994. The Earthquakes of Stable Continental Regions: Volume 1 - Assessment of Large Earthquake Potential, EPRI, TR-102261-V1, A. Johnston, K. Coppersmith, L. Kanter, and C. Cornell, 1994.

Kafka, 1985. Earthquake Activity in the Greater New York City Area: Magnitudes, Seismicity, and Geologic Structures, Bulletin of the Seismological Society of America, Volume 75, Number 5, p 1285-1300, A. Kafka, E. Schlesinger-Miller, and N. Barstow, 1985.

Kafka, 1989. Earthquake activity in the greater New York City area—A faultfinder's guide, in Weiss, D., ed. Field trip guidebook: New York State Geological Association, 61st Annual Meeting, Middletown, New York, October 13-15, 1989, Guidebook, p 177-203, A. Kafka, M. Winslow, and N. Barstow, 1989.

Kafka, 1996. Seismicity in the area surrounding two Mesozoic rift basins in the northeastern United States, Seismological Research Letters, Volume 67, p 69-86, A.L. Kafka and P.E. Miller, 1996.

Karabinos, 2008. External Basement Massifs in the Northern Appalachians: the Link Between Rodinia and angea. Geological Society of America Abstracts with Programs, Vol. 40, No. 6, p. 289, P. Karabinos, 2008.

Keppie, 1989. Tectonic map of Pre-Mesozoic terranes in circum-Atlantic Phanerozoic orogens, Nova Scotia Department of Mines and Energy, Halifax, N.S., scale 1:5,000,000, J. D. Keppie and D. Dallmeyer, 1989.

Kidwell, 1988. Reciprocal sedimentation and noncorrelative hiatuses in marine-paralic siliciclastics: Miocene outcrop evidence, Geology, Volume 16, p 609-612, S. Kidwell, 1988.

Kidwell, 1997. Anatomy of Extremely Thin Marine Sequences Landward of a Passive-Margin Hinge Zone: Neogene Calvert Cliffs Succession, Maryland, Journal of Sedimentary Research, Volume 67, Number 2, p 322-340, S. Kidwell, 1997.

Kim, 2005. The 9 December 2003 Central Virginia Earthquake Sequence: A Compound Earthquake in the Central Virginia Seismic Zone: Bulletin of the Seismological Society of America, Volume 95, Number 6, p 2428-2445, W. Kim and M. Chapman, 2005.

King, 1978. The new York-Alabama lineament: geophysical evidence for a major crustal break in the basement beneath the Appalachian basin, Geology, Volume 6, p 312-318, E. King and I. Zietz, 1978.

Klitgord, 1979. Basin structure of the U.S. Atlantic margin, J. Watkins, L. Montadert, and P. Dickerson, eds, Geological and geophysical investigations of continental margins: American Association of Petroleum Geologists Memoir 29, p 85-112, K. Klitgord and J. Behrendt, 1979.

Klitgord, 1988. U.S. Atlantic continental margin; Structural and tectonic framework, R. Sheridan and J. Grow, eds., The Atlantic Continental Margin, U.S., Geological Society of America, The Geology of North America, Volume I-2, p 19-55, K. Klitgord, D. Hutchinson, and H. Schouten, 1988.

Klitgord, 1995. Mid-Atlantic Continental Margin: The Mesozoic-Cenozoic Continent-Ocean Boundary, in L. Glover III, and K. Klitgord, Chief Compilers, E-3 Southwestern Pennsylvania to Baltimore Canyon Trough, Geological Society of America Continent/Ocean Transect #19, Explanatory Pamphlet, K. Klitgord, C. Poag, L. Glover, R. Sheridan, D. Hutchinson, R. Mixon, and R. Benson, 1995.

Knox, 1969. Glacial Age Marsh, Lafayette Park, Washington, D.C., Science, Volume 165, Number 3895, p. 795-797, A.S. Knox, 1969.

Lane, 1983. Physiographic Provinces of Virginia, Virginia Geographer, Volume XV, Fall-Winter, C. Lane, 1983.

Lash, 1989. Documentation and significance of progressive microfabric changes in Middle Ordovician trench mudstones, Geological Society of America Bulletin, Volume 101, p. 1268-1279, G. G. Lash, 1989.

Lefort, 1989. Is there an Archean crust beneath Chesapeake Bay (abs): Abstracts, 28th International Geological Congress, p 2-227, J. Lefort and M. Max, July 1989.

LeTourneau, 2003. Tectonic and climatic controls on the stratigraphic architecture of the Late Triassic Taylorsville Basin, Virginia and Maryland, P. Olsen, eds., The great rift valleys of Pangea in eastern North America, Sedimentology, Stratigraphy and Paleontology, Volume 2, p 12-58, P. LeTourneau, 2003.

LeVan, 1963. A magnetic survey of the Coastal Plain in Virginia, Virginia Division of Mineral Resources Report of Investigations 4, p 17, D. LeVan and R. Pharr, 1963.

Lyons, 1982. Gravity anomaly map of the United States, Society of Exploration Geophysicists, scale 1:2,500,000, sheets, P. Lyons, N. O'Hara, 1982.

Lindholm, 1978. Triassic-Jurassic in eastern North America – A model based on pre-Triassic structures: Geology, V. 6, p. 365-368. R.C. Lindholm, 1977.

Maguire, 1999. Continuation of Appalachian Piedmont under New Jersey Coastal Plain, in D. W. Valentino and A.E. Gates, eds, The Mid-Atlantic Piedmont: Tectonic Missing Link of the Appalachians: Boulder, Colorado, Geological Society of America Special Paper 330, T. J. Maguire, R. E. Sheridan, R. A. Volkert, M. D. Feigenson, M. D., and L. C. Patino, 1999.

Manspeizer, 1988. Late Triassic-early Jurassic synrift basins of the U.S. Atlantic margin, in R.E. Sheridan and J.A. Grow (eds.), The Atlantic Continental Margin, vol. 1-2 of The Geology of North America, Geological Society of America, Boulder CO., p. 197-216, W. Manspeizer, and H. Cousminer, 1988.

Manspeizer, 1989. Post-Paleozoic Activity, Geology of North America, Volume F-2, The Appalachian-Ouachita Orogen in the United States, Geological Society of America, W. Manspeizer, J. DeBoer, J. Costain, A. Froelich, C. Coruh, P. Olsen, G. McHone, J. Puffer, and D. Prowell, 1989.

Markewich, 1990. Contrasting Soils and Landscapes of the Piedmont and Coastal Plain, Eastern United States, Geomorphology, Volume 3, p 417–447, H. Markewich, M. Pavich, and G. Buell, 1990.

Marple, 1993. Evidence for Possible Tectonic Upwarping Along the South Carolina Coastal Plain from an Examination of River Morphology and Elevation Data, Geology, Volume 21, p 651–654, R. Marple and P. Talwani, 1993.

Marple, 2000. Evidence for a Buried Fault System in the Coastal Plain of the Carolinas and Virginia - Implications for Neotectonics in the Southeastern United Sates, Geological Society of America Bulletin, Volume 112, Number 2, p 200–220, R. Marple and P. Talwani, February 2000.

Marple, 2004a. Relationship of the Stafford fault zone to the right-stepping bends of the Potomac, Susquehanna, and Delaware Rivers and related upstream incision along the U.S. Mid-Atlantic fall line; in Southeastern Geology, Volume 42, Number 3, p 123-144, R. Marple, 2004.

Marple, 2004b. Proposed Shenandoah Fault and East Coast-Stafford Fault System and Their Implications for Eastern U.S. Tectonics, Southeastern Geology, Volume 43, Number 2, p 57-80, R. Marple and P. Talwani, 2004.

Mazzotti, 2010. State of Stress in Central and Eastern North American Seismic Zones, Lithosphere, Volume 2, Number 2, p. 76-83, S. Mazzotti and J. Townend, 2010.

MGS, 2007. Physiographic Provinces and their Subdivisions in Maryland, Maryland Geological Survey, 2007, Website: http://www.mgs.md.gov, Date accessed: June 25, 2007.

McCartan, 1989a. Geologic Map of Charles County, Maryland, Maryland Geological Survey, 1 sheet, Scale 1:62,500, L. McCartan, 1989.

McCartan, 1989b. Geologic Map of St. Mary's County, Maryland: Maryland Geological Survey map, Scale 1:62,500, L. McCartan, 1989.

McCartan, 1989c. Atlantic Coastal Plain Sedimentation and Basement Tectonics Southeast of Washington, D.C., Field Trip Guide Book T214, 28th International Geological Congress, July 13, L. McCartan, 1989.

McCartan, 1990. Geologic Map of the Coastal Plain and Upland Deposits, Washington, D.C., Maryland, and Virginia, U.S. Geological Survey, 1 sheet, Scale 1:24,000, L. McCartan, 1990.

McCartan, 1995. Geologic Map and Cross Sections of the Leonardtown 30 X 60 minute quadrangle, Maryland and Virginia. U.S. Geological Survey Open-file report OFR 95-665, p 38, 1 plate, L. McCartan, W. Newell, J. Owens and G. Bradford, 1995.

McLaughlin, 2002. Results of Trenching Investigations along the New Castle Railroad Survey-1 Seismic Line, New Castle, Delaware, Delaware Geological Survey, Open File Report 43, p 17, P. McLaughlin, S. Baxter, K. Ramsey, T. McKenna, S. Strohmeier, 2002.

Merchat, 2007. The Cat Square terrane: Possible Siluro=Devonian remnant ocean basin in the Inner Piedmont, southern Appalachians, USA, in Hatcher, R,D, et al (eds), 40D Framework of Continental Crust, Geological Society of America Memoir 200, p. 553-565, 2007.

Milici, 1991. Preliminary geologic section across the buried part of the Taylorsville basin, Essex and Caroline Counties, Virginia: Virginia Division of Mineral resources Open File Report 91-1, p 31, R. Milici, K. Bayer, P. Pappano, J. Costain, C. Coruh, J. Cahit, 1991.

Milici, 1995. Structural Section Across the Atlantic Coastal Plain, Virginia and Southeasternmost Maryland, Virginia Division of Mineral Resources, Publication 140, 2 plates, R. Milici, J. Costain, C. Coruh, and P. Pappano, 1995.

Mixon, 1977. Stafford Fault System: Structures Documenting Cretaceous and Tertiary Deformation Along the Fall Line in Northeastern Virginia, Geology, Volume 5, p 437–440, R. Mixon and W. Newell, 1977.

Mixon, 1978. The Faulted Coastal Plain Margin at Fredericksburg, Virginia, Tenth Annual Virginia Geology Field Conference, R. Mixon and W. Newell, October 1978.

Mixon, 1982. Mesozoic and Cenozoic Compressional Faulting Along the Atlantic Coastal Plain Margin, Virginia, in Lyttle ed., Central Appalachian Geology NE-SE Geological Society of America Field Trip Guidebook, p. 29-54, R. B. Mixon, and W. L. Newell, 1982.

Mixon, 1984. Folds and faults in the Inner Coastal Plain of Virginia and Maryland – Their effects on distribution and thickness of Tertiary rock units and local geomorphic history, in Frederiksen, N.O., and Krafft, K., eds., Cretaceous and Tertiary stratigraphy, paleontology, and structure, southwestern Maryland and northeastern Virginia: Field trip volume and guidebook (for field trip held October 17, 1984), Reston, Va. American Association of Stratigraphic Palynologists, p 112-122, R. Mixon and D. Powars, 1984.

Mixon, 1989. Geologic Map and Generalized Cross Sections of the Coastal Plain and Adjacent Parts of the Piedmont, Virginia, U.S. Geological Survey, Miscellaneous Investigations Series Map I-2033, 2 sheets, Scale 1:250,000, R. Mixon, C. Berquist, W. Newell, G. Johnson, D. Powers, J. Schindler, and E. Rader, 1989.

Mixon, 1992. Nature and Timing of Deformation of Upper Mesozoic and Cenozoic Deposits in the Inner Atlantic Coastal Plain, Virginia and Maryland, U.S. Geological Survey Circular C1059, p 65-73, R. Mixon, D. Powars, and D. Daniels, 1992.

Mixon, 2000. Geologic Map of the Fredericksburg 30' x 60' Quadrangle, Virginia and Maryland, U.S. Geological Survey, Geologic Investigations Series Map I-2607, R. Mixon, L. Pavlides, D. Powars, A. Froelich, R. Weems, J. Schindler, W. Newell, L. Edwards, and L. Ward, 2000.

Mixon, 2005. Geologic Map of the Stafford Quadrangle, Stafford County, Virginia, U.S. Geological Survey, Scientific Investigations Map 2841, R.B. Mixon, L. Pavlides, J.W. Horton, Jr., D.S. Powars, and J.S. Schindler, 2005.

Mulvey, 2004. 40Ar/39Ar Constraints on the Age of Fabric Development in the Westminster Terrane, North-Central Maryland, Northeastern Section (39th Annual) and Southeastern Section (53rd Annual) Joint Meeting, B. K. Mulvey, M. J. Kunk, S. Southworth, and R. P. Wintsch, 2004.

Murphy, 2004. Neoproterozoic—Early Paleozoic evolution of peri-Gondwanan terranes: implications for Laurentia-Gondwana connections. International Journal of Earth Sciences, Volume. 93, Number 5, p. 659-682, J. B. Murphy, S. A. Pisarevsky, R. D. Nance and J. D. Keppie, 2004.

Nelson, 1962. Geology and Mineral resources of Albermarle County, Virginia Division of Mineral Resources Bulletin 77, 92 p., 1 folded map, Scale 1:62,500, W. Nelson, 1962.

Nelson, 1980. Determination of Holocene fault movement along the Ramapo fault in southeastern New York using pollen stratigraphy, Geological Society of America Abstracts with Programs, Volume 12, Number 2, p 75, S. Nelson, 1980.

Nelson, 1981. The Clingman Lineament; Aeromagnetic Evidence for a Major Discontinuity in the North American Basement, Geological Society of America, Southeastern Section, Abstracts with Programs, Volume 13, Number 1, p 31, A. Nelson and I. Zietz, January 1981.

Newell, 1976. Detailed Investigation of a Coastal Plain-Piedmont Fault Contact in Northeastern Virginia, U.S. Geological Survey Open-File Report 76-329, W. Newell, D. Prowell, and R. Mixon, 1976.

Newell, 1985. Architecture of the Rappahannock Estuary – Neotectonics in Virginia, in M. Morisawa, and J.T. Hack, editors, Tectonic Geomorphology, Allen and Unwin Publishers, Winchester, Massachusetts, p. 322-342, W.L. Newell, 1985.

Newman, 1983. Holocene neotectonics of the lower Hudson Valley: Geological Society of America Abstracts with Programs, Volume 15, Number 3, p 148, W. Newman, L. Cinquemani, J. Sperling, L. Marcus, and R. Pardi, 1983.

NRC, 1978. Standard Format and Content of Safety Analysis Reports for Nuclear Power Plants, LWR Edition, Regulatory Guide 1.70, Revision 3, U.S. Nuclear Regulatory Commission, November 1978.

NRC, 1997. Identification and Characterization of Seismic Sources and Determination of Safe Shutdown Earthquake Ground Motion, U.S. Nuclear Regulatory Commission, Regulatory Guide 1.165, March 1997.

NRC, 2005. Safety Evaluation Report for an Early Site Permit (ESP) at the North Anna ESP Site – NUREG-1835, Nuclear Regulatory Commission, September 2005.

NRC, 2007. Basis Geologic and Seismic Information, Regulatory Guide 1.206, Section 2.5.1, U.S. Nuclear Regulatory Commission, June, 2007.

Obermier, 1998. Paleoliquefaction Evidence for Seismic Quiescence in Central Virginia During the Late and Middle Holocene Time (abs), Eos Transactions of the American Geophysical Union, Volume 79, Number 17, p S342, S. Obermier and W. McNulty, 1998.

Otton, 1955. Ground-Water Resources of the Southern Maryland Coastal Plain, Maryland Department of Geology, Mines and Water Resources, Bulletin 15, p 347, E. Otton, 1955.

Owens, 1979. Upper Cenozoic Sediments of the Lower Delaware Valley and the Northern Delmarva Peninsula, New Jersey, Pennsylvania, Delaware, and Maryland, Geological Survey Professional Paper 1067-D, U.S. Geological Survey, J. Owens and J. Minard, 1979.

Owens, 1998. Bedrock geologic map of central and southern New Jersey, U.S. Geological Survey M.I. Series Map I-2540-B, 4 sheets, Scale 1:100,000, J. Owens, P. Sugarman, N. Sohl, R. Parker, H. Houghton, R. Volkert, Jr., and R. Orndoff, 1998.

Page, 1968. Seismicity in the vicinity of the Ramapo fault, New Jersey-New York, Bulletin of Seismological Society of America, Volume. 58, p 681-687, R.A. Page, P.H. Molnar, and J. Oliver, 1968.

Pavlides, 1980. Revised Nomenclature and Stratigraphic Relationships of the Fredericksburg Complex and Quantico Formation of the Virginia Piedmont, U.S. Geological Survey Professional Paper 1146, L. Pavlides, 1980.

Pavlides, 1983. Late Cenozoic faulting along the Mountain Run Fault Zone, central Virginia Piedmont, GSA Abstracts with Programs, Volume 15, Number 2, L. Pavlides, 1983.

Pavlides, 1986. Mountain Run Fault Zone of Virginia, U.S. Geological Survey Open-File Report 87-93, 93–94, L. Pavlides, 1986.

Pavlides, 1989. Early Paleozoic Composite Mélange Terrane, Central Appalachian Piedmont, Virginia and Maryland: Its Origin and Tectonic History, Geological Society of America Special Paper 228, p 135–193, L. Pavlides, 1989.

Pavlides, 1994. Early Paleozoic Alkalic and Calc-Alkalic Plutonism and Associated Contact Metamorphism, Central Virginia Piedmont, U.S. Geological Survey Professional Paper 1529, L. Pavlides, J. Arth, J. Sutter, T. Stern, and H. Cortesini Jr, 1994.

Pavlides, 2000. Geology of the Piedmont and Blue Ridge Provinces, Chapter II of the pamphlet to accompany the U.S. Geological Survey, Geologic Investigations Series Map I-2607, L. Pavlides, 2000.

Pazzaglia, 1993a. Stratigraphy, petrography, and correlation of late Cenozoic middle Atlantic Coastal Plain deposits: Implications for late-stage passive-margin geologic evolution, Geological Society of America Bulletin, Volume 105, p 1617-1634, F. Pazzaglia, 1993.

Pazzaglia, 1993b. Fluvial terraces of the lower Susquehanna River, Geomorphology, Volume 8, p 83-113, F. Pazzaglia and T. Gardner, 1993.

Pazzaglia, 1994. Late Cenozoic flexural deformation of the middle U.S. Atlantic passive margin, Journal of Geophysical Research, Volume 99, Number B6, p 12, 143-12, 157, F. Pazzaglia and T. Gardner, 1994.

Pazzaglia, 2006. Rivers, glaciers, landscape evolution, and active tectonics of the central Appalachians, Pennsylvania and Maryland, in Pazzaglia, F.J., ed, Excursions in Geology and History: Field Trips in the Middle Atlantic States: Geological Society of America Field Guide 8. P. 169-197, F.J. Pazzaglia, D.D. Braun, M. Pavich, P. Bierman, N. Potter, D. Merritts, R. Walter, D. Germanoski, 2006.

Pesonen, 2003. Palaeomagnetic configuration of continents during the Proterozoic, Tectonophysics Volume 375, Issues 1-4, Pages 289-324, L. J. Pesonen, S. A. Elming, S. Mertanen, S. Pisarevsky, M. S. D'Agrella-Filho, J. G. Meert, P. W. Schmidt, N. Abrahamsen, and g. Bylundi, 2003.

Poag, 1991. Rise and demise of the Bahama-Grand Banks gigaplatform, northern margin of the Jurassic proto-Atlantic seaway, Marine Geology, Volume 102, p 63-130, C. Poag, 1991.

Poag, 2004. The Chesapeake Bay Crater; geology geophysics of a late Eocene submarine impact structure, Springer-Verland: Berlin, p 522, W. Poag, C. Koeberl, and W. Reimold, 2004.

Poag, 2005. Stratigraphy and Paleoenvironments of Early Postimpact Deposits at the USGS NASA Langley Corehole, Chesapeake Bay Impact Crater, Chapter F of Studies of the Chesapeake Bay Impact Structure - The USGS-NASA Langley Corehole, Hampton, Virginia, and Related Coreholes and Geophysical Surveys, U.S. Professional Paper 1688, pages F1 to F51, Poag, W. and Norris, R.D., 2005.

PEPC, 1973. Preliminary safety analysis report, Douglas Point Nuclear Generating Station, Units 1 and 2, Volume 2, Dames and Moore for the Potomac Electric Power Company, Docket Number 50448-2 and 50449-2, 1973.

Powars, 1999. The effects of the Chesapeake Bay Impact Crater on the Geological Framework and Correlation of Hydrogeologic Units of the Lower York-James Peninsula, Virginia, U.S. Geological Survey Professional Paper 1612, p 82, 9 plates, D. Powars and T. Bruce, 1999.

Powars, 2010a. Coastal Plain Faults Rooted in Crystalline Basement Across the Salisbury Embayment, Virginia and Maryland, Paper No. 89-10, 2010 Annual Meeting of the Geological Society of America, Denver, Colorado, 31 October - 3 November 2010, Geological Society of America Abstracts with Programs, Volume 42, Number 5, p. 219, D.S. Powars and J.W. Horton, Jr., 2010.

Powars, 2010b. Evidence for Basement-Rooted Coastal Plain Faults in the Potomac River Valley and Central Chesapeake Bay Region, Paper No. 29-9, Geological Society of America, Northeastern Section (45th Annual) and Southeastern Section (59th Annual) Joint Meeting, 13-16 March 2010, Geological Society of America Abstracts with Programs, Volume 42, Number 1, p. 100, D.S. Powars, J.W. Horton, Jr., R.W. Harrison, J.S. Schindler, and W.L. Newell, 2010.

Powars, 2011. Basement-Rooted Coastal Plain Faults and their Geomorphic Expressions in Virginia and Maryland, Paper No. 8-1, Geological Society of America Southeastern Section 60th Annual Meeting, March 23-25, 2011, Geological Society of America Abstracts with Programs, Volume 43, Number 2, p. 21, D.S. Powars and J.W. Horton, Jr., 2011.

Pratt, 1988. A geophysical study of the Earth's crust in Central Virginia: Implications for Appalachian Crustal structure: Journal of Geophysical Research, V. 93 p. 6649-6667, T. Pratt, C. Coruh, J. Costain, and L. Glover III, 1988.

Prowell, 1983. Index of Faults of Cretaceous and Cenozoic Age in the Eastern United States, U.S. Geological Survey Miscellaneous Field Studies Map MF-1269, D. Prowell, 1983.

Prowell, 2010. The Fault with the White House: A Study of Late Cenozoic Tectonism in Washington D.C.", Paper No. 29-10, Northeastern Section (45th Annual) and Southeastern Section (59th Annual) Joint Meeting, 13-16 March 2010, Geological Society of America Abstracts with Programs, Vol. 42, No. 1, p. 100, D.C. Prowell and R.A. Christopher, 2010.

PSEG, 2002. Section 2.5, Geology, Seismology, and Geotechnical Engineering, Updated Final Safety Analysis Report, Revision 12, Hope Creek Generating Station, submitted to the NRC (LR-N02-0179), 2002.

Quittmeyer, 1985. Possible implications of recent microearthquakes in southern New York state: Earthquake Notes, Volume 56, p 35-42, R.C. Quittmeyer, C.T. Statton, K.A. Mrotek and M. Houlday, 1985.

Rader, 1993. Geologic map of the Virginia – expanded explanation: Virginia Division of Mineral Resources, E. Rader and N. Evans, eds., 1993.

Rankin, 1989. Pre-orogenic terranes, in Hatcher (Jr), R.D., et al., eds., The Appalachian-Ouachita orogen in the United States: Boulder, Colorado, Geological Society of America, The Geology of North America, Volume F-2, p 7-100, D.W. Rankin, A. A. Drake (Jr), L. Glover, R. Goldsmith, L. M. Hall, D. P Murray, N. M. Ratcliffe, J. F. Read, D. T. Secor (Jr), and R. S. Stanley, 1989.

Ratcliffe, 1971. The Ramapo fault system in New York and Adjacent Northern New Jersey—A case of tectonic heredity, Geological Society of America Bulletin, Volume 82, p 125-142, N. Ratcliffe, 1971.

Ratcliffe, 1980. Brittle faults (Ramapo fault) and phyllonitic ductile shear zones in the basement rocks of the Ramapo seismic zones New York and New Jersey, and their relationship to current seismicity, in Manspeizer, W., ed., Field studies of New Jersey geology and guide to field trips Newark, New Jersey, Rutgers University, Geology Department, U.S., New York State Geological Association, 52nd annual meeting, October 10, 1980, Guidebook, p 278-312, N. Ratcliffe, 1980.

Ratcliffe, 1982. Results of core drilling of the Ramapo fault at Sky Meadow Road, Rockland County, New York, and assessment of evidence for reactivation to produce current seismicity, U.S. Geological Survey Miscellaneous Investigations, Map I-1401, 1 sheet, N. Ratcliffe, 1982.

Ratcliffe, 1983. Fault reactivation models for the origin of eastern United States seismicity, Does the solution to Charleston reside at Charleston, in Hays, W.W., and Gori, P.L., eds., Proceedings of Conference XX: A workshop on the 1886 Charleston, South Carolina, earthquake and its implications for today, US Geological Survey Open-File Report 83-843, N.M. Ratcliffe, 1983.

Ratcliffe, 1985a. Fault reactivation models for origin of the Newark basin and studies related to eastern U.S. seismicity, in Robinson, G.R., and Froelich, A.J., eds., Proceedings of the Second U.S. Geological Survey Workshop on the Early Mesozoic Basins of the Eastern United States, US Geological Survey Circular 946, p 36-45, N.M. Ratcliffe, and W. Burton, 1985.

Ratcliffe, 1985b. Northeast Seismicity and Tectonics, in Jacobson, M.L., and R., R.T., eds., National Earthquake Hazards Reduction Program summaries of technical reports, Volume XX, US Geological Survey Open File Report 85-464, p 54-58, N.M. Ratcliffe, and J. Costain, 1985.

Ratcliffe, 1986a. Seismic Reflection Geometry of the Newark Basin Margin in Eastern Pennsylvania, NUREG/CR-4676, N. Ratcliffe, W. Burton, R. D'Angelo, and J. Costain, 1986.

Ratcliffe, 1986b. Low-angle extensional faulting, reactivated mylonites, and seismic reflection geometry of the Newark basin margin in eastern Pennsylvania, Geology, Volume 14, p 766-770, N.M. Ratcliffe, W. Burton, R.M. D'Angelo, and J.K.Costain, 1986.

Ratcliffe, 1988. Structural analysis of the Furlong fault and the relation of mineralization to faulting and diabase intrusion, Newark basin, Pennsylvania, in Froelich, A.J., and Robinson, G.R., eds., Studies of the early Mesozoic Basins of the Eastern United States, US Geological Survey Bulletin 1776, p 176-193, N.M. Ratcliffe and W.C. Burton, 1988.

Ratcliffe, 1990. Orientation, movement history, and cataclastic rocks of Ramapo fault based on core drilling and trenching along the western margin of the Newark basin near Bernardsville, New Jersey, U.S., Geological Survey Miscellaneous Investigations, Map I-1982, 1 sheet, N. Ratcliffe, W. Burton, and M. Pavich, 1990.

Ratcliffe, 1992. Bedrock geology and seismotectonics of the Oscawana Lake quadrangle, New York, p 38, N.M. Ratcliffe, 1992.

Richardson, 1991. North American Plate Dynamics, Journal of Geophysical Research, Volume 96, R. Richardson and L. Reding, 1991.

Rodgers, 1970. The tectonics of the Appalachians, Wiley-Interscience: New York, NY, p 271, J. Rodgers, 1970.

Root, 1989. Basement control of structure in the Gettysburg rift basin, Pennsylvania and Maryland: Tectonophysics, v. 166, p. 281-292. S.I. Root, 1989.

Sanders, 1963. Late Triassic tectonic history of northeaster United States, American Journal of Science 261, p 501-524, J. Sanders, 1963.

Savy, 2002. Guidance for Performing Probabilistic Seismic Hazard Analysis for a Nuclear Plant Site: Example Application to the Southeastern United States, Nuclear Regulatory Commission, NUREG-CR/6607, J. Savy, W. Foxall, N. Abrahamson, and D. Bernreuter, 2002.

Sbar, 1975. The Delaware-New Jersey earthquake of February 28, 1973, Bulletin of the Seismological Society of America, Volume 65, p 85-92, M. Sbar, R. Jordan, C. Stephens, T. Pickett, K. Woodruff, and C. Sammis, 1975.

Scharnberger, 2006. The Lancaster Seismic Zone of southeast Pennsylvania in relation to the Gettysburg-Newark basin, Geological Society of America Abstracts with Programs, Volume 38, Number 2, p 83, C. Scharnberger, 2006.

Schlische, 1990. Quantitative filling model for continental extensional basins with applications to early Mesozoic rifts of eastern North America, Journal of Geology, 98, p. 135-155, R. Schlische., and P. Olsen., 1990.

Schlische, 1992. Structural and Stratigraphic Development of the Newark Extension Basin, Eastern North America: Evidence for the Growth of the Basin and its Bounding Structures, Geological Society of America Bulletin, Volume 104, p 1246-1263, R. Schlische, October 1992.

Schlische, 1993. Anatomy and evolution of the Triassic-Jurassic Continental Rift System, Eastern North America, Tectonics, v. 12, p. 1026-1042, R.W. Schlische, 1993.

Schlische, 2003a. Progress in Understanding the Structural Geology, Basin Evolution, and Tectonic History of the Eastern North America Rift System, P. LeTourneau and P. Olsen, eds., The Great Rift Valleys of Pangea in Eastern North America, Volume 1, R. Schlische, 2003.

Schlische, 2003b. Relative timing of CAMP, rifting, continental breakup, and inversion: tectonic significance, by The Central Atlantic Magmatic Province: in Hames, W.E., McHone, G.C., Renne, P.R., and Ruppel, C., eds., American Geophysical Union Monograph 136, p. 33-59, R.W. Schlische, M.O. Withjack, and P.E. Olsen, 2003.

Schlische, 2005. The early Mesozoic Birdsboro central Atlantic Margin basin in the Mid-Atlantic region, eastern United States: Discussion, Geological Society of America Bulletin, V. 117, p. 823-828, R.W. Schlische, and M.O. Withjack, 2005.

Schmidt, 1993. Maryland's Geology, Tidewater Publishers, Centreville, Maryland, p 164, M. Schmidt Jr, 1993.

Schruben, 1994. Geology of the conterminous United States at 1:250,000, 000 scale; a digital representation of the 1974 P. B. King and H. M. Beikman map, U.S. Geological Survey Digital Data Series DDS-0011, P. Schruben, R. Arndt, W. Bawiec, and R. Ambroziak, 1994.

Schulte, 2005. An updated global earthquake catalogue for stable continental regions: reassessing the correlation with ancient rifts: Geophys. J. Int., v. 161, p. 707-72. S.M. Schulte, and W.D. Mooney, 2005.

Schwab, 1997a. Initial results of high-resolution sea-floor mapping offshore of the New York–New Jersey metropolitan area using sidescan sonar, Northeastern Geology and Environmental Sciences Volume 9, Number 4, p 243–262, W. Schwab, M. Allison, W. Corso, L. Lotto, B. Butman, M. Bucholtz ten Brink, J. Denny, W. Danforth, and D. Foster, 1997.

Schwab, 1997b. Mapping the sea floor offshore of the New York–New Jersey metropolitan area using sidescan sonar—preliminary report, U.S. Geological Survey Open-File Report 97-61, 3 sheets, W. Schwab, W. Corso, M. Allison, B. Butman, J. Denny, L. Lotto, W. Danforth, D. Foster, T. O'Brien, D. Nichols, B. Irwin, and K. Parolski, 1997.

Scott, 2006. Correlating Late Pleistocene Deposits on the Coastal Plain of Virginia with the Glacial-Eustatic sea-level curve (MS Thesis), Old Dominion University, p 112, T. Scott, May 2006.

Seborowski, 1982. Tectonic implications of recent earthquakes near Annsville, New York, Bulletin of Seismological Society of America, Volume 72, p 1601-1609, D.K. Seborowski, G. Williams, J.A. Kelleher, and C.A. Statton, 1982.

Seeber, 1998. The 1994 Cacoosing Valley earthquakes near Reading, Pennsylvania: A shallow rupture triggered by quarry unloading, Journal of Geophysical Research, Volume 103, Number B10, p 24, 505-24, 521, L. Seeber, J. Armbruster, W. Kim, N. Barstow, and C. Scharnberger, 1998.

Sevon, 2000. Regolith in the Piedmont Upland section, Piedmont Province, York, Lancaster, and Chester Counties, Southeastern Pennsylvania, Southeastern Geology, Volume 39, Number 3 and 4, p 223–241, W. Sevon, October 2000.

Sheridan, 1988a. The Atlantic Continental Margin, U.S.Geological Society of America, The Geology of North America, Volume 1-2, p 610, R. Sheridan and J. Grow, 1988.

Sheridan, 1988b. Geophysical Data, R. Sheridan and J. Grow, eds., The Atlantic Continental Margin, U.S. Geological Society of America, The Geology of North America, Volume 1, p 177-196, R. Sheridan, J. Grow, and K. Klitgord, 1988.

Sheridan, 1993. Deep seismic reflection data of EDGE U.S. mid-Atlantic continental margin experiment: Implications for Appalachian sutures and Mesozoic rifting and magmatic underplating, Geology; Volume 21; Number 6; p 563-567, R. E. Sheridan, D. L. Musser, L. Glover, M. Talwani, J. I. Ewing, W. S. Holbrook, G. M. Purdy, R. Hawman and S. Smithson, 1993.

Sheridan, 1999. Grenville age of basement rocks in Cape May NJ well: new evidence for Laurentian crust in U.S. Atlantic Coastal Plain basement Chesapeake terrane. Journal of Geodynamics, Volume 27, pages 623-633, Sheridan, R.E., Maguire, T.J., Feigenson, M.D., Patino, W. C., Volkert, R.A., 1999

Shumaker, 2000. The New York-Alabama Lineament; An Early Iapetian Wrench Fault?, American Association of Petroleum Geologists Bulletin, Volume 84, Number 9, p 1393, R. Shumaker, September 2000.

Southworth, 2004. Guidebook to Field Trips in the National Capital Region, Central Appalachians: U.S. Geological Survey Circular 1264, p 298, S. Southworth, W. C. Burton and K. Schindler eds., 2004.

Southworth, 2006. Central Appalachian Piedmont and Blue Ridge tectonic transect, Potomac River corridor, in Pazzaglia, F.J., ed., Excursions in Geology and History: Field Trips in the Middle Atlantic States: Geological Society of America Field Guide 8, p 135- 167, S. Southworth, A. A. Drake (Jr), D. K. Brezinski, R. P. Wintsch, M. J. Kunk, J. N. Aleinikoff, C. W. Naeser and N. D. Naeser, 2006.

Southworth, 2007. Geologic Map of the Frederick 30′ × 60′ Quadrangle, Maryland, Virginia, and West Virginia, U.S. Geological Survey Scientific Investigations Map 2889, Scale 1:100,000, 42 pp., S. Southworth, D.K. Brezinski, A.A. Drake, Jr., W.C. Burton, R.C. Orndorff, A.J. Froelich, J.E. Reddy, D. Denenny, and D.L. Daniels, 2007.

Spears, 2002. Geology of the central Virginia Piedmont between the Arvonia syncline and the Spotsylvania high-strain zone, Thirty-Second Annual Virginia Geological Field Conference Guidebook Charlottesville, Virginia, October 11-13, Virginia Division of Mineral Resources. p.36, D. Spears and C. Bailey, 2002.

Spears, 2011. Geology of the Lakeside Village Quadrangle, Virginia, Virginia Department of Mines, Minerals, and Energy, Publication 177, Virginia Division of Geology And Mineral Resources, 23 p., D.B. Spears, 2011.

Spears, 2012. Geologic Framework of the Central Virginia Seismic Zone, Paper No. 5-3, Geological Society of America Southeastern Section 61st Annual Meeting, April 1-2, 2012, Geological Society of America Abstracts with Programs, Vol. 44, No. 4, p. 14, D.B. Spears, 2012.

Spoljaric, 1972. Geology of the Fall Zone in Delaware, Delaware Geological Survey, p 30, N. Spoljaric, March 1972.

Spoljaric, 1973. Normal Faults in Basement Rocks of the Northern Coastal Plain, Delaware, Geological Society of America Bulletin, Volume 84, p 2781-2783, N. Spoljaric, 1973.

Stanford, 1995. Possible Pliocene-Pleistocene Movement on a Reactivated Mesozoic Fault In Central New Jersey, Geological Society of America Abstracts with Programs, Volume 27, Number 1, p 83, S. Stanford, D. Jagel, and D. Hall, 1995.

Stanford, 2002. Surficial Geology of the Monmouth Junction Quadrangle, Somerset, Middlesex, and Mercer Counties, New Jersey, Department of Environment Protection New Jersey Geological Survey Open-File Map OFM 47, 1 plate, Scale 1: 24,000, S. Stanford, 2002.

Steltenpohl, 2010. New York–Alabama Lineament: A Buried Right-Slip Fault Bordering the Appalachians and Mid-Continent North America, Geology, Volume 38, Number 6, p. 571-574, M.G. Steltenpohl, I. Zietz, J.W. Horton, Jr., and D.L. Daniels, 2010.

Stewart, 2002. Late Mississippian paleoseismites from southeastern West Virginia and southwestern Virginia, in Ettensohn, F. F. Rast, N., and Brett, C.E., eds, Ancient seismites: Boulder, Colorado, Geological Society of America Special Paper 359, p 127- 144, K. G. Stewart, J. M. Dennison and M. J. Bartholomew, 2002.

Stoffer, 2003. Geology of the New York City Region, United States Geological Survey, Available Online: http://3dparks.wr.usgs.gov/nyc/common/contents.htm, P.W. Stoffer, 2003.

Stone, 1984. Faults in Pleistocene sediments at trace of Ramapo fault in Geological Survey research, fiscal year 1981, U.S. Geological Survey, Professional Paper 1375, p. 49, B. Stone and N. Ratcliffe, 1984.

Swanson, 1982. Preliminary model for early transform history in central Atlantic rifting, Geology, 10:317-320, M. Swanson, 1982.

Swanson, 1986. Preexisting fault control for Mesozoic basin formation in eastern North America, Geology, v. 14 p. 419-422, M.T. Swanson, 1986.

Sykes, 2008. Observations and Tectonic Setting of Historic and Instrumentally Located Earthquakes in the Greater New York City-Philadelphia Area, Bulletin of the Seismological Society of America, Volume 98, p 1696-1719, L.R. Sykes, J.G. Armbruster, W.Y. Kim, and L. Seeber, 2008.

Tanner, 1987. Gravity Anomaly map of North America, Decade of North American Geology (DNAG), Geological Society of America, Scale 1:5,000,000, 5 plates, J. Tanner, 1987.

Thelin, 1991. Landforms of the Conterminous United States–A Digital Shaded-Relief Portrayal, U.S. Geological Survey, pamphlet to accompany Geological Investigation Series Map I-2206, G. Thelin and R. Pike, April 17 1991.

Thomas, 1989. Tectonic map of the Ouachita orogen: In Hatcher, R.D., Jr., Thomas, W.A., and Viele, G.W., eds., The Appalachian-Ouachita orogen in the United States: Geological Society of America, The Geology of North America, v. F-2, plate 9, W. A. Thomas, G. W. Viele, J. K. Arbenz, R. L. Nicholas, R. E. Denison, W. R. Muehlberger, and P. R. Tauvers, 1989.

Thomas, 2006. Tectonic inheritance at a continental margin: GSA Today, v. 16, no. 2, p. 4–11, W. A. Thomas, 2006.

Thurber, 1985. Crustal structure along the Ramapo fault zone, New York State, Earthquake Notes, Volume 56, p 145-152, C. Thurber and T. Caruso, 1985.

Turcotte, 2002. Geodynamics, Cambridge University Press, p 456, D. Turcotte and G. Schubert, 2002.

URS, 2000. Seismic Characterization study for the expansion of the Williams Gas Pipeline – Transco LNG facility, Cove Point, Maryland, URS Corporation, October 2000.

van Staal, 1998. The Cambrian-Silurian tectonic evolution of the northern Appalachians and British Caledonides: history of a complex, west and southwest Pacific-type segment of Iapetus, Geological Society, London, Special Publications; v. 143; p. 197-242, C. R. van Staal, J. F. Dewey, C. Mac Niocaill and W.S. McKerrow, 1998.

Vigil, 2000. A Tapestry of Time and Terrain, U.S. Geological Survey, pamphlet to accompany U.S. Geological Survey, Geological Investigation Series Map I-2720, J. Vigil, R. Pike, and D. Howell, February 24, 2000.

Walker, 1971. Nondeltaic depositional environments in the Catskill Clastic Wedge (Upper Devonian) of Central Pennsylvania., Geological Society of America Bulletin, Volume 82, Number 5, pgs 1305-1326, R.G. Walker., 1971.

Walsh, 2011a. Stress Changes in the Greater D.C. Metropolitan Area as a Result of the 2010 Germantown, MD, and 2011 Mineral, VA Intraplate Earthquakes, Paper Presented at the 83rd Annual Meeting of the Eastern Section of the Seismological Society of America, October 16-18, 2011, Little Rock, Arkansas, L.S. Walsh, L. G. Montesi, J. M. Sauber, T. R. Watters, W. Kim, A.J. Martin, and R. Anderson, 2011.

Walsh, 2011b. Comparing the Stress Change Characteristics and Aftershock Decay Rate of the 2011 Mineral, VA, Earthquake with Similar Earthquakes from a Variety of Tectonic Settings, Abstract Number S11B-2241, American Geophysical Union, Fall Meeting 2011, L.S. Walsh, L. G. Montesi, J. M. Sauber, T. R. Watters, W. Kim, A.J. Martin, and R. Anderson, 2011.

Walsh, 2012. Implications of the August 2011 Mineral, VA, and July 2010 Germantown, MD, Earthquakes for Seismic Hazard in the National Capital Region, Paper No. 16-1, Geological Society of America Southeastern Section 61st Annual Meeting, April 1-2, 2012, Geological Society of America Abstracts with Programs, Vol. 44, No. 4, p. 60, L.S. Walsh, L.G.J., Montési, and A.J. Martin, 2012.

Ward, 2004. Tertiary Lithology and Paleontology, in Southworth, S. and Burton, W., eds., Geology of the National Capital Region- Field Trip Guidebook: U.S. Geological Survey Circular 1264, p 263-279, L. Ward and D. Powars, 2004.

Watts, 1982. Tectonic Subsidence, Flexure, and Global Changes of Sea Level, Nature, Volume 297, p 469-474, A. Watts, 1982.

Weems, 1998. Newly Recognized En Echelon Fall Lines in the Piedmont and Blue Ridge Provinces of North Carolina and Virginia, With a Discussion of Their Possible Ages and Origins, U.S. Geological Survey Open-File Report 98-374, R. Weems,1998.

Wentworth, 1983, Regenerate Faults of Small Cenozoic Offset - Probable Earthquake Sources in the Southeastern United States, U.S. Geological Survey, Professional Paper 1313-S, C. Wentworth and M. Mergner-Keefer, 1983.

Wheeler, 1992. Geologic Implications of Earthquake Source Parameters in Central and Eastern North America, Seismological Research Letters, Volume 63, Number 4, p 491–505, R. Wheeler and A. Johnston, 1992.

Wheeler, 1995. Earthquakes and the Cratonward Limit of Iapetan Faulting in Eastern North America, Geology, Volume 23, 105–108, R. Wheeler, 1995.

Wheeler, 1996. Earthquakes and the Southeastern Boundary of the Intact Iapetan margin in Eastern North America, Seismological Research letters, Volume 67, Number 5, p 77-83, R. Wheeler, 1996.

Wheeler, 2001. Known and suggested Quaternary faulting in the midcontinent United States, Engineering Geology, Volume 62, p 51-78, R.L. Wheeler, and A.J. Crone, 2001.

Wheeler, 2005. Known or Suggested Quaternary Tectonic Faulting, Central and Eastern United States – New and Updated Assessments for 2005, U.S. Geological Survey, Open File Report 2005-1336, p 37, R. Wheeler, 2005.

Wheeler, 2006. Quaternary tectonic faulting in the Eastern United States, Engineering Geology, Volume 82, p 165-186, R. Wheeler, 2006.

Wheeler, 2008. Paleoseismic Targets, Seismic Hazard, and Urban Areas in the Central and Eastern United States, Bulletin of Seismological Society of America, Volume 98, p 1572-1580, R.L. Wheeler, 2008.

Whitmeyer, 2007. Tectonic Model for the Proterozoic Growth of North America, Geosphere, Volume 3, Number 4, p. 220-259, S.J. Whitmeyer, K.E. Karlstrom, 2007.

Williams, 1983. Appalachian suspect terranes, R. Hatcher Jr, H. Williams and I. Zietz, eds., Contributions to the Tectonics and Geophysics of Mountain Chains, Geological Society of America Memoir 159, p 33-53, H. Williams and R. Hatcher, 1983.

Wilson, 1990. Geology and Hydrologic Assessment of Coastal Plain Aquifers in the Waldorf Area, Charles County, Maryland, Maryland Geological Survey, Report of Investigations No. 53,138 p., 8 plates, J. Wilson and W. Fleck, 1990.

Withjack, 1998. Diachronous rifting drifting, and inversion on the passive margin of eastern North America: An analog for other passive margins, American Association of Petroleum Geologist Bulletin, Volume 82, p 817-835, M. Withjack, R. Schlische, and P. Olsen, 1998.

Withjack, 2005. A review of tectonic events on the passive margin of eastern North America: in Post, P., ed., Petroleum Systems of Divergent Continental Margin Basins:25th Bob S. Perkins Research Conference, Gulf Coast Section of SEPM, p. 203-235., M.O. Withjack, and R. W. Schlische, 2005.

Wolin, 2012. Mineral, Virginia, Earthquake Illustrates Seismicity of a Passive-Aggressive Margin, Geophysical Research Letters, Volume 39, L02305E, p. 1-7, Wolin, S. Stein, F. Pazzaglia, A. Meltzer, A. Kafka, and C. Berti, 2012.

Zietz, 1982. Composite magnetic anomaly map of the United States, Part A: Conterminous United States, U.S. Geological Survey Map GP-54923, Scale 1:2,500,000, I. Zietz, 1982.

Zoback, 1980. State of Stress in the Conterminous United States, Journal of Geophysical Research, Volume 85, p 6113-6156, M.L. Zoback, and M. Zoback, 1980.

Zoback, 1989a. Tectonic Stress Field of the Coterminous United States, in L. C. Pakiser and M. D. Mooney, eds., Geophysical Framework of the Continental United States, Geological Society of America Memoir 172, p 523–539, M. Zoback and M. Zoback, 1989.

Zoback, 1989b. Global patterns of tectonic stress, Nature, Volume 341, p 291-296, M. Zoback, M. Zoback, J. Adams, M. Assumpcao, S. Bell, E. Bergman, P. Blumling, N. Brereton, D. Denham, J. Ding, K. Fuchs, N. Gay, S. Gregersen, H. Gupta, A. Gvishiani, K. Jacob, R. Klein, P. Knoll, M. Magee, J. Mercier, B. Muller, C. Paquin, K. Rajendran, O. Stephansson, G. Suarez, M. Suter, A. Udias, Z. Xu, and M. Zhizhin,. 1989.

Zoback, 1992. Stress Field Constraints on Intraplate Seismicity in Eastern North America, Journal of Geophysical Research, Volume 97, p 11,761–11,782, M. Zoback, 1992.

2.5.2 Vibratory Ground Motion

The U.S. EPR FSAR includes the following COL Item for Section 2.5.2:

> A COL applicant that references the U.S. EPR design certification will review and investigate site-specific details of the seismic, geophysical, geological, and geotechnical information to determine the safe shutdown earthquake (SSE) ground motion for the site and compare site-specific ground motion to the Certified Seismic Design Response Spectra (CSDRS) for the U.S. EPR.

This COL Item is addressed as follows:

{This section provides a detailed description of the vibratory ground motion assessment that was carried out for the CCNPP Unit 3 site, resulting in the development of the CCNPP Unit 3 ground motion response spectra. As the first step in this process, a probabilistic seismic hazard assessment (PSHA) for a hard rock condition was carried out taking into account guidance in NRC Regulatory Guide 1.208 (NRC, 2007a). Inputs to the PSHA consist of: (1) the recently developed seismic source characterization (SSC) for the Central and Eastern United States (CEUS SSC) (EPRI/DOE/NRC, 2012) and (2) the EPRI (2004, 2006) ground motion characterization (GMC) model. Next, taking into account the deaggregation of the PSHA results, a site response analysis is carried out and combined with the PSHA results according to NUREG/CR-6728 (McGuire et al., 2001) to obtain uniform hazard response spectra (UHRS) at the surface and foundation level. Finally, those UHRS are used to develop a performance-based ground motion response spectra (GMRS) for the CCNPP Unit 3 site following Regulatory Guide 1.208 (NRC, 2007a).

NRC Regulatory Guide 1.208, "A Performance Based Approach to Define Site Specific Earthquake Ground Motion (NRC, 2007a) states in Section B, Discussion:

> "The CEUS is considered to be that part of the United States east of the Rocky Mountain front or east of Longitude 105 West (Refs. 13, 14). A Probabilistic Seismic Hazard Analysis in the Central and Eastern United States (CEUS) must account for credible alternative seismic sources through the use of a decision tree with appropriate weighting factors that are based on the most up-to-date information and relative confidence in alternative characterizations for each seismic source, Seismic sources identified and characterized by Lawrence Livermore National Laboratory (LLNL) (Refs. 13-15) and the Electric Power Research Institute (EPRI) (Refs. 16, 17) were used for the CEUS studies in the past. In addition to the LLNL and EPRI resources, the United States geological Survey maintains a large database of seismic sources for both the CEUS and the WUS. The characterization of specific seismic sources found in these databases may still represent the latest information available at the time that a PSHA is to be undertaken. However, if more up-to-date information is available, it should be incorporated."

Currently, the most up-to-date information on seismic sources in the CEUS is EPRI/DOE/NRC (2012). This model provides an updated characterization of the regional seismic sources for use in PSHAs for nuclear facilities. As such, it supercedes and replaces the previous regional seismic source models developed for the CEUS by EPRI and LLNL. Therefore, following the Regulatory Guide 1.208 (NRC, 2007a) guidelines, the CEUS SSC model is used for the PSHA of the CCNPP Unit 3 Site. The model and the methodologies for its development are described in detail in the CEUS SSC report (EPRI/DOE/NRC, 2012).

Appropriate seismic source inputs for the CCNPP Unit 3 PSHA are taken from the hazard input document (HID) provided in the CEUS SSC report (EPRI/NRC/DOE, 2012). A summary of the inputs developed during the CEUS SSC project is presented here.

The EPRI/DOE/NRC CEUS SSC model defines two general types of seismic sources: (1) distributed seismicity sources that cover the entire CEUS region and (2) repeated large magnitude earthquake (RLME) sources. For the first type, the recorded history of seismicity is used to model the frequency and spatial distribution of moderate to large earthquakes ($M_W \geq 5.0$). Two approaches are used to develop distributed seismicity source zones. One is based on areas that are interpreted to have a similar potential for maximum magnitude (the Mmax Zones approach) and the other is based on spatial variations in seismic and tectonic characteristics (the Seismotectonic Zones approach). For both the Mmax and Seismotectonic models alternative configurations are defined.

RLME sources are defined for features or areas with a history of repeated (more than one) large-magnitude (**M** $\geq$ 6.5) earthquakes in the historical or paleoearthquake record. For RLME sources the paleoearthquake record is used to model the frequency and spatial distribution of RLMEs at specific locations.

As part of the development of the updated CEUS SSC model, an updated earthquake catalog covering the entire study region was developed. The catalog includes earthquakes through 2008 and reflects a more rigorous and systematic analysis of earthquake magnitudes than for previous catalogs (e.g., EPRI (1986), USGS (2008) catalog for the National Seismic Hazard Map project). The EPRI/DOE/NRC (2012) earthquake catalog provides a moment magnitude (**M**) value for each earthquake based on an extensive analysis of conversion relations from other magnitude scales and from earthquake intensity data.

Based on the updated seismicity data, earthquake recurrence parameters were calculated for distributed seismicity zones using an updated smoothing procedure. The new procedure provides spatially varying values for both a- and b-values for the truncated exponential model.

The EPRI/DOE/NRC (2012) model also includes a revised assessment of maximum magnitudes (Mmax) and RLME source magnitudes. For distributed seismicity sources, two approaches are used to evaluate Mmax. One employs a Bayesian procedure with a prior distribution based on worldwide observations of the largest earthquakes occurring in stable continental regions believed to be tectonically similar to the CEUS. A second approach is based on the seismicity occurring in each zone. Because seismicity data in some parts of the CEUS is sparse, the second approach cannot be always applied. For RLME sources, the magnitude distribution is characterized based on the evidence of past large earthquakes.

The study region of the CEUS SSC project is shown in Figure 2.5-45. Also shown in the figure is the seismicity of the study region based on the CEUS SSC earthquake catalog (Section 2.5.2.1.1). The study region covers the part of the United States east of longitude 105 W. On the north it extends a minimum of 200 mi north from the U.S.-Canadian border. On the south and east, it includes the offshore area a minimum of 200 mi from the coastline (EPRI/DOE/NRC, 2012).

Section 2.5.2.1 through 2.5.2.3 documents the review of the EPRI/DOE/NRC (2012) CEUS SSC model with respect to seismicity, geologic and tectonic structures, and correlation of features with seismicity.

Section 2.5.2.4 develops PSHA parameters at the site assuming the very hard rock foundation conditions implied by currently accepted ground motion attenuation models.

Section 2.5.2.5 summarizes information about the seismic wave transmission characteristics of the CCNPP Unit 3 site with reference to more detailed discussion of all engineering aspects of the subsurface in Section 2.5.4.

Section 2.5.2.6 describes the development of the horizontal ground motion response spectra (GMRS) for the CCNPP Unit 3 site. The selected ground motion is based on the risk-consistent/ performance-based approach of Regulatory Guide 1.208, A Performance-Based Approach to Define the Site-Specific Earthquake Ground Motion (NRC, 2007a), with reference to NUREG/ CR-6728 (NRC, 2001), NUREG/CR-6769 (NRC, 2002b), and ASCE/SEI 43-05 (ASCE 2005). Horizontal ground motion amplification factors are developed using site-specific data and estimates of near-surface soil and rock properties. These amplification factors are then used to scale the hard rock spectra to develop Uniform Hazard Spectra accounting for site-specific conditions using Approach 2A of NUREG/CR-6728 (NRC, 2001) and NUREG/CR-6769 (NRC, 2002). Horizontal spectra are developed from these soil Uniform Hazard Spectra using the performance-based approach of ASCE/SEI 43-05 (ASCE 2005), as implemented in Regulatory Guide 1.208 (NRC, 2007a). The GMRS is defined at the free ground surface of a hypothetical outcrop at the base of the nuclear island foundation. See Sections 2.5.4 and 2.5.2.5 for further discussion of the subsurface conditions.

Section 2.5.2.6 also describes vertical spectra, which are developed by scaling the horizontal spectra by a frequency-dependent vertical-to-horizontal (V:H) factor.

The spectra that are described in this section are considered performance goal-based (risk-informed) site specific safe shutdown earthquake response spectra. The GMRS, and its specific location at a free ground surface, reflect the seismic hazard in terms of a PSHA and geologic characteristics of the site and represent the site-specific ground motion response spectrum (GMRS) of Regulatory Guide 1.208 (NRC, 2007a). These spectra are expected to be modified as appropriate to develop ground motion for design considerations. The Safe Shutdown Earthquake (SSE) for design is developed in Section 2.5.1.1.2.

2.5.2.1 Seismicity

PSHA methodologies often consider that activity in area seismic sources can be adequately represented by the Gutenberg-Richter (G-R) exponential recurrence relation. A quantitative derivation of the G-R parameters is typically based on seismicity, i.e., on catalogs of historically and instrumentally recorded earthquakes.

2.5.2.1.1 EPRI/DOE/NRC (2012) Earthquake Catalog

As part of the development of the EPRI/DOE/NRC (2012) CEUS SSC model, an updated earthquake catalog was developed. Three specific goals were pursued in developing the CEUS SSC earthquake catalog: (1) inclusion of all known earthquakes in the magnitude range considered important in assessing future earthquake hazard, (2) using a uniform earthquake size measure that is consistent with the ground motion models to be used in the PSHA, and (3) extensive review of the catalog by experienced seismologists. The CEUS SSC report (EPRI/ DOE/ NRC, 2012) provides a detailed explanation of each major step of the earthquake catalog development; a short summary of which is presented here.

The CEUS SSC earthquake catalog is developed in four steps: catalog compilation, assessment of a uniform magnitude for each event, removal of dependent events, and assessment of completeness as a function of location, time, and earthquake magnitude.

Two earthquake catalogs along with their original sources form the basis for the updated CEUS SSC earthquake catalog: (1) The earthquake catalog used by the USGS for seismic hazard mapping in the U.S. (USGS, 2008), and (2) The Geological Survey of Canada (GSC) earthquake catalog for seismic hazard analysis (Adams and Halchuck, 2003). Both the USGS and GSC catalogs are compilation catalogs based on numerous "source" or "primary" catalogs. The GSC catalog forms an important source of seismicity data for the northern portion of the CEUS SSC study region. As part of the CEUS SSC catalog development, the original sources used in the USGS and GSC catalogs have been extensively reviewed to retrieve information that was needed, but not retained in these two compiled catalogs. Additionally, special studies of individual earthquakes and earthquake sequences have been reviewed and used in compiling the CEUS SSC earthquake catalog. Non-tectonic events were identified and removed from the CEUS SSC earthquake catalog.

To develop a uniform moment magnitude (**M**) earthquake catalog, conversion relations between different earthquake size measures and **M** were derived. Because compiled catalogs by the USGS and GSC contain converted magnitudes for many events, original earthquake size measures (such as epicentral intensity, I0) for these events were found from the primary catalogs. These size measures were then directly converted to **M** using conversion relations developed during the CEUS SSC project. Direct conversion to **M** ensures that additional uncertainty (from double or multiple conversions) is not propagated through the PSHA. Conversion relations accounted for magnitude uncertainties so that the catalog can be used to develop unbiased estimated of earthquake recurrence as a function of magnitude.

Dependent events were removed using the EPRI (1988) declustering approach.

Completeness analysis of the CEUS SSC catalog is based on the EPRI (1988) completeness regions for CEUS. Some modifications were applied to these completeness regions to address additional sources of historical earthquakes used in the CEUS SSC catalog and the extension of the completeness regions to cover the entire SSC model.

The final catalog of the CEUS SSC project contains 3298 earthquakes of estimated moment magnitude E[**M**] 2.9 and larger. It covers the entire study region of the CEUS SSC and includes earthquakes for the time period of 1568 through the end of 2008. Information on earthquakes occurring after 2008 was unavailable at the time the CEUS SSC earthquake catalog was compiled. A qualitative examination of earthquakes occurring since 2008 indicated that they are consistent with the historically and instrumentally recorded earthquakes included in the catalog. One significant earthquake that occurred since 2008--the Mineral, VA earthquake of August 2011--is addressed in more detail in Section 2.5.2.1.2

Figure 2.5-46 illustrated the seismicity in the 200-mile Site region based on the CEUS SSC independent earthquake catalog (EPRI/DOE/NRC, 2012)

2.5.2.1.2 Additional Significant Earthquakes

Since the EPRI/DOE/NRC (2012) earthquake catalog was developed, one significant earthquake occurred in the CCNPP Unit 3 site region: The August 23, 2011 Mineral, VA earthquake with **M** 5.8. Its focal depth was 6 km and it was caused by reverse faulting in a plane striking N28E and dipping 50° to the east-southeast (Horton and Williams, 2012). The earthquake was felt widely in the east-central and northeastern United States.

The earthquake was located in the Central Virginia Seismic Zone (CVSZ), an area with an elevated rate of seismicity during historical time compared to most of the CEUS. In the EPRI-SOG seismic source characterization (EPRI, 1986), the CVSZ was characterized as a seismic

source, either explicitly or implicitly, by the ESTs. In most cases, the key factor in defining a source zone based on the CVSZ was the persistent low-level seismicity.

Prior to 2011, the largest earthquake documented in the zone was the 1875 Goochland County event that caused intensity of MMI VII and has an E [**M**] of 4.77 (EPRI/DOE/NRC, 2012). Recorded seismicity also includes an M_W 4.3 earthquake in 2003 (Kim and Chapman, 2005). Seismicity within the CVSZ is shallow (<11 km) and interpreted to occur on faults above the detachment that separates Precambrian basement from overlying Paleozoic and Mesozoic deposits.

Although the 2011 Mineral, VA earthquake occurred after the EPRI/DOE/NRC (2012) CEUS SSC model was developed and was in the final stages of review, the earthquake is consistent with that model. Within the framework of the EPRI/DOE/NRC (2012) CEUSS SSC model the earthquake is located in three source zones representing alternative interpretations of distributed seismicity. Using the CEUS SSC Mmax seismic zonation approach, the earthquake is located in the Study Region source zone and the Mesozoic or Younger Extended Region (MESE) source zone (both narrow and wide interpretations). For the Seismotectonic zonation approach, the earthquake falls in the Extended Continental Crust-Atlantic Margin (ECC-AM) source zone.

For all these sources zones, the **M** of the 2011 Mineral, VA earthquake is less than the entire Mmax distribution assessed by EPRI/DOE/NRC (2012). For the Study Region source zone, the Mmax distribution ranges from 6.5 to 8.1 with the largest weight on **M** 7.2. For the MESE-Wide source zone, the Mmax distribution ranges from 6.4 to 8.1 with the largest weight on **M** 7.3. For the MESE-Narrow source zone, the Mmax distribution ranges from 6.0 to 8.1 with the largest weight on M 7.3. The magnitude of the Mineral, VA earthquake (**M** 5.8) is consistent with all of these distributions.

Two approaches for assessing the Mmax distribution were used in EPRI/DOE/NRC (2012): a Bayesian approach and the approach developed by Kijko (2004). For the Bayesian approach, the maximum observed earthquake in a source zone is used in developing a likelihood function. For the Kijko approach, it is an input parameter. Thus, while the Mineral, VA earthquake is smaller than the existing Mmax distributions, it potentially could impact the assessment the Mmax distribution for each source zone in which it is located. For the Kijko approach the earthquake would also affect the observed seismicity from the catalog that is used to estimate Mmax.

For the Study Region, MESE-Wide, and the MESE-Narrow source zones, the maximum observed earthquake in the existing catalog is in each case larger then the Mineral, VA earthquake. Furthermore, for these source zones, a larger maximum observed earthquake for the Bayesian approach is taken from the paleoearthquake record. Thus there is no impact from the Mineral, VA earthquake on the Mmax distribution using the Bayesian approach. There is also no impact for the Kijko approach because the Kijko approach is not used when the maximum observed earthquake is a paleoearthquake.

For the ECC-AM source zone, the Mineral, VA earthquake impacts the assessment of Mmax, but the impact is small. There is uncertainty in the maximum observed earthquake for the ECC-AM zone. An earthquake in 1755 (**M** 6.1) is nominally the maximum observed, but there is uncertainty in its location and it may not be located in the ECC-AM sources zone. If it is not located in the ECC-AM source zone, then an earthquake in 1638 (E[**M**]=5.32) is the maximum observed. The Mineral, VA earthquake is larger then the 1638 earthquake and would become the maximum observed if the 1755 earthquake is located in a different source zone. For the Bayesian approach, this would shift some weight in the Mmax distribution to higher magnitudes, but there is only a small amount of weight in the existing assessment for

magnitudes less than 5.8 (EPRI/DOE/NRC, 2012, Figure 7.4.2-2). Thus, the impact on the distribution determined using the Bayesian approach is likely to be small.

For the ECC-AM source zone, the Kijko approach receives a weight of only 0.05 in determining the current Mmax distribution. While addition of the Mineral, VA earthquake would potentially impact that weight, any increase in the weight would tend to shift the overall Mmax distribution to lower values. Given these observations, the Mmax distribution for the ECC-AM source zone is not updated to take into account the Mineral, VA earthquake because the impact on hazard would be insignificant.

The Mineral, VA earthquake also potentially affects the seismicity recurrence rates for the source zones in which it is located. For the overall source zone, inclusion of one earthquake of **M** 5.8 is within the uncertainty in rate from the existing EPRI/DOE/NRC (2012) characterization. However, because the recurrence parameters are spatially smoothed, the impact in the vicinity of the earthquake may be more significant. The Mineral, VA earthquake, however, is located about 140 km from the CCNPP Unit 3 site. At this distance, the impact on recurrence rate may produce some effect on the hazard at the Site, but any impact would be within the uncertainty of mean hazard calculations (EPRI/DOE/NRC, 2012, Chapter 9.4).

The Mineral, VA earthquake is also consistent with the future earthquake characteristics (EPRI/DOE/NRC, 2012) assessed for the Study Region, MESE, and ECC-AM source zones.

In summary, the nature of the MVE is adequately characterized by the CEUS SSC model. This is not unexpected because the model was developed using a Senior Seismic Hazard Analysis Committee (SSHAC) Level 3 process to ensure the model captures the center, body, and range of technically defensible interpretations. As such, it is expected to provide a stable regional basis for PSHA in the CEUS. While, if the MVE were to be incorporated into an update of the CEUS SSC model, the computed hazard for the CCNPP Unit 3 site might be affected to some degree, any impact would likely be less than the precision of seismic hazard calculations. Thus, the hazard of the CCNPP Unit 3 is adequately estimated using the published version of the EPRI/DOE/NRC model without any changes based on the MVE.

2.5.2.1.3 Seismicity Zones in the Site Region

2.5.2.1.3.1 Central Virginia Seismic Zone

Seismicity in the CVSZ ranges in depth from about 2 mi (3km) to 8 mi (13 km) (Wheeler, 1992). Coruh and others (Coruh, 1988) suggest that seismicity in the central and western parts of the zone may be associated with west-dipping reflectors that form the roof of a detached antiform, while seismicity in the eastern part of the zone near Richmond may be related to a near-vertical diabase dike swarm of Mesozoic age. However, given the depth distribution of 2 mi (3km) to 8 mi (13 km) (Wheeler, 1992) and broad spatial distribution, it is difficult to uniquely attribute the seismicity to any known geologic structure and it appears that the seismicity extends both above and below the Appalachian detachment.

Two liquefaction features have been found within the CVSZ (Obermeier, 1998). The lack of widespread liquefaction features in the 186 mi (300 km) of stream exposures searched within the CVSZ, despite the presence of mid- to late-Holocene potentially liquefiable deposits, has led some researchers (Obermeier, 1998) to conclude that it is unlikely that an earthquake of magnitude 7 or larger has occurred within the seismic zone in the last 2,000 to 3,000 years, or in the eastern portion of the seismic zone for the last 5,000 years.

Within the CCNPP Unit 3 site region, the paleo-liquefaction features found within the Central Virginia seismic zone are the only two recorded occurrences of Quarternary earthquake-induced geologic failure. Within the CCNPP Unit 3 site region, a literature review, which included compilations of potential Quarternary features by Crone and Wheeler (Crone, 2000), Wheeler (Wheeler, 2005) and Wheeler (Wheeler, 2006), found no other documented evidence of Quarternary earthquake-induced geologic failure, such as earthquake-induced liquefaction, landsliding, land spreading, or lurching. Outside of the CCNPP Unit 3 site region, widespread liquefaction is recorded near Charleston, South Carolina.

In developing the EPRI/DOE/NRC (2012) CEUS SSC model, information on the Central Virginia seismic zone was considered and evaluated. Based on the evaluation and the integration of available data, the CEUS SSC Technical Integration (TI) Team did not identify the Central Virginia seismic zone as a specific seismic source. Future seismicity in the vicinity of the Central Virginia seismic zone is represented by various distributed seismicity seismic sources.

2.5.2.1.3.2 Lancaster Seismic Zone

The Lancaster Seismic Zone (LSZ) of the southeastern Pennsylvania is located about 111 mi (179 km) northwest of the CCNPP Unit 3 site. This region of seismicity in the Appalachian mountains of Pennsylvania is described in Section 2.5.1.1.4.5 and includes roughly two centuries of seismicity. Despite its moderate rate of activity, the largest known earthquake was magnitude mbLg 4.1 (Armbruster and Seeber, 1987). One larger event has been attributed to anthropogenic causes (i.e. Cacoosing Valley Earthquake mbLg 4.6: (Seeber, 1998). No evidence of larger prehistoric earthquakes, such as paleoliquefaction features, has been discovered (Wheeler, 2006).

In developing the EPRI/DOE/NRC (2012) CEUS SSC model, information in the LSZ was considered and evaluated. Based on the evaluation and integration of available data, the CEUS SSC Technical Integration (TI) Team did not identify the LSZ as a specific seismic source. Future seismicity in the vicinity of the LSZ is represented by various distributed seismicity seismic sources. Maximum magnitudes for these seismic sources range from 5.9 to 8.1. These values are significantly larger than the largest reported earthquakes in the LSZ.

2.5.2.1.3.3 Earthquake Swarm of Howard County, Maryland

Howard County of Maryland, located about 12 mi (19 km) southwest of Baltimore, experienced 21 confirmed and probably shallow (less than a kilometer) earthquakes between March and November 1993 (Reger, 1994). The largest earthquakes recorded with m_{bLg} 2.5 and m_{bLg} 2.7, occurred early in the sequence. Analyses of seismicity data define a short (1000 ft (305 m) long) northwest-striking reverse fault with a minor component of left-lateral slip. Researchers speculate that the earthquakes may be associated with a diabase dike either aligned with the inferred reverse fault or offset by the inferred reverse fault; however, the cause of the earthquake swarm remains unknown. Field examination by the Maryland Geological Survey did not find any evidence for surface fault rupture in the region of the inferred surface projection of the fault (Reger, 1994). This earthquake swarm occurred in a region that has no previous history of seismicity.

In developing the EPRI/DOE/NRC (2012) CEUS SSC model, information on the Howard County earthquake swarm was not explicitly considered because of the very small size of the earthquakes. Future seismicity in the vicinity of the Howard County earthquake swarm is represented by various distributed seismicity seismic sources. Maximum magnitudes for these seismic sources range from 5.9 to 8.1. These values are significantly larger than the largest reported earthquakes in the Howard County earthquake swarm.

2.5.2.2 Geologic and Tectonic Characteristics of Site and Region

As described in Section 2.5.1, a comprehensive review of available geological, seismological, and geophysical data has been performed for the CCNPP Unit 3 site region and adjoining areas. As discussed in Section 2.5.1.2.6, excavation mapping is required during construction and any noted deformational zones will be evaluated and NRC notified when excavations are open for inspection. The following sections summarize the seismic source interpretations from the EPRI/DOE/NRC (2012) CEUS SSC model. A review of the model was performed to identify seismic source zones relevant to the assessment of seismic hazard at the CCNPP Unit 3 site. Following the review, inputs related to alternative source models and their weights, seismic source zones and their earthquake recurrence parameters were retrieved from the CEUS SSC Hazard Input Document (EPRI/DOE/NRC, 2012, Appendix H). Various aspects of the model and related input, as needed, are presented in this and following subsections. As documented in Section 2.5.1, no new geologic information was found that would suggest modifications to the EPRI/DOE/NRC (2012) model are required. Potential impacts of the 2011 Mineral, VA earthquake are addressed in Section 2.5.2.1.2.

Section 1.1 of the CEUS SSC report states:

"The Central and Eastern United States Seismic Source Characterization for Nuclear Facilities (CEUS SSC) Project was conducted over the period from April 2008 to December 2011 to provide a regional seismic source model for use in probabilistic seismic hazard analyses (PSHAs) for nuclear facilities. As such, the CEUS SSC model replaces regional seismic source models for this region that are currently accepted by the Nuclear Regulatory Commission (NRC) for assessing seismic design bases and their associated uncertainties satisfying the requirements of the seismic regulation, 10 CFR Part 100.23. The models being replaced are the Electric Power Research Institute-Seismicity Owners Group (EPRI-SOG) SSC model (EPRI, 1988) and the Lawrence Livermore National Laboratory (LLNL) SSC Model (Bernreuter et al., 1989) sponsored by the NRC."

The CEUS SSC Project used a SSHAC level 3 assessment process to ensure compliance with NRC guidance for quantifying uncertainties in PSHA supporting the development of a seismic design basis for nuclear facilities.

The CEUS SSC report states in Section 1.1.1:

"The CEUS SSC Project replaces the SSC components of the landmark seismic hazard projects conducted in the 1980s by EPRI-SOG (EPRI, 1988) and LLNL (Berneruter et al., 1989). Both of these projects developed PSHA models for application in the broad region of the United States to the east of the Rocky Mountains. Recent Licensing applications for nuclear facilities submitted to the NRC have followed regulatory guidance by using the EPRI-SOG SSC model as a starting point, with updates as appropriate on a site-specific basis for site-specific PSHAs. However, while the regional SSC model has been updated for specific sites, it has not been systematically updated to account for the significant new data in the CEUS. The CEUS SSC Project takes full advantage of the following historical and new sources: data used to develop the two previous CEUS models; new data and information developed over the past 20 years, including that developed for the U.S. Geological Survey (USGS) seismic hazard mapping program (Peterson et al., 2008); and other information and hazard analyses that were developed as part of licensing actions for proposed and existing nuclear power facilities. In addition to the new data, updated methods for evaluating the data and quantifying uncertainties have been implemented in the CEUS SSC Project."

Sections 2.5.2.2.1 and 2.5.2.2.2 are added as a supplement to the U.S. EPR FSAR.

2.5.2.2.1 Summary of the CEUS SSC Source Model

The CEUS SSC model contains two general types of seismic sources (EPRI/DOE/NRC, 2012):

1. Distributed seismicity sources covering the entire CEUS study region (Figure 2.5-45). For this type of seismic source the recorded history of seismicity is used to model the frequency and spatial distribution of moderate to large earthquakes (**M** $\geq$ 5). Two approaches are used to characterize the distributed seismicity sources (EPRI/DOE/NRC, 2012). In the first approach, termed the Mmax Zones approach, the distributed seismicity is modeled using seismicity rates that smoothly vary across the entire study region. The study region is subdivided only on the basis of differences in the assessed Mmax distribution. In the second approach, termed the Seismotectonic Zones approach, distributed seismicity is modeled using seismic source zones defined on a seismotectonic basis. In the master logic tree of the CEUS SSC model shown in Figure 2.5-47, the Mmax Zones approach and the Seismotectonic Zones approach are assigned weights of 0.4 and 0.6, respectively.

2. Repeated Large Magnitude Earthquake (RLME) sources are the locations of repeated (more than one) large-magnitude (**M** $\geq$ 6.5) earthquakes (EPRI/DOE/NRC, 2012). For RLME sources, earthquakes in the historical or paleoearthquake record are used to model the frequency and spatial distribution of RLMEs at specific locations. As illustrated in Figure 2.5-47, the RLME sources represent additional sources of seismic hazard that are added to the hazard from the distributed seismicity sources.

For the Mmax Zones, Seismotectonic Zones, and RLME approaches to defining seismic sources, only those relevant to the assessment of seismic hazard at the CCNPP Unit 3 site are discussed here. Relevant sources are taken as those distributed seismicity sources located entirely or partially within the 200-mile region surrounding the CCNPP Unit 3 site, as well as more distant RLME sources that are expected to contribute to the hazard primarily at lower response frequencies. In the calculation of seismic hazard at the CCNPP Unit 3 site, for distributed seismicity source zones that are included and extend beyond the 200-mile (320-km) site region, integration is carried out to a distance of 435 mi (700 km).

2.5.2.2.1.1 Distributed Seismicity Source Zones

2.5.2.2.1.1.1 Mmax Zones

EPRI/DOE/NRC (2012) describes alternative configurations for Mmax source zones. In one configuration the entire study region is considered as a single source zone. In an alternative configuration, the study region is divided into two source zones with different Mmax distributions depending on whether an area was subject to Mesozoic or younger extension (MESE source) or not (NMESE source). Additional configurations depend on alternative interpretations of the extent of the MESE and NMESE sources.

For the CCNPP Unit 3 site, three alternative configurations for the Mmax Zones approach are included in the PSHA. These configurations, referred to herein as Mmax Model M-I, M-II, and M-III, are described below. For each configuration, the RLME sources are also active.

Mmax Model M-I

Mmax Model M-I treats the entire study region as a single source zone (Figure 2.5-45). The model has a weight of of 0.16, resulting from the weight of 0.4 assigned to the Mmax Zones

approach times the weight of 0.4 for the interpretation that the study region has a single Mmax distribution (EPRI/DOE/NRC, 2012).

For the Mmax Model M-I configuration, the Study Region source zone hosts the CCNPP Unit 3 Site and contains the entire site region except for a small area that lies outside the boundaries of the CEUS SSC model in the Atlantic Ocean. Hazard at the Site from the Study Region Mmax source zone is controlled by the spatially smoothed earthquake recurrence parameters and the associated maximum magnitude distribution (Table 2.5-6).

Mmax Model M-II

Mmax Model M-II represents the case for which the study region is divided into two source zones depending on whether an area was subject to Mesozoic or younger extension (MESE) or not (NMESE), and in which a "Wide Interpretation" of the extent of the Mesozoic extension is used (EPRI/DOE/NRC, 2012) (Figure 2.5-48). In an analysis of which geologic and tectonic characteristics of stable continental regions correlate with magnitude, Mesozoic and younger extension was the only characteristic that showed a correlation, although the correlation was weak. From Mmax Model M-II, only Source Zone MESE-W is considered for the PSHA analysis for the CCNPP Unit 3 Site. Source Zone NMESE-W is outside the 200-mile region of the Site.

The M-II source model configuration has a weight of 0.048, resulting from the weight of 0.4 assigned to the Mmax Zones approach, the weight of 0.6 for the interpretation that the study region is separated into Mesozoic or Younger Extended and Non-Extended regions, and the weight of 0.2 for the "Wide Interpretation" of the extent of the Mesozoic extension (EPRI/DOE/NRC, 2012).

For the Mmax Model M-II configuration, the MESE-W source zone hosts the CCNPP Unit 3 Site and contains the site region. Hazard at the Site from the MESE-W source zone is controlled by the spatially smoothed earthquake recurrence parameters and the associated maximum magnitude distribution (Table 2.5-6).

Mmax Model M-III

Mmax Model M-III represents the model for which the study region is divided into MESE and NMESE regions, with a "Narrow Interpretation" of the extent of the Mesozoic extension (EPRI/DOE/NRC, 2012) (Figure 2.5-49). The CCNPP Unit 3 site is located within the boundaries of Source Zone MESE-N. Also, part of Source Zone NMESE-N lies within the 200-mile Site region. Therefore, for Model M-III, both these source zones are included in the PSHA for the CCNPP Unit 3 site.

The M-III source model configuration has a weight of 0.192, resulting from the weight of 0.4 assigned to Mmax Zones approach, 0.6 assigned to the interpretation that the study region is separated into Mesozoic or Younger Extended and Non-Extended regions, and 0.8 for the "Narrow Interpretation" of the extent of the Mesozoic extension (EPRI/DOE/NRC, 2012).

For the Mmax Model M-III configuration, the MESE-N source zone hosts the CCNPP Unit 3 Site. Hazard at the Site from the MESE-N and NMESE-N Mmax source zones is controlled by the spatially smoothed earthquake recurrence parameters and the associated maximum magnitude distributions (Table 2.5-6).

2.5.2.2.1.1.2 Seismotectonic Zones

For the seismotectonic approach to source zonation, the following source zones comprise the CEUS model (EPRI/DOE/NRC, 2012) (Table 2.5-2):

- Atlantic Highly Extended Crust (AHEX)
- Extended Continental Crust-Atlantic Margin (ECC-AM)
- Extended Continental Crust-Gulf Coast (ECC-GC)
- Great Meteor Hotspot (GMH)
- Illinois Basin Extended Basement (IBEB)
- Gulf Highly Extended Crust (GHEX)
- Midcontinent-Craton Alternatives (MidC-A, MidC-B, MidC-C, and MidC-D)
- Northern Appalachians (NAP)
- Oklahoma Aulacogen (OKA)
- Paleozoic Extended Crust narrow and Paleozoic Extended Crust wide (PEZ-N and PEZ-W)
- Reelfoot Rift and Reelfoot Rift including the Rough Creek Graben (RR and RR-RCG)
- St. Lawrence Rift, including the Ottawa and Saguenay grabens (SLR)

The uncertainty in the western boundary of the Paleozoic Extended Crust seismotectonic zone (PEZ) is represented by two alternatives (EPRI/DOE/NRC, 2012): the "Narrow Interpretation" and the "Wide Interpretation". Two alternative interpretations are also provided for the Reelfoot Rift zone: in one the Reelfoot Rift includes the Rough Creek Graben (RR-RGG); in the other it does not (RR). The uncertainties in the western boundary of the PEZ zone and whether or not the Rough Creek Graben is included in the Reelfoot Rift zone together result in four alternative seismotectonic source configurations shown in Figure 2.5-50 through Figure 2.5-53. These configurations are referred to herein as Seismotectonic Models S-I, S-II, S-III, and S-IV. The alternative zonation configurations produce alternative versions of the Mid-Continent source zone designated MidC-A, MidC-B, MidC-C, and MidC-D. Inclusion source zones in the CCNPP Unit 3 PSHA depends on whether the source zones associated with each model extend to within 200 miles (320 km) of the Site.

Seismotectonic Model S-I

Seismotectonic Model S-I represents the case for which the PEZ source zone is interpreted as being narrow (PEZ-N) and the RCG is not part of the RR source zone, leading to the configuration shown in Figure 2.5-50. The version of the Mid-Continent source zone associated with this configuration is designated MidC-A. For this model, the following source zones are included in the PSHA for the CCNPP Unit 3 site: AHEX, ECC-AM, PEZ-N, and MidC-A. The ECC-AM zone hosts the CCNPP Unit 3 site.

Model S-I is assigned a weight of 0.32, resulting from the weight of 0.6 for the Seismotectonic Zones approach, the weight of 0.8 for the "Narrow Interpretation" of the PEZ source zone, and the weight of 0.667 for the interpretation that the RCG is not part of the RR source zone (EPRI/DOE/NRC, 2012).

Seismotectonic Model S-II

Seismotectonic Model S-II represents the case for which the PEZ source zone is interpreted as being narrow and the RCG is part of the RR source zone, leading to the configuration shown in Figure 2.5-51. The version of the Mid-Continent source zone associated with this configuration is designated MidC-B. For this model, the following source zones are included in the PSHA for the Calvert Cliffs Site: AHEX, ECC-AM, PEZ-N, and MidC-B.

Model S-II is assigned a weight of 0.16, resulting from the weight of 0.6 assigned to the Seismotectonic Zones approach, the weight of 0.8 for the "Narrow Interpretation" of the PEZ source zone, and the weight of 0.333 for the interpretation that the RCG is part of the RR source zone. As for Model S-I, the ECC-AM zone hosts the CCNPP Unit 3 Site for this source zone configuration (EPRI/DOE/NRC, 2012).

Seismotectonic Model S-III

Seismotectonic Model S-III represents the case for which the PEZ source zone is interpreted as being wide (PEZ-W) and the RCG is not part of the RR source zone, leading to the configuration shown in Figure 2.5-52. The version of the Mid-Continent source zone associated with this configuration is designated MidC-C. For this model, the following source zones are included in the PSHA for the CCNPP Unit 3 Site: AHEX, ECC-AM, and PEZ-W. The source zone MidC-C is outside the 200-mile region of the Site and, therefore, is not considered in the PSHA input.

Model S-III is assigned a weight of 0.08, resulting from the weights of 0.6 for the Seismotectonic Zones approach, the weight of 0.2 for the "Wide Interpretation" of the PEZ source zone, and the weight of 0.667 for the interpretation that the RCG is not part of the RR source zone (EPRI/DOE/NRC, 2012).

Seismotectonic Model S-IV

Seismotectonic Model S-IV represents the case for which the PEZ source zone is interpreted as being wide (PEZ-W) and the RCG is part of the RR source zone, leading to the configuration shown in Figure 2.5-53. The version of the Mid-Continent source zone associated with this configuration is designated MidC-D. For this model, the following source zones are considered relevant for seismic hazard at the CCNPP Unit 3 site: AHEX, ECC-AM, and PEZ-W. The source zone MidC-D is outside the 200-mile region of the Site and therefore, is not considered in the PSHA input.

Model S-IV is assigned a weight of 0.04, resulting from the weights of 0.6 for the Seismotectonic Zones approach, the weight of 0.2 for the "Wide Interpretation" of the PEZ source zone, and the weight of 0.333 for the interpretation that the RCG is part of the RR source zone (EPRI/DOE/NRC, 2012).

Because the source zones for the CCNPP Unit 3 PSHA from seismotectonic models S-III and S-IV are identical, only one of these models (Seismotectonic Model S-III) is used in the PSHA. It is assigned the combined weight of models S-III and S-IV (i.e., 0.12).

The source models used in the PSHA of the CCNPP Unit 3 Site are summarized in Table 2.5-3.

Brief summaries of the basis for the Seismotectonic source zones included in the CCNPP Unit 3 PSHA are provided below based on EPRI/DOE/NRC (2012):

Atlantic Highly Extended Crust Zone (AHEX)

The AHEX zone is based on the extent of highly extended continental crust that forms a transition between the extended continental crust of the ECC-AM source zone and oceanic crust further offshore (EPRI/DOE/NRC, 2012). The highly extended crust in this zone is thinner than in the ECC-AM source zone, which is interpreted to affect future earthquake characteristics. The highly extended crust also has a more mafic composition resulting from the introduction of significant igneous material during Triassic and Jurassic rifting to create the Atlantic Ocean basin. The East Coast Magnetic Anomaly marks the transition from highly extended crust to oceanic crust and forms the eastern boundary to the AHEX source zone.

The AHEX zone is located within the CCNPP Unit 3 site region for all the seismotectonic model configurations. No uncertainty is included in the CEUS SSC model for the boundary between the AHEX and ECC-AM model (EPRI/DOE/NRC, 2012). Thus, the position of the AHEX zone relative to the CCNPP Unit 3 Site is identical for seismotectonic model S-I through S-IV. At its closest approach to the Site, the zone is more than 100 mi away. Given the low level of seismicity recorded in this source zone (EPRI/DOE/NRC, 2012), which controls the modeled future occurrence of earthquakes, its contribution to hazard at the Site is small.

Extended Continental Crust-Atlantic Margin Zone (ECC-AM)

The ECC-AM zone is based on the extent of extended continental crust associated with the Mesozoic break-up of Pangea to form the Atlantic Ocean basin (EPRI/DOE/NRC, 2012). The terrane is characterized by rift basins and an underlying detachment surface separating Paleozoic and Mesozoic deposits from the Precambrian basement. The extended nature of the crust is the key characteristic defining the zone. It is distinguished from the AHEX zone by a lesser degree of extension and a related thicker crust.

For the Seismotectonic Zones approach to defining distributed seismicity source zones, the ECC-AM zone hosts the CCNPP Unit 3 Site for all configurations. No uncertainty is included in the CEUS SSC model for the zone boundary (EPRI/DOE/NRC, 2012). Thus, the contribution from the source zone to the total hazard is identical for seismotectonic model S-I through S-IV. Concentrations of seismicity in central Virginia and to the northeast of the Site in Maryland, Delaware, New Jersey, and southeastern Pennsylvania lead to relatively elevated activity levels for these areas in modeling future earthquake occurrence (EPRI/DOE/NRC, 2012). The maximum magnitude distribution for the ECC-AM zone is the same as for the AHEX zone to the east and slightly higher than for the PEZ zone to the west (EPRI/DOE/NRC, 2012). Hazard from the ECC-AM zone is a primary contributor to total hazard at the site for mean annual exceedance frequencies of 10^{-4}, 10^{-5}, and 10^{-6}, especially for higher response frequencies (see Section 2.5.2.4.2).

Paleozoic Extended Crust Zone (PEZ)

The PEZ zone is based on the extent of Paleozoic rift-related structures (EPRI/DOE/NRC, 2012). A number of investigators postulate that reactivation of such structures is a cause of contemporary seismicity in portions of the CEUS. The western extent of Paleozoic extension is uncertain. Thus, two alternative configurations of the zone are defined (EPRI/DOE/NRC, 2012): a narrow interpretation (PEZ-N) and a wide interpretation (PEZ-W). While some Paleozoic rift-related structures may have been reactivated during Mesozoic rifting, the zone is distinguished from the ECC-AM zone because evidence for such reactivation is equivocal.

For seismotectonic models S-I through S-IV, the PEZ zone extends within the CCNPP Unit 3 site region. For the narrow interpretation, a portion of the western boundary of the zone is less than 200 mi (322 km) from the Site and, thus, the MidC-A and MidC-B zones also extend within the site region. For the wide interpretation, the western boundary of the PEZ zone lies outside the site region. Thus, the MidC-C and MidC-D zones do not extend within 200 mi (322 km) of the Site. In the portion of the zone closest to the Site, the modeled rates of future earthquake occurrence are somewhat less than for the ECC-AM zone. The maximum magnitude distribution of the PEZ zone also is slightly less than for the ECC-AM zone (EPRI/DOE/NRC, 2012). Hazard from the PEZ zone contributes to the total hazard at the Site, but not as strongly as the hosting ECC-AM zone.

Midcontinent-Craton Zone (MidC)

The MidC zone encompasses the regions of the continental interior that were not involved in the Phanerozoic orogens along continental margins (EPRI/DOE/NRC, 2012). The crust has not been subject to Mesozoic or younger extension. Because of uncertainty in the configuration of the PEZ zone (narrow or wide) and the Reelfoot Rift zone (includes the Rough Creek Graben or not), there are four configurations of the MidC zone, designated MidC-A, MidC-B, MidC-C, and MidC-D. These configurations correspond to seismotectonic models S-I through S-IV, respectively.

The MidC-A and MidC-B zones lie partially within the 200 mi (322 km) site region and are included in the CCNPP Unit 3 Site PSHA. The MidC-C and MidC-D zones lie entirely outside of the site region and are not included in the PSHA. Hazard contributions from the MidC-A and MidC-B zones to the total hazard at the Site are small (Section 2.5.2.4.2). The small contribution derives from their distance from the Site, a rate of activity that is similar or less than that for zones that are closer to the Site, and a maximum magnitude distribution that is lower than for other distributed seismicity zones included in the PSHA.

2.5.2.2.1.1.3 Earthquake Recurrence Parameters for Distributed Seismicity Zones

Magnitude Interval Weighting

In assessment of recurrence parameters, earthquakes with magnitudes as low as E[M] 2.9 are used (EPRI/DOE/NRC, 2012). Because for lower magnitudes the magnitude-recurrence law may deviate from exponential, or the magnitude conversion models or completeness model may be less reliable, lower magnitude bins are assigned lower weights in the estimation of seismicity parameters. In EPRI/DOE/NRC (2012), three alternative cases of magnitude-dependent weights are used for the distributed seismicity source zones: Case A, Case B and Case E, with weights of 0.3, 0.3 and 0.4, respectively (EPRI/DOE/NRC, 2012) (Table 2.5-4).

Assessment of Seismicity Rates

In EPRI/DOE/NRC (2012), seismicity rates for distributed seismicity source zones are determined allowing both the a-value and the b-value of the truncated exponential model to vary spatially (Table 2.5-5). To have the ability to resolve any sharp gradients in parameters that may occur in the more active regions, seismicity parameters are estimated for 1/4 degree longitude by 1/4 degree latitude cells or partial cells for all the distributed seismicity sources except the Mmax sources and MidC sources in the seismotectonic models, for which the cell size 1/2 degree longitude by 1/2 degree latitude is used.

Degree of Smoothing of Seismicity Rates

EPRI/DOE/NRC (2012) use a single approach to select the degree of spatial smoothing used to determine recurrence parameters for each source. For all sources the "Objective" approach is used (Table 2.5-5). The approach is objective in the sense that it determines the optimal degree of smoothing for each source zone based on data.

Uncertainty in Earthquake Recurrence Rates

EPRI/DOE/NRC (2012) represents the uncertainty in recurrence parameters by eight alternative spatial distributions developed from the fitted parameter distributions. The result is eight equally weighted alternative sets of recurrence parameters for each distributed seismicity source zone (Table 2.5-5). Two sets of earthquake recurrence parameters are developed for the distributed seismicity zones: (1) recurrence parameters for PSHA calculations that integrate over magnitude starting from a minimum magnitude of **M** 4.0, which would typically be used for PSHA calculations incorporating the Cumulative Absolute Velocity (CAV) filter, and (2) recurrence parameters for integration from a minimum magnitude of **M** 5.0. This latter set of parameters is used in the PSHA for the CCNPP Unit 3 site.

2.5.2.2.1.1.4 Maximum Magnitude for Distributed Seismicity Sources

The CEUS SSC model provides Mmax distributions in terms of **M** for all seismic sources (EPRI/DOE/NRC, 2012). For distributed seismicity source zones, two approaches are used to evaluate Mmax (EPRI/DOE/NRC, 2012). One is a Bayesian approach with a prior distribution based on worldwide observations of the largest earthquakes occurring in stable continental regions believed to be tectonically similar to CEUS. A second approach, developed by Kijko (2004), is based on the seismicity occurring in each zone. The approaches nominally receive equal weight, but the weight for the Kijko approach is adjusted depending on an assessment of confidence in the determined Mmax. Because seismicity data in some parts of the CEUS is sparse, the Kijko approach often receives low or no weight. Maximum magnitude distributions for Mmax and Seismotectonic Zones are given in Table 2.5-6 and Table 2.5-7, respectively.

2.5.2.2.1.1.5 Rupture Characteristics for Distributed Seismicity Sources

Hazard from distributed seismicity source zones is calculated using virtual ruptures for future earthquakes. The CEUS SSC model, thus, characterizes the aleatory variability for the rupture characteristics of future earthquakes for seismic sources in the model (EPRI/DOE/NRC, 2012). The rupture characteristics for the Mmax and Seismotectonic Zones considered in the PSHA for CCNPP Unit 3 site are summarized in Table 2.5-8.

For all distributed seismicity zones considered in the PSHA, earthquake ruptures are modeled as the result of strike-slip and reverse faulting. The two styles of faulting are assigned weights of 0.666 and 0.334, respectively (EPRI/DOE/NRC, 2012).

The boundaries of all the distributed seismicity sources are considered to be leaky, allowing rupture to extend beyond the source boundary (EPRI/DOE/NRC, 2012).

For each source zone, the area A (in km2) of each modeled earthquake rupture is determined using equation (2.5-1) (EPRI/DOE/NRC, 2012):

$\log_{10}A=M - 4.366$	(2.5-1)

The rupture aspect ratio is 1:1 until the rupture reaches the maximum rupture width (EPRI/DOE/NRC, 2012). The maximum rupture width is defined by the seismogenic crustal thickness and the dip angle of the rupture plane. The distributions of seismogenic crustal thickness values for distributed seismicity zones are given in Table 2.5-9. For ruptures that exceed the available rupture width using a 1:1 aspect ratio, the width is fixed at the maximum value and length is increased to obtain the area given by equation 2.5-1. This model is also used for RLME sources (EPRI/DOE/NRC, 2012).

2.5.2.2.1.2 RLME Sources

RLME sources are defined on the basis of features or areas that have experienced repeated (more than one) large-magnitude (**M** $\geq$ 6.5) earthquakes in the historical or paleoearthquake record (EPRI/DOE/NRC, 2012). Because of the rarity of RLMEs relative to the period of historical observation, evidence for these earthquakes comes largely from the paleoearthquake record, especially from paleo-liquefaction data. As illustrated in Figure 2.5-47, the RLME sources are considered to be additional sources superimposed on the distributed seismicity sources on the seismotectonic branch or on the Mmax branch of the master logic tree for the CEUS SSC model (EPRI/DOE/NRC, 2012).

The RLME sources are (EPRI/DOE/NRC, 2012): (1) Charlevoix; (2) Charleston; (3) Cheraw Fault; (4) Meers Fault; (5) Reelfoot Rift - New Madrid Fault System (NMFS); (6) Reelfoot Rift - Eastern Rift Margin Fault (ERM), consisting of a southern segment (ERM-S) and northern segment (ERM-N); (7) Reelfoot Rift - Marianna; (8) Reelfoot Rift - Commerce Fault Zone; and (9) Wabash Valley. The RLMEs associated with the NMFS are modeled as occurring on three fault sources: (a) the New Madrid South (NMS) fault; (b) the New Madrid North (NMN) fault; and (c) the Reelfoot Thrust (RFT).

Of the RLME sources, the Charleston, Reelfoot Rift (NMFS, ERM, Commerce Fault Zone, and Marianna), and Wabash Valley are included in the PSHA for the CCNPP Unit 3 site to assess their contribution to hazard. The Charlevoix, Cheraw Fault, and Meers Fault RLME sources were judged to have combinations of distance from the CCNPP Unit 3 Site, RLME magnitude, and recurrence rate that would result in negligible contribution to total hazard at the Site. The total hazard results (Section 2.5.2.4.2) show that only the NMFS and Charleston RLME sources make a significant contribution to hazard, especially at lower response frequencies and mean annual frequencies of exceedance greater than 10^{-6}. The RLME sources considered in the PSHA for the CCNPP Unit 3 Site are shown in Figure 2.5-54.

2.5.2.2.1.2.1 Source Geometry and Style of Faulting for RLME Sources

Charleston RLME Source

Three alternative source zone geometries are considered for the Charleston RLME source in the CEUS SSC model (EPRI/DOE/NRC, 2012) (Figure 2.5-55). The geometries and style of faulting for the three cases are specified as follows (Table 2.5-10):

- Charleston Local Source Configuration: The "local" configuration includes the 1886 meizoseismal area, the majority of the 1886 liquefaction features, and numerous postulated faults. Future ruptures are oriented northeast, parallel to the long axis of the zone. Ruptures are modeled as occurring on vertical strike-slip faults. All boundaries of the Charleston Local source are strict, such that ruptures are not allowed to extend beyond the zone boundaries.

- Charleston Narrow Source Configuration: The "narrow" configuration contains postulated north-northeast-striking structures, including the postulated Woodstock fault and the southern segment of the postulated East Coast Fault System. Future ruptures are oriented north-northeast, parallel to the long axis of the zone. Ruptures are modeled as occurring on vertical strike-slip faults. The northeast and southwest boundaries of the Charleston "narrow" source are leaky, whereas the northwest and southeast boundaries are strict.

- Charleston Regional Source Configuration: The "regional" configuration envelops most of coastal South Carolina, including the majority of pre-1886 paleo-liquefaction features and postulated faults. It extends offshore to include the Helena Banks fault zone. Future rupture orientations are represented by two alternatives: (1) future ruptures oriented parallel to the long axis of the source (northeast) with 0.8 weight, and (2) future ruptures oriented parallel to the short axis of the source (northwest) with 0.2 weight. In both cases, future ruptures are modeled as occurring on vertical strike-slip faults. All boundaries of the Charleston "regional" source are strict.

The Charleston RLME source lies between about 350 and 500 mi (560 and 800 km) from the CCNPP Unit 3 Site, depending on which alternative configuration is considered (Figure 2.5-54). The "Local" configuration is given the largest probability (0.5) of representing the Charleston source; the "Regional" configuration, which extends closest to the CCNPP Unit 3 Site, is given the lowest probability (0.2). While distant from the Site regardless of the configuration considered, the combination of the RLME magnitude distribution and the rate of recurrence for the RLME earthquake result in a significant contribution to total hazard. Hazard deaggregation results (Section 2.5.2.4.2) indicate the contribution is primarily for the low response frequency range.

New Madrid Fault System RLME Source

The New Madrid region is the source of the 1811-1812 New Madrid earthquake sequence (EPRI/DOE/NRC, 2012). The earthquake sequence included the three largest earthquakes to have occurred in historical time in the CEUS. The region has also experienced multiple sequences of paleoearthquakes.

The NMFS RLME source consists of three faults (EPRI/DOE/NRC, 2012). Each fault has two alternative geometries (Table 2.5-10). For the NMS fault, the two alternative geometries are the Blytheville Arch-Bootheel Lineament (BA-BL) and the Blytheville Arch-Blytheville fault zone (BA-BFZ) (Figure 2.5-56). Alternative geometries for the NMN fault are New Madrid North (NMN-S) and New Madrid North plus extension (NMN-L) (Figure 2.5-56). For the RFT fault, alternative geometries are Reelfoot thrust (RFT-S) and Reelfoot thrust plus extensions (RFT-L) (Figure 2.5-56). Future NMFS earthquakes are modeled to occur on these faults.

The style of faulting for each of the faults (Table 2.5-10) is based on geologic and seismologic observations (EPRI/DOE/NRC, 2012). The NMS fault is modeled as a vertical right-lateral strike-slip fault. The RFT fault is modeled as a reverse fault dipping an average of 40 degrees southwest. The NMN fault is modeled as a vertical right-lateral strike-slip fault.

The NMFS RLME source lies about 725 to 800 mi (1150 to 1300 km) from the CCNPP Unit 3 Site (Figure 2.5-54). Because of its great distance, alternative configurations have negligible impact on total hazard at the Site. While very distant from the Site, the RLME magnitude distribution and recurrence rate result in a significant contribution to total hazard. Hazard deaggregation results (Section 2.5.2.4.2) indicate the contribution is primarily for the low response frequency range and mean annual frequencies of exceedance greater than 10^{-6}.

Eastern Rift Margin RLME Source

The ERM RLME source consists of a northern (ERM-N) and southern (ERM-S) component (EPRI/DOE/NRC, 2012). There are two alternative geometries for the ERM-S RLME source (EPRI/DOE/NRC, 2012): Eastern Rift Margin South/Crittenden County (ERM-SCC) and the Eastern Rift Margin South/River Picks (ERM-SRP). These are shown on Figure 2.5-57 and listed in Table 2.5-10. A single geometry is specified for the ERM-N RLME source (Figure 2.5-57).

Future ruptures are to be modeled as vertical strike-slip ruptures aligned parallel with the long axis to the RLME source zones (EPRI/DOE/NRC, 2012). Both the northeastern and southwestern ends of the zones are modeled as leaky to allow for uncertainty in the extent of possible reactivated faults along the rift margin.

The ERM RLME source lies about 700 to 800 mi (1125 to 1300 km) from the CCNPP Unit 3 Site. Because of its great distance from the Site, the alternative configurations produce essentially the same contribution to total hazard at the Site. Although included in the PSHA, its RLME magnitude distribution and recurrence rate result in it contributing negligibly to total hazard (Section 2.5.2.4.2).

Marianna RLME Source

A single geometry for the Marianna RLME source is used (EPRI/DOE/NRC, 2012). The geometry is shown on Figure 2.5-57. Two equally weighted alternatives for future ruptures of RLME are modeled: either vertical strike-slip rupture oriented northeast parallel to the sides of the Marianna zone or vertical strike-slip rupture oriented northwest parallel to the sides of Marianna zone. All boundaries of the Marianna zone are modeled as leaky (Table 2.5-10).

The Marianna RLME source lies about 850 mi (1375 km) from the CCNPP Unit 3 Site. Although included in the PSHA, its RLME magnitude distribution and recurrence rate result in it contributing negligibly to total hazard at the Site (Section 2.5.2.4.2).

Commerce Fault Zone RLME Source

A single geometry for the Commerce RLME source is modeled (EPRI/DOE/NRC, 2012) (Figure 2.5-57). The Commerce RLME source is modeled as a zone of vertical strike-slip faulting. Ruptures are oriented N47E, subparallel to the Commerce zone boundary. The northeast and southwest boundaries of the zone are modeled as leaky boundaries.

The Commerce Fault Zone RLME source lies about 725 to 775 mi (1175 to 1250 km) from the CCNPP Unit 3 Site. Although included in the PSHA, its RLME magnitude distribution and recurrence rate result in it contributing negligibly to total hazard at the Site (Section 2.5.2.4.2).

Wabash Valley RLME Source

A single zone geometry is used to model the Wabash Valley RLME (EPRI/DOE/NRC, 2012) (Figure 2.5-57). The boundaries of the Wabash Valley RLME source zone are modeled as leaky boundaries. Future earthquake ruptures are modeled with a random strike (uniform 0 to 360 degree azimuth). The earthquakes are considered to have vertical strike-slip (weight of 2/3) or reverse (weight of 1/3) mechanisms with random dip angles in the range of 40 to 60 degrees.

The Wabash Valley RLME source lies about 625 mi (1000 km) from the CCNPP Unit 3 Site. Although included in the PSHA, its RLME magnitude distribution and recurrence rate result in it contributing negligibly to total hazard at the Site (Section 2.5.2.4.2).

As in the case for distributed seismicity zones (section 2.5.2.2.1.1.5), the rupture area for each RLME source is determined using Equation 2.5-1 (EPRI/DOE/NRC, 2012). The rupture aspect ratio is 1:1 until the rupture reaches the maximum rupture width, which is defined by the seismogenic crustal thickness and the dip angle of the rupture plane. Seismogenic crustal thickness for RLME sources are described in Section 2.5.2.2.1.2.6 and indicated in Table 2.5-11. For larger ruptures the width is fixed at the maximum value and length is increased to obtain the area given by Equation 2.5-1.

2.5.2.2.1.2.2 Temporal Clustering and Tectonic Features for RLME Sources

Some studies of large earthquakes within stable continental regions (SCRs) including the CEUS have concluded that large earthquakes occur as "clusters" of earthquakes that are separated from other clusters by long periods of quiescence. In the CEUS SSC model (EPRI/DOE/NRC, 2012), available data for RLMEs were evaluated to assess whether, (1) temporally clustered behavior has been observed, and (2) if this behavior is observed, whether the source is currently within or outside a temporal cluster. In both cases temporal behavior is modeled as a Poisson process.

Available data have been further evaluated to assess the applicability of the renewal recurrence model to RLME sources (EPRI/DOE/NRC, 2012). Results of the assessments indicated that the renewal models can be applied to the Charleston and New Madrid RLME sources. Available data for other RLME sources were insufficient to allow application of renewal models with confidence (EPRI/DOE/NRC, 2012).

Charleston RLME Source

The Charleston RLME seismic source is modeled as "in" a temporal cluster with a weight of 0.9 and "out" of a temporal cluster with a weight of 0.1 (EPRI/DOE/NRC, 2012) (Table 2.5-12). For the "out" branch, the Charleston RLME source is not included in the determination of total seismic hazard. The approach used for Charleston RLME source is to model future ruptures to occur randomly within the source (i.e., ruptures are not associated with a specific localizing tectonic feature) (Table 2.5-12).

New Madrid Fault System RLME Source

For the NMFS, the issue of temporal clustering is modeled by three alternatives (EPRI/DOE/NRC, 2012) (Table 2.5-12):

- With weight of 0.9 the NMFS RLME is modeled as being in-cluster.
- With weight of 0.05 the RLME is modeled as being out-of-cluster with no earthquake activity occurring on the source.
- With weight of 0.05, the RLME is modeled as being out-of-cluster with a long-term rate assigned to only the RFT.

As mentioned before, the RLMEs associated with the NMFS are modeled as occurring on three fault sources: (1) the NMS fault, (2) the NMN fault, and the RFT (EPRI/DOE/NRC, 2012) (Table 2.5-10).

Eastern Rift Margin Fault RLME Source

The issue of temporal clustering of earthquakes in the present tectonic stress regime is not applicable to the ERM-S and ERM-N RLME sources. Earthquakes in the ERM-S and ERM-N RLME sources are modeled as uniformly distributed in the source zones (EPRI/DOE/NRC, 2012) (Table 2.5-12).

Marianna Zone RLME Source

For the Marianna Zone, the in-cluster model of temporal clustering is assigned a weight of 0.5 and the out-of-cluster model is assigned a weight of 0.5 (EPRI/DOE/NRC, 2012) (Table 2.5-12). On the "out" branch, the Marianna RLME source is not included in calculation of total seismic hazard. RLMEs are modeled as occurring randomly in the Marianna Zone.

Commerce Fault RLME Source

The issue of temporal clustering is not applicable to the Commerce Fault. RLMEs are modeled as occurring randomly in the Commerce Zone (EPRI/DOE/NRC, 2012).

Wabash Valley RLME Source

The issue of temporal clustering is not applicable to this source. RLMEs are modeled as occurring randomly in the Wabash Valley Zone (EPRI/DOE/NRC, 2012).

2.5.2.2.1.2.3 RLME Recurrence Models

Charleston RLME Source

The recurrence data for the Charleston RLME source consists of ages of past RLMEs estimated from the paleo-liquefaction record (EPRI/DOE/NRC, 2012). Therefore, recurrence for the Charleston RLME source is based solely on the "Earthquake Recurrence Intervals" approach (Table 2.5-13). Two alternatives are considered for the length and completeness of the paleo-liquefaction record: the approximately 2,000-year record of Charleston earthquakes with 0.8 weight and the approximately 5,500-year record with weight of 0.2 (EPRI/DOE/NRC, 2012).

Another node of the Charleston logic tree addresses the uncertainty in number of RLMEs that have occurred in the Charleston RLME source (EPRI/DOE/NRC, 2012). For the 2,000-year record, a single model is used. For the 5,500-year, four alternatives are used (Table 2.5-13).

For the regional and local source zones of the Charleston RLME source, only the Poisson model is used as recurrence model. For the more "fault-like" narrow configuration, the Poisson model is assigned 0.90 weight, and the Brownian Passage Time (BPT) renewal model is assigned 0.1 weight (EPRI/DOE/NRC, 2012). Use of the BPT renewal model requires specification of the coefficient of variation of the repeat time, parameter α, for RLMEs. The uncertainty distribution for α is also reported (EPRI/DOE/NRC, 2012) (Table 2.5-13). The coefficient of variation is not applicable to the Poisson model. In total there are 24 uncertainty distributions for the annual frequency of RLMEs from the Charleston source.

New Madrid Fault System RLME Source

For the NMFS RLME source, the "Earthquake Recurrence Intervals" approach is used with weight 1.0 (EPRI/DOE/NRC, 2012) (Table 2.5-14). In-cluster case recurrence rates are based on

the 1811-1812, 1450 AD, and 900 AD sequences. Out-of cluster recurrence rates for the NMFS are based on timing between clusters (EPRI/DOE/NRC, 2012).

In terms of recurrence model, the Poissonian and renewal recurrence models are assigned weights of 0.75 and 0.25, respectively, for the in-cluster case (EPRI/DOE/NRC, 2012). Distribution of parameter α for the renewal model is given in Table 2.5-14.

ERM Fault RLME Source

The "Earthquake Count in a Time Interval" approach is used to assess RLME recurrence frequency for both the ERM-S and ERM-N sources (EPRI/DOE/NRC, 2012) (Table 2.5-15 and Table 2.5-16) respectively. For the ERM-S source, three alternative data sets are used to assess RLME recurrence rates (EPRI/DOE/NRC, 2012): either two, three, or four earthquakes in a 17.7 to 21.7 k.y. period. The three alternatives have equal weight. For the ERM-N source, two alternative data sets are used (EPRI/DOE/NRC, 2012): either one (weight 0.9) or two (weight 0.1) earthquakes in a 12 to 35 k.y. period. The Poisson model is used as the default earthquake recurrence model with weight 1.0 for both the ERM-S and ERM-N sources (EPRI/DOE/NRC, 2012).

Marianna Zone RLME Source

For the Marianna Zone RLME source, the "Earthquake Recurrence Intervals" approach is used with a weight of 1.0 (EPRI/DOE/NRC, 2012) (Table 2.5-17). The two equally weighted data sets consist of either three or four earthquakes with the oldest occurring approximately 9.9 ka. The Poisson model is used as the default earthquake recurrence model with weight 1.0 for the Marianna RLME source (EPRI/DOE/NRC, 2012).

Commerce Fault RLME Source

For the Commerce Fault RLME source, the "Earthquake Recurrence Intervals" approach is used with weight 1.0 (EPRI/DOE/NRC, 2012) (Table 2.5-18). The preferred interpretation (weight 0.75) is that two earthquakes have occurred in the past 23 k.y. with the alternative possibility that the count is three earthquakes. The Poisson model is used as the earthquake recurrence model with weight 1.0 for the Commerce RLME source (EPRI/DOE/NRC, 2012).

Wabash Valley RLME Source

For the Wabash Valley RLME source, the "Earthquake Recurrence Intervals" approach is used with weight 1.0 (EPRI/DOE/NRC, 2012) (Table 2.5-19). The available data for characterizing the recurrence rate of Wabash Valley RLMEs are the estimated ages for the Vincennes-Bridgeport and Skelton paleoearthquakes. The Poisson model is used as the earthquake recurrence model with weight 1.0 for the Wabash Valley RLME source (EPRI/DOE/NRC, 2012).

2.5.2.2.1.2.4 RLME Magnitudes

The RLME sources are intended to model the repeated occurrence of large earthquakes of similar size. The expected magnitude of the RLME is estimated from various sources of data and its uncertainty is expressed by a probability distribution (EPRI/DOE/NRC, 2012). The distributions of magnitudes for RLME sources are given in Table 2.5-20.

2.5.2.2.1.2.5 RLME Rupture Characteristics

Alternative geometries and rupture characteristics of the RME sources are discussed in Section 2.5.2.2.1.2.1 and the related parameters are summarized in Table 2.5-10.

2.5.2.2.1.2.5.1 Seismogenic Crustal Thickness for RLME Sources

In developing the CEUS SSC model (EPRI/DOE/NRC, 2012), crustal thickness, including its uncertainty, was characterized for each seismic source based on the available data. The uncertainty distributions for seismogenic crustal thickness for RLME sources are reported in Table 2.5-11. For the NMFS, Commerce, Marianna, ERM-N, and ERM-S sources, the seismogenic crustal thickness is modeled as being 13 km (weight of 0.3), 15 km (weight of 0.5), or 17 km (weight of 0.2). For the Charleston source the three values of the seismogenic crustal thickness are 13, 17, and 22 km, with the weights of 0.4, 0.4, 0.2, respectively. The values for the Wabash Valley are 17 km and 22 km, with weights of 0.7 and 0.3, respectively (EPRI/DOE/NRC, 2012).

2.5.2.3 Correlation of Earthquake Activity with Seismic Sources

Correlation of earthquakes with seismic sources was one type of information used in EPRI/DOE/NRC (2012) to develop the updated CEUS SSC model. Differences in observed seismicity formed one criterion for defining source zones following the Seismotectonic Zones approach. The focus was on differences in earthquake characteristics rather than recurrence rate because the rate is modeled as spatially varying within a source zone. For features or areas with a history of repeated large (**M**>6.5) earthquakes, RLME sources were defined. For these sources, the correlation of earthquake activity with the feature or area is the primary basis for source definition.

2.5.2.4 Probabilistic Seismic Hazard Analysis and Controlling Earthquake

Sections 2.5.2.4.1 through 2.5.2.4.3 are added as a supplement to the U.S. EPR FSAR.

Using seismic sources from the EPRI/DOE/NRC (2012) CEUS SSC model and the EPRI (2004, 2006) ground motion model, a PSHA was carried out for the CCNPP Unit 3 site. The following sections describe the PSHA and its results.

2.5.2.4.1 Ground Motion Model

Since publication of the 1989 EPRI study (EPRI, 1989a), much work has been done to evaluate strong earthquake ground motion in the central and eastern United States. This work is described in summarized EPRI TR-1009684 (EPRI, 2004) in the form of updated ground motion equations that estimate median spectral acceleration and uncertainty as a function of earthquake magnitude and distance. Epistemic uncertainty is modeled using multiple ground motion equations and multiple estimates of aleatory uncertainty (sigma), all with associated weights. Different sets of equations are recommended for sources that represent rifted versus non-rifted parts of the earth's crust. Equations are available for spectral frequencies of 100 Hz (equivalent to PGA), 25 Hz, 10 Hz, 5 Hz, 2.5 Hz, 1 Hz, and 0.5 Hz, and these equations apply to hard rock conditions.

EPRI published an update, EPRI TR-1014381 (EPRI, 2006a), in 2006 to the estimates of aleatory uncertainty. This update reflected the observation that the aleatory uncertainties in the original EPRI attenuation study (EPRI, 2004) were too large, resulting in over-estimates of seismic hazard. The 2006 EPRI study (EPRI, 2006a) recommends a revised set of aleatory uncertainties

(sigmas) with weights, that can be used to replace the original aleatory uncertainties published in the 2004 EPRI study (EPRI, 2004).

The ground motion model used in the seismic hazard calculations consists of the median equations from the EPRI 2004 study (EPRI 2004), with the updates for the aleatory uncertainties (EPRI, 2006a). EPRI TR-1014381 (EPRI, 2006a) was used in lieu of the Regulatory Guide 1.208 cited document, i.e. EPRI Report 1013105 (EPRI, 2006b). EPRI Report 1013105 (EPRI, 2006b) was an Update Report while EPRI TR-1014381 (EPRI, 2006a) is the final report. For the purposes of revised estimates of aleatory uncertainty in the central and eastern U.S., there is no technical difference between the documents. The "Recommended CEUS Sigma" values and "Conclusions" of both reports are identical.

2.5.2.4.2 Rock Uniform Hazard Response Spectra and Hazard Deaggregation

Using seismic sources from the EPRI/DOE/NRC (2012) CEUS SSC model, as described in Sections 2.5.2.1 through 2.5.2.3, and the EPRI (2004, 2006) ground motion model, described in Section 2.5.2.4.1, a probabilistic seismic hazard analysis was carried out for the CCNPP Unit 3 Site. The annual frequency of exceedance is calculated for 23 values of spectral acceleration ranging from 0.01 g to 5 g. Hazard is determined for peak ground acceleration and spectral acceleration for oscillator frequencies of 0.5, 1, 2.5, 5, 10, and 25 Hz.

The calculation uses a grid approach to integrate the hazard within each distributed seismicity source zone and from the RLME sources. To obtain stable results, especially for the source zones hosting the site, the CEUS SSC recurrence values are re-sampled for 0.125 degree squared cells. Sensitivity analyses indicated that this resolution was adequate; smaller grid spacing had a negligible impact on the calculated hazard. At each grid point, information on the characteristics of future earthquakes from the EPRI/DOE/NRC (2012) model is used to generate a suite of virtual faults for calculation of appropriate distance metrics for evaluating the ground motion equations. A uniform depth distribution is used, taking into account the uncertainty in seismogenic crustal thickness.

In calculating the hazard, integration over distance for the distributed seismicity source zones included in the PSHA is carried out to 435 mi (700 km). For RLME sources, integration is carried out over a distance range that encompasses the source. For all source zones, boundaries are treated as "leaky." While some RLME sources specify some of their boundaries are "strict," because they are distant from the Site (about 350 to 850 mi [550 to 1375 km]), the impact on total hazard at the Site from this deviation will be small.

Hazard results are provided for mean hazard and for the 5th, 15th, 50th, 85th, and 95th fractile of the hazard curve distribution.

Figure 2.5-85 through Figure 2.5-91 are plots of the resulting probabilistic seismic hazard hard rock curves for the seven spectral ordinates (100 Hz (equivalent to PGA), 25 Hz, 10 Hz, 5 Hz, 2.5 Hz, 1 Hz, and 0.5 Hz). The mean and fractile (15%, 50% (median), and 85%) hazard curves are indicated.

Figure 2.5-58 shows mean and median uniform hazard spectra for 10-4, 10-5, and 10-6 annual frequencies of exceedance from these calculations at the seven structural frequencies at which ground motion equations are available. Numerical values of these spectra are documented in Table 2.5-26.

The seismic hazard was deaggregated for implementation of Regulatory Guide 1.208 (NRC, 2007a). That is, the contributions by earthquake magnitude and distance to hazard at the 10^{-4}, 10^{-5}, and 10^{-6} ground motions were determined for 1 Hz, 2.5 Hz, 5 Hz, and 10 Hz.

Additionally, Equation 7 of Regulatory Guide 1.208 (NRC, 2007a), Appendix D, Page D-5, was not used as written in the determination of mean distance for controlling earthquakes.

The deviation is described as follows:

Equation 7 is addressed in Appendix D, Step 3, Determining Controlling Earthquakes, as:

"The mean distance of the controlling earthquake is based on magnitude-distance bins greater than distances of 100 km (63 mi) as discussed in Step 5 and determined according to the following:

$$\ln\{D_c\ (1 - 2.5\ Hz)\} = \Sigma_{d>100}\ln(d)\Sigma_m P{>}100(m, d)_2 \qquad \text{(Equation 7)}$$

where d is the centroid distance value for each distance bin."

The definition of the term "P" is provided in Appendix D, Step 1, Determining Controlling Earthquakes."

P is defined as: This distribution, P>100(m,d), is defined by the following:

$$P > 100\ (m, d)1 \div [\Sigma_m \Sigma_{d>100}[P(m, d)_1]] \qquad \text{(Equation 3)}$$

As written, Equation 7 is in error. The specific error is that the term $P{>}100(m,d)_2$ in Equation 7 should be $P{>}100(m,d)_1$ as defined in Step 1, i.e., difference in subscript 2 in Step 3 versus subscript 1 in Step 1.

By the definition in Step 1, $P{>}100(m,d)_1$ refers to the probability of the fractional contribution of each magnitude and distance bin (beyond 100 km) to the total hazard for the average of 1 and 2.5 Hz, whereas $P{>}100(m,d)_2$ refers to the fractional contribution of each magnitude and distance bin to the total hazard for the average of 5 and 10 Hz. Step 3 explicitly refers to mean magnitude and distance of the controlling earthquakes associated with the ground motions determined in Regulatory Guide 1.208, Appendix D, Step 2 for the average of 1 and 2.5 Hz.

The corrected equation provides for evaluating the mean distance of the controlling earthquake for distances of 100 km or greater for the average of 1 and 2.5 Hz (NRC, 2007a).

The deaggregations for 1 Hz and 2.5 Hz were combined to produce a single mean low-frequency (LF) deaggregation, and the deaggregations for 5 Hz and 10 Hz were combined to produce a single mean high-frequency (HF) deaggregation. These deaggregations were done for ground motions corresponding to mean 10^{-4}, 10^{-5}, and 10^{-6} annual frequencies of exceedance. The resulting deaggregations by magnitude and distance are shown in Figure 2.5-59 and Figure 2.5-60 for 10^{-4}, Figure 2.5-61 and Figure 2.5-62for 10^{-5}, and Figure 2.5-83 and Figure 2.5-84 for 10^{-6}.

Figure 2.5-59 through Figure 2.5-62, Figure 2.5-83, and Figure 2.5-84 show that small, local earthquakes dominate the HF motion, but that a significant contribution to hazard occurs for LF motions from large, distant earthquakes in NMFS. Representative earthquake magnitudes and distances were developed for the 10^{-4} and 10^{-5} ground motions as these are used to

develop the recommended ground motion response spectrum (GMRS). Controlling earthquakes were developed for 10^{-6} ground motions as well.

Controlling earthquakes are determined using the procedure in Regulatory Guide 1.208 (NRC, 2007a), Appendix D for LF and HF.

The deaggregation of seismic hazard at annual frequencies of exceedance of 10^{-4} and 10^{-5} was divided into three groups: those contributions for R < 62 mi) (100 km), those contributions for R > 62 mi (100 km), and contributions from overall distances (R> 0 km). Table 2.5-21 shows the mean magnitudes and distances for each group.

With these deaggregations, the representative LF earthquake was selected using the R > 62 mi (100 km) mean magnitude and mean distance (the shaded cells in Table 2.5-21). For HF ground motion, the mean magnitude and mean distance was selected from the R > 0 km results (the shaded cells in Table 2.5-21).

2.5.2.5 Seismic Wave Transmission Characteristics of the Site

The uniform hazard spectra described in the preceding section are defined on hard rock (shear-wave velocity of 9200 ft/sec (2804 m/sec)), which is located more than 2500 ft (762 m) below the current ground surface at the CCNPP Unit 3 site. The seismic wave transmission effects of this thick soil column on hard rock ground motions are described in this section.

Section 2.5.2.5.1 is added as a supplement to the U.S. EPR FSAR.

2.5.2.5.1 Development of Site Amplification Functions

For the purpose of calculating the Ground Motion Response Spectra (GMRS) for the site, the acceleration response spectra (ARS) amplification functions are developed at the 10^{-4} and 10^{-5} mean annual probability of exceedance (MAPE). The GMRS horizon is defined at a depth of 43.5 ft (13.2 m) or El. 41.5 ft (12.6 m) above MSL from finished ground surface of El. 85 ft (26 m) above MSL within the soil column describing the site conditions in the vicinity of the Nuclear Island (NI). This horizon marks the top-most native soil layer, where the overlying 43.5 ft (13.2 m) of soil are replaced by backfill. The GMRS is calculated at this horizon, after hypothetical excavation of the overlying soil, as a truncated soil column response.

2.5.2.5.1.1 Methodology

The GMRS amplification factors are calculated for the truncated soil column response (TSCR) per the definition of ISG-017 (NRC, 2009).

The calculation of site amplification factors is performed in the following 4 steps:

1. Develop a base-case soil and rock column in which mean low-strain shear wave velocities and material damping values, and strain-dependencies of these properties, are estimated for relevant layers from the hard rock horizon to the surface. At the CCNPP Unit 3 site, hard rock (V_S = 9200 ft/sec (~2.8 km/sec) is at a depth of approximately 2550 ft (777 m).

2. Develop a probabilistic model that describes the uncertainties in the above properties, locations of layer boundaries, and correlation between these properties, and generate a set of 60 artificial "randomized" profiles.

3. Use the seismic hazard results at 10^{-4}, 10^{-5} and 10^{-6} annual frequencies of exceedance to generate smooth spectra, representing LF and HF earthquakes at the three annual frequencies, for input into dynamic response analysis.

4. Use an equivalent-linear site-response formulation together with Random Vibration Theory (RVT) to calculate the dynamic response of the site for each of the 60 artificial profiles, and calculate the mean and standard deviation of site response. This step is repeated for each of the six input motions (10^{-4}, 10^{-5}, and 10^{-6} annual frequencies, HF and LF smooth spectra).

   RVT methods characterize the input rock motion using its power spectrum and duration instead of using time domain earthquake input motions. This spectrum is propagated through the soil to the surface using frequency domain transfer functions and computing peak ground accelerations, spectral accelerations, or peak strains using extreme value statistics. The RVT analysis that was conducted accounted for the strain dependent soil properties in the same manner as time-history based methods.

These steps are described in the following subsections.

2.5.2.5.1.2 Base Case Soil/Rock CCNPP Unit 3 and Uncertainties

Development of a base case soil/rock column is described in detail in Section 2.5.4. Summaries of the low strain shear wave velocity, material damping, and strain-dependent properties of the base case materials are provided below in this section. These parameters are used in the site response analyses.

The geology at the CCNPP Unit 3 site consists of marine and fluvial deposits overlying bedrock. The approximately upper 400 ft (122 m) of the site soils was investigated and characterized using test borings, cone penetration testing, test pits, geophysical methods, and RCTS tests. Information on subsurface conditions below this depth was assembled from available geologic information from various resources.

Natural Soils in the upper 400 ft (122 m) of the site can generally be divided into the following geotechnical strata:

- Stratum I: Terrace Sand
- Stratum IIa: Chesapeake Clay/Silt
- Stratum IIb: Chesapeake Cemented Sand
- Stratum IIc: Chesapeake Clay/Silt
- Stratum III: Nanjemoy Sand

Two borings, B-301 and B-401 provide the deepest site-specific soils information collected during the geotechnical investigation for the CCNPP Unit 3 site, and they were also used to obtain the deepest suspension P-S velocity logging profile at the site. The P-S measurements provide shear and compressional wave velocities and Poisson's ratios in soils at 1.6 ft (0.5 m) intervals to a depth of about 400 ft (122 m).

Various available geologic records were reviewed and communications were made with staff at the Maryland Geological Survey, the United States Geological Survey, the Triassic-Jurassic Study Group, Lamont-Doherty Earth Observatory, and Columbia University to develop estimates of subsurface soil properties below 400 ft (122 m) depth. Further details, including associated references, are presented in Subsection 2.5.1. Soils below 400 ft (122 m) consist of Coastal Plain sediments of Eocene, Paleocene, and Cretaceous eras, extending to an estimated depth of about 2555 ft (779 m) below the ground surface. These soils contain sequences of sand, silt, and clay. Given their geologic age, they are expected to be competent soils, consolidated to at least the weight of the overlying soils.

Several available geologic records were reviewed to estimate bedrock characteristics below the site. Various bedrock types occur in the CCNPP Unit 3 site region, including Triassic red beds, Jurassic diabase, granite, schist, and gneiss. However, only granitoid rocks (metamorphic gneiss, schist, or igneous granitic rocks) similar to those exposed in the Piedmont, could be discerned as the potential regional rock underlying the CCNPP Unit 3 site. This rock type was assumed as the predominant rock type at the CCNPP Unit 3 site.

Two sonic profiles were found for wells in the area that penetrated the bedrock, one at Chester, Maryland (about 40 mi (64 km) north of the site) and another at Lexington Park, Maryland (about 10 mi (16 km) south of the site). These two profiles were digitized and converted to shear wave velocity, based on a range of assumed Poisson's ratios for soil and rock.

Unit weights for the soils beneath the site are in the range of about 115 to 125 pcf (pounds per cubic foot) (1842 kg/m^3 to 2003 kg/m^3). The bedrock unit weight was assigned a value of 162 pcf (2595 kg/m^3). The top 43.5 ft (13.2 m) of native soils are replaced with backfill with a unit weight of 145 pcf (2323 Kg/m^3).

Bedrock was assumed to behave elastically with a damping ratio of 1 percent.

RCTS test results were used to obtain site-specific data on shear modulus and damping characteristics of in situ soils in the upper 400 ft (122 m) and of the backfill material as detailed in Section 2.5.4. The site-specific RCTS-based shear modulus degradation and damping ratio curves were used for all site amplification factor analysis. A subsurface soil profile representing the conditions in the vicinity of the NI including backfill, was used for the calculation of the GMRS. For the development of FIRS in Section 3.7.1, the soil profile appropriate for any given structure was developed from the material properties described and discussed in Section 2.5.4.

2.5.2.5.1.3 Site Properties Representing Uncertainties and Correlations

To account for variations in shear-wave velocity across the site, 60 artificial profiles were generated. These artificial profiles represent the soil column from the top of bedrock (with a bedrock shear-wave velocity of 9,200 ft/s (~2.8 km/sec) to the finished ground surface at El. 85 ft. This model uses as inputs the following quantities:

- The median shear-wave velocity profile, which is equal to the base-case soil and rock profiles described above.
- The standard deviation of ln(Vs) (the natural logarithm of the shear-wave velocity) as a function of depth, which is developed using available site and regional data (refer to Section 2.5.4).
- The correlation coefficient between ln(Vs) in adjacent layers, which is based on generic studies.

- The probabilistic characterization of layer thickness.
- The depth to bedrock, which is randomized to account for epistemic uncertainty in the bedrock-depth data described in Section 2.5.4.
- The median or best-estimate shear stiffness (G/G_{MAX}) and damping curves, which are based on site-specific RCTS test in the upper 400 ft (122 m) of the profile (refer to Section 2.5.4).
- The uncertainty in the shear stiffness (G/GMAX) and damping curves.

Figure 2.5-66 presents the best-estimate (BE) low-strain shear wave velocity profile (also see Figure 2.5-151), where depth is measured starting from finished grade at El. 85 ft (26 m). The total BE soil column thickness is 2,550 ft (777 m). At that depth, bedrock is defined with a shear-wave velocity of 9,200 ft/sec (2804 m/sec). Figure 2.5-67 presents the associated log-standard deviation for the shear wave velocity profile.

This study uses the inter-layer correlation model from Toro for U.S. Geological Survey category "C" as documented in Toro (Toro, 1996) as a guideline for native soils. In the case of the inter-layer correlation between structural fill layers, a correlation coefficient of 0.98 is used to reflect the expected gradual increase in shear-wave velocity with depth, where it is unlikely for velocity reversals to occur.

Section 2.5.4 indicates that the shear-wave velocity of 9,200 ft/s (~2.8 km/sec) (for bedrock) is estimated at a depth of approximately 2550 ft (777 m). This value is taken as the base case or median depth. This information on bedrock depth is based on boreholes located tens of miles away from the site where are discussed in Section 2.5.4. The uncertainty associated with depth to bedrock is characterized by a uniform distribution over the interval of 2550 ft (777 m), plus or minus 50 ft (15 m) (the latter number is one half the contouring interval used to estimate the depth to bedrock). Because bedrock occurs at a large depth, the specific details of modeling uncertainty in this depth are not critical to the calculation of site response.

Figure 2.5-68 illustrates the V_S profiles generated for profiles 1 through 10, using the median, logarithmic standard deviation, and correlation model described. These profiles include uncertainty in depth to bedrock. In total, 60 profiles were generated. Figure 2.5-69 presents the set of 60 simulated low-strain shear wave velocity profiles, which includes the thickness variation of the soil layers. The figure also presents the BE profile used as input for simulation and the simulated median profile, calculated as the log-mean of the 60 simulated profiles, and shows a close match between these two profiles.

The simulated shear strength reduction and damping ratio curves for the uppermost fill layer (Fill 1) are presented in Figure 2.5-70 and Figure 2.5-71, respectively, as an example for simulated strain-dependent property curves. In these figures, the BE and simulated median are compared as well as the input log-standard deviation (Input SD) and simulated log-standard deviation (Simulated SD). Maximum and minimum bounds of twice the SD around the BE are imposed on the strain-dependent property curves. Note that damping curves, in Figure 2.5-71, are truncated at a maximum of 15%, which explains the discrepancy between input and simulated properties once that upper limit is reached. The damping truncation at 15% is a conservative measure with respect to their subsequent use in site response analysis.

This set of 60 profiles, consisting of VS versus depth, depth to bedrock, stiffness, and damping, are used to calculate and quantify site response and its uncertainty, as described in the following sections.

2.5.2.5.1.4 Development of Low-Frequency and High-Frequency Smooth Spectra

To derive smooth spectra for controlling earthquakes corresponding to the 10^{-4}, 10^{-5} and 10^{-6} UHRS, the mean magnitudes and distances summarized in Table 2.5-21 were used in the following way. Realistic spectral shapes for the six representative controlling earthquakes (HF and LF for 10^{-4}, 10^{-5} and 10^{-6} mean annual frequencies of exceedance) were determined from their magnitude and distance using equations from NUREG/CR-6728 (NRC, 2001). For each mean annual frequency of exceedance, the HF shapes were scaled to the mean Uniform Hazard Spectra value (Table 2.5-24) for 5 Hz, 10 Hz, 25 Hz, and 100 Hz. The scaled shapes were used to interpolate between these 4 structural frequencies. Below 5 Hz, the HF spectral shape was extrapolated, without regard to Uniform Hazard Spectra amplitudes at lower frequencies.

Similarly, for each mean annual frequency of exceedance, the LF shapes were scaled to the Uniform Hazard Spectra values (Table 2.5-24) for 0.5 Hz, 1 Hz, and 2.5 Hz. Below 0.5 Hz the spectral shape was extrapolated from 0.5 Hz. Above 2.5 Hz the spectral shape was extrapolated from 2.5 Hz, without regard to Uniform Hazard Spectra amplitudes at higher frequencies.

Creation of smoothed 10^{-4}, 10^{-5} and 10^{-6} spectra in this way ensures that the HF spectra match the 10^{-4}, 10^{-5} and 10^{-6} Uniform Hazard Spectra values at high frequencies (5 Hz and above), and ensures that the LF spectra match the 10^{-4}, 10^{-5} and 10^{-6} Uniform Hazard Spectra values at low frequencies (2.5 Hz and below). In between calculated values, the spectra have smooth and realistic shapes that reflect the magnitudes and distances dominating the seismic hazard (Table 2.5-21).

The LF and HF smooth spectra are shown in Figure 2.5-63 for 10^{-4}, Figure 2.5-64 for 10^{-5} and Figure 2.5-65 for 10^{-6} mean annual frequencies of exceedance. The numerical values for these spectra are given in Table 2.5-22.

2.5.2.5.1.5 Site Response Analysis

The site response analysis performed for the CCNPP Unit 3 site used Random Vibration Theory (RVT). The application of RVT to site response has been described by Schneider (Schneider, 1991), Stepp (Stepp, 1991), Silva (Silva, 1997), and Rathje (Rathje, 2006), and a theoretical description of the method will not be presented here. Given a site-specific soil column and the above studies, the fundamental assumptions are as follows:

- The site response can be modeled using horizontal soil layers and a one-dimensional analysis.
- Vertically-propagating shear waves are the dominant contributor to site response.
- An equivalent-linear formulation of soil nonlinearity is appropriate for the characterization of site response.

These are the same assumptions that are implemented in the SHAKE program (Idriss, 1992) and that constitute standard practice for site-response calculations. In this respect, RVT and SHAKE are similar. Both use an iterative, frequency-domain equivalent-linear calculation to determine site response, and the frequency-domain representation of wave propagation in the the layered medium is identical for both approaches. The difference is that RVT works with ground-motion power spectrum (and its relation to the response spectrum and other peak-response quantities), thus representing an ensemble of ground motions, while SHAKE works with individual time histories and their Fourier transforms, thus representing one specific ground motion. Starting from the same inputs (e.g. the site properties described in Section 2.5.2.5.1.3

and the same rock response spectrum), both procedures will lead to similar estimates of site response (see, for example, Rathje (Rathje, 2006)).

The RVT site-response analysis requires the estimation of an additional parameter, strong motion duration, which does not have a strong influence on the calculated site response. Strong motion durations of the rock motions are calculated from the mean magnitudes and distances of the controlling earthquakes as taken from the deaggregation results. Using the magnitudes (M) of the six input rock motions as documented in Subsection 2.5.2.4, and the relationship between magnitude and duration specified in Table 3-2 of NUREG/CR 6728 (NRC, 2001), the strong motion durations are determined. The magnitudes and corresponding durations are reported in Table 2.5-25.

One parameter that is used by both the RVT method and SHAKE is the effective strain ratio. This parameter is estimated using the expression (**M**-1)/10 (Idriss, 1992), where **M** is the magnitude of the controlling earthquake taken from the deaggregation analysis. As shown in Table 2.5-25, the calculated values are verified to remain within the 0.5 - 0.7 range found empirically by Kramer (Kramer, 1996). As is the case for strong motion duration, computed site response is not very sensitive to estimates of effective strain ratio.

The RVT method starts with the response spectrum of rock motion (for example, the 10^{-4} HF spectrum). It then generates a Fourier spectrum corresponding to that input response spectrum, using an estimate of strong motion duration (calculated as described above) as an additional input. This step is denoted as the Inverse RVT (or IRVT) step. An iterative procedure (similar to that in SHAKE) is then applied to calculate peak and effective shear strains in each layer using RVT, update the stiffness and damping in each layer using the calculated effective strains and the G/G_{max} and damping curves for the layer, and repeat the process until it converges. The final (or strain-compatible) stiffness and damping are then used to calculate the strain-compatible site transfer function. This transfer function is then multiplied by the Fourier spectrum of the input rock motion to obtain the Fourier spectrum of the motion at the top of the profile or at the desired elevation (for either outcrop or in-column conditions), from which response spectra are calculated using RVT.

Note that per ISG-017 (NRC, 2009), the analysis is first performed for the full soil column including the upper 43.5 ft (13.2 m) of backfill. The strain-compatible properties associated with each of the input rock motions are retained, and the site response analysis is repeated using these properties, without further iterations, after removing the upper 43.5 ft (13.2 m) of backfill. In this way, the site amplification factors are calculated at the top of the truncated column, as a free outcrop surface motion at the GMRS horizon.

This process is repeated multiple times, once for each artificial profile. For sixty site profiles, sixty response spectra are calculated, from which statistics of site response are obtained.

The above calculations are repeated multiple times, once for each input rock spectrum. Thus the site response is calculated separately for the 10^{-4} HF, 10^{-4} LF, 10^{-5} HF, 10^{-5} LF, 10^{-6} HF, and 10^{-6} LF spectra.

In comparison to the SHAKE approach, the RVT approach avoids the requirement of performing spectral matching on the input time histories to match an input rock spectrum, and avoids analyzing each individual time history with a site-response program.

The site amplification factor is defined as the TSCR spectral amplitude at each frequency, computed at the GMRS horizon, divided by the input rock spectral amplitude. Figure 2.5-72 shows the logarithmic mean of site amplification factor from the 60 profiles for the 10^{-4} HF

input motion. As would be expected by the large depth of sediments at the site, amplifications are largest at low frequencies, and de-amplification occurs at high frequencies because of soil damping. The maximum strains in the soil column are low for this motion, and this is shown in Figure 2.5-73, which plots the maximum strains calculated for the 60 profiles versus depth. Maximum strains are generally less than 0.02 percent, with some profiles having strains in shallow layers up to 0.04 percent.

Figure 2.5-74 and Figure 2.5-75 show similar plots of amplification factors and maximum strains for the 10^{-4} LF motion. The results are similar to those for the HF motion, with the soil column generally exhibiting maximum strains less than 0.10 percent, with the exception of the backfill layers which exhibit strains up to 0.25 percent.

Figure 2.5-76 through Figure 2.5-79 show comparable plots of amplification factors and maximum strains for the 10^{-5} input motion, both HF and LF. For this higher motion, larger maximum strains are observed, but they are still generally less than 0.3 percent for the in situ soil layers. In the case of the structural fill layers in the top 43.5 ft of the soil column, a few profiles exhibit maximum strains of about 1.3 percent.

Table 2.5-24 documents the mean amplification factors for 10^{-4}, and 10^{-5} rock input motions, and for HF and LF spectra.}

2.5.2.6 Ground Motion Response Spectra

The U.S. EPR FSAR includes the following COL Item in Section 2.5.2.6:

> A COL applicant that references the U.S. EPR design certification will compare the final strain-dependent soil profile with the U.S. EPR design soil parameters and verify that the site-specific seismic response is enveloped by the CSDRS and the soil profiles discussed in Sections 2.5.2, 2.5.4.7 and 3.7.1 and summarized in Table 3.7.1-6, Table 3.7.1-8 and Table 3.7.1-9.

This COL Item is addressed as follows:

Given the nature of the site specific shear wave velocity profile and the site specific Ground Motion Response Spectra (GMRS) described in this Section, a full site specific soil structure interaction (SSI) analysis is performed to reconcile the seismic design of the Category I structures of the CCNPP Unit 3.

Section 2.5.2.6.1 describes the development of the GMRS, and Section 2.5.2.6.2 describes the Seismic Reconciliation.

2.5.2.6.1 Development of the GMRS

The horizontal GMRS was developed starting from the 10^{-4} and 10^{-5} de-aggregated rock LF and HF spectra. The appropriate mean amplification factors, presented in Figure 2.5-72, Figure 2.5-74, Figure 2.5-76, and Figure 2.5-78, were multiplied by the corresponding de-aggregated rock spectra.

Figure 2.5-80 illustrates the resulting site spectra. At high frequencies the HF spectral amplitudes are always greater, and at low frequencies the LF spectral amplitudes are always greater. The two sets of spectral amplitudes cross at 2-4 Hz.

To calculate site spectral amplitudes, the LF and HF 10^{-4} ARS are enveloped resulting in the 10^{-4} UHRS at the GMRS horizon. Similarly, the LF and HF 10^{-5} ARS are enveloped to yield the 10^{-5} UHRS.

This procedure corresponds to Approach 2A in NUREG/CR-6728 (NRC, 2001) and NUREG/CR-6769 (NRC, 2002b), wherein the rock Uniform Hazard Response Spectra (for example, at 10^{-4}) is multiplied by a mean amplification factor at each frequency to estimate the 10^{-4} site Uniform Hazard Spectra.

The performance-based approach described in Regulatory Position 5 of Regulatory Guide 1.208 (NRC, 2007a) was used to derive a GMRS from the 10^{-4} and 10^{-5} site spectra. The spectrum is derived at each structural frequency as follows:

$$A_R = SA(10^{-5})/SA(10^{-4})$$

$$DF = 0.6\ A_R^{0.8}$$

$$GMRS = max(SA(10^{-4}) \times max(1.0, DF), 0.45 \times SA(10^{-5}))$$

The resulting horizontal spectrum is plotted in Figure 2.5-81.

A vertical spectrum was calculated by deriving vertical-to-horizontal (V:H) ratios and applying them to the horizontal spectrum. As background and for comparison purposes, V:H ratios were obtained by the following methods:

1. Rock V:H ratios for the central and eastern United States (CEUS) were calculated from NUREG-6728 (NRC, 2001), using the recommended ratios for PGA < 0.2g, which applies to the horizontal GMRS at this site (see Figure 2.5-82).

2. Soil V:H ratios for the western United States (WUS) were calculated from two publications (Abrahamson, 1997) (Campbell, 1997) that have equations estimating both horizontal and vertical motions on soil. Horizontal and vertical motions were predicted from these two references for **M** = 5.5 and R = 9 mi (15 km). **M** = 5.5 was selected because earthquakes around this magnitude dominate the high frequency motions, and R = 9 mi (15 km) was selected because this distance resulted in a horizontal PGA of approximately 0.1 g at the site, which is close to the PGA associated with the horizontal GMRS. For each reference, the V:H ratio was formed, and the average ratio (average from the two references) was then calculated.

3. The WUS V:H ratios for soil were modified in an approximate way for CEUS conditions by shifting the frequency axis of the V:H ratios. This shifted the WUS peak V:H ratio from about 15 Hz to about 45 Hz.

Figure 2.5-82 shows these three V:H ratios plotted vs. structural frequency. As a conservative choice, the envelope V:H ratio shown as a thick dashed line was selected because this envelops all three approaches. The recommended V:H ratio is 1.0 for frequencies greater than 25 Hz, 0.75 for frequencies less than 5 Hz, and is interpolated (log-linear) between 5 and 25 Hz. Figure 2.5-81 plots the resulting vertical spectrum, calculated in this manner from the horizontal spectrum. Table 2.5-23 lists the horizontal and vertical GMRS amplitudes.

2.5.2.6.2 Seismic Reconciliation

The CCNPP Unit 3 site is not enveloped by the following design parameters used for the design and analysis of the U.S. EPR FSAR:

- The GMRS exceeds the CSDRS. A site SSE has been established as the envelope of the U.S. EPR FSAR European Utility Requirements (EUR) Soft Soil Spectrum anchored at 0.15g and the FIRS of the NI common basemat structure (See Section 3.7.1). Both the GMRS and the Site SSE exceed the CSDRS envelope below approximately 0.7 Hz.

- The shear wave velocities beneath some of the seismic category I structures is less than 1000 fps,

- The site soil column does not meet all of the U.S. EPR FSAR design parameters. Specifically, the dynamic bearing capacity is less than 38,000 lbs/ft^2, the angle of internal friction of the backfill and in situ soil is greater than 30 degrees, the density of the backfill is greater than 134 lb/ft^3, and the coefficient of friction beneath the Category I structures and the NAB is less than 0.5.

Therefore a full site specific soil structure interaction (SSI) analysis and stability analysis has performed to confirm that the U.S. EPR design can be constructed and operated safely at the CCNPP Unit 3 site. The details of the SSI analysis are provided in Section 3.7. Section 3.7.2.5.2.1 and 3.7.2.5.2 present comparisons of the CCNPP Unit 3 ISRS with the certified design ISRS at key locations. It can be seen in the figures that the CCNPP Unit 3 site-specific ISRS, in general, slightly exceed the standard design ISRS at frequencies below 0.7 Hz. Since this exceedance occurs outside the range of any structural frequencies (which are greater than 1 Hz), there is no impact to structural seismic loads used for design. Low frequency motion can affect sloshing. The Pool loads have been evaluated to account for ISRS exceedance. Structural loads are based on zero period acceleration (ZPAs) and are not affected by exceedance in low frequency range.

The standard design Seismic Category I structures (NI Common Basemat Structures, EPGB and ESWB) have been evaluated and the low frequency exceedance does not affect the integrity of the design.

The stability of the standard design Nuclear Auxiliary Building and Access Building have been evaluated using site specific soils and the Site SSE. This analysis confirms that the structures do not interact with Seismic Category I structures. This is discussed in Section 3.7.2.8.

A comparison of CCNPP Unit 3 seismic foundation forces and moments versus the certified design is presented in Section 3.8.5.5. This assessment demonstrates that the foundation forces and moments experienced at CCNPP unit 3 are much smaller than the foundation forces and moments used in the certified design.

2.5.2.7 Conclusions

This section is added as a supplement to the U.S. EPR FSAR.

Calvert Cliffs 3 Nuclear Project, LLC and UniStar Nuclear Operating Services, LLC used the seismic source and ground motion models developed by the Electric Power Research Institute (EPRI), the Department of Energy (DOE), and the USNRC for the Central and Eastern United States (CEUS), Seismic Source Characterization (SSC), (EPRI/DOE/NRC, 2012). As such, FSAR Section 2.5.2 utilizes the most recent seismic interpretations from the learned scientific community. The 2012 CEUS SSC was developed using a Senior Seismic Hazard Analysis

Committee (SSHAC) Level 3 process to ensure that the model captures the center, body, and range of technically defensible interpretations.

Calvert Cliffs 3 Nuclear Project, LLC and UniStar Nuclear Operating Services, LLC also used the guidance of Regulatory Guide 1.208, A Performance–Based Approach to Define the Site-Specific Earthquake Ground Motion, (NRC, 2007a) to develop the Ground Motion Response Spectrum (GMRS).

Calvert Cliffs 3 Nuclear Project, LLC and UniStar Nuclear Operating Services, LLC has provided a characterization of the seismic sources surrounding the site, as required by 10 CFR 100.23. Calvert Cliffs 3 Nuclear Project, LLC and UniStar Nuclear Operating Services, LLC has adequately addressed the uncertainties inherent in the characterization of these seismic sources through a PSHA, and that this PSHA followed the guidance provided in Regulatory Guide 1.208 (NRC, 2007a).

The GMRS developed by UniStar Nuclear Operating Services, LLC uses the performance-based approach described in Regulatory Guide 1.208 (NRC, 2007a), adequately representing the regional and local seismic hazards and accurately includes the effects of the local CCNPP Unit 3 subsurface properties.

The performance-based approach outlined in Regulatory Guide 1.208 (NRC, 2007a) is an advancement over the solely hazard-based reference probability approach recommended in Regulatory Guide 1.165 (NRC, 1997) and it was used where appropriate in the determination of the GMRS. The performance-based approach uses not only the seismic hazard characterization of the site from the PSHA but also basic seismic fragility SSC modeling in order to obtain an SSE that directly targets a structural performance frequency value. Calvert Cliffs 3 Nuclear Project, LLC and UniStar Nuclear Operating Services, LLC conclude that the application for the CCNPP Unit 3 site is acceptable from a geologic and seismologic standpoint and meets the requirements of 10 CFR 100.23(d) (CFR, 2007).

Deviations from the NRC guidance in Regulatory Guide 1.165 (NRC, 1997), Regulatory Guide 1.208 (NRC, 2007a), or review criteria in Standard Review Plan 2.5.2 (NRC, 2007b) have been identified and acceptable alternatives, including technical justification, have been provided.

2.5.2.8 References

This section is added as a supplement to the U.S. EPR FSAR.

Abrahamson, 1997. Empirical Response Spectral Attenuation Relations for Shallow Crustal Earthquakes. N. A. Abrahamson and W. J. Silva, Seismological Research Letter, Volume 68, Number 1, pp. 94-127, 1997.

Adams, 2005. Fourth Generation Seismic Hazard Maps of Canada: Values for over 650 Canadian Localities Intended for the 2005 National Building Code of Canada, Geological Survey of Canada, J. Adams and S. Halchuck, Open File 4459, 155 pp., 2003.

Amick 1990a. Paleoliquefaction Investigations Along the Atlantic Seaboard With Emphasis on the Prehistoric Earthquake Chronology of Coastal South Carolina, D. Amick, unpublished Ph.D. dissertation, University of South Carolina, selected pages, 1990.

Amick, 1990b. Characteristics of Seismically Induced Liquefaction Sites and Features Located In the Vicinity of the 1886 Charleston, South Carolina Earthquake, D. Amick, G. Maurath, and R. Gelinas, Seismological Research Letter, Volume 61, Number 2, pp. 117-130, 1990.

ANSS, 2006. Advanced National Seismic System catalog, catalog-search2_pl_search_090806.htm, obtained from the ANSS website on September 8, 2006. Website: http://www.ncedc.org/anss/catalog-search.html, Date accessed: September 8, 2006.

ASCE, 2005. American Society of Civil Engineers, "Seismic Design Criteria for Structures, Systems, and Components in Nuclear Facilities," American Society for Civil Engineers/Structural Engineering Institute, Report ASCE/SEI 43-05, 2005.

Atkinson, 1987. Stochastic prediction of ground motion and spectral response parameters at hard-rock sites in eastern North America, G. M. Atkinson and D. M. Boore, Seismological Society of America, Bulletin, Volume 77, Number 2, pp. 440-467, 1987.

Atkinson, 1995. Ground-Motion Relations for Eastern North America, G. M. Atkinson and D. M. Boore, Seismological Society of America, Bulletin, Volume 85, Number 1, pp 17-30, 1995.

Bakun, 2004. Magnitudes and Locations of the 1811-1812 New Madrid, Missouri, and the 1886 Charleston, South Carolina, Earthquakes, W. H. Bakun and M. G. Hopper, Seismological Society of America, Bulletin, Volume 94, Number 1, pp. 64-75, 2004

Bechtel, 2006. Update of Charleston Seismic Source and Integration with EPRI Source Models, Bechtel engineering study report 25144-006-V14-CY06-00006, revision 001002, September 8, 2006. S. C Lindvall and R. D. Hartleb. Release was provided by letter AR-07-0883, dated April 19, 2007 from Charles Pierce, Southern Company to Rod Krich, Constellation.

Behrendt, 1981. Cenozoic Faulting in the Vicinity of the Charleston, South Carolina, 1886 Earthquake: Geology, J. C. Behrendt, R. M. Hamilton, H. D. Ackermann, and V. J. Henry, Volume 9, Number 3, pp. 117-122, 1981.

Behrendt, 1983. Marine Multichannel Seismic-reflection Evidence for Cenozoic Faulting and Deep Crustal Structure Near Charleston, South Carolina, C. Behrendt, R. M. Hamilton, H. D. Ackermann, V. J. Henry, and K. C. Bayer, U. S. Geological Survey Professional Paper 1313-J, pp. J1-J29, 1983.

Behrendt, 1987. The Helena Banks Strike-slip (?) Fault Zone in the Charleston, South Carolina, Earthquake Area: Results From a Marine, High-resolution, Multichannel, Seismic-reflection Survey, J. C. Behrendt and A. Yuan, Geological Society of America, Bulletin, Volume 98, pp. 591-601, 1987.

Bernreuter, 1989. Seismic Hazard Characterization of 69 Nuclear Plant Sites East of the Rocky Mountains: U.S. Nuclear Regulatory Commission, NUREG/CR-5250, Volumes 1–8, D.L. Bernreuter, J.B. Savy, R.W. Mensing, J.C. Chen, and B.C. Davis, 1989.

Bollinger, 1977. Reinterpretation of the Intensity Data for the 1886 Charleston, South Carolina, Earthquake in Studies Related to the Charleston, South Carolina, Earthquake of 1886- A Preliminary Report, D. W. Rankin, edition, G. A. Bollinger, U. S. Geological Survey Professional Paper 1028, pp. 17-32, 1977.

Bollinger, 1985. An Analysis of Earthquake Focal Depths in the Southeastern U. S., G. A. Bollinger, M. C. Chapman, M. S. Sibol, and J. K. Costain, American Geophysical Union, Geophysical Research Letter, Volume 12, Number 11, pp. 785-788, 1985.

Bollinger, 1989. Magnitude recurrence relations for the Southeastern United States and its subdivisions, G. A. Bollinger, F. C. Davison Jr., M. S. Sibol, and J. B. Birch, Journal of Geophysical Research, Volume 94, Number B3, pp. 2857-2873, 1989.

Bollinger, 1991. Seismicity of the Southeastern United States; 1698-1986 in Neotectonics of North America, Decade Map Volume to Accompany the Neotectonic Maps, D. B. Slemmons, E. R. Engdahl, M. D. Zoback, and D. D. Blackwell G. A. Bollinger, A. C. Johnston, P. Talwani, L. T. Long, K. M. Shedlock, M. S. Sibol, and M. C. Chapman, pp. 291-308, 1991.

Campbell, 1997. Empirical near-source attenuation relationships for horizontal and vertical components of peak ground acceleration, peak ground velocity, and pseudo-absolute acceleration response spectra, K. W. Campbell, Seismological Society Of America, Seismological Research Letter, Volume 68, Number 1, pp. 154-179, 1997.

Canada, 2006. Canadian catalog is searchable through the on-line bulletin from the Natural Resources Canada, Earthquake Search, Website: http://earthquakescanada.nrcan.gc.ca/stnsdata/nedb/bull_e.php, Date accessed: September 13, 2006.

CFR, 2007. Geologic and Seismic Siting Factors, Title 10, Code of Federal Regulations, Part 100.23(d), 2007.

Chapman, 1994. Seismic Hazard Assessment for Virginia, M. C. Chapman and F. Krimgold, Virginia Tech Seismological Observatory, Department of Geological Sciences, February 1994.

Chapman, 2002. Seismic Hazard Mapping for Bridge and Highway Design in South Carolina, M. C. Chapman and P. Talwani, South Carolina Department of Transportation Report, 2002.

Cook, 1979. Thin-skinned Tectonics in the Crystalline Southern Appalachians: COCORP Seismic Reflection Profiling of the Blue Ridge and Piedmont, F. A. Cook, A. Albaugh, D. S., Brown, L. D., Kaufman, S., Oliver, J. E., Hatcher, R. D. Jr., Geology, Volume 7, pp. 563-567, 1979.

Cook, 1981. COCORP Seismic Profiling of the Appalachian Orogen Beneath the Coastal Plain of Georgia, F. A. Cook, L. D. Brown, S. Kaufman, J. E. Oliver, and T. A. Petersen, Geological Society of America Bulletin, Volume 92, Number 10, pp. 738-748, 1981.

Cornell, 1988. Temporal and Magnitude Dependence in Earthquake Recurrence Models, C. A. Cornell and S. R. Winterstein, Seismological Society of America, Bulletin, Volume 79, pp. 1522-1537, 1988.

Coruh, 1988. Seismogenic structures in the central Virginia seismic zone, C. Coruh, G. A. Bollinger, and J. K Costain, Geology, Volume 16, pp. 748-751, 1988.

Costantino, 1996. Recommendations for Uncertainty Estimates in Shear Modulus Reduction and Hysteretic Damping Relationships, C. J. Costantino, (1996). Published as an appendix in "Description and validation of the stochastic ground motion model," W.J. Silva, N. Abrahamson, G. Toro and C. Costantino. (1997). Report Submitted to Brookhaven National Laboratory, Associated Universities, Inc. Upton, New York 11973, Contract No. 770573.

Cramer, 2001. A Seismic Hazard Uncertainty Analysis for the New Madrid Seismic Zone, C. H. Cramer, Engineering Geology, Volume 62, pp. 251-266, 2001.

Crone, 2000. Data for Quaternary Faults, Liquefaction Features, and Possible Tectonic Features in the Central and Eastern United States, east of the Rocky Mountain front, U.S. Geological Survey Open-File Report 00-260, A. J. Crone and R. L. Wheeler, 2000.

Deere, 1966. Engineering Classification and Index Properties of Intact Rock, University of Illinois, Prepared for Air Force Weapons Laboratory, Technical Report No AFWL-TR-65-116, D. Deere and R. Miller, December, 1966.

Dominion, 2004a. Dominion Nuclear North Anna LLC, Docket No. 52-008, Response to 6/1/04 RAI 2.5.1-5, 2.5.1-6, 2.5.3-2, and 2.5.1-5, Letter No. 5, U.S. Nuclear Regulatory Commission, Serial No. 04-347, 2004.

Dominion, 2004b. Dominion Nuclear North Anna LLC, Docket No. 52-008, Response to 4/15/04 RAI 2.5.1-1 to 2.5.1-4, 2.5.2-2 to 2.5.2-4, and 2.5.3-1, Letter No. 3, U.S. Nuclear Regulatory Committee, Serial No. 04-270, 2004.

Dominion, 2005. Dominion North Anna LLC, Docket No. 52-008, North Anna Early Site Permit Application, Revision 5, Adams Accession No. ML052150253, July 2005.

Ellsworth, 1999. A Physically-Based Earthquake Recurrence Model for Estimation of Long-Term Earthquake Probabilities, W. L. Ellsworth, M. V. Matthews, R. M. Nadeau, S. P. Nishenko, P. A. Reasenberg, and R. W. Simpson, U.S. Geological Survey Open-File Report 99-522, 1999.

EPRI, 1986. Seismic Hazard Methodology for the Central and Eastern United States, Tectonic Interpretations, Electric Power Research Institute, Report NP-4726, Volumes 5–10, July 1986.

EPRI, 1988. Seismic Hazard Methodology for the Central and Eastern United States, Electric Power Research Institute, Report NP-4726-A, Revision 1, Volume 1, Part 2, 1988.

EPRI, 1989a. Probabilistic Seismic Hazard Evaluations at Nuclear Power Plant Sites in the Central and Eastern United States: Resolution of the Charleston Earthquake Issue, Electric Power Research Institute, Report NP-6395-D, 1989.

EPRI, 1989b. EQHAZARD Primer, Electric Power Research Institute, Report NP-6452-D, June 1989.

EPRI, 1992. The stable continental region earthquake database: in Methods for assessing maximum earthquakes in the central and eastern U.S., Electric Power Research Institute, Report RP-2556-12, 1992.

EPRI, 1993. Guidelines for Determining Design Basis Ground Motions, Volume 5: Quantification of Seismic Source Effects, Electric Power Research Institute, Report TR-102293, November 1993.

EPRI, 1994. The earthquakes of stable continental regions, Volume I: Assessment of Large Earthquake Potential, Electric Power Research Institute, Final Report TR-102261-V1, 1994.

EPRI, 2004. CEUS Ground Motion Project Final Report, Electric Power Research Institute, TR-1009684 2004, December 2004.

EPRI, 2006a. Program on Technology Innovation: Truncation of the Lognormal Distribution and Value of the Standard Deviation for Ground Motion Models in the Central and Eastern United States, Electric Power Research Institute, Report TR-1014381, August 2006.

EPRI, 2006b. Program on Technology Innovation: Truncation of the Lognormal Distribution and Value of the Standard Deviation for Ground Motion Models in the Central and Eastern United States, Electric Power Research Institute, Technical Update 1013105, February 2006.

EPRI, 2012. Central and Eastern United States Seismic Source Characterization for Nuclear Facilities, Electric Power Research Institute (EPRI)/U.S. Department of Energy (DOE)/U.S. Nuclear Regulatory Commission, EPRI Report #1021097, DOE Report # DOE/NE-0140, NRC NUREG-2115, 2012.

Exelon, 2005. Letter dated October 31, 2005, T. Mundy, Exelon to NRC, Subject: Response Supplemental Draft Safety Evaluation Report (DSER) Item, page 16 of 112 and page 54 of 112, (Adams Accession Number ML053120131), 2005.

Fletcher, 1978. Seismic Trends and Travel-time Residuals in Eastern North America and Their Tectonic Implications, J. B. Flectcher, M. L. Sbar, and L. R. Sykes, Geological Society of America Bulletin, Volume 89, pp. 1656-1676, 1978.

Grant, 1994. Paleoseismic Evidence of Clustered Earthquakes on the San Andreas Fault in the Carrizo Plain, California, L. B. Grant, and K. Sieh, Journal of Geophysical Research, Volume 99, Number B4, pp. 6819-6841, 1994.

Horton, 2012. The 2011 Virginia Earthquake: What are Scientists Learning?, J.W. Horton and R.A. Williams, American Geophysical Union, Transactions of the American Geophysical Union, Vol. 98, No. 33, pp. 317-318, 2012.

Idriss, 1992. SHAKE91: A computer program for conducting equivalent linear seismic response analyses of horizontally layered soil deposits, I. M. Idriss, and J. I Sun, Department of Civil and Environmental Engineering, Center for Geotechnical Modeling, University of California, Davis, Calif., 1992.

Johnston, 1985. Recurrence rates and probability estimates for the New Madrid seismic zone, A. C. Johnston and S. J. Nava, Journal of Geophysical Research, Volume 90, pp. 6737–6753, 1985.

Johnston, 1996. Seismic Moment Assessment of Earthquake in Stable Continental Regions – III. New Madrid 1811-1812, Charleston 1886 and Lisbon 1755, A. C. Johnston, Geophysical Journal International, Volume 126, pp. 314-344, 1996.

Kramer, 1996. Geotechnical Earthquake Engineering, S. L. Kramer, Prentice-Hall, 1996.

Marple, 1990. Field Investigations of the Woodstock Lineament, R. T. Marple and P. Talwani, Seismological Society of America, Seismological Research Letter, Volume 61, Number 3-4, p. 156, 1990.

Marple, 1993. Evidence For Possible Tectonic Upwarping Along The South Carolina Coastal Plain From An Examination Of River Morphology And Elevation Data, R. T. Marple and P. Talwani, Geology, Volume 21, pp. 651-654, 1993.

Marple, 2000. Evidence for a Buried Fault System in the Coastal Plain of the Carolinas and Virginia - Implications for Neotectonics in the Southeastern United Sates, R. T. Marple and P. Talwani, Geological Society of America Bulletin, Volume 112, Number 2., pp. 200-220, 2000.

Marple, 2004. P., Proposed Shenandoah Fault and East Coast-Stafford Fault System and Their Implications for Eastern U. S. Tectonics, R. T. Marple and P. Talwani, Southeastern Geology, Volume 43, Number 2, pp. 57-80, 2004.

Martin, 1994. G. W., Seismic Parameters from Liquefaction Evidence, J. R. Martin and G. W. Clough, Journal of Geotechnical Engineering, Volume 120, Number 8, pp. 1345-1361, 1994.

McGuire, 2001. Technical Basis for Revision of Regulatory Guidance on Design Ground Motions: Hazard and Risk-consistent Ground Motion Spectra Guidelines, NUREG/CR-6728, U.S. Nuclear Regulatory Commission, R.K. McGuire, W.J. Silva, C.J. Costantino, 2001.

NIST, 2006. NIST/SEMATECH, e-Handbook of Statistical Methods, http://www.itl.nist.gov/div898/handbook/, accessed 11 January 2006, Chapter 1 downloaded in PDF form from http://www.itl.nist.gov/div898/handbook/toolaids/pff/1-eda.pdf.

NRC, 1986. Identification of a Northwest Trending Seismogenic Graben Near Charleston, South Carolina, NUREG/CR-4075, U.S. Nuclear Regulatory Commission 1986.

NRC, 1990. Paleoliquefaction Features Along the Atlantic Seaboard, NUREG/CR-5613, U. S. Nuclear Regulatory Commission, 1990

NRC, 1991. Generic Letter 88-20, Individual Plant Examinations of External Events (IPEEE) for Severe Accident Vulnerabilities, U. S. Nuclear Regulatory Commission, 1991.

NRC, 1997a. Identification and Characterization of Seismic Sources and Determination of Safe Shutdown Earthquake Ground Motion, Regulatory Guide 1.165, U. S. Nuclear Regulatory Commission, March 1997.

NRC, 1997b. Recommendations for Probabilistic Seismic Hazard Analysis: Guidance on Uncertainty and Use of Experts, Prepared by Senior Seismic Hazard Analysis Committee (SSHAC), NUREG/CR-6372, U. S. Nuclear Regulatory Commission, 1997.

NRC, 2001. Technical Basis for Revision of Regulatory Guidance on Design Ground Motions, Hazard- and Risk-Consistent Ground Motion Spectra Guidelines, NUREG/CR-6728, U. S. Nuclear Regulatory Commission, 2001.

NRC, 2002a. Guidance for Performing Probabilistic Seismic Hazard Analysis for a Nuclear Plant Site: Example Application to the Southeastern United States, NUREG/CR-6607, U. S. Nuclear Regulatory Commission, 2002.

NRC, 2002b. Technical Basis for Revision of Regulatory Guidance on Design Ground Motions: Development of Hazard- & Risk-Consistent Seismic Spectra for Two Sites, NUREG/CR-6769, U.S. Nuclear Regulatory Commission, 2002.

NRC, 2005. Safety Evaluation Report for an Early Site Permit (ESP) at the North Anna ESP Site, NUREG-1835, U. S. Nuclear Regulatory Commission, September 2005.

NRC, 2007a. A Performance-Based Approach to Define the Site-Specific Earthquake Ground Motion, U. S. Nuclear Regulatory Commission, Regulatory Guide 1.208, March 2007.

NRC, 2007b. Vibratory Ground Motion, Standard Review Plan, NUREG-0800, Section 2.5.2, Revision 4, U.S. Nuclear Regulatory Commission, March 2007.

NRC, 2007c. Combined License Applications For Nuclear Power Plants (LWR Edition), Regulatory Guide 1.206, U.S. Nuclear Regulatory Commission, March 2007.

NRC, 2009. Interim Staff Guidance on Ensuring Hazard-Consistent Seismic Input for Site Response and Soil Structure Interaction Analyses, DC/COL-ISG-017, U.S. Nuclear Regulatory Commission, 2009.

Obermeier, 1989. Liquefaction evidence for Repeated Holocene Earthquakes in the Coastal Region of South Carolina, S. F. Obermeier, R. E. Weems, R. B. Jacobson, and G. S. Gohn, Annals of the New York Academy of Sciences, Volume 558, pp. 183-195, 1989.

Obermeier, 1998. Paleoliquefaction Evidence for Seismic Quiescence in Central Virginia During the Late and Middle Holocene Time (abs), S. F. Obermier and W. E. McNulty. Eos Transactions, American Geophysical Union, Volume 79, No. 17, p S342, 1998.

Ohio, 2006. Ohio Seismic Network catalog, "http://www.dnr.state.oh.us/OhioSeis, KEY TO COLUMN DATA.htm, Oh_eq_1950 to 1999.htm, and Oh_eq_2000_to_present.htm," Ohio Department of Natural Resources, September 8, 2006. Website: http://www.dnr.state.oh.us/OhioSeis.

Petersen, 2008. Documentation for the 2008 Update of the United States National Seismic Hazard Maps, M. D. Petersen, A.D. Frankel, S.C. Harmsen, C.S. Mueller, K.M. Haller, R.L. Wheeler, R.L. Wesson, Y. Zeng, O.S. Boyd, D.M. Perkins, N. Luco, N.H. Field, C.J. Wills, and K.S. Rukstales, U.S. Geological Survey, Open-File Report 2008-1128, 128 pp., 2008.

Ramsey, 1995. Radiocarbon calibration and analysis of stratigraphy: the OxCal program, C. Bronk Ramsey, C., Radiocarbon, Volume 37, Number 2, pp. 425-430, 1995.

Ramsey, 2001. Development of the radiocarbon program OxCal: Radiocarbon, C. Bronk Ramsey, Volume 43, Number 2A, pp. 355-363, 2001.

Rathie, 2006. Site-Specific Validation of Random Vibration Theory Based Seismic Site Response Analysis, Journal of Geotechnical and Geoenvironmental Engineering, American Society of Civil Engineers, Volume 132, No. 7, G. M. Rathie, C. Ozbey, July, 2006.

Reger, 1994. Summary of the Howard County, Maryland, Earthquakes of 1993, Southeastern U.S. Seismic Network Bulletin No. 28, Appendix A., Website: http://www.geol.vt.edu/outreach/vtso/anonftp/catalog/bul28.list1, J. P. Reger, 1994.

Schneider, 1991. Estimation of Ground Motion at Close Distances Using the Band-Limited White Noise Model, Proceedings 4th International Conference on Seismic Zonation, Vol. 4, Earthquake Engineering Research Institute, J. F. Schneider, W. J. Silva, S. J. Chiou, and J. C. Stepp, Stanford, CA, pp 187-194, 1991.

Seeber, 1981. The 1886 Charleston, South Carolina earthquake and the Appalachian detachment, L. Seeber and J. G. Armbruster, Journal of Geophysical Research, Volume 86, Number B9, pp. 7874-7894, 1981.

Seeber, 1998. The 1994 Cacoosing Valley earthquakes near Reading, Pennsylvania: A shallow rupture triggered by quarry unloading, L. Seeber, J. G. Armbruster, W. Y. Kim, N. Barstow, C. Scharnberger, Journal of Geophysical Research, Volume 103, Number B10, pp. 24,505-24,521, 1998.

SEUSSN, 2006. South Eastern United States Seismic Network catalog, "susn2004cat.txt," Virginia Tech Seismic Observatory, September 8, 2006. Website: http://www.geol.vt.edu/outreach/vtso/.

Sieh, 1989. Precise Chronology of Earthquakes Produced by the San Andreas fault in Southern California, K. Sieh, M. Stuiver, and D. A. Brillinger, Journal of Geophysical Research, Volume 94, Number B1, pp. 603-623, 1989.

Silva, 1997. Description and validation of the stochastic ground motion model, Final report, Brookhaven National Laboratory, Contract No. 770573, W. J. Silva, N. Abrahamson, G. Toro, C. Costantino, Associated Universities, Inc., Upton, N.Y., 1997.

Smith, 1985. Preliminary interpretation of a detailed gravity survey in the Bowman and Charleston, S.C. Seismogenic zones: Abstracts with Programs, W. A. Smith and P. Talwani, Geological Society of America southeastern section, Volume 17, Number 2, p. 137, 1985.

SSA, 1968. Engineering Seismic Risk Analysis, Seismological Society of America, Bulletin, Volume 58, Number 5, pp. 1583-1606, C. A. Cornell, 1968.

SSA, 1981. Results of recent South Carolina seismological studies, Seismological Society of America, Bulletin, Volume 71, Number 6, pp. 1883-1902, A. C. Tarr, P. Talwani, S. Rhea, D. Carver, and D. Amick, 1981.

SSA, 1987. The 23 April 1984 Martic Earthquake and The Lancaster Seismic Zone In Eastern Pennsylvania, Bulletin of the Seismological Society of America, Vol. 77, No. 2, pp. 877-890, J. Armbruster and L. Seeber, 1987.

SSA, 1991. Criticism of Some Forecasts of the National Earthquake Evaluation Council, Seismological Society of America, Bulletin, Volume 81, Number 3, pp. 862-881, J. C. Savage, 1991.

SSA, 1993. Fault Plane Solutions and Relocations of Recent Earthquakes in Middleton Place-Summerville Seismic Zone near Charleston, South Carolina, Seismological Society of America, Bulletin, Volume 83, Number 5, pp. 1442-1466, S. Madabhushi and P. Talwani, 1993.

SSA, 1994. New Empirical Relationships Among Magnitude, Rupture Length, Rupture Width, Rupture Area, and Surface Displacement, Seismological Society of America, Bulletin, Volume 84, Number 4, pp. 974-1002, D. L. Wells and K. J Coppersmith, August 1994.

SSA, 1995. Seismic Hazards in Southern California: Probable earthquakes, 1994 to 2024, Bulletin of the Seismological Society of America, Volume 85, pp. 379-439, Working Group on California Earthquake Probabilities, 1995.

SSA, 2000. Paleoseismology of the Johnson Valley, Kickapoo, and Homestead Valley faults: clustering of earthquakes in the Eastern California shear zone, Seismological Society of America, Bulletin, Volume 90, Number 5, pp. 1200-1236, T. K. Rockwell, S. Lindvall, M. Herzberg, D. Murbach, T. Dawson, and G. Berger 2000.

SSA, 2002. A Brownian model for recurrent earthquakes, Seismological Society of America, Bulletin, Volume 92, pp. 2233-2250, M. V. Matthews, W. L. Ellsworth, and P. A. Reasenberg, 2002.

Stepp, 1991. Site response evaluations based upon generic soil profiles using random vibration methodology. Proceedings 4th International Conference on Seismic Zonation, Vol. 4, Earthquake Engineering Research Institute, J.C. Stepp, W. J. Silva, H.B. Seed, I. M. Idriss, R. McGuire, J. Schneider, Stanford, Calif., pp. 739-746, 1991.

Sykes, 1978. Intraplate Seismicity, Reactivation of Preexisting Zones of Weakness, Alkaline Magmatism, and Other Tectonism Postdating Continental Fragmentation, L. R. Sykes, Reviews of Geophysics, Volume 16, pp. 621-688, 1978.

Talwani, 1982. An internally consistent pattern of seismicity near Charleston, South Carolina, P. Talwani, Geology, Volume 10, pp. 655–658, 1982.

Talwani, 1999. Fault Geometry and Earthquakes in Continental Interiors, P. Talwani, Tectonophysics, Volume 305, pp. 371-379, 1999.

Talwani, 2000. Macroscopic Effects of the 1886 Charleston Earthquake, A Compendium of Field Trips of South Carolina Geology, P. Talwani, South Carolina Geological Survey, pp. 1-6, 2000.

Talwani, 2001. Recurrence Rates of Large Earthquakes in the South Carolina Coastal Plain Based on Paleoliquefaction Data, P. Talwani and W. T. Schaeffer, Journal of Geophysical Research, Volume 106, Number B4, pp. 6621-6642, 2001.

Talwani, 2004. Macroseismic effects of the 1886 Charleston earthquake, P. Talwani and M. Katunam, Carolina Geological Society field trip guidebook, p. 18, 2004.

Toro, 1996. Probabilistic Models of Site Velocity Profiles for Generic and Site-Specific Ground Motion Amplification Studies, G. R. Toro, Published as an appendix in W. J. Silva, N. Abrahamson, G. Toro and C. Costantino, (1997), Description and validation of the stochastic ground motion model, Report Submitted to Brookhaven National Laboratory, Associated Universities, Inc. Upton, New York 11973, Contract No. 770573, 1996.

Tuttle, 2001. The Use of Liquefaction Features in Paleoseismology: Lessons Learned in the New Madrid Seismic Zone, central United States, M. P. Tuttle, Journal of Seismology, Volume 5, pp. 361-380, 2001.

USGS, 1983a. Land multichannel seismic-reflection evidence for tectonic features near Charleston, South Carolina, Studies Related to the Charleston, South Carolina, Earthquake of 1886- Tectonics and Seismicity, U.S. Geologic Survey, Professional Paper 1313-I, pp. I1-I18, R. M. Hamilton, J.C. Behrendt, and H. D. Ackermann, 1983.

USGS, 1983b. Seismicity Near Charleston, South Carolina, March 1973 to December 1979 in Studies Related to the Charleston, South Carolina Earthquake of 1886: Tectonics and Seismicity, G. S. Gohn (ed.), U. S. Geological Survey, Professional Paper 1313, pp. R1-R17, A. C. Tarr and S. Rhea, 1983.

USGS, 1983c. Regenerate Faults of the Southeastern United States, in Studies Related to the Charleston, South Carolina, Earthquake of 1886: Tectonics and seismicity, Gohn, G. S. (ed.), C. M. Wentworth and M. Mergener-Keefer, US Geological Survey Professional Paper 1313, pp. S1-S20, 1983.

USGS, 1992. Specification of Source Zones, Recurrence Rates, Focal Depths, and Maximum Magnitudes for Earthquakes Affecting the Savannah River Site in South Carolina, U.S. Geological Survey, Bulletin 2017, G. A. Bollinger, 1992.

USGS, 1996. National seismic-hazard maps: documentation, U. S Geological Survey, Open-File Report 96-532, A. Frankel, T. Barnhard, D. Perkins, E. V. Leyendecker, N. Dickman, S. Hanson, and M. Hopper, 1996.

USGS, 1997. Geology of the Pringletown, Ridgeville, Summerville, and Summerville Northwest 7.5-minute quadrangles, Berkeley, Charleston, and Dorchester counties, South Carolina: Miscellaneous Investigations Series, U. S. Geological Survey, R. E. Weems, E. M. Lemon, Jr. and M. S. Nelson, 1997.

USGS, 1998. Newly Recognized En Echelon Fall Lines in the Piedmont and Blue Ridge Provinces of North Carolina and Virginia, With a Discussion of Their Possible Ages and Origins, U.S. Geological Survey, Open-File Report 98-374, R. E. Weems, 1998.

USGS, 2002. Documentation for the 2002 Update of the National Seismic Hazard Maps, U.S. Geological Survey Open-File Report 02-420, A. D. Frankel, M. D. Petersen, C. S. Mueller, K. M. Haller, R. L. Wheeler, E. V. Leyendecker, R. L. Wesson, S. C. Harmsen, C. H. Cramer, D. M. Perkins, and K. S. Rukstales, 2002.

USGS, 2003. Earthquake Probabilities in the San Francisco Bay region: 2002-2031, U. S. Geological Survey Open-File Report 03-2134, Working Group on California Earthquake Probabilities, 2003.

Weems, 2002. Structural and tectonic setting of the Charleston, South Carolina, region; evidence from the Tertiary stratigraphic record, R. E. Weems and W. C. Lewis, Geological Society of America, Bulletin, Volume 114, Number 1, pp. 24-42, 2002.

WGCEP, 1995. Working Group on California Earthquake Probabilities, Seismic Hazards in Southern California: Probable earthquakes, 1994 to 2024, Bulletin of the Seismological Society of America, Volume 85, pp. 379-439, 1995.

Wheeler, 1992. Geologic Implications of Earthquake Source Parameters in Central and Eastern North America, Seismological Research Letters, R. L. Wheeler, and A. C. Johnston Volume 63, No. 4, pp. 491–505, 1992.

Wheeler, 2005. Known or Suggested Quaternary Tectonic Faulting, Central and Eastern United States – New and Updated Assessments for 2005, U.S. Geological Survey, Open File Report 2005-1336, R. L. Wheeler, 2005.

Wheeler, 2006. Quaternary tectonic faulting in the Eastern United States, Engineering Geology, Volume 82, pp. 165-186, R. L. Wheeler, 2006.

2.5.3 Surface Deformation

The U.S. EPR FSAR includes the following COL Item in Section 2.5.3:

> A COL applicant that references the U.S. EPR design certification will investigate site-specific surface and subsurface geologic, seismic, geophysical, and geotechnical aspects within 25 miles around the site and evaluate any impact to the design. The COL applicant will evaluate the potential for surface deformation at the site in accordance with the

requirements of 10 CFR 100.23 and 10 CFR 50, Appendix S. If the potential for surface deformation is present at the site, the COL applicant will evaluate the effects of potential surface deformation on the design and operation of the U.S. EPR.

This COL Item is addressed as follows:

{There is no potential for tectonic fault rupture and there are no capable tectonic sources within a 25 mi (40 km) radius of the CCNPP site. A capable tectonic source is a tectonic structure that can generate both vibratory ground motion and tectonic surface deformation, such as faulting or folding at or near the earth's surface in the present seismotectonic regime (NRC, 1997). The following sections provide the data, observations, and references to support this conclusion. Information contained in these sections was developed in accordance with RG 1.165 (NRC, 1997), and is intended to satisfy 10 CFR 100.23, "Geologic and Seismic Siting Criteria" (CFR, 2007a) and 10 CFR 50, Appendix S, "Earthquake Engineering Criteria for Nuclear Power Plants" (CFR 2007b).

Sections 2.5.3.1 through 2.5.3.9 are added as a supplement to the U.S. EPR FSAR.

2.5.3.1 Geological, Seismological, and Geophysical Investigations

The potential for surface deformation within a 25 mi (40 km) radius of the CCNPP Unit 3 site was assessed, in part, through the review of existing geologic and seismologic data for the site vicinity, and a review of the EPRI/DOE/NRC (2012) seismic source characterization for the site region. Details related to the seismic source characterization and the existing geologic and seismologic data for the site vicinity are provided in Sections 2.5.1 and 2.5.2. In addition, existing aerial photographs and satellite and LiDAR imagery for the site vicinity were reviewed for evidence of surface rupturing or related phenomena, as discussed in Section 2.5.1.1.4.4. Additional ground- and aircraft-based field reconnaissance was completed as a supplement to the existing data sets, along with discussions of the site area geology with researchers at the USGS, MGS, and various academic institutions.

The geologic and geotechnical information available for the existing CCNPP Units 1 and 2 site and site vicinity, as well as the proposed CCNPP Unit 3 site, is contained in three principal sources:

1. Work performed for the existing CCNPP Units 1 and 2 and complementary structures (BGE, 1968) (Constellation, 2005); and geotechnical foundation studies for adjacent parking lots (BPC, 1981),

2. Published and unpublished geologic mapping performed primarily by the USGS and MGS, and

3. Seismicity data compiled and analyzed in published journal articles and, more recently, as part of Section 2.5.2.

Existing data and reports related to the CCNPP site provide no evidence of tectonic or geologic instability within the site vicinity. More recent publications, in turn, confirm the stability of the site vicinity and the lack of Quaternary movement on any nearby faults. For example, the CEUS SSC report (EPRI/DOE/NRC, 2012) makes no mention of the only inferred bedrock fault that has been mapped at (or near) the 5 mi (8 km) radius of the CCNPP site (i.e., the Hillville fault (Hansen, 1986)), and acknowledges only the Stafford and Brandywine fault systems, both located beyond the 25 mi (40 mi) site vicinity radius (see also Section 2.5.1.1.4). Specifically, the CEUS SSC (EPRI/DOE/NRC, 2012) indicates that there is no direct evidence for Quaternary

movement on any part of the Stafford fault system, and that activity on the north- to northeast-striking reverse faults of the Stafford and Brandywine systems is difficult to reconcile with the predominantly northeast-southwest orientation of horizontal compressive stress in the Atlantic Coastal Plain.

Nonetheless, this existing information was supplemented by aerial and field reconnaissance within a 25 mi (40 km) radius of the site, and interpretation of aerial photography along all known faults within the 5 mi (8 km) radius of the site. In addition, Light Detection and Ranging (LiDAR) data acquired from surrounding counties (Charles County, St. Mary's County and Calvert County), that covered all known faults within much of the approximately 25 mi (40 km) radius and the entire 5 mi (8 km) radius, was reviewed and interpreted with respect to published Quaternary geologic maps as shown in Figure 2.5-26. Satellite imagery (raster imagery) of the CCNPP site region also was acquired for review and interpretation. These field and office-based studies were performed to verify, where possible, the existence of mapped bedrock faults in the CCNPP site area and to assess the presence or absence of geomorphic features suggestive of potential Quaternary fault activity along the mapped faults, or previously undetected faults. Features reviewed during the field reconnaissance and office-based analysis of aerial photography, satellite imagery, and LiDAR data, were based on a compilation of existing regional geologic information, as well as discussions with experts at the USGS and MGS who have worked in the vicinity of the CCNPP site.

Field reconnaissance of the site and within a 25 mi (40 km) radius of the site was conducted by geologists in teams of two or more. Two field reconnaissance visits in late summer and autumn, 2006 focused on exposed portions of the Calvert Cliffs, other cliff exposures along the west shore of Chesapeake Bay, and roads traversing the site and a 5 mi (8 km) radius of the site. Key observations and discussion items were documented in field notebooks and photographs. A general summary of the key observations includes: (1) the nearly flat-lying Miocene Coastal Plain stratigraphy in the cliffs was generally well exposed and field descriptions matched published literature, (2) no faults were exposed in the Miocene Coastal Plain deposits along the cliffs, and (3) no liquefaction features were identified.

Aerial reconnaissance within a 25 mi (40 km) radius of the site was conducted by two geologists in a top-wing Cessna aircraft on January 3, 2007. The aerial reconnaissance investigated the geomorphology of the Chesapeake Bay area and targeted numerous previously mapped geologic features and potential seismic sources within a 200 mi (322 km) radius of the site (e.g., Mountain Run fault zone, Stafford fault system, Brandywine fault zone, Port Royal fault zone, and Skinkers Neck anticline). The flight crossed over the CCNPP site briefly but did not circle or approach the site closely in order to comply with restrictions imposed by the Federal Aviation Administration. Key observations and discussion items were documented in field notebooks and photographs. In general, the aerial reconnaissance coupled with interpretation of LiDAR data revealed no anomalous geomorphic features suggestive of Quanternary activity (e.g. tonal lineaments, fault scarps or deflected terrace back edges) along the surface-projection of the fault zones.

2.5.3.1.1 Previous Site Investigations

Previous site investigations performed for the existing units are summarized in the CCNPP Units 1 and 2 Preliminary Safety Analysis Report (PSAR) (BGE, 1968) and Independent Spent Fuel Storage Installation (ISFSI) Safety Analysis Report (SAR) (CGG, 2005). These previous investigations provide the following results documenting the absence of Quaternary faults at and within the area of the CCNPP site:

- Interpretation of air photos and topographic maps. This interpretation revealed no evidence of surface rupture, surface warping, or offset of geomorphic features indicative of active faulting.

- Interviews with personnel from government agencies and private organizations. These interviews concluded that no known faults are present beneath the existing CCNPP Units 1 and 2 or CCNPP Unit 3 site areas.

- Seismicity analysis -This analysis showed that: no microseismic activity has occurred in the site area; the site is located in a region that has experienced only infrequent minor earthquake activity; the closest epicentral location is greater than 25 mi (40 km) away. No earthquake within 50 mi (80 km) of the CCNPP site has been large enough to cause significant damage since the region has been populated over the past approximately 300 years. Section 2.5.2 provides a full discussion on the seismicity analysis for the CCNPP site.

- Approximately 85 exploratory boreholes were drilled at the CCNPP Units 1 and 2 site area. Borehole data have provided evidence for the lateral continuity of strata across the existing CCNPP Units 1 and 2 site area and the inspection of soil samples has revealed no adverse effects indicative of geologically recent or active faulting.

- Field reconnaissance of limited surface outcrops at the site and along the western shore of Chesapeake Bay, coupled with geophysical surveys, provided evidence for no faulting at the CCNPP site.

At the time of the original studies for the PSAR (BGE, 1968), there were no published maps showing bedrock faults within a 5 mi (8 km) radius of the CCNPP site. The closest significant bedrock faults mapped prior to 1968 were faults located about 50 mi (80 km) west of the CCNPP site in the Piedmont Province (BGE, 1968). The Geologic Map of Maryland (MGS, 1968) shows no faults within a 25 mi (40 km) radius of the CCNPP site.

2.5.3.1.2 Regional and Local Geological Studies

Since the late 1960's, extensive mapping of the CCNPP site region within the Coastal Plain Province by the MGS (MGS, 1971) (MGS, 1994) (MGS, 2003a) (MGS, 2003b) (MGS, 2003c) (MGS, 1986) and by the USGS (USGS, 1989c) (USGS, 1989d) (USGS, 1979a) (USGS, 1986), (USGS, 1979b) (USGS, 1995) (USGS, 2000b) has been performed to improve the industry's knowledge of the Coastal Plain stratigraphy and geologic structure within the region. Coastal Plain mapping includes geologic cross sections across the CCNPP site area (USGS, 2003b) (USGS, 2003c) and a developed geologic cross section based on mapping and borehole data (Achmad, 1997). In addition, closely-spaced shallow-penetration seismic-reflection profiles in the Chesapeake Bay provide limited below-water information on the Tertiary-Quaternary history of Chesapeake Bay (USGS, 1989a) (USGS, 1989b) (GSA, 1990), as well as limited information on the absence of Middle Miocene faulting. This compilation of previous mapping and exploration studies, coupled with site-specific reconnaissance for CCNPP Unit 3, provides the principal basis for the few, if any, bedrock faults recognized within the site area.

In addition, the USGS completed a compilation of all Quaternary faults, liquefaction features, and possible tectonic features in the eastern U.S. (USGS, 2000a) (USGS, 2005) (Wheeler, 2006). These compilations do not show any Quaternary faults or features within a 25 mi (40 km) or 5 mi (8 km) radius of the site as shown in Figure 2.5-31. The nearest potential Quaternary features (USGS, 2000a) (USGS, 2005) (Wheeler, 2006) are the Stafford fault 47 mi (76 km) west-southwest, and the Upper Marlboro faults 36 mi (58 km) to the northeast, respectively, of the

CCNPP site as shown in Figure 2.5-31. Two documented paleo-liquefaction sites (Obermier, 1998) on the James and Rivanna Rivers within the Central Virginia seismic zone are both located over 25 mi (40 km) from the CCNPP site as shown in Figure 2.5-31. Moreover, independent field reconnaissance following the August 23, 2011 Mineral, Virginia earthquake (GEER, 2011) appears to provide no evidence for ground failure features (liquefaction, slope movements, etc.) produced by the earthquake within the CCNPP site vicinity. Observations of minor liquefaction and slumping along some streams, along with rockfalls, and slope movements were noted only in the epicentral region of the 2011 earthquake, approximately 85 mi (137 km) southwest of the CCNPP.

Local geologic cross-sections oriented northwest-southeast within the site area (5 mi (8 km) radius) depict unfaulted southeast-dipping Eocene-Miocene Coastal Plain sediments that are unconformably overlain by Pliocene Upland deposits (MGS, 1994) (Achmad, 1997) (MGS, 2003b) (MGS, 2003c) as shown in Figure 2.5-13, Figure 2.5-32, and Figure 2.5-33. No faults or folds are depicted on these geologic cross-sections. A review of a PSAR for a proposed nuclear power plant along the eastern shore of the Potomac River (e.g., Douglas Point), located 45 mi (72 km) west-southwest of the CCNPP site, also reported no faults or folds within a 5 mi (8 km) radius of the CCNPP site (PEPCO, 1973). Lastly, review of a seismic source characterization study (URS, 2000) for a liquefied natural gas plant at Cove Point, about 3 mi (4.8 km) southeast of the CCNPP site, also mentions no faults or folds present in the Cove Point area that could project toward the CCNPP site.

The most detailed subsurface exploration of the CCNPP site was performed by Dames and Moore as part of the original PSAR (BGE, 1968) for the CCNPP Units 1 and 2 foundation and supporting structures. This PSAR study included drilling 85 geotechnical boreholes, collecting down-hole geophysical data, and acquiring seismic refraction data across the site. As summarized in the PSAR (BGE, 1968), geologic cross sections were developed extending from Highway 2/4 northwest of the CCNPP site to Camp Conoy on the southeast, which provide valuable subsurface information on the lateral continuity of Miocene Coastal Plain sediments and Pliocene Upland deposits as shown in Figure 2.5-32, Figure 2.5-41, and Figure 2.5-42. Cross-sections C-C′ to D-D′ pre-date site development in the Conoy Landing area, and shadow the existing CCNPP Units 1 and 2 site and the proposed CCNPP Unit 3 site for structures trending north-northeast, parallel to the regional structural grain. These sections depict a nearly flat-lying, undeformed geologic contact between the Eocene Piney Point Formation and the overlying Middle Miocene Calvert Formation at about -200 ft (-61 m) msl as shown in Figure 2.5-41 and Figure 2.5-42.

Geologic cross-sections developed from geotechnical data collected from approximately 85 boreholes as part of the CCNPP Unit 3 study provide additional detailed information for the upper approximately 400 ft (123 km) of strata on the presence or absence of structures directly beneath the footprint of the site. Similar to the previous cross sections prepared for the site, the new geologic borehole data support an interpretation of gently-dipping to flat-lying and unfaulted Miocene and Pliocene stratigraphy at the CCNPP site as shown in Figure 2.5-34, Figure 2.5-39 and Figure 2.5-43. Cross Section E-E′ prepared oblique to previously mapped northeast-trending structures (i.e., the folds, faults, and postulated faults in the site vicinity discussed in Section 2.5.1.1.4, namely the Hillville fault, and unnamed folds and faults identified by the USGS (USGS, 1995) and Kidwell (Kidwell, 1997)) shows nearly flat-lying Miocene and Pliocene stratigraphy directly underling the CCNPP site.Only minor perturbations are present across the Miocene-Pliocene stratigraphic boundary, as well as other subunits within the Miocene Chesapeake Group. Although the stratigraphic contacts between the Calvert and Choptank Formations, as well as the Choptank and St. Mary's Formation, cannot be readily delineated, there are several key lithologic contacts (i.e., cemented sand separated by uncemented sand layers) that exhibit flat-lying bedding and lateral continuity. The

near-horizontal subunits provide evidence for the absence of surface-fault rupture beneath the CCNPP site as shown in Figure 2.5-39. A prominent geologic contact between the Piney Point and Calvert Formations, and Nanjemoy and Piney Point Formations, identified in exploratory boreholes B-303 and B-403 also provides evidence for a very low-gradient, nearly flat-lying Miocene deposit directly beneath the site as shown in Figure 2.5-39.

Geotechnical data collected directly to the south of the CCNPP site were compiled along sections E-E′ and E′-E″ and shown in Figure 2.5-39 and Figure 2.5-43. Although these geotechnical boreholes are limited in depth (from -325 ft to 37.5 ft (-99 to 11.4 m) msl), they provide additional evidence of the lateral continuity between the Pliocene Upland gravel deposits and Miocene St. Mary's Formation, as well as a cemented sand unit in the upper part of the St. Mary's Formation. The nearly flat-lying and undisrupted nature of these shallow Miocene-Pliocene deposits are consistent with sections E-E′ and E′-E″, and observations of the exposed Miocene and Pliocene strata along the western shore of Chesapeake Bay near the existing the CCNPP site as shown in Figure 2.5-44.

2.5.3.2 Geological Evidence, or Absence of Evidence, for Surface Deformation

As shown on Figure 2.5-32, only one inferred bedrock fault (i.e., Hillville fault) has been mapped at or near the 5 mi (8 km) radius of the CCNPP site (Hansen, 1978). In addition to the Hillville fault (Hansen, 1978), several other structures have been proposed within the 5 mi (8 km) radius of the site that have either shown in geologic cross-sections or published papers: (a) that two hypothesized east-facing monoclines are postulated beneath Chesapeake Bay (USGS, 1995) and (b) multiple stratigraphic undulations (inferred folds and warps) and a fault postulated along the western margin of Chesapeake Bay (Kidwell, 1997). The Hillville fault (MGS, 1978) and inferred folds (USGS, 1995) (Kidwell, 1997) are described in Section 2.5.1 and below. None of these features are considered capable tectonic sources, as defined in Appendix A of Regulatory Guide 1.165 (NRC, 1997). Only the Hillville fault has been mapped within or near the 5 mi (8 km) radius of the CCNPP site (Figure 2.5-25), whereas the other features (USGS, 1995) (Kidwell, 1997) are only shown on cross sections.

No deformation or geomorphic evidence indicative of potential Quaternary activity has been reported in the literature for the Hillville fault; whereas the USGS (USGS, 1995) and Kidwell (Kidwell, 1997) features have been loosely inferred to have been active during the Quaternary. No evidence of Quaternary deformation along these inferred structures was identified during aerial and field reconnaissance, as well as during air photo and LiDAR interpretation undertaken for the CCNPP Unit 3 study. The Hillville fault is interpreted as a lithotectonic terrane boundary that coincides with the Sussex-Currioman Bay aeromagnetic anomaly (MGS, 1986), whereas the other postulated features have not been attributed to a known tectonic structure.

2.5.3.2.1 Hillville Fault Zone

The 26 mi (42 km) long Hillville fault (MGS, 1978) approaches to within 5 mi (8 km) of the CCNPP site as shown in Figure 2.5-11, Figure 2.5-26, and Figure 2.5-32. The fault consists of a northeast-striking zone of steep southeast-dipping reverse faults that coincide with the Sussex-Currioman Bay aeromagnetic anomaly (Hansen, 1986). The style and location of faulting are based on seismic reflection data collected about 9 mi (14.5 km) west-southwest of the CCNPP site. Seismic line St M-1 (location shown on Figure 2.5-26) imaged a narrow zone of discontinuities that vertically separate basement by as much as 250 ft (76 m) (MGS, 1978) as shown in Figure 2.5-32. It has been interpreted (MGS, 1986) that this offset is part of a larger lithotectonic terrane boundary that separates basement rocks associated with Triassic rift basins on the west from low-grade metamorphic basement on the east. The Hillville fault may

represent a Paleozoic suture zone that was reactivated in the Mesozoic and Early Tertiary similar to the Brandywine fault system located to the west of the CCNPP site. Based on stratigraphic correlation (e.g., "pinchouts") between boreholes within Tertiary Coastal Plain deposits, it is speculated (MGS, 1986) that the Hillville fault was last active in the Early Paleocene. However, MGS (1986) concludes that the Upper Paleocene Aquia Formation and Miocene Calvert Formation provide evidence for the absence of deformation upsection. For example, a structure contour map of the top of the Eocene Piney Point-Nanjemoy Aquifer appears undeformed in the vicinity of the Hillville fault that likely reflects the absence of considerable faulting of this regionally extensive stratigraphic marker (Figure 2.5-14). Lastly, a geologic cross section prepared by Achmad and Hansen (Achmad, 1997) that intersects the Hillville fault shows no demonstrable offset across the contact between the Piney Point and Nanjemoy Formations (Figure 2.5-13).

Field and aerial (inspection by plane) reconnaissance, coupled with interpretation of aerial photography (review and inspection of features preserved in aerial photos) and LiDAR data shows that there are no geomorphic features indicative of potential Quaternary activity along the surface-projection of the Hillville fault zone. Multiple Quaternary fluvial terraces of the Patuxent and Potomac Rivers previously mapped (USGS, 1989c) (USGS, 1989d) (MGS, 1994) (MGS, 2003b) (MGS, 2003c) were evaluated for features suggestive of tectonic deformation using the LiDAR data as shown in Figure 2.5-26. Furthermore, where the Hillville fault would intersect the steep cliffs of Chesapeake Bay, there is direct observation of no faulting in the exposed Miocene strata. This is consistent with cross sections (Kidwell, 1997) (Achmad, 1997) (MGS, 2003b) (MGS, 2003c) that trend oblique to and across the northeast strike of the Hillville fault and do not show a fault (Figure 2.5-13, Figure 2.5-30, and Figure 2.5-33). Abundant shallow seismic reflection data acquired and interpreted by Colman (1990) in Chesapeake Bay intersect the northeast projection of the Hillville fault (Figure 2.5-29). Colman (1990) makes no mention of encountering the Hillville fault in interpretations of the seismic data. Thus, based on the absence of geomorphic expression and offset of Miocene to Quaternary surficial deposits, it is concluded that the Hillville fault is not a surface-fault rupture hazard at the CCNPP site.

2.5.3.2.2 East Facing Monoclines

Two speculative and poorly constrained east-facing monoclines along the western margin of Chesapeake Bay are depicted in geologic cross sections (USGS, 1995) within the 5 mi (8 km) radius of the CCNPP site. East-facing monoclines are inferred beneath Chesapeake Bay at about 2 and 10 mi (3.2 and 16 km) east and southeast, respectively, of the CCNPP site as shown in Figure 2.5-25. The east-facing monoclines (USGS, 1995) are not depicted on any geologic maps of the area but they are shown on geologic cross-sections (USGS, 1995) that trend northwest-southeast across the CCNPP site and south of the site near the Patuxent River. A partial representation of cross sections A-A' and E-E' is provided in Figure 2.5-40 (USGS, 1995). As mapped in cross Section and inferred in plan view, the monoclines align with the western shore of Chesapeake Bay and by association define a north-trending structure beneath the Chesapeake Bay. The monoclines exhibit a west-side up sense of motion that projects into the Miocene Choptank Formation (USGS, 1995). The monoclines are shown deforming the Lower Paleocene to Upper Miocene strata with approximately 60 to 300 ft (18 to 91 m) of structural relief. The overlying Late Miocene St. Mary's Formation is not shown as warped. Boreholes used to construct the Section are widely spaced and do not provide good constraint on the existence and location of the postulated monoclines (cross sections A-A' and E-E') (USGS, 1995). Although no published geologic data are available to substantiate the existence of the monoclines, it is inferred (USGS, 1995) that the distinct elevation change (about 100 ft (30 m)) between Calvert Cliffs and the Delmarva Peninsula to the east, and the apparent linear nature of the Calvert Cliffs, to be tectonically controlled.

Existing published geologic, aeromagnetic, and gravity data provide evidence for the absence of a prominent north-trending monocline directly underlying Chesapeake Bay. Regional aeromagnetic and gravity maps show that the overall trend of potential structures buried beneath the Coastal Plain and Chesapeake Bay near the site trend northeast or subparallel to mapped faults and folds in the Piedmont Province to the west of the CCNPP site as shown in Figure 2.5-20, Figure 2.5-21, and Figure 2.5-22. A structural contour map of the top of the Middle Eocene Piney Point and Nanjemoy contact shows a northeast-striking undeformed contact across the Chesapeake Bay, consistent with regional bedding, yet inconsistent with a postulated more north-trending structure approximately parallel to the western margin of the Chesapeake Bay as shown in Figure 2.5-14. Lastly, an east-west oriented cross-Section located about 30 mi (48 km) north of the CCNPP site also depicts nearly flat-lying Cretaceous and Paleocene stratigraphy across the Chesapeake Bay, and does not depict a fold or fault (MGS, 1978).

The change in physiographic elevation and geomorphic surfaces between the western and eastern shores of Chesapeake Bay can be explained by erosional processes directly related to the former course of the Susquehanna River, coupled with eustatic sea level fluctuations during the Quaternary (USGS, 1989a) (USGS, 1989b) (GSA, 1990) (USGS, 1979a) (USGS, 1979b). It is interpreted (GSA, 1990) by high resolution, shallow geophysical data to delineate several former river course(s) and provide geometrical constraints on the width and depth of the paleo-Susquehanna River between northern Chesapeake Bay and the southern Delmarva Peninsula as shown in Figure 2.5-29. Paleo-river profiles of the Eastville (150 ka) and Exmore (200 to 400 ka) Susquehanna paleochannels show no distinct elevation changes within the CCNPP site area and along projection features (USGS, 1995), as well as the Hillville fault (MGS, 1978). A submarine geologic map of Tertiary and Pleistocene deposits below the Chesapeake Bay at and near the CCNPP site developed from the shallow, high-resolution seismic reflection profiles has been developed (USGS, 1989a) (USGS, 1989b). No folds, warps or faults are depicted on these maps (USGS, 1989a) (USGS, 1989b) which encompass the hypothesized (USGS, 1995) east-facing monocline. Lastly, structure contour maps of the top of Tertiary deposits, developed from shallow seismic reflection data, show no geomorphic features that could be interpreted as fault or fold related (USGS, 1989b).

In summary, site and aerial reconnaissance, coupled with literature review, do not provide evidence for the existence of the hypothesized east-facing monocline (USGS, 1995). There also is no seismicity spatially associated with these features. If the feature does exist, the Miocene St. Mary's Formation is not depicted (USGS, 1995) to be deformed. Therefore, the inferred monoclines (USGS, 1995) are older than Late Miocene in age and do not represent a surface-fault rupture or deformation hazard at the CCNPP site.

2.5.3.2.3 Stratigraphic Undulations and Hypothesized Fault

Multiple subtle folds or inflections and a postulated fault have been mapped (Kidwell, 1997) in cliff exposures of the Miocene Choptank and St. Mary's Formations along the west side of Chesapeake Bay. Based on structural relations, such as an apparent decrease in warping up-section through the exposed Miocene section, it is suggested (Kidwell, 1997) that the postulated deformation may reflect growth faulting, or the presence of other tensional structures at depth. Over 300 lithostratigraphic columns along an approximately 25 mi (40 km) long stretch of Calvert Cliffs between Chesapeake Beach and Little Cove Point were prepared (Kidwell, 1988) (Kidwell, 1997) as shown in Figure 2.5-30. When these stratigraphic columns are compiled into a cross section, they provide an approximately 25 mi (40 km) long nearly continuous log of Miocene, Pliocene and Quaternary deposits exposed in the cliffs directly east of the CCNPP site as shown in Figure 2.5-30. A stratigraphic analysis (Kidwell, 1997) indicates that the Miocene Coastal Plain deposits strike northeast and dip 1 to 2 degrees to the south

consistent with the findings of others (USGS, 1995) (MGS, 2003b) (MGS, 2003c). However, the very low regional southerly dip is disrupted occasionally by several subtle low amplitude and broad undulations developed within the Miocene Coastal Plain deposits. The stratigraphic undulations (represented at 150 times vertical exaggeration in Figure 2.5-30) are interpreted (Kidwell, 1997) as monoclines and asymmetrical anticlines. The undulatory stratigraphic contacts of the Miocene deposits often coincide with basal unconformities having wavelengths typically on the order of 2.5 to 5 mi (4 to 8 km) and amplitudes of 10 to 11 ft (3 to 3.4 m). South of the CCNPP site, near Little Cove Point, the stratigraphic undulations within the Miocene St. Mary's Formation decrease in wavelength (to approximately 1 mi (1.6 km) and amplitude (to approximately 9 ft (2.7 m) or less). Based on stratigraphic truncations, the inferred warping also appears to decrease up-Section into the overlying upper Miocene St. Mary's Formation near the CCNPP site. Any inferred folding of the overlying Pliocene and Quaternary fluvial strata is very poorly constrained or obscured, because of highly undulatory unconformities within these sand and gravel deposits.

About 1.2 mi (1.9 km) south of the CCNPP site, Kidwell (Kidwell, 1997) interprets an apparent 6 to 10 ft (1.8 to 3 m) elevation change in Miocene strata by extrapolating unit contacts across the approximately 0.6 mile wide (1 km) gap at Moran Landing (Figure 2.5-25 and Figure 2.5-30). Kidwell (Kidwell, 1997) also interprets a 3 to 12 (0.9 to 3.7 m) ft elevation change in younger, possibly Quaternary, fluvial material across this same gap. Because of the lack of cliff exposures at Moran Landing (only the valley margins), no direct observations of these elevation changes can be made. Kidwell (1997) explains the differences in elevation of the Miocene-Quaternary stratigraphy by hypothesizing the existence of a fault at Moran Landing that strikes northeast and accommodates a north-side down sense of separation. However, the postulated fault of Kidwell (Kidwell, 1997) is not shown on any of Kidwell's (Kidwell, 1997) cross-sections, or any published geologic map (e.g., Glaser, 2003b and 2003c). In addition, Hansen (1978) does not describe faulting in seismic reflection line St. M-2 that intersects the inferred southwest projection of the hypothesized Kidwell (Kidwell, 1997) fault (Figure 2.5-27).

The observations of offset younger gravels do not provide any evidence for the existence of a fault because the surface on which the gravels are deposited is an erosional unconformity with extensive variable relief (Kidwell, 1997). Observations made during field reconnaissance, as part of the FSAR preparation, confirmed that this contact was an erosional unconformity with significant topography north and south of Moran Landing consistent with stratigraphic representations in the Kidwell (Kidwell, 1997) profiles. The relatively small elevation change in the Miocene units over such an extensive horizontal distance is at best weak evidence for faulting within the Miocene deposits. For example, subtle elevation variations in Miocene strata characterized along a near-continuous exposure south of Moran Landing contain similar vertical and lateral dimensions as to the inferred elevation change across Moran Landing; however, the features are interpreted as subtle warps and not faults by Kidwell (1997). On the basis of association with similar features to the south and the lack of a continuous exposure, there is little to no evidence to support a fault across Moran Landing.

Field and aerial (inspection by plane) reconnaissance, coupled with interpretation of aerial photography (review and inspection of features preserved in aerial photos) and LiDAR data, conducted for this investigation shows that there are no geomorphic features indicative of potential Quaternary activity along trend with the postulated folds and fault interpreted by Kidwell (Kidwell, 1997). LiDAR data was reviewed for the presence of northeast-striking lineaments in the region of Moran Landing and to the southeast between the Patuxent and Potomac Rivers as shown in Figure 2.5-26. No features suggestive of tectonic deformation were interpreted in the Pliocene (Upland deposits) or Quaternary fluvial surfaces (USGS, 1989c) (USGS, 1989d) (MGS, 2003b) (MGS, 2003c), some of which approach approximately 450 ka in age. Also, there is no seismicity spatially associated with the Kidwell (Kidwell, 1997) features,

nor is there geomorphic evidence to strongly suggest that these features, including the postulated fault, pose a surface-fault rupture hazard at the CCNPP site. The hypothesized fault also is not aligned with any magnetic or gravity anomaly previously interpreted by others, suggesting that the apparent elevation change across Moran Landing is surficial in origin.

In summary, with the exception of Kidwell (Kidwell, 1997), numerous investigations of the Chesapeake Bay coastline by government researchers, stratigraphers, and consultants for Baltimore Gas and Electric have reported no visibly distinct signs of tectonic deformation within the exposed Miocene deposits near the CCNPP site as shown in Figure 2.5-44. Collectively, the majority of published and unpublished geologic information for the CCNPP site area, coupled with regional geologic sections (Achmad, 1997) (MGS, 2003b) (MGS, 2003c) and site and aerial reconnaissance, indicate the absence of Late Miocene and younger faulting and folding. A review of regional geologic sections and interpretation of LiDAR data suggest that the features, if present, are not prominent structures and do not appear to be developed within the Pliocene to Quaternary landscape. In summary, on the basis of regional and site data, there are no known faults within the site area, with the exception of the poorly constrained Hillville fault that lies along the western perimeter of the 5 mi (8 km) radius of the site. The Hillville fault has been documented as being last active in the Paleocene epoch (MGS, 1986).

2.5.3.3 Correlation of Earthquakes with Capable Tectonic Sources

No reported historical earthquake epicenters have been associated with bedrock faults within the 25 mi (40 km) radius of the CCNPP site vicinity as shown in Figure 2.5-25.

2.5.3.4 Ages of Most Recent Deformations

As presented in Section 2.5.3.2, the Hillville fault and postulated folds and faults within 5 mi (8 km) of the CCNPP site do not exhibit evidence of Quaternary activity. It is interpreted (MGS, 1978) that the Hillville fault formed during the Paleozoic Era as part of the regional Taconic orogeny, and locally may have been reactivated during the Paleozoic with the youngest deformation being Paleocene. Based on a review of available published geologic literature, field and aerial (inspection by plane) reconnaissance, and interpretation of aerial photography (review and inspection of features preserved in aerial photos) and LiDAR data, the postulated structures (USGS, 1995) (Kidwell, 1997), if they exist, are constrained to the Miocene and do not appear to affect Pliocene and Quaternary deposits.

2.5.3.5 Relationship of Tectonic Structures in the Site Area to Regional Tectonic Structures

Of the three features evaluated within the 5 mi (8 km) radius of the CCNPP site, only the Hillville fault has been linked with a regional tectonic structure. The Hillville fault zone delineates a possible Paleozoic suture zone reactive in the Mesozoic and Early Tertiary. Tectonic models hypothesize that the crystalline basement underlying the CCNPP site was accreted to a pre-Taconic North American margin in the Paleozoic along a suture that lies about 10 mi (16 km) west of the CCNPP site as shown in Figure 2.5-17 and Figure 2.5-23. The lithosphere plate-scale suture is defined by a distinct north-northeast-trending magnetic anomaly that dips easterly between 35 and 45 degrees and lies about 8 to 9 mi (12.9 to 14.5 km) beneath the CCNPP site (GSA, 1995) as shown in Figure 2.5-17. Directly west of the suture lies the north-to northeast-trending Taylorsville basin and to the east, the postulated Queen Anne Mesozoic rift basin as shown in Figure 2.5-10. The fault zone is interpreted as a lithotectonic terrane boundary that separates basement rocks associated with Triassic rift basins on the west from low-grade metamorphic basement on the east (i.e., Sussex Terrane/Taconic suture (GSA, 1995); see

Figure 2.5-17) (MGS, 1986). The apparent juxtaposition of the Hillville fault zone with the Sussex-Currioman Bay aeromagnetic anomaly suggests that the south flank of the Salisbury Embayment may be a zone of crustal instability that was reactivated during the Mesozoic and Tertiary. Cretaceous activity is inferred (MGS, 1978) and the fault extended up into the Cretaceous Potomac Group. The resolution of the geophysical data does not permit an interpretation for the upward projection of the fault into the younger overlying Coastal Plain deposits. Stratigraphic correlations of Coastal Plain deposits from borehole data were used (MGS, 1978) to speculate that the Hillville fault may have been active during the Early Paleocene.

2.5.3.6 Characterization of Capable Tectonic Sources

Based on previous discussions in Section 2.5.3.4, there are no capable tectonic sources within 5 mi (8 km) of the CCNPP site.

2.5.3.7 Designation of Zones of Quaternary Deformation Requiring Detailed Fault Investigation

There are no zones of Quaternary deformation requiring detailed investigation within the CCNPP site area. A review and interpretation of aerial photography, digital elevation models, and LiDAR data of the site area, coupled with aerial reconnaissance, identified a few discontinuous north to northeast-striking lineaments. None of these lineaments are interpreted as fault-related, or coincident with the Hillville fault or the other previously inferred Miocene-Pliocene structures. Aerial and field reconnaissance of the western shoreline of Chesapeake Bay suggests that some of the lineaments along the western shoreline may be related to a weak to poorly developed, near-vertical, north to northeast-trending fracture or joint set. These fractures provide discontinuities by which large blocks of the St. Mary's and Choptank Formations spall and form colluvial rubble at the base of the steep cliffs; however, these weak fractures do not represent a surface-fault rupture hazard at the site.

2.5.3.8 Potential for Tectonic or Non-Tectonic Deformation at the Site

The potential for tectonic deformation at the site is negligible. This is based on:

1. The nearly flat-lying Miocene stratigraphy beneath the site interpreted from both existing and new borehole data,

2. The absence of faulting in Miocene deposits exposed along the cliffs at the eastern boundary of the CCNPP site as shown in Figure 2.5-43,

3. The interpretation of aerial photography and LiDAR data.

Collectively, these data support the interpretation for the absence of any Quaternary surface faults or capable tectonic sources within the site area. In addition, there is no evidence of non-tectonic deformation at the site, such as glacially induced faulting, collapse structures, growth faults, salt migration, or volcanic intrusion.

2.5.3.9 References

Achmad, 1997. Hydrogeology, model simulation, and water-supply potential of the Aquia and Piney Point-Nanjemoy Aquifers in Calvert and St. Mary's Counties, Maryland, G. Achmad and H. Hansen, 1997.

BPC, 1981. Subsurface Investigation and Foundation Report, North Parking Area, Calvert Cliffs Nuclear Power Plant, Lusby, Maryland, Bechtel Power Corporation, June 1981.

BGE, 1968. Preliminary Safety Analysis Report Calvert Cliffs Nuclear Power Plant Units 1 and 2, Volume 1, Docket 50-317 and 50-318, Baltimore Gas and Electric Company, 1968.

CFR, 2007a. Geologic and Seismic Siting Criteria, Title 10, Code of Federal Regulations, Part 100.23, 2007.

CFR, 2007b. Earthquake Engineering Criteria for Nuclear Power Plants, Title 10, Code of Federal Regulations, Part 50, Appendix S, 2007.

CEG, 2005. Calvert Cliffs Independent Spent Fuel Storage Installation, Updated Environmental Report, Volume 3, Revision 7, Constellation Energy, 2005.

EPRI/DOE/NRC, 2012. Technical Report: Central and Eastern United States Seismic Source Characterization for Nuclear Facilities, Electric Power Research Institute, U.S. Department of Energy, and the U.S. Nuclear Regulatory Commission, 2012.

GEER, 2011. Geotechnical Quick Report on the Affected Region of the 23 August 2011, Geotechnical Extreme Events Reconnaissance (GEER) Association Post-Event Report, October, 2011.

GSA, 1990. Ancient channels of the Susquehanna River beneath Chesapeake Bay and the Delmarva Peninsula, Geological Society of America Bulletin, Volume 102, p 1268-1279, S. Colman, J. Halka, C. Hobbs III, R. Mixon, D. Foster, 1990.

GSA, 1995. E-3 Southwestern Pennsylvania to Baltimore Canyon Trough, Geological Society of America Centennial Continent/Ocean Transect #19, L. Glover III and K. Klitgord, 1995.

Hansen, 1986. The Lithology and Distribution of Pre-Cretaceous Basement Rocks beneath the Maryland Coastal Plain, Department of Natural Resources Maryland Geological Survey Report of Investigations Number 44, 27 pp., H. Hansen and J. Edwards, Jr., 1986.

Kidwell, 1988. Reciprocal Sedimentation and Noncorrelative Hiatuses in Marine-Paralic Siliciclastics: Miocene Outcrop Evidence, Geology, Volume 16, p 609-612, S. Kidwell, 1988.

Kidwell, 1997. Anatomy of Extremely Thin Marine Sequences Landward of a Passive-Margin Hinge Zone: Neogene Calvert Cliffs Succession, Journal of Sedimentary Research, Volume 67, Number 2, p 322-340, S. Kidwell,1997.

MGS, 1968. Geologic Map of Maryland, Scale 1:250,000, Department of Natural Resources, Maryland Geological Survey, E. Cleaves, J. Edwards Jr., and J. Glaser, 1968.

MGS, 1971. Geology and mineral resources of Southern Maryland, Report of Investigations Number 15, p 85, Maryland Geological Survey, J. Glaser, 1971.

MGS, 1978. Upper Cretaceous (Senonian) and Paleocene (Danian) Pinchouts on the South Flank of the Salisbury Embayment, Maryland and their relationship to antecedent basement structures, Report of Investigations Number 29, p 36, Department of Natural Resources, Maryland Geological Survey, H. Hansen, 1978.

MGS, 1986. The Lithology and Distribution of Pre-Cretaceous basement rocks beneath the Maryland Coastal Plain, Report of Investigations Number 44, p 27, Department of Natural Resources, Maryland Geological Survey, H. Hansen and J. Edwards Jr., 1986.

MGS, 1994. Geologic Map of Calvert County, Department of Natural Resources, Maryland Geological Survey, Scale 1:62,500, J. Glaser, 1994.

MGS, 2003a. Geologic Map of Prince George's County, Maryland, Maryland Geological Survey, Scale 1:62,500, J. Glaser, 2003a.

MGS, 2003b. Geologic Map of the Broomers Island Quadrangle, Calvert and St. Mary's Counties, Maryland, Maryland Geological Survey, Scale 1: 24,000, J. Glaser, 2003.

MGS, 2003c. Geologic Map of the Cove Point Quadrangle, Calvert County, Maryland, Maryland Geological Survey, Scale 1:24,000, J. Glaser, 2003c.

NRC, 1997. Identification and Characterization of Seismic Sources and Determination of Safe Shutdown Earthquake Ground Motion, Regulatory Guide 1.165, U.S. Nuclear Regulatory Commission, March 1997.

Obermier, 1998. Paleoliquefaction Evidence for Seismic Quiescence in Central Virginia During the Late and Middle Holocene Time (abs), Eos Transactions of the American Geophysical Union, Volume 79, Number 17, p S342, S. Obermier and W. McNulty, 1998.

PEPCO, 1973. Preliminary Safety Analysis Report, Douglas Point Nuclear Generating Station, Units 1 and 2, Volume 2, Docket Number 50448-2 and 50449-2, Potomac Electric Power Company, 1973.

URS, 2000. Seismic Characterization Study for the Expansion of the Williams Gas Pipeline-Tranco LNG Facility, Cove Point, Maryland, URS Corporation, October 2000.

USGS, 1979a. Upper Cenozoic Deposits of the Central Delmarva Peninsula, Maryland and Delaware, U.S. Geological Survey, Professional Paper 1067-A, J. Owens and C. Denny, 1979.

USGS, 1979b. Upper Cenozoic Sediments of the Lower Delaware Valley and the Northern Delmarva Peninsula, New Jersey, Pennsylvania, Delaware, and Maryland, U.S. Geological Survey, Professional Paper 1067-D, J. Owens and J. Minard, 1979.

USGS, 1986. Geologic Map of Dorchester County, Maryland, U.S. Geological Survey, Scale 1:62,500, J. Owens and C. Denny, 1986.

USGS, 1989a. Quaternary Geology of the Southern Maryland Part of the Chesapeake Bay, U.S. Geological Survey, Miscellaneous Field Studies Map MF-1948-C, Scale 1:125,000, S. Colman and J. Halka, 1989.

USGS, 1989b. Quaternary Geology of the Northern Maryland part of the Chesapeake Bay, U.S. Geological Survey, Miscellaneous Field Studies Map MF-1948-B, Scale 1:125,000, S. Colman and J. Halka, 1989.

USGS, 1989c. Geologic Map of Charles County, Maryland, U.S. Geological Survey, Scale 1:62,500, L. McCartan, 1989.

USGS, 1989d. Geologic Map of St. Mary's County, Maryland, U.S. Geological Survey, Scale 1:62,500, L. McCartan, 1989.

USGS, 1995. Geologic Map and Cross Sections of the Leonardtown 30 X 60 minute quadrangle, Maryland and Virginia, U.S. Geological Survey, L.McCartan, W. Newell, J. Owens, and G. Bradford, 1995.

USGS, 2000a. Data for Quaternary Faults, Liquefaction Features, and Possible Tectonic Features in the Central and Eastern United States, East of the Rocky Mountain Front, Open-File Report 00-260, U.S. Geological Survey, A. Crone and R. Wheeler, 2000.

USGS, 2000b. Geologic Map of the Fredericksburg 30' x 60' Quadrangle, Virginia and Maryland, Geologic Investigations Series Map I-2607, U.S. Geological Survey, R. Mixon, L. Pavlides, D. Powars, A. Froelich, R. Weems, J. Schindler, W. Newell, L. Edwards, L. Ward, 2000.

USGS, 2005. Known or Suggested Quaternary Tectonic Faulting, Central and Eastern United States – New and Updated Assessments for 2005, Open File Report 2005-1336, U.S. Geological Survey, R. Wheeler, 2005.

Wheeler, 2006. Quaternary tectonic faulting in the Eastern United States, Engineering Geology, Volume 82, p 165-186, R. Wheeler, 2006.}

2.5.4 Stability of Subsurface Materials and Foundations

The U.S. EPR FSAR includes the following COL Item for Section 2.5.4:

> A COL applicant that references the U.S. EPR design certification will present site-specific information about the properties and stability of soils and rocks that may affect the nuclear power plant facilities, under both static and dynamic conditions including the vibratory ground motions associated with the CSDRS and the site-specific SSE.

This COL Item is addressed as follows:

{This section addresses site-specific subsurface materials and foundation conditions. It was prepared based on the guidance in relevant sections of NRC Regulatory Guide 1.206, Combined License Applications for Nuclear Power Plants (LWR Edition) (USNRC, 2007a).

The CCNPP Units 1 and 2 Updated Final Safety Analysis Report (UFSAR) (BGE, 1982) contains a summary of the geotechnical information collected previously for the construction of CCNPP Units 1 and 2. The planned CCNPP Unit 3 is approximately 2,000 ft south of the existing units. CCNPP Units 1 and 2 UFSAR (BGE, 1982) contains mostly general information that is quantitatively limited in its extent and depth of exploration relative to the investigation performed for the CCNPP Unit 3. Therefore, comparison to CCNPP Units 1 and 2 is limited, but provided when relevant information is available. The information presented in this section is based on results of a site specific subsurface investigation program implemented at the CCNPP Unit 3 site, and evaluation of the collected data, unless indicated otherwise.

Geotechnical and geophysical site investigations have been completed in three stages as follows:

- **Phase I** – Performed in 2006, this is the initial investigation effort and is reported in the Geotechnical Subsurface Investigation Data Reports (Schnabel, 2007a) (Schnabel, 2007b). The investigation includes the boring program for the CCNPP Unit 3 and

laboratory testing, including the Resonant Column Torsional Shear (RCTS) tests of the in-situ soils.

- **Phase II** – Performed in 2008, the second phase investigation incorporates the following items:
  - Drilling and sampling of 48 additional Standard Penetration Test (SPT) borings.
  - Installation and Development of 7 additional observation wells.
  - 11 Cone Penetration Tests (CPT) with shear wave velocity measurements.
  - Borehole geophysical including P-S suspension tests in the Intake Area.
  - Two pressuremeter tests.

  Information from the Phase II investigation is presented in several geotechnical and laboratory testing data reports (Schnabel, 2009) (MACTEC, 2009a). The investigation incorporates information from additional borings and additional laboratory testing.

- **Phase III** – Performed in 2009, incorporating the following items:
  - Intake samples laboratory testing, including both static and dynamic RCTS tests.
  - Structural fill static testing, including chemical tests, triaxial tests, grain size tests, and Modified Proctor tests.
  - Structural fill dynamic testing (RCTS).

    Information from the Phase III investigation is presented in several geotechnical and laboratory testing data reports (MACTEC, 2009b) (MACTEC, 2009c) (MACTEC, 2009d).

The referenced geotechnical reports for the three phases of the investigation are provided in COLA Part 11J: Geotechnical Data Report and COLA Part 11K: Mactec Report.

The CCNNP3 Unit 3 site covers an area of approximately 460 acres. Figure 2.5-92 provides the site utilization plan. The following areas are identified:

1. Powerblock Area – Safety-related facilities in this area include the Reactor Building (RB), Fuel Building (FB) and Safeguard Buildings (Nuclear Island, NI), Essential Service Water Buildings (ESWB), and Emergency Power Generation Buildings (EPGB); other important facilities are the Nuclear Auxiliary Building (NAB), the Radioactive Waste Processing Building (RWPB), the Access Building (AB), and the Turbine Building (TB). The Powerblock Area is enlarged in Figure 2.5-93.

2. Intake Area – Safety-related facilities in this area include the Ultimate Heat Sink Makeup Water Intake Structure (UHS-MWIS) and the Forebay. Other facilities are the Circulating Water Makeup Intake Structure and the Fish Return. The Intake Area is enlarged in Figure 2.5-94.

3. Utility Corridor Area.

4. Construction Laydown Area (CLA).

5. Unit 3 Switchyard.

6. Unit 3 Cooling Basin and Cooling Tower.

The Powerblock, Construction Laydown Area, switchyard and cooling tower and basin are collectively referred to as the CCNPP Unit 3 Area.

The natural topography at the CCNPP site varies throughout the site with differences in elevation up to 100 ft. In the area where CCNPP Unit 3 is planned, ground surface elevations at the time of the exploration ranged from approximately El. 47 ft to El. 121 ft, with an average of 86 ft. The planned elevation (rough grade) in the Powerblock Area ranges from about El. 75 ft to El. 85 ft, with the centerline of Unit 3 at El. 84.7 ft, or approximately El. 85 ft.

In the Intake Area, ground surface elevations at the time of the exploration ranged from approximately El. 7 ft to 12 ft with an average of approximately 9.5 ft. The planned rough grade in the Intake Area is El. 10 ft.

The focus of Section 2.5.4 is the Powerblock Area and the Intake Area. These zones house the safety-related, Seismic-Category I facilities, with the Utility Corridor Area in between. Numerous natural and man-made slopes are identified across the plan. The safety of slopes is addressed in Section 2.5.5.

The subsurface conditions were established from the information contained in the Geotechnical Subsurface Investigation Data Reports from all Phases of the investigation (MACTEC, 2009a) (MACTEC, 2009b) (MACTEC, 2009c) (MACTEC, 2009d) (Schnabel, 2007a) (Schnabel, 2007b) (Schnabel, 2009). The maximum depth explored was about 400 ft beneath the ground surface at boring locations B-301 and B-401. The maximum depth explored by CPT soundings below the ground surface was 138.0 ft at C-302 and 152.4 ft at C-725 (CPT soundings encountered repeated refusal and, therefore, could not be consistently extended to greater depths). Field tests (borings, CPTs, etc.) identified as 300-series, e.g., B-301 or C-301, are located in the Powerblock Area. Tests identified as 400-series, e.g., B-401 or C-401, are located in an area adjacent to the CCNPP Powerblock Area, hereafter referred to as Construction Laydown Area (CLA). Field tests identified as 700 series, e.g., B-701 or C-701, are located outside of these two areas, and include the proposed cooling tower, switchyard, Utility Corridor, Intake Slope, and intake/discharge piping locations. Locations of various test areas are identified in Figure 2.5-92, Figure 2.5-93, and Figure 2.5-94. The major strata identified from the boring logs are described in detail in the next subsections.

References to elevation values in this subsection are based on the National Geodetic Vertical Datum of 1929 (NGVD29), unless stated otherwise.

2.5.4.1 Geologic Features

The CCNPP Unit 3 is located in the Atlantic Coastal Plain physiographic province. The soils in the site vicinity were formed by ancient rivers carrying large quantities of solids from the northern and western regions into the Atlantic Ocean. These deposits were placed under both freshwater (fluvial) and saltwater (marine) environments, and are about 2,500 ft thick at the site (BGE, 1982). The upper soils are Quaternary, Holocene- and/or Pleistocene-Age deposits formed as beaches or terraces. The lower soils are Miocene-, Eocene-, Paleocene-, and Cretaceous-Age deposits. The Miocene and Eocene soils belong to the Chesapeake and

Nanjemoy groups. The Holocene, Pleistocene, Miocene, and Eocene soils were the subject of a detailed subsurface exploration for the COL investigation.

Detail narrative of the geologic features is provided in Section 2.5.1. Section 2.5.1.1 addresses the regional geologic settings, including regional physiography and geomorphology, regional geologic history, regional stratigraphy, regional tectonic and non-tectonic conditions, and geologic hazards, as well as maps, cross-sections, and references. Section 2.5.1.2 addresses the geologic conditions specific to the site, including site structural geology, site physiography and geomorphology, site geologic history, site stratigraphy and lithology, site structural geology, seismic conditions, and site geologic hazard evaluation, accompanied by figures, maps, and references.}

2.5.4.2 Properties of Subsurface Materials

The U.S. EPR FSAR includes the following COL Item in Section 2.5.4.2:

> A COL applicant that references the U.S. EPR design certification will reconcile the site-specific soil and backfill properties with those used for design of U.S. EPR Seismic Category I structures and foundations described in Section 3.8.

This COL Item is addressed as follows:

{A comprehensive field investigation and associated laboratory testing has been performed for the CCNPP Unit 3 site. This subsection presents the properties of underlying materials encountered. It is divided into five subsections, as follows.

- Section 2.5.4.2.1 provides an introduction to the soil profile and subsurface conditions,
- Section 2.5.4.2.2 provides a description of the field investigation program, including borings, sampling, and in-situ tests,
- Section 2.5.4.2.3 provides a narrative on the origin of the engineered fill soils samples,
- Section 2.5.4.2.4 provides a description of the laboratory testing program,
- Section 2.5.4.2.5 provides the CCNPP Unit 3 soil properties for analysis and design of foundations.

The description of the field investigation and laboratory testing data incorporate information from all three phases of the investigation (Phase I, II, and III).

2.5.4.2.1 Description of Subsurface Materials

The site geology is comprised of deep Coastal Plain sediments underlain by bedrock, which is about 2,500 ft below the ground surface for CCNPP Units 1 and 2 UFSAR (BGE, 1982). The site soils consist of marine and fluvial deposits. The upper 400 ft of the site soils were the subject of the CCNPP Unit 3 subsurface investigation. In general, the soils at the site can be divided into the following stratigraphic units:

- ***Stratum I: Terrace Sand*** – light brown to brown sand with varying amounts of silt, clay, and/or gravel, sometimes with silt or clay interbedded layers.

- ***Stratum IIa: Chesapeake Clay/Silt*** – light to dark gray clay and/or silt, predominantly clay, with varying amounts of sand.

- ***Stratum IIb: Chesapeake Cemented Sand*** – interbedded layers of light to dark gray silty/clayey sands, sandy silts, and low to high plasticity clays, with varying amounts of shell fragments and with varying degrees of cementation. For the purposes of settlement analysis, Stratum IIb was further divided into three sub-layers. The investigation encountered variation of SPT values both in depth and horizontal distribution. The position of the sub layers beneath the Powerblock Area footprint is variable and this condition needs to be accounted for in a detailed three dimensional settlement analysis. Section 2.5.4.10 provides the details of the settlement model.

- ***Stratum IIc: Chesapeake Clay/Silt*** – gray to greenish gray clay/silt soils, they contain interbedded layers of sandy silt, silty sand, and cemented sands with varying amount of shell fragments.

- ***Stratum III: Nanjemoy Sand*** – primarily dark greenish-gray glauconitic sand with interbedded layers of silt, clay, and cemented sands with varying amounts of shell fragments and varying degrees of cementation.

Figure 2.5-95 provides an idealized soil column for the CCNPP Unit 3 site. The actual depth of layer interfaces varies throughout the site. This condition is revealed by the following subsurface profiles identified on Figure 2.5-92, Figure 2.5-93, and Figure 2.5-94:

Figure 2.5-96	Subsurface profile A-A' at the Powerblock looking east through the NI (local plant coordinates).
Figure 2.5-97	Subsurface profile B-B' at the Powerblock looking east through the EPGBs and NI.
Figure 2.5-98	Subsurface profile C-C' at the Powerblock looking south through the NI and TB.
Figure 2.5-99	Subsurface profile D-D' at the Powerblock looking south through 1EPBG, 3ESWB, and the RWPB.
Figure 2.5-100	Subsurface profile E-E' at the Powerblock looking east through the RWPB, NAB, NI (Safeguard North), 2ESWB and 1ESWB.
Figure 2.5-101	Subsurface profile F-F' at the Intake Area, looking east through the UHS-MWIS.

The recommendations for soil properties (Section 2.5.4.2.5) to be used for analysis and design of foundation are provided in tabular form for each layer identified. Table 2.5-27 presents the depths and thicknesses of the layers encountered at the site. The data is provided for the entire site and independently for the Powerblock Area and the Intake Area. Information on deeper soils (below 400 ft) was obtained from literature research and it is discussed in Section 2.5.4.2.5. Identification of Strata I through III was based on their physical and engineering characteristics. The characterization of the soils was based on a suite of tests performed on these soils, consisting of standard penetration tests (SPT) in soil borings including hammer energy measurements, cone penetration test (CPT) soundings, test pits, geophysical suspension P-S velocity logging, field electrical resistivity testing, and observation wells, as well as extensive laboratory testing.

2.5.4.2.1.1 Stratum I – Terrace Sand

The Terrace Sand stratum consists primarily of light-brown to brown sand with varying amounts of silt, clay, and/or gravel, sometimes with silt or clay interbeds. This stratum was fully penetrated by boreholes installed within CCNPP Unit 3 Powerblock Area and the adjoining CLA area (the 300 and 400 series borings) and by a majority of boreholes drilled outside of these two areas including the Intake Slope and the Utility Corridor (the 700 series borings). This stratum was not encountered in low lying areas.

The thickness of Stratum I soils was estimated from the boring logs and CPT logs. In CCNPP Unit 3 area, its thickness with respect to the existing ground surface is shown in Table 2.5-27. The average bottom for Stratum I soils is about El. 62 ft in CCNPP Unit 3 area. Stratum I Terrace Sand does not exist in the Intake Area.

At isolated locations, sandy soils with an appearance similar to Stratum I soils were encountered. Materials that were probably man-made, (hereafter referred to as "fill"), and disturbed soils were encountered, beginning at the existing ground surface at isolated locations at the CCNPP Unit 3 site. These materials were predominantly sand with varying amounts of silt and clay. In the Intake Area (B-701, B-702, B-771 through B-776, B-780 through B-782, and B-821), the depth of these materials varied from approximately 6 to 11 ft below existing grade. They were present at the ground surface and were encountered in 25 borings (B-303, B-309, B-318, B-336, B-340, B-341, B-352, B-356, B-357, B-406, B-409, B-412, B-415, B-419, B-420, B-432, B-437, B-438/A, B-439, B-440, B-701, B-710, B-713, B-768, and B-791). Mainly, they were found in areas which had previously been developed at the site, such as Camp Conoy, roadways, and ball field areas. Their thickness ranged from approximately 0.5 ft to 17 ft, with an average thickness of about 6 ft.

Stratum I soils are characterized, on average, as non-plastic with an average fines content (materials passing No. 200 Sieve) of 20 percent. Grain size analyses indicated that these soils are primarily fine or fine-medium sands. The Unified Soil Classification System (USCS) designations were poorly-graded sand/silty sand, silty sand, well-graded sand, clayey sand, clay of high plasticity, silt, clay, and silt with high plasticity, with the predominant classifications of SP-SM and SM. The often plastic and fine-grained soil classifications are from the interbeds within this stratum.

2.5.4.2.1.2 Stratum IIa – Chesapeake Clay/Silt

The Chesapeake Clay/Silt was encountered at all locations except the Intake Area. When present, it was encountered beneath the Terrace Sand, except in low lying areas where Stratum I soils had been eroded. Stratum IIa typically consists of light to dark gray clay and/or silt, although it is predominately clay, with varying amounts of sand.

The thickness of Stratum IIa soils was estimated from the boring logs and CPT logs. The thickness of this stratum is presented in Table 2.5-27. Only data from borings that fully penetrated the layer were considered for determination of termination elevations.

The stratum IIa soils were characterized, on average, as medium-high plasticity clays. Their predominant USCS designation was clay of high plasticity and silt of high plasticity (CH and MH); sometimes with silty sand, silty sand to clayey sand, and organic clay. The organic designation was based on laboratory (liquid limit) tests. With less than 1 percent organic matter on average, and observations during sampling, these soils are not considered organic.

2.5.4.2.1.3 Stratum IIb – Chesapeake Cemented Sand

The Chesapeake Cemented Sand stratum was encountered beneath Stratum IIa in all the boreholes except at the Intake Area where it was encountered beneath fill. This stratum includes interbedded layers of light to dark gray silty/clayey sands, sandy silts, and low to high plasticity clays, with varying amounts of shell fragments and with varying degrees of cementation. The predominant soils, however, are sandy. The thickness and termination elevations of this layer are presented in Table 2.5-27. Only data from borings that fully penetrated the layer were considered for determination of termination elevations.

Layer IIb is further subdivided into three sub-layers, as shown by Figure 2.5-95. The layers are denominated Layer 1, Layer 2, and Layer 3. In general, Layer 1 is characterized by standard penetration test (SPT) N-values greater than 20, Layer 2 is characterized by SPT N-values less than 20, and Layer 3 is characterized by SPT N-values greater than 20. Additional information on SPT data is provided in Section 2.5.4.2.2.

Grain size analyses indicated that Stratum IIb soils are primarily medium-fine sands. The USCS designations were silty sand, poorly-graded sand to silty sand, clayey sand, silt, silt of high plasticity, clay of high plasticity, clay, and organic clay. The predominant classifications, however, were silty sand, clayey sand, and poorly-graded sand to silty sand (SM, SC, and SP-SM). Three Phase I investigation samples were classified as organic clay or organic silt, although evidence of high organic content was not present during the field exploration. Organic content testing on three samples indicated an average organic content of 1.4 percent. Eleven Phase II samples from Intake Area borings were tested for organic content. The average organic content in the Intake Area was 1.5 percent. Despite the presence of organic matter in these samples, Stratum IIb soils are not considered organic soils since organic materials are virtually absent in these soils. The plastic and fine-grained soil classifications are generally from the clayey/silty interbeds within this stratum. For engineering analysis purposes, and given the predominance of granular proportions, Stratum IIb soils were characterized, on average, as sands with low plasticity, and with fines content of 25 percent.

2.5.4.2.1.4 Stratum IIc – Chesapeake Clay/Silt

Underlying the Stratum IIb sands, another Chesapeake Clay/Silt stratum was encountered, although distinctly different from the soils in Stratum IIa. This stratum was encountered in areas and in borings that were sufficiently deep to encounter these soils. Although primarily gray to greenish gray clay/silt soils, they contain interbedded layers of sandy silt, silty sand, and cemented sands with varying amounts of shell fragments. The greenish tone is the result of glauconite in these soils. Glauconite is a silicate mineral of greenish color with relatively high iron content (about 20 percent). Galuconite oxidizes on contact with air, producing a dark color tone. It is normally found as sand-size, dark green nodules. It can precipitate directly from marine waters or develop as a result of decaying of organic matter in animal shells or bottom-dwellers.

The thickness of Stratum IIc soils was estimated from the boring logs. Only two borings, B-301 and B-401, were sufficiently deep to completely penetrate this stratum. Based on borings B-301 and B-401, the thickness of this stratum is estimated as 190 ft. The stratum thickness and termination elevations of this Stratum are provided in Table 2.5-27.

For engineering analysis purposes, CCNPP Unit 3 Stratum IIc soils were characterized, on average, as high plasticity clay and silt, with an average PI = 50. Their predominant USCS designation was clay of high plasticity and silt of high plasticity (CH and MH), however, sometimes with silty sand, clay, and organic clay classifications indicated. Based on

observations during sampling, the organic soil designation based on laboratory (Liquid Limit) testing is not representative of these soils, and therefore, they are not considered organic soils. The organic designation may be impacted by the glauconite content in the soils. Organic content testing was performed on 53 Stratum IIc soil samples (all areas). Results indicated organic contents ranging from 1.0 to 9.3 percent with an average of 3.3 percent. The measured values are indicative of the presence of slight organics in these soils.

2.5.4.2.1.5 Stratum III – Nanjemoy Sand

Underlying the Chesapeake Clay/Silt stratum are the Nanjemoy soils (Stratum III). Stratum III was encountered in deep borings B-301 and B-401. This stratum consists primarily of dark, greenish-gray glauconitic sand, however, it contains interbedded layers of silt, clay, and cemented sands with varying amounts of shell fragments and varying degrees of cementation. The glauconite in these soils could vary from less than 10 percent to as much as 50 percent.

The thickness of Stratum III soils cannot be estimated from the information obtained from the CCNPP Unit 3 subsurface investigation (boring logs B-301 and B-401), as these borings did not penetrate these soils in their entirety, although they penetrated them by about 100 ft. It is estimated that the Nanjemoy soils are about 200 ft thick at the site (Hansen, 1996), consisting of primarily sandy soils in the upper 100 ft and clayey soils in the lower 100 ft. On this basis, the termination (bottom) of the upper sandy portion can be estimated at about El. -315 ft and the termination of the lower clayey portion can be estimated at about El. -415 ft. Information from borings B-301 and B-401 sufficiently characterizes the upper half of this geologic unit, as these borings were terminated at El. -308 ft and El. -329 ft, respectively.

For engineering analysis purposes, Stratum III soils were characterized, on average, as sand of high plasticity. Their predominant USCS designations were clayey sand and silty sand (SC and SM), although clay of high plasticity and silt of high plasticity were also indicated.

2.5.4.2.1.6 Subsurface Materials below 400 Feet

The field exploration for the CCNPP Unit 3 extended to a maximum depth of about 400 ft below ground. Coastal Plain sediments, however, are known to extend below this depth, to a depth of approximately 2,500 ft, or to top of bedrock (BGE, 1982). The subsurface conditions below 400 ft were addressed through reference to existing literature and work that had been done by others, primarily for the purpose of seismic site characterization. The subsurface conditions below 400 ft are addressed in Sections 2.5.2.5 and 2.5.4.2.5.

2.5.4.2.2 Field Investigation Program

The planning of the field investigation referred to the guidance provided in NRC Regulatory Guide 1.132, "Site Investigations for Foundations of Nuclear Power Plants" (USNRC, 2003a). References to the industry standards used for field tests completed for the CCNPP Unit 3 subsurface investigation are shown in Table 2.5-28. The details and results of the field investigation are included as COLA Part 11J. The work was performed under the Bechtel QA program with work procedures developed specifically for the CCNPP Unit 3 subsurface investigation, including a subsurface investigation plan developed by Bechtel. A complementary Phase II investigation was performed in 2008 as part of the detailed design of the project, with reference to guidance in Regulatory Guide 1.132 (USNRC, 2003a) to verify subsurface uniformity at locations where coverage was not available in the initial phase of the investigation due to shifting locations of some structures. Results of the additional (Phase II) investigation are presented herein, and in the data report (Schnabel, 2009) (MACTEC, 2009a). Locations of the field tests are shown in Figure 2.5-92, Figure 2.5-93, and Figure 2.5-94.

2.5.4.2.2.1 Previous Subsurface Investigations

Based on limited information available from the CCNPP Units 1 and 2 UFSAR (BGE, 1982), the original subsurface investigations for the CCNPP Units 1 and 2 performed in 1967 consisted of a total of 10 exploratory borings, ranging in depth from 146 to 332 ft, with soil samples obtained at various intervals for soil identification and testing. Seven piezometers were also installed for groundwater observation and monitoring. The 1967 investigation included other field investigations (two seismic survey lines using Microtremor) and laboratory testing (moisture content, density, particle size, permeability, cation exchange, and x-ray diffraction). Supplemental investigations in support of detailed design were performed in July 1967 (5 borings), August 1967 (23 borings), December 1968 (18 borings), and 1969 (5 borings). Additional investigations were performed in 1980/1981 (borings, CPT soundings, and observation wells) in order to site a "generic Category I structure," and in 1992 additional investigations (borings, dilatometer soundings, crosshole seismic survey, field resistivity) were performed for an additional Diesel Generator Building (Bechtel, 1992). Various laboratory testing was also performed on selected portions of the recovered soils.

Geological descriptions in CCNPP Units 1 and 2 UFSAR (BGE, 1982) indicate the surficial deposits to be Pleistocene Age soils extending from the ground surface to about El. 70 ft. These soils were estimated to extend to an average El. 60 ft based on the CCNPP subsurface investigation. CCNPP Units 1 and 2 UFSAR (BGE, 1982) indicates that Chesapeake Group soils were encountered in the 1967 investigation between El. 70 ft and El. -200 ft. These soils were estimated to extend to approximately El. -200 ft based on the CCNPP Unit 3 investigation. CCNPP Units 1 and 2 UFSAR (BGE, 1982) indicates that Eocene deposits lie below El. -200 ft and consist of glauconitic sands. Comparable observations were made on these, and the overlying deposits, from the CCNPP Unit 3 subsurface investigation borings. The CCNPP Units 1 and 2 UFSAR (BGE, 1982) remarked that "good correlation of subsurface stratigraphy was obtained between the borings." This remark is corroborated by the results obtained from the CCNPP subsurface investigation.

The CCNPP Unit 3 subsurface investigation involved a significantly larger quantity of testing than performed for the original CCNPP Units 1 and 2. Given the reasonably parallel geologic conditions between CCNPP Units 1 and 2 and the CCNPP Unit 3 site, and the greater intensity in exploration and testing at the CCNPP Unit 3 site which should result in enhanced characterization of the subsurface conditions, findings from previous investigations are not discussed further, unless a differing condition is reported from the previous investigations.

2.5.4.2.2.2 CCNPP Unit 3 Field Investigation

The subsurface investigation program was performed in accordance with the guidance outlined in Regulatory Guide 1.132 (USNRC, 2003a). Deviations are identified at point of use, alternatives and/or basis for deviation are provided. The fieldwork was performed under the contractors QA program and work procedures developed specifically for the CCNPP Unit 3 subsurface investigation.

Regulatory Guide 1.132 (USNRC, 2003a) provides guidance on spacing and depth of borings, sampling procedures, in-situ testing, geophysical investigations, etc. This guidance was used in preparing a technical specification, addressing the basis for the CCNPP Unit 3 subsurface investigation. The quantity of borings and CPTs for Seismic Category I structures was based on a minimum of one boring per structure and the one boring per 10,000-square ft criterion. The maximum depths of the borings for Seismic Category I structures were based on a foundation to overburden stress ratio criterion of 10 percent. The sampling intervals typically exceeded the guidance document by decreasing the sample spacing in the upper 15 ft and maintaining 5-ft

sampling intervals at depths greater than 50 ft, except for the 400-ft borings. Continuous sampling was also performed, and is later described.

Regulatory Guide 1.132 (USNRC, 2003a) provides guidance in selecting the boring depth (dmax) based on a foundation to overburden stress ratio of 10 percent. Regulatory Guide 1.132 (USNRC, 2003a), also indicates that at least one-fourth of the principal borings should penetrate to a depth equal to dmax. Given the previously available knowledge of subsurface conditions as documented in the CCNPP Units 1 and 2 UFSAR (BGE, 1982) indicating stable, geologically old deposits at the site which would not adversely impact foundation stability, it was determined that one boring should be extended to about 400 ft, 4 borings extended to about 200 ft, and 4 borings extended to about 150 ft for the Common Basemat. (The consistency across the site of the Miocene-age Chesapeake Group clays and silts that exist below about 100 ft depth and the underlying Nanjemoy Formation sands that start at around 300 ft depth is aptly demonstrated by the similarity of the shear wave velocity profiles obtained in boreholes almost 1,000 ft apart. Also included were 3 CPT soundings. Borings associated with the Common Basemat extended at least 33 ft below the foundation level. An additional (Phase II) field investigation was completed in 2008 (Schnabel, 2009) (MACTEC, 2009a) in conformance with guidance in Regulatory Guide 1.132.

The current quantity and locations of tests for the combined initial and Phase II investigations, are shown in Figure 2.5-92, Figure 2.5-93, and Figure 2.5-94. These provide the necessary coverage at the footprint structures, although several of the test locations required relocation during the field investigation to reduce cutting trees, and for accessibility for drilling equipment.

A team consisting of a geologist, a geotechnical engineer, and a member of UniStar project management performed a site reconnaissance prior to start of the field investigation. The focus of this task was to observe the site and access conditions, locations of borings and wells, and identify potential test relocation areas. Information on site geology and geotechnical conditions, used as a basis for developing the soils investigation plan for the CCNPP subsurface investigation was obtained from the information contained in the CCNPP Units 1 and 2 UFSAR (BGE, 1982).

Regulatory Guide 1.132, (USNRC, 2003a) provides that boreholes with depths greater than about 100 ft should be surveyed for deviation. In lieu of surveying for deviation in boreholes greater than 100 ft, deviation surveys were used in the 10 suspension P-S velocity logging boreholes to depths ranging from about 200 to 400 ft. The results indicated minimum, maximum, and average deviation of 0.6, 1.6, and 1.0 percent, respectively. The information collected the necessary data for proper characterization of the CCNPP Unit 3 subsurface materials.

Regulatory Guide 1.132, (USNRC, 2003a) provides guidance for color photographs of all cores to be taken soon after removal from the borehole to document the condition of the soils at the time of drilling. For soil samples, undisturbed samples are sealed in steel tubes, and cannot be photographed. SPT samples are disturbed, and by definition they do not resemble the condition of the material in-situ. Sample photography is a practice typically limited to rock core samples, not soils, therefore, it was not used for the initial investigation. However, it was used during the Phase II investigation. X-ray imaging was performed on tube samples selected for RCTS testing.

The Phase I CCNPP Unit 3 subsurface field exploration was performed from April through August 2006; the Phase II exploration was performed from May through December 2008. This

work consisted of an extensive investigation to define the subsurface conditions at the project area. The scope of work and investigation methods was determined to be as follows:

- Surveying to establish the horizontal and vertical locations of exploration points.
- Evaluating the potential presence of underground utilities at exploration points.
- Drilling 200 test borings with SPT sampling and collecting in excess of 275 intact samples (using Shelby push tubes, Osterberg sampler, and Pitcher sampler) to a maximum depth of 403 ft, including 6 borings with continuous SPT samples (B-305, B-409, B-774, B-324, B-417, and B-775), with the first three borings being 150 ft deep each and the last three borings being 100 ft deep each. Note that "continuous sampling" was defined as one SPT sample for every 2.5-ft interval with a one ft distance between each SPT sample. In addition to the 6 continuous borings noted above, 13 borings were continuously sampled between El. 50 ft and El. -20 ft (B-342, B-343, B-344, B-345, B-347, B-348, B-352 through B-357, and B-357A).
- Installing and developing 47 groundwater observation wells to a maximum depth of 122 ft, including Slug testing in each well.
- Excavating 20 test pits to a maximum depth of 10 ft and collecting bulk soil samples.
- Performing 74 CPT soundings, including off-set soundings that required pre-drilling to overcome CPT refusal, to a maximum depth of 152 ft, as well as seismic CPT and 37 pore pressure dissipation measurements.
- Conducting 13 P-S Suspension Logging tests to measure dynamic properties.
- Conducting 2-dimensional field electrical resistivity testing along four arrays.
- Performing borehole geophysical logging, consisting of suspension P-S velocity logging, natural gamma, long- and short-term resistivity, spontaneous potential, 3-arm caliper, and directional survey in 13 boreholes.
- Two pressuremeter tests, one in the CCNPP Unit 3 Powerblock Area and another in the Intake Area.
- Two Dilatometer tests, one in the CCNPP Unit 3 Powerblock Area and another in the Intake Area.
- Conducting SPT hammer-rod combination energy measurements on drilling rigs.

Table 2.5-28 provides a summary of the number of field tests performed. The location of each exploration point was investigated for the presence of underground utilities prior to commencing exploration at that location. Locations of several exploration points had to be adjusted due to proximity to utilities, inaccessibility due to terrain conditions, or proximity to wetlands. Access had to be created to most exploration locations, via clearing roads and creating temporary roads, due to heavy brush and forestation. These areas were restored subsequent to completion of the field investigation.

An on-site storage facility for soil samples was established before the exploration program commenced. Each sample was logged into an inventory system. Samples removed from the facility were noted in the inventory logbook. A chain-of-custody form was also completed for

all samples removed from the facility. Material storage handling was in accordance with ASTM D4220 (ASTM, 2000a).

Complete results of the investigation are in COLA Part 11J. Geophysical test results are discussed and summarized in Section 2.5.4.4. Further details pertaining to field activities related to borings, CPTs, Slug tests, geophysical surveys, and other activities are summarized below.

Borings, Standard Penetration Test and Sampling

Soils were sampled using the SPT sampler in accordance with ASTM D1586 (ASTM, 1999). The soils were sampled at continuous intervals (one sample every 2.5-ft) to 15 ft depth. Subsequent SPT sampling was performed at regular 5 ft intervals. At boring B-401, with a total depth of 401.5 ft, SPT sampling was performed at about 10 ft intervals below a depth of 300 ft. The recovered soil samples were visually described and classified by the engineer or geologist in accordance with ASTM D2488 (ASTM, 2006). A representative portion of the soil sample was placed in a glass jar with a moisture-preserving lid. The sample jars were labeled, placed in boxes, and transported to the on-site storage facility.

Table 2.5-29 provides a summary of all test borings performed. The boring locations are shown in Figure 2.5-92, Figure 2.5-93, and Figure 2.5-94. The boring logs are included in COLA Part 11J. At boring completion, the boreholes were tremie-grouted using cement-bentonite grout.

Soil samples were collected from the borings via SPT and tube samples. Samples were collected more frequently in the upper portion of the borings than in the lower portion, e.g., typically 6 samples were obtained in the upper 15 ft. Thereafter, SPT samples were typically obtained at 5 ft intervals. SPT N-values were measured during the sampling and recorded on the boring logs. SPT N-values in Stratum I soils registered 0 blows/ft (SPT weight of hammer (WOH) or weight of rod (WOR)). The WOH and WOR values were very infrequent in Stratum I soils. A total of 5 WOH and WOR conditions were encountered in borings at CCNPP Unit 3 location, and a total of 5 were observed in all other borings. At the CCNPP Unit 3 location, three of these conditions were in boring B-309 in materials designated as “fill,” which will be removed during construction. The fourth episode was in boring B-314 at the ground surface which will also be removed during construction. The fifth value was in boring B-322 at about El. 70 ft, at the location of the Essential Service Water System (ESWS) Cooling Tower. The cause of this low SPT value is likely due to sampling disturbance. A review of the boring logs and stratigraphic profiles for the same soils at other locations does not indicate this to be the predominant situation. Rather, the low SPT value is an isolated, infrequent situation, most likely caused by factors other than the natural condition of Stratum I soils. Nonetheless, these soils will be removed during excavation for the ESWS Cooling Tower to at least El. 60 ft. In conclusion, at the CCNPP Unit 3 location, the 5 WOH and WOR results are inconsequential to the stability of Stratum I soils.

The data clearly indicates the need to further subdivide Layer IIb into three sub-stratums. Figure 2.5-102 provides a graphic representation of the SPT distribution in the CCNPP Unit 3 Powerblock Area. Figure 2.5-103 provides equivalent information for the Intake Area. SPT data is summarized in Table 2.5-30. For the Powerblock Area, 177 out of 359 N-values are greater than 63 blows/ft, which is approximately 49 percent of the N-values reported. Out of these 177 values, 153 N-values are 100 blows/ft, which is difficult to clearly portray in scatter plots. The plot does not show clearly these 153 points at a N-value of 100 because the deeper layer overrides those points. Values for analysis and design are provided in Section 2.5.4.2.

Intact samples were obtained in accordance with ASTM D1587 (ASTM, 2000c) using the push Shelby tubes, Osterberg sampler, and rotary Pitcher sampler. Upon sample retrieval, the disturbed portions at both ends of the tube were removed, both ends were trimmed square to establish an effective seal, and pocket penetrometer (PP) tests were performed on the trimmed lower end of the samples. Both ends of the sample were then sealed with hot wax, covered with plastic caps, and sealed once again using electrician tape and wax. The tubes were labeled and transported to the on-site storage area. Table 2.5-31 provides a summary of undisturbed sampling performed during the subsurface investigation. A total of 375 sample retrievals were attempted. Intact samples are also identified on the boring logs included in COLA Part 11J.

Energy Measurements

Several drill rigs were used for the Phase I and II COL subsurface exploration. SPT hammer energies were measured for each of the drilling rigs used. Energy measurements were made in 10 borings (B-348, B-354, B-356, B-357, B-401, B-403, B-404, B-409, B-744, and B-791). Because the SPT N-value used in correlations with engineering properties is the value corresponding to 60 percent hammer efficiency, the measured SPT N-values were adjusted in accordance with ASTM D6066 (ASTM, 2004b). A summary of the measured ETR values for each drill rig is shown in Table 2.5-32. The measured SPT N-values from each boring were adjusted using the appropriate ETR value also shown in Table 2.5-32 for the drill rig used.

The energy measurements were made on the hammer-rod system on drilling rigs used in the subsurface investigation. A Pile Driving Analyzer (PDA) was used to acquire and process the data. Energy measurements were made at sampling intervals of 15 ft, with the total number of measurements made per boring ranging from 6 (at boring B-744) to 26 (at boring B-401), depending on boring depth. Energy transfer to the gage locations was estimated using the Case Method, in accordance with ASTM D4633 (ASTM, 2005a). The resultant energy transfer efficiency measurements ranged from 78 to 90 percent, with an average energy transfer efficiency of 84 percent. Detailed results are presented in COLA Part 11J.

Cone Penetration Testing

CPT soundings were performed using an electronic seismic piezocone compression model, with a 15 cm^2 tip area and a 225 cm^2 friction sleeve area. CPT soundings were performed in accordance with ASTM D5778 (ASTM, 2000b), except that tolerances for wear of the cone tip were in accordance with report SGF 1:93E, Recommended Standard for Cone Penetration Tests, (SGS, 1993) which are comparable to ASTM. For the 10-cm^2 base cone, the ASTM D5778 (ASTM, 2005b) specified dimensions for "base diameter," "cone height," and "extension" are a minimum of 34.7 mm, 24 mm, and 2 mm, respectively, compared to the report SGF 1:93E (SGS, 1993) which recommended tolerances of a minimum of 34.8 mm, 24 mm, and 2 mm, for the same cone. The 2-mm SGF Report (SGS, 1993) value accounts for a constant 5-mm porous filter. Pore pressures were measured in the soundings. The equipment was mounted on a track-operated rig dedicated only to the CPT work. Cone tip resistance, sleeve friction, and dynamic pore pressure were recorded every 5 cm (approximately every 2 in) as the cone was advanced into the ground. Seismic shear wave velocity tests were also performed using a geophone mounted in the cone, a digital oscilloscope, and a beam, which was struck on the ground surface with a sledge hammer. Pore pressure dissipation data were also obtained, with the data recorded at 5-sec intervals.

A total of 74 CPT soundings were performed, including additional off-set soundings due to persistent refusal in dense/hard or cemented soils. At selected sounding locations, the soils causing refusal were pre-augered so that deeper CPT penetration could be obtained at the sounding location. Pre-augering was performed at several locations, and often several times at

the same sounding. The sounding depths ranged from about 12 ft to 152 ft. Seismic CPT was performed at eight sounding locations. Pore pressure dissipation tests were performed, with 37 results at various depths. Table 2.5-33 provides a summary of CPT locations. The locations are shown in Figure 2.5-92, Figure 2.5-93, and Figure 2.5-94. The CPT logs, shear wave velocity, and pore pressure dissipation results are contained in COLA Part 11J.

The cone tip resistance, qc, in the Stratum I soils ranged from about 2 to 570 tons per square ft (tsf), with an average of about 120 tsf. The results indicate the qc values in Stratum I soils to be typically limited to about 200 tsf, with values peaking much higher between elevation 80 ft to elevation 90 ft. The CPT results also indicate the presence of clay zones within this stratum, at about elevation 115 ft, elevation 100 ft, and elevation 90 ft. Estimated relative density from CPT data ranges from about 30 to near 95 percent, with an average of about 75 percent. Stratum I Terrace Sand was not encountered in CPTs in the Intake Area. In the Utility Corridor it was present at higher elevations.

For Stratum IIa soils, the cone tip resistance values ranged from about 10 to 200 tsf, with an average value of about 50 tsf. Stratum IIa Chesapeake Clay/Silt was not encountered in the Intake Area. The results also indicate a mild increase in tip resistance with depth.

CPT soundings were attempted in Stratum IIb soils. However, the soils could only be partly penetrated. All CPT soundings experienced refusal when encountering the highly cemented portions of these soils. The CPT soundings could only be advanced after predrilling through the highly cemented zones, and sometimes the predrilling had to be repeated due to the intermittent presence of hard zones at the same sounding. Values of qc from the soundings ranged from about 40 to over 600 tsf. The average qc value ranges from 200 to 300 tsf. The results are consistent with the SPT N-values where the highest N-values were measured in zones that CPT soundings encountered refusal or could not penetrate these soils, approximately between elevation 20 and elevation 40 ft. Stratum IIb Cemented Sand was encountered in the Intake Area with similar but somewhat lower average tip resistance. Average qc value for the Intake Area is approximately 210 tsf. Low SPT N-values and qc values are very infrequent in this stratum, given the influence of cementation. The low values are very likely the result of sampling disturbance, or in one case (at C-406, elevation ~30 ft, qc~10 tsf) the low tip resistance is due to the relatively low overburden pressure at that location. They could also be influenced by groundwater, given that the "confined" groundwater level is roughly near the top of this stratum (refer to Section 2.5.4.6 for groundwater information). The cementation in Stratum IIb soils varies, including zones that are highly cemented and others with little or no cementation. The degree of cementation was subjectively evaluated during the field exploration by observing the degree of shell fragmentation present and testing the soils with diluted hydrochloric acid, as noted on the boring logs. The cementation is affected by the presence of shells in these soils. The influence of iron oxide may also be a factor, although no specific test was performed on the samples for verification of iron contents. These soils, however, have been studied in the past by others, as follows.

Based on a study of soils near Calvert Cliffs (Rosen, et al., 1986), dolomite or calcite, which is present in the local soils, is identified as the cementing agent. The absence of dolomite or calcite in certain parts may be due to low pH groundwater. Abundant iron cement is also reported in some areas near Calvert Cliffs, with significant accumulation of shells that had dissolved. The degree of cementation is affected by the level of dolomitization in the sandy soils, a process that began in the Chesapeake Groups soils once they were covered by the clayey soils above.

The abundant shells in some zones within this stratum render these zones very porous. In a few borings, loss of drilling fluid was noted, (e.g., in borings B-302, B-309, B-354, B-357, B-357A,

B-406, B-414, B-426, B-703, B-710, B-786A and B-790). These zones were encountered either near the upper or the lower part of the stratum. Fluid loss was estimated to be in the range of 300 to 600 gallons at B-354, B-357 and B-357A, and at each of the 400-series borings. The loss was judged to be due to the nested accumulation of coarse materials, particularly shell fragments at these locations. The fluid loss in boring B-309, and in the upper portion of boring B-710, was in suspected fill materials.

Refusal was also encountered for Stratum IIc soils. Profiles of qc versus elevation are shown in Figure 2.5-104 and Figure 2.5-105 for the Powerblock and Intake Areas respectively. The results suggest relative uniformity in qc values with depth and lateral extent, as well as evidence of cemented (or hardened zones) near elevation -40 ft which was similarly reflected in the SPT N-value profiles in Figure 2.5-102. The qc values for CCNPP Powerblock Area range from about 50 to 100 tsf, with an average of about 75 tsf. Stratum IIc Clay/Silt was encountered in the Intake Area with a slightly lower average tip resistance of 70 tsf.

Observation Wells and Slug Testing

A total of 47 observation wells were installed to a maximum depth of 122 ft during the CCNPP Unit 3 subsurface investigation under the full-time supervision of geotechnical engineers or geologists. Wells were installed either in SPT boreholes or at an off-set location, in accordance with ASTM D5092 (ASTM, 2004a). Wells installed in SPT boreholes were grouted to the bottom of the well, and the portion above was reamed to a diameter of at least 6 in using rotary methods and biodegradable drilling fluid. Off-set wells were installed using either 6¼-in ID hollow-stem augers or 6-in diameter holes using the rotary method and biodegradable drilling fluid. Each well was developed by pumping and/or flushing with clean water. Table 2.5-34 provides a summary of the observation well locations and details. The locations are shown in Figure 2.5-92, Figure 2.5-93, and Figure 2.5-94. Complete observation well details are provided in Section 2.4.12.

Slug testing, for the purposes of measuring the in-situ hydraulic conductivity of the soils, was performed in all 47 wells. The tests were conducted using the falling head method, in accordance with Section 8 of ASTM D4044 (ASTM, 2002b). Slug testing included establishing the static water level, lowering a solid cylinder (slug) into the well to cause an increase in water level in the well, and monitoring the time rate for the well water to return to the pre-test static level. Electronic transducers and data loggers were used to measure the water levels and times during the test. Table 2.5-35 provides the hydraulic conductivity values. Details on testing are provided in Section 2.4.12. COLA Part 11J contains the details of well installation records, boring logs for observation wells, and the hydraulic conductivity test results.

Test Pits

A total of 20 test pits were excavated to a maximum depth of 10 ft each using a mechanical excavator. Bulk samples were collected at selected soil horizons in some of the test pits for laboratory testing. Table 2.5-36 provides a summary of the test pit locations. The locations are shown in Figure 2.5-92, Figure 2.5-93, and Figure 2.5-94. COLA Part 11J contains the test pit records.

Field Electrical Resistivity Testing

A total of four field electrical resistivity (ER) tests were performed to obtain apparent resistivity values for the site soils. Table 2.5-37 provides a summary of the ER test locations. ER testing was conducted using an Advanced Geosciences, Inc., Sting resistivity meter, a Wenner four-electrode array, and "a" spacings of 1.5 ft, 3 ft, 5 ft, 7.5 ft, 10 ft, 15 ft, 20 ft, 30 ft, 40 ft, 50 ft, 100 ft,

200 ft, and 300 ft in accordance with ASTM G57 (ASTM, 2001a) and IEEE 81 (IEEE, 1983), except as noted below. The arrays were centered on each of the staked locations R-1 and R-2, R-3, and R-4, and are shown in Figure 2.5-92 and Figure 2.5-93. The electrodes were located using a 300-ft measuring tape along the appropriate bearings using a Brunton compass.

ASTM G57 (ASTM, 2001a) states that electrodes not be driven more than 5 percent of the electrode separation, which is about 0.9 in for the smallest "a" spacing of 1.5 ft used. Electrodes, however, were driven about 2.25 in (or about 12 percent) at locations where leaves and vegetation were present on the ground, to ensure adequate contact with the soils. ASTM G57 (ASTM, 2001a) states that a decade box be used to check the accuracy of the resistance meter. This verification, however, was conducted using a resistor supplied by the equipment manufacturer in compliance with the manufacturer's recommendations. ASTM G57 (ASTM, 2001a) states that measurement alignments be chosen along uniform topography. Given the topography at the site, however, the array alignments along R-1 and R-2 contained topographic variation. Finally, IEEE 81 (IEEE, 1983) states that electrodes not be driven into the ground more than 10 percent of the "a" spacing. As discussed above, at some locations electrodes were driven about 2.25 in (or about 12 percent) into the ground. Despite the noted deviations, the collected resistivity values are considered valid and suitable for use.

The results of field resistivity surveys are presented in COLA Part 11J, and summarized in Table 2.5-38.

Suspension P-S Velocity Logging Survey

Borehole geophysical logging was performed in a total of 13 boreholes. The geophysical survey consisted of natural gamma, long- and short-normal resistivity, spontaneous potential, three-arm caliper, direction survey, and suspension P-S velocity logging. Geotechnical engineers or geologists provided full-time field inspection of borehole geophysical logging activities. Detailed results are provided in COLA Part 11J.

Suspension P-S velocity logging was performed in borings B-301, B-304, B-307, B-318, B-323, B-401, B-404, B-407, B-418, B-423, B-773, B-786, and B-821. The measurement at B-786 was performed directly underneath the UHS-MWIS in the Intake Area during the Phase II investigation. The boreholes were uncased and filled with drilling fluid. Boreholes B-301 and B-401 were approximately 400 ft deep each, while the remaining boreholes were approximately 200 ft deep each. The OYO/Robertson Model 3403 unit and the OYO Model 170 suspension logging recorder and probe were used to obtain the measurements. Details of the equipment are described in Ohya (Ohya, 1986). The velocity measurement techniques used for the project are described in Electric Power Research Institute (EPRI) Report TR-102293, Guidelines for Determining Design Basis Ground Motions, (EPRI, 1993). The results are provided as tables and graphs in COLA Part 11J. Figure 2.5-106 and Figure 2.5-107 present the results of the P-S logging surveys. The values in the figures are presented regardless of location and elevation, and therefore the variability in the plots is only apparent. Variability between measurements in the Powerblock area is best shown by Figure 2.5-228, once the offset in elevations is accounted for and the measurements of distant borings is excluded. The measurements from Boring B-301 are compared with the other measurements in the Powerblock Area. Only B-301, B-304, and B-307 are within the area covered by the Nuclear Island Common Basemat. The shear wave velocity measurements clearly indicate the presence of uniform subsurface conditions. According to these measurements, engineering analyses such as settlement, foundation stability, and site response analysis, can be performed with the use of uniform soil conditions represented by horizontal strata. Figure 2.5-108 provides the test result of the PS log performed in the Intake Area. Overall, the result is consistent with the measurements in the Powerblock Area. Section 2.5.4.2.5.8 and 2.5.4.4 provide the analysis of

the P-S data along with the development of the best estimate soil profiles for the Unit 3 Area and the Intake Area.

The suspension P-S velocity logging used a 23-ft probe containing a source near the bottom, and two geophone receivers spaced 3.3 ft (1 m) apart, suspended by a cable. The probe is lowered into the borehole to a specified depth where the source generates a pressure wave in the borehole fluid (drilling mud). The pressure wave is converted to seismic waves (P-wave and S-wave) at the borehole wall. At each receiver location, the P- and S-waves are converted to pressure waves in the fluid and received by the geophones mounted in the probe, which in turn send the data to a recorder on the surface. At each measurement depth, two opposite horizontal records and one vertical record are obtained. This procedure is typically repeated every 1.65 ft (0.5 m) or 3.3 ft (1 m) as the probe is moved from the bottom of the borehole toward the ground. The elapsed time between arrivals of the waves at the geophone receivers is used to determine the average velocity of a 3.3-ft high column of soil around the borehole. For quality assurance, analysis is also performed on source-to-receiver data.

Ignoring the measurements above El. 85 ft (approximate finished grade), V_p measurements in Stratum I Terrace Sand ranged from about 850 ft/sec to 5,560 ft/sec, with an increasing trend with depth. Vp measurements in Stratum IIa Chesapeake Clay/Silt ranged from about 3,000 ft/ sec to 5,750 ft/sec. V_p measurements in Stratum IIb Chesapeake Cemented Sand ranged from about 2,000 ft/sec to 8,130 ft/sec, with initially increasing trend with depth, however, with fairly uniform values after a few feet of penetration, except at intermittent cemented zones with peak V_p values. V_p measurements in Stratum IIc Chesapeake Clay/Silt ranged from about 4,800 ft/sec to 5,600 ft/sec, with relatively uniform values throughout the entire thickness, except for occasional minor peaks at intermittent depths. V_p measurements in Stratum III Nanjemoy Sand ranged from about 5,420 ft/sec to 7,330 ft/sec, with relatively uniform values, except for occasional minor peaks at intermittent depths. Results are relatively consistent with those reported from CCNPP Units 1 and 2 (Table 2.5-39 and Figure 2.5-109) for similar soils. V_p values below about El. 80 ft are typically at or above 5,000 ft/sec; these measurements reflect the saturated condition of the soils below the referenced elevation.

V_s measurements in Stratum IIa Chesapeake Clay/Silt ranged from about 590 ft/sec to 1,430 ft/ sec, with typically increasing trend with depth. V_s measurements in Stratum IIb Chesapeake Cemented Sand ranged from about 560 ft/sec to 3,970 ft/sec, with significant variation with depth owing to significant changes in density and cementation. V_s measurements in Stratum IIc Chesapeake Clay/Silt ranged from about 1,030 ft/sec to 1,700 ft/sec, with relatively uniform trend in values throughout the entire thickness, except for occasional minor peaks at intermittent depths. V_s measurements in Stratum III Nanjemoy Sand ranged from about 1,690 ft/sec to 3,060 ft/sec, with initially increasing trend in depth, however, relatively uniform at greater depth, except for occasional minor peaks at intermittent depths.

The P-S logging results are discussed in detail in Section 2.5.4.4.

Pressuremeter

Pressuremeter testing was performed in pre-drilled boreholes using a cylindrical probe that expanded radially. The deformation of the borehole wall was measured relative to the stress induced by the pressuremeter on the soil. Geotechnical engineers or geologists were on site to inspect the work. One pressuremeter test was performed in the Unit 3 Powerblock Area to a depth of about 360 ft at borehole PM-301. Another pressuremeter test was performed in the Intake Area to a depth of about 150 ft in borehole PM-701. The data are presented in COLA Part 11J. Sixty-seven (67) tests were completed in PM-301 and 29 in PM-701. Almost all of the tests produced useful data, although not all tests could be completely analyzed for all possible

parameters. In instances where not all parameters could be determined, this was due to borehole disturbance or uneven expansion of the instrument resulting in less than complete information on the soil.

The pressuremeter used was a digital electronic instrument of the Cambridge design and is a much more sensitive instrument than the Menard type specified by ASTM. The pressuremeter data was analyzed to determine the pressuremeter modulus and limit pressure as determined by ASTM D4719 (ASTM, 2007). Additional analyses were performed to determine the unload/reload modulus which usually included one to three cycles per tests at various strain levels. Strength parameters were determined using modeling techniques. Pressuremeter data has been used as means, among other methodologies, to estimate the elastic modulus for settlement. It is also used to establish the ratio of the Unload/Reload Modulus to the Elastic Modulus.

Table 2.5-40 and Table 2.5-41 provide the data recordings of the pressuremeter tests at PM-301 and PM-701. Figure 2.5-110 shows a graphic representation of the data for the Powerblock and Intake Area in the form of elastic modulus. An average for the site is plotted as references. This information is used as one of the criteria to provide a recommendation for elastic modulus.

Dilatometer

An in-situ penetration and expansion test with a steel dilatometer blade with a sharp cutting edge was incrementally forced into the soil in a generally vertical orientation. At a specified depth a flat circular, metallic membrane is expanded into the surrounding soil. Inspected by a geotechnical engineer or geologist, the soil deformation is measured relative to the stress induced on the soil by the expanding membrane. One dilatometer test was performed in the Powerblock Area to a depth of about 350 ft in boring B-301. Another dilatometer test was performed in the Intake Area to a depth of about 150 ft at boring B-701. Due to the large amount of data, the results of the tests are included only in COLA Part 11J.

2.5.4.2.3 Backfill Investigation

During the Phase III investigation, a backfill characterization study was conducted. Structural fill has been identified and the material sampled was sent to the laboratory to establish their static, chemical, and dynamic properties. The results are evaluated to verify that the candidate backfill materials meet the design requirements for structural fill. The structural fill for CCNPP Unit 3 is sound, durable, well graded sand or sand and gravel, with a maximum 25 percent fines content, and free of organic matter, trash, and other deleterious materials. Backfill and related topics are further addressed in Section 2.5.4.5. It is estimated that about 2 million cubic yards of structural backfill are required.

The field sampling campaign was performed as follows:

- Batch 1: sampling of six buckets from Vulcan Quarry in Havre de Grace, Maryland was performed in September of 2008. Sample testing directive to laboratory was performed on unblended samples.

- Batch 2: sampling of six buckets from Vulcan Quarry. Sample testing directive to laboratory was performed on blended samples. Sample testing directive to laboratory was performed on composite samples.

- Batch 3: eight buckets of CR6, eight buckets of GAB, and six buckets of coarse aggregate- 57 sampled from the Vulcan Quarry on December, 2008. Sample testing directive to laboratory was performed on composite samples.

- Batch 4: seventeen buckets of CR6, GAB, and coarse aggregate-57 sampled from the Vulcan Quarry on March, 2009. Sample testing directive to laboratory was performed on composite samples. Batch 4 was used for Resonant Column Torsional Shear Testing.

2.5.4.2.4 Laboratory Testing Program

The laboratory investigations of soils and rock were performed in accordance with the guidance outlined in Regulatory Guide 1.138, Laboratory Investigations of Soils for Engineering Analysis and Design of Nuclear Power Plants (USNRC, 2003b). Deviations are identified and alternatives and/or basis for deviation are provided.

The detailed results of all laboratory tests performed as part of the subsurface investigation is provided in the following reports:

- Geotechnical Subsurface Investigation Data Report (Schnabel, 2007a), with Phase I laboratory testing program.

- Geotechnical Subsurface Investigation Data Report (Schnabel, 2007b).

- Reconciliation of EPRI and RCTS Results Calvert Cliffs Nuclear Power Plant Unit 3 (Bechtel, 2007), with the RCTS data and analysis for the Powerblock Area.

- Revised Laboratory Testing Results, Rev.2 (MACTEC, 2009a).

- Structural Fill Static Laboratory Testing Results, Rev. 1 (MACTEC, 2009b).

- Structural Fill Dynamic Laboratory Testing Results, Rev.1 (MACTEC, 2009c).

- Intake Samples Laboratory Testing Results, Rev. 1 (MACTEC, 2009d).

The referenced reports are included in COLA Part 11J and COLA Part 11K.

The laboratory work was performed under the Bechtel QA program with work procedures developed specifically for the CCNPP Unit 3 subsurface investigation. Soil samples were shipped under chain-of-custody protection from the on-site storage to the testing laboratories. ASTM D4220 (ASTM, 2000a) provides guidance on standard practices for preserving and transporting soil samples. This guidance was referenced in preparing technical specifications for the CCNPP Unit 3 subsurface investigation, addressing sample preservation and transportation, as well as other subsurface investigation and geotechnical requirements.

Laboratory testing consisted of testing soils and groundwater samples obtained from the investigation program. Testing of groundwater samples is addressed in Section 2.4.13. Laboratory testing of soil samples consisted of index and engineering property tests on selected SPT, undisturbed, and bulk samples. The SPT and undisturbed samples were recovered from the borings and the bulk samples were obtained from the test pits.

Testing of index properties included the following items:

- Soil classification,
- Water content,
- Grain size (sieve and hydrometer),
- Atterberg limits,
- Organic content,
- Specific gravity,
- Unit weight.

Chemical tests included:

- pH,
- Chloride content,
- Sulfate content.

Performance and strength tests under static conditions included:

- Consolidation,
- Unconfined compression (UC),
- Unconsolidated-undrained triaxial compression with pore pressure measurement (UU),
- Consolidated-undrained triaxial compression with pore pressure measurement (CU-Bar),
- Direct shear (DS),
- Modified Proctor compaction (Moisture–Density),
- California Bearing Ratio (CBR).

Performance and strength tests under dynamic conditions included:

- Resonant Column Torsional Shear (RCTS) tests.

Unit weight is also obtained from direct volume/mass measurements from miscellaneous tests. The number of tests performed is provided in Table 2.5-42.

Regulatory Guide 1.138 (USNRC, 2003b) provides guidance for laboratory testing procedures for certain specific tests, including related references. Laboratory testing of samples for the CCNPP Unit 3 subsurface investigation used commonly accepted, and updated practices such as more recent ASTM and EPA standards which are equivalent to the testing procedures referenced in the Regulatory Guide. Laboratory testing of samples for the CCNPP Unit 3

subsurface investigation did not rely upon non-U.S. or out-of-date versions of practices or standards.

The soil and rock laboratory tests listed in Regulatory Guide 1.138 (USNRC, 2003b) are common tests performed in most well-equipped soil and rock testing laboratories, and they are covered by ASTM standards. Additional test that are not covered in regulatory guidance were also performed for the CCNPP Unit 3 subsurface investigation (e.g., CBR tests to assess suitability of subgrade or fill materials for pavement, and RCTS tests, which were used in lieu of the resonant column test alone to obtain shear modulus and damping ratio values for a wide range of strains). Results of Cation Exchange Capacity tests are addressed with the groundwater chemistry data in Section 2.4.13.

The following subsections present a summary of the most relevant laboratory testing data. A recommendation of soil properties for use of foundation analysis and design is provided in Section 2.5.4.2.5. The complete set of laboratory test results is included in COLA Part 11J and COLA Part 11K. References are made to property data tables. Each table presents a line item for each of the soil layers and one line item for backfill.

2.5.4.2.4.1 Index Testing

Laboratory index tests and testing for determination of engineering properties were performed on selected samples. Laboratory test quantities are summarized in Table 2.5-42. Sample selection for testing was primarily based on the observed soil uniformity from the field classification, or conversely, the variation in material description based on logging in the field, in order to obtain a quantitative measure of the uniformity, or the variation, respectively.

Values of index testing are provided in Table 2.5-43 and Table 2.5-44. Figure 2.5-111 and Figure 2.5-112 provide a plot of Moisture Content and Atterberg limits as a function of elevation for the Powerblock and Intake Area respectively. Figure 2.5-113 and Figure 2.5-114 provide the plasticity chart for the Powerblock Area and Intake Area respectively.

2.5.4.2.4.2 Chemical Testing

Chemical testing consisted of pH, chloride, and sulfate tests, performed on selected soil samples collected during the COL exploration. The pH tests were performed on samples in both calcium chloride and deionized water. Seventy-seven sets of chemical tests were performed on soil samples collected from depths ranging from the ground surface to 104 ft below the ground surface. The test results are provided in the data report and summarized in Table 2.5-45.

2.5.4.2.4.3 Performance and Strength Tests under Static Conditions

Summary data of performance and strength properties are presented in the following tables:

- Table 2.5-46 and Table 2.5-47 provide the summary of the consolidation test results for the Powerblock Area and Intake Area respectively.

- Table 2.5-48 and Table 2.5-49 provide the summary of shear strength test results for the Powerblock Area and Intake Area respectively; the tests include unconsolidated-undrained triaxial, consolidated-drained triaxial, unconfined compression and direct shear.

- Table 2.5-50 provides the results of Modified Proctor tests for the samples tested for backfill. These samples have been selected based on performance under compaction tests and RCTS tests (Section 2.5.4.2.4.4).

2.5.4.2.4.4 Resonant Column Torsional Shear Tests (RCTS)

Testing was performed on resonant column and torsional shear (RCTS) equipment to measure the material properties (shear modulus and material damping in shear) of soil specimens. The RCTS equipment used is of the fixed-free type, with the bottom of the specimen fixed and shear stress applied to the top. Both the resonant column (RC) and torsional shear (TS) tests were performed in a sequential series on the same specimen over a shearing strain range from about 10^{-4} percent to about 1 percent, depending upon specimen stiffness. RCTS testing was performed on each soil specimen at selected confining pressures of 0.25, 0.5, 1, 2, and 4 times the estimated effective stress. Testing at each successive stage (i.e., confining pressure condition) occurred after the specimens were allowed to consolidate at each pressure step. At each level of shear strain amplitude, the shear modulus and material damping ratio were determined.

EPRI curves were fitted to the data to provide the recommendation (EPRI, 1990). For the Powerblock Area, the EPRI curve fitting is provided in the report "Reconciliation of EPRI and RCTS Results, Calvert Cliffs Nuclear Power Plant Unit 3" (Bechtel, 2007), and is included as COLA Part 11J. Section 2.5.4.2.5 provides a detailed discussion about the criteria for selection of strain dependant property curves based on generic curves and site specific laboratory information.

RCTS testing was performed for the samples in the Powerblock Area, the Intake Area, and Backfill. Table 2.5-51 provides a list of the RCTS samples tested and their index properties. The following samples were used for RCTS testing. The associated figure shows the results for that specific sample.

- Powerblock Area
  - B-437-6 (13.5′), Figure 2.5-115
  - B-301-10 (33.5′), Figure 2.5-116
  - B-305-17 (39.5′), Figure 2.5-117
  - B-404-14 (52.0′), Figure 2.5-118
  - B-401-31 (138.5′), Figure 2.5-119
  - B-401-67 (348.5′), Figure 2.5-120
  - B-401-48 (228.5′), Figure 2.5-121
  - B-301-78 (385.2′), Figure 2.5-122
  - B-306-17 (68.0′), Figure 2.5-123
  - B-409-15 (35.0′), Figure 2.5-124
  - B-404-22 (83.5′), Figure 2.5-125
  - B-401-42 (198.5′), Figure 2.5-126
  - B-409-39 (95.0′), Figure 2.5-127

- Intake Area
  - B-773-2 (15.9′), Figure 2.5-128
  - B-773-3 (27.0′), Figure 2.5-129
  - B-773-4 (37.0′), Figure 2.5-130
  - B-773-5 (47.0′), Figure 2.5-131
  - B-773-6 (57.0′), Figure 2.5-132
  - B-773-7 (66.1′), Figure 2.5-133
  - B-773-9 (87.0′), Figure 2.5-134
  - B-773-11 (107.0′), Figure 2.5-135

- B-773-13 (127.0'), Figure 2.5-136
- B-773-15 (147.0'), Figure 2.5-137

- Backfill
  - CR6 Composite (Bulk), Figure 2.5-138
  - GAB Composite (Bulk), Figure 2.5-139
  - CR6 Vulcan Average (Bulk), Figure 2.5-140

The backfill low strain RCTS test shear wave velocity measurements are used to aid in the development of the best estimate velocity profiles. These measurements are provided in Table 2.5-52. The confining pressures in the test ranged from 0.5 ksf to 17.3 ksf. Since the backfill will be placed near the surface in the uppermost 43.5 feet, and an increase in confining pressures is expected from building facilities, the relevant results correspond to the confining pressures reported in Table 2.5-52.

2.5.4.2.5 Soil Properties for Foundation Analysis and Design

Sections 2.5.4.2.2, 2.5.4.2.3, and 2.5.4.2.4 provide a comprehensive summary of the results from field and laboratory testing. This section uses the data retrieved and develops soil properties to be used for foundation analysis and design. The selection of properties takes into account the wealth of information generated from the field and laboratory, and is developed based on simplified soil profiles that are derived with the use of common geotechnical engineering principles and engineering judgment.

Figure 2.5-95 shows the general soil profile for the CCNPP Unit 3 Site. The profile is applicable throughout the site, though at the Intake Area, due to the difference in elevation and proximity to the shoreline, the Stratum I Terrace Sand and Stratum IIa Chesapeake Clay/Silt are not present. Instead, a man made fill sits on top of Layer IIb Chesapeake Cemented Sand. Figure 2.5-101 shows the conditions at the Intake Area.

The soil properties provided in this section are applicable to the soil layers portrayed by Figure 2.5-95. The settlement analysis for the CCNPP3 Unit 3 Site accounts for a three-dimensional representation of the subsurface conditions. Details of the settlement analysis are provided in Section 2.5.4.10.

2.5.4.2.5.1 General Classification and Index Properties

Stratum I soils are characterized, on average, as non-plastic with an average fines content (materials passing No. 200 Sieve) of 20 percent. Grain size analyses indicated that these soils are primarily fine or fine-medium sands. The Unified Soil Classification System (USCS) designations were poorly-graded sand/silty sand, silty sand, well-graded sand, clayey sand, clay of high plasticity, silt, clay, and silt with high plasticity, with the predominant classifications of SP-SM and SM. The often plastic and fine-grained soil classifications are from the interbeds within this stratum.

Stratum IIa soils are characterized as medium-high plasticity clays. Their predominant USCS designation was clay of high plasticity and silt of high plasticity (CH and MH); sometimes with silty sand, silty sand to clayey sand, and organic clay. The organic designation was based on laboratory (liquid limit) tests. With less than 1 percent organic matter on average, and observations during sampling, these soils are not considered organic.

Stratum IIb soils are primarily medium-fine sands. The USCS designations were silty sand, poorly-graded sand to silty sand, clayey sand, silt, silt of high plasticity, clay of high plasticity,

clay, and organic clay. The predominant classifications, however, were silty sand, clayey sand, and poorly-graded sand to silty sand (SM, SC, and SP-SM).

Stratum IIc soils are characterized as high plasticity clay and silt, with an average PI = 50. Their predominant USCS designation was clay of high plasticity and silt of high plasticity (CH and MH), however, sometimes silty sand, clay, and organic clay classifications were indicated. Based on observations during sampling, the organic soil designation based on laboratory (Liquid Limit) testing is not representative of these soils, and therefore, they are not considered organic soils.

Stratum III soils are characterized as sand of high plasticity. Their predominant USCS designations were clayey sand and silty sand (SC and SM), although clay of high plasticity and silt of high plasticity were also indicated.

Table 2.5-53 provides the USCS classification of soils and index properties for each stratum. Unit weights were determined based on numerous unit weight tests performed on specimens during different types of tests such as unit weight, triaxial, RCTS. The USCS classification is based on the predominant classification of tested samples.

2.5.4.2.5.2 Chemical Properties

Table 2.5-45 provides the data obtained for the CCNPP Unit 3 site. Guidelines for interpretation of chemical test results are provided in Table 2.5-54, based on the following consensus standards, API Recommended Practice 651 (API, 2007), Reinforced Soil Structures (FHWA, 1990), Standard Specification for Portland Cement (ASTM 2005b), Manual of Concrete Practice (ACI, 1994), and Standard Specification for Blended Hydraulic Cement (ASTM, C595). From the average values of available results shown in Table 2.5-45, the field resistivity surveys in Table 2.5-37, and guidelines in Table 2.5-54, the following conclusions were developed:

Attack on Steel (Corrosiveness): The resistivity test results indicate that all soils are "little corrosive," except for Stratum IIc Chesapeake Clay/Silt that may be "little to mildly corrosive." Based on the chloride contents typically being below 10 ppm, all soils are essentially non-corrosive. The pH results, however, indicate that all soils are "corrosive to very corrosive," except for Stratum IIc Chesapeake Clay/Silt that may be "mildly corrosive." Few chemical test results are available from Stratum IIc; however, that should be of no special importance because no Seismic Category I structure (or piping) is anticipated within these soils. The pH data dominate the corrosive characterization of the soils. Nevertheless, all natural soils at the site will be considered corrosive to metals, requiring protection if placed within these soils. Protection of steel against corrosion may include cathodic protection, or other measures. Additional pH testing on groundwater samples obtained from the observation wells (refer to Section 2.4.13) indicate pH values of average 5.5, 6.8, and 7.1 for wells screened in Stratum I, Stratum IIa, and Stratum IIb soils, respectively. Except for values obtained in groundwater associated with Stratum I soils indicating "corrosive" conditions, remaining pH data from other strata only indicate "mildly corrosive" conditions.

Attack on Concrete (Aggressiveness): The sulfate test results in all tested soils indicate a "severe" potential for attack on concrete, except for Stratum IIc Chesapeake Clay/Silt that may cause a "moderate" attack. As noted above, few chemical test results are available for Stratum IIc; however, based on the available information, Seismic Category I structures (or piping) may encounter Stratum IIc soils in the Intake Area. Nevertheless, all natural soils at the site will be considered aggressive to concrete, requiring protection if placed within these soils.

2.5.4.2.5.3 Performance Properties for Settlement Analysis under Static Conditions

The required performance properties under static conditions are the following:

- Cr - Recompression index,
- Cc - Compression index,
- eo - Initial void ratio,
- p'_c - Preconsolidation pressure,
- OCR - Overconsolidation ratio,
- c_v - Coefficient of consolidation,
- k - Permeability (hydraulic conductivity).

The selected values for the consolidation properties are based on average parameters obtained from laboratory testing. Permeability is obtained from well field tests and development and calibration of hydrogeologic models. Details of the tests and models are provided in Sections 2.4.12 and 2.4.13. Hydraulic conductivity for backfill is based on laboratory results of tests performed on bulk samples. Table 2.5-55 provides the soil performance properties for each stratum.

2.5.4.2.5.4 Strength Properties under Static Conditions

The required strength properties under static conditions are the following:

- N - Standard Penetration Test (SPT) Resistance (N);
- c′ - Cohesion under drained conditions;
- Φ′ - Friction angle under drained conditions;
- c - Cohesion under undrained conditions;
- Φ - Friction angle under undrained conditions;
- s_u - Undrained shear strength.

Table 2.5-30 provides the SPT test data. The average SPT N corrected values are used.

For completion purposes and in order to satisfy the documentation requirements of RG 1.206, Table 2.5-56 provides the strength properties according to the laboratory test results for each stratum.

2.5.4.2.5.5 Elastic Properties under Static Loading

The required elastic properties of soil under static loading are the following:

- E - Elastic modulus (large strain).
- $E_{u/r}$ - Unload/Reload Elastic modulus.
- $E_{u/r}$/E- - Ratio of to unload/reload Elastic modulus to Elastic modulus.
- G - Shear modulus (large strain).
- *v* - Poisson's ratio.

The elastic moduli significantly impact settlement estimates and therefore numerous methods have been applied to estimate these parameters. They are determined based heavily on field tests as discussed in Section 2.5.5.2.5.3. The Shear modulus (G) and elastic modulus (E) are estimated for each soil strata using the following three criteria:

1. Geophysical test results: Shear wave velocities (Vs), P-wave velocities (Vp), and Poisson's ratios from borehole surveys are used to estimate the shear modulus (G) and Elastic modulus (E) at depth intervals between 1.6 ft and 1.7 ft below the ground surface. The geophysical survey data are grouped based on the soil strata. Average G and E values and their corresponding standard deviations of each soil layer are estimated. The G and E values estimated based on the geophysical tests correspond to very low strain values; therefore, they are reduced to account for the material's strain softening due to higher strains. The moduli are determined from elasticity theory equations:

   $G = \rho V_s^2$

   $E = 2G(1+v)$

   The value of the static Poisson Ratio is adopted from typical values reported in the literature (Salgado, 2008).

2. Pressuremeter testing data obtained from two borehole locations are used to calculate the shear modulus (G) and elastic modulus (E) for each soil layer. Results from Pressuremeter testing correspond to high strain values, therefore, it is expected that the elastic modulus values fall in the lower bound range.

3. Elastic modulus is calculated using different correlations as a function of corrected SPT N-values and undrained shear strength (su):

$E = 18N_{60}$	Coarse grained Materials (Davie, et al.,1988)
$E = \beta_0\sqrt{OCR} + \beta_1 N_{60}$	Coarse grained materials (Coduto, 2001)
$E = 450s_u$	Fine grained materials (Davie, et al., 1988)
$E = 2G(1 + v)$, $G = s_u$	Fine grained materials (Senapathy, et al., 2001)

Table 2.5-57 provides the estimates of elastic modulus using the previously listed criteria.

The unload/reload modulus ($E_{u/r}$) is required for the estimation of heave and of settlement between excavation and reload. The pressuremeter test data were used to estimate the ratio of unload/reload modulus. The data provided by Table 2.5-40 and Table 2.5-41 indicate that the unload/reload values are consistently above 3.0, with average values above 4.0 and in many instances higher than 6.0. Due to the uncertainty involved in settlement computations and the uncertainty in relating pressuremeter data to actual field conditions it is prudent to adopt a conservative approach. Therefore, the maximum value for the $E_{u/r}/E$ ratio adopted is 3.0 except when the minimum recorded value for a given layer is higher than 3.0. In those instances the minimum value of $E_{u/r}/E$ is adopted. Table 2.5-58 shows the minimum, average, and maximum values of the $E_{u/r}/E$ ratio reported from pressuremeter testing. Table 2.5-59 provides the static elastic properties for each stratum.

By establishing a limit of 3.0, the previous criterion is conservative for the estimation of total settlements. By using a larger value than 3.0 whenever $(E_{u/r}/E)_{min}$ is larger, the previous criterion is conservative for the estimation of tilt. This approach accounts for the asymmetric topographic conditions and the effect that they have on the unloading throughout the footprint of the foundation. Additional explanation is provided in the settlement analysis in Section 2.5.4.10.

2.5.4.2.5.6 Earth Pressure Coefficients

Active, passive, and at-rest static earth pressure coefficients, K_a, K_p, and K_0, respectively, were estimated assuming frictionless vertical walls and horizontal backfill using Rankine's Theory and based on the following relationships (Lambe, et al., 1969):

Active Earth Pressure Coefficient: $K_a = \tan^2\left(45 - \frac{\Phi'}{2}\right)$

Passive Earth Pressure Coefficient: $K_p = \tan^2\left(45 + \frac{\Phi'}{2}\right)$

At Rest Earth Pressure Coefficient: $K_0 = 1 - \sin(\Phi')$

The values for earth pressure coefficients for each stratum are provided in Table 2.5-60.

2.5.4.2.5.7 Coefficient of Friction

Values for the coefficient of friction between the soil and the material it is bearing against (concrete) are provided in Section 3.8 Table 3.8-1.

2.5.4.2.5.8 Low Strain Dynamic Properties

The low strain dynamic properties are the basis to develop the Best Estimate soil profile for the purposes of site amplification analysis. The following properties are discussed:

- γ - Moist unit weight;
- G_o - Low strain shear modulus;
- V_S - Shear wave velocity;

- V_p - Compression wave velocity;
- *v* - Poisson's Ratio;

The moist unit weight is obtained directly from the index properties. Based on all 10 suspension P-S velocity measurements, an average V_s profile was estimated for the upper 400 ft. Poisson's ratio values were determined based on the V_p and V_s measurements. The measurement of dynamic properties reflects the conditions for the approximately upper 400 ft of the site, or to about El. -317 ft. Information on deeper soils, as well as bedrock, was obtained from the available literature.

Shear wave velocity measurements were made using a seismic cone at ten soundings (C-301, C-304, C-307, C-308, C-401, C-404, C-407, C-408, C-724, and C-725). The measurements were made at 3.3 ft (1 m) intervals. At several locations, the soils required pre-drilling to advance the cone, particularly in the cemented zones. Although the deepest CPT sounding was about 142 ft, the combined measurements provided information for the upper approximately 200 ft of the site soils, extending to about elevation -80 ft. Further penetration was not possible due to continued cone refusal. The CPT results are found to be relatively consistent with the suspension P-S velocity logging results. The variations in different soils that were observed in the suspension P-S velocity logging data are readily duplicated by the CPT results, including the peaks associated with cemented or hard zones. Further details on testing and the results are provided, in tables and graphs, in COLA Part 11J and COLA Part 11K.

Given the similarity between the suspension P-S velocity logging and the seismic CPT results, and that the CPT results only extend to limited depth, the suspension P-S velocity logging results were used as the basis for determination of shear wave velocity profile for the site. It is also well established that the P-S logging technique is specifically designed to measure wave velocities and is a superior measurement technique when compared to the CPT.

The best estimate of the shear and compression shear wave velocity profiles are presented by the following four figures:

1. Figure 2.5-155, showing the best estimate velocity profiles in the Powerblock Area;
2. Figure 2.5-156, showing the best estimate velocity profiles in the Powerblock Area, after placement of fill;
3. Figure 2.5-157, showing the best estimate velocity profiles in the Intake Area;
4. Figure 2.5-158, showing the best estimate velocity profiles in the Intake Area, after placement of fill;

In these four figures, 0 depth corresponds to site grade, El 83 ft.

The following apply to the best estimate profiles and the previous figures:

- The figures indicate the position of the groundwater. For the Powerblock Area, the groundwater level at the site has an approximate depth of 16 ft. Once construction is finalized, due to new drainage patterns the expected depth of the groundwater is 30 ft. A detailed discussion related to groundwater is provided in Section 2.4.12.
- The shear wave velocity of the fill has been estimated by adjusting the low strain dynamic properties measured by the RCTS tests to the field conditions. Table 2.5-52

provides the RCTS test results for the range of confining pressures that will prevail after backfill placement. Based on the results, a three-step velocity profile is proposed, as shown by the four previously listed figures. The shear wave velocity for the backfill below the EPGB is 900 fps. This value is below the 1,000 fps specified in the U.S. EPR FSAR. This constitutes a departure. The lower shear wave velocity will be used in the soil-structure interaction analysis in section 3.7.

- For the Intake Area, the best estimate is based in the P-S logging measurement of boring B-773. The shear wave velocity in Stratum II-C, Chesapeake Clay/Silt is consistent with the measurements at the Powerblock Area, though slightly lower with a value of 1150 fps, as opposed to 1250 fps. The measurement at B-773 reached a depth of approximately 150 ft. The values for deeper strata are taken from the best estimate profile in the Powerblock Area.

- The development of the deep soil column, location of bedrock, and location of the 9,200 fps horizon was based on the study of geologic conditions and deep well exploration records in the site vicinity. A detailed discussion with the basis for parameter selection is provided in the following paragraphs.

To develop the deep soil velocity profile, various geologic records were reviewed and communication made with staff at the Maryland Geological Survey, the United States Geological Survey, and the Triassic-Jurassic Study Group of Lamont-Doherty Earth Observatory, Columbia University. The results of this work, and associated references, are addressed in Section 2.5.1. In summary, a soil column profile was prepared, extending from the ground surface to the top of rock. Soils below 400 ft consist of Coastal Plain sediments of Eocene, Paleocene, and Cretaceous eras, extending to an estimated depth of about 2,500 ft below the ground surface. These soils contain sequences of sand, silt, and clay. Given their geologic age, they are expected to be competent soils, consolidated to at least the weight of the overlying soils.

Several available geologic records were also reviewed in order to obtain information on both the depth to bedrock and the bedrock type, as addressed in Section 2.5.1. Accordingly, the estimated depth to bedrock in the proximity of the site is about 2,555 ft, which is consistent with the depth of 2,500 ft reported in the CCNPP Units 1 and 2 UFSAR (BGE, 1982). Top of rock elevation at the CCNPP site is estimated, and adopted, at approximately El. -2,446 ft which corresponds to a depth of about 2,531 ft. Regional geologic data were also researched for information on bedrock type. This revealed various rock types in the region, including Triassic red beds and Jurassic diabase, granite, schist, and gneiss. However, only granitoid rocks (metamorphic gneiss, schist, or igneous granitic rocks), similar to those exposed in the Piedmont, could be discerned as the potential regional rock underlying the CCNPP Unit 3 site. For the purpose of rock response to dynamic loading, granitoid was considered as the predominant rock type at the CCNPP Unit 3 site.

With the geology established below a depth of 400 ft, velocity profiles also needed to be established. The velocity data were found through a research of available geologic information for the area. From the Maryland Geological Survey data, two sonic profiles were discovered for wells in the area that penetrated the bedrock, one at Chester, MD (about 38 miles north the site, (USGS, 1983) and another at Lexington Park, MD (about 13 miles south of the site, (USGS, 1984); their locations relative to the site are shown in Figure 2.5-141. These two sonic profiles were digitized and converted to shear wave velocity, based on a range of Poisson's ratios for the soil and the rock. The two Vs profiles for Chester and Lexington Park are plotted versus elevation, with the superimposed measured velocity profile from the upper 400 ft at the CCNPP site, as shown in Figure 2.5-142 and Figure 2.5-143.

The bottom of the measured Vs profile in the upper 400 ft fits well with the Chester data for which a soil's Poisson's ratio = 0.4 was used, whereas, in the case of Lexington Park data, the bottom of the measured data in the upper 400 ft fits well with the profile for which the soil's Poisson's ratio = 0.45 was used. Geologically, the soils at the two sites are quite comparable. (Refer to Section 2.5.1 for more details on site geology). The reason for the different "fits" is not clear. However, based on actual Poisson's ratio measurement at another deep Coastal Plain site (SNOC, 2006), where suspension P-S velocity logging measurements extended to a depth of over 1,000 ft, a Poisson's ratio of 0.4 was adopted to represent the soil conditions at the CCNPP site, given the geologic similarity of the soils at both sites.

If a Poisson's ratio of 0.4 is used to convert the Chester sonic log to a shear wave velocity log, this shear wave velocity log fits well with the bottom of the site Vs profile measured with suspension logging at comparable elevations. A similarly good fit is obtained for the Lexington Park data when a Poisson's ratio of 0.45 is used.

Although geologically the soils at the Chester and Lexington Park sites are quite comparable, there are reasons why the soils at the elevation of the bottom of the site profile could have slightly different Poisson's ratio values, e.g., the Lexington Park soils may be more cohesive than the Chester soils. Nevertheless, a single Poisson's ratio value was needed for below the bottom of the measured profile for the CCNPP site. Based on actual Poisson's ratio measurements at another deep Coastal Plain site (SNOC, 2006), where suspension P-S velocity logging measurements extended to a depth of over 1,000 ft, a Poisson's ratio of 0.4 was adopted to represent the soil conditions at the CCNPP site, given the geologic similarity of the soils at CCNPP site and the other Coastal Plain site.

Both profiles (particularly the Chester profile) include significant "peaks," giving a visual impression that the difference in the two profiles may be large. To further look at the variation in these two profiles based on the adopted Poisson's ratio of 0.4, both profiles were averaged over 100-ft intervals along the entire depth to "smooth" the peaks. The original profiles for the two sites (based on a Poisson's ratio of 0.4) and the 100-ft interval average for the two measurements are shown in Figure 2.5-144. A comparison of the two 100-ft interval averages show that once the effect of the "peaks" are removed, the two profiles are relatively similar for the same Poisson's ratio of 0.4. Finally, an average of the 100-ft interval data for both sites was taken. This latter profile was compared with an available measured profile in deep Coastal Plain soils (SNOC, 2006); its similarity to the measured profile is indicative of its appropriateness for the geologic setting, as shown in Figure 2.5-145.

Similar to the soil profiles addressed above, two velocity profiles were also available for bedrock, based on the sonic data from Chester (USGS, 1983) and Lexington Park (USGS, 1984) sites. Rock was encountered at different depths at these two sites; however, the elevation difference in top of rock is only 11 ft between the two sites. The bottom portions of Figure 2.5-142 and Figure 2.5-143 (near the soil-rock interface) are enlarged for clarity and are shown in Figure 2.5-146 and Figure 2.5-147 for the Poisson's ratios shown.

A comparison of the shear wave velocity profiles in bedrock for the two sites reveals different velocity responses, regardless of the Poisson's ratio values considered. The Chester profile is somewhat transitional and does not approach 9,200 ft/sec at termination of measurements. The Lexington Park profile is rather abrupt, and is in excess of 9,200 ft/sec. The difference in these two responses is found in the geologic description of the bedrock at the two sites. At Chester, the bedrock is described as more the typical, regional metamorphic rock (granitic, schist, or gneiss). At Lexington Park, the bedrock is described as an intrusive diabase. Based on further evaluation of regional bedrocks, as addressed in Section 2.5.1, the following description was established for the CCNPP Unit 3 site: bedrock is probably granitoid rock, less likely to be

sandstone or shale, even less likely to be diabase. Accordingly, the Lexington Park profile (that is for diabase rock) was excluded from further consideration.

Closer examination of the Chester bedrock velocity results reveal that the velocities are rather "insensitive" to the assumption of Poisson's ratio, as is evident in Figure 2.5-146. For all practical purposes, the assumption of Poisson's ratio of 0.2, 0.25, or 0.3 for the bedrock renders identical velocity profiles. The responses also follow a particular velocity gradient. For a Poisson's ratio of 0.3 for the rock, one could assume a bedrock velocity starting at some value at the soil-rock interface, transitioning to the 9,200 ft/sec at some depth. This approach was followed, as shown in Figure 2.5-148, showing the shear wave velocity profile versus elevation in bedrock. From this figure, starting at Vs of 5,000 ft/sec at the soil-rock interface, the 9,200 ft/sec velocity is reached within about 20 ft depth into rock. Many variations were tried (varying the starting velocity at soil-rock interface, varying the slope of transitioning velocity profile, transition in "slope" or in "step," different Poisson's ratios, etc.); the end result appeared relatively unchanged, i.e., the 9,200 ft/sec velocity is achieved within a short distance of penetrating the rock. On this basis, the "stepped" velocity gradient shown in Figure 2.5-148 was adopted to define the velocity profile for the rock. The recommended velocity profile for bedrock begins with Vs = 5,000 ft/sec at the soil-rock interface, as indicated from the sonic data, transitioning to 9,200 ft/sec in the steps shown in Figure 2.5-148. The top of rock elevation was adjusted to conform to the estimated rock elevation for the CCNPP Unit 3 site, or El. -2,446 ft. (Refer to Section 2.5.1).

Accordingly, based on measured data in the upper 400 ft and data obtained from available literature in areas surrounding the CCNPP site, the shear wave velocity profile in soils at the CCNPP Unit 3 site is shown in Figure 2.5-155 and Figure 2.5-156. For the Intake Area the profiles are provided in Figure 2.5-157 and Figure 2.5-158. The profiles in the figures are considered as the design shear wave velocity profiles. Tabular data related to velocity profiles is provided in Table 2.5-61 and Table 2.5-62 for the Powerblock and Intake Area respectively.

2.5.4.2.5.9 Strain Dependant Properties

The strain dependant properties for the CCNPP3 project are developed by fitting generic curves to the site specific data reported by RCTS tests. EPRI curves from EPRI TR-102293 were used as generic curves (EPRI, 1993). EPRI "sand" curves were used for predominately granular soils and "clay" curves were used for predominately clay soils based on estimated PI values. The EPRI "sand" curves cover a depth range up to 1,000 ft. Since soils at the CCNPP site extend beyond 1,000 ft, similar curves were extrapolated from the EPRI curves, extending beyond the 1,000-ft depth, to characterize the deeper soils. For instance, the "1,000-2,000 ft" curve was extrapolated by "off-setting" this curve by the amount shown between the "250-500 ft" and "500-1,000 ft" curves in EPRI TR-102293 (EPRI, 1993). To assess the adequacy of EPRI curves for the deeper soils, these were compared with the set of curves derived from the RCTS results for the upper soils, as shown in Figure 2.5-222. The comparison indicates that:

- Marlboro Clay and Patuxent/Arundel Clay Curves: the EPRI curves are identical and fall nearly half-way between the RCTS-based curves for the Stratum I Sand (Curve 3) and Strata II and III soils (Curve 2) in their G/Gmax relationship and closer to Curve 3 in their damping relationship. Based on the available RCTS results, it is inconceivable for these soils at such great depths (and expected high strength) to behave as "softly" as Stratum I Sand (Curve 3) which is at relatively shallow depths and primarily non-plastic. Therefore, as a minimum, the Marlboro and Patuxent/Arundel clays are expected to behave closer to that represented by Curve 2. On this basis. Curve 2 is a reasonable representation for these soils and is used for the dynamic characterization of Marlboro Clay and Patuxent/Arundel Clay.

- Aguia/Brightseat Sand and Patapsco Sand: the EPRI curves are nearly identical and follow Curve 2 closely in their G/Gmax and damping relationship. Based on the RCTS results, and given their depths, these soils are expected to behave somewhere in the region represented by Curves 1 and 2, and possibly closer to Curve 1. Given that a number of the RCTS tests on sandy soils banded closely and were represented by Curve 2, the deeper sandy soils of the Aguia/Brightseat and Patapsco are expected to produce relationships that are mimicked by Curve 2, as a minimum. On this basis., Curve 2 is a reasonable representation for these soils and is used for the dynamic characterization of Aguia/Brightseat Sand and Patapsco Sand.

The calculated maximum strains based on the initially adopted EPRI curves for soils below 1000 feet are in the 10^{-3}% to 10^{-2}% range for the 1E-4 and 1E-5 rock input motions, respectively, as shown in Figure 2.5-223. At such strain levels, the difference between the EPRI-based and RCTS-based curves are minor to insignificant as evident in Figure 2.5-222. Therefore the potential impact of variation of the extrapolated curves on the site response analysis is negligible and is conservatively covered by the randomization of the soil column and strain dependant properties as described in Section 2.5.2.

EPRI curve selection for the upper 400 ft of the site soils was based on available soil characterization data from the site investigation.

A detailed description of the RCTS curve fitting process is provided in the report "Reconciliation of EPRI and RCTS Results, Calvert Cliffs Nuclear Power Plant Unit 3" (Bechtel, 2007), and is included as COLA Part 11J.

The strain dependent properties are first developed for the Powerblock Area. After fitting EPRI curves to the RCTS data in the Powerblock, the resulting curves were used as a starting point to fit the data of the Intake Area and develop properties for that zone. The damping ratio curves are truncated at 15 percent, consistent with the maximum damping values that will be used for the site response analysis. The backfill RCTS results were used to develop strain dependent properties following the same fitting approach and using EPRI curves for granular soils. The following tables and figures provide the strain dependant properties for the CCNPP project:

- Table 2.5-63 and Figure 2.5-159 provide the properties for the Powerblock Area.
- Table 2.5-64 and Figure 2.5-160 provide the properties for the Intake Area.
- Table 2.5-65 and Figure 2.5-161 provide the properties for Backfill.

Bedrock Properties

The two velocity profiles for the Chester and Lexington Park sites (Figure 2.5-146 and Figure 2.5-147), indicate the presence of "hard" rock (identified with V_s = 9,200 ft/sec). Hard rocks typically exhibit an elastic response to loading, with little, if any, change is stiffness properties. For the range of shear strains anticipated in the analysis (10^{-4} to 1 percent range), essentially no shear modulus reduction is expected; therefore, for rocks at the site, the estimated shear moduli should remain unaffected, given the relatively high velocity observed from the area rocks.

Hard rocks are considered to have damping, but it is not strain dependent. A damping ratio of 1 percent has been used for bedrock at other sites, e.g., for the Vogtle Early Site Permit application (SNOC, 2006) in order to obtain compatibility with soils above bedrock. Experience on similar work has indicated that using damping ratios of 0.5 percent, 1 percent, 2 percent,

and 5 percent produces essentially identical results (Dominion, 2006). Therefore, for CCNPP Unit 3, a damping ratio of 1 percent was adopted for the bedrock. Bedrock shear modulus was considered to remain constant, i.e., no degradation, in the shear strain range of 10^{-4} percent to 1 percent.

The rock unit weight was estimated from the available literature (Deere, et al., 1996), as 162 pcf.

2.5.4.3 Foundation Interfaces

Subsurface profiles (at the corresponding locations shown in Figure 2.5-92, Figure 2.5-93, and Figure 2.5-94) depicting the inferred subsurface Stratigraphy with the location of the plant's facilities are presented in the following figures:

- Subsurface and excavation profile Powerblock Area A-A': Figure 2.5-149.
- Subsurface and excavation profile Powerblock Area B-B': Figure 2.5-150.
- Subsurface and excavation profile Powerblock Area C-C': Figure 2.5-151.
- Subsurface and excavation profile Powerblock Area D-D': Figure 2.5-152.
- Subsurface and excavation profile Powerblock Area E-E': Figure 2.5-153.
- Subsurface and excavation profile Powerblock Area F-F': Figure 2.5-154.

Excavation and dewatering issues are addressed in Section 2.5.4.5. Settlement and bearing capacity are discussed in Section 2.5.4.10. Slope stability analysis is discussed in Section 2.5.5.

2.5.4.4 Geophysical Surveys

Section 2.5.4.2.2 provides a description of the geophysical surveys performed.
Section 2.5.4.2.5.8 provides a detailed description of the interpretation and recommendation of properties for dynamic soil profiles. The main goal of the surveys was to gather the information to provide a recommendation for velocity profiles underneath foundation footprints.

The best estimate of the shear and compression shear wave velocity profiles are presented by the following four figures:

1. Figure 2.5-155, showing the best estimate velocity profiles in the Powerblock Area.
2. Figure 2.5-156, showing the best estimate velocity profiles in the Powerblock Area, after placement of fill.
3. Figure 2.5-157, showing the best estimate velocity profiles in the Intake Area.
4. Figure 2.5-158, showing the best estimate velocity profiles in the Intake Area, after placement of fill.

2.5.4.5 Excavation and Backfill

Sections 2.5.4.5.1 through 2.5.4.5.4 are added as a supplement to the U.S. EPR FSAR.

2.5.4.5.1 Source and Quantity of Backfill and Borrow

A significant amount of earthwork is anticipated in order to establish the final site grade and to provide for the final embedment of the structures. It is estimated that approximately 3.5 million cubic yards (cyd) of materials will be moved during earthworks to establish the site grade.

The materials excavated as part of the site grading are primarily the surficial soils belonging to the Stratum I Terrace Sand. To evaluate these soils for construction purposes, 20 test pits were excavated at the site. The maximum depth of the test pits was limited to 10 ft. Results of laboratory testing on the bulk samples collected from the test pits for moisture-density and other indices are included in COLA Part 11J and Part 11K. The results clearly indicate that there are both plastic and non-plastic soils included in Stratum I soils, including material designated as fill. These fill soils are predominantly non-plastic. A similar observation was made from the borings that extended deeper than the test pits. Their composition consists of a wide variety of soils, including poorly-graded sand to silty sand, well graded sand to silty sand, clayey sand, silty sand, clay, clay of high plasticity, and silt of high plasticity, based on the USCS. The highly plastic or clay portion of these soils will not be suitable for use as structural fill, given the high percentage of fines (average 59 percent) and the average natural moisture content nearly twice the optimum value of 10 percent. The remaining sand or sandy portion will be suitable; however, these materials are typically fine (sometimes medium to fine) sand in gradation, and likely moisture-sensitive that may require moisture-conditioning. Additionally, the suitable portions of the excavated soils are used for site grading purposes, with very little, if any, remaining to be used as structural fill.

It is estimated that about 2 million cyd of structural backfill are needed. Therefore, structural fill will be obtained from off-site borrow sources. An off-site borrow source of structural fill for CCNPP Unit 3 has been identified, Vulcan Quarry in Havre de Grace, Maryland. Details of the engineering and chemical properties of the backfill are provided in Section 2.5.4.2.4.

2.5.4.5.2 Extent of Excavations, Fills, and Slopes

In the area of CCNPP Unit 3, the current ground elevations range from approximately El. 50 ft to El. 120 ft, with an approximate average El. 88 ft. The finished grade in CCNPP Unit 3 Powerblock Area ranges from about El. 75 ft to El. 85 ft; with the centerline of Unit 3 at approximately El. 85 ft. Earthwork operations are performed to achieve the planned site grades, as shown on the grading plan in Figure 2.5-162. All safety-related structures are contained within the outline of CCNPP Unit 3, except for the water intake structures that are located near the existing intake basin, also shown in Figure 2.5-162. Seismic Category I structures with their corresponding foundation are:

- Nuclear Island Common Basemat (El. 41.5).
- Emergency Power Generating Building (El. 76).
- Essential Service Water Buildings (El. 61.0).
- Ultimate Heat Sink Makeup Water Intake Structure (El. -26.5).

Excavation profiles (at the corresponding locations shown in Figure 2.5-92, Figure 2.5-93, and Figure 2.5-105) are shown in:

- Subsurface and excavation profile Powerblock Area A-A': Figure 2.5-149.
- Subsurface and excavation profile Powerblock Area B-B': Figure 2.5-150.
- Subsurface and excavation profile Powerblock Area C-C': Figure 2.5-151.
- Subsurface and excavation profile Powerblock Area D-D': Figure 2.5-152.
- Subsurface and excavation profile Powerblock Area E-E': Figure 2.5-153.
- Subsurface and excavation profile Intake Area F-F': Figure 2.5-154.

These figures illustrate that excavations for foundations of Seismic Category I structures will result in removing Stratum I Terrace Sand and Stratum IIa Chesapeake Clay/Silt in their entirety, and will extend to the top of Stratum IIb Chesapeake Cemented Sand, except in the Intake Area. In the Intake Area, the foundations are supported on Stratum IIc soils, given the interface proximity of Strata IIb and IIc.

The depth of excavations to reach Stratum IIb is approximately 40 ft to 45 ft below the final site grade in the Powerblock Area. Since foundations derive support from these soils, variations in the top of this stratum were evaluated, reflected as elevation contours for the top of Stratum IIb in CCNPP Unit 3 and in CLA areas, as shown in Figure 2.5-163. The variation in top elevation of these soils is very little, approximately 5 ft or less (about 1 percent) across each major foundation area. The extent of excavations to final subgrade, however, is determined during construction based on observation of the actual soil conditions encountered and verification of their suitability for foundation support. Once subgrade suitability in Stratum IIb soils is confirmed, the excavations are backfilled with compacted structural fill or, if necessary, lean concrete is placed in lieu of structural fill.

The properties of lean concrete are controlled through controlling its compressive strength. A minimum 28-day compressive strength of 2,500 psi is used. Properties of lean concrete are controlled during construction. Detailed project specifications include requirements for mix design, placement, sampling and testing, frequency of testing, applicable standards, and acceptance criteria. Lean concrete may be used in lieu of structural fill in the following cases: below the foundations as leveling mats, to counteract seepage forces at the bottom of the excavation and to help preserve soil subgrade integrity, and in restricted spaces to expedite construction.

Subsequent to foundation construction, the structural fill is extended to the final site grade, or near the final site grade, depending on the details of the final civil design for the project. Compaction and quality control/quality assurance programs for backfilling are addressed in Section 2.5.4.5.3.

To confirm that the excavation has reached the load bearing Stratum IIB, the Geotechnical Engineer will develop a chart that provides a correlation between SPT N-values and the Dynamic Cone Penetration (DCP) values obtained from ASTM STP 399 (ASTM, 1966). ASTM STP 399 provides a correlation between the DCP and SPT; however, using site specific information will increase the accuracy of the correlation. This chart will be developed with the SPT data that has been collected to date and correlated with DCP values after applying a correction for the overburden. Additional testing and correlation will be performed after

excavation has begun and will be completed when the Stratum IIb-Chesapeake Cemented Sand is near the surface. In addition, once Stratum IIb-Chesapeake Cemented Sand has been exposed, as identified by the Geotechnical Engineer, grain size analysis will be performed and the material will be photographed with appropriate color coding.

DCP testing by means of ASTM D7380-08 (ASTM, 2008b) will be utilized due to its ease of use in the field. Once the design elevation is reached during excavation, DCP testing will be performed to characterize the subsurface conditions. In addition, samples will be collected for grain size analysis. The suitability of the design elevation will be determined based on DCP test correlation, grain size, and the soil color code. The grain size and soil color will help differentiate between Stratum IIa - Chesapeake Clay/Silt and Stratum IIb - Chesapeake Sand.

Structural backfill placement will not begin until the unsuitable material of the final excavation grade has been verified and approval received from the Geotechnical Engineer. The Geotechnical Engineer will be responsible for final approval of the foundation soils. A geologist will map the exposed stratum. Photos and videotape of the exposed stratum will be collected for documentation. Finally, acceptance will be documented on a Final Foundation Acceptance form that is completed by the responsible parties and included in the report.

Permanent excavation and fill slopes, created due to site grading, are addressed in Section 2.5.5. Temporary excavation slopes, such as those for foundation excavation, are graded on an inclination not steeper than 2:1 horizontal:vertical (H:V) or even extended to inclination 3:1 H:V, if found necessary, and having a factor of safety for stability of at least 1.30 for static conditions.

Excavation for the Ultimate Heat Sink Makeup Water Intake Structure is different than that for other CCNPP Unit 3 structures, as shown in Figure 2.5-154. Given the proximity of this excavation to the Chesapeake Bay, this excavation is made by installing a sheetpile cofferdam that not only provides excavation support but also aids with the dewatering needs. This is addressed further in Section 2.5.4.5.4.

Excavation for Seismic Category I electrical duct banks and pipes in the Powerblock Area involve the removal of Stratum I Terrace Sand in its entirety to the top of Stratum IIa Chesapeake Clay/Silt. Such excavation is required since the Stratum I layer has potential for liquefaction, as indicated in Section 2.5.4.8.

2.5.4.5.3 Compaction Specifications

Testing of structural backfill is described in Section 2.5.4.2.4. For foundation support and backfill against walls, structural fill should be granular in nature, with well-graded sand, gravel or crushed gravel, and typically should not contain more than 10 percent by weight of material passing No. 200 sieve and no less than 95 percent by weight passing the 3/4-inch sieve. The maximum allowable aggregate size shall be 1 inch. Gradation shall be determined in accordance with ASTM D422 and D1140. Structural fill should consist of durable materials free from organic matters or any other deleterious or perishable substances, and of such a nature that it can be compacted readily to a firm and non-yielding state.

Structural fill will be compacted at a moisture content of ±3 percent of the optimum, and compaction will be done to 95 percent of Modified Proctor optimum dry density. The maximum dry density and optimum moisture content is determined in accordance with ASTM D1557, "Standard Test Methods for Laboratory Compaction Characteristics of Soil Using Modified Effort (56,000 ft-lbf/ft^3(2700 kN-m/m^3))," (ASTM, 2009).

Fill materials need to be placed in horizontal layers usually not greater than 8 inches in loose thickness. Each layer is required to be spread evenly and mixed thoroughly to obtain uniformity of material and moisture in each layer. When the moisture content of the fill material is below that specified, water needs to be added until the moisture content is as specified. When the moisture content of the fill material is too high, the fill material needs to be aerated through blading, mixing, or other satisfactory methods until the moisture content is as specified. After each fill layer has been placed, mixed and spread evenly, it needs to be thoroughly compacted to the specified degree of compaction. Compaction needs to be accomplished by acceptable types of compacting equipment. The equipment is required to be of such design and nature that it is able to compact the fill to the specified degree of compaction. Compaction should be continuous over the entire area and the equipment should make sufficient passes to obtain the desired uniform compaction.

Continuous geotechnical engineering observation and inspection of fill placement and compaction operations is required to certify and ensure that the fill is properly placed and compacted in accordance with the project plans and specifications. Field density tests in accordance with ASTM D1556 "Standard Test Method for Density and Unit Weight of Soil in Place by Sand-Cone Method, American Society for Testing and Materials" (ASTM, 2007b) are required to be performed for each layer of fill. Moisture content may be determined in the laboratory in accordance with ASTM D2216, "Standard Test Methods for Laboratory Determination of Water (Moisture) Content of Soil and Rock by Mass" (ASTM, 2005c) or in the field using nuclear methods in accordance with ASTM D6938 "Standard Test Method for In-Place Density and Water Content of Soil and Soil-Aggregate by Nuclear Methods (Shallow Depth)," (ASTM, 2008b). If the surface is disturbed, the density tests are to be made in the compacted materials below the disturbed zone. When these tests indicate that the degree of compaction of any layer of fill or portion thereof does not meet the specified minimum requirement, the particular layer or portions requires reworking until the specified relative compaction is obtained.

At least one in-place moisture content and field density test are required on every 10,000 square feet of each lift of fill, and further placement is not allowed until the required relative compaction has been achieved. The number of tests is increased if a visual inspection determines that the moisture content is not uniform or if the compacting effort is variable and not considered sufficient to meet the project specification. For critical areas, at least one in-place moisture content and field density test are required at least every 200 cubic yards of compacted fill.

Testing and analysis will be performed to confirm the structural fill shear wave velocity at the bottom of the basemats for Seismic Category I structures meets or exceeds the requirements in Part 10 ITAAC Table 2.4-1. The testing will consist of shear wave velocity (V_S) measurements using Spectral Analysis of Surface Waves (SASW). The testing frequency will be selected to produce a V_S profile with depth, at three locations per SASW line. The initial SASW testing will be performed at the foundation elevation along a line (either east-west or north-south) beneath the center line of each structure. A second line, parallel to the first line (and at the same elevation) will be carried out adjacent to each structure in areas free from foundations or other structures. The third and final SASW line will be performed at the final rough or finished grade elevations directly above the second line tested in the area free from foundations. The first and second lines of testing allow direct comparison of the fill quality and variability at the level of the foundation. The second and final testing allows assessment of the increase in VS with increasing confining pressure due to the backfill loading at the same vertical location. Given the consistency between the first and second SASW lines, conclusions can be drawn regarding the relationship between V_S and confining pressure beneath the structure. The recorded V_S measurements will also be compared with V_S measurements from RCTS testing at

comparable confining pressures, allowing correlation of design (laboratory-based) and actual (field-based) measurements.

In addition to SASW testing, a second geophysical method (e.g., down-hole testing) will be utilized to measure VS at one location at final rough or finished grade for each structure for redundancy and confirmation purposes. The NRC will be informed of critical dates for testing of structural fill so they may observe the testing process.

The backfill supplier will submit samples of backfill prior to placement to perform tests such as Modified Proctor, grain size and chemical properties. The number of samples should adequately cover each of the backfill supply batches. Samples should be collected in accordance with ASTM D75. Each sample should be representative of the material from a single source. Testing will be performed by an independent qualified laboratory.

Careful inspection and testing during fill placement will be enforced and fill placement progress interrupted if required. The number of tests will be sufficient to adequately represent the backfill for each lift. The number of samples and quality control testing will be indicated by the testing specification.

2.5.4.5.4 Dewatering and Excavation Methods

Groundwater control is required during construction. Groundwater conditions and dewatering are addressed in Sections 2.4.12.5 and 2.5.4.6.

Given the soil conditions, excavations are performed using conventional earth-moving equipment, likely using self-propelled scrapers with push dozers, excavators and dump trucks. Most excavations should not present any major difficulties. Blasting is not anticipated. The more difficult excavations would have been in Stratum IIb Cemented Sand, due to the cemented nature and proximity to groundwater, but the cemented portions are not planned to be excavated, except where minor excavations are needed due to localized conditions or due to deeper foundation elevations such as at the Ultimate Heat Sink Makeup Water Intake Structure area. Excavations in localized, intermittent cemented soils may require greater excavating effort, such as utilizing hoe-rams or other ripping tools; however, these zones are very limited in thickness, with probably only occasional need for expending additional efforts. Excavations for the CCNPP Unit 3 powerblock foundations are planned as open cut. Upon reaching the final excavation levels, all excavations are cleaned of any loose materials, by either removal or compaction in place. All final subgrades are inspected and approved prior to being covered by backfill or concrete. The inspection and approval procedures are addressed in the foundation and earthworks specifications developed during the detailed design stage of the project. These specifications include measures, such as proof-rolling, excavation and replacement of unsuitable soils, and protection of surfaces from deterioration.

As discussed in Section 2.5.4.5.2, excavation for the Ultimate Heat Sink Makeup Water Intake Structure requires the installation of a sheetpile cofferdam. The sheetpile structure extends from the ground surface to a depth of about 50 ft. The full scope of the sheetpile cofferdam is developed during the detailed design stage of the project. Excavation of soils in this area should not present any major difficulties given their compactness.

Foundation rebound (or heave) is monitored in excavations for selected Seismic Category I structures. Rebound estimates are addressed in Section 2.5.4.10. Monitoring program specifications are developed during the detailed design stage of the project. The specification document addresses issues, such as the installation of a sufficient quantity of instruments in the

excavation zone, monitoring and recording frequency, and evaluation of the magnitude of rebound and settlement during excavation, dewatering, and foundation construction.

2.5.4.6 Groundwater Conditions

Sections 2.5.4.6.1 through 2.5.4.6.5 are added as a supplement to U.S. EPR FSAR.

2.5.4.6.1 Groundwater Conditions

Details of available groundwater conditions at the site are given in Section 2.4.12. The shallow (surficial) groundwater level in the CCNPP Unit 3 area ranges from approximately El. 68 to El. 85.7 ft, or an average El. of 80 ft. This elevation is considered as the in-situ, current condition groundwater elevation. Similarly, the groundwater level associated with the deeper hydrostatic surface was found to range from approximately El. 16 ft to El. 42 ft, with an average El. of 34 ft. Available observation well data indicate the groundwater table in the Intake Area is at about El. 3 ft.

The shallow groundwater should have little to no impact on the stability of foundations, as the site grading and excavation plans will implement measures to divert these flows away from excavations, i.e., through runoff prevention measures and/or ditches. There are no Seismic Category I foundations planned within the upper water-bearing soils. Groundwater in the powerblock after construction is expected to be at El. 55. Additional detail is provided in Section 2.4.12.

2.5.4.6.2 Dewatering During Construction

Temporary dewatering is required for groundwater management during construction. On the basis of defined groundwater conditions, groundwater control/construction dewatering is needed at the site during excavations for the Powerblock Area foundations. Groundwater associated with seepage in the shallow (upper) zones (Surficial aquifer) is controlled through site grading and/or a system of drains and ditches, as previously discussed. This may also consist of more positive control, including a series of sumps and pumps strategically located in the excavation area to effectively collect and discharge the seepage that enters the excavation, in addition to ditches, drains, or other conveyance systems.

The drainage ditches are installed below grade level, at the peripheries, as the excavation progresses. These ditches are oriented in approximately north-south and east-west directions, i.e., at excavation corners or more frequently as warranted during construction. Once at the final subgrade, stone-filled drains are installed in the excavation interior for control of upward seepage, if any. These drains are in turn connected to exterior ditches and sumps. Each sump is equipped with a pump of sufficient capacity for efficient groundwater removal. Based on the estimated lateral groundwater flow rate derived in Section 2.4.12.5, a total of four pumps with capacity of 100 gpm each will be used for the dewatering.

Temporary dewatering is required for the excavation of the Ultimate Heat Sink Makeup Water Intake Structure and other neighboring structures. A sheetpile cofferdam, designed to aid with dewatering, needs to be extended into low permeability soils; however, some level of groundwater control is still required to maintain a relatively “dry” excavation during construction. As a minimum, pumps are installed to control and/or lower the groundwater level inside the cofferdam. Given the limited excavation size, one 100 gpm pump is sufficient for control of groundwater in this excavation.

Additional auxiliary pumps are available for removal of water from excavations during periods of unexpected storm events. The groundwater level in excavations will be maintained at a minimum of 3 ft below the final excavation level.

2.5.4.6.3 Analysis and Interpretation of Seepage

Analysis of the groundwater conditions at the site is ongoing at this time, given continued groundwater monitoring that is still in progress, as addressed in Section 2.4.12. A groundwater model, based on information currently available, has been prepared for the overall groundwater conditions at the site and is addressed in detail in Section 2.4.15. The groundwater program and milestones are provided in Section 2.4.12.

2.5.4.6.4 Permeability Testing

Testing for permeability of the site soils was performed using Slug tests, as discussed in Section 2.5.4.2.3. A detailed description of the tests and the results is provided in Section 2.4.12. A summary of the hydraulic conductivity values is presented in Table 2.5-35.

2.5.4.6.5 History of Groundwater Fluctuations

A detailed treatment of the ground water conditions is provided in Section 2.4.12.

2.5.4.7 Response of Soil and Rock to Dynamic Loading

The spectra developed in Section 2.5.2.6 and its specific location at a free ground surface reflect the seismic hazard in terms of PSHA and geologic characteristics of the site and represent the site-specific ground motion response spectrum. These spectra are modified to develop ground motion for design considerations. Detailed descriptions on response of site soils and rocks to dynamic loading are addressed in Section 2.5.2, a Site SSE for design is developed in Section 3.7.1.

2.5.4.8 Liquefaction Potential

The potential for soil liquefaction at the CCNPP Unit 3 site was evaluated following NRC Regulatory Guide 1.198 (USNRC, 2003c). The soil properties and profiles utilized are those described in Section 2.5.4.2.

Sections 2.5.4.8.1 through 2.5.4.8.6 are added as a supplement to the U.S. EPR FSAR.

2.5.4.8.1 Previous Liquefaction Studies

Two liquefaction studies are cited in the CCNPP Units 1 and 2 UFSAR (BGE, 1982), as follows. The same reference cites a horizontal ground acceleration of 0.08 g and a Richter magnitude of 4 to 5 for the OBE case, and a horizontal ground acceleration of 0.15 g and a Richter magnitude of 5 to 5.5 for the SSE case.

CCNPP Units 1 and 2 UFSAR (BGE, 1982) reports that the liquefaction potential at the site was evaluated using data from standard penetration test borings, laboratory test results, in-place density determinations, and geologic origin of the site soils. The results showed that the site soils did not possess the potential to liquefy. Quantitative values for the factor of safety against liquefaction were not given.

CCNPP Units 1 and 2 UFSAR (BGE, 1982) also reports on results of a liquefaction study for the siting of the Diesel Generator Building in the North Parking area as a part of CCNPP Units 1 and 2 development. This liquefaction evaluation was performed on data from standard penetration test borings, resulting in computed factors of safety from 1.3 to 2.4, with a median value of 1.8. On this basis, it was determined that the site of the Diesel Generator Building had adequate factor of safety against liquefaction (Bechtel, 1992).

2.5.4.8.2 Soil and Seismic Conditions for CCNPP Unit 3 Liquefaction Analysis

Preliminary assessments of liquefaction for the CCNPP Unit 3 soils were based on observations and conclusions contained within CCNPP Units 1 and 2 UFSAR (BGE, 1982). The site soils that were investigated for the design and construction of CCNPP Units 1 and 2 did not possess the potential to liquefy. Given the relative uniformity in geologic conditions between existing and planned units, the soils at CCNPP Unit 3 were preliminarily assessed as not being potentially liquefiable for similar ground motions, and were further evaluated for confirmation, as will be described later in this subsection. Based on this assessment, it was determined that aerial photography as outlined in Regulatory Guide 1.198 (USNRC, 2003c) would not add additional information to the planning and conduct of the subsurface investigation; therefore, was not conducted.

A common stratigraphy was adopted for the purpose of establishing soil boundaries for liquefaction evaluation. The adopted stratigraphy was that shown generically in Figure 2.5-95 and also by the velocity profiles shown in Figure 2.5-156 and Figure 2.5-158. Only soils in the upper 400 ft of the site were evaluated for liquefaction, based on available results from the CCNPP Unit 3 subsurface investigation. Soils below a depth of 400 ft are considered geologically old and sufficiently consolidated. These soils are not expected to liquefy, as will be further discussed in Section 2.5.4.8.4.

The liquefaction analysis was performed using a peak ground acceleration (PGA) of 0.15 g from the Site Safe Shutdown Earthquake (SSE) developed in Section 3.7.1. A sensitivity calculation was developed to study the impact that a distant, higher magnitude event, with lower acceleration would have in the Factor of Safety against liquefaction. The controlling distant event with magnitude 6.9 was used along with a maximum ground acceleration of 0.1g. The sensitivity analysis indicates that the Factor of Safety against liquefaction is about 14% larger for such scenario.

2.5.4.8.3 Liquefaction Evaluation Methodology

Liquefaction is defined as the transformation of a granular material from a solid to a liquefied state as a consequence of increased pore water pressure and reduced effective stress (Youd, et al., 2001). The prerequisite for soil liquefaction occurrence (or lack thereof) are the state of soil saturation, density, gradation and plasticity, and earthquake intensity. The present liquefaction analysis employs state-of-the-art methods (Youd, et al., 2001) for evaluating the liquefaction potential of soils at the CCNPP Unit 3 site. Given the adequacy of these methods in assessing liquefaction of the site soils, and the resulting factors of safety which will be discussed later in this subsection, probabilistic methods were not used.

In brief, the present state-of-the-art method considers evaluation of data from SPT, Vs, and CPT data. Initially, a measure of stress imparted to the soils by the ground motion is calculated, referred to as the cyclic stress ratio (CSR). Then, a measure of resistance of soils to the ground motion is calculated, referred to as the cyclic resistance ratio (CRR). Finally, a factor of safety (FOS) against liquefaction is calculated as a ratio of cyclic resistance ratio and cyclic stress ratio. Details of the liquefaction methodology and the relationships for calculating CSR, CRR, FOS,

and other intermediate parameters such as the stress reduction coefficient, magnitude scaling factor, accounting for non-linearity in stress increase, and a host of other correction factors, can be found in Youd (Youd, et al., 2001). A magnitude scaling factor (MSF) of 1.93 was used in the calculations based on the adopted earthquake magnitude and guidelines in Youd (Youd, et al., 2001). Below are examples of liquefaction resistance calculations using the available SPT, Vs, and CPT data in the Powerblock Area and Intake Area. Calculations were performed mainly using spreadsheets, supported by spot hand-calculations for verification.

2.5.4.8.4 FOS Against Liquefaction Based on SPT Data

The equivalent clean-sand $CRR_{7.5}$ value, based on SPT measurements, was calculated following recommendations in Youd (Youd, et al., 2001), based on corrected SPT N-values $(N_1)_{60}$, including corrections based on hammer-rod combination energy measurements at the site. The soils at CCNPP site include clean granular soils with $(N_1)_{60}30$ that are considered too dense to liquefy and are classified as non-liquefiable (Youd, et al., 2001). Similarly, corrections were made for the soils fines contents, based on average fines contents and the procedure recommended in Youd (Youd, et al., 2001).

The collected raw (uncorrected) SPT N-values are shown in Figure 2.5-102 and Figure 2.5-103. SPT data from the figures were used for the liquefaction FOS calculations for over 2000 SPT N-value data points. The results are shown in Figure 2.5-165 for the Powerblock Area and Figure 2.5-166 for the Intake Area.

For completeness, all data points, including data for clay soils and data above the groundwater level, were included in the FOS calculation, despite their known high resistance to liquefaction. The SPT N-values shown in Figure 2.5-102 and Figure 2.5-103 were mostly taken at 5-ft intervals. SPT in the deepest borings (B-301 and B-401) extended to about 400 ft below the ground surface.

Of the over 2,000 SPT N-value data points for which FOS values were calculated, no points resulted with FOS<1.1 below foundation grade.

Soils indicating FOS<1.1 are either at elevations that will eventually be lowered during construction which would result in the removal of these soils, or are at locations where no structures are planned. Hence, the low FOSs are not a concern for these samples. Based on SPT data, there is no potential for liquefaction for the CCNPP3 Unit 3 Powerblock and Intake Areas.

2.5.4.8.5 FOS Against Liquefaction Based on Shear Wave Velocity Data

Similar to the FOS calculations for the SPT values, equivalent clean-sand $CRR_{7.5}$ values, based on V_s measurements, were calculated following recommendations in Youd (Youd, et al., 2001). Soils at the CCNPP site include soils with normalized shear wave velocity (VS_1) exceeding a value of 215 m/s (705 fps). Clean granular soils with V_{S1} larger than 215 m/s (705 fps) are considered too dense to liquefy and are classified as non-liquefiable (Youd, et al., 2001). The limiting upper value of VS1 for liquefaction resistance is referred to as V_{S1}*; the latter varies with fines content and is 215 m/s (705 fps) and 200 m/s (656 fps) for fines contents of less than 5 percent and larger than 35 percent, respectively. As such, when values of V_{S1} are larger than V_{S1}*, the soils were considered too dense to liquefy, and therefore, the maximum CRR value of 0.5 was used in the FOS calculations.

Shear wave velocity data from the P-S logging measurements were used for the FOS calculations. The collected raw (uncorrected) V_s data are shown in Figure 2.5-107 and Figure 2.5-108 for the Powerblock and Intake Areas respectively. Suspension P-S velocity

logging measurements were made at 0.5-m intervals (~1.6-ft). The two deepest measurements (at borings B-301 and B-401) extended to about 400 ft below the ground surface. Approximately 1,400 V_s data points were used for the FOS calculations. The results showing FOS against liquefaction using the shear wave velocity data are provided in Figure 2.5-167 and Figure 2.5-168.

The results show that all calculated FOSs exceeded 1.1 with significant margin; almost all are at least 4.0, with a few scattered values at about 2.0. The high calculated FOS values are the result of V_{S1} values typically exceeding the limiting V_{S1}* values, indicating no potential for liquefaction. Based on shear wave velocity data, there is no potential for liquefaction for the CCNPP Unit 3 Powerblock and Intake Areas.

2.5.4.8.6 FOS Against Liquefaction Based on CPT Data

The CPT testing at the CCNPP Unit 3 site included the measurement of both commonly measured cone parameters (tip resistance, friction, and pore pressure) and shear wave velocity. The evaluation of liquefaction based on both the commonly measured parameters and shear wave velocity is addressed herein. The CCNPP Powerblock CPT data was reviewed and correlated with the applicable SPT data and compared with guidelines in Robertson (Robertson, et al., 1988). This review process verified the CPT data by correlation to the CCNPP Unit 3 site-determined SPT values.

The equivalent clean-sand $CRR_{7.5}$ value, based on CPT tip measurements, was calculated following recommendations in Youd (Youd, et al., 2001), based on normalized clean sand cone penetration resistance (qc1N)cs and other parameters such as the soil behavior type index, Ic.

Cone tip resistance values from CPT soundings are shown in Figure 2.5-104 and Figure 2.5-105 for the Powerblock and Intake Areas respectively. The CPT soundings encountered repeated refusal in the cemented sand layer, and could only be advanced deeper after pre-drilling through these soils, indicative of their high level of resistance to liquefaction. The deepest CPT sounding (C-407) penetrated 142 ft below the ground surface, encountering refusal at that depth, terminating at approximately El. -80 ft. Tip resistance measurements were made at 5-cm intervals (~2-in). The results showing FOS against liquefaction using the CPT data are provided in Figure 2.5-169 and Figure 2.5-170 for the Powerblock and Intake Areas, respectively. For completeness, all data points, including data for clay soils, were included in the calculation, despite their known high resistance to liquefaction.

Only data points in the upper layers resulted in FOS < 1.1. CPT-based CRR relationship was intended to be conservative, not necessarily to encompass every data point; therefore, the presence of a few data points beyond the CRR base curve is acceptable (Youd, et al., 2001). The soils in Stratums I and IIa will be removed during construction. In addition an extremely conservative margin is adopted by using a PGA value of 0.15 g. Based on CPT data, there is no potential for liquefaction for the CCNPP3 Powerblock and Intake Areas.

2.5.4.8.7 Liquefaction Resistance of Soils Deeper Than 400 Feet

Liquefaction evaluation of soils at the CCNPP Unit 3 site was focused on soils in the upper 400 ft. The site soils, however, are much deeper, extending to approximately 2,500 ft below the ground surface. Geologic information on soils below a depth of 400 ft was gathered from the available literature, indicating that these soils are from about 50 to over 100 million years old. Liquefaction resistance increases markedly with geologic age, therefore, the deeper soils are geologically too old to be prone to liquefaction. Additionally, their compactness and strength are only anticipated to increase with depth, compared with the overlying soils. The Pleistocene

soils have more resistance than Recent or Holocene soils and pre-Pleistocene sediments are generally immune to liquefaction (Youd, et al., 2001). Additionally, liquefaction analyses using shear wave velocity values of about 2,000 ft/sec near the 400-ft depth did not indicate any potential liquefaction at that depth, with the FOSs exceeding 5.0. With shear wave velocities increasing below the 400-ft depth, in the range of about 2,200 ft/sec to 2,800 ft/sec as indicated in Figure 2.5-155 through Figure 2.5-158, high resistance to liquefaction would be expected from these deeper soils. On this basis, liquefaction of soils at the CCNPP Unit 3 site below a depth of 400 ft is not considered possible.

2.5.4.8.8 Potential for Liquefaction of Backfill

Section 2.5.4.5 describes material specifications and compaction for structural fill. For foundation backfill, compaction will be done to 95 percent of Modified Proctor optimum dry density. The fill will be compacted to within 3 percent of its optimum moisture content.

Liquefaction in an engineered fill is not an issue if the recommended compaction practices are followed. Liquefaction occurs in loose sands and/or silts with poor gradation. An engineered fill is a compacted and well graded soil structure. Compaction practices need to be monitored during construction. Liquefaction of granular engineered fills will be prevented by assuring that the fill specifications are met during the implementation stages. Particular attention will be placed on the grain size and compaction requirements to ensure the specifications are fully met. Specifications for fill will include requirements for an on-site testing laboratory for quality control, especially material gradation and plasticity characteristics, the achievement of specified moisture-density criteria, fill placement/compaction, and other requirements to ensure that the fill operations conform to the earthwork specification for CCNPP Unit 3.

Regardless of the non-liquefiable nature of engineered fills, the liquefaction potential was also evaluated with the shear wave velocity approach. Figure 2.5-156 indicates that the values for the backfill are 790, 900, and 1080 fps. The 790 fps backfill will not be exposed to saturated conditions since it only corresponds to the first six ft from the surface. The results of the analysis are shown in Figure 2.5-171. Based on shear wave velocity data, there is no potential for liquefaction for the CCNPP3 backfill.

2.5.4.8.9 Concluding Remarks on Liquefaction Analysis

It is evident, from the collective results, that soils at the CCNPP Unit 3 site are overly-consolidated, geologically old, and sometimes even cemented. They are not susceptible to liquefaction due to acceleration levels from the anticipated earthquakes. A very limited portion of the data at isolated locations indicated potentially liquefiable soils, however, this indication cannot be supported by the overwhelming percentage of the data that represent these soils. Moreover, the state-of-the-art methodology used for the liquefaction evaluation was intended to be conservative, not necessarily to encompass every data point; therefore, the presence of a few data points beyond the CRR base curve is acceptable (Youd, et al., 2001). Additionally, in the liquefaction evaluation, the effects of age, overconsolidation, and cementation were ignored. These factors tend to increase resistance to liquefaction. Finally, the earthquake acceleration and magnitude levels adopted for the liquefaction analysis are conservative. More importantly, there is no documented liquefaction case for soils in the State of Maryland (USGS, 2000). Therefore, liquefaction is not a concern. A similar conclusion was arrived at for the original CCNPP Units 1 and 2 (BGE, 1982).

A significant level of site grading is anticipated at the CCNPP Unit 3 site during construction. This primarily results in the removal of geologically younger materials (the upper soils) from the higher elevations, and the placement of dense compacted fill in lower elevations. Limited

man-made fill may be already present at the CCNPP Unit 3 site at isolated locations. These soils will be removed during construction.These activities, further improve the liquefaction resistance of soils at the site.

2.5.4.8.10 Regulatory Guide 1.198

Before and during the liquefaction evaluation, guidance contained in NRC Regulatory Guide 1.198 (USNRC, 2003c) was used. The liquefaction evaluation conforms closely to the NRC Regulatory Guide 1.198 guidelines.

Under "Screening Techniques for Evaluation of Liquefaction Potential," NRC Regulatory Guide 1.198 (USNRC, 2003c) lists the most commonly observed liquefiable soils as fluvial-alluvial deposits, eolian sands and silts, beach sands, reclaimed land, and uncompacted hydraulic fills. The geology at the CCNPP site includes fluvial soils and man-made fill at isolated locations. The liquefaction evaluation included all soils at the CCNPP site. The man-made fill, which is suspected only at isolated locations, will be removed during the site grading operations. In the same section, NRC Regulatory Guide 1.198 (USNRC, 2003c) indicates that clay to silt, silty clay to clayey sand, or silty gravel to clayey gravel soils can be considered potentially liquefiable. This calculation treated all soils at the CCNPP Unit 3 site as potentially liquefiable, including the fine-grained soils. The finer-grained soils at the CCNPP Unit 3 site contain large percentages of fines and/or are plastic and are, therefore, considered non-liquefiable, as also indicated by the calculated FOSs for these soils. In fact, all soils at the CCNPP Unit 3 site contain some percentage of fines and exhibit some plasticity, which tends to increase their liquefaction resistance. The same section of NRC Regulatory Guide 1.198 (USNRC, 2003c) confirms that potentially liquefiable soils that are currently above the groundwater table, are above the historic high groundwater table, and cannot reasonably be expected to become saturated, pose no potential liquefaction hazard. In the liquefaction analyses, the groundwater level was taken at elevation 80 ft. This water level may be a "perched" condition, situated above Stratum IIa Chesapeake Clay/Silt, with the actual groundwater level near the bottom of the same stratum in the Chesapeake Cemented Sand, or at about an average El. 39 ft. Despite the adopted higher groundwater level (a higher piezometric head of more than 40 ft), the calculated FOS overwhelmingly exceeded 1.1. The site historic groundwater level is not known, however, it is postulated that the groundwater level at the site has experienced some fluctuation due to pumping from wells in the area and climatic changes. Groundwater levels at the site are not expected to rise beyond El. 55 ft in the future given the relief and topography of the site, promoting drainage. Similarly, NRC Regulatory Guide 1.198 (USNRC, 2003c) indicates that potentially liquefiable soils may not pose a liquefaction risk to the facility if they are insufficiently thick and of limited lateral extent. At the CCNPP Unit 3 site, the soil layers are reasonably thick and uniformly extend across the site, except where they have been eroded, yet the FOSs overwhelmingly exceeded 1.1. Soils identified as having FOS<1.1, regardless of the thickness, will be removed during grading operations or are located where no structures are planned.

Under "Factor of Safety Against Liquefaction," NRC Regulatory Guide 1.198 (USNRC, 2003c) indicates that FOS=1.1 is considered low, FOS=1.1 to 1.4 is considered moderate, and FOS = 1.4 is considered high. A FOS = 1.1 appears to be the lowest acceptable value. On the same issue, the Committee on Earthquake Engineering of the National Research Council (CEE, 1985) states that "There is no general agreement on the appropriate margin (factor) of safety, primarily because the degree of conservatism thought desirable at this point depends upon the extent of the conservatism already introduced in assigning the design earthquake. If the design earthquake ground motion is regarded as reasonable, a safety factor of 1.33 to 1.35... is suggested as adequate. However, when the design ground motion is excessively conservative, engineers are content with a safety factor only slightly in excess of unity." This, and a minimum

FOS = 1.1 in NRC Regulatory Guide 1.198 (USNRC, 2003c), are consistent with the FOS = 1.1 adopted for the assessment of FOSs for the CCNPP Unit 3 site soils, considering the conservatism adopted in ignoring the cementation, age, and overconsolidation of the deposits, as well as the seismic acceleration and magnitude levels. Such level of conservatism in the evaluation, in conjunction with ignoring the geologic factors discussed above, justifies the use of FOS = 1.1 for liquefaction assessment of the CCNPP site soils.

2.5.4.9 Earthquake Site Characteristics

Section 2.5.2.6 describes the development of the horizontal ground motion response spectra (GMRS) for the CCNPP Unit 3 site. The selected ground motion is based on the risk-consistent/ performance-based approach of NRC Regulatory Guide 1.208, "A Performance-Based Approach to Define the Site-Specific Earthquake Ground Motion" (USNRC, 2007b) with reference to NUREG/CR-6728 (REI, 2001) and ASCE/SEI 43-05 (ASCE, 2005). Any deviation from the guidance provided in Regulatory Guide 1.208 is discussed in Section 2.5.2. Horizontal ground motion amplification factors are developed in Section 2.5.2.5 using site-specific data and estimates of near-surface soil and rock properties presented in Section 2.5.4. These amplification factors are then used to scale the hard rock spectra, presented in Section 2.5.2.4, to develop a soil Uniform Hazard Spectra (UHS), accounting for site-specific conditions using Approach 2A of NUREG/ CR-6769 (USNRC, 2002). Horizontal spectra are developed from these soil UHS, using the performance-based approach of ASCE/SEI 43-05, accepted by Regulatory Guide 1.208. The motion is defined at the free ground surface of a hypothetical outcrop at the base of the foundation. Section 2.5.2.6 also describes vertical ground motion, which was developed by scaling the horizontal ground motion by a frequency-dependent vertical-to-horizontal (V:H) factor, presented in Section 2.5.2.6. Section 3.7.1 develops a Site Safe Shutdown Earthquake (Site SSE) that satisfies the minimum Safe Shutdown Earthquake Ground Motion for design identified in paragraph (d)(1) of 10 CFR 100.23 (CFR, 2007).

2.5.4.10 Static Stability

The CCNPP Powerblock Area is graded to establish the final site elevation, which will range from about El. 81 ft to 85 ft. An average grade elevation of 83 ft is assumed. The Reactor, Safeguards, and Fuel Buildings are seismic Category I structures and are supported on a common basemat. For a basemat thickness of 10 ft and top of basemat about 31.5 ft below grade, the bottom of the basemat would be 41.5 ft below the final site grade, or El. 41.5 ft. The common basemat has an irregular shape, approximately 80,000 square feet (sq ft) in plan area, with outline dimensions of about 363 ft x 345 ft. For bearing capacity and settlement estimation, a representative foundation is used. Table 2.5-66 presents the values for elevation, depth, area, and loads of the seismic Category I structures and the main structures in the Powerblock area. This information is also shown in Figure 2.5-172.

Construction of the common basemat requires an excavation of about 41 to 42 ft (from approximately El. 83 ft). The resulting rebound (heave) in the ground due to the removal of the soils is expected to primarily take place in Stratum IIc Chesapeake Clay/Silt soils. A rebound of about 4 in is estimated due to excavation for the common basemat, and is expected to take place concurrent with the excavation. Ground rebound is monitored during excavation. The heave estimate is made based on the elastic properties of the CCNPP site soils and the response to the unloading of the ground by the excavation. The magnitude and rate of ground heave is a function of, among other factors, excavation speed and duration that the excavation remains open. Other factors remaining unchanged, shorter durations culminate in smaller values of ground heave.}

2.5.4.10.1 Bearing Capacity

The U.S. EPR FSAR includes the following COL Items in Section 2.5.4.10.1:

A COL applicant that references the U.S. EPR design certification will verify that site-specific foundation soils beneath the foundation basemats of Seismic Category I structures have the capacity to support the bearing pressure with a factor of safety of 3.0 under static conditions, or 2.0 under dynamic conditions, whichever is greater.

A COL applicant that references the U.S. EPR design certification will perform a site-specific analysis to determine the bearing pressure demand and peak displacement of the NAB. The foundation soils beneath the NAB foundation basemat shall have the capacity to support the bearing pressure with a factor of safety of 3.0 under static conditions, or 2.0 under combined static and dynamic conditions, whichever is greater. The minimum required separation distance is a factor of two times the calculated absolute sum of the maximum combined site-specific NAB and U.S. EPR NI design displacements, but not less than 30 inches.

These COL Items are addressed as follows:

{The ultimate bearing capacity of safety-related buildings and the NAB is estimated using the closed form solutions proposed by Vesic (Vesic, et al., 1975) and Meyerhof (Meyerhof, et al., 1978). Factors of safety are obtained for different soil profile cases and compared with standard practice allowable values.

The NAB bearing pressure, displacement and separation distance from the NI are discussed in Section 3.7.2.8.1.

The soil profiles of CCNPP Unit 3 and Intake Areas are used in the analysis in order to determine the corresponding layer thickness and material properties. Stratum thicknesses and elevations are presented in Table 2.5-27.

Weighted average values of soil parameters are used in the analysis; weight factors are based on the relative thickness of each stratum within a specific depth (i.e. depth equal to the least lateral dimension of the building).

The water table in the Powerblock Area is conservatively considered to be at El. 83 ft, which corresponds to the average grade surface elevation. For the Intake Area, the water table is considered to be at El. 10 ft, which also corresponds to the average grade surface elevation. With the higher groundwater level, the bearing capacity estimate will be more conservative since overburden resistance is diminished by increased buoyant effect.

Average values of the soil strength parameters (c', Φ', s_u, γ) are considered in the analysis. Average unit weights are calculated using data from the entire CCNPP Unit 3 area (limited number of samples were available for strength parameters in the Powerblock Area, therefore data from the Construction Laydown Area (CLA) area are included in the calculation of the average values). Sand layers present a relatively low cohesion due to the presence of fine particles, based on laboratory tests results. However, for this analysis the cohesion for sand layers is conservatively not considered ($c' = 0$).

The ultimate static bearing capacity of a footing supported on homogeneous soils can be estimated using the following equation (Vesic, et al., 1975):

$$q_{ult} = cN_c s_c d_c i_c g_c b_c + \frac{1}{2}\gamma' B' N_\gamma s_\gamma d_\gamma i_\gamma g_\gamma b_\gamma r_\gamma + qN_q s_q d_q i_q g_q b_q$$

Where:

q_{ult} → Ultimate bearing capacity;

c → Cohesion;

N_c , N_γ , N_q → Bearing capacity factors;
$N_q = e^{\pi \tan\Phi}\tan^2(45 + \Phi/2)$;
$N_c = (N_q - 1)\cot\Phi$;
$N_\gamma = 2(N_q + 1)\tan\Phi$;

Φ → Friction angle;

s_c , s_γ , s_q → Foundation shape correction factors;

d, i, g, b → Shape, depth, and inclination factors;

r_γ → Foundation size correction factor;

γ' → Effective unit weight of foundation media;

B′ → Effective foundation width;

Three different cases are considered in the analysis:

a. Soil subsurface including all strata: For this case, weighted average values of the strength parameters are used based on relative thickness of each stratum in the zone between the bottom of the footing and a depth B below this point, where B is the least lateral dimension of the building. For this case, effective soil parameters are used (drained conditions). (Vesic, et al. 1975)

b. Soil subsurface considering only stratum IIb Chesapeake Cemented Sand. Soil parameters of this layer are used for the entire depth. For this case, effective soil parameters are used (drained conditions). (Vesic, et al. 1975)

c. The ultimate static bearing capacity of a footing supported on a dense sand stratum over a soft clay stratum can be estimated using the punching shear failure with a circular slip path (Meyerhof, et al., 1978):

$$q_{ult} = q_{u,b} + \frac{2\gamma_1 H_t^2}{B}\left(1 + \frac{2D}{H_t}\right)K_{ps}\tan\Phi_1 - \gamma_1 H_t \le q_{ut}$$

$$q_{u,b} = c_2 N_{c_2}\zeta_{c_2} + \frac{1}{2}\gamma'_2 B' N_{\gamma_2}\zeta_\gamma 2r\gamma + \gamma'_1(H_t + D)N_{q_2}\zeta_{q_2}$$

$$q_{ut} = c_1 N_{c_1}\zeta_{c_1} + \frac{1}{2}\gamma'_1 B' N_{\gamma_1}\zeta_{\gamma 1} r_\gamma + \gamma'_b D N_{q_1}\zeta_{q_1}$$

Where:

q_{ult} → Ultimate bearing capacity;

$q_{u,b}$ → Ultimate bearing capacity of a very thick bed of the bottom soft clay layer;

q_{ut} → Ultimate bearing capacity of upper dense sand layer;

γ'_1 → Effective unit weight of the upper sand layer;

γ'_2 → Effective unit weight of the lower clay layer;

γ'_β → Effective unit weight of backfill;

Φ_1 → Friction angle of upper sand layer;

Φ_2 → Friction angle of lower clay layer;

c_1 → Cohesion of upper sand layer;

c_2 → Cohesion of lower clay layer;

H_t → Depth from footing base to soft clay;

D → Depth from of footing base below ground surface;

K_{ps} → Punching shear coefficient;

B′ → Effective foundation width;

ζ_q , ζ_c , ζ_γ → Geometry Factors;

N_c , N_γ , N_q → Bearing capacity factors;

Buildings are considered to have an equivalent rectangular foundation with the same area and moment of inertia as the original footprint shape. The analysis is preformed using uniformly distributed loads in all buildings. For the NI Common Mat, an average uniform load is used including the loads from the Reactor, Safeguard and Fuel Buildings. The vertical load imposed by adjacent structures is conservatively not included in the calculation of bearing capacity of each building, only the surcharge imposed by the backfill is considered.

The vertical loads and dimensions of the buildings that comprise the NI common mat are not symmetrical. This will result in overturning moments around the centroid of the common mat that will reduce the contact area of the foundation and hence the bearing capacity. To account for this reduction in the contact area, an effective area is used in the bearing capacity equations. The length (L) and width (B) of the foundation's footprint are reduced in proportion to the eccentricity of the resultant vertical force. For the CCNPP3 NI common mat the asymmetry in dimensions and static loads is not significant; the effective area is approximately 98% of the total area.

The Meyerhof model represents a more realistic approach to calculate the bearing capacity of the soil subsurface at CCNPP 3, by considering a dense sand layer overlying a softer clay layer. This model considers a punching shear failure mechanism between both layers.

A summary of the calculated allowable static and dynamic bearing capacities using both the layered and the homogeneous soil conditions are presented in Table 2.5-67. A factor of safety of 3.0 for static loads (dead plus live loads) and 2.0 for dynamic loading are typically considered to be acceptable. For the NI, the dynamic bearing capacity value of 35.2 ksf reported in Table 2.5-67 is lower than the U.S. EPR bearing pressure of 38 ksf for soft soils. Therefore, there is a departure related to the dynamic bearing capacity. Site specific bearing pressure, stability, and structural analyses have been performed with the use of actual soil conditions. As indicated in Section 3.7.2.14.1, the site-specific structural analyses indicate that bearing demands are lower than the allowable bearing capacities.

A dynamic bearing capacity analysis was performed to assess the impact of seismic forces that produce overturning moments in the foundation. During overturning, the effective supporting area is reduced, resulting in a decrease in the bearing capacity of the subsurface. To take into account this effect and simulate the potential for higher edge pressures during dynamic loading, the seismic bearing capacity is calculated for three different foundation widths: B1 = 270 ft, B2 = 203 ft, and B3 = 135 ft, which correspond to the original foundation width, and two reduced values. The reduction for B2 and B3 is 25% and 50% are considered as a sensitivity analysis of the effective bearing area. The results of the analysis are provided in Table 2.5-76.

Even if the foundation width is reduced by half (B3 = 135 ft), the allowable dynamic bearing capacity (58.5 ksf) is larger than the AREVA design certification requirement of 26 ksf. For the case with average soil strength parameters and the original foundation width (B1=270 ft), the allowable dynamic bearing capacity is 72.9 ksf.

The dynamic bearing capacity of 72.9 ksf is lower than the allowable static bearing capacity of 87.8 ksf (Vesic method). The deduction due to seismic forces in this case is around 17%. For the same case, the deduction of ultimate static bearing capacity is approximately 45%. Lower deductions are expected for allowable bearing capacities since a smaller factor of safety is considered for the dynamic case. The factors of safety are FOS = 3 for static loading and FOS = 2 for dynamic loading.

Table 2.0-1 compares CCNPP Unit 3 site Characteristic Values with U.S. EPR FSAR design Parameters. The static and dynamic bearing capacity exceed the requirements established for the NI, EPGB and ESWB as shown in Table 2.0-1.

For static and dynamic loading conditions, and based on a factor of safety of 3.0 (static) and 2.0 (dynamic), the site provides adequate allowable bearing capacity.}

2.5.4.10.2 Settlement

The U.S. EPR FSAR includes the following COL Items in Section 2.5.4.10.2:

A COL applicant that references the U.S. EPR design certification will provide an assessment of predicted settlement values across the basemat of Seismic Category I structures during and post construction. The assessment will address both short term (elastic) and long term (heave and consolidation) settlement effects with the site specific soil parameters, including the soil loading effects from adjacent structures.

A COL applicant that references the U.S. EPR design certification will verify that the predicted tilt settlement value of ½ inch per 50 ft in any direction across the foundation basemat of a Seismic Category I structure is not exceeded. Settlement values larger than this may be demonstrated acceptable by performing additional site specific evaluations.

These COL Items are addressed as follows:

{The surface topography and subsurface conditions of the CCNPP Unit 3 Powerblock Area make the estimation of settlement and building tilt complex. The objective of the settlement analysis of the CCNPP Powerblock Area is to provide an estimate of the time dependant settlement and heave distribution throughout the footprint of the Powerblock Area, including maximum settlement and tilt estimated for each of the facilities.

The settlement analysis of the CCNPP Powerblock Area was carried out under the following premises:

- Develop a three-dimensional model capable of capturing irregular subsurface conditions, realistic foundation footprint shapes, and asymmetric building loads;
- Perform a time-dependant simulation, that provides settlement and tilt estimates as a function of time through and after construction;
- Incorporate a construction sequence and examine the behavior of settlement and tilt as buildings are erected;
- Account for asymmetric topography, by recognizing that reloading time to original consolidation pressure after excavation will be variable throughout the foundation footprint;
- Perform the settlement analysis simultaneously for the NI and adjacent facilities, including the detached safety related structures (EPBG and ESWB);

2.5.4.10.2.1 Settlement Calculation Methodology

In order to address the issues described above, a Finite Element Method (FEM) model of the subsurface and structural interfaces was developed. The FEM has the capability of providing a numerical solution to the general equations of elasticity in continuous media. The settlement analysis of the CCNPP Powerblock Area is performed with the computer application PLAXIS 3D Foundation v2 (PLAXIS3D) (DUTP, 2007). The application has been validated and verified under the Paul C. Rizzo Associates, Inc. (RIZZO) Quality Assurance Program. The settlement computations have also been performed under RIZZO QA Program.

PLAXIS3D provides a FEM solution of the virtual work equation defining equilibrium conditions and natural boundary conditions in a differential equation form. The program calculates displacements with the use of numerical integration methods. In addition to the typical capabilities of a general FEM application for elastic solids, PLAXIS incorporates advanced constitutive models, (stress vs. strain relationships) that are capable of simulating the response of soils to external loading. Such response includes both elastic/elastoplastic displacement and consolidation. This feature makes PLAXIS3D a unique application for the analysis of foundation systems and its applicability to the CCNPP Powerblock settlement problem is ideal. The application allows for the elaboration of a three-dimensional representation of the subsurface conditions and the building geometries. The model is capable of capturing variation of soil properties below the footprints of the foundation and therefore it is possible to better assess differential settlement. All structures in the Powerblock Area are modeled simultaneously and load increments are applied in different steps in time.

The Mohr-Coulomb constitutive model is selected for the analysis. Other soil hardening constitutive models introduce further sophistication to account for the stress-dependency of

the stiffness, but are slightly less conservative when compared to the Mohr-Coulomb model. This analysis accounted for increased unload and reload elastic moduli with the use of conservative ratios applied at different time steps during the unloading and loading sequence. This approach provided a better understanding of the effect that irregular topographic conditions had in settlement and tilt. Further details are provided in the following sections.

2.5.4.10.2.2 Settlement and Heave Analysis in the CCNPP Powerblock Area

The settlement analysis of the Powerblock Area is based on an FEM model of approximately 2500 ft x 2500 ft x 840 ft (Length x Width x Depth). The area occupied by the buildings is approximately 1100 ft by 1100 ft. There are 42,130 elements in the model. The boundary conditions for the sides of the model included allowing the vertical displacement, and restraining the two horizontal displacement components. The bottom of the model was restrained in vertical and horizontal directions. The free drainage conditions for consolidation were adapted on the model boundaries. Since the model boundaries were far enough from the loaded areas, the primary direction for the water flow is the vertical direction. In other words, the sides of the model are far enough from the loaded areas so that the consolidation behavior is not impacted by the free-drainage conditions implemented on the sides of the model.

Soil profiles, such as those shown by Figure 2.5-96, were taken as the basis for the geotechnical input of the FEM model. In addition, data from boreholes B-311, B-313, B-334, B-335, B-344, and B-357A were included to adequately represent the three-dimensional nature of the model. PLAXIS3D interpolates information between borehole locations to obtain the three-dimensional representation of the subsurface conditions, as shown in Figure 2.5-173. The figure presents a reduced version of one of the excavation profiles to illustrate how the FEM geometry conforms to the subsurface conditions. The CCNPP Powerblock Area model is a comprehensive mathematical representation of the physical conditions at the site.

The analysis depth is approximately twice the width of the NI foundation footprint. Therefore, given the dimensions of the NI common basemat, the model depth was extended to El. -760 ft. This was achieved by extending the Nanjemoy sand (the continuous soil layer deeper than -208 ft elevation) to the bottom of the model.

Two separate models were developed for the CCNPP Powerblock Area:

1. An Excavation and Dewatering Model (ED Model).

2. Construction and Post-Construction Model (CPC Model).

Heave Analysis: Excavation and Dewatering (ED Model)

On saturated soils, prior to excavation, it is necessary to dewater the excavation area. As water is extracted from the voids, soils will consolidate and settlement due to dewatering will take place. In addition, soils beneath dewatered areas will experience increased loading as consolidation of upper layers takes place. The effect that dewatering has on settlement depends on the soil properties, the hydrogeologic conditions, and to some extent on the pumping rates.

At the CCNPP Powerblock Area, the Stratum IIa Chesapeake Clay/Silt isolates the upper surficial aquifer from the layers beneath. The surficial aquifer is confined by the first clay layer and it does not influence the soils at and beneath foundation elevation. Therefore, dewatering will not produce settlement at the foundation level. In consequence soils will not experience

increased stress due to dewatering and such increase need not be accounted for as an excess consolidation pressure as it is typically done if the surficial aquifer was not confined.

Heave will be experienced after excavation and the ED FEM model was used to estimate its magnitude. For this model, the Powerblock Area was divided in three zones considering different average ground elevations for each zone. The subdivision was performed based on the site topography information, as shown in Figure 2.5-174. The zones are:

- Zone I: low areas North East (Plant Local Coordinate System) with an average ground elevation of 60 ft;
- Zone II: South areas (Plant Local Coordinate System) with an average ground elevation of 80 ft;
- Zone III: high areas with an average ground elevation of 105 ft.

The division was done to capture the difference in heave resulting from different depths of excavation. As shown by the resulting variable heave distribution in Figure 2.5-175, the effect of topography is adequately captured. As expected, the magnitude of heave is directly related to the surface topography. Between the end of excavation and the beginning of construction, the maximum reported heave at the center of containment (Point C) is 4.7 in. Most of the heave is elastic and is experienced immediately after excavation. Table 2.5-68 provides heave results for the four locations shown in Figure 2.5-175.

Once excavation is completed, the foundation surface will be prepared for the placement of foundations. Settlement in the following sections will be reported from the beginning of construction or the initial reloading of the soil.

Settlement Analysis: Construction and Post-Construction (CPC Model)

The CPC model was designed to evaluate the settlements during and after construction. This model is not a continuation of the ED model. The excavation and dewatering stages included in ED model were assumed to be completed, and the excess pore pressure generated due to excavation and dewatering fully dissipated. As previously stated, settlement will be reported from the beginning of construction and beyond. The analysis also assumes that the ground surface was re-leveled after the immediate heave. As previously stated, long term heave is a small fraction of the total displacement when compared to the immediate elastic value.

The initial effective stress condition for the CPC model was in accordance with the post-excavation overburden geometry. The model assumes an average surface Elevation of 83 ft. The effect of asymmetric topography is evaluated by performing sensitivity analysis on the value of the initial ground surface elevation (i.e., initial overburden stress). A detailed discussion is provided later in this Section.

The building loads were applied in eight sequential steps as specified by Table 2.5-69. The table corresponds to the construction schedule. The loading sequence is also shown in Figure 2.5-176. Settlement analysis is conducted at the application of each step, accounting for both immediate and consolidation settlements. After the application of the last loading sequence and finalization of construction, partial rewatering occurs in the construction area. The final groundwater elevation is El. 55 ft. The construction schedule affects the timing of the settlement and tilt during construction. However, end values will be similar if variations that are typical during construction take place.

Backfill between El. 41.5 ft and El. 83 ft was placed in the first five steps indicated by Table 2.5-69 as follows:

1. During Step 1, backfill is placed between El. 41.5 ft and El. 48 ft.
2. During Step 2, additional backfill is placed between El. 48 ft and El. 61 ft.
3. During Step 3, additional backfill is placed between El. 61 ft and El. 66 ft.
4. During Step 4, additional backfill is placed between El. 66 ft and El. 76 ft.
5. During Step 5, additional and final backfill is placed between El. 76 ft and El. 83 ft.

The groundwater elevation in the Powerblock Area was modeled at El. 38 ft during construction to account for dewatering. Around the Powerblock Area, the groundwater elevation was maintained at El. 69 ft. For the post-construction conditions, groundwater elevation in the Powerblock Area was increased up to El. 55 ft and remained constant at that level, while the groundwater elevation around the Powerblock Area remained at El. 69 ft. Post construction groundwater levels will have little impact on the construction settlement.

The stiffness of the foundation mats is also accounted for in the analysis. As the construction proceeds, the deflection pattern of the foundations is expected to be closer to the rigid body motion due to the additional stiffness introduced into the foundation by the structure itself. The stiffness of the foundation mat was transitioned from an initial value based on a 10 ft thick concrete mat to a stiff, rigid-body like condition at the end of construction.

The soil properties used in the settlement analysis are provided in Section 2.5.4.2.5. The soil properties that directly impact the settlement analysis are:

- Unit Weight,
- Permeability,
- Strength parameters, used in the Mohr-Coulomb constitutive model,
- Elastic Modulus and Poisson Ratio,
- Ratio of Unload/Reload Modulus to Elastic Modulus.

The elastic modulus in the deeper Nanjemoy Sand was increased linearly, as a function of depth from its estimated value of 3,170 ksf at the interface with Layer IIC. The value of E at the lower boundary of the FEM model is 4,600 ksf, which corresponds to a rate increase of 2.6 ksf/ ft. The increase was performed according to the following relationship (DUTP, 2007) (Schanz, et al., 1999) applicable to a sand with no cohesion:

$$E = E_{ref}\sqrt{\frac{(1-\sin\Phi)\sigma'_1}{P_{ref}}}$$

Where:

$E \rightarrow$ Elastic modulus at desired depth (El. -760 ft, end of FEM model);

$E_{ref} \rightarrow$ Reference elastic modulus, calculated with effective vertical stress at El. -207.5 (Nanjemoy Sand top horizon elevation);

$\Phi \rightarrow$ Friction angle (40°);

$p_{ref} \rightarrow$ Reference pressure (100 pressure units);

$\sigma'_1 \rightarrow$ Effective vertical stress;

During the analysis, it was required to account for the asymmetric distribution of surface topography throughout the Powerblock Area. This condition is especially important for the NI common basemat. Figure 2.5-164 clearly shows that the existing surface grade at the NI changes up to 50 ft in elevation. At the lower portions, the construction of the plant will reach the original pre-consolidation pressure relatively soon. On the contrary, for high elevation points, this condition will be reached at later stages into the construction. During the first six steps of construction, some points throughout the foundation footprint will be experiencing reloading, while others are subject to loads that are higher than the original overburden pressure. This fact will have direct influence in the estimation of tilt. The topographic conditions suggest that there is potential for the NI common basemat to present additional tilt towards the North or North East (Local Coordinates) direction along the cross section indicated in Figure 2.5-164.

In order to incorporate the influence of surface topography into the settlement estimates, sensitivity on the initial average surface elevation was performed according to the following cases:

1. *Settlement Representative of Low Surface Elevation Zones*: The unloading/ reloading modulus was used until the end of the second loading step, when the reloading for the North East part of the Powerblock Area is expected to be completed. For Step three the elastic modulus value was reverted to its lower counterpart (loading Elastic modulus). This case represents the stress-stiffness correspondence for the parts of the Powerblock Area with an initial pre-excavation ground surface of about El. 60 ft.

2. *Settlement Representative of Medium Surface Elevation Zones*: The unloading/reloading modulus was used until the end of the third [Medium Elevation E Revert (1)] and fourth [Medium Elevation E Revert (2)] loading steps. These cases represent the stress-stiffness correspondence for the parts of the Powerblock Area with an initial pre-excavation ground surface of about El. 80 ft. These two cases cover the elevation range of most of the Powerblock Area.

3. *Settlement Representative of High Surface Elevation Zones*: The unloading/ reloading modulus was used until the end of the fifth loading step, when reloading is expected to be completed for the totality of the footprint area. This case represents the stress-stiffness correspondence for the parts of the Powerblock Area with an initial pre-excavation ground surface of about El. 105 ft.

By performing the settlement analysis under multiple scenarios, it is possible to assign the most representative case for each point throughout the foundation footprint, and obtain a reliable estimate of the increase of tilt for each structure, specifically the NI. Figure 2.5-177 provides a

conceptual representation of the three cases previously described. Depending on the original surface elevation with respect to plant grade, each zone throughout the footprint will be best represented by one of the three cases.

Settlement Analysis Results

The following plots and tables are provided for the purposes of presenting settlement and tilt estimates:

- Figure 2.5-179: Settlement vs. Time for center point of NI;

  This figure presents the calculation of settlement for cases that consider different initial elevations of surface topography. As previously discussed, revert from reloading to loading modulus occurs sooner for low elevation points and therefore the low elevation case indicates larger settlement. Using conservatism, the case that best represents settlement at center point of containment is the case denominated "Medium Elevation E Revert (2)". According to this case, total settlement at centerline of the reactor building is estimated at 12.7 in.

  Tilt across the NI, especially running West to East and South West to North East (Local Plant coordinates) will be heavily influenced by the variation of surface topography throughout the NI footprint. The relevance of such influence is directly related to the difference in settlement reported by the analysis cases shown in Figure 2.5-179.

- Figure 2.5-178: Settlement contour plot from FEM model (Medium Elevation Topography);

  The contour plots provide the incremental settlement from the Medium Elevation E Revert(2) case, reported after the application of each loading sequence. The maximum settlement for the NI footprint is estimated at 12.7 in. The plots shows the influence that the Nuclear Island has over the rest of the buildings. In general, the Powerblock Area will present a tilt tendency from the perimeter to the center of the footprint. Long term settlement beyond construction will be influenced by secondary consolidation and rewatering.

- Table 2.5-70: Settlement vs. Time for center point of each foundation (Medium Elevation Topography) and Figure 2.5-180, Settlement at the Center Point of Safety Related Buildings;

- Table 2.5-70 presents the tabular data of settlement under the footprint of each facility from the Medium Elevation E Revert(2) case. As expected, the Fuel Building and NI present the highest settlement. Figure 2.5-180 is the graphical representation of the settlement data provided by Table 2.5-70;

- Figure 2.5-181: Settlement tracking cross-sections;

  Tilt was recorded for several cross sections, as indicated by Figure 2.5-181. The selection of the cross-sections was done to assure that maximum tilt is captured.

- Figure 2.5-182: Foundation base settlement for four sections of the NI and Turbine Building;

The figure indicates how the foundation settles after each step of the construction sequence. The results in the figure correspond to data resulting from the topography case that conservatively provides settlement at the centerline of the reactor ("Medium Elevation E Revert (2)").

- Table 2.5-75 presents differential settlements between the NI and adjacent buildings. The differential settlements are also shown in Table 2.5-75. Figure 2.5-181 shows the location of points considered for differential settlements.

  Differential settlements between the NI and each adjacent building are determined for pairs of points at the center of the NI and each surrounding building, and also for pairs of points at the edges of the NI and each surrounding building. For the edge to edge case, the closest points for the selected building pairs are considered. Also considered is the differential settlement between RWPB and NAB.

  While calculating the differential settlement, the effect of the construction sequence is considered. The output from the model consists of settlements at the end of each one of 8 loading steps. The construction sequence indicates that construction of different buildings start at different loading steps. For example, EPGB construction starts at the 6th loading step, and any deformation obtained from the model prior to 6th loading step should be subtracted from the total deformation obtained at the end of 8th loading step. This correction aims to address the fact that construction for each building is expected to start on a level ground.

  Differential settlements (Δu_y) for the pairs were computed by using the definition below:

  $$(\Delta u_y) = (u_y)_{Adj.Bldg.} - (u_y)_{NI}$$

  where $(u_y)_{Adj.Bldg.}$ and $(u_y)_{NI}$ are the settlements at the end of 8th loading step and at the base of the adjacent building and NI, respectively.

  The U.S. EPR standard design does not include specific requirements for the differential settlements between buildings. As shown in Table 2.5-75, the largest inter-building differential settlement was close to 9.8 inches between the center of the NI and the center of EPGB2. This difference will be minimized by the time interval in construction, much of the NI settlement will have occurred prior to connection being made between the buildings. The side-by-side Seismic Category I Buildings have edge-to-edge differential settlements of less than an inch. Thus, differential settlements expected between Cat I buildings do not pose a construction concern.

- Table 2.5-71: Maximum recorded tilt for the structures in the Powerblock Area.

- Figure 2.5-183: provides the settlement underneath each facility corresponding to the cases that analyze the sensitivity on surface topography. Low elevation points will have an increase in settlement after adjustment and high elevation points will see their settlement estimates reduced.

Long Term Settlement (Creep and Rewatering)

Long term settlements related to secondary consolidation or rewatering are estimated to be very small and both aspects will counteract each other. The stress increase induced by loading are consistently lower than the pre-consolidation condition. At CCNPP the ratio of final applied

stress to the preconsolidation pressure always remains below 0.7 for the Stratum IIc Chesapeake Clay layer. The effective stress is always in the recompression range and secondary settlement is not significant (Terzaghi, et al., 1995).

Settlement Monitoring

A settlement monitoring program will be enforced to record heave of the excavation bottom, the effect of dewatering and the effect of Nuclear Island Basemat loading during and after construction. This is necessary to confirm that the estimated rate of heave and settlement is consistent with the field observations. The purpose of this monitoring program is to assess and document the actual settlements in comparison with the predicted and the acceptable limits. The settlement monitoring program consists of three primary elements:

- Piezometers to measure effects of dewatering and pore pressures in a soil layer prone to consolidation type settlement. Vibrating wire piezometers are preferred for this purpose as they are adequately sensitive and responsive and easily record positive and negative changes on a real time basis. Piezometers should be screened in Stratum II-B (Chesapeake Cemented Sand) and Stratum II-C (Chesapeake Clay/Silt).

- Settlement monuments placed directly on concrete, preferably on the Mud Mat and on the corners of the structures at grade that are accessible with conventional surveying equipment.

- Settlement sensors and extensometers if monuments are not practical or if fills are used over consolidation type soils and it is necessary to monitor settlement of the consolidation type soils independent of the consolidation of the fill.

The instrumentation plan for the Powerblock Area of the site will consist of horizontal settlement sensors, Vibrating Wire (VW) piezometers, surface monuments, concrete anchored monuments, extensometers and one accelerometer. The definitive number of instruments needs to be established during design stages of the monitoring system. The tentative locations of the instruments are shown on Figure 2.5-224.

Tested and calibrated settlement sensors will be used to monitor settlement and heave within the excavation footprint. Settlement sensors will be installed at the bottom of the proposed foundation (bench mark El. 40) before the excavation of the Powerblock Area is started. The sensors will be placed at the approximate locations shown on Figure 2.5-224 and the required cables will be routed away from the fill area.

The settlement sensors have two important components, the sensor and the reservoir. The sensor will be located inside the limits of the structural backfill while the reservoir is located outside the fill limits in a borehole attached by a Borros anchor (Dunnicliff, 1988). The reservoir needs to be located on stable ground because it reads difference in settlement between the reservoir and sensor. The wires connecting the sensor to the reservoir are suited for direct burial. The wires shall be buried below the frost line for protection and to minimize temperature differentials that could result in erroneous settlement or heave measurements.

Figure 2.5-224 shows a tentative distribution and placement of VW piezometers to be installed around the Perimeter of the Powerblock Area. The VW piezometers will be used to measure ground water elevations and associated changes in pore pressure during dewatering, excavation, structural backfill placement, and plant construction.

Extensometers shall be installed in the Powerblock Area. These will be installed adjacent to the Reactor building, bench mark elevation 41.5, adjacent to the Turbine building, adjacent to the Essential Service Water Building (ESWB) Nos. 1, 2, and adjacent to ESWB Nos. 3 and 4. At least one extensometer will be installed adjacent to the Radioactive Waste Processing Building. The bench mark for the Turbine Building, ESWB and Radioactive Processing Building is El. 59.5. The extensometers shall be calibrated rod type borehole extensometers. The extensometers will either be protected by raising the standpipe out of the ground approximately one foot or by placing the extensometer approximately 10 to 12 inches below top of the ground surface.

Concrete survey monuments to monitor the settlement of EPGB and ESWB basemats will be placed as shown in Figure 2.5-225. Similarly, the settlement of the CBIS will be monitored using the concrete survey monuments shown in Figure 2.5-226. The final location of the monitoring points is subject to modification to adjust for construction limitations. The number of monitoring points is sufficient to check against the predicted settlements.

After the structural backfill has been placed to the final grade, Surface Monuments (SM), bench mark El. 80 shall be placed on the surface of the backfill at approximate locations shown on Figure 2.5-224. The monuments shall consist of a one foot diameter concrete cylinders placed a minimum of three feet below final grade and be fitted with a brass dome cap with a point for survey use.

Additional concrete survey monuments will be placed on the interior of the NI to monitor the settlement throughout the NI common basemat, as shown in Figure 2.5-227. The number of settlement monitoring points is sufficient to check against the predicted settlements. The final location of the monitoring points is subject to modification to adjust for construction limitations. However, the number and distribution of points will be similar to those proposed in Figure 2.5-227.

On the side of foundation mats, no later than 28 days after construction, National Geodetic Survey (NGS) (USDC, 1978) survey disks will be placed by drilling a cavity on the side of foundation mats. The cavity will be backfilled with a mortar mix and the survey disk will be anchored into the foundation mat. The disk needs to be located at strategic points of the mat and have a direct view to a benchmark or to other survey points that can relate to a benchmark.

One accelerometer shall be installed to record any seismic events that occur during or after construction. The accelerometer shall be placed within the mat foundation of the Reactor Building.

The Instrumentation Plan for the Makeup Water Intake Structure (MWIS) will consist of settlement sensors, extensometers, surface monuments and one accelerometer. Tentative location of these instruments is shown on Figure 2.5-226. Calibrated settlement sensors will be used to monitor settlement and heave within the excavation footprint of the UHS. Extensometers will be installed adjacent to the Circulating Water Makeup Intake Structure and adjacent to the UHS Makeup Water Intake Structure. The bench mark for the extensometers is El. -26.5. The extensometers shall be calibrated rod type borehole extensometers. The extensometers will either be protected by raising the standpipe out of the ground approximately one foot or placing the extensometer approximately 10 to 12 inches below top of the ground surface. Finally, one accelerometer shall be installed to record any seismic events that occur during or after construction. The accelerometer shall be placed within the foundation of the MWIS.

Each instrument will be read to determine baseline conditions after installation. For the settlement sensors, the baseline readings will be taken before any site earthwork has been

performed. The baseline survey should be completed with a minimum of three different readings taken over several days to verify that the readings have stabilized.

Each instrument should be read at least twice a day in the initial stages of this project. During later stages of the project, the reading frequency may be adjusted to once per day and longer at the discretion of the Engineer.

Plots showing movement (settlement or heave) versus time should be maintained during construction, along with estimated load versus time curves. The site should remain dewatered until the curves go asymptotic, at which time connections between buildings can be made. Monitoring should continue after these connections are made in order to assure asymptotic conditions. After construction is completed, all instruments will be monitored for at least one year. At that time, the Engineer will define frequency and instruments to maintain a long-term monitoring program.

Conclusions – Settlement Analysis

The analysis and careful examination of the settlement results provide the following conclusions apply.

- Total average settlement at the end of construction beneath the Reactor Building footprint is estimated at 12.7 in. Settlement for other facilities is provided in Table 2.5-70 and Figure 2.5-183 for the medium topography case.

- Long term settlements related to secondary consolidation or rewatering are estimated to be very small and both aspects will counteract each other.

- Maximum tilt for each building is provided in Table 2.5-71. Maximum tilt is highest for Section CC' of the NI running from south west to north east (Local Coordinates), and Section BB' running west to east.

  Differential settlement or tilt depends on (1) the asymmetric nature of loads, (2) the irregular thickness of the subsurface strata, and (3) the asymmetry in surface topography. The first two are naturally captured by the FEM simulation. The third, influence of asymmetric topography, is captured by means of sensitivity analyses.

- The differential settlement between the NI and TB is provided after each loading step. Since both facilities are founded on different basemats, a discontinuity shows the magnitude of the differential settlement. The same condition applies between the NI and the NAB. The differential settlement between the NI and these two adjacent facilities is estimated to be in the order of one to two inches. Tilt between NAB and RB occurs in opposite directions, and both facilities tilt towards each other. This condition needs to be accounted for in the final design and construction.

- Groundwater is below foundation grade during construction. After construction, groundwater is expected to rise to El. 55. The settlement estimates are not sensitive to variations in the groundwater rebound level, if such variations are in the order of plus or minus ten feet.

The U.S. EPR FSAR Section 2.5.4.10.2 identifies tilt settlement as a required parameter to be enveloped, defined as "½ inch per 50 ft in any direction across the foundation basemat of a Seismic Category I structure" and that "values larger than this may be demonstrated acceptable by performing additional site specific evaluations."

The estimated tilt settlements for ESWB 1 and ESWB 2 do not meet the U.S. EPR FSAR requirement of ½ inch per 50 ft (or 1/1,200) and EPGB 1 is at ½ inch per 50 ft (see Table 2.5-71); however, additional site specific evaluations will be performed to demonstrate their acceptability, as follows.

To verify that foundations perform according to estimates, and to provide an ability to make corrections, if needed, major structure foundations are monitored for rate of movement during and after construction.

Foundations are designed to safely tolerate the anticipated total and differential settlements. Additionally, engineering measures are incorporated into design for control of differential movements between adjacent structures, piping, and appurtenances sensitive to movement, consistent with settlement estimates. This includes the development and implementation of a monitoring plan that supplies and requires evaluation of information throughout construction and post-construction on ground heave, settlement, pore water pressure, foundation pressure, building tilt, and other necessary data. This information provides a basis for comparison with design conditions and for projections of future performance.

The estimated differential settlements represent departures from the U.S. EPR FSAR requirements. Additional discussion of the acceptability of these estimated differential settlements is provided in Section 3.8.5.

2.5.4.10.2.3 Settlement in the Intake Area

The settlement model in the Intake Area is developed in a similar form. The model is much simpler and the influence of neighboring structures is negligible. The size of the foundation is very small compared to the variability in layer thickness throughout the footprint. Soil layers, as shown in Figure 2.5-154 are horizontal. There is no additional complication introduced by asymmetric topography. The loading sequence for the Intake Area facilities is applied in a single step. Figure 2.5-184 provides the FEM model for the UHS MWIS.

The total settlement at the end of construction for the facilities in the Intake Area is provided in Table 2.5-72. The maximum total settlement is 3.6 in and the maximum estimated tilt is 0.4 in/50 ft.}

2.5.4.10.3 Uniformity and Variability of Foundation Support Media

The U.S. EPR FSAR includes the following COL Item in Section 2.5.4.10.3:

> A COL applicant that references the U.S. EPR design certification will investigate and determine the uniformity of the soil layer(s) underlying the foundation basemats of Seismic Category I structures.

This COL Item is addressed as follows:

{Three criteria are identified in the U.S. EPR FSAR for establishing uniformity in foundation support media, namely, (1) presence of soil and rock, (2) dip angle of soil layers, and (3) shear wave velocity. Each is addressed below:

1. Foundations of all Seismic Category I structures at the CCNPP Unit 3 site are supported on compacted structural fill which is in turn supported on natural soils. Bedrock at the site is very deep, at about 2,500 ft below ground surface. Given the considerable depth

to bedrock, non-uniform foundation conditions resulting from combined soil-rock support are not applicable to foundations at the CCNPP Unit 3 site.

2. Detailed subsurface information is presented in Section 2.5.4. Stratigraphic profiles indicate that the stratigraphic lines delineating various soil units have gentle slopes, mostly sloping about 1 to 2 degrees. This is consistent with the regional dip of 1 to 2 degrees in Coastal Plain deposits (refer to Section 2.5.1 for more details). However, at isolated CCNPP Unit 3 locations, stratigraphic units dip steeper, up to about 10 degrees which may be due to inherent assumptions in developing the stratigraphic lines or paleochannels and/or irregular erosional surfaces. Regardless, these steeper angles are less than the dip angle of 20 degrees from the horizontal identified in the U.S. EPR FSAR as the criterion for determining levelness of layers. On this basis, the soil layers at the CCNPP Unit 3 site are considered horizontal.

3. Classification of uniformity (or non-uniformity) in foundation support media resides with the geotechnical engineer, per the U.S. EPR FSAR. Shear wave velocity (Vs) measurements are used for this determination because they are a) in-situ measurements reflecting the natural ground conditions and b) important input to the safety evaluation of structures such as in soil-structure interaction and seismic analyses. The shear wave velocity measurements clearly indicate the presence of uniform subsurface conditions. For engineering analyses purposes, specifically: settlement, foundation, stability, and site response analysis, the shear wave velocity profiles are equivalent and the substrata can be considered uniform. This conclusion is supported by the information and analysis provided in Section 2.5.4.2.2.2.

Based upon the above, CCNPP Unit 3 is considered a Uniform Site.}

2.5.4.10.4 Site Investigation for Uniform Sites

No departures or supplements.

2.5.4.10.5 Site Investigations for Non-uniform Sites

No departures or supplements.

{Section 2.5.4.10.6 is added as a supplement to the U.S. EPR FSAR.

2.5.4.10.6 Earth Pressure

Static and seismic lateral earth pressures are addressed for below-grade walls. Seismic earth pressure diagrams are structure-specific. They are only addressed generically herein. Specific earth pressure diagrams are developed for specific structures based upon each structure's final configuration. Passive earth pressures are not addressed; they are excluded for conservatism for general purpose applications. Engineering properties for structural fill are used to estimate earth pressures. The properties of backfill are provided in Section 2.5.4.2.5.9. Structural backfill material is verified to meet the design requirements prior to use during construction. A surcharge pressure of 500 psf applied at the ground surface is assumed. The validity of this assumption will be confirmed during detailed design. In addition to earth pressures associated with the effective pressure distribution of the backfill materials, subsurface structures and walls may also be subjected to surcharge loads caused by heavy equipment operating close to the structure and by increased permanent lateral earth pressures caused by compaction of backfill material with heavy equipment. Compaction-induced earth pressures can cause a significant increase in the permanent lateral earth pressures acting on a vertical wall of a structure. The

magnitude of the increase in lateral pressure is dependent, among other factors, on the effective weight of the compaction equipment and the weight, earth pressure coefficient, and Poisson's ratio of the backfill material.

The lateral pressure that will be generated due to the compaction of the backfill is calculated based on the assumption that the equipment can operate to within 6 inches of the wall. Significant reductions in lateral pressures occur as the closest allowable distance to the wall is increased. A 3.2-ton vibratory roller compactor is used to estimate lateral pressures due to compaction. The critical lateral pressure in excess of active and at-rest pressure associated with this equipment is considered to be 400 psf; the critical depth at which this critical pressure is reached, Dc, is 1.7 ft. However, the critical depth is conservatively considered as Dc = 0.

In developing the earth pressure diagrams, the following are assumed:

- Ground surface behind walls is horizontal,
- The side of the wall in contact with the backfill is vertical and there is no friction between the backfill and the wall,
- Retaining walls designed for the active earth pressure are allowed to move laterally, and building walls designed for the at-rest condition are prevented from moving laterally;
- Properties of backfill relevant to the earth pressure calculations are unit weight and angle of shearing resistance. These are provided in Table 2.5-53 and Table 2.5-56 respectively. The values are obtained from laboratory testing of backfill bulk samples and these are 145 pcf and 40°;
- Active and at rest earth pressure coefficients are provided in Table 2.5-60. These values are: $k_A = 0.22$, and $k_0 = 0.36$;
- For active and surcharge pressures, earthquake-induced horizontal ground accelerations are addressed by the application of $k_h g$. Vertical ground accelerations ($k_v g$) are considered negligible and are ignored (Seed, et al., 1970). A seismic horizontal acceleration of 0.15 g is conservatively assumed (consistent with the plant SSE).

2.5.4.10.6.1 Static Lateral Earth Pressures

The static active earth pressure is estimated with the following equation (Lambe, et al., 1969):

$$p_{AS} = K_{AS}\gamma z$$

Where:

p_{AS} → Static active earth pressure;

K_{AS} → Active earth pressure coefficient from Table 2.5-60;

γ → Unit Weight of backfill;

z → Depth below ground surface;

The static at-rest earth pressure is estimated with the following equation (Lambe, et al., 1969):

$$p_{0S} = K_{0S}\gamma z$$

Where:

p_{AS} → At rest earth pressure;

K_{AS} → At rest earth pressure coefficient from Table 2.5-60;

γ → Unit Weight of backfill;

z → Depth below ground surface;

Hydrostatic pressure is accounted for by assuming Groundwater Level at El. 55 ft, which is 13.5 ft above foundation level of the NI.

2.5.4.10.6.2 Seismic Lateral Earth Pressure

The active seismic pressure, pAE, is given by the Mononobe-Okabe equation (Whitman, 1991), represented by:

$$p_{AE} = \Delta K_{AE}\gamma(H - z)$$

Where:

p_{AE} → Active seismic pressure;

ΔK_{AE} → Coefficient of active seismic earth pressure ($K_{AE} - K_{AS}$);

K_{AE} → Mononobe-Okabe coefficient of active seismic earth thrust

$$K_{AE} = \frac{\cos^2(\Phi' - \theta)}{\cos^2\theta\left(\sqrt{\frac{\sin\Phi'\sin(\Phi' - \theta)}{\cos\theta}}\right)^2}$$

θ → $\theta = \tan^{-1}(k_h)$

k_h → Seismic coefficient (0.15 g)

γ → Unit Weight of backfill;

H → Below-grade height of wall;

z → Depth below the top of the backfill;

The value ΔK_{AE} can be estimated as 0.75 k_h for k_h values less than about 0.25 g, regardless of the angle of shearing resistance of the backfill (Seed, et al., 1970).

The seismic at-rest pressure ΔK_{0E}, for below-grade walls for Category I structures is evaluated using a method that recognizes the frequency content of the design motion, limited building wall movements due to the presence of floor diaphragms, and uses the soil shear wave velocity and damping as input (Ostadan, 2004). To predict lateral seismic soil pressures for below-grade

structural walls resting on firm foundations and assuming non-yielding walls, the method involves the following steps:

1. For conservatism, define the ground motion as the CCNPP Unit 3 Safe Shutdown Earthquake (SSE) peak ground acceleration. This value is the maximum spectral acceleration of the site specific spectra (See Section 3.7).

2. Compute the total mass for a representative Single Degree of Freedom (SDOF) system using Poisson's ratio and the mass density of the soil, m:

$$m = \frac{1}{2}\frac{\gamma}{g}H^2\psi_v$$

Where:

$\gamma/g \rightarrow$ Total mass density of the structural backfill;

$H \rightarrow$ Height of wall

$\psi v \rightarrow$ Factor to account for Poisson's ratio (v), with $|v| = 0.3$ adopted for structural backfill for unsaturated conditions, and 0.45 was considered for saturated conditions

$$\psi_v = \frac{2}{\sqrt{(1-v)(2-v)}}$$

3. Obtain the lateral seismic force as the product of the total mass obtained from Step 2, and 0.15 g.

4. Obtain the maximum lateral seismic soil pressure at the ground surface by dividing the lateral force obtained from Step 3 by the area under the normalized seismic soil pressure, or 0.744 H.

5. Obtain the soil pressure profile by multiplying the maximum pressure from Step 4 by the following pressure distribution relationship:

$p(y) = -0.0015 + 5.05y - 15.84y^2 + 28.25y^3 - 24.59y^4 + 8.14y^5$

Where:

$y \rightarrow$ Normalized height ratio (y/H). "y" is measured from bottom of the wall and y/H ranges from a value of zero at the bottom of the wall to a value of 1.0 at the top of the wall.

For well-drained backfills, seismic groundwater pressures need not be considered (Ostadan, 2004). Since granular backfill is used for the project, only hydrostatic pressures are taken into consideration. Seismic groundwater thrust greater than 35 percent of the hydrostatic thrust can develop for cases when $k_h > 0.3g$ (Whitman, 1990). Given the relatively low seismicity at the CCNPP Unit 3 site ($k_h < 0.1g$), seismic groundwater considerations can be ignored.

Representative earth pressure diagrams are provided in Figure 2.5-185}.

2.5.4.11 Design Criteria

No departures or supplements.

2.5.4.12 Techniques to Improve Subsurface Conditions

{Major structures derive support from the very dense cemented soils or compacted structural backfill. Given the planned foundation depths and soil conditions at these depths, no special ground improvement measures are warranted. Ground improvement is limited to excavation of unsuitable soils, such as existing fill or loose/soft soils, and their replacement with structural backfill or lean concrete. It also includes proof-rolling of foundation subgrade for the purpose of identifying any unsuitable soils for further excavation and replacement, which further densifies the upper portions of the subgrade. In absence of subsurface conditions at the site that require ground improvement, ground control, i.e., maintaining the integrity of existing dense or stiff foundation soils, is the primary focus of earthworks during foundation preparation. These measures include groundwater control, use of appropriate measures and equipment for excavation and compaction, subgrade protection, and other similar measures.

2.5.4.13 References

This section is added as a supplement to the U.S. EPR FSAR.

ACI, 1994. ACI, 1994. Manual of Concrete Practice, Part 1, Materials and General Properties of Concrete, American Concrete Institute [Report] - 1994.

API, 2007. Cathodic Protection of Aboveground Petroleum Storage Tanks, API Recommended Practice Number 651, American Petroleum Institute [Report] - 2007.

ASCE, 2005. American Society of Civil Engineers, "Seismic Design Criteria for Structures, Systems, and Components in Nuclear Facilities," American Society for Civil Engineers/Structural Engineering Institute, Report ASCE/SEI 43-05 [Report] - 2005.

ASTM, 1966. ASTM STP 399, "Dynamic Cone for Shallow In-Situ Penetration Testing," American Society for Testing and Materials (ASTM), 1966.

ASTM, 1999. Standard Test Method for Penetration Test and Split-Barrel Sampling of Soils, American Society for Testing and Materials, ASTM D1586-99. [Report] - 1999.

ASTM, 2000a. Standard Practices for Preserving and Transporting Soil Samples, American Society for Testing and Materials, ASTM D4220-95(2000) [Report] - 2000.

ASTM, 2000b. Standard Test Method for Performing Electronic Friction Cone and Piezocone Penetration Testing of Soils, American Society for Testing and Materials, ASTM D5778-95 (reapproved 2000), [Report] - 2000.

ASTM, 2000c. Standard Practice for Thin-Walled Tube Sampling of Soils for Geotechnical Purposes, American Society for Testing and Materials, ASTM D1587-00. [Report] - 2000.

ASTM, 2001a. Standard Test Method for Field Measurement of Soil Resistivity Using the Wenner Four-Electrode Method, American Society for Testing and Materials, ASTM G57-95 (reapproved 2001). [Report] - 2001.

ASTM, 2002a. Standard Test Methods for Laboratory Compaction Characteristics of Soil Using Modified Effort (56,000 ft-lbf/ft^3 (2,700 kN-m/m^3)), American Society for Testing and Materials, ASTM D1557-02 [Report] - 2002.

ASTM, 2002b. Standard Test Method (Field Procedure) for Instantaneous Change in Head (Slug) Tests for Determining Hydraulic Properties of Aquifers, American Society for Testing and Materials, ASTM D4044-96 (reapproved 2002). [Report] - 2002.

ASTM, 2004a. Standard Practice for Design and Installation of Ground Water Monitoring Wells, American Society for Testing and Materials, ASTM D5092-04. [Report] - 2004.

ASTM, 2004b. Standard Practice for Determining the Normalized Penetration Resistance of Sands for Evaluation of Liquefaction Potential, ASTM D6066 - 96(2004) [Report] - 2004.

ASTM, 2005a. Standard Test Method for Energy Measurement for Dynamic Penetrometers, American Society for Testing and Materials, ASTM D4633-05. [Report] - 2005.

ASTM, 2005b. Standard Specification for Portland Cement, American Society for Testing and Materials, ASTM C150-05. [Report] - 2005.

ASTM, 2005c. Standard Test Methods for Laboratory Determination of Water (Moisture) Content of Soil and Rock by Mass, American Society for Testing and Materials, ASTM 2216-05 [Report], 2009.

ASTM, 2006. Standard Practice for Description and Identification of Soils (Visual-Manual Procedure), American Society for Testing and Materials, ASTM D2488-06. [Report] - 2006.

ASTM, 2007a. Standard Test Method for Prebored Pressuremeter Testing in Soils, American Society for Testing and Materials, ASTM D4719-07 [Report] - 2007.

ASTM, 2007b. Standard Test Method for Density and Unit Weight of Soil in Place by Sand-Cone Method, American Society for Testing and Materials, ASTM 1556-07 [Report], 2009.

ASTM, 2008a. Standard Test Method for Soil Compaction Determination at Shallow Depths Using 5-lb (2.3 kg) Dynamic Cone Penetrometer, ASTM D7380-08 [Report], 2009.

ASTM, 2008b. Standard Test Method for In-Place Density and Water Content of Soil and Soil-Aggregate by Nuclear Methods (Shallow Depth), American Society for Testing and Materials, ASTM 6938-08a, [Report], 2009.

ASTM, 2009. Standard Test Methods for Laboratory Compaction Characteristics of Soil Using Modified Effort (56,000 ft-lbf/ft3(2700 kN-m/m3)), American Society for Testing and Materials, ASTM 1557-09 [Report], 2009.

Bechtel, 1992. Subsurface Investigation and Foundation Report for Calvert Cliffs Nuclear Plant Diesel Generator Project, Prepared for Baltimore Gas and Electric Company, Bechtel Power Corporation [Report] - 1992.

Bechtel, 2007. Reconciliation of EPRI and RCTS Results, Calvert Cliffs Nuclear Power Plant Unit 3, Bechtel Power Corporation, December 2007. [Report] - 2007.

BGE, 1982. Updated Final Safety Analysis Report, Calvert Cliffs Nuclear Power Plant (Units 1 and 2), Docket 50-317 and 50-318, Calvert County, Maryland, Baltimore Gas and Electric Company, Baltimore, Maryland [Report] - 1982.

CEE, 1985. Liquefaction of Soils During Earthquakes, National Research Council, Committee on Earthquake Engineering, National Academy Press [Report] - 1985.

CFR, 2007. Geologic and Seismic Siting Criteria, Title 10 Code of Federal Regulations, part 100.23, 2007.

Coduto, 2001. Coduto D.P., Foundation Design, Second Edition, p. 233 [Book] - 2001.

Davie, et al., 1988. Davie L. and Lewis M., Settlement of Two Tall Chimney Foundations [Conference] // Proceedings 2nd International Conference on Case Histories in Geotechnical Engineering. - pp 1309-1313 - 1988.

Deere, et al., 1996. Deere D. and Miller R. Engineering Classification and Index Properties of Intact Rock, University of Illinois, Prepared for Air Force Weapons Laboratory, Technical Report Number AFWL-TR-65-116 [Report] - 1996.

Dominion, 2006. North Anna Early Site Permit Application, Revision 9 Docket Number. 05200008, Dominion Nuclear North Anna LLC [Report] - 2006.

Dunnicliff, 1988. Geotechnical Instrumentation for Monitoring Field Performance, John Dunnicliff, John Wiley & Sons, Inc., 1988.

DUTP, 2007. PLAXIS 3D Foundation Version 2, Delft University of Technology & PLAXIS [Report] - 2007.

EPRI, 1990. Manual on Estimating Soil Properties for Foundation Design, F. Kulhawy and P. Mayne, Electric Power Research Institute, Report EL-6800 [Report] - 1990.

EPRI, 1993. Guidelines for Determining Design Basis Ground Motions, Electric Power Research Institute, Report Number TR-102293. [Report] - 1993.

FHWA, 1990. Reinforced Soil Structures, Vol. 1, Design and Construction Guidelines, Federal Highway Administration, Federal Highway Administration Report Number FHWA-RD-89-043 [Report] - 1990.

Hansen, 1996. Hansen H., Hydrostratigraphic Framework of the Piney Point-Nanjemoy Aquifer and Aquia Aquifer in Calvert and St. Mary's Counties, Maryland, Open-File Report No. 96-02-8, 1996. [Report] - [s.l.]: Maryland Geological Survey - 1996.

IBC 2006. International Building Code, International Code Council, Inc., Country Club Hills, IL, Table 1804.2 [Report] - 2006.

IEEE, 1983. Guide for Measuring Earth Resistivity, Ground Impedance, and Earth Surface Potentials of a Ground System Part 1: Normal Measurements, Institute of Electrical and Electronics Engineers, IEEE 81 [Report] - 1983.

Lambe, et al., 1969. Lambe T. and Whitman R. Soil Mechanics [Book] - New York: John Wiley and Sons Inc. -1969.

MACTEC, 2009a. Revised Laboratory Testing Results, Rev 2, Calvert Cliffs Nuclear Power Plant Unit 3, Report by MACTEC Engineering and Consulting, Inc., Charlotte, North Carolina [Report] - 2009.

MACTEC, 2009b. Structural Fill Static Laboratory Testing Results, Rev. 1, Report by MACTEC Engineering and Consulting, Inc., Charlotte, North Carolina [Report] - 2009.

MACTEC, 2009c. Structural Fill Dynamic Laboratory Testing Results, Rev. 1, Report by MACTEC Engineering and Consulting, Inc., Charlotte, North Carolina [Report] - 2009.

MACTEC, 2009d. Intake Samples Laboratory Test Data Report, Report by MACTEC Engineering and Consulting, Inc., Charlotte, North Carolina [Report] - 2009.

Meyerhof, et al., 1978. Ultimate Bearing Capacity of Foundation on Layered Soil Under Inclined Load, G. Meyerhof and A. Hanna, Canadian Geotechnical Journal, Volume 15, Number 4, pp 565-572 [Journal] - 1978.

Ohya, 1986. In-Situ P and S Wave Velocity Measurement, Proceedings of In Situ '86, American Society of Civil Engineers -1986.

Ostadan, 2004. Seismic Soil Pressure for Building Walls-An Updated Approach, F. Ostadan, 11th International Conference on Soil Dynamics and Earthquake Engineering and 3rd International Conference on Earthquake Geotechnical Engineering, University of California, Berkeley [Conference] - 2004.

REI, 2001. Technical Basis for Revision of Regulatory Guidance on Design Ground Motions: Hazard- and Risk-consistent Ground Motion Spectra Guidelines: NUREG/CR 6728", Risk Engineering Inc., U.S. Nuclear Regulatory Commission [Report] - 2001.

Robertson, et al., 1988. Guidelines for Geotechnical Design Using CPT and CPTU, P. K. Robertson, and R. G. Campanella, Soil Mechanics Series No. 120, University of British Columbia [Journal] - 1988.

Rosen, et al., 1986. Rosen M. and Holdren G., Origin of Dolomite Cement in Chesapeake Group (Miocene) Siliciclastic Sediments: An Alternative Model to Burial Dolomatization [Journal] // Journal of Sedimentary Petrology. - Volume 56, Number 6, pp 788-798 -1986.

Salgado, 2008. The Engineering of Foundations, Salgado R. [Book] - 2008.

Schantz, et al., 1999. Schanz T., Vermeer P.A. and Bonnier P.G. The hardening soil model: Formulation and verification, Beyond 200 in Computational Geotechnics - 10 Years of PLAXIS [Conference] - 1999.

Schnabel, 2007a. Geotechnical Subsurface Investigation Data Report (Revision No. 1), CGG Combined Operating License Application (COLA) Project, Calvert Cliffs Nuclear Power Plant (CCNPP), Calvert County, Maryland, Schnabel Engineering North, LL [Report] - 2007.

Schnabel, 2007b. Geotechnical Subsurface Investigation Data Report Addendum No. 3 (RCTS Test Results), Revision 2, CGG Combined Operating License Application (COLA) Project, Calvert Cliffs Nuclear Power Plant (CCNPP), Report by Schnabel Engineering North, LLC [Report]. - Calvert County, Maryland: [s.n.] - 2007.

Schnabel, 2009. Geotechnical Subsurface Investigation Data Report, CGG Combined Operating License (COL) Project - Phase 2, Calvert Cliffs Nuclear Power Plant, Calvert County, Maryland, Report by Schnabel Engineering North, LLC [Report] - 2009.

Seed, et al., 1970. Seed H.B. and Whitman R.V., Design of Earth Retaining Structures for Dynamic Loads, Proc. Specialty Conference on Lateral Stresses in the Ground and Design of Earth-Retaining Structures, ASCE, New York, pp 103-147 [Conference] - 1970.

Senapathy, et al., 2001. Senapathy H., Clemente J. and Davie J. Estimating Dynamic Shear Modulus in Cohesive Soils, [Conference] // XVth International Conference on Soil Mechanics and Geotechnical Engineering - 2001.

SGS, 1993. Swedish Geotechnical Society, Recommended Standard for Cone Penetration Tests, Report SGF 1:93E, Stockholm, Sweden, 1993 [Report] - 1993.

SNOC, 2006. Vogtle Early Site Permit Application, Revision 1, Docket No. 052011, Southern Nuclear Operating Company, Inc. [Report] - 2006.

Terzaghi, et al., 1995. Terzaghi K., Peck R.B. and Mesri G., Soil Mechanics in Engineering Practice, Terzaghi, K., Peck, R.B., Mesri, G., John Wiley & Sons, Inc, New York, NY. [Book] - 1995.

USDC, 1978. National Oceanic and Atmospheric Administration (NOAA) Manual NOS NGS 1, Geodetic Benchmarks, U.S. Department of Commerce, 1978.

USGS, 1983. Preliminary Analysis of Geohydrologic Data from Test Wells Drilled Near Chester, on Kent Island, Queen Anne's County, MD, Open File Report 82-854, Mack F. [Report]. - [s.l.]: U.S. Geological Survey - 1983.

USGS, 1984. Summary of Hydrogeologic Data from a Deep (2,678 ft) Well at Lexington Park, St. Mary's County, Maryland, U.S. Geological Survey, Open File Report 84-02-1, Maryland Geological Survey, H. Hansen and J. Wilson [Report] - 1984.

USGS, 2000. Data for Quaternary Faults, Liquefaction Features, and Possible Tectonic Features in the Central and Eastern United States, East of the Rocky Mountain Front, U.S. Geological Survey, Open File Report 00-260, J. Crone and R. Wheeler [Report] - 2000.

USNRC, 2002. Technical Basis for Revision of Regulatory Guidance on Design Ground Motions: Development of Hazard- & Risk-Consistent Seismic Spectra for Two Sites, NUREG/CR-6769, U.S. Nuclear Regulatory Commission [Report] - 2002.

USNRC, 2003a. Site Investigations for Foundations of Nuclear Power Plants, Regulatory Guide 1.132, U.S. Nuclear Regulatory Commission [Report] - 2003.

USNRC, 2003b. Laboratory Investigations of Soils for Engineering Analysis and Design of Nuclear Power Plants, Regulatory Guide 1.138, Revision 2, U.S. Nuclear Regulatory Commission [Report] - 2003.

USNRC, 2003c. Procedures and Criteria for Assessing Seismic Soil Liquefaction at Nuclear Power Plant Sites, Regulatory Guide 1.198, U.S. Nuclear Regulatory Commission [Report] - 2003.

USNRC, 2007a. Combined License Applications For Nuclear Power Plants (LWR Edition), Regulatory Guide 1.206 [Report]. - [s.l.]: U.S. Nuclear Regulatory Commission -2007.

USNRC, 2007b. Regulatory Guide 1.208, A Performance-Based Approach to Define the Site-Specific Earthquake Ground Motion [Report] - 2007.

Vesic, et al., 1975. Bearing Capacity of Shallow Foundations, Foundation Engineering Handbook, A. Vesic, H. Winterkorn and H. Fang, Editors, Van Nostrand Reinhold Co [Journal] - 1975.

Whitman, 1990. Seismic Design and Behavior of Gravity Walls, Proceedings, Specialty Conference on Design and Performance of Earth-Retaining Structures, R. Whitman, ASCE, NY, pp 817-842 [Conference] - 1990.

Whitman, 1991. Seismic Design of Earth Retaining Structures, R. Whitman, Proceedings 2nd International Conference on Recent Advances in Geotechnical Earthquake Engineering and Soil Dynamics, pp 1767-1778 [Journal] - 1991.

Youd, et al, 2001. Youd T. L. [et al.] Liquefaction Resistance of Soils: Summary Report from the 1996 NCEER and 1998 NCEER/NSF Workshops on Evaluation of Liquefaction of Soils, ASCE Journal of Geotechnical and Geoenvironmental Engineering, Volume 127, Number 10, pp 817-833 [Journal] - 2001.}

2.5.5 Stability of Slopes

The U.S. EPR FSAR includes the following COL Item for Section 2.5.5:

> A COL applicant that references the U.S. EPR design certification will evaluate site-specific information concerning the stability of earth and rock slopes, both natural and manmade (e.g., cuts, fill, embankments, dams, etc.), of which failure could adversely affect the safety of the plant.

This COL Item is addressed as follows:

{This section addresses the stability of constructed and natural slopes. It was prepared based on the guidance in relevant sections of NRC Regulatory Guide 1.206, "Combined License Applications for Nuclear Power Plants (LWR Edition)" (NRC, 2007). Constructed slopes evolve as part of the overall site development.

The site of the Calvert Cliffs Nuclear Power Plant (CCNPP) Unit 3 is comprised of rolling topography. The site is planned to be graded in order to establish the final grade for the project, resulting in cuts and fills, as well as slopes. The stability of these slopes and their potential impact on safety-related structures are evaluated herein. Natural slopes at the site consist of the Calvert Cliffs; they are steep slopes undergoing continuous erosion. The impact of naturally-occurring erosion on these cliffs and their potential impact on safety-related structures are also evaluated.

Information on site conditions and geologic features is provided in Section 2.5.1. Section 2.5.4 presents a discussion of the properties of the underlying soil and the backfill.

All elevations referenced in this section are based on National Geodetic Vertical Datum of 1929 (NGVD 29).

Sections 2.5.5.1 through 2.5.5.5 are added as a supplement to the U.S. EPR FSAR.

2.5.5.1 Slope Characteristics

The characteristics of constructed and natural slopes are described below.

2.5.5.1.1 Characteristics of Constructed Slopes

Site grading for CCNPP Unit 3 structures will include such areas as the powerblock, switchyard, cooling tower (collectively identified as the CCNPP Unit 3 area), the intake area and the utility corridor between the CCNPP Unit 3 area and the intake area. The powerblock includes the Reactor Building, Fuel Building, Safeguard Buildings, Emergency Power Generating Building (EPGB), Essential Service Water Building (ESWB), Nuclear Auxiliary Building (NAB), Access Building, Radioactive Waste Building, Turbine Building, Fire Protection Building and Switchgear Building. The intake area includes the Ultimate Heat Sink Makeup Water Intake Structure (UHS MWIS), Circulating Makeup Water Intake Structure (CW MWIS), Forebay and Fish Return. All the safety related structures are in these two areas. Natural ground surface elevations within the powerblock range from approximately Elevation 47 ft to Elevation 121 ft, and approximately Elevation 8 ft to Elevation 11 ft within the intake area, as shown in Figure 2.5-92. The centerline of the CCNPP Unit 3 powerblock is graded to approximately Elevation 85 ft. The finished grade in each major area will be approximately:

- Powerblock: Elevation 80 ft to Elevation 85 ft.
- Intake Area: Elevation 10 ft.
- Switchyard: Elevation 90 ft to 98 ft.
- Cooling Tower: Elevation 94 ft to 100 ft.
- Utility Corridor: Elevation 80 ft near proposed CCNPP Unit 3 to Elevation 8 ft near the Barge Slip.

Locations of these areas and associated structures, and a schematic of the overall grading configuration, are shown in Figure 2.5-186. The site grading within the powerblock will require both cut and fill, currently estimated at approximately 40 ft and 45 ft, respectively. The cut and fill operations will result in permanent slopes around the powerblock and Category I structures in the powerblock area. The maximum height of new slopes in the area of CCNPP Unit 3 powerblock is approximately 50 ft, located on the eastern side of the powerblock, sloping down from the powerblock.

The hill to the west of the intake area is approximately 90 ft high with a slope towards the east. The intake slope is constructed such that its toe is at least 100 ft from the intake structure.

An access road connects the CCNPP Unit 3 area and the Intake area. The cooling-water pipes and electrical duct banks are routed along the same alignment. This area is referred to as the 'Utility Corridor'. The maximum height of the slopes along the Utility Corridor is about 45 ft (from the road elevation 30 ft to top of slope elevation 75 ft).

Permanent slopes, whether cut or fill, will have an inclination of approximately 3:1 (horizontal to vertical). Earthworks for slope construction, including fill control, compaction, testing, etc. are addressed in Section 2.5.4.5.

Seven cross-sections that represent the typical site grading configuration were selected for evaluation based on location (e.g., proximity to Category I structures), slope geometry (e.g.,

height), and soil conditions. These cross-sections and their locations are shown in Figure 2.5-186 through Figure 2.5-188. Sections A, C, D and E are located in the powerblock area, Section B in the Construction Layout Area (CLA), Section F extends across the Utility Corridor, and Section G extends across the Intake Slope and Intake area. Slope stability calculations were made for these cross-sections; the results are discussed in Section 2.5.5.2.

2.5.5.1.2 Characteristics of Natural Calvert Cliffs

The CCNPP Unit 3 site area is located about 1,000 ft west of the steep cliffs known as the Calvert Cliffs, as shown in Figure 2.5-186. These cliffs make up the Chesapeake Bay shoreline and reach elevations as high as 100 ft at their closest point to the CCNPP Unit 3 powerblock area. Stability of the Calvert Cliffs is discussed in Section 2.5.5.2.

2.5.5.1.3 Exploration Program and Geotechnical Conditions

The geotechnical exploration program, groundwater conditions, sampling, materials and properties, liquefaction potential, and other geotechnical parameters are addressed in Section 2.5.4. A summary relevant to the slope stability evaluation is presented below.

A geotechnical subsurface investigation was performed to characterize the upper 400 ft of soil at the CCNPP Unit 3 site. The site geology, based on geotechnical borings beneath the CCNPP Unit 3 site is comprised of fluvial and marine deposits that are about 2500 ft thick. Only the deposits in the upper 150 ft are of interest for the slope stability analyses. The subsurface, in the upper 150 ft, is divided into the following stratigraphic units:

- Stratum I: Terrace Sand
- Stratum IIa: Chesapeake Clay/Silt
- Stratum IIb: Chesapeake Cemented Sand
- Stratum IIc: Chesapeake Clay/Silt

Identification of soil layers was based on their physical and engineering characteristics. The characterization of the subsurface materials was based on a suite of tests consisting of standard penetration tests (SPT), in-soil borings including auto-hammer energy measurements, geophysical testing, and laboratory testing. Figure 2.5-95 provides an idealized profile for CCNPP Unit 3. Overall, the subsurface conditions encountered throughout the site are relatively uniform, as presented in detail in Section 2.5.4.

The first two soil layers, Terrace Sand and Chesapeake Clay/Silt IIa are not adequate foundation strata for safety related structures or facilities that will impose high contact pressures. These soils are susceptible to unacceptable levels of both elastic and long-term settlements. These soils will be removed in the powerblock area and replaced with Category I structural fill.

Based on the information provided in Section 2.4.12, in the powerblock area, shallow and deep groundwater regimes are present. For conservatism, the average groundwater level of Elevation 80 ft was chosen for slope stability evaluation in the powerblock, where in-situ soils were present. In locations where Category I structural fill replaced in-situ soils, the groundwater level was chosen as 55 ft. In the Intake Area, Intake Slope and Utility Corridor, the groundwater conditions are also based on the subsurface investigation and monitoring of observation wells. For conservatism, the groundwater levels in the Intake Area, Intake Slope and Utility Corridor were chosen as Elevations 10 ft, 37 ft and 24 ft, respectively. In naturally low-lying areas, that is,

in area with ground surface elevations lower than groundwater level, the ground may be saturated. These areas will be inspected during construction for groundwater condition. Should these areas appear saturated and if they are to receive fill during construction, a layer of highly permeable drainage material will be placed between the natural soils and the fill to preclude saturation of the fill and to maintain the groundwater level near the bottom of the fill.

The geotechnical parameters for the purpose of slope stability evaluation are based on material properties derived from the data collected during the exploration program. For the evaluation of the Utility Corridor, material properties based on data from the powerblock area were conservatively selected.

2.5.5.2 Design Criteria and Analysis

The stability of constructed slopes was assessed using limit equilibrium methods, which generally consider moment or force equilibrium of a potential sliding mass by discretizing the mass into vertical slices. This approach results in a Factor of Safety (FOS) that can be defined as (Duncan, 1996):

$$FOS = \frac{\text{Shear Strength of Soil}}{\text{Shear Stress Required for Equilibrium}}$$

Various limit equilibrium methods are available for slope stability evaluation, including the Ordinary method (Fellenius, 1936), Bishop's simplified method (Bishop, 1955), Janbu's simplified method, (Janbu, 1968), and Morgenstern-Price method (Morgenstern, 1965). These methods are routinely used for the evaluation of slopes, and their limitations and advantages are well documented. The main differences are:

1. Static equilibrium equations.

2. Interslice forces that are included in the analysis.

3. Assumed relationship between the interslice shear and normal forces.

The Ordinary method (Fellenius, 1936) is one of the earliest methods developed. It ignores all interslice forces and satisfies only moment equilibrium. Bishop's (Bishop, 1955) and Janbu's (Janbu, 1968) simplified methods satisfy only moment equilibrium and horizontal force equilibrium, respectively. Both Bishop's simplified method (Bishop, 1955) and Janbu's (Janbu, 1968) include the interslice normal force, but ignore the interslice shear force. The Morgenstern-Price method (Morgenstern, 1965) considers both shear and normal interslice forces, and it satisfies both moment and force equilibrium. The Ordinary method (Fellenius, 1936), Bishop's simplified method (Bishop, 1955) and Morgenstern-Price method (Morgenstern, 1965) were used to calculate FOSs for constructed slopes at the CCNPP Unit 3 site.

Dynamic analysis of the slopes can be performed using a pseudo-static approach, which represents the effects of seismic vibration by accelerations that induce inertial forces. These forces act in the horizontal and vertical directions at the centroid of each slice, and are defined as:

$$F_h = \left(\frac{a_h}{g}\right) W = k_h W$$

$$F_v = \left(\frac{a_v}{g}\right) W = k_v W$$

Where a_h and a_v are horizontal and vertical ground accelerations, respectively, W is the slice weight, and g is the gravitational acceleration constant. The inertial effect is specified by k_h and k_v coefficients, based on site seismic considerations.

Typical minimum acceptable values of FOS are 1.5 for normal long-term loading conditions and 1.0 to 1.2 for infrequent loading conditions (Duncan, 1996), e.g., during earthquakes.

2.5.5.2.1 Stability of Constructed Slopes

The slope stability analysis was performed using SLOPE/W (GEO-SLOPE, 2007). SLOPE/W 2007 has been independently validated and verified using the Ordinary (Fellenius, 1936), Bishop's (Bishop, 1955) and Morgenstern-Price methods. The software searches for a critical slip surface by attempting several hundred combinations of surfaces of different shapes. Both static and pseudo-static analyses were performed for the selected cross-sections, allowing the program to select the critical surface.

The initial code for SLOPE/W was developed by Professor D. G. Fredlund at the University of Saskatchewan in Canada. During the 1980s, the PC version became available. SLOPE/W contains formulation for 10 different methods for evaluating the stability of slopes, each with various assumptions in its development of the respective mathematical model. Some of these assumptions were described earlier in Section 2.5.5.2, with the main difference being in the treatment of interslice forces. SLOPE/W contains a variety of options for the shape of trial surfaces, e.g., circular, planar, composite, or block type, and locates the critical surface with the lowest possible FOS. The reasonableness of the surface, however, should be determined by the user as SLOPE/W, or other similar applications, cannot be expected to make these judgments. SLOPE/W also allows for the incorporation of forces due to water, as well as negative porewater (suction) and externally applied forces, when needed. Material properties may simply be defined in terms of unit weight, friction and/or cohesion, or made a function of other parameters, e.g., change in stress. SLOPE/W has two options for evaluating slopes subjected to rapid loading; namely, pseudo-statically or using results from other dynamic analyses such as a companion program that obtains dynamic stresses and porewater pressure. A complete description of SLOPE/W and slope stability formulations is given in SLOPE/W user manual (GEO-SLOPE, 2007).

The effect of surcharge loading was excluded from the analyses. Planned structures are sufficiently set back from edges of slopes so that they do not impose surcharge loading on the slope. The location and relative positions of safety-related structures to slopes in Sections A′, G′ and G″ for the powerblock and intake area are shown in Figure 2.5-189 and Figure 2.5-190. The site soils are not considered liquefiable for the seismic conditions of the site; therefore, liquefaction is not applicable to stability of slopes at the site. Liquefaction potential is addressed in detail in Section 2.5.4.8.

For the pseudo-static analysis in the CCNPP Unit 3 site, the inertial effect coefficient $k_h = 0.15$ was used, based on $a_h = 0.15g$, from the Site Safe Shutdown Earthquake (Site SSE) developed in Section 3.7.1. The vertical component, k_v, was chosen as 0.075.

In the static analysis, a Mohr-Coulomb failure criterion based on effective stress conditions was used. For the sand layers, it is assumed that the effective cohesion, c′, is equal to zero. This is a conservative approach which yields a lower factor of safety (FOS). The sand layers at the site contain varying amounts of clay and silt as shown in the boring logs provided in COLA Part 11J: Geotechnical Subsurface Investigation Data Report. The effective friction angle (Φ') for the sand layers is based on standard penetration and cone penetration tests correlations, direct

shear and CIU-bar triaxial compression tests. For the clay/silt layers, c′ and Φ′ were obtained from the CIU-bar triaxial compression and direct shear tests.

Two cases were considered for the dynamic analysis:

- A Mohr-Coulomb failure criterion based on total stress conditions was used, to account for the hydrostatic pressure buildup. For the sand layers, total strength parameters (cohesion, c, and friction angle, Φ) were obtained from CIU triaxial compression and direct shear tests. For the clay/silt layers, the undrained shear strength, s_u, obtained from Unconsolidated Undrained (UU) and Unconfined Compression (UC) tests was used (Table 2.5-56).

- A Mohr-Coulomb failure criterion based on effective stress conditions, using the same parameters as in the static analysis.

Material properties for the slope stability analysis are presented for the powerblock, utility corridor, and the intake slope and intake area in Table 2.5-73.

Result of the static and pseudo-static slope stability analyses for critical surfaces, that is, surfaces with the lowest FOS, are shown in Figure 2.5-191 through Figure 2.5-199. In these figures, TSA and ESA represent total stress analysis and effective stress analysis, respectively. The computed FOSs shown on these figures are based on the Morgenstern-Price method (Morgenstern, 1965). Various runs were conducted on each slope to determine the lowest FOS. Sloughing or surficial failures that appeared during analyses were evaluated and disregarded when appropriate. For Sections A and B in the CCNPP Unit 3 area, two cases were considered: a) groundwater at the boundary between structural backfill and Chesapeake Sand, and b) groundwater located at Elevation 55 ft within structural backfill. In addition to the Morgenstern-Price method (Morgenstern, 1965), FOSs were also calculated using the Ordinary method and Bishop's simplified method (Bishop, 1955) for comparison. All three methods are implemented in SLOPE/W. The FOSs for these methods are summarized in Table 2.5-74, for effective stress and total stress conditions. The Ordinary method errs on the conservative side and yields lower FOSs because all interslice forces are ignored and only moment equilibrium is satisfied. The Bishop's method considers moment equilibrium and the normal interslice force. The Morgenstern-Price method considers moment and force equilibrium, and the interslice normal and shear forces. Both Bishop's and Morgenstern-Price methods yield higher FOSs.

An examination of the FOSs in Table 2.5-74 indicates that for the pseudo-static analyses (dynamic), the effective stress conditions yields lower FOSs. However, total stress conditions are more representative of dynamic conditions at the site since porewater pressures do not have time to dissipate. Results reported hereafter for pseudo-static analyses are based on total stress conditions.

In the powerblock and adjacent areas (Cross-sections A through E in Figure 2.5-187), all slopes show FOSs greater than 1.8 for the static case and greater than 1.6 for the pseudo-static case, based on the Morgenstern-Price method (Morgenstern, 1965), as shown in Figure 2.5-191 through Figure 2.5-197.

Along the Utility Corridor, at Cross-section F shown in Figure 2.5-188, a static FOS of 2.34 and a pseudo-static FOS of 2.82 was obtained with the Morgenstern-Price method, as shown in Figure 2.5-198.

In the intake area, at Cross-section G shown in Figure 2.5-188, a static FOS of 2.05 and a pseudo-static FOS of 1.93 were obtained using the Morgenstern-Price method, as shown in Figure 2.5-199.

As stated previously, typical minimum acceptable values of FOS are 1.5 for normal long-term loading conditions and 1.0 to 1.2 for infrequent loading conditions. The calculated FOSs for all slopes exceed the minimum acceptable values. Therefore, the slopes in the powerblock, intake area and utility corridor have sufficient static and dynamic stability against slope failure.

There are no dams or embankments that would affect the CCNPP Unit 3. Probable Maximum Flood (PMF) at the CCNPP Unit 3 area is accounted for by assuming a high groundwater level of 37 ft at the Intake Slope. A maximum flood level of 33.9 ft is postulated, this would only affect the Intake Slope.

2.5.5.2.2 Stability of Natural Calvert Cliffs

The Calvert Cliffs are steep, near-vertical slopes, formed by erosion processes over the last several thousand years. These processes are addressed in more detail in Section 2.4.9. The on-going erosion results in the cliffs failing along irregular, near-vertical surfaces. The failures are the result of shoreline erosion undermining the cliffs at the beach line. With sufficient undermining, the weight of the overlying deposits that make up the cliffs exceeds their shear strength, resulting in the undermined portion falling to the shoreline. Long-term and short-term processes, e.g., waves, tidal fluctuations, and extreme weather conditions, affect the Calvert Cliffs. The cliffs are estimated to undergo erosion near the CCNPP Unit 3 site area of about 2 ft to 4 ft per year, as described in Section 2.4.9.

In the proximity of CCNPP Unit 3, the cliffs rise to elevations in the range of about Elevation 30 ft to Elevation 100 ft, with a major portion maintaining about Elevation 90 ft, as shown in Figure 2.5-186. Given the past performance of the high cliffs, there is no reason to expect their future performance would appreciably differ; therefore, these cliffs are anticipated to continue to be globally stable, owing to the relatively high strength of the soil deposits that make up the cliffs (refer to Section 2.5.4.2 for strength data for these soils). Consistent with the results of the preconstruction exploration, all soils that make up the cliffs also include some level of plasticity, as well as a moderate amount of fines, resulting in moderate capillary forces and, therefore, enhanced stability and resistance to erosion.

The easternmost boundary of the CCNPP Unit 3 powerblock is set back a distance of about 1,000 ft from the cliffs, with at least 1,200 ft to the nearest Category I structure, as shown in Figure 2.5-186. This set back area will be free from any major construction, surcharge, re-grading, or other activities that could modify the ground or the loading conditions which would adversely impact the cliffs or their stability. Therefore, they are anticipated to remain unaffected by construction factors.

Although not expected, should the global stability of the cliffs, due to unforeseen conditions, be adversely impacted such that a major cliff failure could ensue, hypothesized failure scenarios may be in the form of (1) a wedge (or a plane) portion of the cliffs sliding into the Chesapeake Bay at an inclined angle, or (2) a portion of the cliffs separate and topple into the Chesapeake Bay. For the wedge-shaped hypothesis, conservatively assuming that an inclined angle of 45 degrees from the base of the cliffs could form a wedge that daylights at the top of the cliffs, only an area of approximately 100 ft from the cliffs' edge would be impacted by such an unexpected scenario, and the remaining 900-plus ft setback area would still be intact to provide sufficient global stability to CCNPP Unit 3. For the toppling hypothesis, except for cases associated with erosion that will be discussed below, the hydrogeologic conditions that are

prerequisite to this failure situation are not known to exist at the site, such as fractured bedrock or soils with planes of weakness due to fissures, slickensides, faults, or discontinuities; excessive seepage forces that could promote such failures; or prior failure history of the type hypothesized. Therefore, massive toppling failure of the Calvert Cliffs that could have an immediate, adverse impact on CCNPP Unit 3 is not kinematically possible.

The Calvert Cliffs, however, are expected to continue to erode, as they have in the past. Based on the estimated rate of erosion of 2 ft to 4 ft annually, at a constant rate, it will take approximately 25 to 50 years to erode about 100 ft of the cliffs. Or, it would take approximately 125 to 250 years for the cliffs to erode to within a distance of 500 ft from CCNPP Unit 3 outline (or 700 ft from any Category I structure). The estimated period of 125 to 250 years is appreciably more than the anticipated operating life of CCNPP Unit 3; therefore, stability of Calvert Cliffs due to erosion should not pose any immediate risk to the stability of soils supporting CCNPP Unit 3 in its lifetime.

2.5.5.2.3 Concluding Remarks

Based on analyses provided in this Section, the constructed and natural slopes at the site are sufficiently stable and present no failure potential that would adversely affect the safety of the proposed CCNPP Unit 3.

2.5.5.3 Logs of Borings

Logs of borings, and associated references, are provided in COLA Part 11J: Geotech Data Report.

2.5.5.4 Compacted Fill

Compacted fill, and associated references, are addressed in Section 2.5.4.5.

2.5.5.5 References

BGE, 1992. Updated Final Safety Analysis Report, Calvert Cliffs Nuclear Power Plant (Units 1 and 2), Calvert County, Maryland, Docket Numbers 50-317 and 50-318, Baltimore Gas and Electric Company, 1992.

Bishop, 1955. The Use of the Slip Circle in the Stability Analysis of Slopes, A. W. Bishop, Geotechnique, Vol. 5 (1), 7-17, 1955.

Duncan, 1996. State of the art: Limit equilibrium and finite-element analysis of slopes, J. M. Duncan, Journal of Geotechnical Engineering, ASCE, Vol. 122 (7), 577-596, 1996.

Fellenius, 1936. Calculation of Stability of Dams, W. Fellenius, Second Congress on Large Dams Transactions, Vol. 4, 445-462, 1936.

GEO-SLOPE, 2007. Stability Modeling with SLOPE/W 2007, An Engineering Methodology, Second Edition, Geo-Slope/W International Ltd., 2007.

Janbu, 1968. Slope Stability Computations. N. Janbu, Soil Mechanics and Foundation Engineering, The Technical University of Norway, 1968.

Morgenstern, 1965. The Analysis of the Stability of General Slip Surfaces, N.R. Morgenstern and V. E. Price, Geotechnique, Vol. 15(1), 79-93, 1965.

NRC, 2007. Combined License Applications for Nuclear Power Plants (LWR Edition), Regulatory Guide 1.206, Revision 0, U.S. Nuclear Regulatory Commission, March 2007.}

2.5.6 References

No departures or supplements.

Table 2.5-1 — {Definitions of Classes Used in the Compilation of Quaternary Faults, Liquefaction Features, and Deformation in the Central and Eastern United States}

Class Category	Definition
Class A	Geologic evidence demonstrates the existence of a Quaternary fault of tectonic origin, whether the fault is exposed for mapping or inferred from liquefaction to other deformational features.
Class B	Geologic evidence demonstrates the existence of a fault or suggests Quaternary deformation, but either (1) the fault might not extend deeply enough to be a potential source of significant earthquakes, or (2) the currently available geologic evidence is too strong to confidently assign the feature to Class C but not strong enough to assign it to Class A.
Class C	Geologic evidence is insufficient to demonstrate (1) the existence of tectonic fault, or (2) Quaternary slip or deformation associated with the feature.
Class D	Geologic evidence demonstrates that the feature is not a tectonic fault or feature; this category includes features such as demonstrated joints or joint zones, landslides, erosional or fluvial scarps, or landforms resembling fault scarps, but of demonstrable non-tectonic origin.

Table 2.5-2 — {Seismotectonic Source Zones for the CEUS SSC Model}

Zone Acronym	Seismotectonic Source Zone
AHEX	Atlantic Highly Extended Crust
ECC-AM	Extended Continental Crust—Atlantic Margin
ECC-GC	Extended Continental Crust—Gulf Coast
GMH	Great Meteor Hotspot
IBEB	Illinois Basin Extended Basement
GHEX	Gulf Highly Extended Crust
MidC-A, MidC-B,MidC-C, MidC-D	Midcontinent-Craton alternatives
NAP	Northern Appalachians
OKA	Oklahoma Aulacogen
PEZ-N and PEZ-W	Paleozoic Extended Crust narrow and Paleozoic Extended Crust wide
RR and RR-RCG	Reelfoot Rift and Reelfoot Rift including the Rough Creek Graben
SLR	St. Lawrence Rift, including the Ottawa and Saguenay grabens

Source: Table H-4-1 of Appendix H of the CEUS SSC Report (EPRI/DOE/NRC, 2012).

Table 2.5-3 — {Alternative Seismic Source Models and Associated Weights}

Each source model consists of a superimposition of selected RLME sources on one or several distributed seismicity sources.

Alternative SourceModels		Mmax Model / Seismotectonic Model		RLME Sources
Name	**Weight**	**Name**	**Source Zones**	
SourceModel I	0.160	M-I	STUDY-R	NMFS, Commerce, ERM-S,ERM-N, Marianna, Wabash, Charleston
SourceModel II	0.048	M-II	MESE-W	NMFS, Commerce, ERM-S, ERM-N, Marianna, Wabash, Charleston
SourceModel III	0.192	M-III	MESE-N, NMESE-N	NMFS, Commerce, ERM-S,ERM-N, Marianna, Wabash, Charleston
SourceModel IV	0.320	S-I	AHEX, ECC-AM, PEZ-N, MidC-A	NMFS, Commerce, ERM-S,ERM-N, Marianna, Wabash, Charleston
SourceModel V	0.160	S-II	AHEX, ECC-AM, PEZ-N, MidC-B	NMFS, Commerce, ERM-S,ERM-N, Marianna, Wabash, Charleston
SourceModel VI	0.120	S-III	AHEX, ECC-AM, PEZ-W	NMFS, Commerce, ERM-S, ERM-N Marianna, Wabash, Charleston

Table Acronyms

AHEX = Atlantic Highly Extended Seismotectonic Source Zone
ECC-AM = Extended Continental Crust-Atlantic Margin Seismotectonic Source Zone
ERM-N = Eastern Rift Margin-North
ERM-S = Eastern Rift Margin-South
MESE-N = Mesozoic and younger Extended Mmax Source Zone (Narrow interpretation)
MESE-W = Mesozoic and younger Extended Mmax Source Zone (Wide interpretation)
MidC-A, MidC-B = Midcontinental Seismotectonic Source Zone (Case A and B)
NMESE-N = Non-Mesozoic and younger Extended Mmax Source Zone (Narrow interpretation)
NMFS - New Madrid Fault System RLME Source
PEZ-N = Paleozoic Extended Seismotectonic Source Zone (Narrow Interpretation)
PEZ-W = Paleozoic Extended Seismotectonic Source Zone (Wide Interpretation)
STUDY-R = Study Region Mmax Source Zone

Table 2.5-4 — {Alternative Cases of Magnitude-Dependent Weights for the Estimation of Seismicity Parameters for Distributed Seismicity Sources}

Weighting Schemes		Magnitude (MW) Bin and Weight					
Case	**Weight**	**2.9-3.6**	**3.6-4.3**	**4.3-5.0**	**5.0-5.7**	**5.7-6.4**	**> 6.4**
A	0.3	1.0	1.0	1.0	1.0	1.0	1.0
B	0.3	0.1	1.0	1.0	1.0	1.0	1.0
E	0.4	0.0	0.3	1.0	1.0	1.0	1.0

Source: Table 5.3.2-1 of the CEUS SSC Report (EPRI/DOE/NRC, 2012).

Table 2.5-5 — {Alternative Earthquake Recurrence Parameters for Distributed Seismicity Sources}

Source Zone	Magnitude Range Weighting		Spatial Variability Approach		Smoothing Approach		Seismicity Parameters	
	Case	Weight	Approach	Weight	Approach	Weight	Realization	Weight
STUDY-R MESE-W MESE-N NMESE-N AHEX ECC-AM MidC-A MidC-B PEZ-N PEZ-W	Case A	0.3	Variable *a* - and *b*-value	1.0	"Objective"	1.0	"01" "02" "03" "04" "05" "06" "07" "08"	0.125 0.125 0.125 0.125 0.125 0.125 0.125 0.125
	Case B	0.3	Variable *a* - and *b*-value	1.0	"Objective"	1.0	"01" "02" "03" "04" "05" "06" "07" "08"	0.125 0.125 0.125 0.125 0.125 0.125 0.125 0.125
	Case E	0.4	Variable *a* - and *b*-value	1.0	"Objective"	1.0	"01" "02" "03" "04" "05" "06" "07" "08"	0.125 0.125 0.125 0.125 0.125 0.125 0.125 0.125

Source: EPRI/DOE/NRC (2012, Appendix H)

Table Acronyms
AHEX = Atlantic Highly Extended Seismotectonic Source Zone
ECC-AM = Extended Continental Crust-Atlantic Margin Seismotectonic Source Zone
MESE-N = Mesozoic and younger Extended Mmax Source Zone (Narrow interpretation)
MESE-W = Mesozoic and younger Extended Mmax Source Zone (Wide interpretation)
MidC-A, MidC-B = Midcontinental Seismotectonic Source Zone (Case A and B)
NMESE-N = Non-Mesozoic and younger Extended Mmax Source Zone (Narrow interpretation)
PEZ-N = Paleozoic Extended Seismotectonic Source Zone (Narrow Interpretation)
PEZ-W = Paleozoic Extended Seismotectonic Source Zone (Wide Interpretation)
STUDY-R = Study Region Mmax Source Zone

Table 2.5-6 — {Maximum Magnitude Distribution for the Sources of Distributed Seismicity in Source Model I, II and III}

Maximum Magnitude for:				Weight
STUDY-R	MESE-W	MESE-N	NMESE-N	
6.5	6.5	6.4	6.4	0.101
6.9	6.9	6.8	6.8	0.244
7.2	7.3	7.2	7.1	0.310
7.7	7.7	7.7	7.5	0.244
8.1	8.1	8.1	8.0	0.101

Source: Table H-3-3 of Appendix H of the CEUS SSC Report (EPRI/DOE/NRC, 2012).

Table Acronyms

MESE-N = Mesozoic and younger Extended Mmax Source Zone (Narrow interpretation)
MESE-W = Mesozoic and younger Extended Mmax Source Zone (Wide interpretation)
NMESE-N = Non-Mesozoic and younger Extended Mmax Source Zone (Narrow interpretation)
STUDY-R = Study Region Mmax Source Zone

Table 2.5-7 — {Maximum Magnitude Distributions for the Distributed Source Zones in Source Model IV, V and VI}

Maximum Magnitude for:				Weight
AHEX	ECC-AM	PEZ-N PEZ-W	MidC-A, MidC-B	
6.0	6.0	5.9	5.6	0.101
6.7	6.7	6.4	6.1	0.244
7.2	7.2	6.8	6.6	0.310
7.7	7.7	7.2	7.2	0.244
8.1	8.1	7.9	8.0	0.101

Source: Table H-4-4 of Appendix H of the CEUS SSC Report (EPRI/DOE/NRC, 2012).

Table Acronyms

AHEX = Atlantic Highly Extended Seismotectonic Source Zone
ECC-AM = Extended Continental Crust-Atlantic Margin Seismotectonic Source Zone
MidC-A, MidC-B = Midcontinental Seismotectonic Source Zone (Case A and B)
PEZ-N = Paleozoic Extended Seismotectonic Source Zone (Narrow Interpretation)
PEZ-W = Paleozoic Extended Seismotectonic Source Zone (Wide Interpretation)

Table 2.5-8 — {Aleatory Distribution for Characterization of Earthquake Rupture for Distributed Seismicity}

Source Zone	Source Boundary Characteristics[§]	Style of Faulting		Rupture Strike		Rupture Dip	
		Mechanism	Weight	Value	Weight	Value	Weight
STUDY-R MESE-N	Leaky	Strike-slip	0.666	310° 0° 35° 60° 90°	0.20 0.20 0.40 0.10 0.10	Uniformly distributed 60° to 90°	Equally likely
MESE-W NMESE-N		Reverse	0.334	310° 0° 35° 60° 90°	0.20 0.20 0.40 0.10 0.10	Uniformly distributed 60° to 90°	Equally likely
AHEX ECC-AM MidC-A MidC-B PEZ-N PEZ-W	Leaky	Strike-slip	0.666	310° 0° 35° 60° 90°	0.20 0.20 0.40 0.10 0.10	Uniformly distributed 60° to 90°	Equally likely
		Reverse	0.334	310° 0° 35° 60° 90°	0.20 0.20 0.40 0.10 0.10	Uniformly distributed 60° to 90°	Equally likely

Note:

[§]) Leaky boundary denotes the case were earthquake rupture are centered on the earthquake epicenter, the epicenters are contained within the source boundary, but the rupture is allowed to extend beyond the source boundary.

Source: Table H-3-2 and H-4.3 of Appendix H of the CEUS SSC Report (EPRI/DOE/NRC, 2012).

Table Acronyms

AHEX = Atlantic Highly Extended Seismotectonic Source Zone
ECC-AM = Extended Continental Crust-Atlantic Margin Seismotectonic Source Zone
MESE-N = Mesozoic and younger Extended Mmax Source Zone (Narrow interpretation)
MESE-W = Mesozoic and younger Extended Mmax Source Zone (Wide interpretation)
MidC-A, MidC-B = Midcontinental Seismotectonic Source Zone (Case A and B)
NMESE-N = Non-Mesozoic and younger Extended Mmax Source Zone (Narrow interpretation)
PEZ-N = Paleozoic Extended Seismotectonic Source Zone (Narrow Interpretation)
PEZ-W = Paleozoic Extended Seismotectonic Source Zone (Wide Interpretation)
STUDY-R = Study Region Mmax Source Zone

Table 2.5-9 — {Alternative Seismogenic Crustal Thickness Values and Weights for Distributed Seismicity Sources}

Source Zone	Seismogenic Thickness	
	Value (km)	Weight
STUDY-R, MESE-W, MESE-N, NMESE-N	13	0.40
	17	0.40
	22	0.20
AHEX	8	0.50
	15	0.50
ECC-AM, MidC-A, MidC-B, PEZ-N, PEZ-W	13	0.40
	17	0.40
	22	0.20

Source: Tables H-3-1 and H-4-2 of Appendix H of the CEUS SSC Report (EPRI/DOE/NRC, 2012).

Table Acronyms

AHEX = Atlantic Highly Extended Seismotectonic Source Zone
ECC-AM = Extended Continental Crust-Atlantic Margin Seismotectonic Source Zone
MESE-N = Mesozoic and younger Extended Mmax Source Zone (Narrow interpretation)
MESE-W = Mesozoic and younger Extended Mmax Source Zone (Wide interpretation)
MidC-A, MidC-B = Midcontinental Seismotectonic Source Zone (Case A and B)
NMESE-N = Non-Mesozoic and younger Extended Mmax Source Zone (Narrow interpretation)
PEZ-N = Paleozoic Extended Seismotectonic Source Zone (Narrow Interpretation)
PEZ-W = Paleozoic Extended Seismotectonic Source Zone (Wide Interpretation)
STUDY-R = Study Region Mmax Source Zone

Table 2.5-10 — {Aleatory Distribution for Characterization of Earthquake Rupture for RLME Sources}

(Page 1 of 2)

RLME Source		Source Geometry		Source Boundary Characteristics§	Style of Faulting		Rupture Strike		Rupture Dip	
		Geometry	Weight		Mech.	Weight	Value	Weight	Value	Weight
Charleston		Local	0.5	Strict	Strike- slip	1.0	NE † (parallel to long axis)	1.0	90°	1.0
		Narrow	0.3	Leaky NE and SW Strict NW and SE boundaries	Strike- slip	1.0	NNE † (parallel to long axis)	1.0	90°	1.0
		Regional	0.2	Strict	Strike- slip	1.0	NE † (parallel to long axis)	0.8	90°	1.0
					Strike- slip	1.0	NW † (parallel to short axis)	0.2	90°	1.0
NMFS	NMS	BA-BL	0.6	-	Strike- slip	1.0	Parallel to the Fault Trace†	1.0	90°	1.0
		BA-BFZ	0.4	-	Strike- slip	1.0	Parallel to the Fault Trace†	1.0	90°	1.0
	NMN	NMN-S	0.7	-	Strike- slip	1.0	Parallel to the Fault Trace†	1.0	90°	1.0
		NMN-L	0.3	-	Strike- slip	1.0	Parallel to the Fault Trace†	1.0	90°	1.0
	RFT	RFT-S	0.7	-	Reverse	1.0	Parallel to the Fault Trace†	1.0	40°	1.0
		RFT-L	0.3	-	Reverse	1.0	Parallel to the Fault Trace†	1.0	40°	1.0
ERM-S		ERM-SCC	0.6	Leaky NE and SW	Strike- slip	1.0	NE † (parallel to long axis)	1.0	90°	1.0
		ERM-SRP	0.4	Leaky NE and SW	Strike- slip	1.0	NE † (parallel to long axis)	1.0	90°	1.0
ERM-N		ERM-	1.0	Leaky NE and SW	Strike- slip	1.0	NE † (parallel to long axis)	1.0	90°	1.0

Table 2.5-10 — {Aleatory Distribution for Characterization of Earthquake Rupture for RLME Sources}

(Page 2 of 2)

RLME Source	Source Geometry		Source Boundary Characteristics[§]	Style of Faulting		Rupture Strike		Rupture Dip	
	Geometry	Weight		Mech.	Weight	Value	Weight	Value	Weight
Marianna	Marianna Zone	1.0	Leaky	Strike- slip	1.0	NE [†] (parallel to Zone Sides)	0.5	90°	1.0
						NW [†] (parallel to Zone Sides)	0.5	90°	1.0
Commerce	Commerce Zone	1.0	Leaky NE and SW	Strike- slip	1.0	47°	1.0	90°	1.0
Wabash Valley	Wabash Valley Zone	1.0	Leaky	Strike- slip	0.666	Uniformly distributed 0° to 360°	Equally Likely	90°	1.0
				Reverse	0.334	Uniformly distributed 0° to 360°	Equally Likely	40° to 60°	Equally Likely

Note:

[§]) Leaky boundary denotes the case where earthquake ruptures are centered on the earthquake epicenter, the epicenters are contained within the source boundary, but the rupture is allowed to extend beyond the source boundary. Strict boundary denotes the case where earthquake ruptures are not allowed to extend beyond the zone boundaries.

[†]) Rupture strike for these source zones will be determined in a separate (hazard) calculation from the corresponding geographical coordinates provided in the EPRI/DOE/NRC (2012) report.

Source: EPRI/DOE/NRC (2012, Appendix H)

Table Acronyms

BA-BL = Blytheville Arch - Bootheel Lineament
BA-BFZ = Blytheville Arch - Blytheville fault zone
NMN = New Madrid North
NMN-S = New Madrid North with no extension
NMN-L = New Madrid North plus extension
>NMS = New Madrid South
RFT = Reelfoot Thrust
RFT-S = Reelfoot Thrust with no extension
RFT-N = Reelfoot Thrust plus extension
ERM-N = Eastern Rift Margin - North
ERM-S = Eastern Rift Margin - South
ERM-SCC = Eastern Rift Margin - South Crittenden County
ERM-SRP = Eastern Rift Margin - South River Profile

Table 2.5-11 — {Alternative Seismogenic Crustal Thickness Values and Weights for RLME Sources}

RLME Source	Seismogenic Thickness	
	Value (km)	Weight
NMFS, Commerce, Marianna, ERM-S, ERM-N	13	0.40
	15	0.40
	17	0.20
Wabash Valley	17	0.70
	22	0.30
Charleston	13	0.40
	17	0.40
	22	0.20
Table Acronyms ERM-N = Eastern Rift Margin - North ERM-S = Eastern Rift Margin - South NMFS = New Madrid Fault System		
Source: EPRI/DOE/NRC (2012, Appendix H)		

Table 2.5-12 — {Temporal Clustering and Tectonic Features for RLME Sources}

RLME Source	Temporal Clustering		Localizing Tectonic Features	
	In/Out	Weight	Feature	Weight
Charleston	In-cluster	0.9	Random in Zone	1.0
	Out-of-cluster	0.1	Default to background	-
NMFS	In-cluster	0.9	NMS, NMN, RFT	1.0
	Out-of-cluster	0.05	None, default to background	-
	Out-of-cluster except RFT	0.05	Only RFT Fault	1.0
ERM-S	N/A	-	Random in Zone	1.0
ERM-N	N/A	-	Random in Zone	1.0
Marianna	In-cluster	0.5	Random in Zone	1.0
	Out-of-cluster	0.5	Default to background	-
Commerce	N/A	-	Random in Zone	1.0
Wabash Valley	N/A	-	Random in Zone	1.0

Note: N/A stands for "Not Applicable"

Table Acronyms

ERM-N = East Rift Margin - North
ERM-S = East Rift Margin - South
NMFS = New Madrid Fault System
NMN = New Madrid North
NMS = New Madrid South
RFT = Reelfoot Thrust

Source: EPRI/DOE/NRC (2012, Appendix H)

Table 2.5-13 — {Alternative Recurrence Parameters for the Charleston RLME Source}

(Page 1 of 5)

RLME Source	Source Geometry	Recurrence Method		Time Period		Earthquake Count		Earthquake Recurrence Model		Coefficient of Variation (*a*)		RLME Annual Frequency	
		Method	Wt.	Period (Yrs)	Wt.	Count	Wt.	Model	Wt.	Value	Wt.	Freq.	Wt.
Charleston	Regional	Earthquake Recurrence Intervals	1.0	2,000	0.8	1886,A,B,C	1.0	Poisson	1.0	N/A	-	4.7E-03	0.101
												3.1E-03	0.244
												2.1E-03	0.310
												1.3E-03	0.244
												6.8E-04	0.101
				5,500	0.2	1886,A,B,C	0.2	Poisson	1.0	N/A	-	4.7E-03	0.101
												3.1E-03	0.244
												2.1E-03	0.310
												1.3E-03	0.244
												6.8E-04	0.101
						1886,A,B,C,D	0.3	Poisson	1.0	N/A	-	2.7E-03	0.101
												1.9E-03	0.244
												1.3E-03	0.310
												8.8E-04	0.244
												5.0E-04	0.101
						1886,A,B,C,E	0.2	Poisson	1.0	N/A	-	1.9E-03	0.101
												1.3E-03	0.244
												9.2E-04	0.310
												6.4E-04	0.244
												3.4E-04	0.101
						1886,A,B,C,D,E	0.3	Poisson	1.0	N/A	-	2.2E-03	0.101
												1.5E-03	0.244
												1.1E-03	0.310
												7.8E-04	0.244
												4.6E-04	0.101
				2,000	0.8	1886,A,B,C	1.0	Poisson	1.0	N/A	-	4.7E-03	0.101
												3.1E-03	0.244
												2.1E-03	0.310
												1.3E-03	0.244
												6.8E-04	0.101

Table 2.5-13 — {Alternative Recurrence Parameters for the Charleston RLME Source}

(Page 2 of 5)

RLME Source	Source Geometry	Recurrence Method		Time Period		Earthquake Count		Earthquake Recurrence Model		Coefficient of Variation (*a*)		RLME Annual Frequency	
		Method	Wt.	Period (Yrs)	Wt.	Count	Wt.	Model	Wt.	Value	Wt.	Freq.	Wt.
Charleston	Local	Earthquake Recurrence Intervals	1.0	5,500	0.2	1886,A,B,C	0.2	Poisson	1.0	N/A	-	4.7E-03 3.1E-03 2.1E-03 1.3E-03 6.8E-04	0.101 0.244 0.310 0.244 0.101
						1886,A,B,C,D	0.3	Poisson	1.0	N/A	-	2.7E-03 1.9E-03 1.3E-03 8.8E-04 5.0E-04	0.101 0.244 0.310 0.244 0.101
						1886,A,B,C,E	0.2	Poisson	1.0	N/A	-	1.9E-03 1.3E-03 9.2E-04 6.4E-04 3.4E-04	0.101 0.244 0.310 0.244 0.101
						1886,A,B,C,D,E	0.3	Poisson	1.0	N/A	-	2.2E-03 1.5E-03 1.1E-03 7.8E-04 4.6E-04	0.101 0.244 0.310 0.244 0.101
				2,000	0.8	1886,A,B,C	1.0	Poisson	0.9	N/A	-	4.7E-03 3.1E-03 2.1E-03 1.3E-03 6.8E-04	0.101 0.244 0.310 0.244 0.101
										0.3	0.2	6.4E-05 7.6E-06 9.5E-07 8.5E-08 2.3E-09	0.101 0.244 0.310 0.244 0.101
												1.4E-03	0.101

Table 2.5-13 — {Alternative Recurrence Parameters for the Charleston RLME Source}

(Page 3 of 5)

RLME Source	Source Geometry	Recurrence Method		Time Period		Earthquake Count		Earthquake Recurrence Model		Coefficient of Variation (*a*)		RLME Annual Frequency	
		Method	Wt.	Period (Yrs)	Wt.	Count	Wt.	Model	Wt.	Value	Wt.	Freq.	Wt.
Charleston	Narrow	Earthquake Recurrence Intervals	1.0					Renewal	0.1	0.5	0.5	3.8E-04 9.5E-05 1.7E-05 1.0E-06	0.244 0.310 0.244 0.101
										0.7	0.3	2.6E-03 9.8E-04 3.2E-04 7.1E-05 5.6E-06	0.101 0.244 0.310 0.244 0.101
				5,000	0.2	1886,A,B,C	0.2	Poisson	0.9	N/A	-	4.7E-03 3.1E-03 2.1E-03 1.3E-03 6.8E-04 6.8E-05 8.0E-06	0.101 0.244 0.310 0.244 0.101 0.101 0.244
										0.3	0.2	1.0E-06 9.2E-08	0.310 0.244
								Renewal	0.1			2.5E-09 1.4E-03 3.9E-04	0.101 0.101 0.244
										0.5	0.5	9.8E-05 1.7E-05 1.1E-06 2.7E-03	0.310 0.244 0.101 0.101
										0.7	0.3	9.9E-04 3.3E-04 7.3E-05 5.8E-06 2.7E-03 1.9E-03	0.244 0.310 0.244 0.101 0.101 0.244

Table 2.5-13 — {Alternative Recurrence Parameters for the Charleston RLME Source}

(Page 4 of 5)

RLME Source	Source Geometry	Recurrence Method		Time Period		Earthquake Count		Earthquake Recurrence Model		Coefficient of Variation (*a*)		RLME Annual Frequency	
		Method	Wt.	Period (Yrs)	Wt.	Count	Wt.	Model	Wt.	Value	Wt.	Freq.	Wt.
								Poisson	0.9	N/A	-	1.3E-03	0.310
												8.8E-04	0.244
												5.0E-04	0.101
												3.5E-07	0.101
												2.5E-08	0.244
										0.3	0.2	2.2E-09	0.310
												1.4E-10	0.244
						1886,A,B,C,D	0.3					2.7E-12	0.101
												2.2E-04	0.101
												4.5E-05	0.244
								Renewal	0.1	0.5	0.5	9.3E-06	0.310
												1.4E-06	0.244
												7.6E-08	0.101
												1.0E-03	0.101
												3.3E-04	0.244
										0.7	0.3	9.5E-05	0.310
												2.0E-05	0.244
												1.5E-06	0.101
												1.9E-03	0.101
												1.3E-03	0.244
								Poisson	0.9	N/A	-	9.2E-04	0.310
												6.4E-04	0.244
												3.4E-04	0.101
												4.5E-09	0.101
												2.0E-10	0.244
										0.3	0.2	1.2E-11	0.310
						1886,A,B,C,E	0.2					5.4E-13	0.244
												6.4E-15	0.101
								Renewal	0.1			5.2E-05	0.101
												8.2E-06	0.244
										0.5	0.5	1.4E-06	0.310

Table 2.5-13 — {Alternative Recurrence Parameters for the Charleston RLME Source}

(Page 5 of 5)

RLME Source	Source Geometry	Recurrence Method		Time Period		Earthquake Count		Earthquake Recurrence Model		Coefficient of Variation (*a*)		RLME Annual Frequency	
		Method	Wt.	Period (Yrs)	Wt.	Count	Wt.	Model	Wt.	Value	Wt.	Freq.	Wt.
												1.7E-07	0.244
												7.0E-09	0.101
										0.7	0.3	5.2E-04	0.101
												1.4E-04	0.244
												3.4E-05	0.310
												6.1E-06	0.244
												3.9E-07	0.101
												2.2E-03	0.101
												1.5E-03	0.244
								Poisson	0.9	N/A	-	1.1E-03	0.310
												7.8E-04	0.244
												4.6E-04	0.101
												1.5E-08	0.101
												8.7E-10	0.244
										0.3	0.2	7.0E-11	0.310
												4.4E-12	0.244
						1886,A,B,C,D,E	0.3					8.2E-14	0.101
												7.0E-05	0.101
												1.3E-05	0.244
								Renewal	0.1	0.5	0.5	2.5E-06	0.310
												3.7E-07	0.244
												2.1E-08	0.101
												5.7E-04	0.101
												1.6E-04	0.244
										0.7	0.3	4.5E-05	0.310
												9.2E-06	0.244
												7.6E-07	0.101

Note: N/A stands for "Not Applicable"

Notes:
Wt. = weight
Freq. = Annual Frequency of Occurrence
Yrs = years
* Coefficient of Variation is applicable only to the Renewal Earthquake Recurrence Model; otherwise "N/A" (not applicable)
*For Earthquake Count, letters refer to various paleoearthquakes interpreted from paleo-liquefaction data
Source: EPRI/DOE/NRC (2012, Appendix H)

Table 2.5-14 — {Alternative RLME Recurrence Parameters for the NMFS RLME Source}

RLME Source	In or Out of Cluster	Recurrence Method		Recurrence Data		Earthquake Recurrence Model		Coefficient of Variation (a)		RLME Annual Frequency	
		Method	Wt.	Sequences/Clusters	Wt.	Model	Wt.	Value	Wt.	Freq.	Wt.
NMFS	In-Cluster	Earthquake Recurrence Intervals	1.0	1811-1812 1450, and 900 AD	1.0	Poisson	0.75	N/A	-	6.0E-03	0.101
										3.7E-03	0.244
										2.4E-03	0.310
										1.4E-03	0.244
										6.2E-04	0.101
						Renewal	0.25	0.3	0.2	3.5E-03	0.101
										1.1E-03	0.244
										3.2E-04	0.310
										6.4E-05	0.244
										4.7E-06	0.101
								0.5	0.5	4.8E-03	0.101
										2.2E-03	0.244
										8.9E-04	0.310
										2.6E-04	0.244
										3.1E-05	0.101
								0.7	0.3	4.4E-03	0.101
										2.2E-03	0.244
										1.0E-03	0.310
										3.4E-04	0.244
										4.7E-05	0.101
	Out-of-Cluster Except RFT	Earthquake Recurrence Intervals	1.0	2000 BC and 1000 AD Clusters	1.0	Poisson	1.0	N/A	-	1.3E-03	0.101
										7.2E-04	0.244
										4.2E-04	0.310
										2.2E-04	0.244
										8.0E-05	0.101

Note: N/A stands for "Not Applicable"

Source: EPRI/DOE/NRC (2012, Appendix H)

Table 2.5-15 — {Alternative RLME Recurrence Parameters for the ERM-S RLME Source}

RLME Source	Recurrence Method		Recurrence Data		Earthquake Recurrence Model		RLME Annual Frequency	
	Method	Wt.	Sequences/Clusters	Wt.	Model	Wt.	Freq.	Wt.
ERM-S	Earthquake Count in a Time Interval	1.0	2 Earthquakes in 17.7-21.7 k.y.	0.333	Poisson	1.0	3.5E-04	0.101
							2.1E-04	0.244
							1.4E-04	0.310
							8.0E-05	0.244
							3.6E-05	0.101
			3 Earthquakes in 17.7-21.7 k.y.	0.334	Poisson	1.0	4.3E-04	0.101
							2.8E-04	0.244
							1.9E-04	0.310
							1.2E-04	0.244
							6.2E-05	0.101
			4 Earthquakes in 17.7-21.7 k.y.	0.333	Poisson	1.0	5.0E-04	0.101
							3.4E-04	0.244
							2.4E-04	0.310
							1.6E-04	0.244
							9.0E-05	0.101

Table 2.5-16 — {Alternative RLME Recurrence Parameters for the ERM-N RLME Source}

RLME Source	Recurrence Method		Recurrence Data		Earthquake Recurrence Model		RLME Annual Frequency	
	Method	Wt.	Sequences/ Clusters	Wt.	Model	Wt.	Freq.	Wt.
ERM-N	Earthquake Count in a Time Interval	1.0	1 Earthquake in 12-35 k.y.	0.9	Poisson	1.0	2.9E-04	0.101
							1.5E-04	0.244
							8.0E-05	0.310
							4.0E-05	0.244
							1.4E-05	0.101
			2 Earthquakes in 12-35 k.y.	0.1	Poisson	1.0	3.9E-04	0.101
							2.2E-04	0.244
							1.3E-04	0.310
							7.2E-05	0.244
							3.2E-05	0.101

Table 2.5-17 — {Alternative RLME Recurrence Parameters for the Marianna Zone RLME Source}

RLME Source	Recurrence Method		Recurrence Data		Earthquake Recurrence Model		RLME Annual Frequency	
	Method	Wt.	Sequences/ Clusters	Wt.	Model	Wt.	Freq.	Wt.
Marianna	Earthquake Recurrence Intervals	1.0	3 Earthquakes in 9.6-10.2 k.y.	0.5	Poisson	1.0	6.9E-04	0.101
							4.2E-04	0.244
							2.7E-04	0.310
							1.6E-04	0.244
							7.2E-05	0.101
			4 Earthquakes in 9.6-10.2 k.y.	0.5	Poisson	1.0	8.4E-04	0.101
							5.5E-04	0.244
							3.7E-04	0.310
							2.4E-04	0.244
							1.2E-04	0.101

Table 2.5-18 — {Alternative RLME Recurrence Parameters for the Commerce RLME Source}

RLME Source	Recurrence Method		Recurrence Data		Earthquake Recurrence Model		RLME Annual Frequency	
	Method	Wt.	Sequences/ Clusters	Wt.	Model	Wt.	Freq.	Wt.
Commerce	Earthquake Recurrence Intervals	1.0	2 Earthquakes in 18.9-23.6 k.y.	0.75	Poisson	1.0	2.5E-04	0.101
							1.4E-04	0.244
							8.0E-05	0.310
							4.0E-05	0.244
							1.4E-05	0.101
			3 Earthquakes in 18.9-23.6 k.y.	0.25	Poisson	1.0	3.3E-04	0.101
							2.0E-04	0.244
							1.3E-04	0.310
							7.6E-05	0.244
							3.4E-05	0.101

Table 2.5-19 — {Alternative RLME Recurrence Parameters for the Wabash Valley RLME Source}

RLME Source	Recurrence Method		Recurrence Data		Earthquake Recurrence Model		RLME Annual Frequency	
	Method	Wt.	Sequences/ Clusters	Wt.	Model	Wt.	Freq.	Wt.
Wabash Valley	Earthquake Recurrence Intervals	1.0	2 Earthquakes in 11-13 k.y.	1.0	Poisson	1.0	4.4E-04	0.101
							2.5E-04	0.244
							1.4E-04	0.310
							7.2E-05	0.244
							2.4E-05	0.101

Table 2.5-20 — {Maximum Magnitude Distributions for RLME Sources}

(Page 1 of 2)

RLME Source	Maximum Magnitude	
	Value	Weight
NMS	7.9	0.167
	7.8	0.167
	7.6	0.250
	7.2	0.083
	6.9	0.250
	6.7	0.083
RFT	7.8	0.167
	7.7	0.167
	7.8	0.250
	7.4	0.083
	7.3	0.250
	7.1	0.083
NMN	7.6	0.167
	7.5	0.167
	7.5	0.250
	7.2	0.083
	7.0	0.250
	6.8	0.083
Commerce	6.7	0.15
	6.9	0.35
	7.1	0.35
	7.3	0.10
	7.7	0.05
ERM-S	6.7	0.15
	6.9	0.20
	7.1	0.20
	7.3	0.20
	7.5	0.20
	7.7	0.05
ERM-N	6.7	0.30
	6.9	0.30
	7.1	0.30
	7.4	0.10

Table 2.5-20 — {Maximum Magnitude Distributions for RLME Sources}

(Page 2 of 2)

RLME Source	Maximum Magnitude	
	Value	**Weight**
Marianna	6.7	0.15
	6.9	0.20
	7.1	0.20
	7.3	0.20
	7.5	0.20
	7.7	0.20
Wabash Valley	6.75	0.05
	7.0	0.25
	7.25	0.35
	7.5	0.35
Charleston	6.7	0.10
	6.9	0.25
	7.1	0.30
	7.3	0.25
	7.5	0.10

Source: Tables H-5.1-1, H-5.2-1, H-5.5-1, H-5.6-1, H-5.6-2, H-5.7-1, H-5.8-1, and H-5.9-1 of Appendix H of the CEUS SSC Report (EPRI/DOE/NRC, 2012)

Table Acronyms

ERM-N = Eastern Rift Margin - North

ERM-S = Eastern Rift Margin - South

NMN = New Madrid Fault System, New Madrid North fault

NMS = New Madrid Fault System, New Madrid South fault

RFT = New Madrid Fault System, Reelfoot Thrust fault

Table 2.5-21 — {Mean Magnitudes and Distances from Deaggregations}

Struct. frequency	Annual Freq. Exceed.	Overall hazard R>0 km		Hazard from R<100 km		Hazard from R>100 km	
		M	R, km	M	R, km	M	R, km
1 & 2.5 Hz	1E-04	6.8	174	6	29	7.3	502
5 & 10 Hz	1E-04	6.1	52	5.8	28	6.7	206
1 & 2.5 Hz	1E-05	6.7	60	6.3	20	7.5	483
5 & 10 Hz	1E-05	6	18	6	15	7.2	171
1 & 2.5 Hz	1E-06	6.8	23	6.7	17	7.7	356
5 & 10 Hz	1E-06	6.3	12	6.3	12	7.8	154

Notes:

M = moment magnitude

R = epicentral distance

Hz = Hertz (cycles per second)

Annual Freq. Exceed. = mean annual frequency of exceedance

Shaded combinations of magnitude and distance represent the low frequency (1 & 2.5 Hz) and high frequency (5 & 10 Hz) controlling earthquakes for the given mean annual frequency of exceedance

Table 2.5-22 — {HF and LF Rock Smooth Spectra}

Freq. [Hz]	SA, g					
	10^{-4} HF	10^{-4} LF	10^{-5} HF	10^{-5} LF	10^{-6} HF	10^{-6} LF
0.1	0.0005	0.0035	0.0014	0.0094	0.0051	0.0215
0.125	0.0008	0.0049	0.0023	0.0134	0.0084	0.0310
0.15	0.0011	0.0065	0.0034	0.0179	0.0121	0.0415
0.2	0.0020	0.0101	0.0060	0.0279	0.0207	0.0652
0.3	0.0039	0.0186	0.0123	0.0524	0.0414	0.1222
0.4	0.0062	0.0292	0.0198	0.0827	0.0662	0.1908
0.5	0.0088	0.0419	0.0285	0.1185	0.0950	0.2689
0.6	0.0118	0.0450	0.0383	0.1258	0.1277	0.2962
0.7	0.0151	0.0478	0.0492	0.1320	0.1641	0.3192
0.8	0.0187	0.0502	0.0612	0.1370	0.2037	0.3377
0.9	0.0225	0.0523	0.0741	0.1406	0.2460	0.3521
1	0.0266	0.0540	0.0878	0.1429	0.2904	0.3626
1.25	0.0376	0.0672	0.1243	0.1828	0.4063	0.4743
1.5	0.0489	0.0779	0.1621	0.2162	0.5223	0.5726
2	0.0705	0.0917	0.2343	0.2638	0.7350	0.7308
2.5	0.0894	0.0985	0.2976	0.2936	0.9148	0.8536
3	0.1057	0.1105	0.3524	0.3262	1.0688	0.9415
4	0.1332	0.1284	0.4460	0.3752	1.3306	1.0781
5	0.1567	0.1417	0.5275	0.4116	1.5575	1.1820
6	0.1725	0.1520	0.5935	0.4400	1.7638	1.2648
7	0.1862	0.1603	0.6529	0.4628	1.9518	1.3326
8	0.1982	0.1671	0.7064	0.4816	2.1234	1.3891
9	0.2085	0.1728	0.7545	0.4972	2.2794	1.4367
10	0.2175	0.1776	0.7974	0.5104	2.4204	1.4771
12.5	0.2472	0.1866	0.9117	0.5352	2.8052	1.5542
15	0.2701	0.1927	1.0001	0.5519	3.1147	1.6066
20	0.3004	0.1996	1.1174	0.5709	3.5537	1.6664
25	0.3171	0.2024	1.1815	0.5785	3.8249	1.6907
30	0.3106	0.2026	1.1652	0.5789	3.7568	1.6928
35	0.3007	0.2006	1.1339	0.5731	3.6450	1.6762
40	0.2880	0.1964	1.0905	0.5608	3.4972	1.6404
45	0.2726	0.1896	1.0356	0.5414	3.3144	1.5837
50	0.2545	0.1803	0.9698	0.5148	3.0985	1.5061
60	0.2132	0.1561	0.8169	0.4457	2.6023	1.3037
70	0.1734	0.1305	0.6671	0.3726	2.1199	1.0900
80	0.1427	0.1101	0.5514	0.3143	1.7484	0.9195
90	0.1227	0.0967	0.4757	0.2761	1.5057	0.8078
100	0.1108	0.0890	0.4308	0.2541	1.3613	0.7435

Table 2.5-23 — {Horizontal and Vertical GMRS Amplitudes and Common V/H Ratios}

Frequency [Hz]	Horizontal GMRS (g)	V/H Ratio	Vertical GMRS (g)
0.1	7.38E-03	0.750	5.54E-03
0.125	1.22E-02	0.750	9.17E-03
0.15	1.98E-02	0.750	1.48E-02
0.2	4.34E-02	0.750	3.26E-02
0.3	6.05E-02	0.750	4.54E-02
0.4	7.17E-02	0.750	5.37E-02
0.5	1.16E-01	0.750	8.71E-02
0.6	1.48E-01	0.750	1.11E-01
0.7	1.58E-01	0.750	1.18E-01
0.8	1.69E-01	0.750	1.27E-01
0.9	1.79E-01	0.750	1.34E-01
1	1.84E-01	0.750	1.38E-01
1.25	2.15E-01	0.750	1.61E-01
1.5	2.17E-01	0.750	1.63E-01
2	1.99E-01	0.750	1.50E-01
2.5	2.17E-01	0.750	1.63E-01
3	2.58E-01	0.750	1.93E-01
4	2.86E-01	0.750	2.15E-01
5	2.84E-01	0.750	2.13E-01
6	2.73E-01	0.778	2.12E-01
7	2.65E-01	0.802	2.13E-01
8	2.55E-01	0.823	2.10E-01
9	2.40E-01	0.841	2.02E-01
10	2.29E-01	0.858	1.97E-01
12.5	2.04E-01	0.892	1.82E-01
15	1.82E-01	0.921	1.68E-01
20	1.54E-01	0.965	1.48E-01
25	1.38E-01	1.000	1.38E-01
30	1.29E-01	1.000	1.29E-01
35	1.23E-01	1.000	1.23E-01
40	1.20E-01	1.000	1.20E-01
45	1.18E-01	1.000	1.18E-01
50	1.17E-01	1.000	1.17E-01
60	1.16E-01	1.000	1.16E-01
70	1.15E-01	1.000	1.15E-01
80	1.15E-01	1.000	1.15E-01
90	1.15E-01	1.000	1.15E-01
100	1.15E-01	1.000	1.15E-01

Table 2.5-24 — {Calvert Cliffs Site Amplification Factors for 10^{-4} and 10^{-5} Input Motions and HF and LF Rock Spectra}

Frequency [Hz]	1E-4 LF	1E-4 HF	1E-5 LF	1E-5 HF
0.1	1.58	1.71	1.61	1.74
0.125	1.81	1.87	1.86	1.91
0.15	2.18	2.16	2.27	2.28
0.2	3.26	3.15	3.16	3.47
0.3	2.64	2.67	2.31	2.57
0.4	1.83	1.87	1.76	1.81
0.5	1.99	2.02	2.02	2.01
0.6	2.58	2.67	2.37	2.50
0.7	2.68	2.75	2.39	2.53
0.8	2.68	2.68	2.48	2.51
0.9	2.81	2.80	2.54	2.60
1	2.87	2.88	2.55	2.61
1.25	2.73	2.77	2.32	2.46
1.5	2.37	2.40	1.99	2.15
2	1.81	1.85	1.50	1.66
2.5	1.61	1.64	1.34	1.50
3	1.62	1.69	1.28	1.52
4	1.42	1.55	1.05	1.32
5	1.19	1.31	0.85	1.11
6	1.03	1.16	0.71	0.94
7	0.93	1.04	0.63	0.83
8	0.84	0.96	0.56	0.74
9	0.76	0.86	0.51	0.65
10	0.70	0.79	0.47	0.59
12.5	0.60	0.63	0.41	0.45
15	0.53	0.52	0.37	0.37
20	0.46	0.40	0.34	0.28
25	0.43	0.33	0.33	0.24
30	0.42	0.31	0.33	0.22
35	0.42	0.30	0.33	0.22
40	0.42	0.30	0.33	0.23
45	0.44	0.31	0.34	0.23
50	0.46	0.33	0.36	0.25
60	0.53	0.39	0.42	0.29
70	0.63	0.48	0.50	0.36
80	0.74	0.57	0.59	0.43
90	0.84	0.67	0.67	0.50
100	0.92	0.74	0.73	0.55

Table 2.5-25 — {Input Rock Motions and Associated Parameters}

Rock Motion	Magnitude (M)	Duration [sec)	Effective Strain Ratio
LF 1E-4	7.3	26.3	0.63
HF 1E-4	6.1	8.4	0.51
LF 1E-5	7.5	26.3	0.65
HF 1E-5	6.0	3.7	0.50
LF 1E-6	7.7	26.3	0.67
HF 1E-6	6.3	5.1	0.53

Table 2.5-26 — {Values of UHS (Hard Rock Conditions)}

Frequency, Hz	10^{-4} SA, g	10^{-4} SA, g	10^{-5} SA, g	10^{-5} SA, g	10^{-6} SA, g	10^{-6} SA, g
	Mean	Median	Mean	Median	Mean	Median
0.5	0.04188	0.02664	0.1185	0.06994	0.2689	0.17608
1	0.05398	0.04231	0.1429	0.11404	0.3626	0.30618
2.5	0.09846	0.08840	0.2936	0.26626	0.8536	0.77104
5	0.1567	0.14465	0.5275	0.48708	1.557	1.40839
10	0.2175	0.19970	0.7974	0.70486	2.42	2.16353
25	0.3171	0.26357	1.182	1	3.825	3.13551
100	0.1108	0.09966	0.4308	0.39287	1.361	1.16210

Table 2.5-27 — {Summary Thickness and Termination Elevation}

ENTIRE SITE		Thickness [feet]			Termination Elevation [feet]		
		Min	Max	Avg	Min	Max	Avg
Stratum I - Terrace Sand		1	68	28	32	82	61
Stratum IIa - Chesapeake Clay/Silt		4	36	19	5	67	43
Stratum IIb - Chesapeake Cemented Sand	Layer 1	3	69	24	-2	46	22
	Layer 2	3	55	23	-17	30	0
	Layer 3	4	39	16	-31	-9	-22
Stratum IIc - Chesapeake Clay/Silt		190	195	193	-215	-208	-211
Stratum III - Nanjemoy Sand		>101*	>115*	>108*	-	-	-
** Data based on borings B-301 and B-401*							

POWERBLOCK AREA		Thickness [feet]			Termination Elevation [feet]		
		Min	Max	Avg	Min	Max	Avg
Stratum I - Terrace Sand		1	52	21	45	79	62
Stratum IIa - Chesapeake Clay/Silt		4	30	18	34	55	45
Stratum IIb - Chesapeake Cemented Sand	Layer 1	8	45	26	3	43	20
	Layer 2	4	55	23	-17	28	-3
	Layer 3	5	39	16	-31	-9	-23
Stratum IIc - Chesapeake Clay/Silt		190	190	190	-208	-208	-208
Stratum III - Nanjemoy Sand		>101*	>101*	>101*	-	-	-
** Data based on borings B-301*							

INTAKE AREA		Thickness [feet]			Termination Elevation [feet]		
		Min	Max	Avg	Min	Max	Avg
Stratum I - Terrace Sand (NP)		-	-	-	-	-	-
Stratum IIa - Chesapeake Clay/Silt (NP)		-	-	-	-	-	-
Stratum IIb - Chesapeake Cemented Sand	Layer 1	5	5	5	3	3	3
	Layer 2	3	31	15	-12	-1	-8
	Layer 3	9	24	15	-28	-17	-22
Stratum IIc - Chesapeake Clay/Silt		>13	>141	>57	-	-	-
Stratum III - Nanjemoy Sand		-	-	-	-	-	-
** Data based on borings B-775 (NP) Not Present*							

Table 2.5-28 — {Summary of Field Tests}

Field	Test Standard	Number of Tests
Test Borings	ASTM D1586/1587	200
Observation Wells	ASTM D5092	47
CPT Soundings(1)	ASTM D5778	74*
Suspension P-S Velocity Logging	EPRI TR-102293	13
Test Pits	N/A	20
Field Electrical Resistivity Arrays	ASTM G57/IEEE 81	4
SPT Hammer Energy Measurements	ASTM D4633	10
Pressuremeter	ASTM D4719	2
Dilatometer	ASTM D6635	2
Notes: - (1) Includes additional off-set soundings		

Table 2.5-29 — {Summary of As-Conducted Boring Information}

(Page 1 of 5)

Location	Depth [ft]	Termination Elevation (Bottom) [ft]	Coordinates [ft], Maryland State Plane (NAD 1927)		Surface Elevation [ft] (NGVD 1929)	Date of As Built Survey
			North	East		
B-301	403.0	-308.5	217024.1	960815.1	94.5	9/15/2006
B-301A	350.0	-253.3	217011.1	960816.8	96.7	11/21/2008
B-301B	120.0	-23.2	217002.6	960819.2	96.8	11/21/2008
B-302	200.0	-123.6	217122.2	960767.0	76.4	9/15/2006
B-303	200.0	-112.6	217016.9	960867.7	87.4	9/15/2006
B-304	200.0	-132.0	217188.6	960896.9	68.0	9/15/2006
B-305	151.5	-79.5	217166.3	960686.7	72.0	9/15/2006
B-306	150.0	-31.4	217024.3	960681.8	118.6	9/15/2006
B-307	201.5	-82.2	216955.3	960690.1	119.3	9/15/2006
B-308	150.0	-42.9	216906.7	960771.3	107.1	9/15/2006
B-309	150.0	-49.9	216949.2	960890.7	100.1	9/15/2006
B-310	100.0	-8.4	217081.4	960616.6	91.6	5/15/2006
B-311	150.0	-91.6	217268.6	960771.8	58.4	9/15/2006
B-312	99.5	-44.2	217293.0	960740.0	55.3	5/15/2006
B-313	150.0	-99.3	217372.3	960713.7	50.7	9/15/2006
B-314	100.0	-47.2	217321.9	960654.5	52.8	9/15/2006
B-315	100.0	-34.5	217184.7	960559.4	65.5	9/15/2006
B-316	100.0	8.1	216767.2	960864.4	108.1	9/15/2006
B-317	100.0	-5.6	217094.7	961249.2	94.4	5/15/2007
B-318	200.0	-102.2	217019.3	961227.2	97.8	5/15/2006
B-319	100.0	2.9	216963.6	961123.0	102.9	9/15/2006
B-320	150.0	-43.6	216943.5	961044.1	106.4	5/15/2006
B-321	150.0	-79.3	217152.5	960333.2	70.7	5/25/2006
B-322	100.0	-10.1	217170.0	960202.7	89.9	9/15/2006
B-323	200.0	-92.5	217028.0	960060.9	107.5	9/15/2006
B-324	101.5	3.7	216906.4	960114.4	105.2	9/15/2006
B-325	100.0	-15.0	216949.0	960549.7	85.0	9/15/2006
B-326	100.0	3.1	216859.2	960652.3	103.1	9/15/2006
B-327	150.0	-63.1	216865.7	960573.4	86.9	9/15/2006
B-328	150.0	-73.7	216828.9	960493.2	76.3	9/19/2006
B-329	100.0	-25.2	216800.4	960379.4	74.8	9/19/2006
B-330	100.0	-14.5	216715.4	960523.7	85.5	9/15/2006
B-331	100.0	-31.7	216970.6	960481.8	68.3	9/15/2006
B-332	100.0	-34.6	217127.4	960400.5	65.4	9/15/2006
B-333	98.8	-9.3	216657.0	960386.2	89.5	9/15/2006
B-334	100.0	-13.3	216515.5	960556.6	86.8	9/15/2006
B-335	100.0	-0.5	216732.7	960703.3	99.5	5/15/2006
B-336	100.0	-3.1	216632.9	960750.3	96.9	9/15/2006
B-337	100.0	-28.2	217257.9	960264.4	71.8	9/15/2006
B-338	99.6	-1.6	217121.1	960150.1	98.0	5/25/2006
B-339	100.0	-8.0	217095.2	960212.0	92.0	9/15/2006
B-340	100.0	-15.4	217171.3	961225.2	84.6	9/15/2006
B-341	100.5	-2.3	217036.4	961104.5	98.2	9/15/2006
B-342	250.0	-174.3	217217.6	960272.9	75.7	11/21/2008
B-343	250.0	-166.9	217037.8	960306.8	83.1	11/21/2008

Table 2.5-29 — {Summary of As-Conducted Boring Information}

(Page 2 of 5)

Location	Depth [ft]	Termination Elevation (Bottom) [ft]	Coordinates [ft], Maryland State Plane (NAD 1927)		Surface Elevation [ft] (NGVD 1929)	Date of As Built Survey
			North	East		
B-344	250.0	-177.7	216976.8	960358.0	72.3	5/14/2008
B-345	250.0	-180.4	217097.3	960392.9	69.6	11/21/2008
B-346	100.0	-38.2	217206.4	960400.4	61.8	5/14/2008
B-347	200.0	-139.8	217214.2	960531.8	60.2	5/14/2008
B-348	200.0	-131.6	217148.9	960567.4	68.4	11/21/2008
B-349	100.0	-45.6	217396.4	960537.5	54.4	5/15/2008
B-350	100.0	-53.4	217516.2	960789.0	46.6	5/14/2008
B-351	100.0	-29.9	217072.1	960538.3	70.1	11/21/2008
B-352	200.0	-90.7	216829.4	960893.9	109.3	11/21/2008
B-353	200.0	-89.1	216772.7	960972.2	110.9	5/13/2008
B-354	251.5	-159.1	217131.1	961098.9	92.4	11/20/2008
B-355	250.0	-161.8	217052.6	960993.5	88.2	5/13/2008
B-356	250.0	-129.0	216965.3	961264.9	121.0	11/20/2008
B-357	105.0	-1.9	216923.1	961175.4	103.1	11/20/2008
B-357A	250.0	-147.0	216928.8	961167.0	103.0	11/20/2008
B-401	401.5	-329.4	216344.1	961516.8	72.1	9/15/2006
B-402	200.0	-117.8	216405.1	961463.5	82.2	5/15/2006
B-403	200.0	-136.6	216305.8	961562.9	63.4	5/15/2006
B-404	200.0	-132.1	216441.3	961596.5	67.9	9/21/2006
B-405	150.0	-28.0	216487.4	961408.7	122.0	9/15/2006
B-406	150.0	-31.6	216315.6	961352.0	118.4	9/15/2006
B-407	200.0	-118.4	216239.0	961412.5	81.6	9/15/2006
B-408	150.0	-81.6	216261.7	961482.0	68.4	9/15/2006
B-409	150.0	-88.5	216253.8	961614.8	61.6	4/20/2006
B-410	55.0	64.1	216374.3	961323.7	119.1	4/20/2006
B-410A*	98.7	20.4	216381.3	961323.7	119.1	4/20/2006
B-411	150.0	-68.6	216556.3	961517.2	81.5	9/15/2006
B-412	98.9	-6.7	216589.2	961495.4	92.2	9/15/2006
B-413	150.0	-27.1	216694.9	961413.3	122.9	9/15/2006
B-414	100.0	21.2	216630.2	961354.5	121.2	9/15/2006
B-415	98.7	20.6	216480.9	961264.2	119.3	4/20/2006
B-416	100.0	-13.8	216084. 5	961596.3	86.2	9/15/2006
B-417	101.5	-52.3	216435.8	961901.1	49.2	9/15/2006
B-418	200.0	-156.3	216340.3	961976.7	43.7	9/22/2006
B-419	100.0	-44.7	216267.8	961895.6	55.3	9/21/2006
B-420	150.0	-87.4	216213.5	961670.4	62.6	9/15/2006
B-421	150.0	-34.4	216497.6	961019.8	115.6	9/15/2006
B-422	100.0	4.0	216478.2	960915.0	104.0	9/15/2006
B-423	201.5	-91.4	216331.8	960850.2	110.1	9/15/2006
B-424	100.0	18.9	216263.3	960818.6	118.9	4/26/2006
B-425	101.5	16.9	216247.5	961274.7	118.4	4/20/2006
B-426	100.0	-16.3	216193.0	961386.6	83.7	9/21/2006
B-427	150.0	-33.7	216164.1	961272.7	116.3	9/19/2006
B-428	150.0	-35.9	216109.2	961210.1	114.1	9/19/2006
B-429	100.0	3.7	216087.9	961119.3	103.7	9/19/2006

Table 2.5-29 — {Summary of As-Conducted Boring Information}

(Page 3 of 5)

Location	Depth [ft]	Termination Elevation (Bottom) [ft]	Coordinates [ft], Maryland State Plane (NAD 1927)		Surface Elevation [ft] (NGVD 1929)	Date of As Built Survey
			North	East		
B-430	100.0	2.5	216006.9	961193.1	102.5	9/19/2006
B-431	101.5	16.9	216271.1	961177.3	118.4	4/20/2006
B-432	100.0	18.6	216399.0	961139.1	118.6	4/20/2006
B-433	100.0	-2.5	215963.8	961107.5	97.5	4/27/2006
B-434	100.0	5.2	215827.1	961244.3	105.2	5/2/2006
B-435	100.0	7.7	216020.1	961404.7	107.7	9/15/2006
B-436	100.0	8.3	215923.9	961441.6	108.3	9/22/2006
B-437	100.5	10.1	216521.8	960968.8	110.6	9/15/2006
B-438	6.5	99.5	216414.9	960848.9	106.0	9/28/2006
B-438A	100.0	6.6	216412.0	960867.3	106.6	9/28/2006
B-439	100.0	13.8	216340.5	960948.7	113.8	9/15/2006
B-440	100.0	-43.7	216349.5	961813.7	56.3	9/21/2006
B-701	75.0	-66.3	219485.5	960507.6	8.7	9/21/2006
B-702	50.0	-39.7	218980.6	961183.2	10.3	9/21/2006
B-703	100.0	-54.6	218171.0	960957.0	45.4	9/21/2006
B-704	50.0	-10.4	217991.1	960926.1	39.6	9/21/2006
B-705	50.0	-3.3	217581.3	960917.9	46.8	4/19/2006
B-706	50.0	27.4	217140.1	961339.7	77.4	9/21/2006
B-707	50.0	17.4	217397.0	961481.8	67.4	9/21/2006
B-708	100.0	-62.7	217585.8	961810.6	37.4	9/28/2006
B-709	50.0	-18.8	217642.8	961978.2	31.3	9/28/2006
B-710	75.0	-27.0	217542.5	962136.9	48.0	9/28/2006
B-711	50.0	3.0	216755.7	961743.5	53.0	4/19/2006
B-712	50.0	-7.6	216506.2	961997.6	42.4	9/22/2006
B-713	50.0	8.0	216117.7	962283.2	58.0	9/28/2006
B-714	50. 0	66.0	215705.7	962034.4	116.0	10/16/2006
B-715	50.0	36.3	214951.8	962639.6	86.3	10/17/2006
B-716	49.5	32.9	215003.2	961364.6	82.4	10/16/2006
B-717	50.0	40.7	214302.5	962349.3	90.7	10/17/2006
B-718	50.0	67.5	214130.5	961929.1	117.5	10/18/2006
B-719	49.4	25.8	213978.7	961500.2	75.2	10/18/2006
B-720	75.0	-1.5	215674.5	962378.5	73.5	9/28/2006
B-721	100.0	1.3	215545.8	962462.1	101.3	5/4/2006
B-722	73.9	25.9	215386.1	962467.0	99.8	5/4/2006
B-723	75.0	15.0	215108.0	963000.8	90.0	4/28/2006
B-724	100.0	-3.0	214780.0	963106.2	97.0	4/28/2006
B-725	75.0	-16.0	214664.3	963219.4	59.0	4/28/2006
B-726	75.0	3.3	215564.7	961709.6	78.3	10/16/2006
B-727	100.0	4.9	215300.9	961885.0	104.9	10/16/2006
B-728	75.0	37.3	215163.6	961910.1	112.3	10/16/2006
B-729	75.0	42.3	214861.9	962454.6	117.3	10/17/2006
B-730	75.0	40.4	214728.5	962523.8	115.4	10/17/2006
B-731	99.3	16.4	214546.5	962547.9	115.7	10/17/2006
B-732	75.0	15.7	215034.1	961594.7	90.7	5/11/2006
B-733	100.0	-12.1	214866.8	961697.7	87.9	5/11/2006

Table 2.5-29 — {Summary of As-Conducted Boring Information}

(Page 4 of 5)

Location	Depth [ft]	Termination Elevation (Bottom) [ft]	Coordinates [ft], Maryland State Plane (NAD 1927)		Surface Elevation [ft] (NGVD 1929)	Date of As Built Survey
			North	East		
B-734	75.0	30.7	214589.6	961812.5	105.7	5/9/2006
B-735	75.0	16.2	214805.5	961021.8	91.2	10/16/2006
B-736	75.0	23.3	214681.7	961154.3	98.3	10/16/2006
B-737	100.0	-36.5	214511.9	961147.4	63.5	10/16/2006
B-738	75.0	12.3	213826.3	961679.6	87.3	10/19/2006
B-739	99.8	0.5	213719.6	961793.3	100.4	10/19/2006
B-740	75.0	-0.7	213605.1	961781.1	74.3	10/19/2006
B-741	75.0	6.4	213760.5	961029.8	81.4	10/18/2006
B-742	100.0	2.4	213472.8	961217.2	102.4	10/18/2006
B-743	75.0	28.6	213315.7	961232.0	103.6	5/9/2006
B-744	100.0	13.3	216377.3	959963.4	113.3	9/29/2006
B-745	75.0	36.7	215971.2	960529.0	111.7	9/29/2006
B-746	75.0	7.8	215743.4	960721.4	82.8	9/29/2006
B-747	75.0	15.3	216176.3	959945.0	90.3	9/29/2006
B-748	100.0	-17.6	216039.7	960288.7	82.4	9/29/2006
B-749	75.0	27.5	215775.1	960332.2	102.5	9/29/2006
B-750	73.9	-1.6	215849.2	959930.1	72.4	9/29/2006
B-751	73.9	18.3	215588.9	960146.2	92.2	9/29/2006
B-752	100.0	-4.2	215489.2	960257.6	95.8	9/29/2006
B-753	40.0	8.8	217831.2	960648.9	48.8	9/21/2006
B-754	50.0	17.0	217369.8	960290.4	67.0	9/21/2006
B-755	40.0	55.0	215923.7	961637.9	95.0	9/22/2006
B-756	50.0	56.9	215504.6	961215.1	106.9	4/21/2006
B-757	40.0	66.9	215135.1	960760.6	106.9	10/16/2006
B-758	40.0	42.6	215133.3	960332.7	82.6	10/16/2006
B-759	100.0	-1.7	214526.3	960025.3	98.4	10/19/2006
B-765	102.0	-4.6	216424.5	959701.2	97.4	9/29/2006
B-766	50.0	58.9	216932.9	959791.5	108.9	9/19/2006
B-768	100.0	-51.6	217116.0	962243.0	48.4	9/28/2006
B-769	50.0	4.2	216589.8	962559.5	54.2	9/28/2006
B-770	50.0	71.6	215466.6	962827.0	121.6	10/18/2006
B-771	100.0	-89.4	219268.2	960931.9	10.6	7/1/2008
B-772	100.0	-89.4	219323.9	960876.1	10.6	7/1/2008
B-773	165.0	-157.1	219241.3	961045.9	7.9	7/1/2008
B-773A	150.0	-141.7	219233.1	961052.9	8.3	11/25/2008
B-773B	150.0	-142.0	219248.1	961039.9	8.0	11/25/2008
B-774	150.0	-139.9	219196.0	961000.5	10.1	7/1/2008
B-775	100.0	-90.3	219105.3	961091.5	9.7	7/1/2008
B-776	51.5	-41.9	219143.0	961053.7	9.6	7/14/2008
B-778	121.5	-7.9	219075.0	960739.6	113.6	11/25/2008
B-779	102.0	-1.2	218941.1	960604.8	100.8	7/2/2008
B-780	6.0	3.7	219546.2	960610.0	9.7	11/25/2008
B-780A	8.0	1.2	219542.4	960604.1	9.2	11/25/2008
B-780B	50.0	-40.8	219532.9	960625.2	9.2	11/25/2008
B-781	50.0	-39.6	219400.9	960780.8	10.4	7/14/2008

Table 2.5-29 — {Summary of As-Conducted Boring Information}

(Page 5 of 5)

Location	Depth [ft]	Termination Elevation (Bottom) [ft]	Coordinates [ft], Maryland State Plane (NAD 1927)		Surface Elevation [ft] (NGVD 1929)	Date of As Built Survey
			North	East		
B-782	51.5	-41.6	218936.5	961232.1	9.9	7/1/2008
B-785	70.0	28.1	218155.9	960637.4	98.1	11/25/2008
B-786	11.5	50.5	217943.5	960500.5	62.0	11/25/2008
B-786A	80.0	-17.9	217943.2	960496.4	62.1	11/25/2008
B-786B	115.0	-60.8	217914.6	960460.7	54.2	11/25/2008
B-787	100.0	-50.6	217780.9	960598.1	49.4	11/25/2008
B-788	50.0	2.1	217495.9	960896.1	52.1	11/21/2008
B-789	100.0	-42.7	217401.7	960986.9	57.3	11/21/2008
B-790	49.7	23.0	217278.1	961110.5	72.7	5/13/2008
B-791	100.0	-12.5	217143.5	961245.1	87.5	5/13/2008
B-821	50.0	-41.1	218736.3	961124.6	8.9	7/1/2008
B-821A	115.0	-89.6	218571.3	960962.8	25.4	11/25/2008
B-821B	7.6	-1.3	218727.2	961275.2	6.3	11/25/2008
B-821C	30.0	-22.6	218739.5	961258.1	7.4	11/25/2008
B-822	50.0	-11.2	218440.2	960840.8	38.8	7/2/2008

Table 2.5-30 — {Summary of Standard Penetration Test Data}

ENTIRE SITE		SPT N VALUE [Blows/ft]			SPT N CORRECTED [Blows/ft]		
		Min	Max	Avg	Min	Max	Avg
Stratum I - Terrace Sand		0	70	11	0	91	16
Stratum IIa - Chesapeake Clay/Silt		3	100	10	4	100	14
Stratum IIb - Chesapeake Cemented Sand	Layer 1	4	100	59	6	100	82
	Layer 2	0	100	16	0	100	22
	Layer 3	10	100	43	14	100	60
Stratum IIc - Chesapeake Clay/Silt		5	100	20	7	100	28
Stratum III - Nanjemoy Sand		28	100	56	36	100	72
POWERBLOCK AREA		**SPT N VALUE [Blows/ft]**			**SPT N CORRECTED [Blows/ft]**		
		Min	**Max**	**Avg**	**Min**	**Max**	**Avg**
Stratum I - Terrace Sand		0	70	10	0	91	14
Stratum IIa - Chesapeake Clay/Silt		3	50	11	4	70	15
Stratum IIb - Chesapeake Cemented Sand	Layer 1	6	100	63	9	100	89
	Layer 2	1	100	17	1	100	24
	Layer 3	12	100	45	16	100	63
Stratum IIc - Chesapeake Clay/Silt		9	100	21	14	100	30
Stratum III - Nanjemoy Sand		34	100	58	44	100	75
INTAKE AREA		**SPT N VALUE [Blows/ft]**			**SPT N CORRECTED [Blows/ft]**		
		Min	**Max**	**Avg**	**Min**	**Max**	**Avg**
Stratum I - Terrace Sand		-	-	-	-	-	-
Stratum IIa - Chesapeake Clay/Silt		-	-	-	-	-	-
Stratum IIb - Chesapeake Cemented Sand	Layer 1	26	26	26	35	35	35
	Layer 2	1	100	12	1	100	17
	Layer 3	12	100	39	16	100	54
Stratum IIc - Chesapeake Clay/Silt		5	44	16	7	59	22
Stratum III - Nanjemoy Sand		-	-	-	-	-	-

Notes:
- A cut-off value of 100 blows/ft is used

Table 2.5-31 — {Summary Undisturbed Tube Samples}

(Page 1 of 9)

Boring	Drill Rig	Date	Sample No.	Depth [ft]	Rec [in]	Field Remarks
B-301	U. TRUCK	5/25/2006	UD-1	33.5 - 35.5	24	MH
			UD-2	43.5 - 45.3	21	MH
			UD-3	88.5 - 90.5	0	
			UD-4	98.5 - 99.8	6	SM
			UD-5	138.5 - 140.5	4	SC / SM
		5/30/2006	UD-6	158.5 - 159.6	13	13" push, CL with fine sand
			UD-7	168.5 - 170.5	9	CL / MH
			UD-8	183.5 - 184.3	10	MH
B-301A	U. TRUCK	8/18/2008	UD-1	58.0 - 58.8	9	SP
			UD-2	60.0 - 61.9	23	SC
			UD-3	68.0 - 69.8	22	SM
			UD-4	198.0 - 199.9	23	MH
			UD-5	218.0 - 219.9	23	SM
			UD-6	238.0 - 239.9	23	MH
			UD-7	258.0 - 260.0	24	MH
			UD-8	268.0 - 269.8	22	MH
			UD-9	278.0 - 279.9	23	MH
			UD-10	288.0 - 290.0	24	MH
			UD-11	298.0 - 300.0	24	MH
			UD-12	308.0 - 309.9	23	SC
			UD-13	318.0 - 319.9	23	SC
			UD-14	328.0 - 330.0	24	SC
			UD-15	338.0 - 339.8	22	SC
			UD-16	348.0 -350.0	24	SM
B-301B	U. TRUCK	8/25/2008	UD-1	78.0 - 80.0	24	SM
			UD-2	88.0 - 89.9	23	SM
			UD-3	98.0 - 100.0	24	SM
			UD-4	108.0 -110.0	24	SM
			UD-5	118.0 -120.0	24	SM
B-302	C. ATV	5/30/2006	UD-1	83.5 - 84.9	16	16" push SM with fine sand, shell
			UD-2	128.5 - 130.5	12	MH
B-303	U. TRUCK	5/9/2006	UD-1	28 - 30	24	CL
				38 - 39.6	19	19" push, SC
B-304	U. ATV	5/30/2006	UD-1	73.5 - 75.5	22	SM
			UD-2	98.5 - 99.5	12	12" push, SC
			UD-3	138.5 - 139.3	10	MH
B-305	C.ATV	7/17/2006	UD-1	12.5 - 14.3	22	CH
			UD-2	19.5 - 21.2	16	MH
			P-3	35 - 37	5	pitcher, cemented sand
			P-4	39.5 - 41.5	22	pitcher, SM
			UD-5	52.5 - 53.5	7	f. sandy silt, shell
			P-6	89.5 - 91.5	8	pitcher, sand
B-306	U. TRUCK	5/5/2006	UD-1	58 - 60	24	CL
			UD-2	68 - 70	24	CL

Table 2.5-31 — {Summary Undisturbed Tube Samples}

(Page 2 of 9)

Boring	Drill Rig	Date	Sample No.	Depth [ft]	Rec [in]	Field Remarks
B-307	U. TRUCK	5/15/2006	UD-1	123.5 - 124.7	14	SM
			UD-2	178.5 - 180.4	23	MH
B-308	U. TRUCK	5/3/2006	UD-1	43 - 45	24	CL
		5/4/2006	UD-2	53 - 55	16	CL
		5/4/2006	UD-3	63 - 65	0	sand
B-309	C. TRUCK	5/11/2006	UD-1	33.5 - 35.5	23	CL
		5/11/2006	UD-2	43.5 - 45.5	24	CL
		5/11/2006	UD-3	53.5 - 55.5	23	SC
B-310	C. ATV	6/15/2006	UD-1	78.5 - 79.8	15	SC
B-312	C. ATV	5/18/2006	UD-1	10.5 - 12.3	17	21" push, CH
		5/18/2006	UD-2	38.5 - 38.6	0	0.5" push
		5/18/2006	UD-3	98.5 - 99.5	12	12" push, MH
B-313	U. ATV	5/22/2006	UD-1	93.5 - 94.7		CL
			UD-2	123.5 - 124.3		ML
B-314	U. ATV	5/22/2006	UD-1	13.5 - 15.5	12	CH
B-315	C. ATV	5/22/2006	UD-1	23.5 - 25.5	14	CH
B-316	C. TRUCK	5/4/2006	UD-1	43.5 - 45.5	24	CL
		5/4/2006	UD-2	53.5 - 55.5	24	CL
B-317	C. TRUCK	5/5/2006	UD-1	28.5 - 30.5	24	CL
		5/5/2006	UD-2	38.5 - 40.5	24	CH
		5/5/2006	UD-3	48.5 - 50.3	21	SC
B-318	U. ATV	6/3/2006	UD-1	148.5 - 149.1	3	7" push, f. sandy SILT
B-319	U. ATV	5/5/2006	UD-1	33.5 - 35.5	24	MH
		5/5/2006	UD-2	43.5 - 45.5	27	MH
		5/5/2006	UD-3	53.5 - 54.3	10	MH
B-320	C. TRUCK	5/8/2006	UD-1	38.5 - 40.5	24	MH
		5/9/2006	UD-2	48.5 - 50	18	18" push, clayey sand
B-321	C. ATV	6/5/2006	UD-1	23.5 - 25	18	CH
		6/6/2006	UD-2	73.5 - 75.5	24	SM
B-322	U. ATV	5/18/2006	UD-1	28.5 - 30.5	28	CL
			UD-2	38.5 - 39.9	27	SM
			UD-3	48.5 - 49.3	9	SC
B-323	U. ATV	6/7/2006	UD-1	83.5 - 84.8	15	MH
			UD-2	178.5 - 179.1	0	MH
B-324	U. ATV	6/7/2006	UD-1	60 - 62	24	CH
			P-2	69 - 71	22	SM
			P-3	85.5 - 87.5	5	SM
B-326	U. ATV	5/4/2006	UD-1	33.5 - 35.5	28	CL
		5/4/2006	UD-2	43.5 - 45.5	28	MH
		5/4/2006	UD-3	53.5 - 55.5	27	sandy lean clay, bottom 2" bent
B-327	C. ATV	5/25/2006	UD-1	113.5 - 114.2	9	ML
			UD-2	138.5 - 140.5	10	SM
B-328	C.ATV	6/19/2006	UD-1	63.5 - 65.5	24	SM
			UD-2	93.5 - 94.6	12	SC
			UD-3	123.5 - 124.4	11	ML, shell

Table 2.5-31 — {Summary Undisturbed Tube Samples}

(Page 3 of 9)

Boring	Drill Rig	Date	Sample No.	Depth [ft]	Rec [in]	Field Remarks
B-329	C.ATV	6/13/2006	UD-1	63.5 - 65.3	22	SM
			UD-2	73.5 - 75.5	24	SM
B-330	U. ATV	5/25/2006	UD-1	28.5 - 29.2	0	
B-331	C. ATV	5/24/2006	UD-1	18.5 - 20.5	24	MH
B-332	C. ATV	6/2/2006	UD-1	73.5 - 74.6	13	SM
B-333	U. ATV	5/17/2006	UD-1	28.5 - 30.5	24	MH
			UD-2	38.5 - 40.5	24	CL
			UD-3	48.5 - 48.8	4	SM
B-334	U. TRUCK	5/24/2006	UD-1	23 - 25	24	CL
			UD-2	33 - 35	13	CL
B-335	U. ATV	5/3/2006	UD-1	31 - 33	24	CL
			UD-2	38.5 - 40.5	24	CH
			UD-3	48.5 - 50.5	24	CL
			UD-4	58.5 - 58.8	3	tube deformed, SPT @ bottom, sand with shell
B-336	U. ATV	5/15/2006	UD-1	33.5 - 35.5	24	CH
			UD-2	43.5 - 45.5	24	CH
			UD-3	53.5 - 55.5	15	SC
B-337	C. ATV	6/7/2006	UD-1	53.5 - 54.6	13	ML
B-338	C.ATV	6/13/2006	UD-1	48.5 - 50.5	24	MH / ML
			UD-2	94.5 - 95.0	?	not on boring log
			UD-3	95 - 97	?	not on boring log
			UD-4	98.5 - 99.6	7	SM
B-340	C.TRACK	8/4/2006	P-1	66 - 68	12	SC, cemented
B-341	C.TRACK	8/4/2006	UD-1	88.5 - 90.5	24	SM
			UD-2	98.5 - 100.5	24	SP-SM
B-344	C. ATV	7/24/2008	UD-1	181.5 - 182.8	16	SM
			UD-2	191.5 - 193.4	23	SM
			UD-3	201.5 - 202.5	12	SM
			UD-4	204.0 - 206.0	24	SM
			UD-5	211.5 - 213.5	24	SM
			UD-6	221.5 - 223.5	24	ML
			UD-7	231.5 - 233.5	24	ML
			UD-8	241.5 - 243.5	24	ML
B-354	C. ATV	7/3/2008	UD-1	196.5 - 197.3	10	SM
			UD-2	197.3 - 199.3	24	SM
			UD-3	206.5 - 208.5	24	SM
			UD-4	216.5 - 218.5	24	SP-SM
			UD-5	226.5 - 228.5	24	SM
			UD-6	236.5 - 238.5	24	SM
			UD-7	246.5 - 248.1	19	SM
B-355	C. ATV	7/15/2008	UD-1	191.5 - 193.4	23	ML
			UD-2	201.5 - 203.4	23	SM

Table 2.5-31 — {Summary Undisturbed Tube Samples}

(Page 4 of 9)

Boring	Drill Rig	Date	Sample No.	Depth [ft]	Rec [in]	Field Remarks
B-356	C-TRUCK	7/16/2008	UD-1	221.5 - 222.6	13	ML
			UD-2	223.0 - 224.5	18	ML
			UD-3	231.5 - 233.5	24	SM
			UD-4	241.5 - 243.5	24	SM
B-401	U.TRUCK	6/20/2006	UD-1	68.5 - 70.5	23	SM
			UD-2	98.5 - 99.8	15	ML
			UD-3	123.5 - 124.8	16	CL
			UD-4	138.5 - 140.5	23	MH
		6/21/2006	UD-5	158.5 -159.3	10	MH
		6/21/2006	UD-6	173.5 - 174.4	11	MH
		6/22/2006	UD-7	198.5 - 200.5	21	ML
		6/22/2006	UD-8	213.5 - 214.6	13	ML
			UD-9	228.5 - 229.6	13	ML
			UD-10	243.5 - 244.4	8	ML
			UD-11	348.5 - 350.5	7	
B-403	C.ATV	6/21/2006	UD-1	63.5 - 64.9	20	SM
			UD-2	98.5 - 99.5	12	ML
			UD-3	123.5 - 124.5	12	ML
B-404	U.ATV	6/23/2006	UD-1	52 - 53.6	18	SP-SM
			UD-2	66 - 67.5	18	SC
			UD-3	83.5 - 85.1	17	SC
B-405	C. TRUCK	5/16/2006	UD-1	58.5 - 60.5	22	CL
			UD-2	68.5 - 70.5	24	CL
B-406	U. TRUCK	5/17/2006	UD-1	63.5 - 65.5	24	CH
			UD-2	73.5 - 75.2	12	21" push, SC
B-407	U. ATV	5/14/2006	UD-1	53.5 - 54.5	11	12" push, SM with shell
		5/15/2006	UD-2	78.5 - 79	4	tube bent, SM
		5/15/2006	UD-3	128.5 - 129	6	ML with sand
		5/15/2006	UD-4	153.5 - 153.9	5	tube bent, MH
B-409	C.TRUCK	6/22/2006	P-1	35	13	Pitcher, SP
			UD-2	17.5 - 19	24	SC
			UD-3	50 - 52	24	SM
			UD-4	62.5 - 64.5	24	SM
			UD-5	95 - 96.6	19	ML, sandy SILT
		6/27/2006	UD-6	137.5 - 139	18	MH
B-410	C. TRUCK	5/1/2006	UD-1	53.5 - 55.5	0	shelby tube lost in hole, not accepted
		5/1/2006	UD-2	60.5 - 62.5	15.5	remnant tube recovered, not accepted
B-410A	C. TRUCK	5/1/2006		53.5 - 55.5	24	CH, not on log
		5/1/2006	UD-2	63.5 - 65.5	7	CH
		5/2/2006	UD-3	73.5 - 75	18	CH, f. sand at bottom
B-411	C.ATV	7/26/2006	UD-1	23 - 25	16	CH
B-413	U. TRUCK	5/15/2006	UD-1	73 - 75	24	CL
B-414	U. TRUCK	5/11/2006	UD-1	58 - 60	24	CL
		5/11/2006	UD-2	68 - 70	24	CL

Table 2.5-31 — {Summary Undisturbed Tube Samples}

(Page 5 of 9)

Boring	Drill Rig	Date	Sample No.	Depth [ft]	Rec [in]	Field Remarks
B-420	U. TRUCK	6/6/2006	UD-1	63.5 - 65.5	24	SM
		6/7/2006	UD-2	128.5 - 130.3	22	CL
B-421	C. TRUCK	5/10/2006	UD-1	48.5 - 50.5	24	ML
		5/10/2006	UD-2	58.5 - 60.5	24	CL
B-422	C. ATV	5/4/2006	UD-1	38.5 - 40.5	24	CL
		5/4/2006	UD-2	48.5 - 50.5	23	CH
		5/4/2006	UD-3	58.5 - 59.3	8	CH / SC
B-423	C. ATV	5/4/2006	UD-1	103.5 - 105.3	21	SM
			UD-	113.5 - 113.8	0	
			UD-2	158.5 - 160.1	19	CL
			UD-3	178.5 - 179.8	16	MH
			UD-4	188.5 - 189.2	8	MH
B-425	U. TRUCK	5/1/2006	UD-1	57 - 59	24	CH
		5/1/2006	UD-2	65 - 67	24	CH
		5/1/2006	UD-3	75 - 77	24	CH
B-427	C. TRUCK	5/2/2006	UD-1	63.5 - 65.5	24	CH
		5/2/2006	UD-2	73.5 - 74.8	15	SC
B-428	U. TRUCK	5/2/2006	UD-1	57 - 59	21	CH, bottom 10" bent
		5/2/2006	UD-2	60 - 62	24	CL, bent
		5/2/2006	UD-3	63 - 65	20	CL, bottom 10" bent
		5/2/2006	UD-4	66 - 68	24	CL, bottom 5" bent
		5/2/2006	UD-5	69 - 71	7	CL, bottom 3" bent
B-429	U. ATV	5/1/2006	UD-1	45 - 47	24	CH
		5/1/2006	UD-2	53.5 - 55.5	0	
		5/1/2006	UD-3	58.5 - 60	18	SC
B-430	C. ATV	5/1/2006	UD-1	30 - 32	10	ML
		5/1/2006	UD-2	38.5 - 39.2	5	SC
		5/1/2006	UD-3	48.5 - 50.1	18	MH
		5/1/2006	UD-4	58.5 - 59.3	18	ML
B-433	C. TRUCK	5/17/2006		28.5 - 30.5	24	not on log
		5/17/2006	UD-2	38.5 - 40.5	24	CL
		5/17/2006	UD-3	48.5 - 48.8	4	CL from log
B-434	C. ATV	5/9/2006	UD-1	43.5 - 45.5	6.5	CL
		5/9/2006	UD-2	53.5 - 55	18	CH
		5/10/2006	UD-3	63.5 - 64.3	14	CH
B-436	C. ATV	5/9/2006	UD-1	48.5 - 50.5	18	CL
B-437	U.TRUCK	7/10/2006	UD-1	13.5 - 15.5	23	SM
			UD-2	98.5 - 100.5	22	SM
B-438a	U.TRUCK	7/10/2006	UD-1	93.5 - 95.5	14	SM
B-440	U. ATV	6/6/2006	UD-1	51 - 53	24	SM
			UD-2	58.5 - 58.6	0	
B-701	C.TRUCK	6/28/2006	UD-1	43.5 - 44.9	17	ML
B-703	C.TRUCK	6/28/2006	UD-1	18.5 - 20.5	19	CH
			UD-2	73.5 - 75.5	10	SM
B-708	U. ATV	5/9/2006	UD-1	78.5 - 79.5	12	12" push, sand
B-714	U. ATV	5/9/2006	UD-1	48 - 50	24	SC

Table 2.5-31 — {Summary Undisturbed Tube Samples}

(Page 6 of 9)

Boring	Drill Rig	Date	Sample No.	Depth [ft]	Rec [in]	Field Remarks
B-722	U.ATV	7/18/2006	UD-1	13 - 15	24	SM
B-723	C.TRACK	6/1/2006	UD-1	28.5 - 30.2	20	SP-SC
			UD-2	38.5 - 40.5	24	CL
B-724	C. TRACK	6/5/2006	UD-1	73.5 - 75.5	21	SM
B-725	C. TRACK	6/6/2006	UD-1	63.5 - 65.5	24	SM
B-726	C.TRACK	8/1/2006	UD-1	10.5 - 12.5	0	No Recovery
		8/1/2006	UD-2	23.5 - 25.5	19.5	CH
B-727	C. ATV	5/10/2006	UD-1	48.5 - 50.5	22	
		5/11/2006	UD-2	63.5 - 65.5	20	24" push
B-728	C. ATV	5/11/2006	UD-1	53.5 - 55.5	23	CH
B-729	C. TRUCK	5/19/2006	UD-1	68.5 - 70.5	24	CH
B-730	C. TRUCK	5/18/2006	UD-1	53.5 - 55.5	0	No Recovery
			UD-2	68.5 - 70.5	24	CH
B-731	C. TRACK	5/31/2006	UD-1	58.5 - 60.5	24	SM
B-732	C.TRACK	6/8/2006	UD-1	15 - 17	24	SM
B-733	C. TRACK	6/8/2006	UD-1	23.5 - 25.5	24	CL
			UD-2	88.5 - 90.5		CH/MH
B-734	C. TRACK	6/7/2006	UD-1	48.5 - 50.5	24	CL
B-735	C.TRACK	6/28/2006	UD-1	28 - 30	24	sand
B-737	C.TRACK	7/19/2006	UD-1	10.5 - 12.5	24	SC / CL
B-739	C. TRACK	6/15/2006	UD-1	51- 52	12	SC
			UD-2	83.5 - 84	5	CL
			UD-3	96 - 96.8	9	SP-SM
B-742	C. TRACK	6/15/2006	UD-1	78.5 - 78.6	0	
			UD-2	88.5 - 88.8	3	SM, sample placed in jar
B-743	U.ATV	7/10/2006	UD-1	23.5 - 25.5	21	SM
			UD-2	38 - 40	0	
B-746	C. TRACK	7/18/2006	UD-1	13.5 -15.5	24	SM
B-748	C.TRACK	7/17/2006	UD-1	13.5 - 15.5	24	ML
B-749	C. TRUCK	5/23/2006	UD-1	43.5 - 45.5		
B-750	C.TRACK	7/10/2006	UD-1	28.5 - 30.5	0	
			UD-2	48.5 - 49.5	11	clayey sand, shells
B-751	C. TRUCK	5/22/2006	UD-1	33.5 - 35.5		
			UD-2	43.5 - 45.5		
B-752	C.TRACK	7/5/2006	UD-1	58 - 59.5	18	clay
B-759	C.TRACK	7/5/2006	UD-1	56.5 - 57	0	
			UD-2	66 - 68	24	CH
			UD-3	98 - 98.5	5	SC, tube bent
B-765	C. TRACK	7/12/2006	P-1	70 - 72	8	cemented fine sandy silt, trace clay, trace shells
			P-2	100 - 102	20	clayey fine sandy silt
B-768	C.TRUCK	6/20/2006	UD-1	43.5 - 45.3	20	SM
			UD-2	73.5 - 75.5	24	SM

Table 2.5-31 — {Summary Undisturbed Tube Samples}

(Page 7 of 9)

Boring	Drill Rig	Date	Sample No.	Depth [ft]	Rec [in]	Field Remarks
B-771	C. TRACK	7/24/2008	UD-1	31.5 -33.5	24	SM
			UD-2	41.5 - 43.5	24	SM
			UD-3	51.5 - 53.5	24	SP-SM
			UD-4	61.5 - 63.5	24	SM
			UD-5	71.5 - 73.5	24	ML
			UD-6	81.5 - 83.5	24	ML
			UD-7	91.5 - 93.5	24	ML
B-772	C. TRACK	7/29/2008	UD-1	41.5 - 43.5	24	SM
			UD-2	51.5 - 52.6	13.5	SM
			UD-3	56.5 - 58.5	24	ML
B-773A	C. TRUCK	8/7/2008	UD-1	13.0 - 15.0	24	SM
			UD-2	23.0 - 24.3	15.5	SC
			UD-3	33.0 - 34.6	9	ML
			UD-4	43.0 - 45.0	24	SM
			UD-5	53.0 - 55.0	24	SM
			UD-6	63.0- 65.0	24	SM
			UD-7	73.0 - 75.0	24	MH
			UD-8	83.0 - 84.6	19	MH
			UD-9	93.0 - 94.8	21	SC
			UD-10	103.0 - 105.0	24	MH
			UD-11	113.0 - 114.8	22	SM
			UD-12	123.0 - 124.9	23	SM
			UD-13	136.0 - 137.8	22	SM
			UD-14	148.0 - 150.0	24	MH
B-773B	U. TRUCK	10/16/2008	UD-1	5.0 - 7.0	24	SM
			UD-2	15.0 - 16.8	22	SM
			UD-3	25.0 - 26.8	21	SC
			UD-4	35.0 - 37.0	24	ML
			UD-5	45.0 - 46.9	23	SM
			UD-6	55.0 - 57.0	24	SM
			UD-7	65.0 - 67.0	24	SM
			UD-8	75.0 - 77.0	24	MH
			UD-9	85.0 - 87.0	24	MH
			UD-10	95.0 - 97.0	24	SC
			UD-11	105.0 - 107.0	24	MH
			UD-12	115.0 - 116.5	18	SM
			UD-13	125.0 - 127.0	24	SM
			UD-14	135.0 - 137.0	24	SM
			UD-15	145.0 - 147.0	24	MH

Table 2.5-31 — {Summary Undisturbed Tube Samples}

(Page 8 of 9)

Boring	Drill Rig	Date	Sample No.	Depth [ft]	Rec [in]	Field Remarks
B-774	U.ATV	7/30/2008	UD-1	11.5 - 13.1	19	SP-SM
			UD-2	16.5 -17.9	16.5	SM
			UD-3	21.5 - 23.4	23	SM
			UD-4	31.5 - 33.4	23	SM
			UD-5	41.5 - 43.5	24	SM
			UD-6	51.5 - 53.5	24	SM
			UD-7	81.5 - 83.3	22	MH
			UD-8	101.5 - 103.5	24	SM
			UD-9	111.5 - 113.4	23	SM
			UD-10	121.5 - 123.0	18	SM
			UD-11	131.5 - 133.4	22.5	SM
			UD-12	141.5 - 143.2	20	MH
B-776	C. TRACK	7/22/2008	UD-1	36.5 - 38.2	20	ML
			UD-2	46.5 - 47.8	16	SM
B-778	C. TRACK	8/18/2008	UD-1	6.5 - 8.5	24	SM
			UD-2	11.5 - 13.5	24	SM
			UD-3	21.5 - 22.4	11	SM
			UD-4	23.5 - 24.5	12	SP-SM
			UD-5	31.5 - 32.5	12	SP-SM
			UD-6	33.5 - 34.4	10.5	SP-SM
			UD-7	41.5 - 43.1	19	CL
			UD-8	51.5 - 53.5	24	ML
			UD-9	61.5 - 63.5	24	GP
			UD-10	71.5 - 73.5	24	ML
			UD-11	81.5 - 83.5	24	ML
			UD-12	91.5 - 92.5	12	GP
			UD-13	93.5 - 94.7	14	SP
			UD-14	101.5 - 103.2	20	SP
			UD-15	111.5 - 113.5	24	SM
B-779	C. TRACK	8/13/2008	UD-1	6.5 - 8.3	21	SP
			UD-2	11.5 -13.5	24	SM
			UD-3	21.5 - 23.5	24	CL
			UD-4	31.5 - 33.5	24	SP
			UD-5	41.5 - 43.5	24	SM
			UD-6	51.5 - 52.5	12	ML
			UD-7	53.5 - 55.5	24	ML
			UD-8	61.5 - 63.5	24	ML
			UD-9	71.5 - 73.3	22	SM
			UD-10	81.5 - 82.8	16	SP-SM
			UD-11	96.5 - 97.7	14	SP-SM
			UD-12	100.0 - 102.0	24	SP-SM
B-782	C. TRACK	7/23/2008	UD-2	46.5 - 47.3	9	SM

Table 2.5-31 — {Summary Undisturbed Tube Samples}

(Page 9 of 9)

Boring	Drill Rig	Date	Sample No.	Depth [ft]	Rec [in]	Field Remarks
B-786B	C. TRACK	11/6/2008	UD-1	5.0 - 7.0	24	SP-SM
			UD-2	15.0 -16.5	18	SM
			UD-3	25.0 - 26.0	12	SP
			UD-4	27.0 - 28.8	21	CH
			UD-5	35.0 - 36.7	20	CL
			UD-6	45.0 - 46.5	18	SM
			UD-7	55.0 - 57.0	24	SP-SM
			UD-8	65.0 - 66.8	22	SP-SM
			UD-9	75.0 - 76.8	21	SP-SM
			UD-10	85.0 -87.0	24	ML
			UD-11	95.0 - 97.0	24	SM
B-821A	C. TRACK	11/11/2008	UD-1	10.0 - 11.2	14	SP-SM
			UD-2	12.0 - 13.0	12	SP-SM
			UD-3	20.0 - 22.0	24	SP-SM
			UD-4	30.0 - 32.0	24	SM
			UD-5	40.0 - 41.5	18	SM
			UD-6	50.0 - 52.0	24	ML
			UD-7	60.0 - 62.0	24	ML
			UD-8	70.0 - 71.0	12	SM
			UD-9	72.0 - 73.0	12	SM
			UD-10	80.0 - 82.0	24	ML
			UD-11	90.0 - 90.9	11	ML
			UD-12	92.0 - 93.6	19	SM
			UD-13	100.0 - 101.8	21	ML

Table 2.5-32 — {Summary of Hammer Rod Energy Measurements}

Drill Rig	Boring	ETR Range [%]	Average ETR [%]	Adjustment [ETR%/60%]
Failing 1500 Truck	B-401	67-88	78	1.3
CME 550X ATV	B-403	73-92	84	1.4
CME 750 ATV	B-404	78-90	87	1.45
CME 75 Truck	B-409	69-90	84	1.4
Diedrich D50 ATV	B-744	73-84	81	1.35
CME 75 ATV (Phase II)	B-348 & B-357	77-95	90	1.5
CME 550X ATV (Phase II)	B-354	79-90	83	1.38
Diedrich D50 ATV (Phase II)	B-791	74-85	81	1.35
CME 75 Truck (Phase II)	B-356	86-92	90	1.5

Table 2.5-33 — {Summary As-Conducted CPT Information}

(Page 1 of 2)

Location	Depth [ft]	Bottom Elevation [ft]	Coordinates [ft], Maryland State Plane (NAD 1927)		Ground Surface Elevation [ft] (NGVD 1929)	Date of As Built Survey	Remarks PD: Pre-Drill S: Seismic D: Dissipation		
			North	East			PD	S	D
C-301	52.3	42.5	217041.78	960820.13	94.84	9/15/2006		×	·
C-302	61.7	29.2	217088.9	960833.77	90.94	9/15/2006		·	×
C-302-2*	55.3	39.2	217026.56	960817.55	94.51	7/26/2006		·	·
C-302-2a*	138	-43.5	217026.56	960817.55	94.51	7/26/2006	×85 ft	·	×
C-303	25.4	36.2	217230.6	960804	61.58	4/24/2006		·	
C-303a*	47.1	14.5	217230.6	960804	61.58	7/25/2006	×45 ft	·	·
C-303a-1*	71.4	-9.8	217230.6	960804	61.58	7/25/2006	×50 ft	·	·
C-303b*	123.4	-61.8	217230.6	960804	61.58	7/25/2006	×80 ft	·	×
C-304	26.7	34.3	217235.29	960606.73	60.95	9/15/2006		×	×
C-305	74.3	41.6	216876.5	960961.5	115.91	4/24/2006		·	·
C-306	56.9	40.4	217042.12	961184.89	97.31	9/15/2006		·	×
C-306a*	102.5	-5.2	217038.92	961181.69	97.31	7/27/2006	×80 ft	·	·
C-307	75.3	42.3	216853.68	961079.64	117.64	9/15/2006		×	·
C-308	48.2	36.1	217129.9	960263.7	84.33	5/1/2006		×	·
C-309	70.1	35.9	217045.62	960110.76	106.04	9/15/2006		·	×
C-311	34.9	39.1	216869.75	960488.16	73.97	9/15/2006		·	·
C-312	56.4	43.4	216799.2	960596.36	99.75	9/15/2006		·	·
C-313	37.2	42.7	216757.92	960336.75	79.93	9/15/2006		·	·
C-314	39.5	40.6	216531.4	960493.83	80.09	9/15/2006		·	·
C-401	28.1	39.4	216384.26	961574.09	67.46	9/15/2006		×	·
C-401-2a*	81.9	-14.4	216381.06	961570.89	67.46	7/27/2006	×55 ft	×	·
C-401-2b*	131.2	-63.7	216381.06	961570.89	67.46	7/27/2006	×85 ft	×	×
C-402	34.5	38.6	216333.85	961494.18	73.13	9/15/2006		·	×
C-403	43.8	39.2	216517.33	961511.47	82.96	9/15/2006		·	·
C-404	80.1	39.1	216524.3	961308.9	119.21	4/20/2006		×	×
C-405	40	35.5	216163.49	961666.32	75.54	9/15/2006		·	·
C-406	15.6	28.3	216380.92	961901.51	43.89	9/28/2006		·	×
C-407	32.3	30.9	216159.2	961732.2	63.23	6/22/2006		×	×
C-407-2a*	96.3	-33.1	216161.5	961726.7	63.23	7/28/2006	×50 ft	·	×
C-407-b*	142.4	-79.2	216161.5	961726.7	63.23	7/31/2006	×95 ft	·	×
C-408	77.4	40.8	216396.64	961001.81	118.18	9/15/2006		×	·
C-408a*	98.3	19.9	216398.76	960999.69	118.18	7/24/2006	×98 ft	×	·
C-408-2a*	123.7	-5.5	216393.81	961004.64	118.18	7/31/2006	×105 ft	×	·
C-409	80.5	38.6	216288.45	960760.56	119.12	9/15/2006		·	×
C-411	80.4	36.2	216178.94	961178.21	116.6	9/19/2006		·	×
C-412	76.8	37.5	216093.75	961306.66	114.31	9/28/2006		·	·
C-413	13.6	86.3	216045.53	961037.78	99.9	9/28/2006		·	·
C-414	62.5	39.9	215893.42	961201.1	102.36	9/28/2006		·	×
C-415	20	36.6	216305.7	961857.4	56.63	5/26/2006			
C-701	29.5	-18.6	219262.19	960933.61	10.95	9/21/2006	·	·	×
C-701a*	28.1	-17.2	219265.39	960936.81	10.95	7/21/2006	·	·	·
C-702	20.3	-9	218720.05	961033.95	11.34	9/21/2006	·	·	·

Table 2.5-33 — {Summary As-Conducted CPT Information}

(Page 2 of 2)

Location	Depth [ft]	Bottom Elevation [ft]	Coordinates [ft], Maryland State Plane (NAD 1927)		Ground Surface Elevation [ft] (NGVD 1929)	Date of As Built Survey	Remarks PD: Pre-Drill S: Seismic D: Dissipation		
			North	East			PD	S	D
C-703	32.6	35.2	217361.27	961165.03	67.82	10/17/2006	·	·	×
C-704	48.2	-2.8	217500.74	961710.02	45.36	9/28/2006	·	·	·
C-705	34	-2.9	217637.26	961983.1	31.08	9/28/2006	·	·	·
C-706	50	55.3	216958.95	961494.86	105.28	9/21/2006	·	·	·
C-707	19.5	20.9	216308.12	962079.42	40.35	9/22/2006	·	·	·
C-708	50	63	215658.28	961962.86	112.97	10/16/2006	·	·	·
C-709	50	61.7	215027.59	962824.89	111.73	10/18/2006	·	·	·
C-710	21.2	85	214875.83	961187.31	106.15	10/16/2006	·	·	·
C-711	34.9	65.6	214222.13	962176.75	100.54	10/17/2006	·	·	·
C-712	29.7	29.4	213909.83	961370.06	59.05	10/18/2006	·	·	×
C-713	41.8	21.3	215855.86	962296.57	63.11	9/28/2006	·	·	·
C-714	85.1	24.2	214920.3	963057.62	109.32	10/18/2006	·	·	×
C-715	57.3	33.6	215445.62	961798.99	90.85	10/16/2006	·	·	·
C-716	20.5	75.7	214432.49	962659.44	96.21	10/17/2006	·	·	·
C-717	66.6	35.8	214698.14	961692.58	102.35	10/16/2006	·	·	×
C-718	34.1	33.6	214343.71	961205.59	67.67	10/16/2006	·	·	·
C-719	12	78.2	214025.3	961636.9	90.21	10/18/2006	·	·	·
C-720	70.7	28	213593.77	961134.09	98.66	10/18/2006	·	·	×
C-721	52	35.6	216157.88	960330.47	87.62	9/29/2006	·	·	·
C-722	38.4	36.1	215478.76	960648.26	74.52	10/16/2006	·	·	·
C-723	68.7	28.9	215988.18	959760.36	97.6	9/29/2006	·	·	×
C-724	152.2	-144.3	219309.8	960973.5	7.9	8/6/2008	×	×	·
C-724A	13.3	-5.4	219309.3	960973.9	7.9	8/6/2008		×	·
C-725	152.4	-144.2	219157.7	961143.9	8.2	8/7/2008	×	×	·
C-726	52.5	-43.3	219479.9	960691.8	9.2	8/6/2008		·	·
C-727	101.1	-92.9	219368.3	960914.9	8.2	8/6/2008	×	·	×
C-728	52.8	-42.8	218975.5	961193	10	8/5/2008	·	·	·
C-747	52.8	-43.7	218860.2	961248.5	9.1	8/4/2008	×	·	·
C-748	41.3	-8.9	218521.4	960909.8	32.4	8/20/2008	·	·	·
C-748A	52	-19.7	218518.9	960908.7	32.3	8/21/2008	·	·	·
C-749	18.4	43.9	218344.5	960737.8	62.3	8/20/2008	·	·	·
C-749A	41.2	21.1	218346.4	960740	62.3	8/21/2008	×	·	·

Notes:
- (*) Location and elevation approximated based on offset observed in the field and recorded on Field Checklist

Table 2.5-34 — {Summary of As-Conducted Observation Well Information}

(Page 1 of 2)

Location	Depth [ft]	Termination Elevation (Bottom) [ft]	Coordinates [ft], Maryland State Plane (NAD 1927)		Surface Elevation [ft] (NGVD 1929)	Elevation (Top of Concrete at Base of Well Head Protector) [ft]	Elevation GW Level Measuring Point (V-Notch) [ft]	Date of As Built Survey
			North	East				
OW-301	80	14.5	217048.02	960814.47	94.51	94.78	96.27	9/15/2006
OW-313A	57.5	-6.5	217367.31	960705.3	51.03	51.31	53.2	9/15/2006
OW-313B	110	-59.3	217372.34	960713.67	50.73	51.16	53.54	9/15/2006
OW-319A	35	68.1	216962.56	961116.12	103.13	103.31	104.91	9/15/2006
OW-319B	85	18.5	216957.32	961125.02	103.53	103.85	105.35	9/19/2006
OW-323A	43.5	63.5	217034.46	960057.07	106.96	107.55	109.69	9/19/2006
OW-328	72	4.3	216828.86	960493.21	76.29	76.55	77.85	9/19/2006
OW-336	74	23.1	216643.18	960746.61	97.11	97.5	99.07	9/16/2006
OW-401	77.5	-6.1	216348.86	961530.99	71.38	71.91	73.49	9/21/2006
OW-413A	50	73.2	216703.14	961418.81	123.15	123.51	125.04	9/15/2006
OW-413B	125	-2.1	216694.88	961413.25	122.9	123.25	124.85	9/15/2006
OW-418A	40	3.7	216340.41	961966.46	43.66	44.31	45.83	9/22/2006
OW-418B	92	-48.3	216340.25	961976.71	43.67	44.13	45.77	9/22/2006
OW-423	43	68.1	216339.99	960882.24	111.12	111.67	113.16	9/15/2006
OW-428	50	63.9	216105.21	961212.38	113.92	114.32	115.92	9/19/2006
OW-436	50	58.1	215922.47	961446.87	108.13	108.53	110.39	9/22/2006
OW-703A	49	-5	218171.23	960967.72	44.02	44.44	45.65	9/21/2006
OW-703B	80	-34.4	218171.67	960958.91	45.57	45.97	47.53	9/21/2006
OW-705	52	-4.3	217566.62	960917.18	47.71	47.77	50.22	9/15/2006
OW-708A	34	3.4	217586.23	961803.52	37.44	37.82	39.61	9/28/2006
OW-711	50	2.9	216748.48	961741.61	52.92	53.26	55.31	9/22/2006
OW-714	50	66	215705.73	962034.37	116.02	116.32	117.98	10/16/2006
OW-718	43	75.5	214133.58	961924.87	118.53	118.96	120.41	10/18/2006
OW-725	60	-2	214649.3	963212.73	58.04	58.38	59.94	10/18/2006
OW-729	42	76.9	214872.58	962445.93	118.88	119.44	121.11	10/17/2006
OW-735	72	19.2	214805.48	961021.83	91.2	91.81	93.44	10/16/2006
OW-743	55	48.7	213320.62	961234.01	103.65	104.05	105.89	10/18/2006
OW-744	50	47.5	216405.37	960089.41	97.5	97.96	99.81	9/29/2006
OW-752A	37	58.3	215482.18	960250.12	95.3	95.73	97	9/29/2006
OW-752B	97	-1.2	215489.21	960257.57	95.79	96.09	97. 41	9/29/2006
OW-754	44	23	217369.78	960290.37	67	67.21	68.85	9/15/2006
OW-756	42	64.6	215497.07	961212.39	106.56	107.07	108.77	10/16/2006
OW-759A	35	62.8	214536.47	960055.02	97.78	98.05	99.69	10/19/2006
OW-759B	90	8.4	214526.25	960056.32	98.35	98.72	100.14	10/19/2006
OW-765A	29	68.4	216424.51	959701.22	97.37	97.92	99.6	9/29/2006
OW-765B	102	-5.8	216420.42	959693.64	96.82	97.19	98.47	9/29/2006
OW-766	37	71.9	216932.89	959791.5	108.89	109.32	110.72	9/19/2006

Table 2.5-34 — {Summary of As-Conducted Observation Well Information}

(Page 2 of 2)

Location	Depth [ft]	Termination Elevation (Bottom) [ft]	Coordinates [ft], Maryland State Plane (NAD 1927)		Surface Elevation [ft] (NGVD 1929)	Elevation (Top of Concrete at Base of Well Head Protector) [ft]	Elevation GW Level Measuring Point (V-Notch) [ft]	Date of As Built Survey
			North	East				
OW-768A	42	6.5	217106.06	962238.98	48.48	48.96	49.84	9/28/2006
OW-769	42	12.2	216589.75	962559.47	54.23	54.39	56.43	9/28/2006
OW-770	42	79.6	215466.6	962826.95	121.59	121.79	123.08	10/18/2006
OW-304	72.8	-4	217158.1	960920.8	68.8	69.28	71.01	7/17/2008
OW-308	103	8.4	216928	960750	111.4	111.95	113.62	7/17/2008
OW-774A	23	-13.3	219187.3	961030.5	9.7	10.2	12.2	7/31/2008
OW-774B	52.8	-42.7	219176.7	961020.2	10.1	10.5	12.55	7/31/2008
OW-778	52	61.3	219100.6	960728.6	113.3	113.7	115.45	8/27/2008
OW-779	52.5	48.4	218958.7	960587.3	100.9	101.3	102.94	8/27/2008
OW-781	53	-42.7	219421.3	960764.4	10.3	10.8	12.87	7/29/2008

Table 2.5-35 — {In-Situ Hydraulic Conductivity (Slug) Test Results}

Location	Screened Interval Depth [ft]	USCS Soil Classification	Hydraulic Conductivity [fps]
OW-301	65 - 75	SP	1.58X10-4
OW-313A	40 - 50	SM, ML	7.50X10-6
OW-313B	95 - 105	CL, ML, MH	2.74X10-7
OW-319A	20 - 30	SP-SM, SC, CH, CL	2.89X10-6
OW-319B	70 - 80	SM	3.42X10-5
OW-323A	30 - 40	SP, SP-SM	6.24X10-5
OW-328	60 - 70	SM, OH	3.79X10-6
OW-336	60 - 70	SP-SM, SM	2.10X10-5
OW-401	63 - 73	SM	6.77X10-6
OW-413A	35 - 45	SP-SM	1.21X10-5
OW-413B	110 - 120	SP-SM, SM	2.78X10-6
OW-418A	25 - 35	SP-SM	4.41X10-6
OW-418B	75 - 85	SC, SM	2.16X10-7
OW-423	28 - 38	SP-SM, SM, SC	6.86X10-5
OW-428	35 - 45	SM, SC	1.19X10-5
OW-436	29 - 39	SC, SM	2.80X10-6
OW-703A	35 - 45	SM	1.34X10-5
OW-703B	68 - 78	SM, ML	1.08X10-6
OW-705	40 - 50	SC, SM	4.99X10-6
OW-708A	22 - 32	SM	2.56X10-5
OW-711	35 - 45	SM	6.04X10-6
OW-714	38 - 48	SP-SM, SC	2.81X10-6
OW-718	30 - 40	SP-SM	4.44X10-6
OW-725	48 - 58	SM	7.54X10-6
OW-735	60 - 70	SP-SM, SM	5.48X10-5
OW-743	40 - 50	SP-SM, SM	6.23X10-7
OW-744	38 - 48	CL, SC, SM	1.07X10-6
OW-752A	25 - 35	CH, SM	7.03X10-5
OW-752B	85 - 95	SP-SM	3.35X10-6
OW-754	32 - 42	CL, SM	5.29X10-6
OW-756	30 - 40	SP-SM, SP-SC	2.01X10-4
OW-759A	20 - 30	SM, SC, MH	4.64X10-7
OW-759B	75 - 85	SM, SP, SP-SM	1.17X10-6
OW-765A	17 - 27	SP-SM	1.00X10-5
OW-765B	82 - 92	SM	1.36X10-6
OW-766	20 - 30	SP-SM	1.10X10-6
OW-768A	30 - 40	SM	5.29X10-6
OW-769	32 - 42	SM, SC	1.74X10-6
OW-304	60 - 70	SM	4.31X10-6
OW-308	90 - 100	SP-SM	1.87X10-5
OW-774A	20-Oct	SM	2.72X10-5
OW-774B	40 - 50	SC	1.44X10-7
OW-778	40 - 50	ML,CH	Dry
OW-779	40 - 50	CH	Dry
OW-781	40 - 50	SM,ML	4.01X10-7

Table 2.5-36 — {Summary As-Conducted Test Pit Information}

Location	Depth [ft]	Termination Elevation (Bottom) [ft]	Coordinates [ft], Maryland State Plane (NAD 1927)		Surface Elevation [ft] (NGVD 1929)	Date of As Built Survey
			North	East		
TP-B307	6.7	112.7	216957.53	960690.62	119.35	9/19/2006
TP-B314	9	43.8	217320.35	960658.25	52.78	9/15/2006
TP-B315	8.5	57.3	217182.5	960563.12	65.8	9/15/2006
TP-B334	10	77	216515.64	960560.94	87.03	9/19/2006
TP-B335	8	91.6	216730.79	960706.97	99.64	9/19/2006
TP-B407	7	74.3	216391.76	961465.02	81.25	9/21/2006
TP-B414	6.5	114.3	216631.18	961530.95	120.83	9/15/2006
TP-B415	6.5	112.4	216490.91	961298.37	118.92	9/15/2006
TP-B423	8	97.9	216414.95	960849.03	105.86	9/19/2006
TP-B434	8.5	96.7	215825.9	961244.18	105.24	9/22/2006
TP-B435	10	97.7	216020.06	961404.74	107.71	9/19/2006
TP-B715	8.5	79.7	214964.18	962637.77	88.16	10/17/2006
TP-B716	8.8	88.3	214983.83	961289.79	97.13	10/16/2006
TP-B717	8	82.5	214297.68	962346.36	90.53	10/17/2006
TP-B719	8	64.3	213966.93	961493.94	72.28	10/18/2006
TP-B727	7	97.3	215299.14	961883.13	104.33	10/16/2006
TP-B744	6.5	106.8	316377.3	959963.38	113.28	9/29/2006
TP-B758	9	73.6	215133.29	960332.67	82.63	10/16/2006
TP-C309	8	100.5	217020.05	960105.24	108.45	9/19/2006
TP-C723	7	89.8	215989.07	959754.78	96.75	9/29/2006

Table 2.5-37 — {Summary of Field Electrical Resistivity Information}

Location	Depth [ft]	Coordinates [ft], Maryland State Plane (NAD 1927)		Surface Elevation [ft] (NGVD 1929)	Date of As Built Survey
		North	East		
R-1	6.7	215837.3	960255.8	85.45	5/3/2006
R-2	9	215837.3	960255.8	85.45	5/3/2006
R-3	8.5	216622.5	960406.8	89.12	5/2/2006
R-4	10	215915.4	961114	99.4	4/27/2006

Table 2.5-38 — {Field Electrical Resistivity}

Spacing [ft]	Location				Min [ohm -m]	Max [ohm -m]	Avg [ohm -m]
	R1 El. 85.5	R2 El. 85.5	R3 El. 89.1	R4 El. 99.4			
	Measured Resistivity [ohm -m]						
1.5	1210	1520	3070	471	471	3070	1568
3.0	2480	2410	3750	640	640	3750	2320
5.0	3220	2780	4550	660	660	4550	2803
7.5	3110	2890	5440	806	806	5440	3062
10.0	2490	2700	6240	1130	1130	6240	3140
15.0	1870	2780	5370	1340	1340	5370	2840
20.0	1570	1960	4100	1790	1570	4100	2355
30.0	1310	2060	1960	1640	1310	2060	1743
40.0	739	1590	1010	1280	739	1590	1155
50.0	314	1080	415	975	314	1080	696
100.0	45	487	69	463	45	487	266
200.0	37	116	38	57	37	116	62
300.0	48	76	31	41	31	76	49

Table 2.5-39 — {Geophysical Data from CCNPP Units 1 and 2 UFSAR}

STATION	Compressional Velocities							
	Surficial Sediments (Pleistocene)		Unconsolidated Sediments (Tertiary)		Intermediate Sediments (Cretaceous)		Basement Rock	
	Wave Velocity [fps]	Thickness [ft]	Wave Velocity [fps]	Thickness [ft]	Wave Velocity [fps]	Thickness [ft]	Wave Velocity [fps]	Thickness [ft]
Solomons Shoal	-	-	5900	3080	-	-	15,170	3130
Solomons Deed	-	-	6080	1070	6980	1900	18,100	3080
Site	2200	40	5500	-	-	-	-	-
Site	-	-	5900	-	-	-	-	-

Table 2.5-40 — {Pressuremeter Test Results, PM-301}

(Page 1 of 2)

Test	Depth [ft]	El. [ft]	Layer/Material		G [ksf]	$G_{u/r}$ [ksf]	*v*	E [ksf]	$E_{u/r}$ [ksf]	$E_{u/r}$ / E
CC30	9.0	85.5	I	sand, some gravels	38	63	0.30	99	164	1.6
CC31	18.0	76.5	I	sand, some gravels	148	993	0.30	386	2581	6.7
CC32	29.5	65.0	I	clayey sand, silt	80	787	0.30	209	2045	9.8
CC33	28.0	66.5	I	clayey sand, silt	104	993	0.30	271	2581	9.5
CC34	41.0	53.5	IIa	sandy clay, lean clay	219	619	0.45	635	1795	2.8
CC35	39.5	55.0	IIa	sandy clay, lean clay	230	583	0.45	668	1690	2.5
CC36	51.0	43.5	IIb-1	interbedded fat clay with silty sand	508	1758	0.30	1322	4571	3.5
CC37	49.5	45.0	IIb-1	interbedded fat clay with silty sand	454	999	0.30	1179	2598	2.2
CC38	60.8	33.7	IIb-1	clayey sand, some cementation	859	3517	0.30	2232	9143	4.1
CC39	59.3	35.2	IIb-1	clayey sand to sand	572	1985	0.30	1488	5162	3.5
CC40	70.4	24.1	IIb-1	interbedded cemented sand, silt	963	9600	0.30	2504	24960	10.0
CC41	68.9	25.6	IIb-1	interbedded cemented sand, silt	637	6600	0.30	1656	17160	10.4
CC42	80.9	13.6	IIb-2	interbedded sand and clay	644	4705	0.30	1674	12232	7.3
CC43	79.4	15.1	IIb-2	interbedded sand and clay	255	3136	0.30	663	8155	12.3
CC44	91.0	3.5	IIb-2	interbedded cemented sand, silt	625	5280	0.30	1625	13728	8.4
CC45	89.5	5.0	IIb-2	interbedded cemented sand, silt	731	9827	0.30	1900	25551	13.4
CC46	101.0	-6.5	IIb-2	silty sand, some cementation	510	3517	0.30	1326	9143	6.9
CC47	99.5	-5.0	IIb-2	silty sand	508	2271	0.30	1322	5904	4.5
CC48	111.0	-16.5	IIb-3	silty sand, trace clay, cementation	1017	6273	0.30	2643	16310	6.2
CC49	109.5	-15.0	IIb-3	silty sand, trace clay	731	2839	0.30	1900	7382	3.9
CC50	120.8	-26.3	IIb-3	interbedded silty sand, sandy clay	731	3517	0.30	1900	9143	4.8
CC51	119.3	-24.8	IIb-3	interbedded cemented sand, silt	907	6273	0.30	2359	16310	6.9
CC52	131.0	-36.5	IIc	sandy clay, clayey sand, silt	510	2358	0.45	1479	6839	4.6
CC53	129.5	-35.0	IIc	sandy clay, clayey sand, silt	454	1985	0.45	1315	5757	4.4
CC54	141.0	-46.5	IIc	clayey sand, sandy clay	417	2580	0.45	1208	7482	6.2
CC55	139.5	-45.0	IIc	clayey sand, sandy clay	510	1999	0.45	1479	5797	3.9
CC56	151.0	-56.5	IIc	sandy clay	564	2580	0.45	1637	7482	4.6
CC57	149.5	-55.0	IIc	sandy clay	461	1999	0.45	1337	5797	4.3
CC58	161.0	-66.5	IIc	interbedded silty sand, sandy clay	740	2271	0.45	2145	6585	3.1
CC59	159.5	-65.0	IIc	interbedded silty sand, sandy clay	740	1758	0.45	2145	5099	2.4
CC60	171.0	-76.5	IIc	clayey sand, sandy clay	510	2358	0.45	1479	6839	4.6
CC61	169.5	-75.0	IIc	clayey sand, sandy clay	625	2166	0.45	1813	6283	3.5
CC62	181.0	-86.5	IIc	sandy elastic silt, trace clay	770	2358	0.45	2234	6839	3.1
CC63	179.5	-85.0	IIc	sandy elastic silt, trace clay	693	2278	0.45	2010	6607	3.3
CC64	191.0	-96.5	IIc	sandy elastic silt	907	2580	0.45	2631	7482	2.8
CC65	189.5	-95.0	IIc	sandy elastic silt	693	1999	0.45	2010	5797	2.9
CC66	201.0	-106.5	IIc	sandy elastic silt, clay	693	1999	0.45	2010	5797	2.9
CC67	199.5	-105.0	IIc	sandy elastic silt, clay	731	2166	0.45	2119	6283	3.0
CC68	210.9	-116.4	IIc	interbedded clayey sand, silty sand	731	1851	0.45	2119	5369	2.5

Table 2.5-40 — {Pressuremeter Test Results, PM-301}

(Page 2 of 2)

Test	Depth [ft]	El. [ft]	Layer/Material		G [ksf]	$G_{u/r}$ [ksf]	*v*	E [ksf]	$E_{u/r}$ [ksf]	$E_{u/r}$ / E
CC69	209.4	-114.9	IIc	interbedded clayey sand, silty sand	770	1999	0.45	2234	5797	2.6
CC70	221.0	-126.5	IIc	clayey sand to sandy clay	417	3147	0.45	1208	9125	7.6
CC71	219.5	-125.0	IIc	clayey sand to sandy clay	376	2166	0.45	1091	6283	5.8
CC72	231.0	-136.5	IIc	clayey sand to sandy clay	357	1851	0.45	1036	5369	5.2
CC73	229.5	-135.0	IIc	clayey sand to sandy clay	357	1999	0.45	1036	5797	5.6
CC74	241.0	-146.5	IIc	clayey sand	461	1851	0.45	1337	5369	4.0
CC75	239.5	-145.0	IIc	clayey sand	417	1720	0.45	1208	4989	4.1
CC76	251.0	-156.5	IIc	clay to sandy clay	510	1851	0.45	1479	5369	3.6
CC77	249.5	-155.0	IIc	clay to sandy clay	693	1999	0.45	2010	5797	2.9
CC78	261.0	-166.5	IIc	interbedded clay and sandy silt	396	2166	0.45	1148	6283	5.5
CC79	259.5	-165.0	IIc	interbedded clay and sandy silt	396	1720	0. 45	1148	4989	4.3
CC80	271.0	-176.5	IIc	interbedded clay and sandy silt	417	1603	0.45	1208	4650	3.8
CC81	269.5	-175.0	IIc	interbedded clay and sandy silt	693	2358	0.45	2010	6839	3.4
CC82	281.0	-186.5	IIc	elastic silt, trace sand	510	1720	0.45	1479	4989	3.4
CC83	279.5	-185.0	IIc	elastic silt, trace sand	625	1851	0.45	1813	5369	3.0
CC84	291.0	-196.5	IIc	interbedded elastic silt and clay	461	1720	0.45	1337	4989	3.7
CC85	289.5	-195.0	IIc	interbedded elastic silt and clay	536	1498	0.45	1556	4345	2.8
CC86	301.0	-206.5	IIc	interbedded elastic silt and clay	594	2580	0.45	1722	7482	4.3
CC87	299.5	-205.0	IIc	interbedded elastic silt and clay	461	2358	0.45	1337	6839	5.1
CC88	310.7	-216.2	III	cemented sand, behaved like rock	Unsuccessful Test					
CC89	321.0	-226.5	III	interbedded clayey sand, clay	1096	3870	0.30	2850	10062	3.5
CC90	319.5	-225.0	III	interbedded clayey sand, clay	1220	4720	0.30	3171	12272	3.9
CC91	328.5	-234.0	III	cemented sand, behaved like rock	Unsuccessful Test					
CC92	338.5	-244.0	III	clayey sand	1156	3537	0.30	3005	9197	3.1
CC93	350.0	-255.5	III	clayey sand	807	3568	0.30	2098	9278	4.4
CC94	348.5	-254.0	III	clayey sand	768	3969	0.30	1996	10320	5.2
CC95	361.0	-266.5	III	clayey sand	990	3232	0.30	2573	8404	3.3
CC96	359.5	-265.0	III	clayey sand	695	3568	0.30	1808	9278	5.1

Notes:

- G - Shear Modulus; $G_{u/r}$ - Unload/Reload Shear Modulus

- v - Poisson Ratio

- E - Elastic Modulus; $E_{u/r}$ - Unload/Reload Elastic Modulus

Table 2.5-41 — {Pressuremeter Test Results, PM-701}

Test	Depth [ft]	El. [ft]	Layer/Material		G [ksf]	$G_{u/r}$ [ksf]	*v*	E [ksf]	$E_{u/r}$ [ksf]	$E_{u/r}$ / E
CC03	23.5	-14.8	IIc	interbedded silts, sand, some gravel	578	3960	0.45	1676	11484	6.9
CC04	30.7	-22.0	IIc	silty sand, trace clay, shell fragments	494	3960	0.45	1432	11484	8.0
CC05	29.2	-20.5	IIc	silty sand, trace clay, shell fragments	382	2360	0.45	1109	6844	6.2
CC06	40.9	-32.2	IIc	sandy clay, silt	382	1625	0.45	1109	4712	4.2
CC07	39.3	-30.6	IIc	sandy clay, silt	610	2638	0.45	1768	7649	4.3
CC08	51.0	-42.3	IIc	silty sand, shell fragments	346	1935	0.45	1002	5611	5.6
CC09	49.5	-40.8	IIc	silty sand, shell fragments	346	3406	0.45	1002	9877	9.9
CC10	60.5	-51.8	IIc	elastic silt, clay + sand	762	2129	0.45	2211	6175	2.8
CC11	59.0	-50.3	IIc	elastic silt, clay + sand	913	3406	0.45	2647	9877	3.7
CC12	70.5	-61.8	IIc	silty sand, trace clay, shell fragments	329	1832	0.45	953	5313	5.6
CC13	69.0	-60.3	IIc	silty sand, trace clay, shell fragments	364	2360	0.45	1054	6844	6.5
CC14	80.7	-72.0	IIc	sandy silt, some clay	402	1625	0.45	1167	4712	4.0
CC15	79.2	-70.5	IIc	sandy silt, some clay	762	1769	0.45	2211	5129	2.3
CC16	90.6	-81.9	IIc	elastic silt, clay + sand	382	1290	0.45	1109	3742	3.4
CC17	89.1	-80.4	IIc	elastic silt, clay + sand	808	1625	0.45	2344	4712	2.0
CC18	100.5	-91.8	IIc	silty sand, trace clay, shell fragments	282	1935	0.45	818	5611	6.9
CC19	99.0	-90.3	IIc	silty sand, trace clay, shell fragments	913	2638	0.45	2647	7649	2.9
CC20	110.7	-102.0	IIc	sandy elastic silt, clay	644	1935	0.45	1867	5611	3.0
CC21	109.2	-100.5	IIc	sandy elastic silt, clay	469	1625	0.45	1359	4712	3.5
CC22	120.1	-111.4	IIc	silty sand, some clay	610	1499	0.45	1768	4348	2.5
CC23	118.6	-109.9	IIc	silty sand, some clay	382	1769	0.45	1109	5129	4.6
CC24	130.8	-122.1	IIc	silty sand	297	2129	0.45	861	6175	7.2
CC25	129.3	-120.6	IIc	silty sand	329	2129	0.45	953	6175	6.5
CC26	140.8	-132.1	IIc	silty sand to sandy silt, some clay	297	1499	0.45	861	4348	5.0
CC27	139.3	-130.6	IIc	silty sand to sandy silt, some clay	578	1935	0.45	1676	5611	3.3
CC28	150.9	-142.2	IIc	sandy elastic silt	494	2048	0.45	1432	5939	4.1
CC29	149.4	-140.7	IIc	sandy elastic silt	423	2129	0.45	1227	6175	5.0

Notes:
- G - Shear Modulus; $G_{u/r}$ - Unload/Reload Shear Modulus
- v - Poisson Ratio
- E - Elastic Modulus; $E_{u/r}$ - Unload/Reload Elastic Modulus

Table 2.5-42 — {Summary of Laboratory Tests and Quantities}

Test		Standard/Method	Number of Tests (1)		
			PB	IA	BF
Index	Unified Soil Classification System (USCS)	ASTM D2488	591	10	3
	Natural moisture content	ASTM D2216	1048	10	18
	Grain size analysis (sieve)	ASTM D422	546	10	9
	Grain size analysis (hydrometer)	ASTM D6913	546	10	6
	Atterberg limits	ASTM D4318	423	10	3
	Organic content	ASTM D2974	79	10	3
	Specific gravity	ASTM D854	126	10	3
	Unit Weight	Not Specified	126	10	-
Chemical	pH	ASTM D4972	116	-	3
	Chloride	EPA 300.0	116	-	3
	Sulfate	EPA 300.0	116	-	3
	Resistivity	ASTM G187	-	-	14
Static Performance/Strength	Consolidation	ASTM D2435	79	-	3
	Permeability(2)	AST 2434	-	-	3
	Unconfined compression (UC)	ASTM D2166	25	-	-
	Unconsolidated-Undrained Triaxial (UU)	ASTM D2850	110	-	-
	Consolidated-Undrained Triaxial (CU-)	ASTM D4767	10	-	3
	Consolidated-Drained Triaxial (CD)	Unspecified	-	-	3
	Direct Shear (DS)	ASTM D3080	43	-	-
	Modified Proctor (Moisture-Density)	ASTM D1557	-	-	4
	California Bearing Ratio	ASTM D1883	12	-	2
Dynamic Resonant Column Torsional Shear		Not Specified	13	10	8

Notes:
- (1) PB: Powerblock Area (Includes Construction Laydown, Cooling and Transmission Corridor)
  IA: Intake Area
  BF: Backfill
- (2) Description of slug tests and the results are provided in Section 2.4.12.

Table 2.5-43 — {Index Properties, Powerblock Area}

POWERBLOCK AREA		USCS	Stat	γ_{moist} [%]	w [%]	LL [%]	PL [%]	PI [%]	Fines [%]
Stratum I - Terrace Sand		SM, SP-SMC	Min	120.0	4.5	NV	NP	NP	4.6
			Max	124.0	36.2	55.0	20.0	37.0	72.0
			Avg	121.3	15.8	19.7	8.0	11.7	21.8
Stratum IIa - Chesapeake Clay/ Silt		CH MH	Min	103.0	15.1	27.0	11.0	8.0	50.0
			Max	122.3	42.5	79.0	36.0	54.0	99.7
			Avg	115.4	31.2	57.4	20.7	36.6	79.5
Stratum IIb - Chesapeake Cemented Sand	Layer 1	SM SP	Min	117.0	13.5	NV	NP	NP	2.1
			Max	128.4	36.2	72.0	32.0	50.0	72.7
			Avg	122.2	24.1	24.8	12.0	12.8	26.2
	Layer 2	SM SP-SM	Min	120.5	25.0	NV	NP	NP	10.6
			Max	126.0	44.2	72.0	41.0	40.0	87.0
			Avg	122.5	30.5	19.7	10.6	9.1	23.3
	Layer 3	SM	Min	123.0	16.1	NV	NP	NP	9.8
			Max	123.0	38.7	49.0	28.0	28.0	35.9
			Avg	123.0	26.0	17.3	9.5	7.8	23.7
Stratum IIc - Chesapeake Clay/ Silt		MH SM	Min	86.5	27.5	39.0	20.0	9.0	19.6
			Max	117.0	109.8	199.0	119.0	133.0	99.5
			Avg	103.9	51.2	95.4	42.9	52.5	59.9
Stratum III - Nanjemoy Sand		SC SM	Min	123.5	13.4	36.0	14.0	18.0	13.9
			Max	132.0	44.5	79.0	36.0	59.0	44.6
			Avg	127.0	29.1	57.1	22.6	34.5	23.3
Backfill		GP GM	Min	136.8	7.1	NV	NP	NP	7.2
			Max	150.4	5.6	NV	NP	NP	11.4
			Avg	146.2	6.3	NV	NP	NP	9.3

Notes:

- γ_{moist}: Moist Unit Weight
- w: Water Content
- LL: Liquid Limit
- PL: Plastic Limit
- NP: Non Plastic
- NV: Non Viscous
- NA: Not Available

Table 2.5-44 — {Index Properties, Intake Area}

INTAKE AREA		USCS	Stat	γ_{moist} [%]	w [%]	LL [%]	PL [%]	PI [%]	Fines [%]
Stratum I - Terrace Sand		SM, SP-SM	Min	NA	NA	NA	NA	NA	NA
			Max	NA	NA	NA	NA	NA	NA
			Avg	NA	NA	NA	NA	NA	NA
Stratum IIa - Chesapeake Clay/ Silt		CH MH	Min	NA	NA	NA	NA	NA	NA
			Max	NA	NA	NA	NA	NA	NA
			Avg	NA	NA	NA	NA	NA	NA
Stratum IIb - Chesapeake Cemented Sand	Layer 1	SM SP	Min	NA	7.9	NA	NA	NA	16.5
			Max	NA	7.9	NA	NA	NA	16.5
			Avg	NA	7.9	NA	NA	NA	16.5
	Layer 2	SM SP-SM	Min	NA	9.4	NV	NP	NP	6.3
			Max	NA	36.0	27.0	17.0	10.0	44.2
			Avg	NA	24.4	5.4	3.4	2.0	18.9
	Layer 3	SM	Min	118.2	15.4	NV	NP	NP	8.4
			Max	123.4	37.4	42.0	23.0	22.0	37.9
			Avg	120.4	25.5	13.3	9.2	4.1	25.9
Stratum IIc - Chesapeake Clay/ Silt		SM MH	Min	93.6	22.4	NV	NP	NP	11.0
			Max	118.4	94.5	143.0	79.0	110.0	98.3
			Avg	108.2	48.5	72.5	32.6	39.9	49.0
Stratum III - Nanjemoy Sand		SC SM	Min	Not Encountered					
			Max						
			Avg						
Backfill		GP GM	Min	136.8	7.1	NV	NP	NP	7.2
			Max	150.4	5.6	NV	NP	NP	11.4
			Avg	146.2	6.3	NV	NP	NP	9.3

Notes: -γ_{moist}: Moist Unit Weight
- w: Water Content
- LL: Liquid Limit
- PL: Plastic Limit
- NP: Non Plastic
- NV: Non Viscous
- NA: Not Available

Table 2.5-45 — {Summary of Soils Chemical Testing Data}

CCNPP Unit 3		USCS	Stat	pH [CaCl2]	pH [H2O]	Sulfate (1)	Chloride (2)
Stratum I - Terrace Sand		SM, SP-SM	Min	2.6	2.7	0.0	<10
			Max	6.7	7.6	2.6	48.6
			Avg	4.6	5.5	0.2	<12
Stratum IIa - Chesapeake Clay/Silt		CH MH	Min	2.6	2.5	0.0	<10
			Max	4.9	5.8	2.6	10.7
			Avg	3.1	3.6	0.7	<10
Stratum IIb - Chesapeake Cemented Sand	Layer 1	SM SP	Min	2.4	2.5	0.0	<10
			Max	7.4	8.0	3.1	145.0
			Avg	5.7	5.8	0.6	<22
	Layer 2	SM SP-SM	Min	2.4	2.5	0.0	<10
			Max	7.4	8.0	3.1	145.0
			Avg	5.7	5.8	0.6	<22
	Layer 3	SM	Min	2.4	2.5	0.0	<10
			Max	7.4	8.0	3.1	145.0
			Avg	5.7	5.8	0.6	<22
Stratum IIc - Chesapeake Clay/Silt		SM MH	Min	6.6	7.0	0.2	<10
			Max	6.6	7.0	0.2	<10
			Avg	6.6	7.0	0.2	<10
Stratum III - Nanjemoy Sand		SC SM	Min	NA	NA	NA	NA
			Max	NA	NA	NA	NA
			Avg	NA	NA	NA	NA
Backfill		GP GM	Min	8.3	-	204.0	<2.1
			Max	8.5	-	446.0	2.2
			Avg	8.4	-	325.0	2.1

Notes:
(1) Expressed as [%] for in-situ soils and as [mg/Kg] for backfill
(2) Expressed as [ppm] for in-situ soils and as [mg/Kg] for backfill
- NA: Not Available

Table 2.5-46 — {Consolidation Test Results, Powerblock Area}

POWERBLOCK AREA		USCS	Stat	C_r	C_c	e_o	p'_c [ksf]	OCR
Stratum I - Terrace Sand		SM, SP-SM	Min	0.009	0.37	0.85	11.40	4.26
			Max	0.009	0.37	0.85	11.40	4.26
			Avg	0.009	0.37	0.85	11.40	4.26
Stratum IIa - Chesapeake Clay/ Silt		CH MH	Min	0.013	0.46	0.82	11.20	4.91
			Max	0.043	0.68	1.15	35.00	15.40
			Avg	0.026	0.54	1.03	21.66	8.10
Stratum IIb - Chesapeake Cemented Sand	Layer 1	SM SP	Min	0.006	0.04	0.63	20.20	2.82
			Max	0.012	0.32	0.92	30.00	22.61
			Avg	0.010	0.19	0.80	24.40	9.99
	Layer 2	SM SP-SM	Min	0.003	0.11	0.71	4.20	1.00
			Max	0.003	0.11	0.90	23.80	4.68
			Avg	0.003	0.11	0.80	14.00	2.84
	Layer 3	SM	Min	NA	NA	NA	NA	NA
			Max	NA	NA	NA	NA	NA
			Avg	NA	NA	NA	NA	NA
Stratum IIc - Chesapeake Clay/ Silt[(1)]		SM MH	Min	0.007	0.35	1.01	21.40	2.14
			Max	0.169	1.73	2.41	42.30	5.66
			Avg	0.060	0.95	1.61	33.30	3.21
Stratum III - Nanjemoy Sand		SC SM	Min	0.021	0.26	0.73	29.20	1.76
			Max	0.092	0.91	1.42	32.80	1.90
			Avg	0.045	0.53	1.00	30.40	1.85
Backfill		GP GM	Min	Large preconsolidation pressure of 54 ksf reported in one instance. It was not possible to define the virgin compression slope and the preconsolidation pressure.				
			Max					
			Avg					

Notes: -
C_r: Recompression index
- C_c: Compression index
- e_o: Initial void ratio
- p'_c: Preconsolidation pressure
- (1) Properties given for clay portions of layer

Table 2.5-47 — {Consolidation Test Results, Intake Area}

INTAKE AREA		USCS	Stat	C_r	C_c	e_o	p'_c [ksf]	OCR
Stratum I - Terrace Sand		SM, SP-SM	Min	NA				
			Max					
			Avg					
Stratum IIa - Chesapeake Clay/ Silt		CH MH	Min					
			Max					
			Avg					
Stratum IIb - Chesapeake Cemented Sand	Layer 1	SM SP	Min					
			Max					
			Avg					
	Layer 2	SM SP-SM	Min					
			Max					
			Avg					
	Layer 3	SM	Min	0.006	0.135	0.635	32.5	17.7
			Max	0.006	0.135	0.635	32.5	17.7
			Avg	0.006	0.135	0.635	32.5	17.7
Stratum IIc - Chesapeake Clay/Silt		SM MH	Min	0.020	0.371	0.97	25.7	3.7
			Max	0.155	1.641	1.95	40.8	9.2
			Avg	0.085	1.036	1.47	32.4	7.1
Stratum III - Nanjemoy Sand		SC SM	Min	Not Encountered				
			Max					
			Avg					
Backfill		GP GM	Min	Large preconsolidation pressure of 54 ksf reported in one instance. It was not possible to define the virgin compression slope and the preconsolidation pressure.				
			Max					
			Avg					

Notes:
- C_r: Recompression index
- C_c: Compression index
- e_o: Initial void ratio
- p'_c: Preconsolidation pressure
- NA: Not Available

Table 2.5-48 — {Shear Strength Laboratory Testing Data, Powerblock Area}

POWERBLOCK AREA		USCS	Stat	Triaxial Test				Direct Shear		s_u [ksf]	
				c' [ksf]	f' [°]	c [ksf]	f' [°]	c [ksf]	f' [°]	UC	UU
Stratum I - Terrace Sand		SM, SP-SM S	Min	0.55	27.9	1.16	13.3	0.42	24.9	1.72	1.20
			Max	0.55	27.9	1.16	13.3	0.89	26.0	1.72	1.46
			Avg	0.55	27.9	1.16	13.3	0.66	25.5	1.72	1.33
Stratum IIa - Chesapeake Clay/ Silt		CH MH	Min	0.44	31.0	0.72	12.5	0.64	19.0	1.14	1.42
			Max	0.98	32.1	2.06	17.0	1.38	30.1	4.06	4.60
			Avg	0.71	31.6	1.39	14.8	1.01	22.9	2.50	2.38
Stratum IIb - Chesapeake Cemented Sand	Layer 1	SM SP	Min	0.30	33.5	0.59	19.5	NA	NA	NA	0.80
			Max	0.30	33.5	0.59	19.5	NA	NA	NA	2.44
			Avg	0.30	33.5	0.59	19.5	NA	NA	NA	5.76
	Layer 2	SM SP-SM M	Min	0.04	30.0	1.94	13.4	NA	NA	NA	0.90
			Max	1.00	34.6	3.36	20.0	NA	NA	NA	0.90
			Avg	0.52	32.3	2.65	16.7	NA	NA	NA	0.90
	Layer 3	SM	Min	NA	NA	NA	NA	NA	NA	NA	NA
			Max	NA	NA	NA	NA	NA	NA	NA	NA
			Avg	NA	NA	NA	NA	NA	NA	NA	NA
Stratum IIc - Chesapeake Clay/Silt		SM MH	Min	NA	NA	NA	NA	0.00	29.0	3.74	1.80
			Max	NA	NA	NA	NA	1.58	35.0	5.24	9.58
			Avg	NA	NA	NA	NA	0.79	32.0	4.49	6.37
Stratum III - Nanjemoy Sand		SC SM	Min	NA	NA	NA	NA	NA	NA	NA	4.56
			Max	NA	NA	NA	NA	NA	NA	NA	7.66
			Avg	NA	NA	NA	NA	NA	NA	NA	5.78
Backfill		GP GM	Min	0.00	42.5	-	-	NA	NA	-	-
			Max	0.00	43.5	-	-	NA	NA	-	-
			Avg	0.00	43.0	-	-	NA	NA	-	-

Notes:
- NA: Not Available
- UC: Unconfined compression
- UU: Unconsolidated undrained triaxial test

Table 2.5-49 — {Shear Strength Laboratory Testing Data, Intake Area}

INTAKE AREA		USCS	Stat	Triaxial Test c' [ksf]	Triaxial Test f' [°]	Triaxial Test c [ksf]	Triaxial Test f' [°]	Direct Shear c [ksf]	Direct Shear f' [°]	s_u [ksf] UC	s_u [ksf] UU
Stratum I - Terrace Sand		SM, SP-SM	Min	NA							
			Max								
			Avg								
Stratum IIa - Chesapeake Clay/ Silt		CH MH	Min								
			Max								
			Avg								
Stratum IIb - Chesapeake Cemented Sand	Layer 1	SM SP	Min								
			Max								
			Avg								
	Layer 2	SM SP-SM	Min								
			Max								
			Avg								
	Layer 3	SM	Min	0.00	38.0	NA	NA	0.46	28.2	NA	NA
			Max	0.00	38.0	NA	NA	0.46	28.2	NA	NA
			Avg	0.00	38.0	NA	NA	0.46	28.2	NA	NA
Stratum IIc - Chesapeake Clay/Silt		SM MH	Min	0.00	19.4	2.69	0.0	0.00	24.4	NA	1.92
			Max	3.63	37.3	7.68	18.7	2.10	38.7	NA	8.32
			Avg	1.52	31.9	4.35	11.9	0.73	30.8	NA	4.83
Stratum III - Nanjemoy Sand		SC SM	Min	Not Encountered							
			Max								
			Avg								
Backfill		GP GM	Min	0.00	42.5	-	-	NA	NA	-	-
			Max	0.00	43.5	-	-	NA	NA	-	-
			Avg	0.00	43.0	-	-	NA	NA	-	-

Notes:
- NA: Not Available
- UC: Unconfined compression
- UU: Unconsolidated undrained triaxial test
γ dry

Table 2.5-50 — {Modified Proctor Tests on Backfill Samples}

Sample	Modified Proctor						98% MP		90% MP	
	Uncorrected			Corrected						
	w [%]	γ dry [pcf]	γ moist [pcf]	w [%]	γ dry [pcf]	γ moist [pcf]	γ dry [pcf]	γ moist [pcf]	γ dry [pcf]	γ moist [pcf]
CR6 Composite FUGRO	6.9	145.2	155.2	6.0	148.0	156.9	145.0	153.7	133.2	141.2
CR6 Composite MACTEC	6.4	144.0	153.2	6.0	145.3	154.0	142.4	150.9	130.8	138.6
GAB Composite MACTEC	6.4	145.9	155.2	5.7	148.6	157.1	145.6	153.9	133.7	141.4
GAB Composite FUGRO	7.1	145.3	155.6	6.5	148.5	158.2	145.5	155.0	133.7	142.3
Min	6.4	144.0	153.2	5.7	145.3	154.0	142.4	150.9	130.8	138.6
Max	7.1	145.9	155.6	6.5	148.6	158.2	145.6	155.0	133.7	142.3
Avg	6.7	145.1	154.8	6.1	147.6	156.5	144.6	153.4	132.8	140.9

Notes:
- USCS: GP-GM

Table 2.5-51 — {RCTS Testing Samples}

Sample		Depth [ft]	USCS	Type	γ dry [pcf]	w [%]
POWERBLOCK AREA	B-437-6	13.5	SP-SM	UD	124.1	7.2
	B-301-10	33.5	CH	UD	117.5	31.1
	B-305-17	39.5	SC	UD	117.2	34.7
	B-404-14	52.0	SP-SM	UD	117.6	27.7
	B-401-31	138.5	CH	UD	104.1	44.1
	B-401-67	348.5	SM	UD	116.4	35.6
	B-401-48	228.5	MH	UD	98.2	58.6
	B-301-78	383.5	SM	Jar	116.4	34.4
	B-306-17	68.0	CH	UD	115.8	30.7
	B-409-15	35.0	SP-SM	UD	124.8	23.3
	B-404-22	83.5	SM	UD	115.4	32.2
	B-401-42	198.5	SM	UD	101.2	48.8
	B-409-39	95.0	SM	UD	109.3	33.1
INTAKE AREA	B-773-2	15.9	SM	UD	125.7	23.3
	B-773-3	27.0	SC	UD	111.6	35.0
	B-773-4	37.0	CH	UD	103.0	53.6
	B-773-5	47.0	SC	UD	110.9	34.1
	B-773-6	57.0	CH	UD	106.4	44.5
	B-773-7	66.1	CH	UD	110.1	33.5
	B-773-9	87.0	CH	UD	99.1	59.2
	B-773-11	107.0	CH	UD	102.5	55.1
	B-773-13	127.0	SC	UD	108.3	45.2
	B-773-15	147.0	CH	UD	101.5	52.3
BACKFILL	CR6 Composite(1)	-	GP-GM	Bulk	145.4	6.4
	GAB Composite(1)	-	GP-GM	Bulk	147.3	5.8
	CR6 Vulcan Average(1)	-	GP-GM	Bulk	143.1	5.5

Notes:
(1) Test results reported for target unit weight of 95% Modified Proctor

Table 2.5-52 — {Low Strain Results for Backfill Samples}

Source	γ dry [pcf]	Moisture Content [%]	Confining Pressure [ksf]	G_{max} [ksf]	V_s [fps]	D [%]
CR-6 Composite	145.4	6.4	1.08	2680	770	4.61
			2.16	3851	922	4.1
			4.32	5846	1133	3.41
CR-6 Vulcan Avg	143.1	5.5	1.08	3741	917	2.31
			2.16	5196	1080	1.96
			4.32	7054	1257	1.88
GAB Composite	147.3	5.8	1.08	3904	923	3.91
			2.16	5444	1089	3.33
			4.32	7427	1270	2.99

Table 2.5-53 — {USCS Classification and Index Properties}

STRATUM			USCS	γ moist [pcf]	w [%]	LL [%]	PL [%]	PI [%]	Fines [%]
POWERBLOCK AREA	I - Terrace Sand		SM, SP-SM	120.0	16.0	20.0	8.0	12.0	21.8
	IIa - Chesapeake Clay/Silt		CH MH	115.0	31.0	57.0	21.0	36.0	79.5
	IIb - Chesapeake Cemented Sand	L1	SM SP	120.0	24.0	26.0	13.0	13.0	26.2
		L2	SM SP-SM	120.0	31.0	20.0	11.0	9.0	23.3
		L3	SM	120.0	26.0	17.0	9.0	8.0	23.7
	IIc - Chesapeake Clay/Silt		MH SM	105.0	51.0	95.0	42.0	53.0	59.9
	III - Nanjemoy Sand		SC SM	125.0	29.0	57.0	22.0	35.0	23.3
INTAKE AREA	I - Terrace Sand		SM, SP-SM	NA	NA	NA	NA	NA	NA
	IIa - Chesapeake Clay/Silt		CH MH	NA	NA	NA	NA	NA	NA
	IIb - Chesapeake Cemented Sand	L1	SM SP	NA	8.0	NA	NA	NA	16.5
		L2	SM SP-SM	NA	24.0	5.0	3.0	2.0	18.9
		L3	SM	120.0	26.0	13.0	9.0	4.0	25.9
	IIc - Chesapeake Clay/Silt		SM MH	110.0	49.0	73.0	33.0	40.0	49.0
	III - Nanjemoy Sand		SC SM	125.0	29.0	57.0	22.0	35.0	23.3
BACKFILL			GP GM	145.0	6.0	NV	NP	NP	9.0

Notes:
- NP: Non Plastic
- NV: Non Viscous
- NA: Not Available

Table 2.5-54 — {Guidelines for Soil Chemistry Evaluation}

Soil Corrosiveness					
Property	**Range for Steel Corrosiveness**				
	Little Corrosive	**Mildly Corrosive**	**Moderately Corrosive**	**Corrosive**	**Very Corrosive**
Resistivity [ohm-m]	>100(A), (B)	20-100(A) 50-100(B) >30(C)	10-20(A) 20-50(B)	5-10(A) 7-20(B)	<5(A) <7(B)
pH		>5.0 and <10(B)		5.0-6.5(A)	<5.0(A)
Chlorides (ppm)		<200(B)		300-1,000(A)	>1,000(A)
Soil Aggressiveness Recommendations for Normal Weight Concrete Subject to Sulfate Attack					
Concrete Exposure	Water Soluble Sulfate (SO_4) in Soil, Percent		Cement Type		Max W/C Ratio
Mild	0.00-0.10		---		---
Moderate	0.10-0.20		II, IP(MS), IS(MS)		0.5
Severe	0.20-2.0		V(1)		0.45
Very Severe	Over 2.0		V with pozzolan		0.45

Notes:
- (A) API, 2007
- (B) FHWA, 1990
- (C) ACI, 1994
- (1) Or a blend of Type II cement and a ground granulated blast furnace slag or a pozzolan that gives equivalent sulfate resistance

Table 2.5-55 — {Performance Properties under Static Loading}

STRATUM			C_r	C_c	e_o	p'_c [ksf]	OCR	c_v [ft^2/year]	kh [ft/s]	kv [ft/s]
POWERBLOCK AREA	I - Terrace Sand		0.009	0.37	0.85	11.40	4.26	NA	NA	NA
	IIa - Chesapeake Clay/Silt		0.026	0.54	1.03	21.66	8.10	316.0	1.62E-09	1.62E-09
	IIb - Chesapeake Cemented Sand	L1	0.010	0.19	0.80	24.40	9.99	2018.0	9.84E-06	9.84E-07
		L2	0.003	0.11	0.80	14.00	2.84	2018.0	9.84E-06	9.84E-07
		L3	0.010	0.19	0.80	24.40	9.99	2018.0	9.84E-06	9.84E-07
	IIc - Chesapeake Clay/Silt		0.06	0.95	1.61	33.30	3.21	1913.0	1.62E-09	1.62E-09
	III - Nanjemoy Sand		0.05	0.53	1.00	30.40	1.85	2018.0	9.84E-07	9.84E-08
INTAKE AREA	I - Terrace Sand		NP	NP	NP	NP	NP	NP	NP	NP
	IIa - Chesapeake Clay/Silt		NP	NP	NP	NP	NP	NP	NP	NP
	IIb - Chesapeake Cemented Sand	L1	NP	NP	NP	NP	NP	NP	NP	NP
		L2	NA	NA	NA	NA	NA	NA	NA	NA
		L3	0.01	0.14	0.64	32.50	17.69	2018.0	9.84E-06	9.84E-07
	IIc - Chesapeake Clay/Silt		0.09	1.04	1.47	32.44	7.11	1913.0	1.62E-09	1.62E-09
	III - Nanjemoy Sand		0.05	0.53	1.00	30.40	1.85	2018.0	9.84E-07	9.84E-08
BACKFILL			Consolidation in backfill material will not be significant						9.50E-03	9.50E-04

Notes:
- NP: Not Present
- NA: Not Available
- c_v Values correspond to an applied pressure of 8 ksf for IIA, 32 ksf for IIb, and 64 ksf for IIc
- k_h is horizontal hydraulic conductivity; k_v is vertical hydraulic conductivity
- Intake area values for deeper strata are obtained from Powerblock recommendation

Table 2.5-56 — {Strength Properties of Soils}

STRATUM			c' [ksf]	f' [°]	c [ksf]	f [°]	S_u [ksf]
POWERBLOCK AREA	I - Terrace Sand		0.0	27.9	1.2	13.3	1.5
	IIa - Chesapeake Clay/Silt		0.7	31.6	1.4	14.8	2.4
	IIb - Chesapeake Cemented Sand	L1	0.0	33.5	1.2	19.5	5.8
		L2	0.0	32.3	2.7	16.7	0.9
		L3	0.0	31.7	1.2	19.5	5.8
	IIc - Chesapeake Clay/Silt		0.8	32.0	1.4	14.8	5.4
	III - Nanjemoy Sand(1)		0.0	40.0	1.2	19.5	5.8
INTAKE AREA	I - Terrace Sand		NP	NP	NP	NP	NP
	IIa - Chesapeake Clay/Silt		NP	NP	NP	NP	NP
	IIb - Chesapeake Cemented Sand	L1	NP	NP	NP	NP	NP
		L2	NP	NP	NP	NP	NP
		L3	0.0	33.1	NA	NA	5.8
	IIc - Chesapeake Clay/Silt		1.5	31.1	4.3	11.9	4.8
	III - Nanjemoy Sand(1)		0.0	40.0	1.2	19.5	2.9
BACKFILL			0.0	40.0	-	-	-

Notes:
(1) Friction of 40 degrees assumed, recommendation at Intake taken from Powerblock
NA: Not Available
NP: Not Present

Table 2.5-57 — {Estimation of Elastic Modulus}

STRATUM			E [ksf] from various methods						
			Vs (1)	PM	SPT		s_u		Avg
					(2)	(3)	(4)	(5)	
POWERBLOCK AREA	I - Terrace Sand		729	241	504	268	-	-	436
	IIa - Chesapeake Clay/Silt		1210	652	-	-	1098	1415	1094
	IIb - Chesapeake Cemented Sand	L1	4090	1575	3204	1226	-	-	2525
		L2	1300	1573	864	375	-	-	1028
		L3	5120	2200	2268	914	-	-	2625
	IIc - Chesapeake Clay/Silt		1560	1555	-	-	2772	3573	2365
	III - Nanjemoy Sand		4300	2500	2700	-	-	-	3166
INTAKE AREA	I - Terrace Sand		NP	NP	NP	NP	NP	NP	NP
	IIa - Chesapeake Clay/Silt		NP	NP	NP	NP	NP	NP	NP
	IIb - Chesapeake Cemented Sand	L1	NP	NP	NP	NP	NP	NP	NP
		L2	941	-	612	308	-	-	620
		L3	1840	-	1944	752	-	-	1512
	IIc - Chesapeake Clay/Silt		1290	-	-	-	2169	1928	1796
	III - Nanjemoy Sand(6)		4300	2500	2700	-	-	-	3166
BACKFILL			1920		-	-	-	-	1920

Notes:
- (1) Calculated from $G_{dyn}/G_{static} = 10$;
- (2) $E = 18N_{60}$ (Davie, 1988); [tsf]
- (3) $E = ß_0 \text{ sqrt(OCR)} + ß_1 N_{60}$; [psf]
- (4) $E = 450\ s_u$ (Davie, 1988); [tsf]
- (5) $E = 2G(1+\boldsymbol{v})$; $G = 200\ s_u$ (Senapathy, 2001); [tsf]
- (6) Values adopted from Powerblock Area
- NP: Not Present

Table 2.5-58 — {Basis for Recommendation of $E_{u/r}/E$ Ratio}

STRATUM			$E_{u/r}/E$			
			Min	Max	Avg	Rec
POWERBLOCK AREA	I - Terrace Sand		1.6	9.8	6.9	3.0
	IIa - Chesapeake Clay/Silt		2.5	2.8	2.7	3.0
	IIb - Chesapeake Cemented Sand	L1	2.2	10.4	5.6	3.0
		L2	4.5	13.4	8.8	4.5
		L3	3.9	6.9	5.4	3.9
	IIc - Chesapeake Clay/Silt		2.4	7.6	4.0	3.0
	III - Nanjemoy Sand(1)		3.1	5.2	4.1	3.1
INTAKE AREA	I - Terrace Sand		NP	NP	NP	NP
	IIa - Chesapeake Clay/Silt		NP	NP	NP	NP
	IIb - Chesapeake Cemented Sand	L1	NP	NP	NP	NP
		L2	NA	NA	NA	4.5
		L3	-	-	-	3.0
	IIc - Chesapeake Clay/Silt		2.0	9.9	4.8	3.0
	III - Nanjemoy Sand		-	-	-	3.0
BACKFILL			-	-	-	-

Notes:
- Values from pressuremeter tests at B-301 (Powerblock Area) and B-701 (Intake Area)
- NP: Not Present
- NA: Not Available

Table 2.5-59 — {Elastic Properties Under Static Conditions}

STRATUM			E [ksf]	$v^{(1)}$	G [ksf]	$E_{u/r}/E$
POWERBLOCK AREA	I - Terrace Sand		436	0.30	168	3.0
	IIa - Chesapeake Clay/Silt		1094	0.45	377	3.0
	IIb - Chesapeake Cemented Sand	L1	2525	0.30	971	3.0
		L2	1028	0.30	395	4.5
		L3	2625	0.30	1010	3.9
	IIc - Chesapeake Clay/Silt		2365	0.45	815	3.0
	III - Nanjemoy Sand		3166	0.30	1218	3.1
INTAKE AREA	I - Terrace Sand		NP	NP	NP	NP
	IIa - Chesapeake Clay/Silt		NP	NP	NP	NP
	IIb - Chesapeake Cemented Sand	L1	NP	NP	NP	NP
		L2	620	0.30	239	4.5
		L3	1512	0.30	581	3.0
	IIc - Chesapeake Clay/Silt		1796	0.45	619	3.0
	III - Nanjemoy Sand[(2)]		3166	0.30	1218	3.0
BACKFILL			1920	0.35	711	not used

Notes:
- (1) Adopted from typical values reported in the literature (Salgado, 2008).
- (2) Adopted from Powerblock Area
- NP: Not Present

Table 2.5-60 — {Earth Pressure Coefficients}

STRATUM			K_a	K_P	K_0
POWERBLOCK AREA	I - Terrace Sand		0.36	2.76	0.53
	IIa - Chesapeake Clay/Silt		0.31	3.20	0.48
	IIb - Chesapeake Cemented Sand	L1	0.29	3.46	0.45
		L2	0.30	3.30	0.47
		L3	0.31	3.21	0.47
	IIc - Chesapeake Clay/Silt		0.31	3.25	0.47
	III - Nanjemoy Sand		Not Required		
INTAKE AREA	I - Terrace Sand		NP	NP	NP
	IIa - Chesapeake Clay/Silt		NP	NP	NP
	IIb - Chesapeake Cemented Sand	L1	NP	NP	NP
		L2	NA	NA	NA
		L3	0.29	3.41	0.45
	IIc - Chesapeake Clay/Silt		0.32	3.14	0.48
	III - Nanjemoy Sand		Not Required		
BACKFILL			0.22	4.60	0.36

Notes:
NP: Not Present
NA: Not Available
- values of f are used to determine K coefficients
$Ka = \tan^2(45-f'/2)$; $K_p = \tan^2(45+f'/2)$; $K_0 = 1 - \sin(f')$

Table 2.5-61 — {Dynamic Properties for Powerblock Area}

POWERBLOCK AREA	El [ft msl]	D [ft]	γ [pcf]	G_o [ksf]	V_s [fps]	V_p [fps]	ν	Damping [%]	
								$S^{(1)}$	$P^{(2)}$
Backfill 1	85.0	0.0	145.0	2810	790	1645	0.35	1.50	0.50
Backfill 2	79.0	6.0	145.0	3650	900	1915	0.36	1.50	0.50
Backfill 3	63.0	22.0	145.0	5250	1080	2260	0.35	1.50	0.50
I, Terrace Sand	85.0	0.0	120.0	2330	790	2903	0.46	1.40	0.47
IIA, Chesapeake Clay/Silt	60.0	25.0	115.0	4320	1100	4623	0.47	1.30	0.43
IIB-1, Che. Cem. Sand	45.0	40.0	120.0	7840	1450	4800	0.45	1.30	0.43
IIB-2, Che. Cem. Sand	30.0	55.0	120.0	12070	1800	5970	0.45	1.30	0.43
IIB-3, Che. Cem. Sand	15.0	70.0	120.0	4760	1130	5762	0.48	1.30	0.43
IIB-4, Che. Cem. Sand	0.0	85.0	120.0	11280	1740	5771	0.45	1.30	0.43
IIc, Chesapeake Clay/Silt	-15.0	100.0	105.0	5100	1250	5254	0.47	1.10	0.37
III, Nanjemoy Sand (NS1)	-200.0	285.0	125.0	12440	1790	5937	0.45	1.30	0.43
III, Nanjemoy Sand (NS2)	-220.0	305.0	125.0	21070	2330	6274	0.42	1.30	0.43
III, Nanjemoy Sand (NS3)	-230.0	315.0	125.0	16000	2030	5793	0.43	1.30	0.43
III, Nanjemoy Sand (NS4)	-270.0	355.0	125.0	14460	1930	5896	0.44	1.30	0.43
I1, Deep Soil	-317.0	402.0	115.0	17290	2200	5389	0.40	1.30	0.43
I2, Deep Soil	-1000.0	1085.0	115.0	19390	2330	5707	0.40	1.30	0.43
I3, Deep Soil	-1500.0	1585.0	115.0	23220	2550	6246	0.40	1.30	0.43
I4, Deep Soil	-2000.0	2085.0	115.0	28000	2800	6859	0.40	1.30	0.43
I5, Bedrock	-2446.0	2531.0	162.0	125780	5000	9354	0.30	1.30	0.43
I6, Bedrock	-2456.0	2541.0	162.0	246520	7000	13096	0.30	1.30	0.43
I7, Bedrock	-2466.0	2551.0	162.0	425830	9200	17212	0.30	1.30	0.43
Base	-3000.0	3085.0	162.0	425830	9200	17212	0.30	1.30	0.43

Notes:
- (1) Shear damping based on RCTS test results
- (2) P damping assumed as 1/3 of S damping

Table 2.5-62 — {Dynamic Properties for Intake Area}

INTAKE AREA	El [ft msl]	D [ft]	γ [pcf]	G_o [ksf]	V_s [fps]	V_p [fps]	ν	Damping [%]	
								$S^{(1)}$	$P^{(2)}$
Backfill 1	10.0	0.0	145.0	2810	790	1645	0.35	1.50	0.50
Backfill 2	4.0	6.0	145.0	3650	900	1915	0.36	1.50	0.50
Backfill 3	-12.0	22.0	145.0	5250	1080	2260	0.35	1.50	0.50
IIB-3, C. Cemented Sand	-0.3	8.2	120.0	2270	780	1610	0.35	1.30	0.43
IIB-4, C. Cemented Sand	-2.3	10.2	120.0	6890	1360	5580	0.47	1.30	0.43
IIC-1, C. Clay/Silt	-18.7	26.6	115.0	4720	1150	5250	0.47	1.30	0.43
IIC-2, C. Clay/Silt	-43.0	50.9	105.0	4310	1150	5250	0.47	1.30	0.43
IIC-3, C. Clay/Silt	-105.0	112.9	115.0	4720	1150	5250	0.47	1.30	0.43
IIC-4, C. Clay/Silt	-131.0	138.9	105.0	4310	1150	5250	0.47	1.30	0.43
III, Nanjemoy Sand (NS1)	-200.0	207.9	125.0	12440	1790	5937	0.45	1.10	0.37
III, Nanjemoy Sand (NS2)	-220.0	227.9	125.0	21070	2330	6274	0.42	1.30	0.43
III, Nanjemoy Sand (NS3)	-230.0	237.9	125.0	16000	2030	5793	0.43	1.30	0.43
III, Nanjemoy Sand (NS4)	-270.0	277.9	125.0	14460	1930	5896	0.44	1.30	0.43
I1, Deep Soil	-317.0	324.9	115.0	17290	2200	5389	0.40	1.30	0.43
I2, Deep Soil	-1000.0	1007.9	115.0	19390	2330	5707	0.40	1.30	0.43
I3, Deep Soil	-1500.0	1507.9	115.0	23220	2550	6246	0.40	1.30	0.43
I4, Deep Soil	-2000.0	2007.9	115.0	28000	2800	6859	0.40	1.30	0.43
I5, Bedrock	-2446.0	2453.9	162.0	125780	5000	9354	0.30	1.30	0.43
I6, Bedrock	-2456.0	2463.9	162.0	246520	7000	13096	0.30	1.30	0.43
I7, Bedrock	-2466.0	2473.9	162.0	425830	9200	17212	0.30	1.30	0.43
Base	-3000.0	3007.9	162.0	425830	9200	17212	0.30	1.30	0.43

Notes:
- (1) Shear damping based on RCTS test results
- (2) P damping assumed as 1/3 of S damping

Table 2.5-63 — {Strain Dependant Properties for Powerblock Area}

Strata	Strain	G/G_{max}	Damping [%]
I-Terrace Sand	0.0001	1.0000	1.40
	0.0003	1.0000	1.50
	0.0010	0.9800	1.80
	0.0030	0.9150	2.30
	0.0100	0.7600	3.80
	0.0300	0.5600	6.50
	0.1000	0.3400	10.50
	0.3000	0.2000	14.80
	1.0000	0.1000	-
IIC-Chesapeake Clay/Silt	0.0001	1.0000	1.10
	0.0003	1.0000	1.10
	0.0010	1.0000	1.10
	0.0030	1.0000	1.13
	0.0100	0.9900	1.20
	0.0300	0.9400	1.50
	0.1000	0.8000	2.40
	0.3000	0.6300	4.10
	0.6000	0.5000	5.80
	1.0000	0.4000	7.40
All Other Natural Soils	0.0001	1.0000	1.30
	0.0003	1.0000	1.30
	0.0010	1.0000	1.40
	0.0030	0.9900	1.60
	0.0100	0.9400	2.20
	0.0300	0.8200	3.20
	0.1000	0.6200	5.40
	0.3000	0.4200	8.40
	0.6000	0.3100	10.60
	1.0000	0.2500	12.60

Table 2.5-64 — {Strain Dependant Properties for Intake Area}

Strata	Strain	G/G_{max}	Damping [%]		Strata	Strain	G/G_{max}	Damping [%]
IIB, IIC-1 & III	0.0001	1.0000	1.30		IIC-3	0.0001	1.0000	1.10
	0.0003	1.0000	1.30			0.0003	1.0000	1.10
	0.0010	1.0000	1.40			0.0010	1.0000	1.10
	0.0030	0.9900	1.60			0.0030	0.9700	1.13
	0.0100	0.9400	2.20			0.0100	0.8600	1.20
	0.0300	0.8200	3.20			0.0300	0.7400	1.50
	0.0548	0.7200	4.30			0.0548	0.6500	1.95
	0.1000	0.6200	5.40			0.1000	0.5600	2.40
	0.1732	0.5200	6.90			0.1732	0.4700	3.25
	0.3000	0.4200	8.40			0.3000	0.3900	4.10
	0.4243	0.3650	9.50			0.4243	0.3400	4.95
	0.6000	0.3100	10.60			0.6000	0.3000	5.80
	1.0000	0.2500	12.60			1.0000	0.2400	7.40
IIC-2	0.0001	1.0000	1.10		IIC-4	0.0001	1.0000	0.80
	0.0003	1.0000	1.10			0.0003	1.0000	0.80
	0.0010	1.0000	1.10			0.0010	1.0000	0.80
	0.0030	0.9900	1.13			0.0030	0.9900	0.90
	0.0100	0.9400	1.70			0.0100	0.9400	1.12
	0.0300	0.8200	3.20			0.0300	0.8200	1.50
	0.0548	0.7200	4.30			0.0548	0.7200	1.95
	0.1000	0.6200	5.40			0.1000	0.6200	2.40
	0.1732	0.5200	6.90			0.1732	0.5200	3.25
	0.3000	0.4200	8.40			0.3000	0.4200	4.10
	0.4243	0.3650	9.50			0.4243	0.3650	4.95
	0.6000	0.3100	10.60			0.6000	0.3100	5.80
	1.0000	0.2500	12.60			1.0000	0.2500	7.40

Table 2.5-65 — {Strain Dependant Properties for Backfill}

Strata	Strain	G/G_{max}	Damping [%]
BACKFILL	0.0001	1.0000	1.49
	0.0003	0.9700	1.57
	0.0010	0.8900	1.84
	0.0032	0.7400	2.71
	0.0100	0.5300	5.02
	0.0316	0.3000	9.38
	0.1000	0.1300	15.00
	0.3160	0.0600	-
	1.0000	0.0382	-

Table 2.5-66 — {Building Elevation, Depth, Area, and Load}

Building		El. [ft]	Depth [ft]	Area [ft^2]	Load [kips]	Pressure [ksf]	Eq. Shape [ft] (1)
Nuclear Island	Reactor Building (RB)	41.5	41.5	26268	313477	11.9	270 x 300
	Fuel Building (FB)	41.5	41.5	14545	216806	14.9	
	Safeguard Building 1 (SB1)	41.5	41.5	9198	108064	11.7	
	Safeguard 2&3 Buildings (SB23)	41.5	41.5	20952	200814	9.6	
	Safeguard Building 4 (SB4)	41.5	41.5	9247	104079	11.3	
Other Buildings	Nuclear Auxiliary Building (NAB)	48.0	35.0	12559	122000	9.7	105 x 120
	Access Building (AB)	48.0	35.0	7620	49300	6.5	95 x 80
	Rad. Waste Building (RWPB)	47.0	36.0	16970	109700	6.5	130 x 130
	E. Power Gen. Buildings (EPGB)	76.0	7.0	12611	40200	3.2	84 x 150
	E. Service Water Building (ESWB)	61.0	22.0	16284	88700	5.4	105 x 155
	Turbine Building (TB)	60.5	22.5	101305	446600	4.4	270 x 380
Intake Area	UHS Makeup Water Intake Structure (UHS MWIS)	-27.5	37.5	5162	34146	7.1	58 x 89
	Notes: *- (1) Equivalent Rectangular shape* *Depth is based on average site grade elevation of 83 ft*						

Table 2.5-67 — {Bearing Capacity}

Building	Building Load [ksf]	Ultimate Bearing Capacity q_{ult} [ksf]			Allowable Bearing Capacity qa [ksf] (1)	
		VESIC		MEYERHOF	STATIC	DYNAMIC
		Case a	Case b	Case c (2)		
NI Common Mat	11.8	192.7	228.9	70.5	23.5	35.2
NAB	9.7	170.7	179.1	105.8	35.3	52.9
EPGB	3.2	113.6	102.2	115.0	34.1	51.1
ESWB	5.4	145.7	153.8	118.0	39.3	59.0
UHS MWIS (3)	7.1	NA	35.2	NA	11.7	17.6

Notes:
- (1) With FS = 3.0 for static conditions and FS = 2.0 for dynamic condition (minimum q_{ult} used)
- (2) Case c, Dense sand over soft clay
- (3) Case b with Stratum II-C used for UHS, other scenarios are not applicable (NA).

Table 2.5-68 — {Heave after Excavation}

Measured at NI Foundation Level

Location	Vertical Displacement after Excavation [in]	
	Immediate	1 Year
A	-2.2	-2.4
B	-3.0	-3.5
C	-4.7	-5.3
D	-3.1	-3.5

Table 2.5-69 — {Foundation Loading Sequence}

Building Name		Loads [ksf]								
	Step	0	1	2	3	4	5	6	7	8
	Day	0	60	140	300	500	800	1000	1400	2000
	Month	0	2	4	10	16	26	33	46	66
	Year	0	1	1	1	2	3	3	4	6
Reactor (RB)		0.0	0.1	0.2	2.1	3.8	7.5	9.6	9.8	11.9
Fuel (FB)		0.0	0.0	1.0	1.7	2.0	5.7	9.0	14.9	14.9
Safeguard 1 (SB1)		0.0	0.0	0.8	3.8	5.9	8.6	11.8	11.8	11.8
Safeguard 2&3 (SB23)		0.0	0.0	1.0	1.7	2.6	5.4	8.2	9.6	9.6
Safeguard (SB4)		0.0	0.0	0.8	3.6	5.6	8.2	11.3	11.3	11.3
Nuclear Auxiliary (NAB)		0.0	0.0	0.9	1.8	3.5	5.3	7.1	9.7	9.7
Access (AB)		0.0	0.0	0.9	1.9	2.8	4.6	5.6	6.5	6.5
Radioactive Waste (RWPB)		0.0	0.0	0.0	0.0	0.0	0.7	2.2	6.5	6.5
Emergency Power Gen. (EPGB)		0.0	0.0	0.0	0.0	0.0	0.0	0.5	3.2	3.2
Emergency Service Water (ESWB)		0.0	0.0	0.0	0.0	0.0	1.6	5.5	5.5	5.5
Turbine (TB)		0.0	0.0	0.0	0.6	1.8	3.2	4.4	4.4	4.4
Turbine Extension (TBE)		0.0	0.0	0.0	0.6	1.8	3.2	4.4	4.4	4.4

Table 2.5-70 — {Building Center Point Settlement Estimates}

Building Name		Settlement [in] (Medium Elevation Surface Topography)(1)							
	Step	1	2	3	4	5	6	7	8
	Day	60	140	300	500	800	1000	1400	2000
	Month	2	4	10	16	26	33	46	66
	Year	1	1	1	2	3	3	4	6
Reactor (RB)		0.3	1.1	2.0	3.1	7.1	10.2	12.1	12.7
Fuel (FB)		0.3	1.3	2.0	3.0	6.8	9.8	12.4	13.0
Safeguard 1 (SB1)		0.3	1.4	2.3	3.3	7.1	10.1	11.4	12.0
Safeguard 2&3 (SB23)		0.3	1.4	2.2	3.2	7.0	9.9	11.1	11.6
Safeguard (SB4)		0.3	1.3	2.2	3.2	6.9	9.8	12.1	12.5
Nuclear Auxiliary (NAB)		0.4	1.4	2.2	3.2	6.5	9.1	12.0	12.3
Access (AB)		0.4	1.6	2.4	3.5	7.0	9.8	11.4	11.7
Radioactive Waste (RWPB)		0.5	1.3	1.9	2.7	5.1	6.9	9.4	9.6
E. Service Water 1 (ESWB1)		0.0	1.6	2.0	2.6	4.7	7.0	7.4	7.4
E. Service Water 2 (ESWB2)		0.0	1.7	2.2	2.9	5.5	8.3	8.9	9.1
E. Service Water 3 (ESWB3)		0.0	2.0	2.5	3.3	6.0	8.8	9.1	9.2
E. Service Water 4 (ESWB4)		0.0	1.9	2.3	3.0	5.3	7.9	8.1	8.2
E. Power Generating (EPBG1)		0.0	0.0	0.0	3.8	5.9	7.6	9.5	9.6
E. Power Generating (EPBG2)		0.0	0.0	0.0	3.7	5.7	7.1	8.5	8.7

Notes:
- (1) Settlement estimates correspond to Medium Elevation Surface Topography 2, Revert after 4th Step

Table 2.5-71 — {Maximum Tilt at End of Construction}

Building	Section	Tilt Direction (1)	Tilt [in/50 ft]	
			Tilt Average Elevation Case(2)	Construction Baseline(3)
NI	AA	N	-0.10	-0.10
	BB	E	0.27	0.27
	CC	SW	-0.21	-0.21
	DD	SE	0.32	0.32
ESWB1	EE	NW	-0.80	-0.59
	FF	NE	-0.17	-0.18
ESWB2	GG	SW	0.29	0.23
	HH	NW	-0.88	-0.72
ESWB3	II	NE	0.13	-0.17
	JJ	SE	0.19	0.13
ESWB4	KK	SW	0.36	0.28
	LL	SE	0.53	0.42
EPBG1	MM	SW	0.35	0.16
	NN	SE	0.68	0.49
EPBG2	OO	NE	0.72	-0.42
	PP	NW	0.37	-0.14

Notes
- (1) Local Plant Coordinates
- (2) Tilt recorded with calculation for Medium Elevation Surface Topography Revert 2
Sign is positive for clockwise tilt and negative for counter-clockwise
- (3) Correction to subtract the observed tilt before the construction of the building

Table 2.5-72 — {Settlement and Tilt for UHS Facilities}

Building	? Center [in]	Maximum Tilt (1) [in/50 ft]
Ultimate Heat Sink Makeup Water Intake Structure (UHS MWIS)	3.5	0.1
Forebay	3.4	0.1
Cooling Water Makeup Intake Structure (CW MIS)	3.6	0.4
Notes *- (1) Adjustment for construction not incorporated.*		

Table 2.5-73 — {Material Properties for Slope Stability}

Stratum	Material Property	Powerblock(1)	Intake Area & Intake Slope	Utility Corridor
Structural Backfill	Unit Weight (pcf)	145	-	-
	c (psf)	0	-	-
	f (degrees)	40	-	-
	c' (psf)	0	-	-
	f' (degrees)	40	-	-
Stratum I: Terrace Sand	Unit Weight (pcf)	120	120	120
	c (psf)	1100	1100	1100
	f (degrees)	13	13	13
	c' (psf)	0	0	0
	f' (degrees)	32	32	32
Stratum IIa: Chesapeake Clay/ Silt	Unit Weight (pcf)	115	115	115
	c (psf)	2500	3400	2500
	f (degrees)	0	0	0
	c' (psf)	900	1400	900
	f' (degrees)	25	28	25
Stratum IIb: Chesapeake Cemented Sand	Unit Weight (pcf)	120	120	120
	c (psf)	2800	2800	2800
	f (degrees)	17	17	17
	c' (psf)	0	0	0
	f' (degrees)	34	34	34
Stratum IIc: Chesapeake Clay/ Silt	Unit Weight (pcf)	105	110	105
	c (psf)	5000	4800	5000
	f (degrees)	0	0	0
	c' (psf)	2300	1000	2300
	f' (degrees)	26	26	26

Notes:
(1) Powerblock includes the Construction Laydown Area CCNPP

Table 2.5-74 — {Computed Factors of Safety for Critical Slip Surface}

Slope Section	Affected Area	Effective Stress Conditions						Total Stress Conditions[1]		
		Static Analysis			Pseudo-static (Dynamic) Analysis			Pseudo-static (Dynamic) Analysis		
		Ordinary	Bishop	M-P	Ordinary	Bishop	M-P	Ordinary	Bishop	M-P
A - Case a	Powerblock	1.92	2.19	2.18	1.32	1.47	1.47	1.73	1.76	1.76
A - Case b		1.63	1.89	1.89	1.14	1.27	1.28	1.61	1.68	1.68
B - Case a		1.95	2.22	2.22	1.35	1.49	1.49	1.76	1.81	1.81
B - Case b		1.85	2.12	2.12	1.23	1.40	1.41	1.74	1.78	1.79
C		1.96	2.02	2.02	1.31	1.36	1.36	3.15	3.24	3.24
D		1.93	1.97	1.97	1.32	1.38	1.38	4.09	4.14	4.14
E		1.98	2.05	2.05	1.34	1.41	1.41	3.15	3.15	3.15
F	Intake Area	2.20	2.34	2.34	1.57	1.68	1.69	2.73	2.81	2.82
G	Utility Corridor	1.87	2.04	2.05	1.24	1.34	1.35	1.86	1.92	1.93

Notes:
Ordinary = Ordinary method
Bishop = Bishop's simplified method
M-P = Morgenstern-Price method
Typical minimum acceptable values of FOS are 1.5 for static conditions and 1.0 to 1.2 for pseudo-static (e.g., earthquake) conditions (Duncan, 1996)
(1) Total stress conditions are more representative of dynamic conditions are not used in the discussion.

Table 2.5-75 — {Building Points with Associated Differential Settlements}

Building Name		Pair of Point No.		u_y (in.)		?u_y (in.)
		NI	Adj. Bldg.	NI	Adj. Bldg.	
Emergency Power Generating Building 1 (EPBG1)	Center	1	54	12.7	3.7	9.1
	Edge	21	57	10.7	3.9	6.8
	Edge	22	56	12.1	4.4	7.7
	Edge	26	56	11.6	4.4	7.2
Emergency Power Generating Building 2 (EPBG2)	Center	1	59	12.7	3.0	9.8
	Edge	12	60	11.4	3.5	7.8
	Edge	14	60	10.9	3.5	7.4
	Edge	19	63	10.4	3.1	7.2
Emergency Service Water Building 2 (ESWB2)	Center	1	74	12.7	6.2	6.6
	Edge	12	77	11.4	6.5	4.8
	Edge	12	78	11.4	7.4	3.9
	Edge	30	75	12.4	5.8	6.6
	Edge	30	78	12.4	7.4	4.9
	Edge	31	77	12.3	6.5	5.7
	Edge	31	78	12.3	7.4	4.8
Emergency Service Water Building 3 (ESWB3)	Center	1	69	12.7	5.9	6.8
	Edge	21	70	10.7	6.1	4.6
	Edge	21	71	10.7	6.1	4.6
	Edge	21	72	10.7	5.5	5.1
	Edge	26	70	11.6	6.1	5.4
	Edge	26	71	11.6	6.1	5.5
Turbine Building (TB)	Center	1	84	12.7	8.9	3.9
	Edge	19	86	10.4	10.3	0.0
	Edge	20	85	10.7	10.3	0.4
	Edge	20	86	10.7	10.3	0.3
	Edge	21	85	10.7	10.3	0.4
Nuclear Auxiliary Building (NAB)	Center	1	42	12.7	11.9	0.8
	Edge	22	40	12.1	11.4	0.7
	Edge	23	39	12.6	13.3	0.7
	Edge	28	36	12.3	12.3	0.0
	Edge	33	38	12.7	13.3	0.6
	Edge	34	37	12.7	13.3	0.6
	Edge	36	28	12.3	12.3	0.0
Access Building (AB)	Center	1	45	12.7	11.3	1.4
	Edge	16	46	12.1	12.3	0.2
	Edge	21	47	10.7	11.2	0.5
	Edge	25	44	12.1	12.6	0.4
	Edge	26	43	11.6	11.6	0.1
		RWPB	NAB	RWPB	NAB	
Radwaste Building (RWPB) - Nuclear Auxiliary Building (NAB)		51	41	7.3	10.1	2.7
		52	40	8.7	11.4	2.6
u_y (NI) - Settlements at the end of the 8th loading step at the base of the N						
u_y (Adj. Bldg)- Settlements at the end of the 8th loading step at the base of the adjacent building						
?u_y - Differential Settlements						

Table 2.5-76 — {Seismic Bearing Capacity Results}

Dynamic Bearing Capacity	Foundation Width (ft)		
	$B_1 = 270$	$B_2 = 203$	$B_3 = 135$
Ultimate, q_{ult} (ksf)	145.8	131.9	117.0
Allowable, q_a (ksf) (1)	72.9	66.0	58.5
Notes: (1) Factor of Safety for dynamic forces is FOS = 2.0. i.e., $_{qa} = q_{ult}/FOS$			

Figure 2.5-1 — {Map of Physiographic Province}

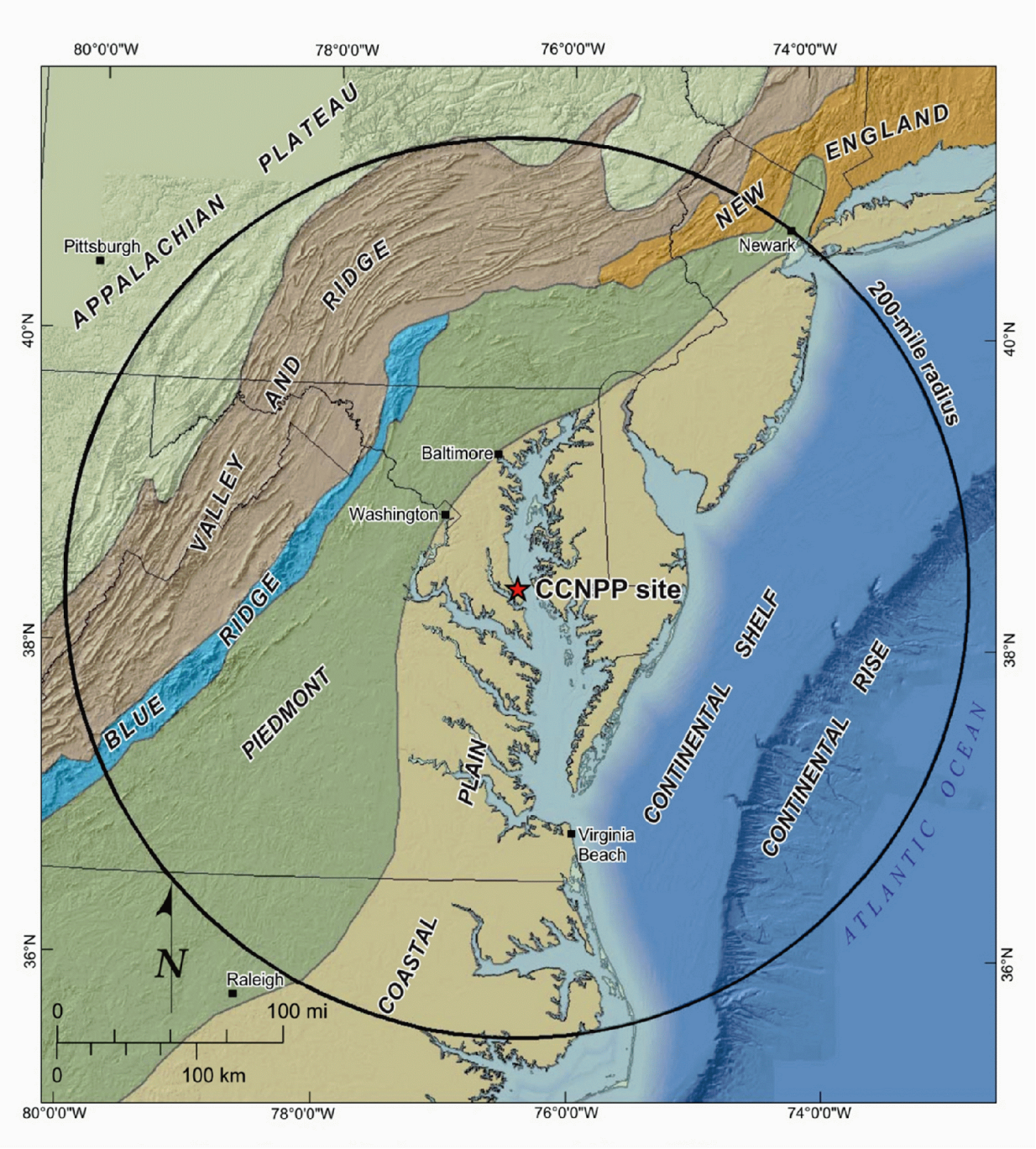

Figure 2.5-2 — {Site Vicinity Topographic Map 25-Mile (40-Km) Radius}

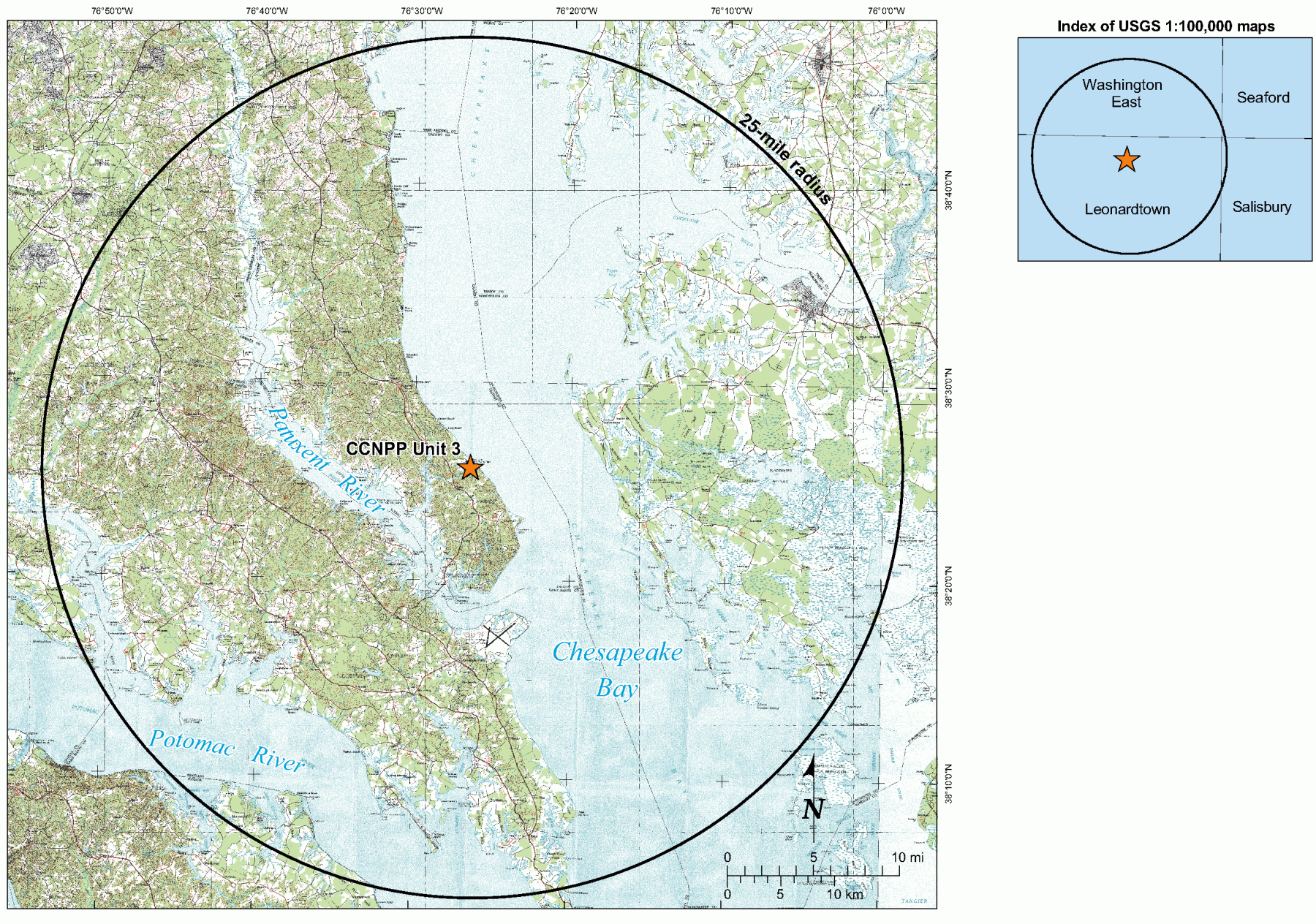

Figure 2.5-3 — {Site Area Topographic Map 5-Mile (8-Km) Radius}

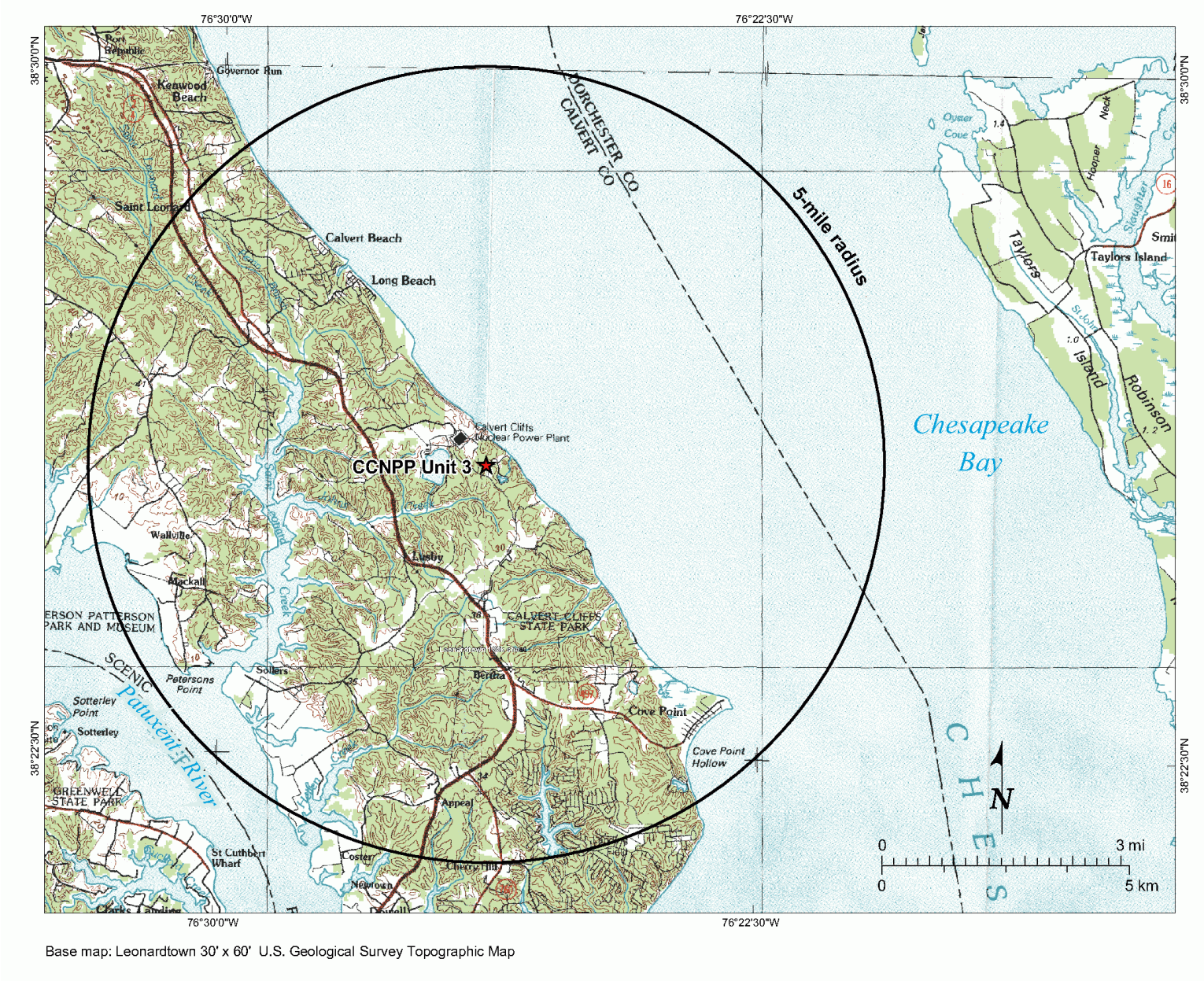

Base map: Leonardtown 30' x 60' U.S. Geological Survey Topographic Map

Figure 2.5-4 — {Site Topographic Map 0.6-Mile (1-Km) Radius}

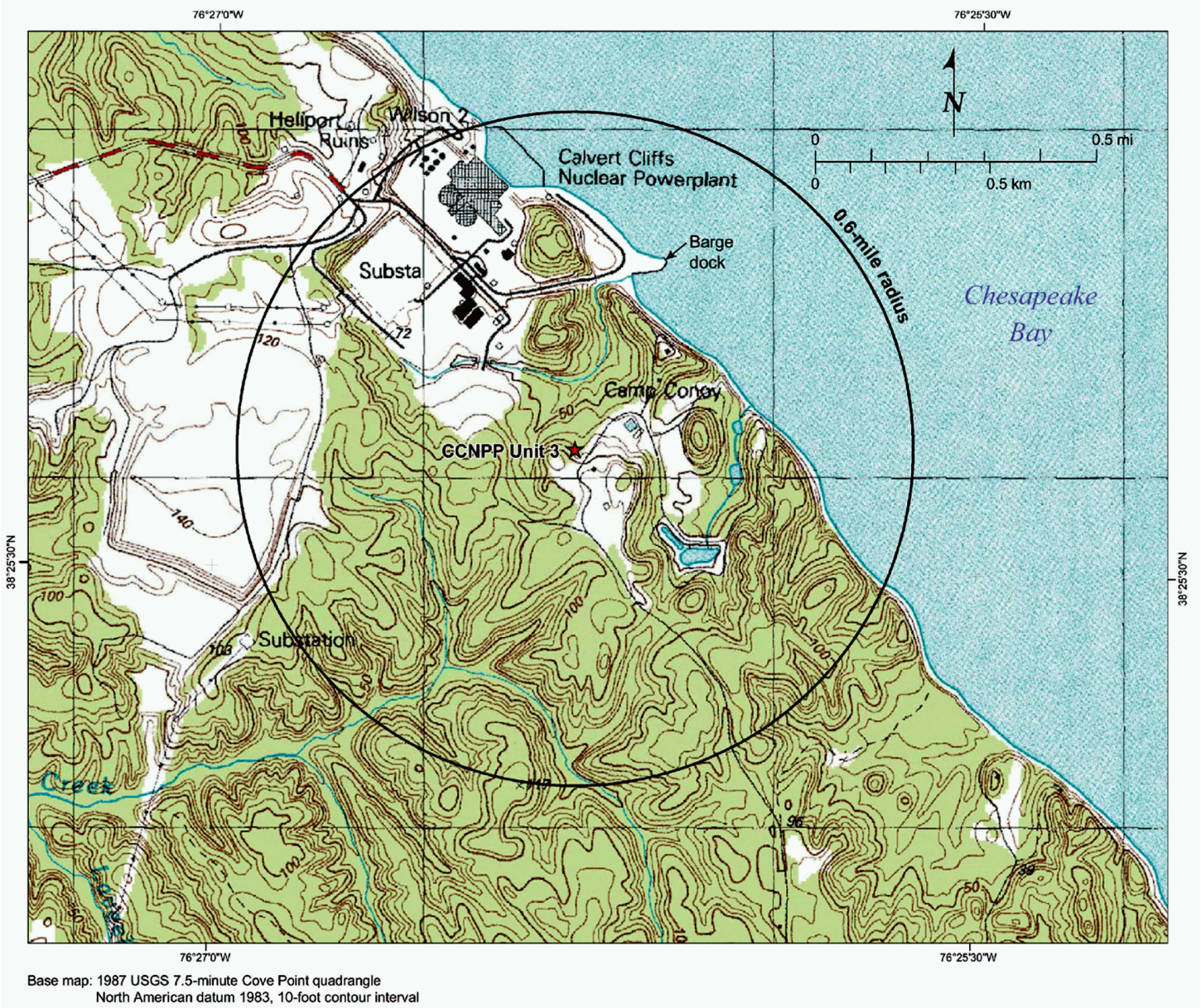

Figure 2.5-5 — {Regional Geologic Map 200-Mile (320-Km) Radius}

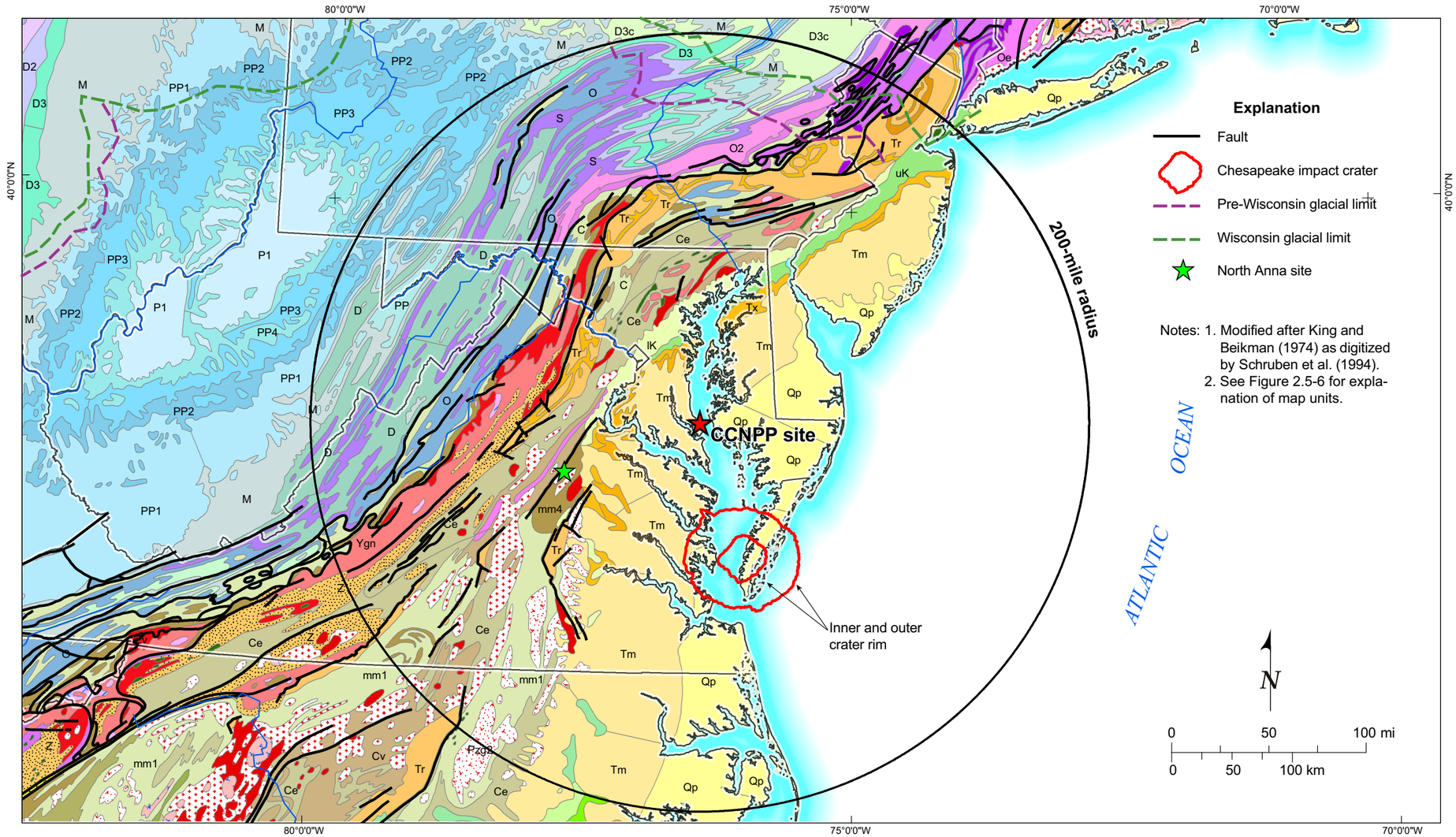

Figure 2.5-6 — {Regional Geologic Map 200-Mile (320-Km) Radius Explanation}

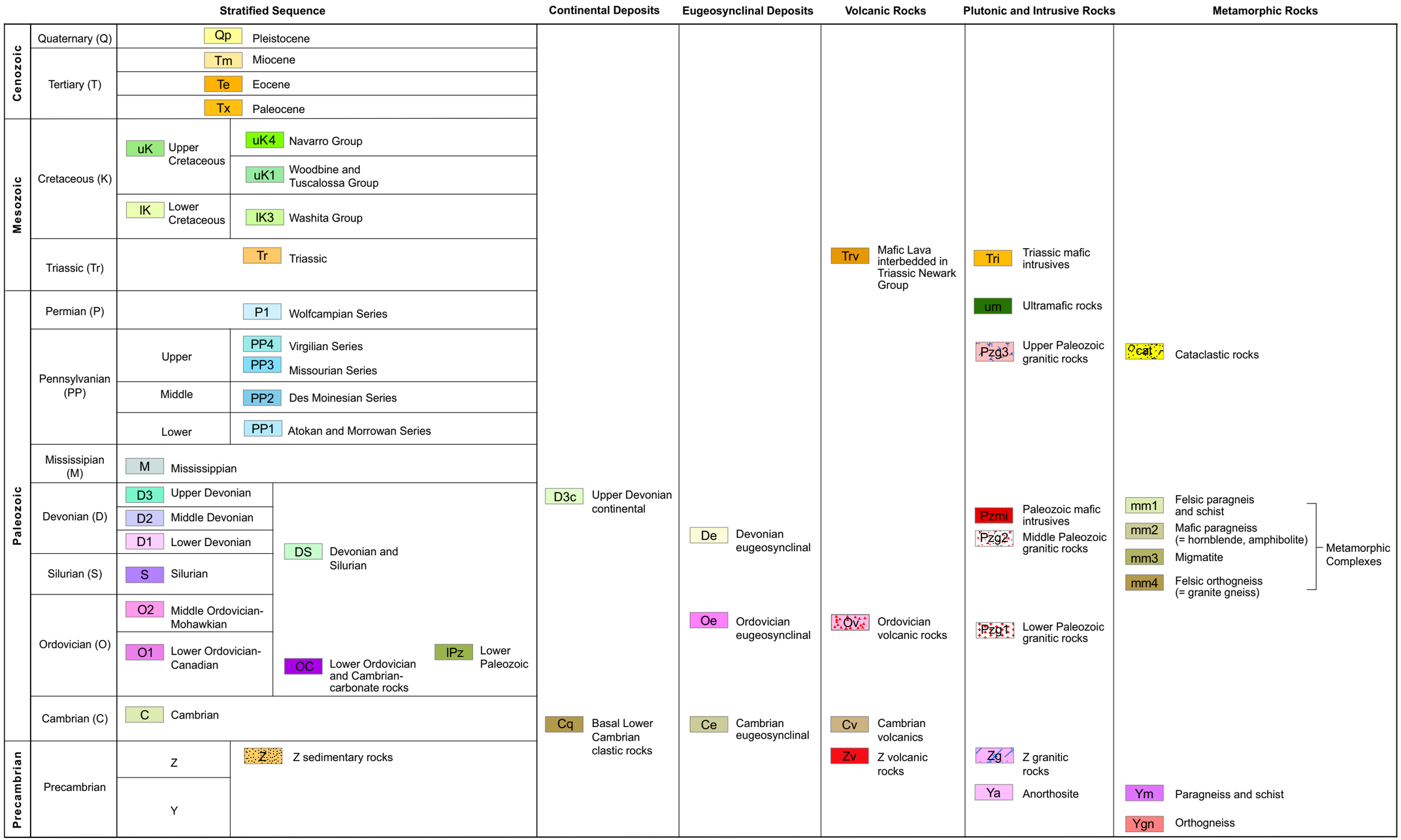

Figure 2.5-7 — {Physiographic Map of Maryland}

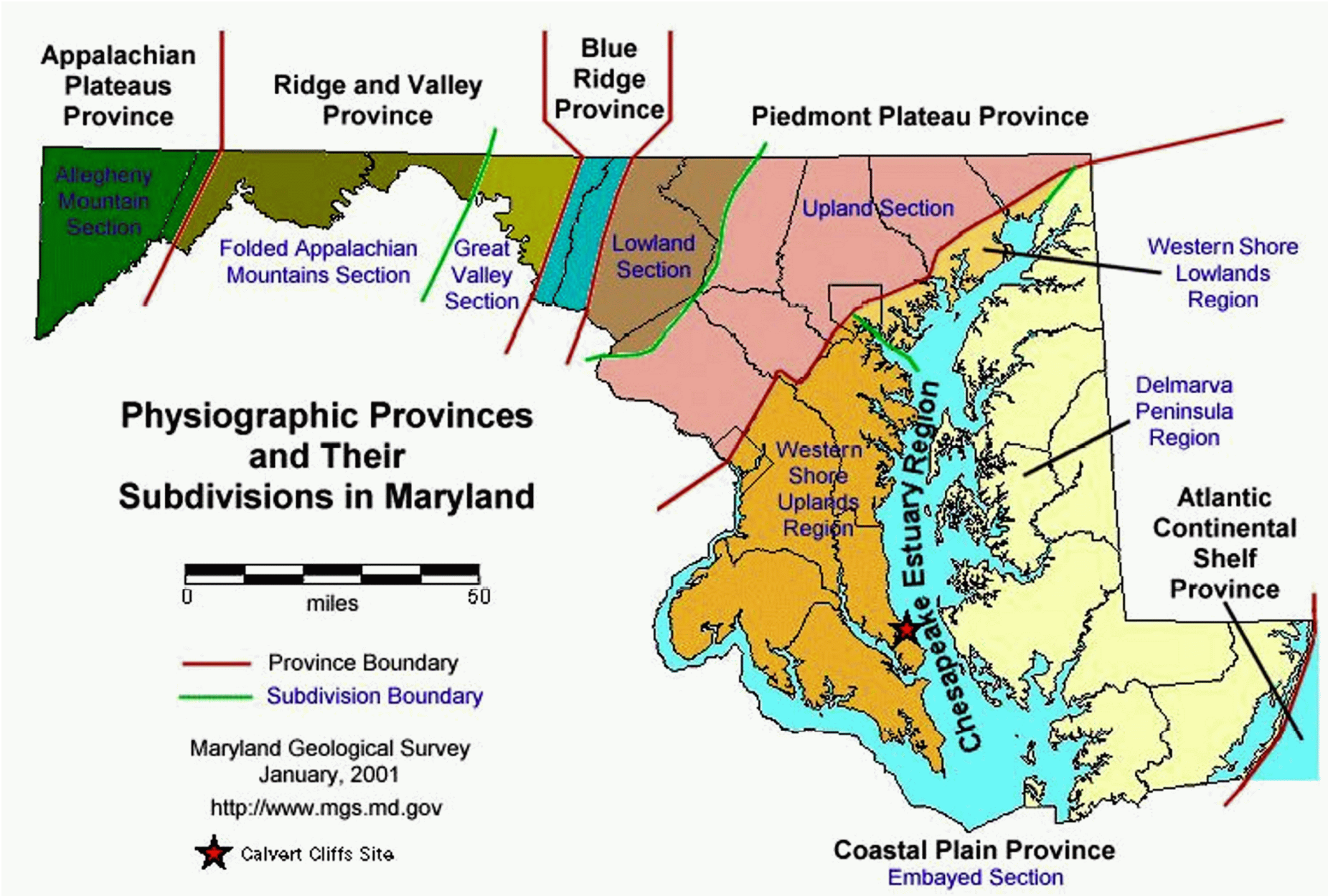

Figure 2.5-8 — {Evolution of the Appalachian Orogen}

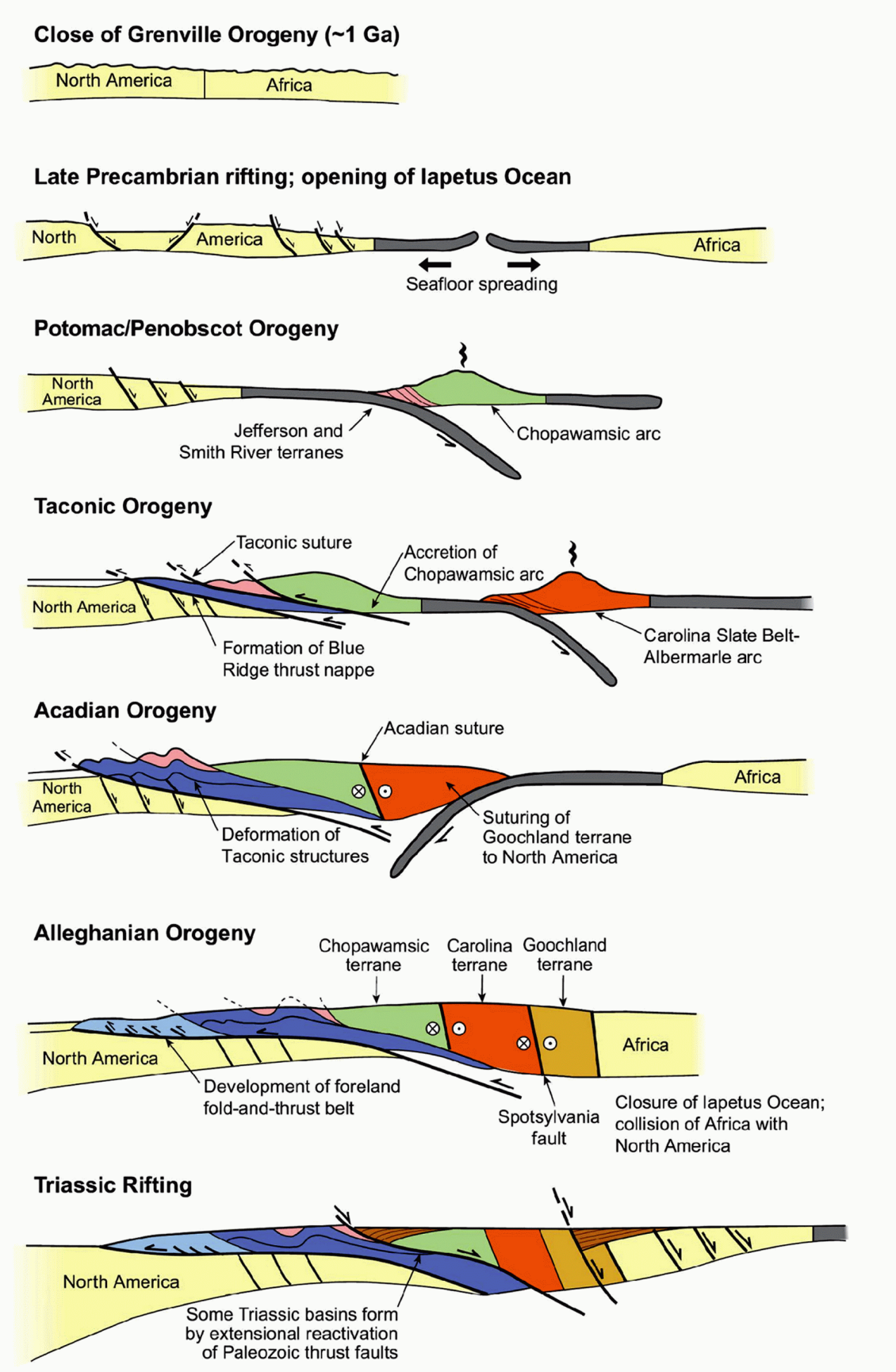

Figure 2.5-9 — {General Technostatigraphic Terrane Map 200-mile (320 km) Radius (modified from Horton 1991)}

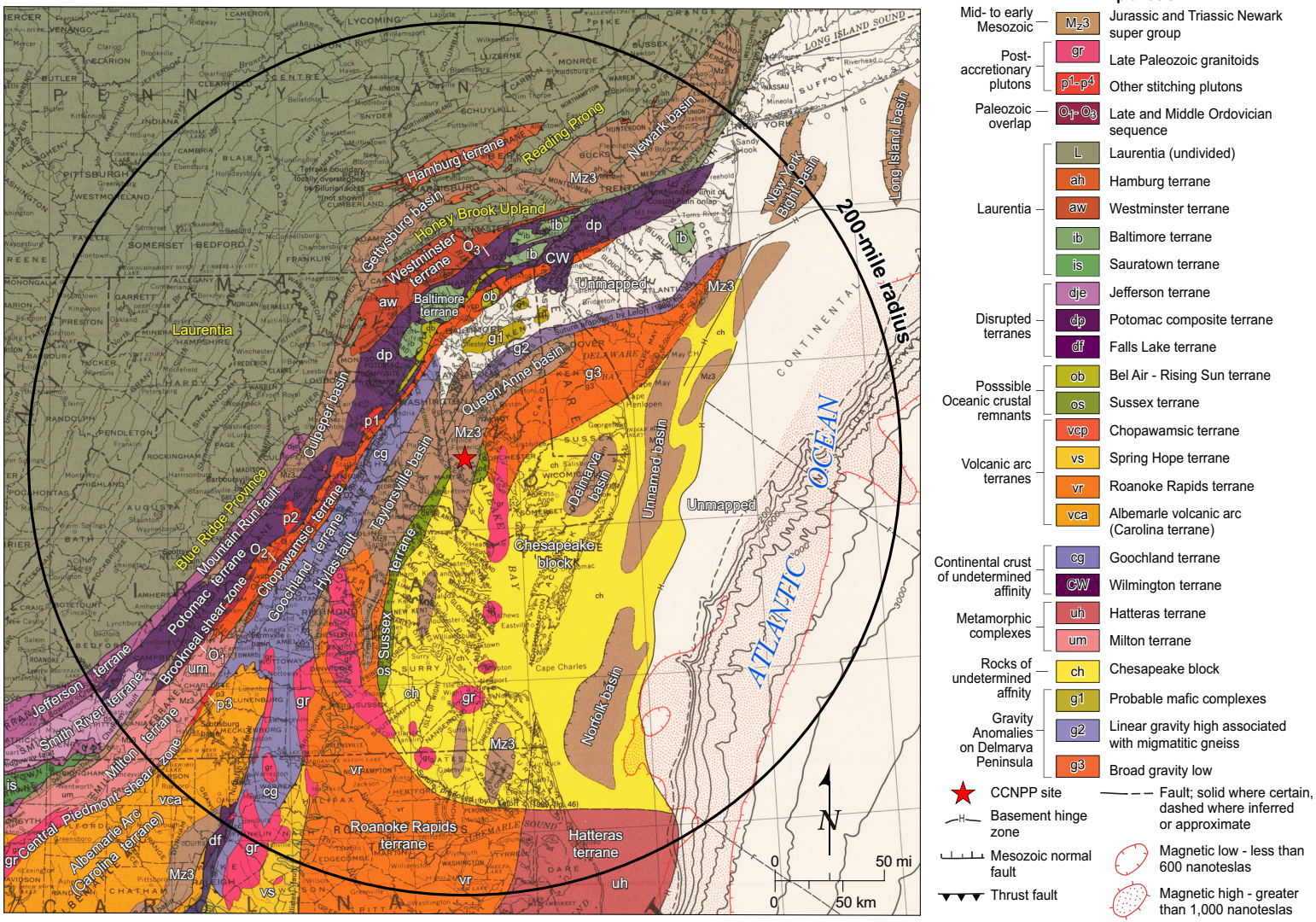

Explanation

Mid- to early Mesozoic	M_z3	Jurassic and Triassic Newark super group
Post-accretionary plutons	gr	Late Paleozoic granitoids
	p^1–p^4	Other stitching plutons
Paleozoic overlap	O_1–O_3	Late and Middle Ordovician sequence
Laurentia	L	Laurentia (undivided)
	ah	Hamburg terrane
	aw	Westminster terrane
	ib	Baltimore terrane
	is	Sauratown terrane
Disrupted terranes	dje	Jefferson terrane
	dp	Potomac composite terrane
	df	Falls Lake terrane
Possible Oceanic crustal remnants	ob	Bel Air - Rising Sun terrane
	os	Sussex terrane
Volcanic arc terranes	vcp	Chopawamsic terrane
	vs	Spring Hope terrane
	vr	Roanoke Rapids terrane
	vca	Albemarle volcanic arc (Carolina terrane)
Continental crust of undetermined affinity	cg	Goochland terrane
	CW	Wilmington terrane
Metamorphic complexes	uh	Hatteras terrane
	um	Milton terrane
Rocks of undetermined affinity	ch	Chesapeake block
Gravity Anomalies on Delmarva Peninsula	g1	Probable mafic complexes
	g2	Linear gravity high associated with migmatitic gneiss
	g3	Broad gravity low

CCNPP site
Basement hinge zone
Mesozoic normal fault
Thrust fault
Fault; solid where certain, dashed where inferred or approximate
Magnetic low - less than 600 nanoteslas
Magnetic high - greater than 1,000 nanoteslas

Figure 2.5-10 — {Map of Mesozoic Basins}

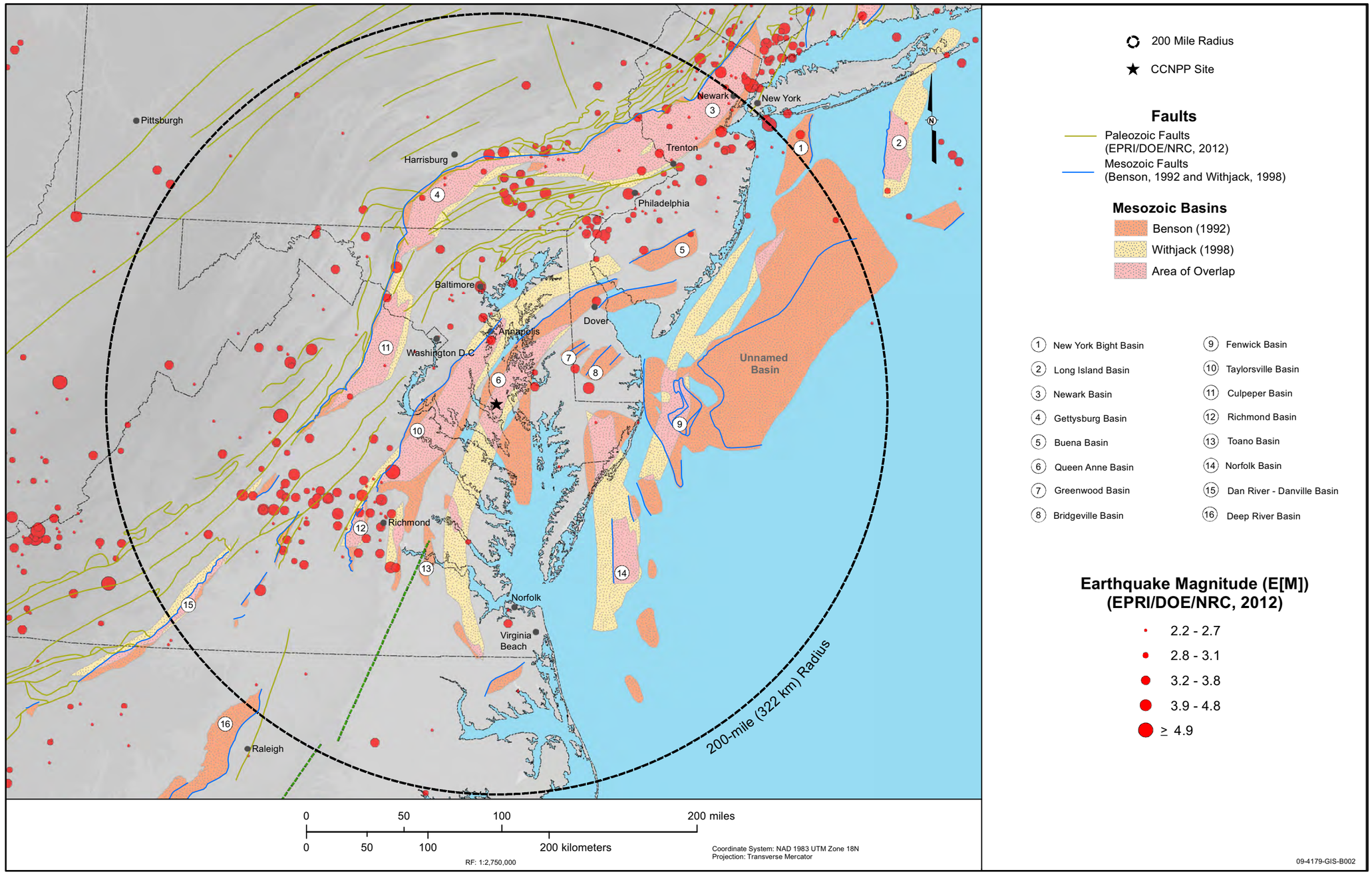

Figure 2.5-11 — {Lithologies of Basement Rocks from Coastal Plain Wells}

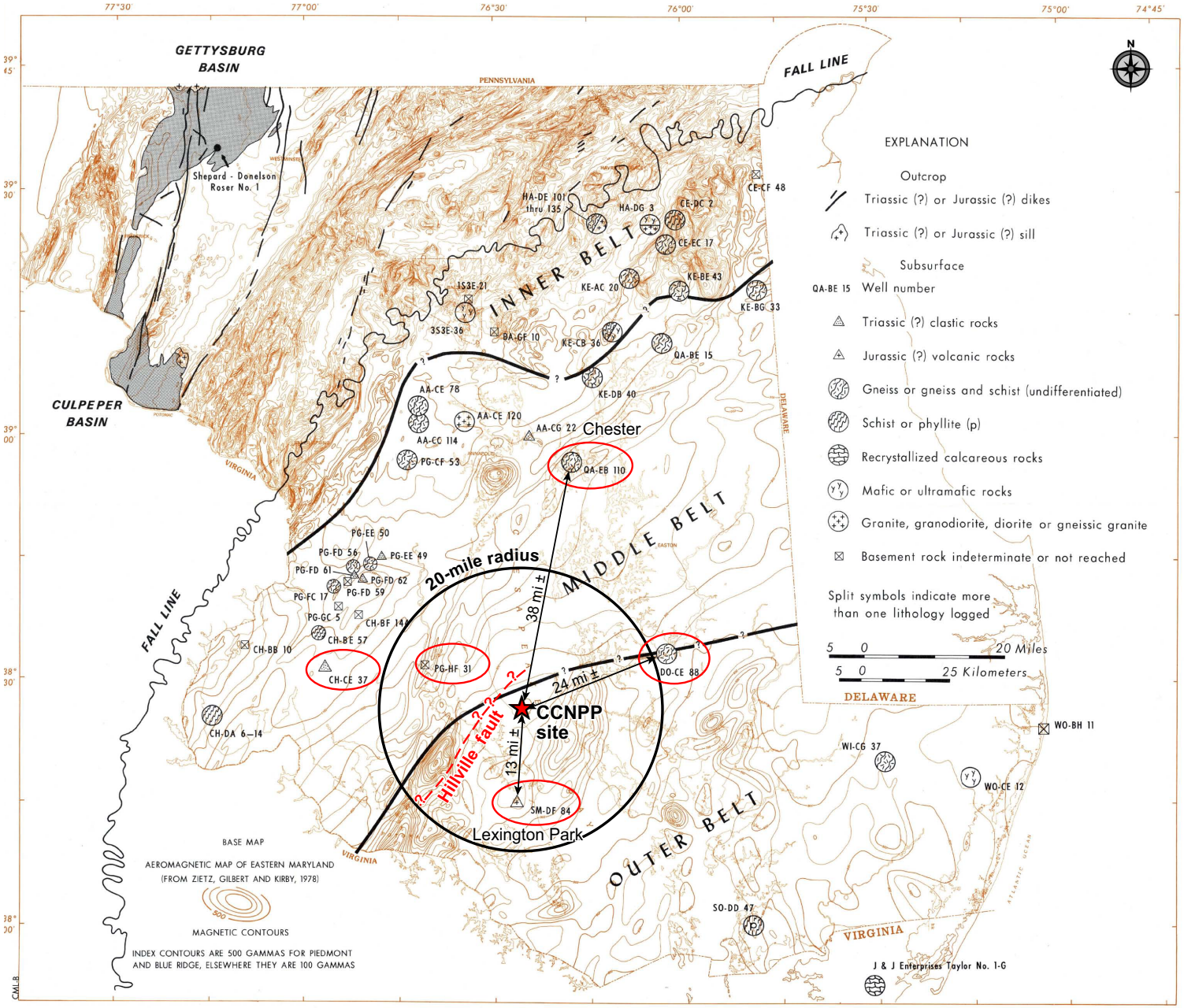

Figure 2.5-12 — {Tectonic Features of the Mid-Atlantic Passive Margin}

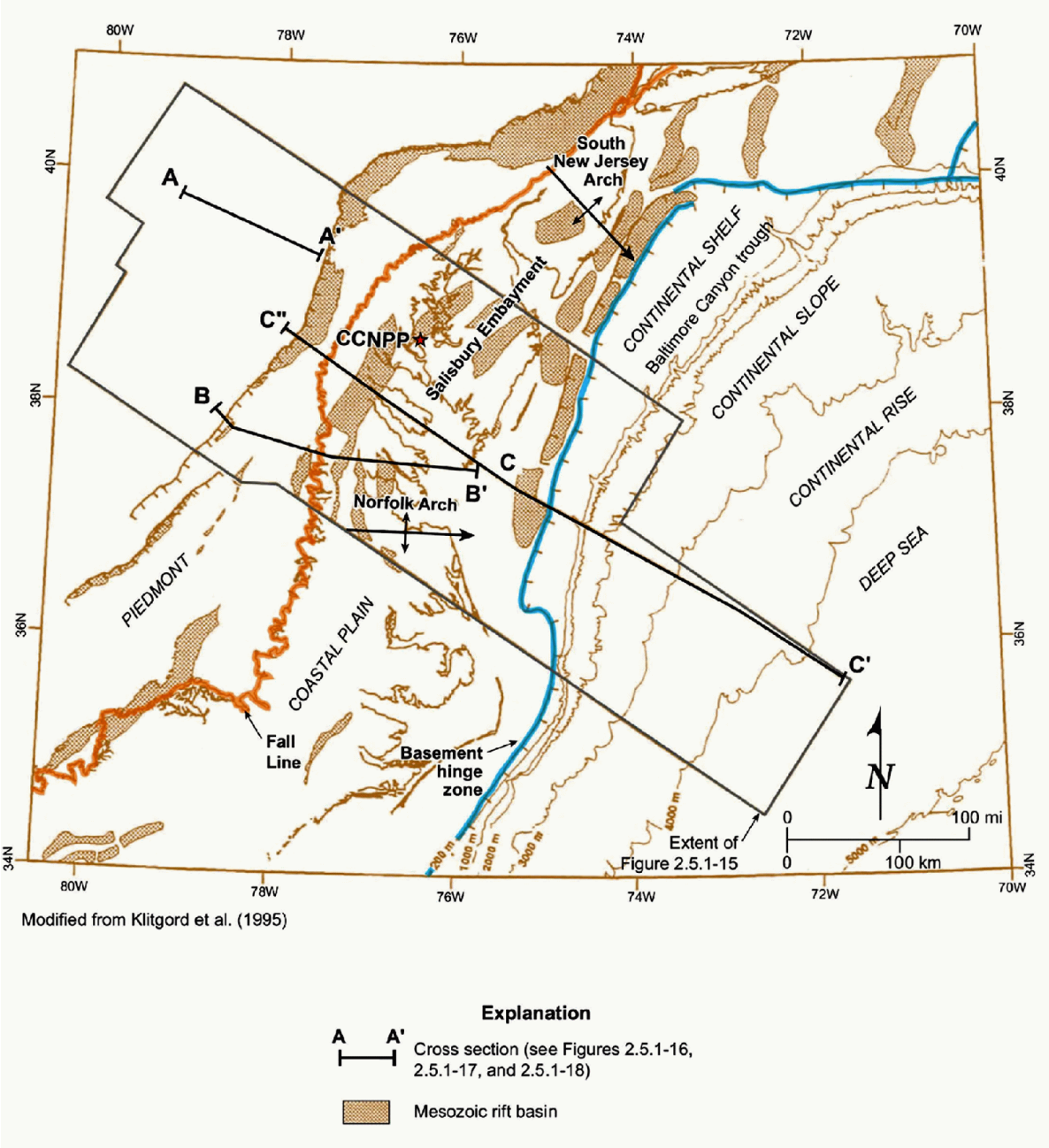

Figure 2.5-13 — {Stratigraphic Cross-Section Through Anne Arundel, Calvert and St. Mary's Counties}

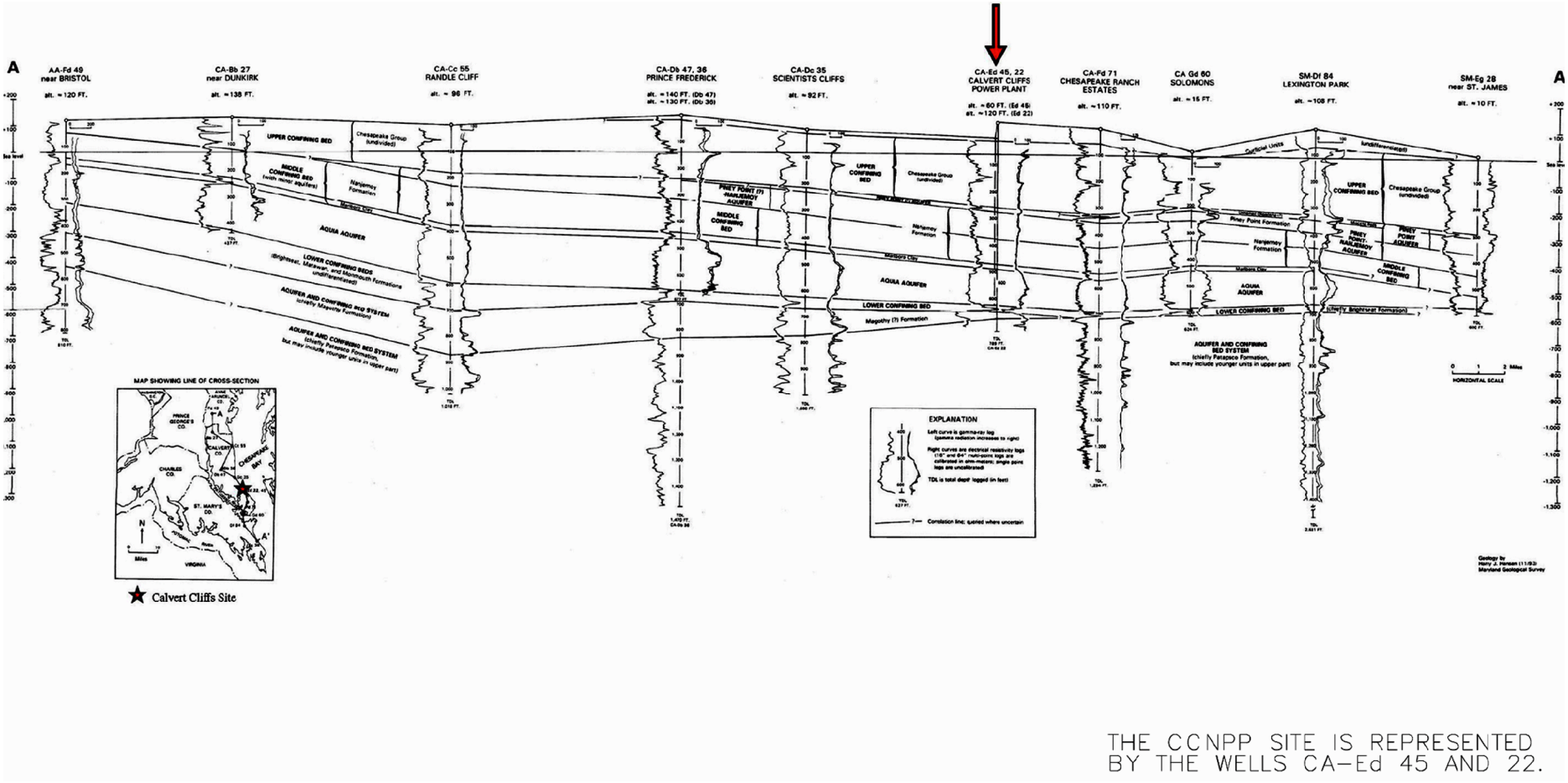

Figure 2.5-14 — {Structure-Contour Map of the Top of the Piney Point-Nanjemoy Aquifer}

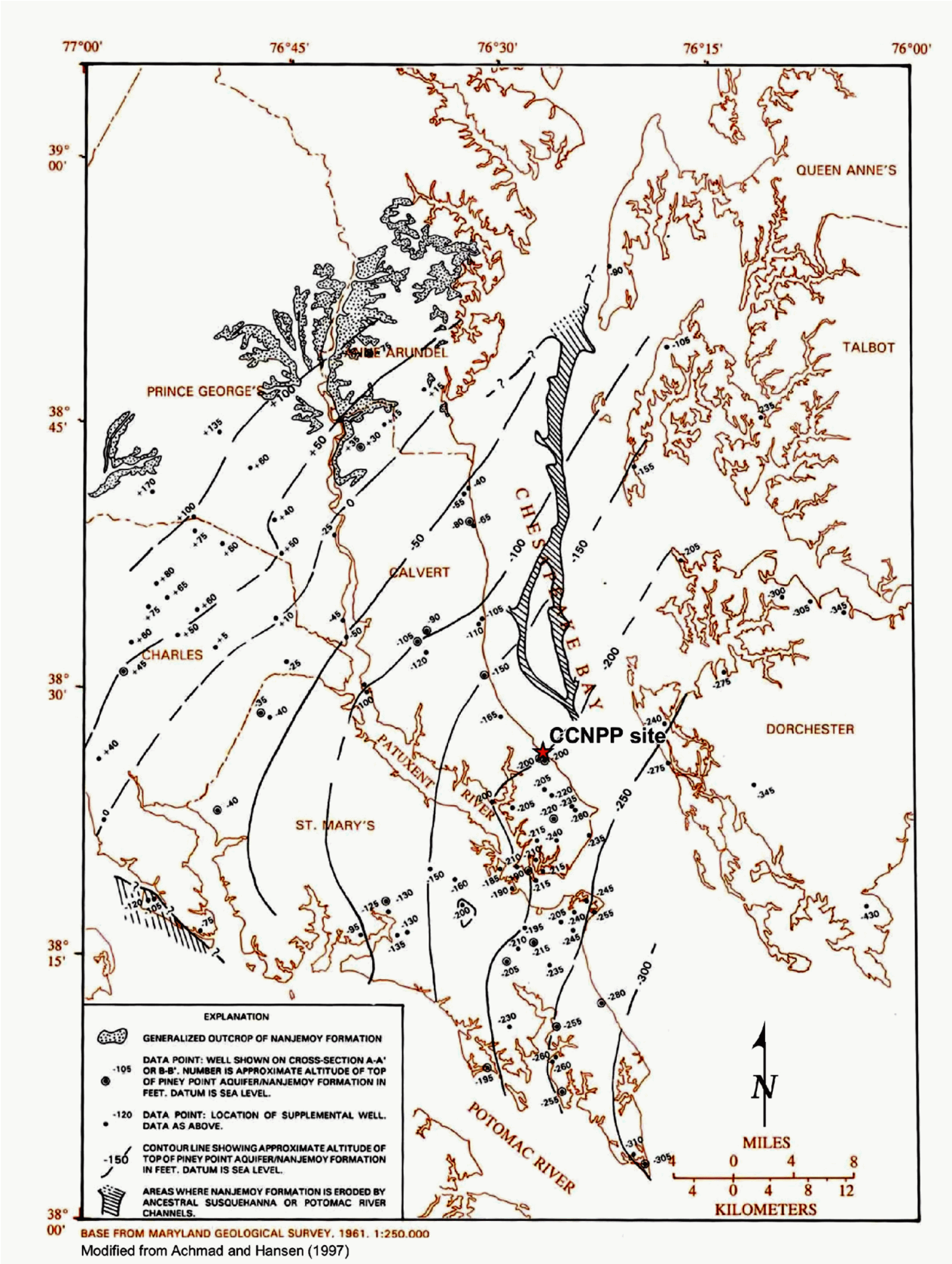

Modified from Achmad and Hansen (1997)

Figure 2.5-15 — {Tectonic Age of Crust}

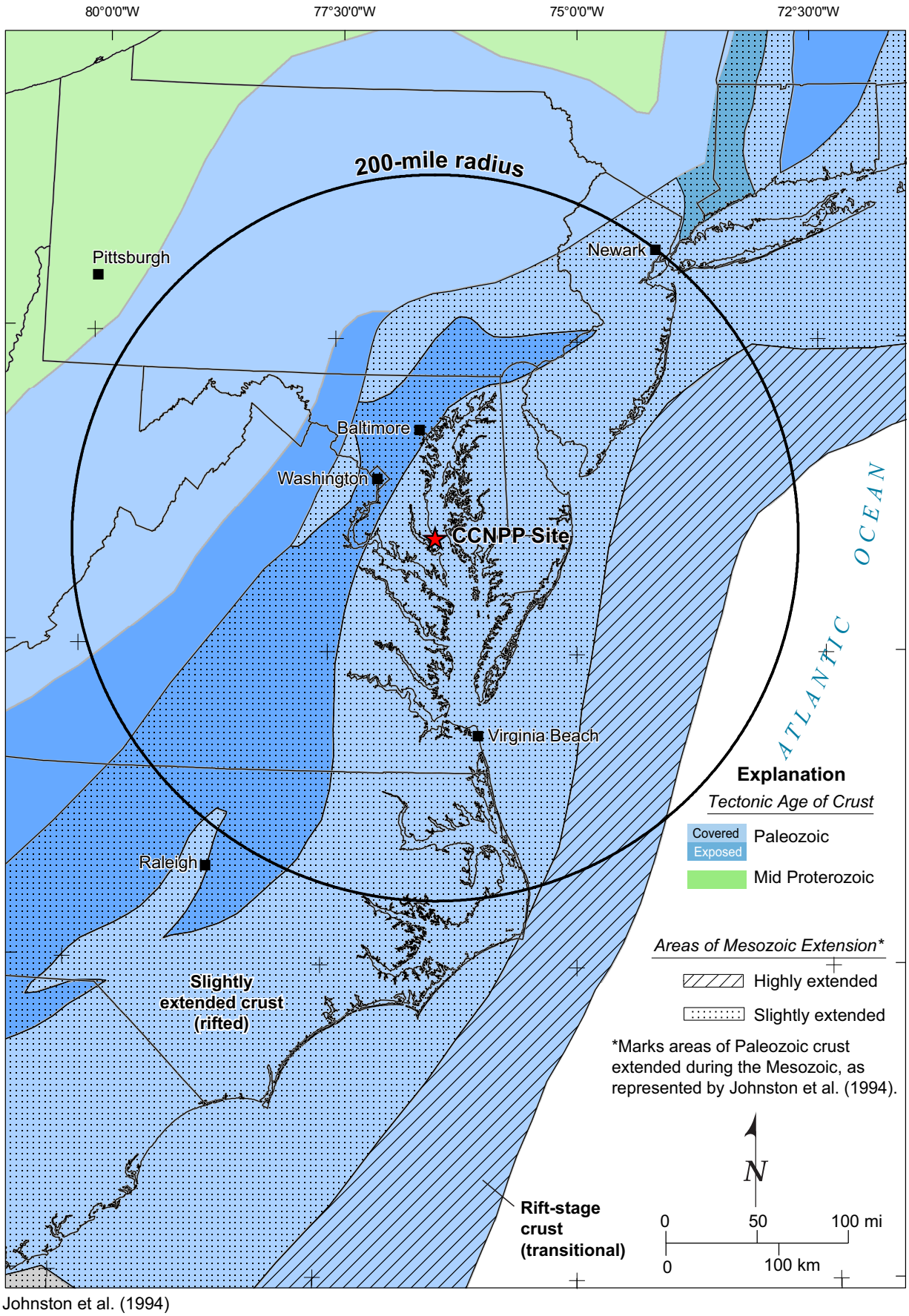

Johnston et al. (1994)

Figure 2.5-16 — {Regional Strip Maps Showing Tectonostratigraphic Divisions and Regional Cross-Section Lines}

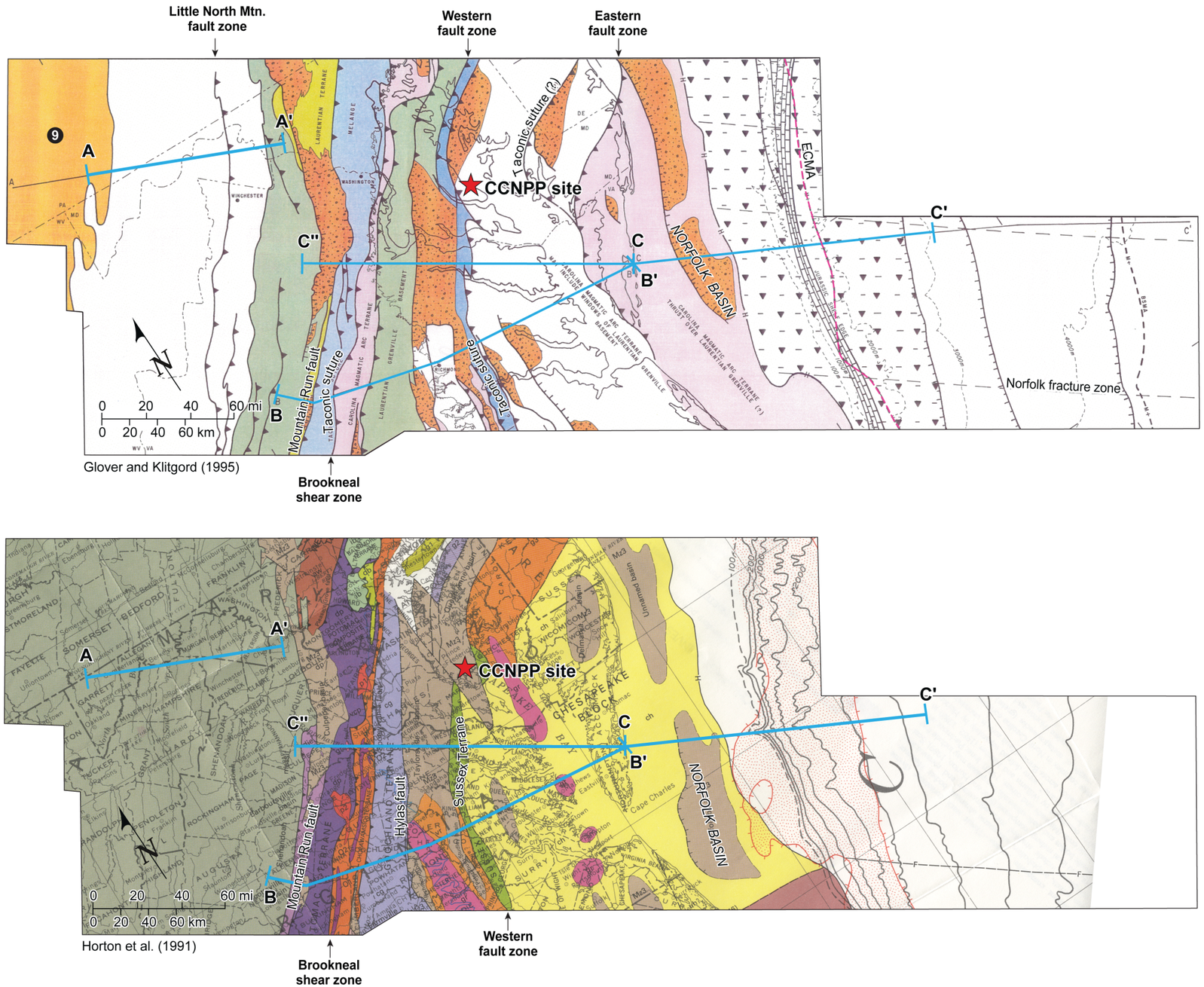

Explanation
(Glover and Klitgord, 1995)

Symbols	*Map Units*
Bathymetric isobath	Cenozoic
Normal fault	Early Mesozoic basin
Basement hinge zone	Cretaceous - stratified rock
C C' Cross section (see Figures 2.5.-17, 18, and 19)	Permian - Upper Mississippian straified rock
Magnetic lineament	Lower Jurassic - Upper Triassic stratified rock
	Jurassic volcanic wedge
	Cambrian - stratified rock
	Cambrian - intrusive rock

Explanation
(Horton et al., 1991)

Symbols	*Map Units*
Basement hinge zone	M_z3 Jurassic and Triassic Newark super group
Mesozoic normal fault	gr Late Paleozoic granitoids
Thrust fault	p^1, p^2 Other stitching plutons
C C' Cross-section line (see Figures 2.5-17, 18, and 19	O_2 O_1 Late and Middle Ordovician sequences interpreted as Taconian successor basin deposits
Fault; solid where certain, dashed where inferred or approximate	L Laurentia (undivided)
Magnetic low - less than 600 nanoteslas	aw Westminster terrane
Magnetic high - greater than 1,000 nanoteslas	ib Baltimore terrane
	dje Jefferson terrane
	dp Potomac composite terrane
	ob Bel Air - Rising Sun terrane
	os Sussex terrane
	vcp Chopawamsic terrane
	vr Roanoke Rapids terrane
	cg Goochland terrane
	ch Chesapeake block
Gravity Anomalies on Delmarva Peninsula	g1 Probable mafic complexes
	g2 Linear gravity high associated with migmatitic gneiss
	g3 Broad gravity low

Figure 2.5-17 — {Crustal-Scale Cross Section Through the Appalachian Orogen and Coastal Plain}

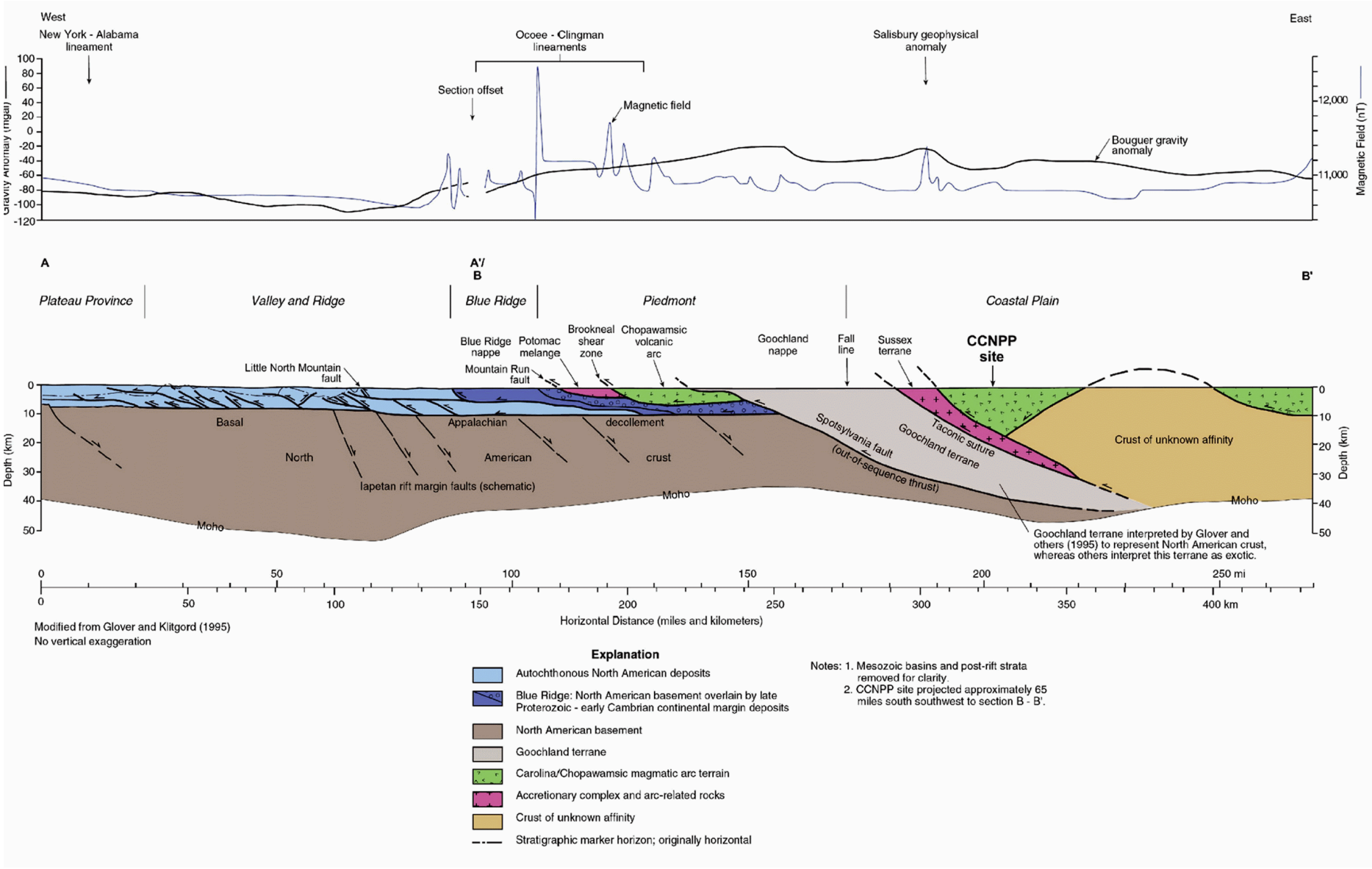

Figure 2.5-18 — {Crustal-Scale Cross Section Across the Mid-Atlantic Continental Shelf, Slope and Rise}

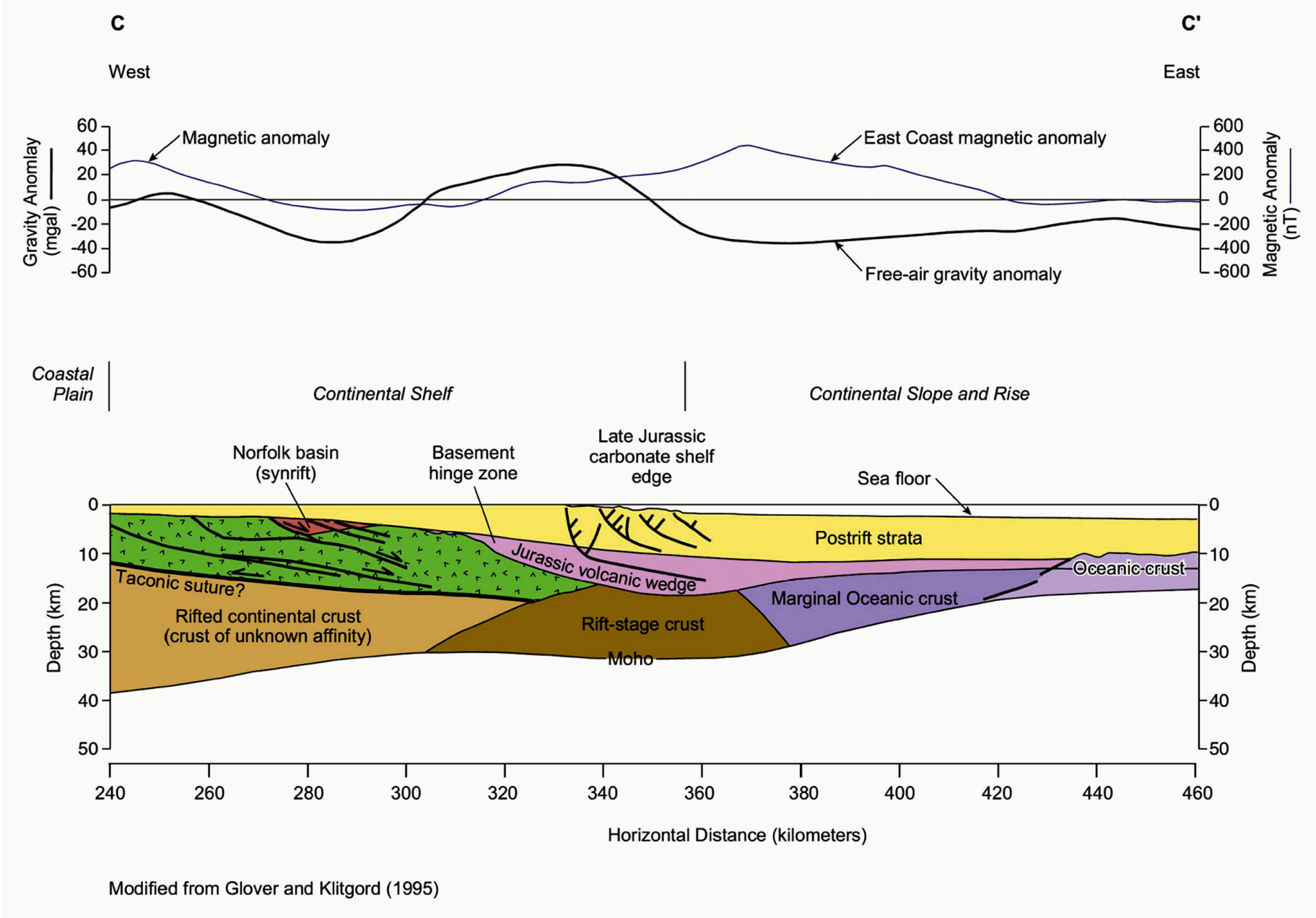

Modified from Glover and Klitgord (1995)

Figure 2.5-19 — {Crustal-Scale Cross Section of the Mid-Atlantic Passive Margin}

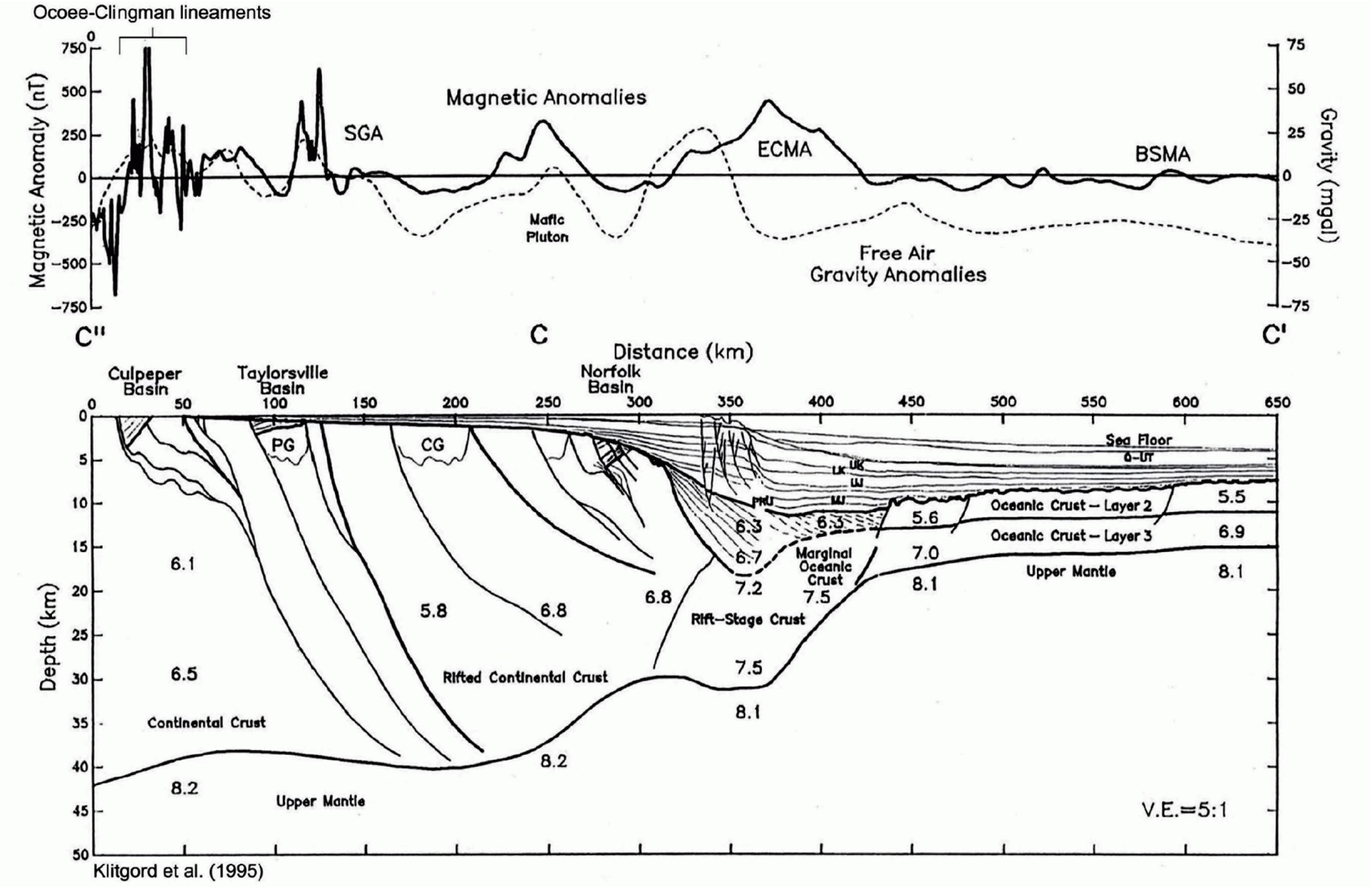

Cross section along line C" - C - C' displaying selected crustal fractures. Surface features along segment C" - C are taken directly from the geologic map panel. Subsurface features have been projected northward onto the profile from cross section B - B'. Magnetic and gravity anomaly profiles along the section and selected refraction velocity values (in km/sec) are shown. Major sub-horizontal crustal boundaries are indicated by heavy lines. Sedimentary strata are indicated by the light lines above the upper heavy line. SGA - Salisbury geophysical anomaly; ECMA = East Coast magnetic anomaly; BSMA = Blake Spur magnetic anomaly; PG = Petersburg Granite; CG = Chesapeake Granite. See Figure 2.5.1-15 for section location. C- C' is the same as Figure 2.5.1-17, but represents an alternative interpretation.

Figure 2.5-20 — {Regional Magnetic Anomaly Map}

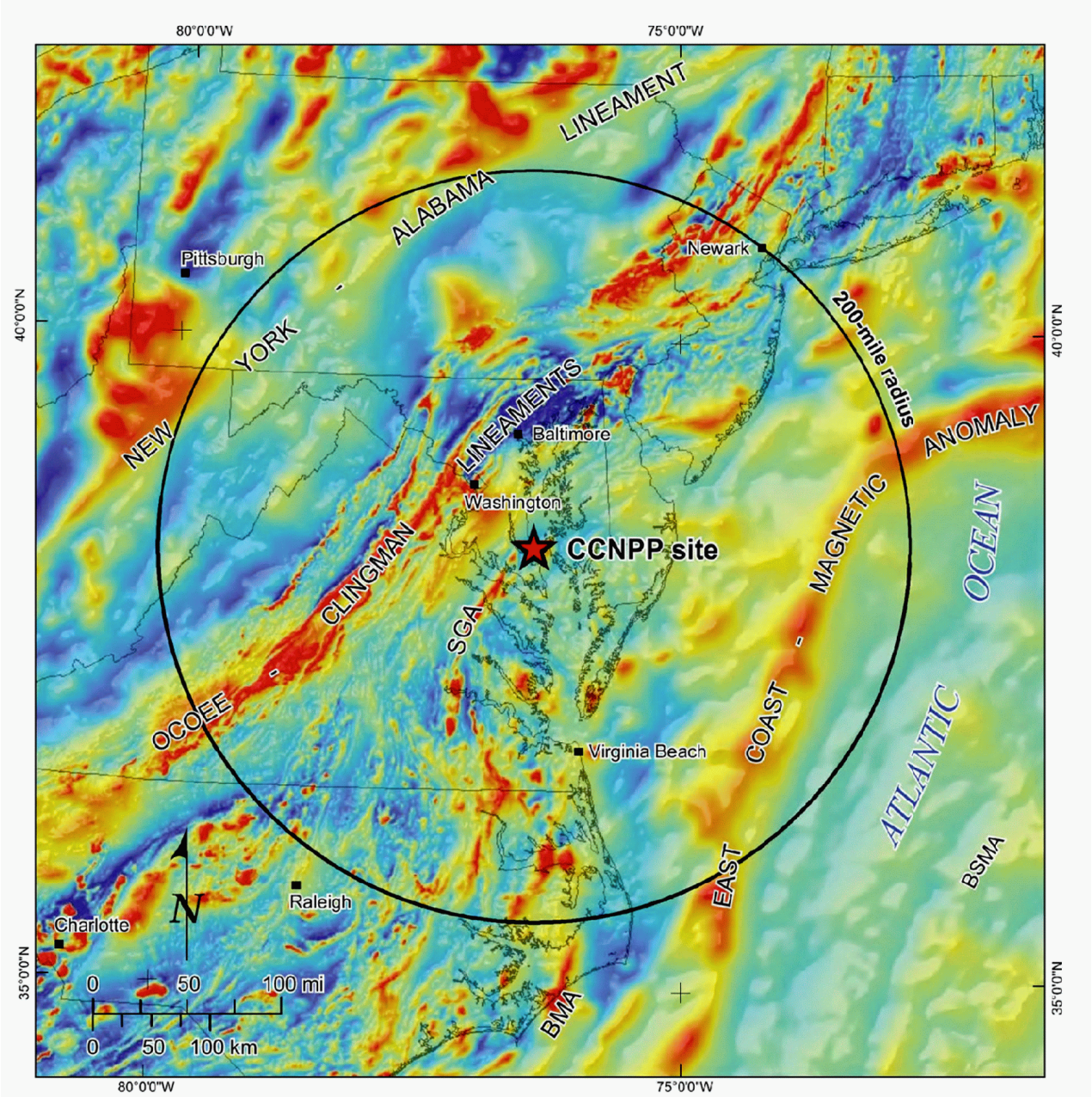

Explanation

BMA	Brunswick magnetic anomaly
BSMA	Blake Spur magnetic anomaly
SGA	Salisbury geophysical anomaly

Aeromagnetics (Bankey et al., 2002)

8215 nanoteslas

0

-1730 nanoteslas

Note: Aeromagnetic data from Bankey et al. (2002).